AD 702659
AGARD CP No. 48

AGARD

ADVISORY GROUP FOR AEROSPACE RESEARCH & DEVELOPMENT

Aerodynamics of Atmospheric Shear Flows

This document has been approved for public release and sale; its distribution is unlimited.

DDC
RECEIVED
MAR 30 1970

NORTH ATLANTIC TREATY ORGANIZATION

Reproduced by the
CLEARINGHOUSE
for Federal Scientific & Technical
Information Springfield Va. 22151

INITIAL DISTRIBUTION IS LIMITED
FOR ADDITIONAL COPIES SEE BACK COVER

436

Conference Proceedings No.48

NORTH ATLANTIC TREATY ORGANIZATION

ADVISORY GROUP FOR AEROSPACE RESEARCH AND DEVELOPMENT

(ORGANISATION DU TRAITE DE L'ATLANTIQUE NORD)

THE AERODYNAMICS OF ATMOSPHERIC SHEAR FLOW

Papers presented at the Fluid Dynamics Panel Specialists' Meeting held at Munich, Germany, 15-17 September 1969

The material in this publication has been produced directly from copy supplied by each author.

551.511.32:533.6.011

Published February 1970

Printed by Technical Editing and Reproduction Ltd
Harford House, 7-9 Charlotte Street, London W1P 1HD

AGARD FLUID DYNAMICS PANEL

PANEL CHAIRMAN Professor R.N.Cox, The City University, London, UK.
PANEL DEPUTY CHAIRMAN Professor W.R.Sears, Cornell University, Ithaca, US.

PROGRAMME COMMITTEE MEMBERS

Professor A.D.Young, University of London, UK. (Chairman)
Mr E.Dobbinga, Delft Technical University, Netherlands.
Professor J.J.Ginoux, Von Kármán Institute, Rhode-St-Genèse, Belgium.
Professor E.Truckenbrodt, Technische Hochschule München, Germany.
Professor J.Valensi, Institut de Mécanique des Fluides de l'Univ. d'Aix-Marseille, France.
Professor B.W.Marschner, Colorado State University, US.

FDP EXECUTIVE, Dr R.Barth

FOREWORD

The decision to hold a Specialists' Meeting on "The Aerodynamics of Atmospheric Shear Flows" was taken as a result of a Round Table Discussion of the Fluid Dynamics Panel in September, 1967, at Göttingen.

The subject is a very wide one and could readily be extended well outside the realm of aeronautical problems. It was felt, however, that in the context of this AGARD meeting the emphasis should be on aspects of direct aeronautical interest. Nevertheless, it was agreed that other aspects should not be rigidly excluded, since certain developments aimed at non-aeronautical problems can readily have relevance to aeronautical and space needs.

The Programme Committee decided that papers should be invited under three headings; namely: I. The Structure of Atmospheric Shear Flows; II. Basic Problems Related to Atmospheric Shear Flow; III. Industrial Problems.

The final programme is made up of 10 papers under Topic I, 10 papers under Topic II, and 4 papers under Topic III. In addition associated with each topic is a general review paper by a leading exponent in that field. It is hoped that the final coverage of meteorological aspects, laboratory and simulation techniques and behaviour of structures in shear flows will prove a balanced one and will provide a useful basis for discussion and a stimulus for further work.

The contributions to the programme derive from six NATO countries.

A. D. Young

CONTENTS

	Page
PANEL MEMBERS AND PROGRAMME COMMITTEE	iii
FOREWORD	iv

TOPIC I - STRUCTURE OF ATMOSPHERIC SHEAR FLOWS

	Reference
THE STRUCTURE OF ATMOSPHERIC SHEAR FLOWS by H.Panofsky	1
THE ORIGINS AND FORMS OF DYNAMIC INSTABILITY IN CLEAR AIR AT HIGH ALTITUDE by R.S.Scorer	2
MOUNTAIN WAVES IN THE STRATOSPHERE MEASURED BY AN AIRCRAFT OVER THE WESTERN USA DURING FEBRUARY 1967 by A.McPherson and J.M.Nicholls	3
DEUX REMARQUABLES EXEMPLES DE CISAILLEMENT DANS LA STRATOSPHERE CONCERNANT LE VENT ET LA TEMPERATURE par G.D.Barbé	4
TURBULENCE STRUCTURE IN THE ATMOSPHERIC BOUNDARY LAYER OVER THE OPEN OCEAN by C.N.Gibson and R.B.Williams	5
LONGITUDINAL AND LATERAL SPECTRA OF TURBULENCE IN THE ATMOSPHERIC BOUNDARY LAYER by G.H.Fichtl and G.E.McVehil	6
TURBULENCE STRUCTURE IN FLOW REGIMES OF VANISHING MEAN SHEAR by H.Lettau	7
DETERMINATION OF VERTICAL TRANSPORTS OF MOMENTUM AND HEAT AND RELATED SPECTRA OF ATMOSPHERIC TURBULENCE IN THE MARITIME BOUNDARY LAYER by L.Hasse, M.Dunckel and D.Schriever	8
MEAN WIND-PROFILE AND TURBULENCE-CONSIDERATIONS OF A SIMPLE MODEL by R.Roth	9
ON THE DEVELOPMENT OF CYCLONES IN A STATIONARY LONG-WAVE BASIC STATE by J.Egger	10
MODELE AERO (HYDRO) DYNAMIQUE POUR LE CALCUL DU REGIME DES ONDES DE RELIEF par R.Zeytounian	11

Reference

TOPIC II - BASIC PROBLEMS RELATED TO ATMOSPHERIC SHEAR FLOWS

PROBLEMS OF ATMOSPHERIC SHEAR FLOWS AND THEIR LABORATORY SIMULATION
by J.E.Cermak and S.P.S.Arya 12

METHODS AND CONSEQUENCES OF ATMOSPHERIC BOUNDARY LAYER SIMULATION
by D.J.Cockrell and B.E.Lee 13

A METHOD OF SIMULATING A NEUTRAL ATMOSPHERIC BOUNDARY LAYER IN A WIND TUNNEL
by J.Counihan 14

LABORATORY INVESTIGATIONS OF ATMOSPHERIC SHEAR FLOWS USING AN OPEN WATER CHANNEL
by J.W.Clark 15

WAKE CHARACTERISTICS OF A BLUFF BODY IN A SHEAR FLOW
by D.J.Maull 16

ETUDE D'UNE SOUFFLERIE POUR RECHERCHES SUR LES ECHANGES D'ENERGIE ATMOSPHERE - OCEANS
par M.Coantic, P.Bonmarin, B.Pouchain et A.Favre 17

ON THE USE OF DIFFUSION DETECTOR GASES IN THE STUDY OF ATMOSPHERIC SHEAR LAYERS WITH ADVERSE PRESSURE GRADIENTS
by J.E. de Krasinski 18

THE VERTICAL TRANSFER OF MOMENTUM THROUGH THE BOUNDARY LAYER
by F.B.Smith 19

THE ORIENTATION OF VORTICES DUE TO INSTABILITY OF THE EKMAN-BOUNDARY LAYER
by F.Wippermann 20

DIFFUSION IN THE ATMOSPHERIC SURFACE LAYER: COMPARISON OF SIMILARITY THEORY WITH OBSERVATIONS
by W.Klug 21

SOME MEASUREMENTS OF INSTABILITIES AND TURBULENCE IN EKMAN-BOUNDARY LAYERS
by D.R.Caldwell and C.W. Van Atta 22

TOPIC III - INDUSTRIAL PROBLEMS RELATED TO ATMOSPHERIC SHEAR FLOWS

A REVIEW OF INDUSTRIAL PROBLEMS RELATED TO ATMOSPHERIC SHEAR FLOWS
by C.Scruton 23

Reference

FLUCTUATING FORCES ON BLUFF BODIES IN TURBULENT FLOW
by P.W.Bearman 24

WIND EXCITED BEHAVIOUR OF CYLINDRICAL STRUCTURES - ITS RELEVANCE TO AEROSPACE DESIGN
by D.J.Johns 25

STATISTICAL ANALYSIS OF GUST VELOCITIES FOR SPACE LAUNCHER DESIGN
by E.Albanese, F.Bevilacqua and E.Vallerani 26

AERODYNAMIQUE DES PAROIS PERFOREES- APPLICATION AU PROJET D'ECRANS DE PROTECTION CONTRE LE VENT - ETUDE DU FONCTIONNEMENT DE CES ECRANS
par J.Valensi et J.M.Rebont 27

APPENDIX A - Discussions

APPENDIX B - Round Table Discussion

THE STRUCTURE OF ATMOSPHERIC SHEAR FLOWS - A REVIEW

H. A. Panofsky*
The Pennsylvania State University

*Evan Pugh Research Professor of Atmospheric Sciences

SUMMARY

Atmospheric shear flows near the ground are discussed in some detail, and characteristics of elevated shear flows are not so well understood and are mentioned only briefly.

The behavior of the structure of atmospheric shear flows near the ground is discussed in terms of three similarity hypotheses:

1) Monin-Obukhov similarity in the surface layer

2) Kolmogorov similarity

3) Davenport geometric similarity

Monin-Obukhov similarity makes it possible to combine the effects of shear and buoyancy. It describes well the wind profile in the surface layer, as well as the spectra of vertical wind and temperature, and the cospectra of heat flux and Reynolds stress. Spectra of the horizontal components do not obey Monin-Obukhov similarity, probably due to the effect of large-scale roughness.

Due to the high Reynolds numbers, well-developed inertial subranges exist in all spectra at high frequencies, except in very stable air. In stable air, buoyant subranges have been observed. The inertial ranges permit estimation of dissipation.

Davenport geometrical similarity predicts that the relation between wind fluctuations for given ratios of height difference and wavelength is a function of Richardson number only. This hypothesis agrees with observations at many sites. Fluctuations occur first at higher levels, then spread downwards. The delay for the lateral components is larger than for the horizontal components.

Spectra of elevated shear layers (clear-air turbulence) clearly show the inertial range. At lower frequencies, longitudinal rolls are indicated in the case of clear-air turbulence.

THE STRUCTURE OF ATMOSPHERIC SHEAR FLOWS - A REVIEW

H. A. Panofsky*

The Pennsylvania State University**

I. Introduction

Atmospheric shear flows have been studied most extensively in the atmospheric boundary layer, which is, on the average, about 1 km thick. Most of this paper will deal with properties of this layer. In addition, however, there exist, on occasion, strong shear layers in the upper air, with a maximum probability about 10 km above the surface, which give rise to "clear-air turbulence" (CAT). Some information concerning the mechanism and structure of CAT has only recently become available and will be discussed.

Atmospheric and oceanic shear zones differ in two important aspects from boundary layers usually studied in wind tunnels: first, the Reynolds numbers are so large that they cease to be important, except, perhaps right near the ground. Second, the vertical temperature stratification plays a dominant role in determining the characteristics of the shear flow; if temperature increases with height, it tends to damp out turbulence; if it decreases with height by more than the adiabatic rate γ_d (1°C/100 m), heat convection is added to the "mechanical" turbulence produced by the shear. Therefore, the most relevant non-dimensional number for atmospheric shear flow becomes the Richardson number, defined by

$$Ri = \frac{g(\gamma_d - \gamma)}{T\left(\frac{\partial u}{\partial z} + \frac{\partial v}{\partial z}\right)^2} \qquad (1)$$

According to Batchelor (1953), this number determines dynamic similarity; qualitatively it can be thought of representing the relative importance of heat convection and mechanical turbulence. Here, g is gravity, T temperature, z height, $\gamma = -\partial T/\partial z$, and u and v are two Cartesian horizontal wind components. Ri is defined in such a way that large negative numbers imply relatively strong heat convection; zero Ri, pure mechanical turbulence; small positive Ri, mechanical turbulence, damped by the temperature stratification; and large positive Ri, no vertical turbulence at all. Between the last two categories there exists a "critical" Richardson number, separating vertical turbulence from no vertical turbulence; its numerical value is probably around 0.25. In practice, $B \equiv gz^2(\gamma_d - \gamma)/u^2T$ is sometimes used instead of Ri because it can be measured more easily.

II. Vertical Wind Structure in the Boundary Layer

a. The surface layer. Within the atmospheric boundary layer, we distinguish two regions: the "surface layer" and the "Ekman layer". The surface layer, which extends up to a height of 10 meters or so, has the following relatively simple properties (over homogeneous terrain): the wind direction is constant; and the vertical variation of stress, heat flux and other vertical fluxes can be neglected. In the Ekman layer, the earth's rotation becomes important and the wind turns with increasing height. Also, the vertical fluxes decrease significantly in magnitude.

Over homogeneous terrain, for zero or negative Richardson numbers (the normal configuration at daytime), the vertical wind distribution over homogeneous terrain is given by

$$V = 2.5\, u_*[\ln(z/z_o) - \psi(Ri)] \qquad (2)$$

---

*Evan Pugh Research Professor of Atmospheric Sciences

**Contribution No. 68-66 from the College of Earth and Mineral Sciences

Here u_*, the friction velocity, is defined as $u_* = \sqrt{\tau/\rho}$, where τ is the stress and ρ the air density, z_o is the usual roughness length, which varies from about 0.1 cm over smooth sand to several meters over some cities. $\psi(Ri)$ appears to be a universal function, which has been tabulated and is available in graphical form (Panofsky, 1963). It is positive if Ri is negative. For positive Richardson numbers, Eq. (2) is probably not valid, because radiative heat transfer becomes important; further, winds at different levels become more independent of each other, and u_* decreases rapidly with height.

Equation (2) does not really describe the distribution of wind with height, because the vertical distribution of Ri is not known a priori; however, the equation in this form is quite useful for evaluating u_* from given roughness, winds and temperatures.

The distribution of wind with height can be described explicitly by introducing L, the Lettau-Monin-Obukhov length, which is defined by

$$L = -\frac{u_*^3 c_p \rho T}{0.4\, gH} \qquad (3)$$

Here H is the vertical heat flux (to be modified when moisture affects the buoyancy of the air), and c_p the specific heat at constant pressure. In the surface layer, L is essentially independent of height, and $|L/30|$ represents the height below which mechanical turbulence is dominant in producing vertical fluxes, and above $|L/30|$, buoyant turbulence (heat convection). L is treated as a scaling length in Monin-Obukhov similarity along with u_* as scaling velocity. According to this theory, z/L is a universal function of Ri in the surface layer. In fact, for practical purposes, Ri and z/L appear to be equal when both are negative (daytime). We can then rewrite the low-level wind profile:

$$V = 2.5\, u_* \left[\ln(z/z_o) - \psi(z/L)\right] \qquad (4)$$

b. Wind distribution in the Ekman layer. In the Ekman layer, the wind tends to turn clockwise with increasing height in the northern hemisphere, counterclockwise in the southern. The wind speed increases rapidly at first, more slowly later on. The exact distribution depends on many factors, particularly, the vertical distribution of the horizontal pressure gradient, and the vertical distribution of Richardson numbers.

Many models exist for this distribution; of particular importance is the ratio between surface friction velocity and free-stream velocity, and the angle between surface stress and direction of free-stream velocity. Both these ratios depend primarily on the "surface Rossby number" V_g/fz_o, some form of bulk Richardson number, and the distribution of pressure gradient. Here f is the Coriolis parameter $2\omega\sin\phi$, and V_g the free-stream velocity. ω is the earth's rate of rotation and ϕ the latitude.

III. The Behavior of the Variances in the Boundary Layer

According to Monin-Obukhov similarity theory, the non-dimensional ratios σ_u/u_*, σ_v/u_* and σ_w/u_* are functions of Ri or z/L only. Here σ stands for standard deviation, and subscripts, u, v and w for longitudinal, lateral and vertical velocity components, respectively.

Figures 1 and 2 show these relationships, as determined by Prasad and Panofsky (1967) from observations at many locations. The Monin-Obukhov prediction fits best to the statistics of vertical velocity. In fact, over the range $-0.5 < Ri < 0.2$, the ratio σ_w/u_* is essentially constant and equal to 1.3; this fact a. Eq. (2) make it possible to determine the fluctuations of vertical velocity from measured wind, temperature gradients and ground roughness. For negative Ri of large magnitude ("free convection"), σ_w/u_* varies as $(z/L)^{1/3}$, even up to heights exceeding that of the surface layer (see Myrup, 1967).

The ratios σ_u/u_* and σ_v/u_* show systematic variations from place to place, suggesting that certain features of larger scales than those characterized by z_o influence their behavior. Also, there is a tendency for the ratio σ_v/u_* to increase toward large positive Ri, suggesting the existence of small-scale, horizontal motions besides mechanical turbulence and heat convection. In general, there is very little vertical variation of the various standard deviations in the surface layer. A final characteristic of the various ratios appears to be that they are relatively unaffected by terrain heterogeneities.

According to Monin-Obukhov similarity theory, the standard deviations of scalars such as temperature (σ_T) are described by

$$\sigma_T/T_* = \phi_T(z/L) \qquad (5)$$

where T_* is given by $-H/0.4\, c_p \rho u_*$ and ϕ_T is a universal function. Equation (5) appears to fit the few existing data, but is not well established. For negative Ri, ϕ_T is given approximately by

$$\phi_T = (1 - 18\ z/L)^{-1/2} \qquad (6)$$

Presumably, the same expression describes the behavior of the fluctuations of other scalars.

IV. Spectra of Atmospheric Variables at High Frequencies

a. Spectra of wind components. There exists now considerable evidence that Taylor's frozen-wave hypothesis is satisfied at high frequencies; more will be said about the applicability of this hypothesis later. In any case, it is possible to interpret local time spectra of meteorological variables, particularly at high frequencies, to represent one-dimensional Eulerian space spectra in the direction of the mean wind.

There now exists overwhelming evidence that Kolmogorov's law for the inertial subrange fits spectra of the horizontal velocity components in neutral and unstable air well, provided that the height is equal to or larger than the wavelength. In fact, the law:

$$S(k) = b\varepsilon^{2/3}k^{-5/3} \qquad (7)$$

fits one-dimensional longitudinal spectra even to smaller wave numbers k. Here ε is the dissipation rate. The "universal constant" b, in Eq. (7) is now well determined at about 0.5 for longitudinal spectra when k is measured in radians per unit length. This result fits observations in the sea, the air and in the wind tunnel. Of course, the constant for lateral spectra is about 0.66.

Because the constants can now be regarded as well known, it is possible to use Eq. (7) to determine the dissipation ε from measured spectra. This estimate of dissipation can then be combined with estimates of the production rates of turbulent energy, and of the turbulent divergence of energy flux, in order to understand the turbulent energy budget. So far, to the author's knowledge, all these terms have been measured only by Record and Cramer at MIT, Round Hill Field Station, South Dartmouth, Massachusetts (1966). Here, as reanalyzed by Busch and Panofsky (1968) dissipation was balanced locally by mechanical and buoyant production, with the divergence term being unimportant. This result contradicts an earlier conclusion based on the less complete observations at Brookhaven (see Lumley and Panofsky, 1964).

Recently, spectra of wind components were obtained from six levels (18 m to 150 m) on the tower at Cape Kennedy, Florida, during convective conditions. The results were complex; at 18 m, the dissipation could be balanced by mechanical production alone, implying that buoyant production was balanced by the divergence term. On the other hand, the dissipation at the five levels between 30 m and 150 m could be fitted to the equation:

$$\varepsilon = \frac{u_{*c}^3}{0.4z}\left[\left(1 - 18\ Ri_{eff}\right)^{-1/4} - Ri_{eff}\right] \qquad (8)$$

derived from the assumption of a local balance of buoyant production, mechanical production and dissipation. In this equation, Ri_{eff} is an effective Richardson number obtained by vertical linear extrapolation of the measured Richardson number between 18 and 30 m. u_{*0} is the friction velocity at the surface. These results agree with Businger's hypothesis (unpublished) that the flux divergence term is most important at low levels. In any case, Eq. (8) can be used in practice to estimate dissipation rates up to 150 m and therefore the high-frequency components of the spectra of velocity components at these levels, from observations near the ground only.

The existence of an inertial range in the spectrum of the vertical velocity is less clear. Observations quite close to the ground often suggest less energy in the vertical velocities than in the longitudinal velocities at high frequencies. South Dartmouth observations, analyzed by Busch and Panofsky (1968) and recent unpublished spectra obtained from aircraft flying in the U.S. Air Force LO-LOWT project and in CAT (Fig. 3) suggest that the -5/3 law with the proper universal constant for lateral components exists only as long as the height is at least seven times the wavelength. In other words, local isotropy exists only for wavelengths much shorter than often assumed, and for wavelengths much shorter than those for which the horizontal velocity components obey the Kolmogorov law.

Some new observations have become available recently which point to the existence of a buoyant range in the boundary layer. Lumley (1967) suggested that the most likely place for a buoyant range would be in turbulence maintained by import from another region. A similar conclusion was reached by Lin, Panchev and Cermak (1969). In particular, then, buoyant subranges might be found in a slightly hydrostatically stable layer above an unstable layer near the ground. Evidence for the correctness of this suggestion has recently come from three independent sources. In two papers (Myrup, 1968 and Lenschow and Johnson, 1968), spectra in elevated stable layers were measured from airplanes; in the third (Busch and Panofsky, 1968), spectra of vertical velocity had been obtained by sonic anemometer on the 1500-ft tower near Dallas, Texas by Kaimal and Haugen (1967). In all

cases, the spectra are consistent with the hypothesis that the spectral densities vary as k^{-3}. Unfortunately no spectra of scalars have been obtained under these conditions.

b. Spectra of scalars at high frequencies. According to inertial-range theory, the high frequency portion of the one-dimensional spectra of scalars (except pressure) follow the equation:

$$S_q(k) = c\varepsilon^{-1/3}N_q k^{-5/3} \qquad (9)$$

Here, q represents an arbitrary scalar, and N_q the rate of dissipation of fluctuations of this scalar.

There now exist numerous spectra of temperature, moisture and refractive index, obtained from towers and aircraft, showing that the spectral densities indeed vary as $k^{-5/3}$. Some of these were summarized by Obukhov and Yaglom (1967).

In spite of the difficulty of obtaining estimates of N, there is now considerable agreement about the constant c in Eq. (3). Largely as a result of studies by Gibson and Schwarz (1963), Grant et al. (1962), Gurvich and Zubkovski (1966), Gurvich and Kelashkin (1966) Panofsky (1969) it now appears that c equals about 0.7, if k is measured in radians per unit length. Of course, the corresponding constant in the structure function is about 2.8. The knowledge of this constant now makes it possible to estimate N from fluctuation statistics of wind and of the scalar, or from statistics of wind fluctuations and properties of scattered waves. So far, within the errors of measurement, N seems to be equal to the rate of production of the fluctuations of the scalar -- a statement which cannot possibly have much generality, particularly over heterogeneous terrain.

Spectral intensities of pressure should vary as $k^{-7/3}$ in the inertial range. Actual measurements (Gorshikov, 1967) do not contradict this possibility, but there is so much variation in the spectra from case to case to make any definitive statement of the power of this law impossible as yet.

V. Eulerian Time Spectra in the Energy-Containing Range

a. The spectrum of vertical velocity. According to Monin-Obukhov similarity theory, the spectrum of a velocity component in the surface layer is given by

$$\frac{kS(k)}{u_*^2} = F(kz, z/L) \qquad (10)$$

where $f \equiv kz$.

Up to a height of about 50 m, the observations of vertical velocity agree quite well with Eq. (10). Further, for a large range of stabilities, we can replace u_*^2 on the left of Eq. (10) by $0.6\,\sigma_w^2$ where σ_w^2 is the variance of vertical velocity. Only for extreme instability, u_*^2 is smaller relative to σ_w^2.

There is now considerable evidence that the relation between F and kz for a given Ri is nearly universal (Fig. 4). Here spectra of vertical velocity are brought together from many sources, in neutral or unstable air. Under such conditions, the value of F has a maximum of about 0.43 for kz about 0.3 -- that is, for a wavelength between 3 and 4 times the height. In stable air, the value of kz at the maximum shifts to higher values.

Since the shape of the vertical velocity spectra seems so nearly universal, attempts have been made to fit F by empirical expressions which are proportional to kz for small kz and vary as $(kz)^{-2/3}$ for large kz. Thus, Busch and Panofsky (1968) recommend for neutral and moderately unstable air:

$$\frac{kS_w(k)}{u_*^2} = \frac{3.36\,f}{1 + 10f^{5/3}} \qquad (11)$$

Actually Fig. 4 does show some differences between the shapes of the different vertical-velocity spectra; in particular, over the ocean, and in the New Jersey saltmarsh more low-frequency energy is indicated than in the other time spectra. One possible explanation is this: there is now considerable evidence that there exist, near the ground, large longitudinal "eddies" with axes slightly inclined to the direction of the geostrophic wind (see, e.g., Faller and Kaylor, 1966 and Angell and Dickson, 1968). Over the oceans, or generally flat terrain, these eddies are slowly carried past a stationary observer, thus contributing to the low-frequency energy. Over rough terrain, such eddies are likely to be broken up; however, there are isolated instances where bursts of strong updrafts every 15 minutes or so have appeared at such sites as Sublette, Kansas (Haugen et al., 1969) and Brookhaven, New York, where the general countryside is quite flat. Such vortices also form characteristic cloud patterns which have been observed from satellites. These eddies would add low-frequency energy which is not described by Monin-Obukhov similarity theory. The airplane spectrum in Fig. 4 also shows some extra low-frequency energy which could be due to longitudinal rolls.

Up to 50 m, the value of kz at the maximum is essentially constant, implying that the scale of the turbulence increases linearly with height. Above this level, the spectral shapes in neutral and unstable air remain the same, but kz at the maximum increases, showing that the scale of turbulence increases less rapidly with height and eventually becomes constant. Figure 5, taken from the Dallas measurements to which some LO-LOCAT airplane spectra have been added, show this behavior. As pointed out, at these higher levels, spectra in stable air no longer obey the $k^{-5/3}$ law at high frequencies, so that the shape of F now varies with stability.

b. Spectra of longitudinal wind components. In recent years, spectra of longitudinal wind components (or wind speeds) have become available from many sites. Some are published (Barman, 1965); others come from various research reports and unpublished records, covering such places as Cape Kennedy, Obninsk, USSR, White Sands, N.M., South Dartmouth, Mass., as well as various cities. It is quite clear that these spectra do not follow similarity theory, although the high-frequency portions obey the Kolmogorov law, often to wavelengths as long as five times the height.

If $kS_u(k)$ is plotted as function of k, the peak shifts little or not at all with height; if similarity theory applied, it would be a linear function of height. Figure 6 shows an assortment of u-spectra, mostly obtained in strong winds, and therefore small Richardson numbers. It is clear that the shapes of the spectra from various sites differ widely. In particular, the wavelength at the maximum varies from several 100 to several 1000 meters. It is particularly long for cities. This suggests that mesoscale features determine the characteristics of the low-frequency portions of the u-spectra, not just the roughness length z_o which is a measure of local roughness. Attempts have been made to fit u-spectra to empirical formulae; however, such fits can be only of limited use for application over terrain for which they have been derived.

The low-frequency portions of u-spectra react to changes in atmospheric stability, decreasing somewhat as the stability is increased; for more detail, the reader is referred to the paper by Busch et al. (1968).

c. Spectra of lateral velocities. Spectral densities of lateral velocities (or wind direction) behave very much as those of longitudinal velocities, only more so; the k value at the peak of $kS_v(k)$ is nearly invariant with height. Further, the low-frequency portions of the spectra are extremely sensitive to changes of stability, so that in stable air, there is very little energy for frequencies of order one cycle/minute or smaller (Fig. 7). Since the energy of the u-components at these wavelengths is still quite large, "eddies" in stable and neutral air are elongated along the wind.

However, with light winds, in very stable air, meanders in wind directions with periods of order one half hour are possible; thus the v-spectra sometimes show gaps between this very low-frequency domain and the high-frequency mechanical turbulences (see Lumley and Panofsky, 1964).

d. Spectra of scalars. According to similarity theory, the spectrum of temperature is given by

$$\frac{kS_T(k)}{\overline{T}^2_*} = G(f, Ri) \qquad (12)$$

So far, there are very few places where Eq. (12) has been tested, since usually not all the quantities in Eq. (12) were evaluated. The few observations used to test Eq. (12) show tentatively that it is correct. As an example of the normalized temperature spectrum, see Fig. 8.

It is likely that the spectra of moisture and refractive indices behave in an analogous manner as that of temperature but observations are not yet available.

VI. Space-Time Structure

a. Space-time structure of velocity components. According to Taylor's hypothesis, space correlations in the x-direction with time lag zero are equal to local Eulerian time correlations, provided $x = \bar{u}t$. This test of Taylor's hypothesis has recently been repeated by Melnichuk (1968) from an analysis of Doppler radar records of rain at 60 m. Taylor's hypothesis is remarkably good at that height for values of x up to 400 m.

Melnichuk also shows a series of complete space-time correlation curves, which indicate again that the time scale of turbulence for air following the mean motion is three to four times larger than the local Eulerian time scale of turbulence. In other words, the correlation function following the mean motion is not very different from a Lagrangian correlation function.

The behavior of lateral and vertical correlations with varying time lapse is most conveniently analysed through the behavior of the coherence between wind components at various points, and of the time delay between the arrival of the signal at these points or the "slope" of the eddies. Davenport (1961) suggested a kind of geometric similarity, according to which the coherence should depend only on a stability factor and on the ratio of separation between the two points to wavelength, Δf. Figure 9 shows from an example at White Sands, New Mexico, that this hypothesis is well satisfied; coherences from many different pairs of levels fall on the same line if plotted

as function of Δf. Similar graphs were prepared with data from Brookhaven, South Dartmouth and Cape Kennedy; the Davenport similarity theory seems valid everywhere. Moreover, in each case, a simple exponential fits the coherence-Δf graphs satisfactorily.

In order to analyze the dependence of vertical coherence on stability, the value of Δf for a coherence of 0.5 was plotted as function of Richardson number (Fig. 10). In general, coherence increases with decreasing stability. However, in unstable air, the coherence at Cape Kennedy is significantly less than elsewhere. The reason is unknown. Lateral velocity behaves in a similar fashion.

In neutral air (strong winds), the coherence of wind speed has been analyzed at additional sites by Davenport (1967) and Shiotani (1968). All data agree fairly well with the equation:

$$\mathrm{coh}(n) = e^{-16\,\Delta f} \tag{13}$$

where Δf can be computed from $\Delta f = n\Delta z/V$ (Δz is the vertical separation, n Eulerian frequency and V the mean wind in the layer Δz).

In shear flow, a gust will arrive at the top of a tower before it arrives lower down. The "eddies" slope with the wind shear. Such slopes defined by $\Delta x/\Delta z$ were analyzed at four separate locations, and were always larger (longer delay between arrival at different levels) for the lateral component v than for u. Generally, the slopes varied between 0.5 and 1 for the u-components and between 1 and 3 for the v-components. They tended to decrease with height (see, e.g., Fig. 11).

Shiotani (1967) has analyzed lateral coherence between wind components at 40-m height in strong winds, with separations up to 100 m. Again, Davenport's hypothesis is correct, and exponentials fit the relations between coherence and ratio of separation to wavelength. In fact, Eq. (9) is valid if Δf is redefined as the ratio of lateral separation to wavelength. The same relation is also valid in wind tunnels (see Davenport, 1963). Of course, it should be remembered that Shiotani's observations were taken in strong winds, and therefore Eq. (9) applies to lateral coherence when Richardson numbers are small. The fact that Eq. (9) applies both in the vertical and lateral direction suggests circular symmetry in vertical planes at right angles to the wind in hydrostatically neutral air, suggesting streamwise vortices. It would be tempting to suggest, for the wind speed or longitudinal wind component:

$$\mathrm{coh}(n) = e^{-16\,\frac{rn}{V}} \tag{14}$$

where r is any separation in a plane at right angles to the mean wind, and V is the mean wind speed.

b. Space-time correlations for scalars. M. C. Thompson (1968) determined structural characteristics of refractive index by measuring cross correlations in three Cartesian directions, for separations up to 150 cm near the ground. He did not, unfortunately, test Davenport geometric similarity. A later examination of his data suggested that Eq. (13) is valid for the largest separation measured, but the coherence decreases more slowly with Δf for smaller separations. As in the case of the wind components, the index fluctuations at the top of the vertical mast precede those at the bottom, and the slope again, is of order one. The same result follows from an analysis of temperature fluctuations at South Dartmouth where the delay of the temperature is about the same as that for the longitudinal wind component.

Also, the refractive index correlations along the wind were highest when the separation and time delay are related by $x = ut$ in agreement with Taylor's hypothesis. Thompson also shows that the lateral scale of the refractive index is considerably smaller than the longitudinal scale, and vertical scale is near the lateral, again making circular symmetry a possibility in strong winds.

Finally, some comments will be made on Lagrangian time correlations. Their scale seems to be about the same as that of Eulerian correlations following the mean motion.

Angell's study (1964) of constant-level tetrahedral balloons, compared to records made by a vertical vane at 2500 feet suggests that the ratio of the scale of Lagrangian time correlations to that of local Eulerian time correlations is inversely proportional to the relative turbulence intensity. It is here suggested that this ratio β is best represented by

$$\beta = \frac{0.45\,V}{\sigma} \tag{15}$$

where σ is the standard deviation of the velocity component involved. This result fits Angell's results fairly well as well as those summarized by Lumley and Panofsky (1964).

VII. Structure of CAT

In the free atmosphere, shear layers can develop which are analogous to "fronts": air masses of differing temperatures and motions are brought together along a narrow, sloping volume, across which both temperature gradients and wind shears are large. The vertical extent of such layers is from about 100 to 1000 m. Since the Richardson numbers are inversely proportional to the square of the vector wind shear, they can become small and dip below the critical value. At that point, unstable Kelvin-Helmholtz develop, grow and change into turbulent flow. This process has also been observed in the laboratory and in the ocean.

As mentioned before, spectra obtained in CAT invariably show a $k^{-5/3}$ region and local isotropy for high wave numbers. There is less agreement about the structure at lower wave numbers. Flights along and across the flow suggest the existence of longitudinal rolls, as discussed for the turbulence in the atmospheric boundary layer.

There is also some indication that the impetus for the breaking of the waves may be given by mountain waves, which have wavelengths of order of several kilometers. These waves are sometimes seen in the registrations of the velocity components. It is also clear that mountains produce locally subcritical Richardson numbers, even when the average Richardson numbers are too large for turbulence. This accounts for the spottiness of some of the CAT, as well as for the fact that it tends to be relatively frequent and severe over mountains.

In general, the total turbulent energy in CAT tends to increase with the vector wind difference across the "front", and is not well correlated with the Richardson number, provided that the Richardson number is small enough to permit the formation of CAT.

References

Angell, J. K., 1964: Measurements of Lagrangian and Eulerian properties of turbulence at a height of 2500 feet. Quart. J. R. Met. Soc., 90, 57-71.

Angell, J. K. and C. R. Dickson, 1968: A Lagrangian study of helical circulation in the planetary boundary layer. J. Atmos. Sc., 25, 700-717.

Batchelor, G. K., 1953: The conditions for dynamical similarity of motions of a frictionless perfect-gas atmosphere. Quart. J. R. Met. Soc., 79, 224-235.

Berman, S., 1965: Estimating the longitudinal wind spectrum near the ground. Quart. J. R. Met. Soc., 91, 302-317.

Busch, N. E., J. A. Frizzola and I. A. Singer, 1968: The micrometeorology of the turbulent flow field in the atmospheric surface boundary layer. Acta Polytech. Scand. Phys. inc., Nucleonics Ser., No. 59.

Busch, N. E. and H. A. Panofsky, 1968: Recent spectra of atmospheric turbulence. Quart. J. R. Met. Soc., 94, 132-148.

Davenport, A. G., 1961: The spectrum of horizontal gustiness near the ground in high winds. Quart. J. R. Met. Soc., 87, 194-211.

Davenport, A. G., 1963: The relation of wind structure to wind loading. *Symposium on Wind Loading on Structures.* Inst. Civ. Eng., Inst. Struct. Eng., and the Nat. Phys. Lab., Teddington, England. June 26-28.

Davenport, A. G., 1967: The dependence of wind loads on meteorological parameters. *International Research Seminar, 11-15 September 1967, Ottawa, Canada: Wind Effects on Buildings and Structures.*

Faller, A. J. and R. E. Kaylor, 1966: A numerical study of the instability of the laminar Ekman layer. J. Atmos. Sci., 23, 466-480.

Gibson, C. H. and W. H. Schwarz, 1963: The universal equilibrium spectra of turbulent velocity and scalar fields. J. Fluid Mech., 16, 365-384.

Gorshikov, N. F., 1967: Measurement of the spectrum of pressure micropulsations in the near-earth layer of the atmosphere. Izv. Atmos. and Ocean. Phys., 447-451.

Grant, H. L., B. A. Hughes, W. M. Vogel and A. Moilliet, 1968: The spectrum of temperature fluctuations in turbulent flow. J. Fluid Mech., 34, 423-442.

Gurvich, A. S. and B. N. Meleshkin, 1966: The determination of the microscale of turbulence from light intensity fluctuations. Izv. Atmos. and Ocean. Phys., 2, 688-694.

References (continued)

Gurvich, A. S. and S. L. Zubkovski, 1966: Evaluation of structural characteristics of temperature pulses in the atmosphere. Izv. Atmos. and Ocean. Phys., 2, 202-204.

Haugen, D. A., J. C. Kaimal and E. F. Bradley, 1969: Some characteristics of turbulent transport of heat momentum in the boundary layer. Paper No. M21, Annual Washington Meeting, Amer. Geophys. Union.

Kaimal, J. C. and D. A. Haugen, 1967: Characteristics of vertical velocity fluctuations on a 430-m tower. Quart. J. R. Met. Soc., 93, 305-317.

Lenschow, D. H. and W. B. Johnson, 1968: Current airplane and balloon measurements of atmospheric boundary layer structure over a forest. J. Appl. Meteor., 7, 79-89.

Lin, J.-T., S. Panchev and J. E. Cermak, 1969: Turbulence spectra in the buoyancy subrange of thermally stratified shear flows. Project Thermis Rep. 1, Colorado State University Contract No. N00014-68-A-0493-0001.

Lumley, J. L., 1967: Theoretical aspects of research on turbulence in stratified flows. *Moscow Symposium on Atmospheric Turbulence and Radio Wave Propagation*, pp. 105-110. Publishing House Nauka, Moscow.

Lumley, J. L. and H. A. Panofsky, 1964: *The Structure of Atmospheric Turbulence*. Interscience Monographs and Texts in Physics and Astronomy, v. XII, John Wiley & Sons, Inc., New York, 239 + xi pp.

Mather, G. K., 1967: Some measurements of mountain waves and mountain wave turbulence made using the NAE T-33 turbulence research aircraft. National Aeronautical Establishment, National Research Council, Canada.

Melnichuk, Y. V., 1966: Measuring turbulence in precipitation with a Doppler Radar Station. Izv. Atmos. and Ocean. Phys., 2, 695-704.

Myrup, L. O., 1967: Temperature and vertical velocity fluctuations in strong convection. Quart. J. R. Met. Soc., 93, 350-360.

Myrup, L. O., 1968: Atmospheric measurements of the buoyant subrange of turbulence. J. Atmos. Sci., 25, 1160-1164.

Obukhov, A. M. and A. M. Yaglom, 1967: Progress in atmospheric turbulence investigations. Izv. Atmos. and Ocean. Phys., 3, 335-366.

Panofsky, H. A., 1963: Determination of stress from wind and temperature measurements. Quart. J. R. Met. Soc., 89, 85-94.

Panofsky, H. A., 1969: The spectrum of temperature. *IUCRM Colloquium on Spectra of Meteorological Variables*. Stockholm, 9 June 1969.

Prasad, B. and H. A. Panofsky, 1967: Properties of variances of the meteorological variables at Round Hill. Chapter 7 in Final Report on Properties of Wind and Temperature at Round Hill, South Dartmouth, Mass. ECOM-0035-F, pp. 65-92. The Pennsylvania State University.

Record, F. A. and H. E. Cramer, 1966: Turbulent energy dissipation and exchange processes above a non-homogeneous surface. Quart. J. R. Met. Soc., 92, 519-532.

Shiotani, M., 1967: Lateral structures of gusts in high winds. Interim Report. The Physical Science Laboratory, Nihon University at Narashino, Funabashi, Chiba, Japan.

Shiotani, M., 1968: Structures of gusts in high winds. Interim Report Part 2. The Physical Science Laboratories, Nihon University at Narashino, Funabashi, Chiba, Japan.

Thompson, M. C., Jr., 1968: Refractive index microstructure. J. Geophys. Res., 73, 6429-6433.

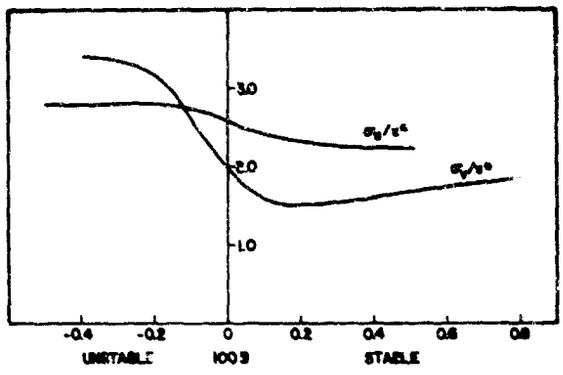

Figure 1. The ratios σ_u/u_* and σ_v/u_* as function of B at many sites.

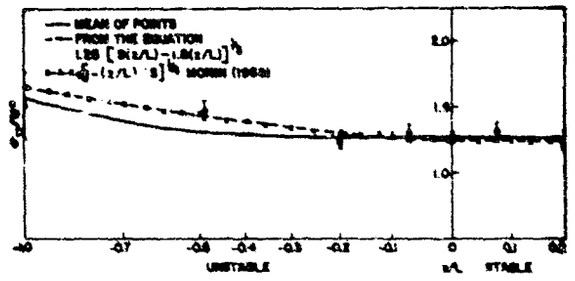

Figure 2. The ratio σ_w/u_* as function of z/L according to many sources. Confidence intervals represent standard deviation of means, assuming all observations are independent of each other.

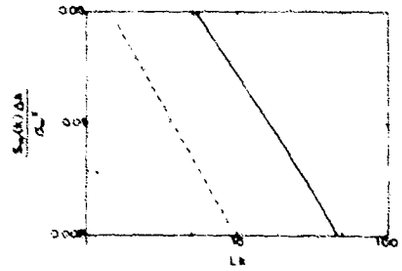

Figure 3. Spectra of vertical velocity as measured by the National Aeronautical Establishment of Canada. Solid line: observed. Broken line: -5/3 law. (Mather, 1967).

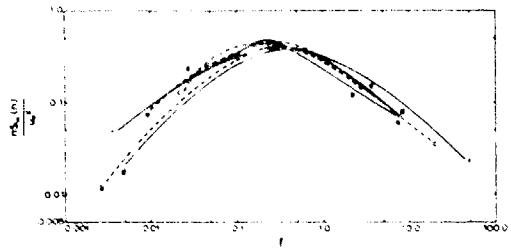

Figure 4. Comparison of vertical-velocity spectra in neutral to slightly unstable air at various locations. a. LO-LOCAT, 76 m (averaged neutral and unstable. b. South Dartmouth, 15 to 91 m (neutral). c. Dallas, 46 m (unstable). d. Hanford, 3 and 6.1 m (neutral). e. New Jersey saltmarsh, 2 to 4 m (moderately unstable). f. Over sea near Vancouver (unstable).

Figure 5 Variation of vertical-velocity spectra with height in neutral to slightly unstable air. Dallas: a. 46 m; b. 137 m; c. 229 m; d. 320 m. LO-LOCAT: e. 229 m.

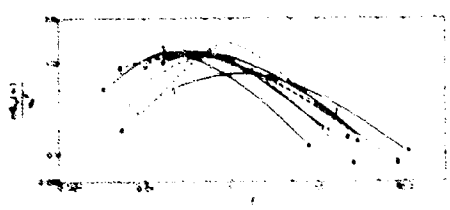

Figure 6. Assorted longitudinal-velocity spectra in neutral air at various locations. a. St. Louis, 76 m. b. New York City, Telephone Bldg., SW winds, 177 m. c. Brookhaven, 91 m. d. South Dartmouth, 15 to 46 m (neutral and unstable). e. New York City, Wall St. Tower, NW winds, 280 m. f. Montreal, 76 m. g. Hanford, 3 and 6.1 m. h. Cape Kennedy, 90 and 120 m.

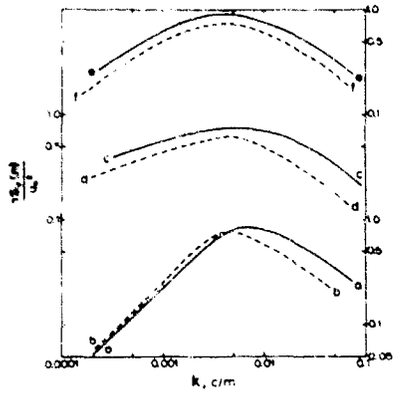

Figure 7. Spectra of lateral velocity at South Dartmouth, Mass. Stable: a. height 46 m; b. height 91 m. Unstable: c. heights 15 and 16 m; d. heights 40 and 46 m. Neutral: e. heights 15 and 16 m; f. heights 40 and 46 m.

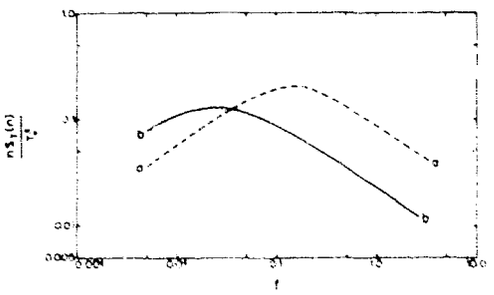

Figure 8. Spectra of temperature at South Dartmouth, Mass. a. stable, heights 15 to 91 m; b. unstable, heights 15 to 46 m.

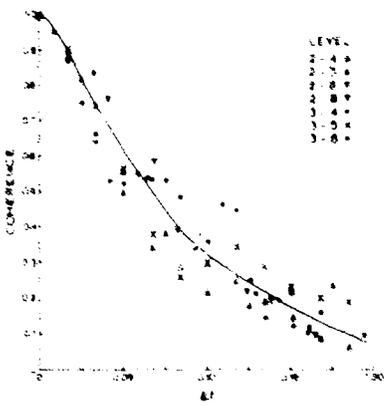

Figure 9. Typical dependence of coherence on Δf. White Sands, New Mexico, levels: 2 at 22.9 m, 3 at 29.1 m, 4 at 53.3 m, 5 at 68.6 m, 6 at 91.4 m, 8 at 152.4 m.

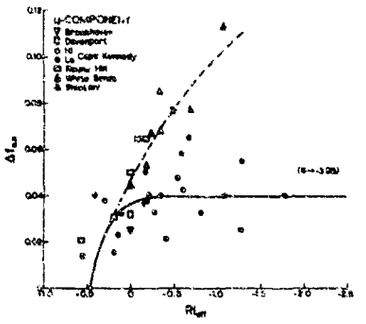

Figure 10. Dependence of $f_{0.5}$ on Ri_{eff} for the u-component. Solid line, fit to Cape Kennedy site; broken line, fit to sites other than Cape Kennedy.

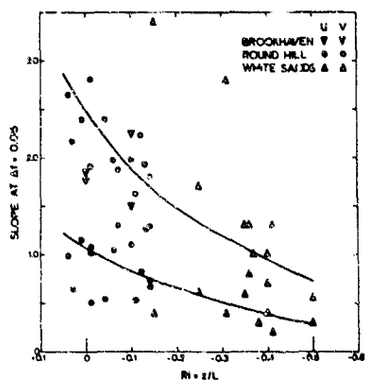

Figure 11. Slope of eddies for the u- and v-components of the wind as function of z/L.

The Origins and Forms of Dynamic Instability in Clear Air at High Altitude

by R. S. Scorer

Imperial College, London.

The first term vanishes because it represents the integral of an odd function which vanishes at ∞ . The integral in the second term is equal to π and so

$$u_o = \tfrac{1}{2}\eta\Delta z Ak$$

and
$$u = \tfrac{1}{2}\eta\Delta z Ak \, Cos kx \tag{2.1}$$

The rate of increase of vorticity by advection at a point x , which is equal to $-\eta\Delta z \, \partial u/\partial x$, is therefore

$$-\tfrac{1}{2}(\Delta z)^2 Ak^2 \sin kx \tag{2.2}$$

At the same time the slope of the density discontinuity is such as to increase the vorticity at the point x along the layer at the rate

$$-g\beta\Delta z \frac{\partial}{\partial x} A \, Cos kx = g\beta\Delta z Ak \, Sin kx \tag{2.3}$$

where β is the stable stratification in the layer. If the sum of (2.2) and (2.3) is positive where $\sin kx$ is negative there will be a total accumulation of vorticity at the downward sloping nodes, towards which it is being advected; and consequently the wave disturbance will grow if

$$\tfrac{1}{2}(\eta\Delta z)^2 k > g\beta\Delta z$$

i.e.
$$k > 2g\beta/\eta^2\Delta z \tag{2.4}$$

The classical theory of the instability of a vortex sheet shows that waves grow like $\exp i\sigma_i t$ where, in the conventional notation,

$$i\sigma_i = \frac{k}{\rho_1+\rho_2}\left\{\rho_1\rho_2(U_1-U_2)^2 - \frac{g}{k}(\rho_1+\rho_2)(\rho_1-\rho_2)\right\}^{\frac{1}{2}} \tag{2.5}$$

when $k > k_c$ and

$$k_c = \frac{(\rho_1-\rho_2)(\rho_1+\rho_2)}{\rho_1\rho_2(U_1-U_2)^2} g \simeq \frac{2g\Delta\rho}{U^2\rho} \tag{2.6}$$

The velocity and density discontinuities are $\eta\Delta z$ and $\beta\Delta z$ and so

$$k_c = 2g\beta/\eta^2\Delta z \tag{2.7}$$

which gives the same result as (2.4).

Thus the instability arises because of the accumulation of the vorticity of the layer at the alternate nodes of a wavelike disturbance. In most steady flows there is a balance of forces and instability merely means that in a displacement the balance is disturbed so as to produce an acceleration in the direction of the displacement. But in the flow due to a horizontal

vortex layer in an inviscid fluid the hydrostatic pressure gradient balances gravity and so the physical forces are always stabilising. What happens is that the deformation of the layer produces curved flow and the creation of new pressure gradients by centrifugal forces. Some particles travel down the new pressure gradients and are accelerated, so that energy available from the mean motion becomes concentrated locally in the vortices. Evidently a concentrated vortex layer is necessary for a very deep layer of uniform vorticity is not unstable in this sense. A discontinuity is unstable for all wave numbers greater than k_c, and so the thickening of the layer excludes waves at the small end of the length range from instability. The general problem of layers of finite thickness has not been solved but the critical wave number for a layer of uniform η and β and thickness h must, if the Boussinesq approximation be made, satisfy an equation of the form

$$F(\frac{g\beta}{\eta^2}, k_c h) = 0 \qquad (2.8)$$

with a similar equation for K_c, the wave number at the small wavelength end of the unstable range. According to (2.7)

$$k_c = 2g\beta/\eta^2 h$$

or
$$\tfrac{1}{2}k_c h = Ri = g\beta/\eta^2 \qquad (2.9)$$

while for a given Ri and form of stream profile, we must also have

$$K_c h = \text{const} \qquad (2.10)$$

which implies the already rather obvious conclusion that an increase in layer thickness increases the wavelength at the small wavelength end of the unstable range.

When instability sets in on account of a decrease in Ri, a unique finite wavelength, determined by h and the profile of Ri, becomes unstable first. If the mechanisms decreasing Ri continue to operate while the instability gets going, the actual growth rate may be fairly large, and is likely to be a maximum at a wavelength close to that which first became unstable.

This view of the sequence of events does not require the imposition of an additional criterion to select, from a range of unstable wavelengths, one that will actually occur.

When billows occur a cat's eyes pattern of motion develops in which the phase of the waves is opposite above and below the layer, whereas initially the phase is the same at all heights. Within the cat's eyes is

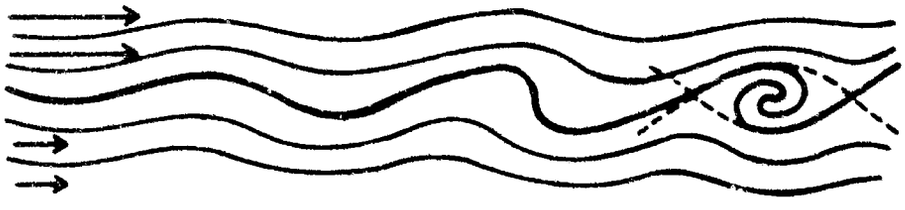

Fig. 2 Development of cat's-eye pattern.

a region of multiple static instability once the vortex layer has become sufficiently rolled up, and this must become mixed up into a region of uniform potential temperature. As the internal motion degenerates the mixed region spreads out under gravity into a horizontal layer whose depth H is related roughly to the original wavelength $2\pi/k$ by (Scorer 1951)

$$kH \doteq 2\pi/2.7 \tag{2.11}$$

Since the original instability set in at a Richardson number of less than 1/4 we must have, according to (2.9) and (2.11) that

$$H/h \doteq \frac{2\pi}{5.4Ri} > 5$$

and so the instability actually effects the mixing of a layer at least five times the depth of the original vortex layer.

When the mixing is complete the original stable layer has been replaced by stable layers at the top and bottom of the original layer. According to Thorpe's experiments (1968), cusped waves are then likely to occur at these two discontinuities with the well-mixed fluid protruding in cusps into the unstirred region.

3. The generation of small Richardson number layers

If the flow remains laminar and adiabatic the static stability may be altered by a velocity field which varies the distances between isentropic surfaces. But the vorticity is altered according to the equation

$$\frac{D\underline{\omega}}{Dt} = -\underline{\omega}\,\mathrm{div}\,\underline{v} + (\underline{\omega}.\underline{\mathrm{grad}})\,\underline{v} + \underline{\beta} \times (\underline{g} - \frac{D\underline{v}}{Dt}) \tag{3.1}$$

$$\text{where } \underline{\beta} = -\frac{1}{\tau}\,\underline{\mathrm{grad}}\,\tau \quad , \quad \theta = \frac{1}{\tau} = \text{potential temperature} \tag{3.2}$$

and the flow is inviscid. The equation takes this form because we can write $\frac{1}{\rho}\,\underline{\mathrm{grad}}\,p$ for the usual $\underline{\mathrm{grad}}\,p$ in the equation of motion where

$$\rho = \frac{1}{T}\left(\frac{p}{p_1}\right)^{\frac{\gamma-1}{\gamma}} \rho \quad , \quad \tau = \frac{\gamma R}{\gamma-1}\left(\frac{p}{p_1}\right)^{\frac{\gamma-1}{\gamma}} \tag{3.3}$$

p_1 being a standard pressure, and the other symbols having their usual meaning.

The term in (3.1) in $\mathrm{div}\,\underline{v}$ produces a negligible effect. The term $(\underline{\omega}.\underline{\mathrm{grad}})\,\underline{v}$ is zero in 2D motion, and in the third term $g \gg D\underline{v}/Dt$, at any rate before billows develop. If the motion is steady and q is the air speed. β is the magnitude of $\underline{\beta}$, and suffix 0 denotes the initial state in horizontal motion, continuity in 2D motion requires that

$$\frac{q}{\beta} = \text{const} = \frac{q_0}{\beta_0} \tag{3.4}$$

The transverse component of vorticity changes at the rate

$$\frac{D\eta}{Dt} = q\frac{\partial\eta}{\partial s} = g\beta\sin\psi \qquad (3.5)$$

where ψ is the inclination of the isentropic flow surfaces to the horizontal. Thus

$$\delta\eta = g\frac{\beta}{q}\delta s \sin\psi$$

$$= g\frac{\beta_o}{q_o} z \qquad (3.6)$$

where δz is the vertical displacement of the fluid as it travels along the streamline. In unsteady flow the corresponding equation would be

$$\delta\eta = g\beta\delta t \sin\psi \qquad (3.7)$$

The Richardson number of the layer is given by

$$Ri = g\beta/(\ _o + \ )^2$$

$$= g\beta/(\ _o + g\frac{\beta_o}{q_o} z)^2 \quad \text{by (3.6)} \qquad (3.8)$$

The most interesting case is where β_o is large in a shallow layer initially, without any shear, after which the Ri is decreased by tilting of the layer. Thus $Ri_o = \infty$, and subsequently

$$Ri = \beta q_o^2/g\beta_o^2(\delta z)^2$$

$$= q^2/g\beta(\delta z)^2 \qquad (3.9)$$

In this it is seen that the vortex layer, where Ri is smallest, will tend to occur where β is largest, where (δz) is largest, and q is smallest. This is the most important case for us to consider.

If there is initially a streamwise component of vorticity ξ it is increased by stretching in 2D motion in a region of acceleration of the flow. At the same time the static stability is increased by a decrease in the streamline spacing. Thus

$$q\frac{\partial\xi}{\partial s} = \xi\frac{\partial q}{\partial s} \qquad (3.10)$$

and

$$Ri = \frac{g\beta}{\xi} = \frac{g\beta_o q/q_o}{\xi_o(1+\delta\xi/\xi)^2}$$

$$= \frac{g\beta_o}{\xi_o}\frac{q}{q_o}(1+\frac{\delta q}{q})^{-2}$$

$$= Ri_o\,(1-\delta q/q) \quad \text{approximately} \qquad (3.11)$$

This shows that a streamwise acceleration does decrease Ri even though β is increased; but the effect is not large. By contrast if there is only a transverse component of vorticity η in a region of streamwise acceleration, since η is unaltered Ri is increased by the increase in β.

In 3D motion the situation is very complicated but even so the most significant effects are due to tilting and are effectively represented by (3.8) and (3.9). The most common cause of tilting is the inclination of the streamlines in mountain waves. The vertical displacement ζ satisfies the following equation in steady 2D flow

$$\nabla^2\zeta + 2\alpha_o \frac{\partial\zeta}{\partial z} + \frac{g\beta_o}{U^2}\zeta = 0$$

for small and moderate amplitudes of ζ. Here $\alpha_o = U^{-1}\,\partial u/\partial z$ in the undisturbed stream, and this does not initially have particularly large values at levels where β_o is large. The horizontal derivatives of ζ cannot vary significantly with height, and so where β_o is large $\partial^2\zeta/\partial z^2$ must also be large because $\partial\zeta/\partial z$ cannot be large in a shallow layer without $\partial^2\zeta/\partial z^2$ also being large. This means that at this level the curvature of the profile of ζ is exceptionally large, and so usually ζ has a well defined maximum at that level. Consequently, levels of large β_o are very likely to be the levels of greatest (δz), which emphasises the effects of mountain waves in changing Ri.

4. The origin of the statically stable layers

It has long been well known to glider pilots that the wave amplitude in mountain and lee waves has a maximum at the top of a cloud layer. This happens because cloud layers are cooled more than the air immediately above them by infra-red radiation to space, and so they are layers of large β_o and therefore of maximum ζ.

Subsidence inversions are not commonly produced in situations otherwise favourable for mountain waves, but when they act as a limit to cumulus convection the subsidence causes widespread evaporation of the cumulus tops and a cooling of the upper part of the convection layer. In general this can happen to any convection layer in which clouds participate.

A less obvious source of stable layers is a larger scale instability in an airstream with a vertical gradient of wind. In a geostrophic air stream of static stability β, with wind gradients $\partial u/\partial z$ and $\partial u/\partial y$ in the vertical and low pressure directions, a parcel displaced a vertical distance c would experience a buoyancy force $g\beta c$ and so, in being displaced a distance c would absorb work of amount

$$\int_0^c g\beta c\,dc = \tfrac{1}{2}g\beta c^2 \qquad (4.1)$$

It would then have a velocity anomaly $c\partial u/\partial z$ as a result of the displacement, and would experience a coriolis force anomaly $fc\partial u/\partial z$. If it underwent a horizontal transverse displacement b in the direction of this force it would receive work equal to

$$fbc\,\partial u/\partial z \qquad (4.2)$$

In this displacement b it would acquire a velocity anomaly $b(\partial u/\partial y - f)$ and the work done by the resulting coriolis force anomaly would be

$$\tfrac{1}{2}f\left(\frac{\partial u}{\partial y} - f\right) b^2 \qquad (4.3)$$

If all the particles in a cell of aspect ratio b/c circulated in vertical planes transverse to the motion the circulation would gain energy if (4.2) and (4.3) together exceeded (4.1). The disturbance would therefore be unstable if

$$f\left(\frac{\partial u}{\partial y} - f - 2\frac{c}{b}\frac{\partial u}{\partial z}\right) > g\beta\frac{c^2}{b^2} \qquad (4.4)$$

This criterion can be derived (at much greater length) by conventional perturbation techniques.

It is unusual for $\partial u/\partial y$ to exceed f and is more generally of the order of $\tfrac{1}{2}f$ in typical cases. But c/b can be negative, and so can $\partial u/\partial z$, and a real value of c/b exists to satisfy (4.4) if

$$\left(\frac{\partial u}{\partial z}\right)^2 > \frac{g\beta}{f}\left(f - \frac{\partial u}{\partial y}\right) \qquad (4.5)$$

If we write equality in (4.4) and (4.5) we have that

$$\frac{c}{b} = \left\{\frac{f\left(f - \frac{\partial u}{\partial y}\right)}{2g\beta}\right\}^{\frac{1}{2}} \qquad (4.6)$$

which is typically of the order of 10^{-3}. Thus if it were n km wide the cell would be n metres deep, and for a typical case in which $\partial u/\partial y = \tfrac{1}{2}f$ we require that

$$\frac{\partial u}{\partial z} > (\tfrac{1}{2}g\beta)^{\frac{1}{2}} \qquad (4.7)$$

for instability. The right of (4.7) is typically of the order of 5×10^{-3} so that a wind shear in excess of 5 m sec^{-1} km^{-1}, which is quite common, would produce instability.

The growth rate is necessarily of the order of an e-fold increase in a day because the coriolis forces are the source of the instability but layers a few tens of metres thick with large vertical gradients of T could be generated in an airstream of large $\partial u/\partial z$ which is necessarily one of large $\partial T/\partial y$.

In jet streams over the ocean these could easily be generated rapidly to produce billows as soon as they are displaced vertically by flow over a mountain.

5. The significance of billow clouds

The forms of clouds are mostly dominated by the motions produced by buoyancy forces due to the latent heat released by condensation. We have, therefore, to distinguish clearly those in which the cloud is simply a passive tracer of motion. Often a pattern of motion exists which becomes visible at the moment cloud first forms and which is modified when the buoyancy forces become large. Generally, when cloud is only just above its condensation level it is a good passive tracer, and the wavy motion overturning into rolls can often be seen. Billows are by far the most common clear air motion pattern seen in this way. Various features of convection from hot ground can be seen when the thermals just begin to reach the condensation level, and cirrus streaks and aircraft condensation trails show up various rather slow motions deforming the air: otherwise only billows are common, and show that the billow form of dynamic instability is the most important one. We are concerned therefore with a quite specific form of 'turbulence', and not with a vague kind of 3D eddying motion presumed to draw its energy from the shear of larger scale motion.

On the other hand not all billow clouds are formed by the generation of shear at very stable layers. Many are a form of cellular overturning which is arranged in rolls by a rather small shear in the overturning layer. It is not profitable to think of such motions in terms of cellular convection patterns in viscous fluids and it is probably more appropriate to think of the reduction of the Richardson number by a decrease in β which eventually becomes slightly negative than an increase in the Rayleigh number in which the coefficients of heat and momentum transfer are quite meaningless in this context.

The radiative heat loss from the top of a layer of cloud fairly quickly renders the cloud layer statically unstable. The overturning is nevertheless very slow by comparison with that in Helmholtz instability. The cells are arranged across the shear vector because the vorticity generated by the buoyancy forces is small compared with that already present which, therefore, determines the direction of overturning. The fact that the upper and lower surfaces are not rigid means that a pattern of motion like the cats-eye vortices can develop, with all the cells rotating in the same direction, since they do not have any common boundaries on which velocities of opposite sign would have to be present. When the vorticity generated by buoyancy forces is dominant the motion takes the form of streets aligned along the shear vector, with opposing rotation in adjacent cells.

If the billows formed in the way described are indeed a form of Helmholtz instability the velocities will clearly be small, when Ri is reduced by a decrease in β, compared with the other case in which η is increased.

Convection or billows in cloud layers can leave a cellular pattern of humidity in the air when the cloud evaporates. The pattern reappears when condensation of cloud next occurs. In the meantime the air can remain unstirred with the decrease in density due to high humidity being exactly compensated for by a lower temperature ΔT which is approximately equal to one sixth of the wet bulb anomaly.

When a stable layer is overturned and well mixed, it is replaced by two, probably thinner, stable layers at the top and bottom of the mixed layer. Consequently, in passing through mountain waves billows of different wavelengths and orientations may be formed at almost the same level. Each set of billows may leave its imprint on the humidity distribution, so that a cloud layer may appear to have several sets of billows in it simultaneously.

6. Other forms of clear air turbulence

In emphasising billows as the dominant form of dynamical instability in the free air we must not appear to assert that it is the only form of clear air turbulence at these altitudes. There are other possibilities, but most of the likely ones invoke hydrostatic instability or the presence of rough ground. In particular, all other forms of 'turbulence' in gravity waves require hydrostatic instability, and they come outside the scope of this paper. Reference may be made to the books and papers listed at the end.

Scorer, R. S. 1951 Billow clouds. Quart.J.R.Met.Soc. 77, 235.

1954 Theory of airflow over mountains III Airstream characteristics (esp. fig. 2) Quart.J.R.Met.Soc. 80, 417.

1958 Natural Aerodynamics, pp. 153-4 and 243-4. (Pergamon)

1961 Paper no. 7 in R.A.E. Symposium - Atmospheric turbulence in relation to aircraft operation. (H.M.S.O.)

1970 A Colour Encyclopaedia of Clouds, Chapter 6 - Billows. (Pergamon, in press).

Scorer, R. S. and Wexler, H. 1963 A Colour Guide to Clouds, plates 32, 33. (Pergamon)

1968 Cloud Studies in Colour, plates 61-64 and fig. 9. (Pergamon)

Thorpe, S. A. 1968 A method of producing shear flow in a stratified fluid. J.Fluid Mech. 32, 693.

MOUNTAIN WAVES IN THE STRATOSPHERE MEASURED BY AN AIRCRAFT OVER THE WESTERN USA DURING FEBRUARY, 1967

by

A McPherson and J.M Nicholls

Royal Aircraft Establishment,
Bedford, England

Mountain Waves in the Stratosphere Measured by an Aircraft over the Western U.S.A. during February, 1967

A. McPherson
J.M. Nicholls

Royal Aircraft Establishment, Bedford, England

1. INTRODUCTION

Mountain waves are one possible source of high altitude disturbances* sufficient to affect the operation of an aircraft (the other chief source is, of course, thunderstorms). Clear air turbulence (CAT) encounters are common at and below the tropopause in conjunction with wave activity over mountainous terrain. It is also known, from experience in gliders and from "mother of pearl" clouds, that mountain waves propagate through the tropopause well into the stratosphere. Information on the wavelengths, amplitudes and associated turbulence of stratospheric waves is, however, rather sparse and, in view of the growing interest in the stratosphere with the advent of the supersonic transport aircraft, it was felt to be important to gain a greater understanding of the nature and magnitude of disturbances in the stratosphere. The stratosphere is, in general, a stable layer in which it was anticipated that disturbances transmitted through the tropopause would be damped out. It was known, however, that in some conditions disturbances could propagate into and be amplified in the stratosphere but it was not clear under what conditions or how frequently this occurred[1,2].

While the primary purpose of the present tests was to investigate the nature and magnitude of disturbances in the stratosphere, it was also considered important to assess their predictability. Tropospheric mountain waves can be predicted with some confidence from meteorological considerations[3] and it was hoped that this exercise would provide data from which the propogation of tropospheric waves into the stratosphere could be forecast with similar success. In addition it was hoped to gain a feel for the circumstances in which mountain waves contained marked turbulence and changes in outside air temperature.

The Canberra PR 7/9 WH 793 operated by Aero Flight, RAE Bedford, was based at the NASA Ames Research Center, California from late January until the end of February, 1967 on Project WAVERIDER, a part of the general RAE programme of research on High Altitude Atmospheric Disturbances. Thirteen flights were made over mountainous terrain, mainly in California and Nevada, but on one occasion over Utah (see Fig. 1). A T33 aircraft operated by the Canadian National Aeronautical Establishment (NAE) was also based at Ames during February and, on many occasions, it flew at the same time and in the same area as the Canberra. The latter flew at and above the tropopause up to 50,000 ft (once to 54,000 ft) while the T33 flew at and just below the tropopause.

Each flight was planned on the basis of a tropospheric mountain wave forecast (see Appendix A) made by a member of the trials team based on information provided by the Weather Bureau Office at San Francisco International Airport. Mountain waves are likely to be found when there is a fairly strong wind component at right angles to a mountain range (20 kt or more at mountain top height, increasing at greater height) and the temperature profile shows stability near mountain top height. Upper air reports from civil airlines and hourly cloud reports from the surface were also taken into account. Whenever possible the aircraft flew over an area where strong tropospheric lee wave activity was forecast. On some occasions, however, strong wave activity was out of range, and on these days flights were made in the area nearest to base where any wave activity was expected. Several horizontal legs displaced at height intervals of from one to five thousand feet from one another were normally flown from about 20 nm upwind of the mountain to 80 nm downwind. On a few occasions the track was across-wind, parallel to the ridge and some 20 nm on the downwind side. The flight levels were chosen in early flights on the basis of the height of the tropopause but in later flights, in the light of experience gained, the aircraft flew at the height of discontinuities in the wind or temperature profile in the stratosphere. Most of the runs were in the lowest 10,000 ft of the stratosphere. When the T33 accompanied the Canberra, it patrolled the region of the tropopause along the same ground track and at the same time.

Nine of the 13 flights yielded valuable data and these form the basis of the discussion. The results obtained by the T33, which is also fully instrumented, are published separately[3].

2. THE ISSC AIRCRAFT AND INSTRUMENTATION

Canberra WH 793 is the PR 9 prototype developed from the PR7 by increasing the wing area, fitting more powerful engines and powered aileron and rudder controls. The aircraft is fitted

---

* "Disturbances" is used throughout this paper to indicate any phenomenon, such as gusts or changes in outside air temperature, which might affect the operation of an aircraft.

with wing-tip tanks one of which contains a weather radar antenna and the other a forward looking 16 mm camera. There is also a nose pole carrying an incidence vane and a pitot head, supplying pitot and static pressure to the pilot's instruments but pitot pressure only to the recorder. The static pressure for the recorder is provided by vents on the side of the fuselage and this gives rise to a difference between pilot reported and recorded height and airspeed which has been allowed for in the analysis. Navigation aids include TACAN and doppler.

Recordings were made on two oscillograph recorders running "slow" and "fast" respectively. The slow recorder measures airspeed, barometric height, normal acceleration, outside air temperature, elevator angle and pitch attitude. In addition this recorder was used to give time synchronisation by means of "event" marks by the pilot or navigator, and by synchronous pulses from the fast recorder and camera. The fast recorder duplicates measurements of outside air temperature, elevator angle and pitch attitude in addition to measuring incidence, pitch rate and a more sensitive normal acceleration.

The slow recorder, which ran throughout the flight, was used to calculate the long wavelength components of the waves, to edit the fast recorder records, and to provide temperature information at varying heights to supplement the conventional meteorological radiosonde measurements. The fast recorder has limited duration and is only switched on when the pilot considers that a significant event is occurring or is about to occur. The fast recorder records were used to measure fine detail and true gust velocities in the more turbulent regions.

The transducers used for the recordings are conventional instruments with inductive pick-off, except for the pitch attitude information which is obtained from a standard aircraft horizon gyro unit with a potentiometer fitted. Outside air temperature is measured by a Rosemount 102E rapid response open platinum element total temperature sensor[6]. All instruments were calibrated before and after the exercise.

3. RESULTS OF FLIGHTS OVER MOUNTAINOUS TERRAIN

The Canberra is well-instrumented for gust research studies. True air motion is established by well-tried methods from measurements in turbulence[4] but new methods had to be established to deduce the longer wavelengths associated with mountain waves. The first of these, a method of isentropic analysis, is based on the assumption that the vertical profile of temperature is the same in disturbed flow over mountains as it is upwind of a ridge. The method is summarised in fig. 2 and is now described. A composite upwind stratospheric vertical temperature profile is assembled (left side of fig. 2) which usually includes two or more radiosonde ascents and the aircraft-measured temperature upwind of the mountain range. From this profile a potential temperature profile is deduced by assigning to each height the temperature the air at that height would achieve if it was descended adiabatically to the 1,000 mb level (approximately to sea level). The aircraft-measured temperature along a run at constant height is converted to true outside air temperature by including the effects of kinetic heating and further converted to potential temperature (right side of fig. 2). From these measurements isentropes (i.e. lines of constant potential temperature) can be drawn as shown in fig. 2. If air has a velocity relative to an isentropic surface and if the isobaric or height gradients on the surface remain constant with time, then the air is flowing along the isentropic surface. A vertical section through the surface along the wind direction will produce an isentrope which will be a trajectory of airflow. In mountain wave conditions the measured isentropes will closely correspond to waves.

The second method makes use of the principle of conservation of energy. If the aircraft is trimmed and the power is not changed then waves will cause changes in height and airspeed. If it is assumed that the wind speed is approximately constant along the path of the aircraft, then the measured airspeed changes can be converted to equivalent height changes (i.e. kinetic energy is transformed into potential energy). These height changes are added to the actual height changes measured to give the effective wave motion. Both methods, which show reasonable agreement, are used in the analysis of the results.

Canberra WH 793 was based at the NASA Ames Research Center, Moffett Field NAS, California from January 30 to February 24, 1967. In that time 13 experimental and 2 other flights were made in 39½ hours flying time. Significant disturbances were found on February 3, 9, 13 and 14 and lesser disturbances were noted on January 30, February 7, 10, 15 and 24. On the remaining four experimental flights (January 31, February 6, 16 and 20) no disturbances were found and none were anticipated. On two occasions (February 13, run 6 and February 14, run 2) the disturbances were so severe that the pilot partially lost control of the aircraft and did not regain full control until several thousand feet of height had been lost. It is clear that very marked disturbances can exist in the stratosphere but the frequency of occurrence of such events cannot be deduced directly from the results of an exercise such as this where comparatively few flights are made in areas selected because they are likely to contain disturbed air. Some general inferences can however, be made on the meteorological conditions prevailing when the disturbances were found, and these and some general implications to the operation of aircraft are discussed in section 4.

3.1 Wave Motion

In general, on days when the tropospheric wave intensity was probably slight to moderate or less, the stratospheric disturbances were in the main irregular with amplitudes of 1,000 ft or less (January 30, February 15 and 24). Amplitudes do, however, appear to vary little with height. Trains of stratospheric waves appeared on only two of these days, February 15 and 24, at one height on each day. The lee wave amplitudes were less than 300 ft and wavelengths were approximately equal to the natural wavelength and less than the calculated tropospheric wavelength (see Appendix A). It may be concluded that on the days of little tropospheric wave activity stratospheric disturbances are also slight. The data from February 7 is not included since the only part of that flight in the stratosphere was over non-mountainous terrain.

When the probable intensity of the tropospheric waves was moderate to strong or greater (February 9, 10, 13 and 14) well developed waves, as indicated by the isentropes, were present in the stratosphere. On February 9 and 10 there were negligible temporal variations in the atmospheric parameters governing wave structure. The isentropic patterns were stationary, wave amplitudes were about 1,500 ft with no damping with height, and wavelengths were greater than the calculated tropospheric wavelength and much greater than the natural wavelength.

On February 13 and 14 the aircraft encountered violent disturbances which caused the pilot temporarily to lose control. The pilot described the incident on February 13 run 6 in these terms: "At 50,000 ft the aircraft encountered a strong draught and as power was reduced to flight idle the aircraft accelerated to 0.82 IMN (0.02 above MNE) in a 1,000 ft min^{-1} rate of descent (note: power idle!). An estimated 40 lb one-handed pull on the stick produced little or no response to elevator. Both hands were then used and an 80 lb pull reduced speed to 0.80 IMN. The aircraft was finally levelled at 47,000 ft". The pilot described the incident on February 14 run 2 as follows: "The aircraft entered a climb at 2,000 ft min^{-1} with 87% rpm with the IMN increasing from 0.775 to about 0.79! Suddenly, and without any warning at all, the IAS dropped in under one second from about 198 kt to 150 kt at 47,[illegible]0 ft (approximately 100 kt true air speed change). The airflow could be heard breaking away from the canopy and I was conscious of the aircraft continuing upward even as I applied about ½ forward stick (this could easily be the effect of -ve g). The aircraft bunted over at about 150 kt. No pre-stall buffet was felt although the airflow was distinctly heard as it broke away over the canopy. After the aircraft was diving satisfactorily the speed increased slowly and then jumped suddenly to 200 kt/0.81 IMN. I held the aircraft at 0.8 and descended to 42,000 ft to gather my wits. A check on the g meter showed -1 g". Both days were characterised by strong tropospheric wave conditions, by some change in the controlling meteorological parameters during the period of the flight and by adjacent layers of high and low stability in the stratosphere. The stratospheric isentropes corresponding to the waves are shown in fig. 3. The amplitude to wavelength ratios of the isentropes were the greatest of the flight series (with the exception of February 3, which is discussed below). The wavelengths were close to the natural wavelength, and the vertical variation of wavelength on each day suggests that wavelengths in changing meteorological conditions were determined by the vertical variation of the wind and temperature fields: the data from February 15 supports this view. Frequently, in changing conditions wave amplitudes appeared to increase with increasing height or time. If the increase is time dependent then it could be due to temporal changes in meteorological parameters over a particular mountain range.

On February 3 the flight was made more or less across wind so that the measured isentropes do not correspond to waves but merely indicate the presence of wave flow. On this day there were large amplitude (second to those of February 14), short wavelength disturbances at the tropopause. Although no temporal changes were occurring during the flight period in the meteorological parameters governing tropospheric lee wave intensity, the stratospheric lapse rate was again characterised on this day by adjacent layers of high and low stability.

It is impossible on the evidence of these few flights to assess how far stratospheric wave parameters are dependent on topography. All the flights were made over mountainous terrain, but it should be noted that the large amplitude waves of February 13 occurred to the lee of mountains whose crests were only 3,000 or 4,000 ft above the general terrain.

3.2 Turbulence and Temperature Changes

In mountain wave conditions encountered during WAVERIDER there appeared to be a relationship between temperature change and turbulence. The air in the troughs of mountain waves in the stratosphere is at a higher temperature than the surrounding air since the wave has caused the air to descend from a greater height and during this descent its temperature increases adiabatically. As shown below, turbulence tended to occur in the troughs so that there was a relationship between turbulence and temperature increase in mountain wave conditions. Not all troughs contained patches of turbulence and in some cases the turbulence extended over neighbouring crests, however an increase in temperature indicated the presence of the most likely location of turbulence. In addition, the most marked and rapid temperature changes were associated with the areas of marked turbulence.

3.2.1 Turbulence

The Canberra encountered moderate or severe turbulence on February 3, 13 and 14; the T33 flew at the same time and in the same area but at lower heights on February 13 and 14 encountering marked turbulence on February 14 but not on February 13[5]. In many cases when turbulence was encountered it occurred with no warning - the indicated air speed trace of fig. 4 (a) shows the sudden onset. This sudden entry into turbulence was most common on runs along the direction of the wind. On February 3 the turbulence increased slowly from slight to severe (the indicated airspeed trace of fig. 4 (b)) when the aircraft was flying more or less across wind.

In most cases, particularly where the turbulence occurred in patches, the disturbance was found in the trough of a wave. This is indicated in fig. 3, though it will be noted that some of the most marked troughs were completely smooth. The sudden onset of turbulence in along-wind flights and the location of turbulence in wave troughs suggests that, in the horizontal plane, the turbulence patches are elongated ellipses with considerable length across wind and small width along wind. There is little evidence on which to base a suggested vertical extension of this picture (Fig. 3 (a)) and none at all to indicate the nature of the temporal dimension.

Considering the three flights with marked turbulence, it is not possible to construct a "climatology" of turbulence from so little data but there are some common features in the meteorological environment on these days which can be compared with results of previous studies[2,7]. Tropospheric wave activity was moderate or strong on the days of severe turbulence, but this was also the case on February 9 and 10 when little turbulence was encountered. As shown in fig. 5 February 13 and 14 were characterised by marked vertical lapse rate changes in the stratosphere (as was February 3), whereas no such fine structure was present on February 9 and 10. The temperature of the turbulent air on February 3 and 13 indicated that turbulence was occurring in the top of the semi-adiabatic and base of the stable layers (fig. 5).

3.2.2 Temperature Changes

The greatest temperature changes occurred when strong stratospheric waves were accompanied by severe turbulence. When the aircraft encountered strong stratospheric waves without turbulence, e.g. February 9 and 13 (runs 3 and 4), the temperature changes were not more than 6°C in 2 nm (3°C per nm) and 10°C in 5 nm (2°C per nm). With the exception of February 14, temperature changes at times of strong stratospheric waves and marked turbulence, e.g. February 13 (run 6), were about 7°C in 1 nm (7°C per nm) and 10.5° in 2 nm (5.2°C per nm). These are comparable with the largest changes found near thunderstorms. The greatest changes measured, on February 14, were about 12°C in 0.2 nm (60° per nm) and 20°C in 1 nm (20°C per nm). The U2[1] reported changes of 6°C in 0.1 nm (60° per nm) and 13.5°C in 3 nm (4.5°C per nm) at 60,000 ft over Bishop in moderate turbulence.

4. DISCUSSION OF RESULTS

Tropospheric lee wave studies have been made previously but there have been few reports of flights above the tropopause in conditions suitable for tropospheric lee waves. Only two papers are known to have reported disturbances in the stratosphere in possible lee wave situations[1,7]. Of these only one[1], describing two flights over the Sierra Nevada by the HICAT U2, contains the meteorological and positional information which allows the results to be incorporated in this discussion. The present results add considerably to the fund of knowledge on stratospheric airflow in conditions suitable for tropospheric waves. The implications of these results are developed below but it must be stressed that more flights will be needed to establish the generality of the conclusions. In addition, work should be extended to greater heights to establish the vertical extent of disturbances, and to areas where there is a single tropopause in contra-distinction to the latitudes of the Sierra Nevada where a second tropopause at about 60,000 ft was frequently evident.

The two U2 flights[1] were made in unchanging meteorological conditions over the Sierra Nevada up to 65,000 ft. On both flights tropospheric waves were probably moderate and lee wave-trains were found in the stratosphere with wavelength 17 nm (much larger than the tropospheric or natural wavelength). The data used in constructing the isentropes was averaged over one minute with consequent lack of resolution of short wavelengths and reduction in amplitude. However, more detailed data on a run at 60,000 ft on the first flight indicated a disturbance of amplitude 2,500 ft on the lee of the main Sierra crest. The report also indicates that the wave crests and troughs tilted upwind with increasing height with the gradient of each axis (i.e. the line through crests at different heights) given by $z : x :: 1.5 : 1$. Lack of wind data and accurate information on aircraft position made such calculations impossible from the data reported here. Spillane[2] also found a strong correlation over flat terrain between turbulence encounters and the presence and height of marked vertical variations in the stratospheric lapse rate. HICAT flights over the Australian Alps appear to indicate that the severity of the turbulence increases over mountainous terrain.

The severe turbulence encountered by the Canberra on February 14 at 46,000 ft (whereas no turbulence was found 20 minutes earlier and 12 nm south at 45,000 ft) was probably the result of rapid changes in the parameters governing tropospheric wave structure. However, it may also have been due to reduction of Richardson's number (Ri. No.) by ageostrophic motion or by streamline cramping in the disturbed flow, or by some combination of these circumstances (see Appendix A for an explanation of these terms). The reduction of Ri. No. in disturbed flow was considered as a cause of turbulence occurring in the wave troughs in the two U2 flights over the Sierra Nevada[1]. On three occasions, all at 60,000 ft moderate CAT was encountered by the U2 with no more than a few patches of light turbulence at 38,000, 44,000, 52,500 and 65,000 ft., the other heights flown. There was evidence of marked fine structure in the stratospheric lapse rate centred at about 63,000 ft which may have contributed to the turbulence at 60,000 ft. It was shown that the Ri. No. in the disturbed flow was reduced when streamline cramping occurred. It was also shown that Ri. No. is further reduced in wave flow containing tilting crests with the minimum value occurring just upstream of the wave troughs in normal stratospheric flow.

If ageostrophic motion is present in a stratospheric layer above a jet stream it may cause destabilisation of part of the layer with corresponding decrease in Ri. No. If tropospheric stability criteria are satisfied the jet will also cause strong tropospheric wave activity and hence stratospheric wave activity. If, as has been suggested, the waves tilt backwards there will be a further decrease in Ri. No. in the wave troughs and just upstream of them; any cramping of the isentropes will result in a reduction of Ri. No. in the locality of the cramping. The combination of ageostrophic motion and strong stratospheric wave activity appears to be conducive to severe turbulence near the level of the ageostrophic motion. The severity may well be increased by interference caused by changes in the meteorological parameters or geographical effects.

To summarise, it appears that in unchanging meteorological conditions and when stratospheric lapse rates show no fine structure, stratospheric waves are characterised by long wavelengths, little variation of amplitude with height and smoothness. Their presence is primarily due to the underlying topography and their intensity primarily dependent on the tropospheric mountain and lee wave intensity.

When meteorological conditions are changing with time in a specific location, or when stratospheric lapse rates show marked fine structure, short wavelength, large amplitude waves of some sort are present, frequently superimposed on the longer wavelength topographically-induced mountain and lee waves. These short wavelength features are frequently mobile and turbulent and it is probable that their presence is dependent on the existence of the longer wavelength waves as well as on the meteorological conditions. They also appear to be centred at the level of lapse rate change, but in changing meteorological conditions they could possibly exist at all levels.

In view of the correlation between increase in temperature and areas prone to turbulence in mountain wave conditions, some remarks are appended on the value of remote temperature sensing as an aid to avoiding turbulence. The postulated elongated elliptical shape of turbulence patches would make it almost impossible for an aircraft flying along wind to avoid turbulence by horizontal manoeuvres and lack of knowledge of the vertical structure of the turbulence makes climb or descent manoeuvres a matter of chance. For an aircraft flying across wind the turbulence could be avoided only if the temperature sensing device was able to scan in the horizontal plane. A temperature sensor would, however, be able to detect the existence of the waves themselves, if it had adequate range resolution. At least until more is known about the persistence of particular turbulence patches, such detection might be more valuable than that of the turbulence itself.

5. CONCLUSIONS

The 13 flights over mountainous terrain reported in this paper have provided valuable information from which it has been possible to extend our understanding of stratospheric flow. However, more flights would be needed to give the greatest generality to the results. In particular, flights at greater heights would be most valuable.

One particularly violent incident, on February 14, serves to set the limit, within our present experimental knowledge, of the savagery of which the stratosphere is capable. The aircraft flew through air which had been brought down from at least 7,000 and possibly 9,000 ft above (fig. 3 (b)). In this air mass it encountered a 100 kt change in true air speed and a temperature change of 12°C in 0.2 nm. The pilot partially lost control of the aircraft and during the incident -1 g was measured. While such an incident may be uncommon, or even rare, it can happen.

Significant waves were found in the stratosphere only when moderate to strong or greater waves were probable in the troposphere. Practically all the evidence suggests that there is no reduction in wave amplitude with height, a result opposite to that expected before the start of the exercise. The waves were most pronounced on days when meteorological parameters affecting wave production were changing in the flight area at the time of the flight.

In strong wave conditions and at heights where there are anomalies in the vertical temperature profile, severe turbulence is most likely. Associated with the turbulence there will probably be large and rapid changes in outside air temperature.

In summary, it is fairly certain that the conventional techniques for forecasting tropospheric waves (Appendix A) give a clear estimate of the severity of stratospheric waves. It is unlikely that severe disturbances will exist in the stratosphere unless the probable tropospheric wave activity is moderate to strong or greater. Even when marked stratospheric waves are likely to be present they will probably be of moderate amplitude if meteorological conditions are constant. The most dangerous situation occurs when strong tropospheric (and hence stratospheric) waves are probable in rapidly changing meteorological conditions or where marked fine structure exists in the stratospheric vertical temperature profile. Severe turbulence and rapid temperature changes seem to require a combination of strong stratospheric waves and anomalies in the vertical temperature profile in the stratosphere. The indications are that neither wave amplitude nor turbulence severity depend on the magnitude of the mountainous terrain.

REFERENCES

1. HELVEY, R.A. — Observations of stratospheric clear air turbulence and mountain waves over the Sierra Nevada Mountains. An analysis of the U2 flights of 13-14 May 1964. AFCRL - 68-0001

2. SPILLANE, K.T. — Clear air turbulence at high levels and supersonic transport. Nature 214 (5085) 237-239. 1967

3. SCORER, R.S. — Forecasting dangerous flying conditions near mountains. Met. Research Committee, MRP 814. 1953

4. ZBROSEK, J.K. RIDLAND, D.M. — A measured power spectrum of the vertical component of atmospheric turbulence. Unpublished RAE Paper. 1960

5. MATHER, G.K. — Some measurements of mountain waves and mountain wave turbulence made using the RAE T-33 turbulence research aircraft. Quarterly Bulletin of the Div. of Mech. Eng. and the NAE DME/NAE 1967(2) April-June (p1)

6. WOODFIELD, A.A. HAYNES, P.J. — Measurements of air temperature on an aircraft travelling at high subsonic and supersonic speeds. ARC CP 809. 1965

7. COLEMAN, T.L. STEINER, R. — Atmospheric turbulence measurements obtained from airplane operations at altitudes between 20,000 and 75,000 ft for several areas in the northern hemisphere. NASA TN D-540. 1960

APPENDIX A METEOROLOGICAL ASPECTS OF THE STUDY

A1 Forecasting mountain waves

Predicting quantitative details such as amplitude and wavelength of lee waves, and their variations with height of the tropospheric airflow over and in the lee of individual mountain ranges is a lengthy task. It is however possible, in the time available in field trials such as WAVERIDER, to forecast with some confidence the presence of waves for the mountain ranges under consideration. The following criteria were used.

The theoretical requirement for the presence of tropospheric lee waves is that the parameter $l^2 = \frac{g\beta}{u^2}$ should have a maximum value in the lower or middle troposphere (at or about mountain top height) with lower values in the upper troposphere. In the formula β, a stability factor, is given by $\frac{1}{\theta}\frac{d\theta}{dz}$ where θ is the potential temperature and z is height; u is the wind component normal to the range, and g is the acceleration due to gravity.

In terms of stability this means that the upstream vertical temperature profile should show marked static stability at levels where the airstream is disturbed by the mountain (i.e. large $\frac{d\theta}{dz}$) with lower stability above. Synoptically this condition is frequently satisfied by the presence of a subsidence inversion, a frontal inversion, or warm sector isothermal or near-isothermal layer near mountain top height. Of course other synoptic situations exist in which the required profile would be produced.

Another necessary condition for the presence of tropospheric waves is that there must be a reasonable component of the wind current normal to the range. Also, for the necessary reduction in ℓ^2 with height, it is preferable for this component to increase with height. This too has synoptic implications since this increase is often found in or near jet-streams. In practice it is found that marked wave activity is absent if the wind direction is not within about 30° of the normal to the range or if marked directional changes occur with height. The most common situation in which both stability and wind criteria are satisfied is in the vicinity of fronts on the equatorial side of depressions.

When forecasting tropospheric waves any foreseeable changes in the synoptic situation must of course be taken into account, for example the movement of fronts will cause the height of the stable layer to vary at a fixed location. Observational evidence of waves in the form of wave clouds (which are by no means always present) and pilot reports are also important.

A few factors governing wave amplitude and wavelength are sometimes of help to the forecaster and will be mentioned here. The tropospheric lee wavelength (in km) is approximately equal to half the mean tropospheric wind speed (in m sec^{-1}). If the lee wavelength is approximately equal to the horizontal "scale" of the mountain range, the amplitude will be much larger than for broader or narrower mountains. The amplitude is approximately proportional to the mountain height and is also dependent on the symmetry of the range, asymmetric ridges producing greater disturbances. The natural wavelength is given by $\frac{2\pi}{\ell}$

All other factors being equal, amplitudes are largest when the wave forming criteria are only just satisfied. Thus, in this region, the amplitude depends critically on the airstream characteristics and large amplitude changes may result from small changes in the wind or temperature profiles. Also, larger amplitude waves are formed in airstreams containing a shallow layer of great stability than for a broad layer of slight stability, but in the first case the amplitudes will fall off greatly with height.

No criteria had been evolved before this exercise from which stratospheric disturbances could be forecast. Here "stratospheric disturbances" means mountain waves (a distortion of the flow just due to ground undulation with no following lee waves), lee waves, or turbulence in association with these waves. However, it was assumed that the magnitude of the stratospheric disturbances would be proportional to the magnitude of the tropospheric disturbance, and also that possible breakdown of the flow could be associated with large wind shear and possibly with marked changes in lapse rate.

A.2 Isentropes and Waves

An isentropic surface (in the meteorological context) is a surface on which air has the same potential temperature. If the air has a velocity relative to that surface and if it can be shown that the isobaric or height gradients on the surface remain constant with time, then the air is flowing along the isentropic surface. In this case, if a vertical section is taken through the surface along the wind direction, the isentrope so produced is a trajectory of the airflow and vertical air speeds can be directly deduced from the isentropic gradients and a knowledge of the wind speed in the undisturbed upstream flow. A mountain lee wave is indicated by a periodic disturbance in a stationary isentrope to the lee of a mountain range.

It is difficult to attach physical significance to disturbances in an isentrope unless it can be shown to be stationary. In non-stationary cases in which the isentrope shows wavelike disturbances it may not be possible to say more than that the disturbances must have been caused somewhere locally and their amplitude and period must be representative of the air oscillations somewhere in the flight area.

The onset of ageostrophic motion (i.e. motion due to the component of wind normal to the isobars or height contours), usually present between the 200 and 50 mb layers above a jet stream, results in destabilisation of certain stratospheric layers if macroscale horizontal temperature variations are present in the area of onset. The decrease in stability results in a reduction of Ri. No. and is a possible contributory cause of turbulence. Where streamline cramping occurs it will also cause a reduction in Richardson's number (Ri. No. - $\frac{\frac{g}{\theta}\frac{\partial\theta}{\partial z}}{\left(\frac{\partial u}{\partial z}\right)^2}$)

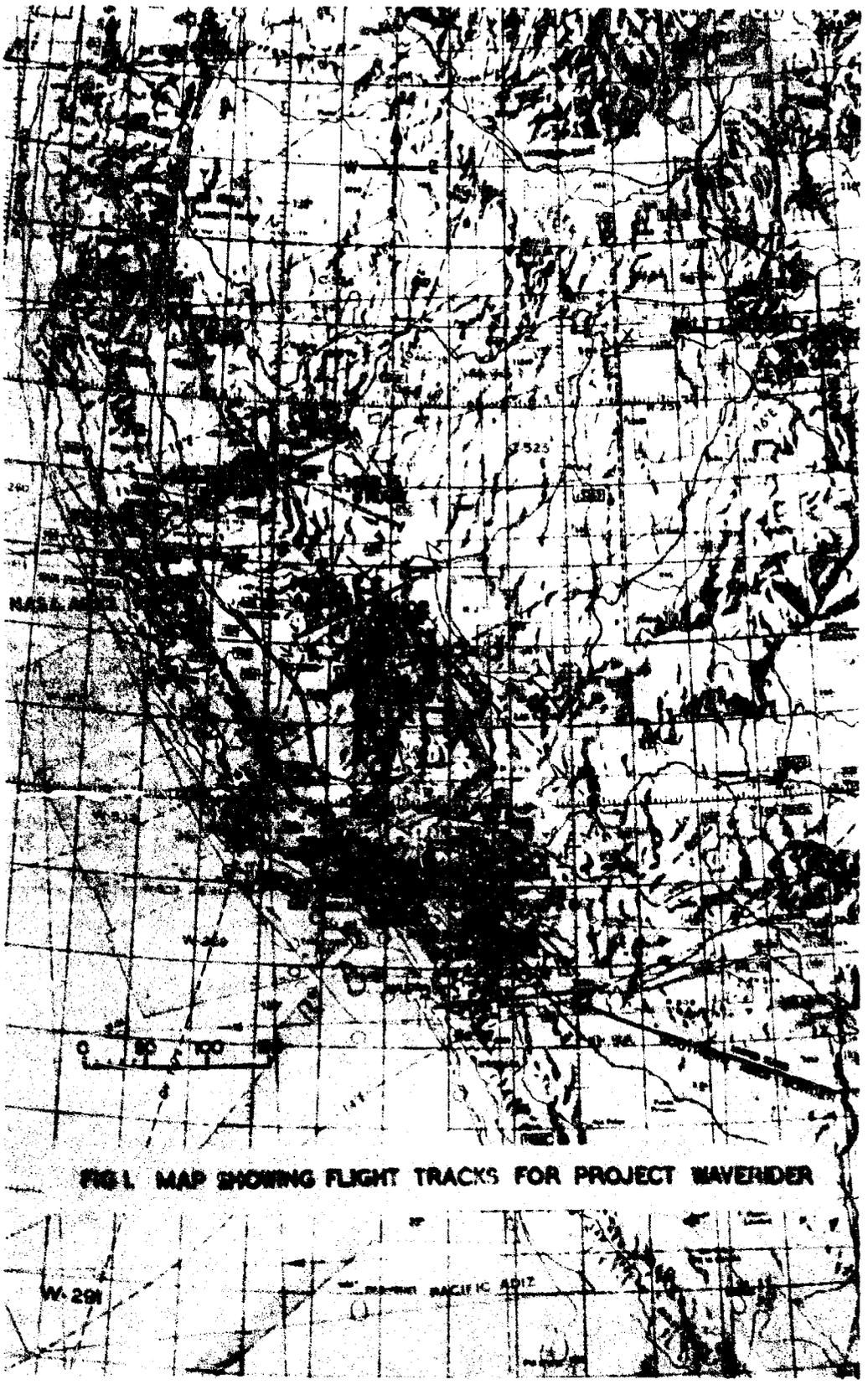

FIG 1. MAP SHOWING FLIGHT TRACKS FOR PROJECT WAVERIDER

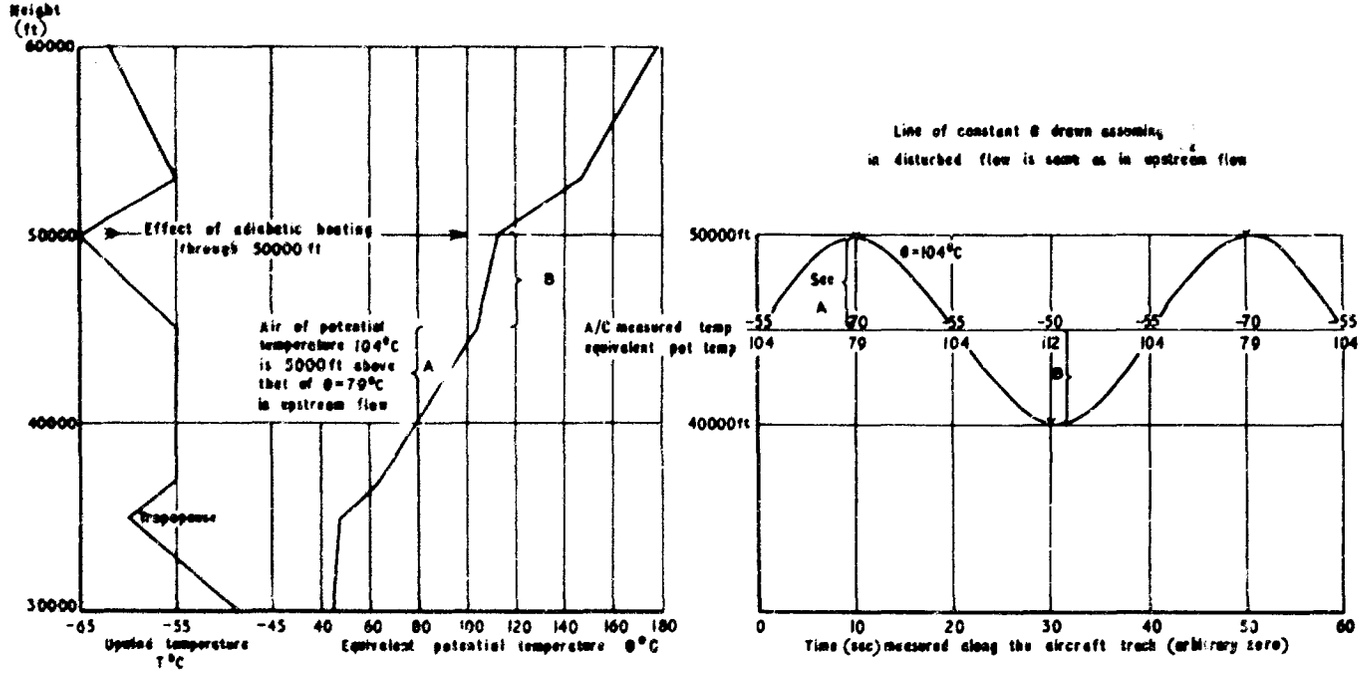

Fig. 2 Construction of line of constant potential temperature for a run at 45000 ft

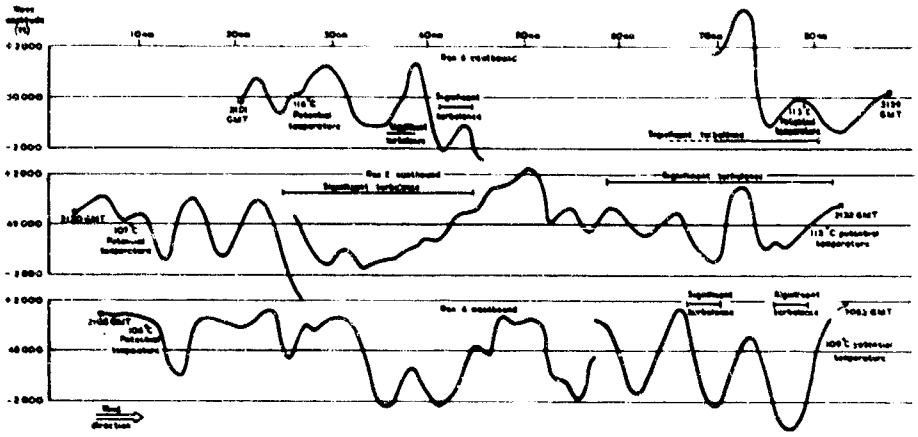

Fig. 3a Wave motion on february 13

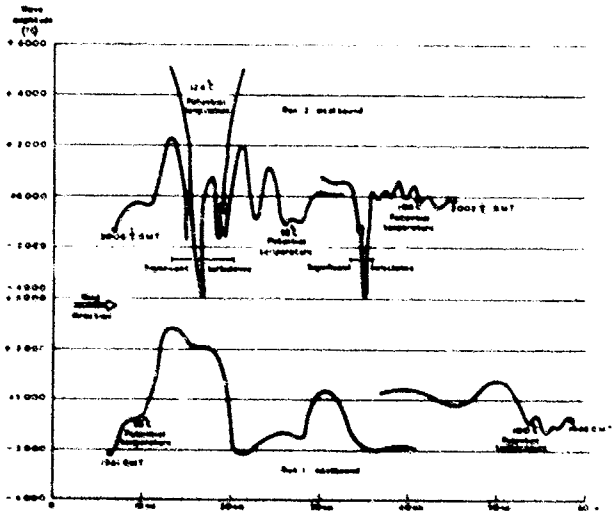

Fig. 3b Wave motion on february 14

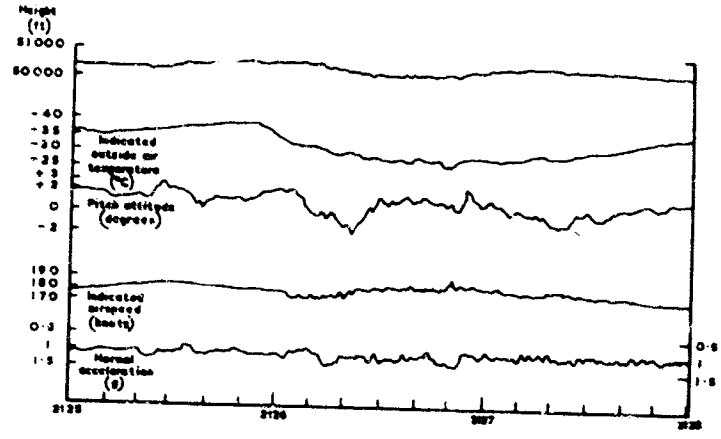

Fig. 4a Copies of original record
for run 5 on february 13

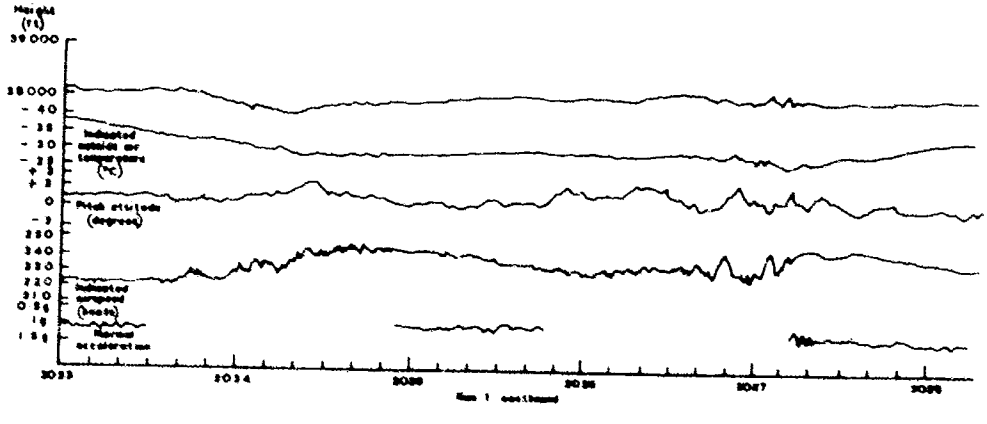

Fig. 4b Copies of original record on february 3

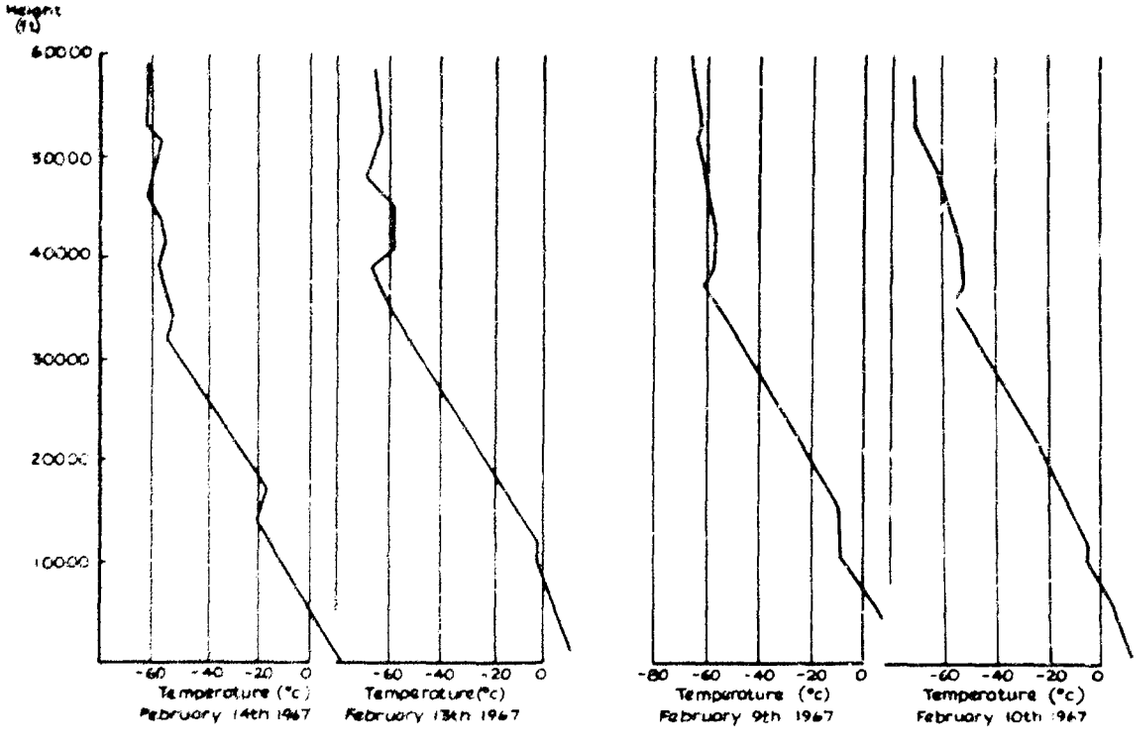

Fig.5 Vertical temperature profiles on days of marked stratospheric waves

DEUX REMARQUABLES EXEMPLES DE CISAILLEMENTS DANS LA STRATOSPHERE CONCERNANT LE VENT ET LA TEMPERATURE

par

G.D.Barbé

Météorologie Nationale, France

SOMMAIRE

Le service "HAUTE ATMOSPHERE" de l'Etablissement d'Etudes et de Recherches Météorologiques de la Météorologie Nationale poursuit depuis plusieurs années des recherches expérimentales et théoriques sur la circulation stratosphérique (de 10 à 40/45 km d'altitude) à l'échelle moyenne (mesoscale).

Les résultats expérimentaux obtenus mettent en évidence que la stratosphère considérée à cette échelle est un milieu plus perturbé que la troposphère.

Premier exemple - Cas du 11 au 12 mars 1968 : 25 sondages horaires consécutifs de vent dans la couche 10-30 km à Magny-les-Hameaux.

La structure de la stratosphère basse et moyenne présente de forts et réguliers cisaillements de la vitesse et de la direction du vent, autour d'une valeur moyenne, de variation lente avec l'altitude. L'interprétation de tels résultats est difficile et semble devoir faire appel à une analyse ondulatoire.

Second exemple - Cas du 21 au 22 novembre 1968 : 9 sondages tri-horaires de vent et température en chacun des points d'un triangle d'environ 50 kilomètres de côté au sud de Paris.

Cette campagne a été effectuée avec la participation de l'avion CANBERRA du Meteorological Research Flight. Le 21 novembre 1968, au milieu de la journée, une turbulence en air limpide a été détectée vers la tropopause (environ 12500/12600 m), alors qu'une variation de température de l'ordre de +8°C a été relevée sur une tranche d'environ 300 mètres d'épaisseur juste au-dessus de ladite tropopause, avec simultanément cisaillement marqué sur les deux modules du vent.

DEUX REMARQUABLES EXEMPLES DE CISAILLEMENTS DANS LA STRATOSPHERE CONCERNANT LE VENT ET LA TEMPERATURE

par G.D. BARBE[1]
Météorologie Nationale - France

I - MOYENS DU SERVICE "HAUTE ATMOSPHERE".

Le service "Haute Atmosphère" de l'Etablissement d'Etudes et de Recherches Météorologiques de la Météorologie Nationale française dispose depuis juillet 1967 d'un ensemble opérationnel "évolué" en temps réel comprenant trois points de mesure situés aux sommets d'un triangle approximativement équilatéral d'environ 50 kilomètres de côté :

- Magny-les-Hameaux (Yvelines)
- Chartres (Eure-et-Loir)
- Pithiviers (Loiret).

Chacun de ces points est équipé d'une station de radar-vent et de radiosondage de température (réception sur 28 MHz actuellement, 403 MHz ultérieurement). Des ballons emportant un ou deux réflecteurs passifs et une sonde de température dont le capteur est une thermistance peuvent être suivis jusqu'à une distance de 140 km par radar COT/AL modifié (2). L'ensemble des trois points de mesure permet de choisir judicieusement le lieu de lancer d'un ballon haute performance et d'assurer éventuellement une poursuite complémentaire avec le radar d'une deuxième station; le ballon peut alors être suivi jusqu'à 190 km de distance; ceci présente un intérêt pratique en hiver par régime de vents forts troposphériques et stratosphériques (de secteur Ouest).

La mesure des trois données primaires définissant la position du ballon (distance oblique radar-ballon, angles de site et de gisement) est assurée toutes les 30 secondes (ou toutes les minutes), avec "lissage" sur 9 secondes effectué par un ordinateur digital IBM 1800 (voir ci-dessous) en ce qui concerne les deux angles. La mesure de la fréquence de l'émission correspondant à la température de la thermistance est assurée "en continu", avec prélèvement toutes les secondes transmis à l'ordinateur.

Ces données "analogiques" sont "digitalisées" en chacun des points de mesure par un convertisseur analogique/numérique et transmises pour chacun des deux points périphériques (Chartres et Pithiviers) par une liaison téléphonique spécialisée à l'ordinateur central IBM 1800 stationné au troisième point de mesure (Magny-les-Hameaux).

Cet ordinateur calcule en temps réel, suivant des programmes comportant des variantes, les données ci-après correspondant à un intervalle de mesure :

- Vecteur vent horizontal : direction et vitesse, vent transversal, vent radial, vent zonal, vent méridien,
- Vitesse verticale du ballon et variation de cette vitesse,
- Température : instantanée (lissage sur 4 secondes de part et d'autre de la seconde correspondant à l'altitude de mesure) et moyenne (couche correspondant à 30 ou 60 secondes d'ascension),

.../...

(1) Ingénieur Général de la Météorologie, Chef du Service "Haute Atmosphère" de l'Etablissement d'Etudes et de Recherches Météorologiques de la Météorologie Nationale française.

(2) Sa précision de mesure a été améliorée par l'adjonction d'amplificateur paramétrique ou de tube à ondes progressives.

- Pression obtenue par itération à partir de la pression au niveau du sol en tenant compte de la différence de pression correspondant à l'épaisseur de la couche considérée entre deux mesures consécutives de l'altitude du ballon. Cette pression peut être comparée à celle "prévue" pour les niveaux standards et éventuellement "recalés" par programme du calculateur.

Le dispositif est complété par un traceur de courbes et un perforateur de cartes travaillant en temps réel. Par ailleurs, des programmes spéciaux "de recherche" en évolution constante sont déjà élaborés pour sortir en temps réel ou éventuellement en temps différé les éléments caractéristiques correspondant à des ondes de gravité (ou assimilées) susceptibles de rendre compte de la structure mésoscalaire de la circulation stratosphérique et de son évolution à court terme : projection horizontale de la trajectoire du ballon, hodogramme de ce mouvement, nombre de Richardson, etc...

Toute singularité détectée dans cette circulation l'étant en temps réel, grâce à la conception moderne de l'ensemble, il est ainsi possible de déclencher une série de mesures rapprochées dans le temps (à l'aide de lâchers de ballons à intervalles fixes) et dans l'espace (trois points de mesure), afin d'étudier la durée, l'extension et l'évolution de l' "accident".

Il est à noter qu'au point de vue technologique, ainsi que cela a été reconnu au cours du symposium sur la stratosphère tenu à Londres du 17 au 29 juillet 1967, les mesures de vent et de température à partir du sol en utilisant des ballons haute performance demeureront à l'avenir indispensables pour compléter - en ce qui concerne la couche 30-50 km - le réseau de fusées météorologiques destiné à l'étude de la couche 30-80 km.

Mentionnons au passage que l'altitude record atteinte en France par un ballon haute performance (type KAYSAM 140 D) est de 48667 m le 26 avril 1968 à Magny-les-Hameaux.

II - BUTS DE RECHERCHE.

L'étude de la circulation dans la basse et moyenne stratosphère (1), conduite par le service "Haute Atmosphère" à l'échelle dite "mésoscale" (la centaine de mètres, c'est-à-dire entre 100 mètres et 1 kilomètre, selon la verticale; la dizaine de kilomètres, c'est-à-dire entre 10 et 100 à 400 kilomètres, dans le plan horizontal; la dizaine de minutes, c'est-à-dire de 30 minutes à plusieurs heures pour le temps), a pour but :

a) Recherche fondamentale : une contribution à l'établissement d'une théorie valable de la circulation générale de l'atmosphère en vue de permettre l'amélioration des modèles actuellement utilisés dans les grands ordinateurs digitaux pour la prévision synoptique et globale;

b) Recherche appliquée : étude et prévision de la turbulence en atmosphère limpide (CAT).

L'énergie cinétique présente dans l'atmosphère se partage en plusieurs catégories - liées entre elles - de perturbations qui se différencient par leur échelle (2), les périodes correspondantes variant de quelques jours pour les perturbations synoptiques (dimensions horizontales de l'ordre du millier de kilomètres) à quelques minutes pour les mouvements turbulents (échelle "aéronautique" vraisemblablement comprise entre quelques mètres et quelques kilomètres).

D'après G.D. ROBINSON (3), l'hypothèse admise par la GARP (Global Atmospheric Research Project) de s'en tenir aux deux seules catégories de mouvements précitées limite à 5 jours l'échéance probable des prévisions à l'échelle globale. Il importe donc de procéder à des expériences préliminaires, consistant "en particulier à une investigation directe du spectre des mouvements atmosphériques"; c'est le cas précisément des mesures mésoscalaires effectuées par le service "Haute Atmosphère".

.../...

(1) G.D. Barbé : "La circulation atmosphérique à moyenne échelle (mesoscale) dans la basse et moyenne stratosphère", Technical Note N°95, WMO-N°227.TP.121, pp.272-284.

(2) Van Der Hoven : "Power spectrum of horizontal wind speed in the frequency range from 0.0007 to 900 cycles per hour", J. Meteo., 14, 160, 1957.

(3) G.D. Robinson : Adresse présidentielle du 19 avril 1967 (Quarterly Journal of the Royal Meteorological Society, Vol. 93, N°398, octobre 1967, pp. 409-418).

Par ailleurs, l'utilisation croissante de ballons haute performance permet d'apporter des précisions sur les phénomènes de la moyenne et haute stratosphère (couche 30-45/50 km) encore insuffisamment connus, tels que :

a) Périodes et modes d'établissement et de disparition de la mousson stratosphérique d'été (1), du secteur Est, respectivement 15 avril - 15 mai (début mars pour certaines années) et 15 août-15 septembre.

b) "Evènements à vents d'Est" et réchauffements explosifs qui leur sont liés en hiver et au printemps (1).

Ces derniers phénomènes, dont la liaison avec l'absorption ionosphérique a pu être mis en évidence, attirent l'attention sur le fait que l' "environnement" de la planète constitue un tout, ce qui est particulièrement vrai pour l'atmosphère dans ses différentes couches : ionosphère, mésosphère, stratosphère, troposphère, dont l'interaction ne saurait ainsi être mise en doute.

III - RESULTATS EXPERIMENTAUX OBTENUS.

Les premiers résultats obtenus avec le dispositif opérationnel en trois points confirment ceux déjà connus précédemment, tant par nos propres mesures en un ou deux points qu'à l'étranger, à savoir que les "accidents" (cisaillements du vecteur vent, soit en direction, soit en vitesse, soit pour les deux modules) sont suffisamment fréquents dans la circulation stratosphérique pour que le caractère quasi-périodique puisse y être considéré comme un mode fréquent des fluctuations du vecteur vent en fonction de l'altitude (structure feuilletée).

Il est permis d'avancer que, contrairement à ce qu'on aurait pu penser auparavant, la stratosphère considérée à l'échelle "mesoscale", c'est-à-dire à l'intérieur de couches élémentaires d'une épaisseur comprise entre 100 et 500 mètres (environ), est un milieu plus perturbé que la troposphère.

Compte tenu des intervalles de mesure qui n'ont pas jusqu'à présent été abaissés au-dessous de la demi-heure, la variabilité temporelle est nettement plus marquée que la variabilité spatiale dans le triangle opérationnel; en effet, il n'est pas rare que les "accidents" du vecteur vent soient pratiquement "coïncidents" (altitude, épaisseur et intensité) pour les trois stations à un moment donné alors que d'une heure à l'autre des déformations ou des déplacements de ces "accidents" selon la verticale peuvent être manifestes pour chacune des stations.

Il existe néanmoins des situations pour lesquelles il est possible de suivre facilement(2) le même "accident" pendant plusieurs heures. Mieux même, il semble que pour des périodes

.../...

(1) Des recherches de même nature sont poursuivies à la station météorologique des Kerguelen (hémisphère Sud) depuis janvier 1963 avec un radar COT/AL modifié.

(2) Il n'est pas toujours aisé d'identifier avec certitude un "accident" d'un sondage à l'autre en cas de variation d'altitude ou de dédoublement. A noter à ce sujet l'intérêt de l'ozone comme "traceur" de la circulation stratosphérique à des altitudes inférieures à 25/30 km. La structure feuilletée de sa distribution verticale, qui semble être stable - au moins dans certains cas - à l'échelle de la demi-journée dans ce domaine, est susceptible de faciliter le travail d'identification des "accidents" du vent. Des contacts sont en cours avec l'Institut Royal Météorologique de Belgique où M. FLANDRE effectue régulièrement depuis deux ans des sondages d'ozone à l'Observatoire d'UCCLE-Bruxelles.

allant jusqu'à 24 heures, il existe des secteurs d'altitudes privilégiées, ne variant guère de plus de 1 km, pour lesquelles une persistance d' "accident" se retrouve, non sans des interruptions et, le plus souvent, de forts changements d'intensité ou de forme (phases alternatives de croissance et de décroissance, maximum absolu ou relatif s'atténuant pour devenir minimum relatif ou absolu, etc...).

A titre indicatif, pour un degré de permanance d' "accident" sur plusieurs kilomètres selon la verticale à l'échelle de l'heure, les cisaillements observés peuvent être de l'ordre de 40% par rapport à la vitesse moyenne et de plusieurs dizaines de degrés par rapport à la direction moyenne.

Nous traiterons maintenant plus en détail deux remarquables exemples de cisaillements dans la stratosphère relevés à l'occasion de campagnes de mesures.

IV - CAS DU 11 au 12 MARS 1968.

Il s'agit d'une série de 25 sondages horaires de vent (sans température) effectuée à Magny-les-Hameaux entre 10 et 30/32 km d'altitude du 11 mars 1968 à 07.00 TU au 12 mars 1968 à 07.00 TU. Toutes les 3 heures, à partir de 07.00 TU, le sondage était double (1), c'est-à-dire que deux ballons étaient lancés à cinq minutes d'intervalle et poursuivis alternativement toutes les 30 secondes. Ce procédé permet d'obtenir deux sondages complets et indépendants effectués sur deux ballons séparés en altitude par une distance d'environ 1500 mètres. La pratique montre que les courbes représentatives (vitesse et direction du vent en fonction de l'altitude) correspondant aux deux sondages sont pratiquement superposées; c'est bien ce qui résulte de l'examen de la figure 1 pour le sondage double du 11 mars 1968 à 22.00/22.05 TU dont les résultats sont donnés à titre d'exemple. L'écart entre les courbes indique à la fois l'erreur - fortuite - de la mesure et la variation - en cinq minutes - de la grandeur mesurée.

L'ensemble des graphiques (vitesse et direction du vent, vitesse ascensionnelle) correspondant à cette campagne de mesures a déjà été reproduit dans la Technical Note N°95 de l'O.M.M. précitée (cf. figures 10 - 11 et ..., pp. 280-282) et de leur examen résulte la mise en évidence des caractéristiques communes suivantes :

- La structure de la stratosphère basse et moyenne présente de forts et réguliers cisaillements de la vitesse et de la direction du vent autour d'une valeur moyenne de variation progressive en fonction de l'altitude (de 2400 m/mn - 145 km/h - au niveau 10 km à 1000 m/mn - 60 km/h - au voisinage de 20 km, pour croître au-dessus, surtout à partir de 27/28 km jusqu'à 2600 m/mn - 155 km/h - au niveau 32 km pour la vitesse; de 340/360° - nord-nord-ouest/nord - au niveau 10 km à 270° - ouest - au niveau 30 km pour la direction). D'une manière générale, la variabilité des deux modules du vent (vitesse et direction) en fonction de l'altitude est plus accentuée et semble plus périodique pour les sondages de nuit (entre 18.00 et 03.00 TU.).

- Ces cisaillements présentent dans le temps un grand degré de permanence, de l'ordre de 12 heures et même plus si l'on tient compte de certains niveaux privilégiés tels que 19 km environ (extremums à caractère maximal) et 15 km environ (extremums à caractère minimal).

- On observe également ces cisaillements sur les composantes zonales et méridiennes du vent (voir figure 2 relative au sondage du 11 mars 1968 à 22.00 TU) avec le même degré de permanence de 12 heures et plus dans le temps.

- Les hodogrammes horaires du vent réel en fonction de l'altitude mettent en relief une rotation continue dans le sens rétrograde (sens des aiguilles d'une montre) d'un vent résiduel autour du vent moyen dont la direction varie lentement, comme indiqué ci-dessus, du nord à l'ouest. Une rotation de 360° du vent résiduel s'effectue dans des épaisseurs de couche de l'ordre de 2 à 3 km, ainsi que c'est le cas dans la figure 3 traitant le sondage du 11 mars 1968 à 22.00 TU.

Ce phénomène est particulièrement net dans les tranches d'atmosphère présentant des "accidents" définis par un nombre appréciable de niveaux de mesure. Alors que la cadence des mesures permet d'obtenir un point représentatif environ tous les 300 m., seuls les points les plus significatifs ont été reportés sur les figures 2 et 3.

.../...

(1) G.D. Barbé : Données sur le vent en altitude jusqu'à 30 km et au-delà (emploi d'un radar à poursuite automatique et du procédé du "sondage double"), Journal Scientifique de la Météorologie, N°38, avril-juin 1958.

Un tel feuilletage de l'atmosphère sur les paramètres du vent ne peut pratiquement pas être expliqué par la distribution verticale de la température. Afin de s'en rendre compte, il suffit d'admettre que, pour les sondages des 11 et 12 mars 1968 où la température n'a pas été mesurée, sa répartition verticale était conforme à celle de l'atmosphère standard type OACI.

En supposant une station X distante de Magny-les-Hameaux de 100 km dans une direction perpendiculaire au vent zonal, il est possible de calculer, pour une tranche d'altitude où $\frac{dv}{dz}$ peut être considéré comme constant, la température moyenne nécessaire au-dessus de la station X pour justifier ledit vent zonal dans l'hypothèse du vent thermique.

Le calcul du gradient théorique de la température moyenne d'une couche qui devrait exister entre les stations de Magny-les-Hameaux et X peut nous permettre, par l'analyse de son ordre de grandeur, de juger de la validité de l'hypothèse géostrophique nécessaire à l'emploi de l'équation classique du vent thermique :

$$\frac{\delta v}{\delta z} = \frac{1}{\omega \sin\varphi} \cdot \frac{g}{T} \cdot \frac{\delta T}{\delta x}$$

Pour le cas particulier du 11 mars 1968 à 22,00 TU, la séparation des différentes couches à $\frac{\delta v}{\delta z}$ constant est indiqué sur le graphique du vent zonal (figure 2). Numériquement, la formule se réduit à :

$$T_x - T_M = \Delta T = 1,22\, T_M \frac{\delta v}{\delta z}$$

avec :

T_M = Température moyenne de la couche à Magny-les-Hameaux

T_x = " d° " la station X

$\frac{\delta v}{\delta z}$ = gradient du vent zonal pour la couche considérée

La figure 4 indique les résultats obtenus, en supposant les températures en altitude conformes à l'atmosphère standard à Magny-les-Hameaux.

Il apparaît qu'au-dessus de la station X les écarts de température moyenne nécessaires pour justifier dans l'hypothèse géostrophique le vent observé varient de 1,8°C à environ 10°C pour des couches adjacentes. D'autre part, dans une même couche, des écarts de température entre Magny-les-Hameaux et la station X varient de 0,4°C à 7,4°C dans le cadre de cette hypothèse.

Or, tous les chiffres ainsi donnés correspondent à des températures <u>moyennes</u> de couche, ce qui infère des écarts plus importants pour des températures à un niveau donné. Leur ordre de grandeur est alors nettement supérieur à tout ce qui peut être observé habituellement; il est donc permis d'affirmer que les "accidents" de vent étudiés sont certainement de nature ageostrophique.

Les caractéristiques de ces résultats sont très proches de celles de J.S. SAWYER (1) et de A.I. WEINSTEIN, E.R. REITER et J.R. SCOGGINS (2). Pour ces derniers auteurs un tel schéma est analogue à celui qui serait provoqué par des ondes dites d'inertie ou de quasi-inertie : vecteur vent horizontal réel résultant de la superposition d'un vecteur vent moyen géostrophique et d'un vecteur vent résiduel rotatoire en fonction de l'altitude. D'autres auteurs (3) (4) (5) (6) font appel aux ondes de gravité (ou à des ondes similaires) et nos propres recherches sont orientées dans ce sens.

.../...

(1) J.S. SAWYER : Quasi-periodic wind variations with height in the lower stratosphere, Quarterly Journal of the Royal Meteorological Society, 1961, 87, 371, pp. 24-33.

(2) A.I. WEINSTEIN, E.R. REITER et J.R. SCOGGINS : Mesoscale structure of 11-20 km winds, Journal of Applied Meteorology, 1965, 5, p.49.

(3) C.O. HINES : Internal atmospheric gravity waves at ionospheric heights, Canadian Journal of Physics, 1960, 38, pp. 1441-1481.

(4) C.O. HINES : Atmospheric gravity waves : a new toy for the wave theorist, Journal of Geophysical Research, 1965, 69, 3, p.575.

(5) R.E. NEWELL, J.R. MAHONEY et R.W. LENHARD Jr : A pilot study of small-scale wind variations in the stratosphere and mesosphere, Quarterly Journal of the Royal Meteorological Society, 1966, 92, 391, pp. 41-54.

(6) B. LETTAU : An analysis of vertical scale structure and wind shear in the mesosphere from falling sphere data, Journal of Geophysical Research, 1966. 71, 4, pp. 1003-1010.

Une analyse plus complète de nos résultats, particulièrement des périodes de rotation, de leur variation en fonction de l'altitude et du temps ainsi que de leur liaison avec la valeur du gradient de vent moyen (cf. méthodes de l'analyse harmonique et des coefficients de corrélation) devrait permettre de caractériser avec plus de précision les phénomènes observés et d'en déduire les paramètres nécessaires à leur compréhension.

Il est certain que la répartition de l'énergie cinétique en altitude, telle qu'elle résulte de la figure 5 pour le cas du 11 mars 1968 à 22.00 TU, pose un problème puisqu'un remarquable accroissement de 100% peut être relevé à l'occasion de certains cisaillements de vitesse du vent.

V - CAS DU 21 au 22 NOVEMBRE 1968.

Il s'agit d'une campagne en trois points (Magny-les-Hameaux, Chartres, Pithiviers) comportant pour chacune des stations une série de 9 sondages tridimensionnels de vent et de température entre 09.30 TU le 21 novembre 1968 et 09.30 TU le 22 novembre 1968. Les mesures de vent et de température ont été effectuées toutes les 30 secondes, ce qui correspond à des couches élémentaires d'une épaisseur de 150 à 300 m.

Cette campagne a été effectuée avec la participation de l'avion CANBERRA du Meteorological Research Flight de Farnborough (Grande-Bretagne), spécialement équipé (centrale à inertie)(1) pour la mesure de paramètres météorologiques tels que le vent, la température, la turbulence, etc... L'avion a survolé le triangle de mesures selon une direction méridienne entre 38000 et 44000 pieds (11600 et 13400 m) de 11.30 à 13.30 TU le premier jour et entre 40000 et 45000 pieds (12200 et 13700 m) de 09.00 à 11.00 TU le second jour; lors de chaque opération, 4 allers et retours à altitude constante ont ainsi été exécutés, intéressant 8 niveaux distants d'environ 300 mètres selon la verticale.

Les résultats des mesures sont rapportés succinctement dans les figures suivantes :

1°) Figure 6 donnant la répartition verticale de la température et du vent (vitesse et direction) en chacun des trois points de mesure entre les niveaux 8 et 25 km le 21 novembre 1968 à 12.30 TU.

La courbe de la température de Chartres semble-vraisemblablement en raison d'une erreur systématique de mesure - décalée d'environ 300 m par rapport aux courbes représentatives de Magny-les-Hameaux et Pithiviers qui sont sensiblement confondues; par suite d'un blocage de radiosonde, le sondage de Pithiviers s'est arrêté à une altitude un peu supérieure à 14 km.

Par ailleurs, la température mesurée par l'avion CANBERRA entre 11.30 et 13.30 TU figure sous la forme d'une courbe en trait point qui est en excellent accord avec les précédentes entre 11500 et 13500 mètres. Enfin est reportée sur le graphique la répartition verticale de la température dans l'atmosphère OACI (courbe en trait plein).

La tropopause est extrêmement bien marquée à une altitude de l'ordre de 12500 m avec une température d'environ -72°C, remontant rapidement au-dessus (-65,5°C à 12800 m); après un stationnement relatif (-65,0 à -65,5°C) sur 1000 mètres d'épaisseur, on observe une nouvelle saute de température d'environ +4,5°C sur 300 m, d'où une température de -61,0° à 14100 m supérieure de 1°C à celle de la tropopause. A remarquer que, pour le sondage de Chartres du 21 novembre 1968 à 09.30 TU, la saute de température mesurée à la tropopause a été de près de 8°C (de -71,4°C à -63,8°C) sur moins de 300 mètres d'épaisseur.

La vitesse et la direction du vent présentent également un cisaillement marqué : défini par les mesures faites à la fois à l'aide des trois ballons (lancés simultanément des trois points) et à l'aide de l'avion CANBERRA (plateforme à inertie). C'est ainsi que la vitesse du vent varie de 12/14 m/s entre 11700 et 12000 m à 24 m/s, c'est-à-dire environ le double, vers 12650/12700 m, pour s'abaisser jusqu'à environ 8/10 m/s vers 13500 m. Simultanément la direction du vent passe de 270° (Ouest) vers 12500 m à 330° (Nord-Ouest 1/4 Nord) vers 13500 m pour revenir à 270° (Ouest) vers 14000 m.

.../...

(1) D.N. AIFORD : On the accuracy of wind measurements using an inertial platform in an aircraft, and an example of a measurement of the vertical mesostructure of the atmosphere (Journal of Applied Meteorology, août 1968, Vol.7, N° 4, pp. 645-666).

Ce remarquable "cisaillement" de vent et de température a été accompagné d'une légère turbulence en air limpide rencontrée par le CANBERRA tant à la montée qu'à la descente :

a) Dans une couche située entre 41000 et 41300 pieds (12493 - 12645 m), c'est-à-dire juste au-dessus de la tropopause et en coïncidence avec un "shear" de vent (variation détectée à la fois par les mesures radar aux trois points et les mesures faites à bord du CANBERRA) bien marqué sur la vitesse : accroissement de 15 à 24 m/s, soit 9 m/s, et sur la direction : rotation de 270° (Ouest) à 300° (Nord-ouest 1/4 ouest), soit 30°.

b) Dans une couche située entre 43100 et 43300 pieds (13133 - 13194 m), correspondant à la zone de température stationnaire au-dessus de la tropopause signalée ci-dessus tandis que le vent a amorcé en vitesse et va le faire en direction une variation inverse à la précédente.

2°) Figure 7 sous forme de tableau donnant la répartition verticale de la température entre les niveaux 10 et 25/26 km pour chacun des 9 sondages tri-horaires. La température reportée est celle mesurée par Magny-les-Hameaux, généralement peu différente de la température mesurée aux deux autres points.

Pour les sondages de 15,30 TU à 21,30 TU, la tropopause (-71°C/-69°C) reste nettement marquée, mais l'épaisseur de la couche de température minimale tend à s'accroître jusqu'à 300, puis 1000 m. Ensuite, son altitude tend à s'élever légèrement (12600 m) ainsi que sa température (-70,0°C puis -67,5°C), la couche de température minimale s'amincissant en fin de période.

Au-dessus, jusqu'au niveau 16000 m, les "accidents" de température semblent liés à l'évolution de la tropopause. C'est ainsi qu'aux sondages de 09,30 et 12,30 TU trois réchauffements sont notés vers 13000 m (-64/65°C), 14000 m (-62/63°C) et 15500 m (-62/63°C), séparés par deux zones de refroidissement vers 13500 m (-66/67°C) et 14700 m (-65/66°C). Aux sondages suivants, avec l'épaississement de la couche de transition, ces "accidents" de température s'atténuent et finissent même par disparaître presque totalement en fin de période.

De 16000 à 19000 m, la température reste stationnaire ou baisse progressivement (de -62° à -65°C).

Dans la couche de 19000 à 26000 m, la décroissance de température est nette, avec -69/70°C vers 25000m. A noter, aux sondages de 15,30 et 21,30 TU, la naissance d'"accidents" de température peu importants entre 19500 et 22000 m qui, d'ailleurs, s'atténuent puis disparaissent aux sondages suivants.

•

• •

J'exprime mes vifs remerciements à M. C.J.M. AANENSEN, chef du Meteorological Research Flight (Grande-Bretagne), qui a bien voulu participer si obligeamment à nos campagnes de mesures de novembre et décembre 1968 et nous autoriser à faire état des données d'observations obtenues à partir du CANBERRA.

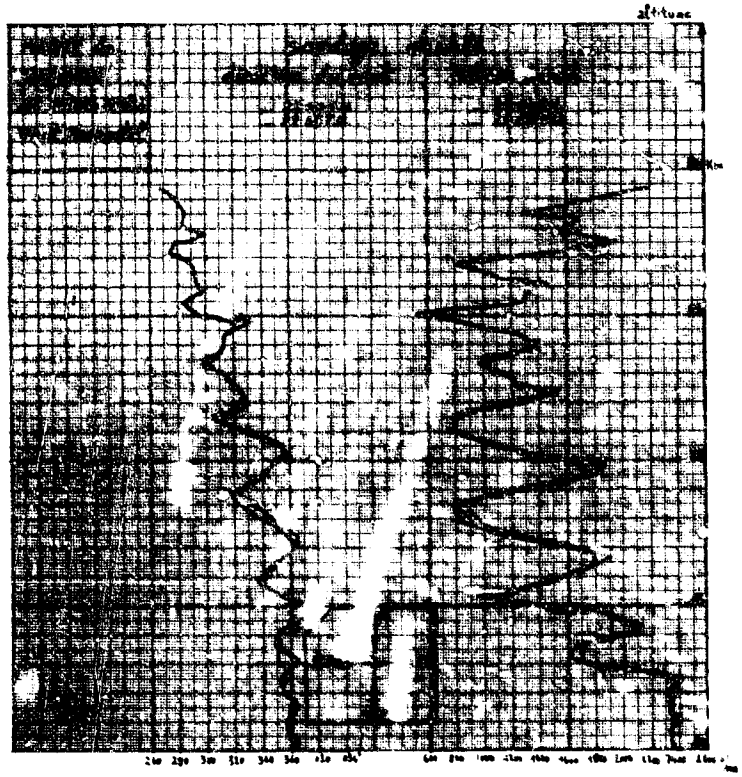

Figure 1 - Sondage double de vent à Magny-les-Hameaux le 11 mars 1968 à 22.00/22.05 TU. Direction (en degrés) et vitesse (en m/mn) en fonction de l'altitude.

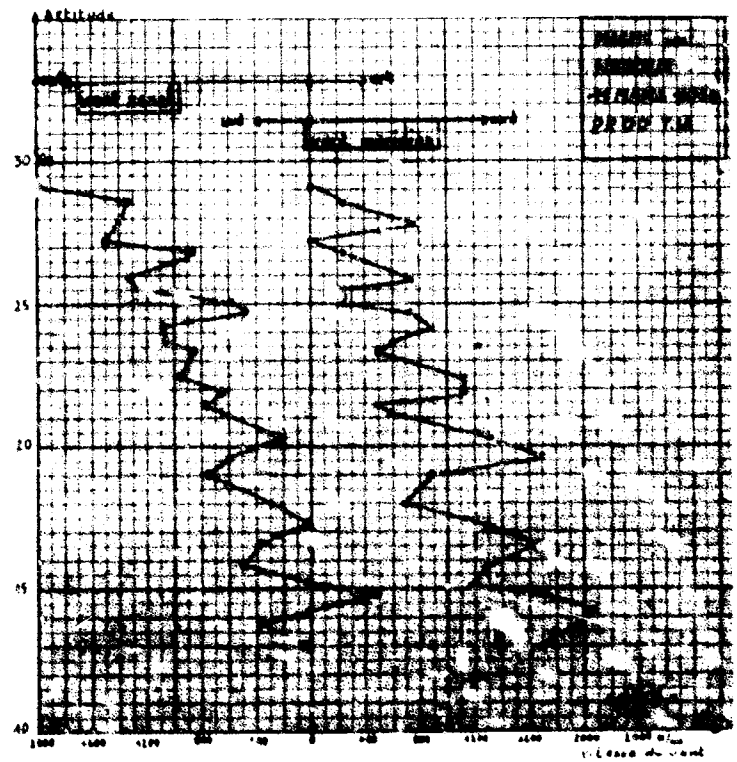

Figure 2 - Sondage de vent à Magny-les-Hameaux le 11 mars 1968 à 22.00 TU. Composantes zonales (en m/mn) et méridiennes (en m/mn) en fonction de l'altitude.

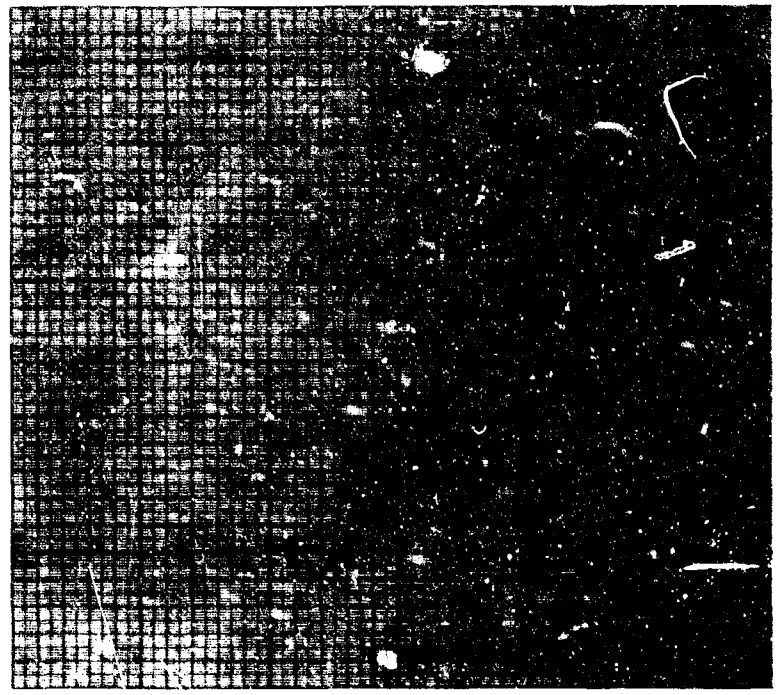

Figure 3 - Sondage de vent à Magny-les-Hameaux le 11 mars 1968 à 22.00 TU. Hodogramme du vent réel en fonction de l'altitude.

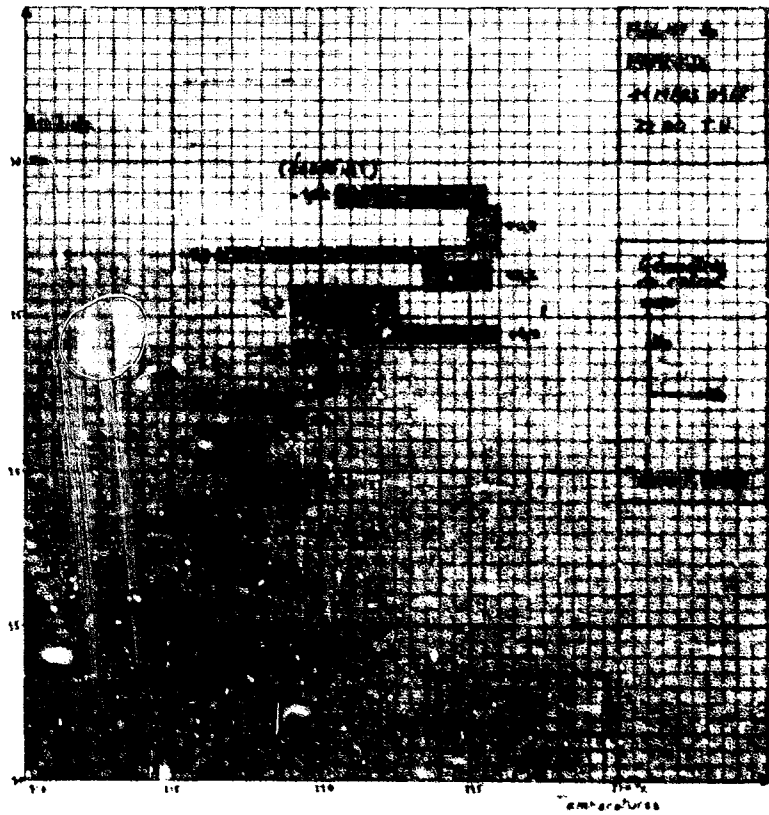

Figure 4 - Sondage de vent à Magny-les-Hameaux le 11 mars 1968 à 22.00 TU - Température (Tx) en altitude (par tranches) à 100 kilomètres de Magny-les-Hameaux dans une direction perpendiculaire au vent zonal en supposant l'hypothèse géostrophique et une température standard OACI (T_M) à Magny-les-Hameaux.

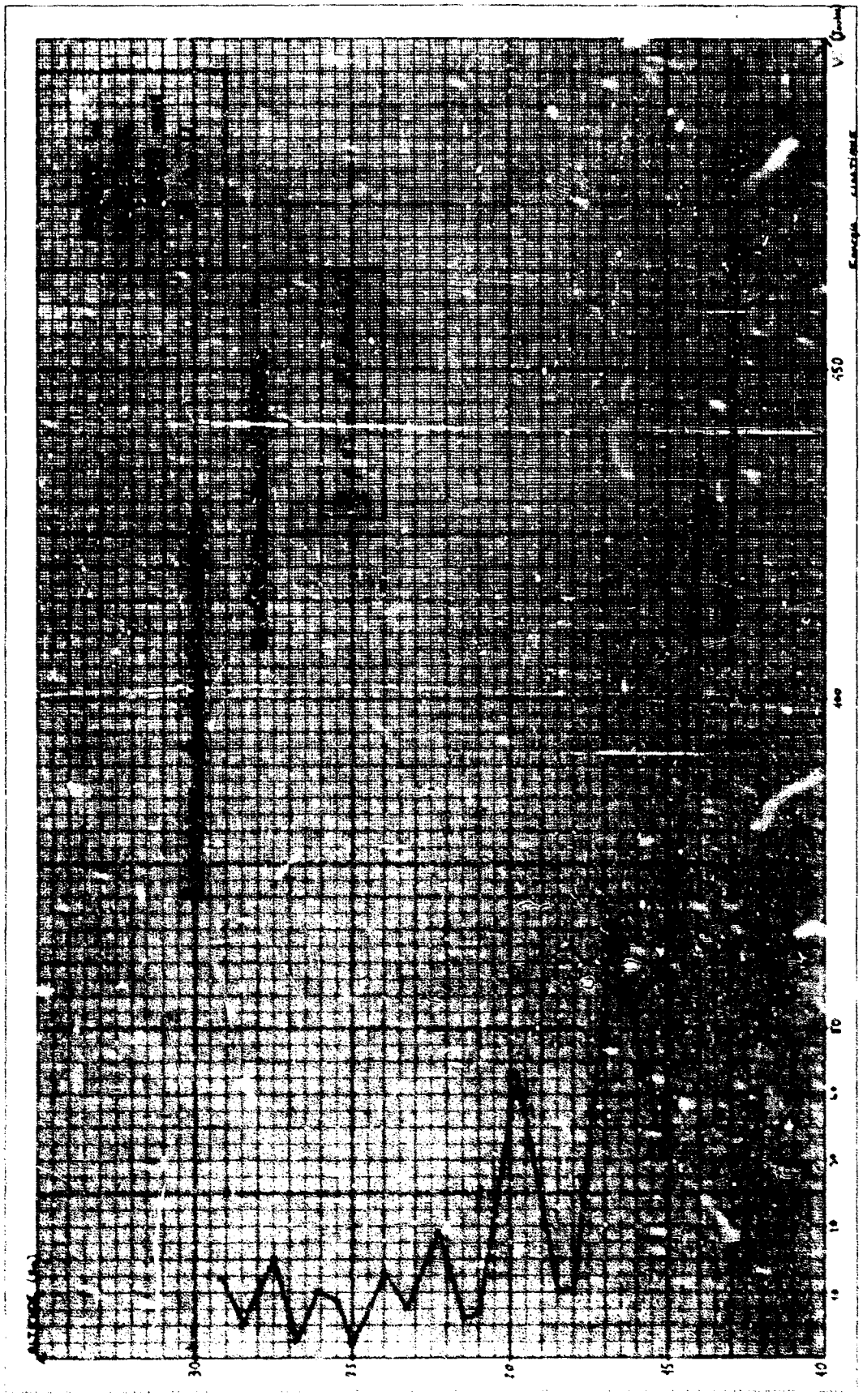

Figure 5 - Sondage de vent à Magny-les-Hameaux le 11 mars 1968 à 22.00 TU.
Répartition de l'énergie cinétique (en joules) en fonction de l'altitude.

Figure 1 - Sondage de vent et température en trois points le 21 novembre 1968 à 12.30 TU.

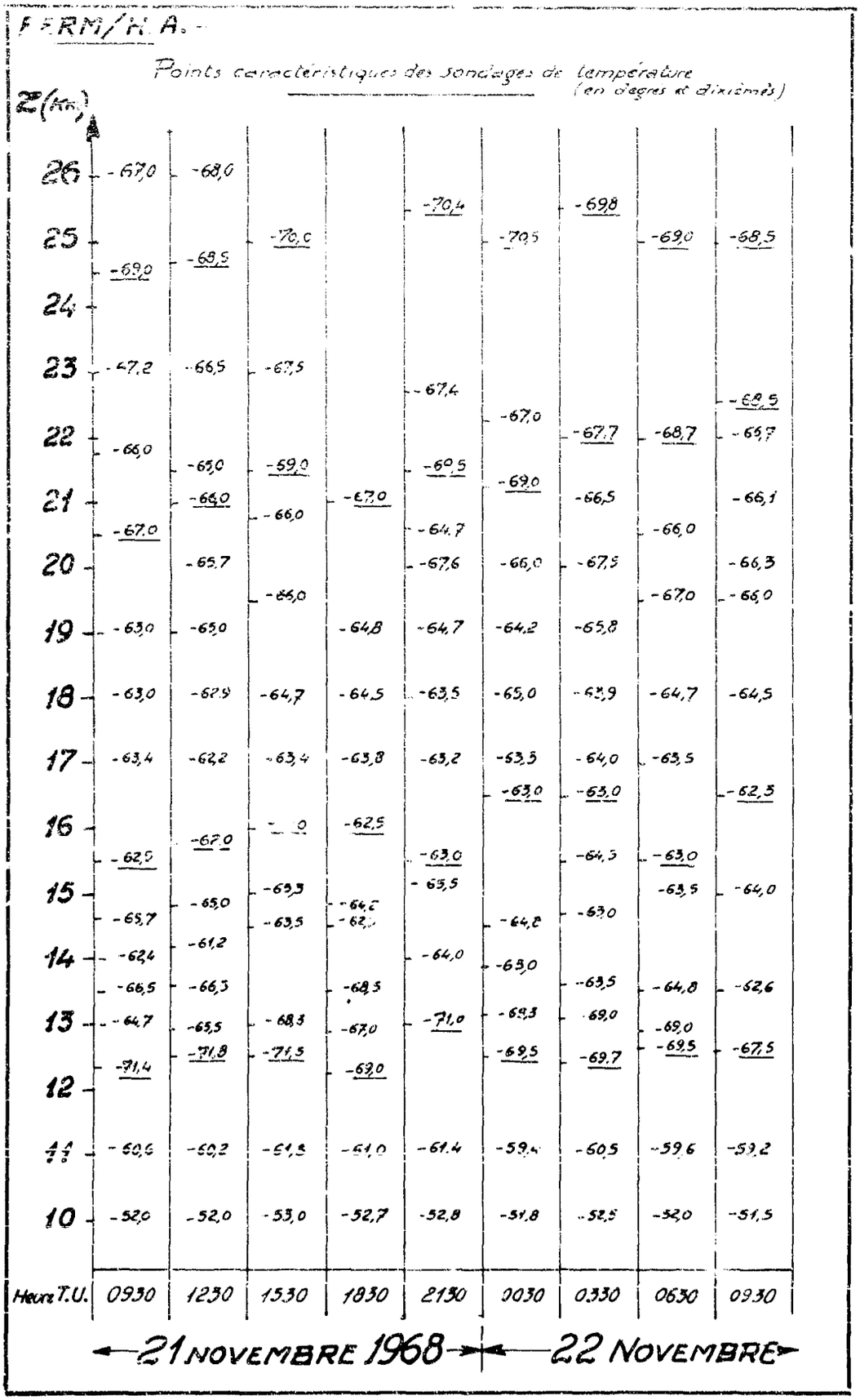

Figure 7 - Tableau donnant les points caractéristiques des sondages tri-horaires de température à Magny-les-Hameaux du 21 novembre 1968 à 09.30 TU au 22 novembre 1968 à 09.30 TU.

"TURBULENCE STRUCTURE IN THE ATMOSPHERIC BOUNDARY LAYER OVER THE OPEN OCEAN"*

by

Carl H. Gibson† and R. Bruce Williams‡

Department of Aerospace and Mechanical Engineering Sciences
and
Scripps Institution of Oceanography
University of California, San Diego
La Jolla, California 92037 U.S.A.

*This research was supported jointly by the Office of Naval Research under Contract NONR 2216(23) and Project THEMIS which is sponsored by the Air Force Office of Scientific Research, Office of Aerospace Research, United States Air Force, under Contract F 44620-68-C-0010.

†Assistant Professor

‡Graduate Student

SUMMARY

Measurements of turbulence statistics at various heights above mean sea level are described. Digital data acquisition and processing techniques were used to analyze signals from a linearized constant temperature anemometer. Mean viscous dissipation rates measured from the velocity derivative were found to be inversely proportional to the height as expected for a constant stress, neutrally stratified boundary layer. Streamwise velocity spectra exhibit extensive inertial subranges, even at scales larger than the height. Probability distribution functions for the velocity differences between points separated by 1 cm are compared with lognormal predictions of Kolmogoroff and Yaglom.

INTRODUCTION

In this paper some hot wire measurements of turbulence a few meters above the surface of the open ocean are described. Such measurements are of interest for several reasons. Many elementary propositions of turbulence theory have been difficult to compare with experiment simply because high Reynolds number flows are difficult to generate and measure in the laboratory and because the requirements of power, weight and protection for the instrumentation required for the measurements can hardly be supplied anywhere else. Consequently it was over twenty years before Kolmogoroff's second similarity hypothesis[1] was conclusively tested by Grant, Stewart and Moilliet[2] by measurements of turbulence in a tidal channel at Reynolds numbers of order 10^8. A number of hot wire measurements in the wind over the bay near Vancouver have been reported[3-4] but few if any similar measurements have been made over the open ocean despite the fact that a large fraction of the earth's surface is covered by open ocean and important turbulent transport processes occur in the turbulent boundary layer in the air near this surface. Therefore one purpose of the present experiment was to explore some aspects of the turbulence structure in this little known but important boundary layer, and to develop techniques and procedures for later studies.

An elementary result of the theory of high Reynolds number, constant stress turbulent boundary layers which is very difficult to test in the laboratory is the prediction that the viscous dissipation rate ϵ should be inversely proportional to the distance from the surface. Klebanoff[7] found it was necessary to measure various derivatives of velocity components to accurately determine ϵ, since local isotropy was not obtainable at his laboratory Reynolds numbers. Bradshaw[8] determined ϵ by difference in his energy balance, and remarks that it is a difficult and inaccurate quantity to measure. The effective Reynolds number for the present study is several orders of magnitude larger than the largest possible for boundary layers measurable in a laboratory. Based on mean velocity and height above mean sea level the Reynolds number Uy/ν for the present study varied from 2×10^5 to 7×10^6.

An important property of high Reynolds number turbulence is the tendency for the small scale structure to become quite variable, or "intermittent". The extreme variability of the local dissipation rate at high Reynolds number induced Kolmogoroff to refine[9] his previous[1] universal similarity hypotheses based on the mean dissipation $\langle\epsilon\rangle$. Kolmogoroff assumed that the local dissipation should be a log-normal random variable. Yaglom[10] has provided some physical basis for this assumption by showing that at high Reynolds number the local dissipation can be written as the product of a large number of independent identically distributed random variables using an assumption much like the usual cascade hypothesis. Thus, by applying the central limit theorem, the logarithm of the local dissipation should be Gaussian.

EXPERIMENTAL ARRANGEMENT

The crucial requirement of a stable instrument platform was satisfied by the Scripps Institution of Oceanography Floating Instrument Platform (FLIP) shown in Figure 1. In the vertical mode FLIP typically has horizontal motions of less than five feet and has had measured vertical displacements of only three inches in 36-foot waves. She is equipped with sufficient laboratory space for several instrument racks, and ample regulated power is available.

The experiments described in this paper were carried out on FLIP about 50 miles off the Mexican coast with the wind from the west over the open Pacific ocean. Wind velocities in the streamwise direction was measured using a Thermosystems linear constant temperature anemometer circuit. A platinum hot wire two mm long and 7.62 micron in diameter was used, as well as a tungsten wire 1 mm long and 3.8 microns in diameter.

The probes were mounted on a fin stabilized "fish" suspended by cable from the end of the 37 foot port boom as shown in Figure 2. Pendulum motions were prevented by tag lines attached to the cable above the fish. The probe was positioned in the boundary layer by pulling up the support cable on a winch.

The cable connecting the hot wire in the anemometer bridge was 200 feet long, and consequently it was necessary to modify the anemometer bridge circuit to achieve stable operation. Some loss of frequency response was observed above about 2,000 hz, but this is adequate for the present measurements.

The local viscous dissipation rate per unit mass ϵ is given by

$$\epsilon = 2\nu e_{ij} e_{ij} \tag{1}$$

where ν is the kinematic viscosity of the fluid and e_{ij} is the rate of strain tensor $1/2(\partial u_i/\partial x_j + \partial u_j/\partial x_i)$. Summation over repeated indices is assumed. For locally isotropic turbulence the mean dissipation rate $\langle\epsilon\rangle$ may be measured from the mean square streamwise gradient of the streamwise velocity $\partial u_1/\partial x_1$

$$\langle\epsilon\rangle = 15\nu \left(\partial u_1/\partial x_1\right)^2 \tag{2}$$

Since the output voltage e of a linearized hot wire anemometer circuit is

$$e = A u_1 \tag{3}$$

and since

$$\frac{1}{e}\frac{de}{dt} = \frac{d(Au_1)}{Au_1 dt} = \frac{du_1}{dx_1} \tag{4}$$

it is clear that $\langle \epsilon \rangle$ may be measured without knowing the calibration constant A in (3) since, from (3), (4) and (2)

$$\langle \epsilon \rangle = 15\nu \left\langle \left(\frac{1}{e}\frac{de}{dt}\right)^2 \right\rangle \cong \frac{15\nu}{\langle e \rangle^2} \left\langle \left(\frac{de}{dt}\right)^2 \right\rangle \tag{5}$$

The approximation that $\langle ((de/dt)/e)^2 \rangle$ is $\langle (de/dt)^2 \rangle / \langle e \rangle^2$ is valid if the voltage and its derivative are independent or if e is nearly constant. These restrictions were satisfied to a sufficient degree for the present experiments.

RESULTS

Figure 3 shows the calibration curve for the linearized hot wire anemometer measured in the Aerospace and Mechanical Engineering Sciences Department wind tunnel after the operation at sea using the same circuit and cables. Clearly the response is linear within experimental error. The zero point was tested immediately before and after each of the measurements at sea and no measurable shift was observed.

Figure 4 shows a log-log plot of ϵ (hereafter, average brackets on ϵ are assumed) estimated using the approximate form of equation (4). The linearized anemometer output was recorded on a strip chart and the mean value $\langle e \rangle$ determined directly from the trace. The mean square derivative $\langle (de/dt)^2 \rangle$ was estimated from a simultaneous strip chart recording of the Hewlett Packard 3400A RMS Voltmeter DC average output with twenty second time constant. The input derivative signal was obtained by preamplifying the anemometer output, band pass filtering from 0.2 to 2,000 hz, and differentiating this signal using Tektronix O-unit operational amplifiers and a Krohn-Hite 330-A filter.

During the measurements the mean velocity at 10 meters was about 720 cm/sec measured using the anemometer calibration curve of Figure 3. It might be noted that this velocity is about 30 per cent lower than the value indicated by the ship's cup anemometer. As shown in Figure 1, FLIP's anemometer is close to the ship's hull where the flow might be accelerated by this amount, and this is assumed to have been the case.

The heights above mean sea level are accurate to about ± 1 foot in Figure 3. Vertical motions at the end of the boom were approximately ± 6 inches.

Wave heights during the test were about 2 meters peak-to-peak so that the 1 meter point on Fig. 4 was actually below the crests of the higher waves. Shortly after the probe was moved up to the 2 meter position a wave immersed the bottom of the fish, narrowly missing the probe. The point at 14.2 meters was obtained by mounting the probe on the radio antenna extending from the upper deck.

The data in Fig. 4 is compared with a line of slope minus one which might be expected for a constant stress turbulent boundary layer. Assuming that energy flux is lost only by viscous dissipation using u_*/Ky for the mean velocity gradient leads to the result[11]

$$\epsilon = u_*^3/Ky \tag{6}$$

where u_* is the friction velocity $(\sigma/\rho)^{1/2}$, σ is the stress, ρ is the density, K is Von Karman's constant 0.41 and y is the distance from the boundary. Close to the surface but far from the viscous sublayer a high Reynolds number equilibrium turbulent boundary layer should have constant stress, so ϵ should be inversely proportional to y as given by (5). Hence, by measuring ϵ and y given K and ρ, it should be possible to determine the stress σ using (5) and the definition of u_*.

Figure 5 shows the data of Fig. 4 plotted as $1/\epsilon$ versus y, in order to determine a virtual origin y_o for the expression

$$1/\epsilon = \frac{K}{u_*^3}(y - y_o) \tag{7}$$

In this way u_* was found to be 19.6 cm/sec, corresponding to a stress of 0.47 dyne/cm^2 and a drag coefficient $C_{10} \equiv (u_*/U_{10})^2$ of 7.5×10^{-4}. The virtual origin y_o was 1/2 ± 1/2 meter, much smaller than the height of the waves. U_{10} is the mean velocity at 10 meters.

The indicated drag coefficient is rather low compared to most recent measurements[12] which give values about twice as large based on profile measurements or direct measurements of stress. It is not clear at this time why the dissipation technique should give a lower value for C_{10} than the conventional methods, and further work is in progress to answer this question. It is conceivable

that the low C_{10} value occurred because the boundary layer was stable since the air and water temperatures were not measured at the time of the measurements. However, since measurements on previous days indicated air temperatures slightly cooler than the water, and since the measurements were made in the afternoon of a windy, sunny day, it seems probable that the boundary layer was neutral or slightly unstable.

Figures 6a, b, and c show streamwise velocity spectra measured at heights of 1, 2, and 7 meters above the mean sea level. Velocity signals were recorded on a magnetic tape as 12 bit samples at 350 samples/sec. Spectra were computed using the fast Fourier transforms of 2048 sample records averaged over 20 records for each position. The spectra are compared with the -5/3 slope expected from Kolmogoroff's second similarity hypothesis. An interesting feature of the spectra is a slight but significant dip which appears for heights of 1 and 2 meters at wavenumber $k = 2\pi/y$, or wavelength $\lambda = y$. For the spectrum at 7 meters the dip, if any, is less distinct. Pond[4] mentions a similar distortion in his spectra measured in the wind over waves in a bay.

Data used to calculate the spectra of Fig. 6 were also used to calculate the statistics of the velocity difference for small separation shown in Fig. 7. Since the mean velocity for each set of data was approximately 350 cm/sec and the turbulent intensity (standard deviation) was only 4 to 5 % the samples in time correspond to samples separated in space by a distance of about one centimeter. Since the spectra of Fig. 6 show viscous cut-off, it is also clear that this separation is smaller than the viscous scale so that velocity differences between successive samples approximate values of the velocity derivative du_1/dx_1.

Figure 7 shows the calculation of the probability distribution functions for the logarithm of the velocity difference squared for the data at the three elevations. The probability coordinate has been stretched in such a way that Gaussian distribution functions lie on straight lines so that the data can be compared with the log-normal distribution predicted by Kolmogoroff[9] and Yaglom[10] for turbulence at very high Reynolds number. Also shown in Figure 7 are kurtosis and skewness values for the velocity difference Δu. Kurtosis is defined as the fourth moment about the mean of a random variable divided by the square of the second moment, and skewness is defined as the third moment divided by the 3/2 power of the second.

It is clear from the plot that all the measured distribution functions can be fitted adequately by straight lines over the range of probabilities from 50 to 99.9%, corresponding to log-normal behavior. Reynolds numbers based on mean velocity and height above mean sea level ranged from 2×10^5 to 2×10^6. Values of kurtosis were about 20, which is very large compared to 3 corresponding to a Gaussian distribution and illustrates the phenomenon of small scale intermittency for high Reynolds number turbulence. Using a method suggested by Batchelor,[7] a kurtosis value of 21 corresponds to a Gaussian derivative concentrated in only 15 per cent of the fluid volume. It is interesting to note that the measured values of kurtosis do not show a tendency to increase with height, and hence Reynolds number, as expected if Reynolds number is the only factor determining intermittency. The implication is that it is not. Skewness factors were very large and negative, consistent with previous evidence that turbulent fluid elements tend to be stretched into sheets, but inconsistent with a great number of measurements which give about -0.4 for this quantity at lower Reynolds numbers. Skewness values are notoriously difficult to measure accurately, and it may be that 4×10^4 samples are inadequate for convergence. The fact that three sets of samples this size gave consistent magnitudes and trends for both kurtosis and skewness does seem to suggest approximate convergence, however. Because the velocity differences were usually only a few bits in magnitude in spite of the large dynamic range provided by 12 bit velocity samples, it is possible that a systematic round-off error could affect the moment calculations. Examination of the individual distributions did not indicate that the deviation of the skewness factors from -0.4 could be accounted for in this way, however.

ACKNOWLEDGMENTS

The authors would like to gratefully acknowledge the assistance of several people in the course of this work; in particular, Richard Ackermann, and Robert Renner who can find faulty transistors at sea, Russ Davis, Ian Hirschsohn, Gilbert Stegen and the crew of FLIP.

REFERENCES

1. Kolmogoroff, A. N., Compt. Rend. Acad. Sci. U. R. S. S. 30, 301 (1941) [Sov. Phys. Usp. 10, 734 (1968)].
2. Grant, H. L., R. W. Stewart and A. Moilliet, J. Fluid Mech. 12, 241 (1962).
3. Pond, S., S. D. Smith, P. F. Hamblin and R. W. Burling, J. Atm. Sci. 23, 376-386 (1966).
4. Pond, S., R. W. Stewart and R. W. Burling, J. Atm. Sci. 20, 319-324 (1963).
5. Weiller, H. S. and R. W. Burling, J. Atm. Sci. 24, 653-664 (1967).
6. Pond, S. and R. W. Stewart, Izv. Akad. Nauk SSSR, Phys. Ocean Atmos. 1, 914-919 (1965).
7. Klebanoff, P. S., NACA TN 3178 (1955).
8. Bradshaw, P., J. Fluid Mech. 29, 625-645 (1967).
9. Kolmogoroff, A. N., J. Fluid Mech. 13, 1, 82 (1962).
10. Yaglom, A. M., Soviet Physics - Doklady 11, 1, 26 (1966).
11. Landau, L. D. and E. M. Lifshitz, Fluid Mechanics, Pergamon Press, Addison-Wesley (1959) p. 163.
12. Paulson, C. A., Ph. D. Thesis, Department of Atmospheric Sciences, University of Washington, Seattle (1967).
13. Batchelor, G. K., Homogeneous Turbulence, Cambridge University Press (1953), p. 184.

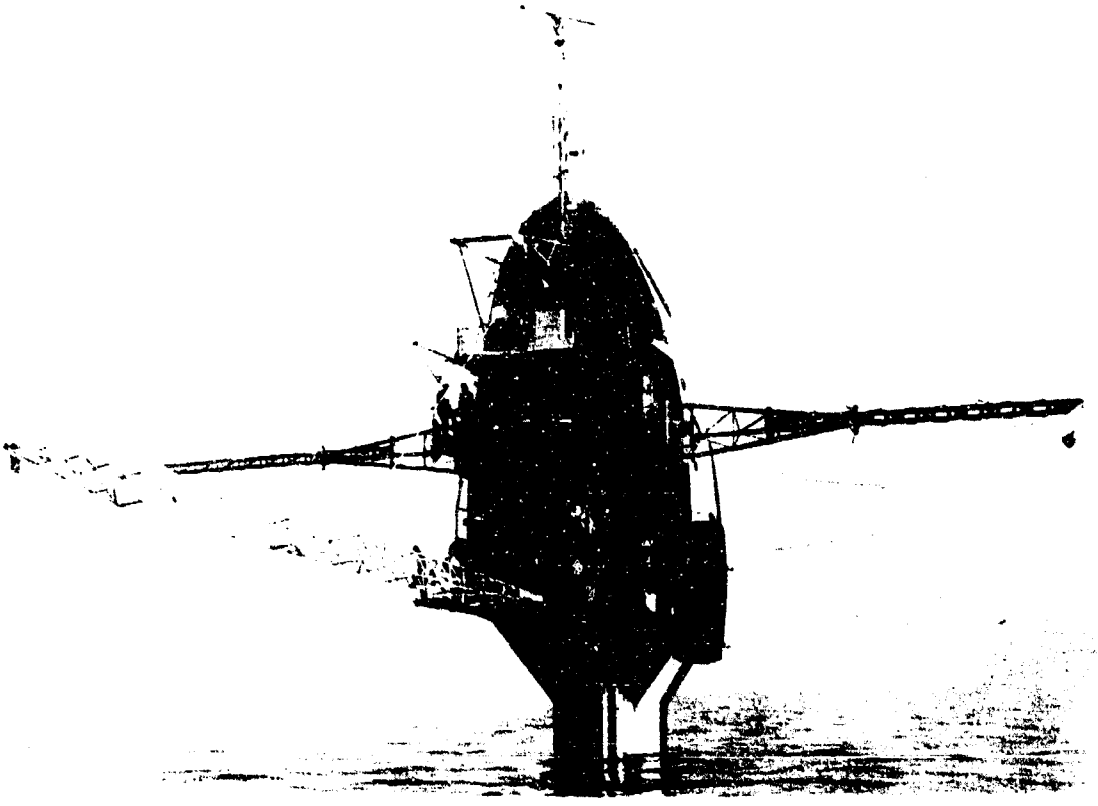

Figure 1 Scripps Institution of Oceanography Floating Instrument Platform - FLIP

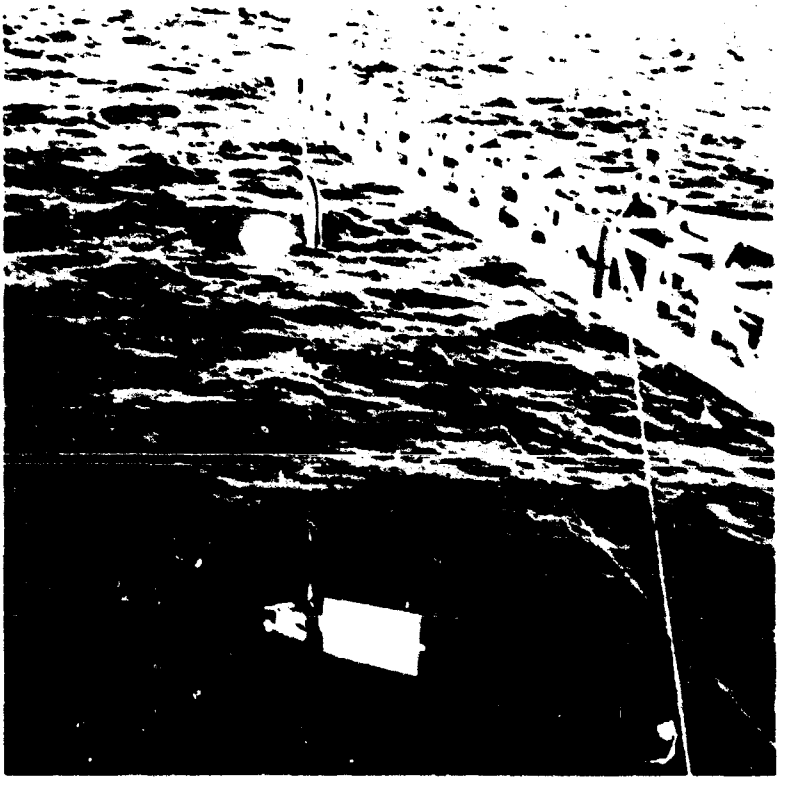

Figure 2 Hot wire probe mounted on "fish" suspended from boom. Tag lines below prevent pendulum motion.

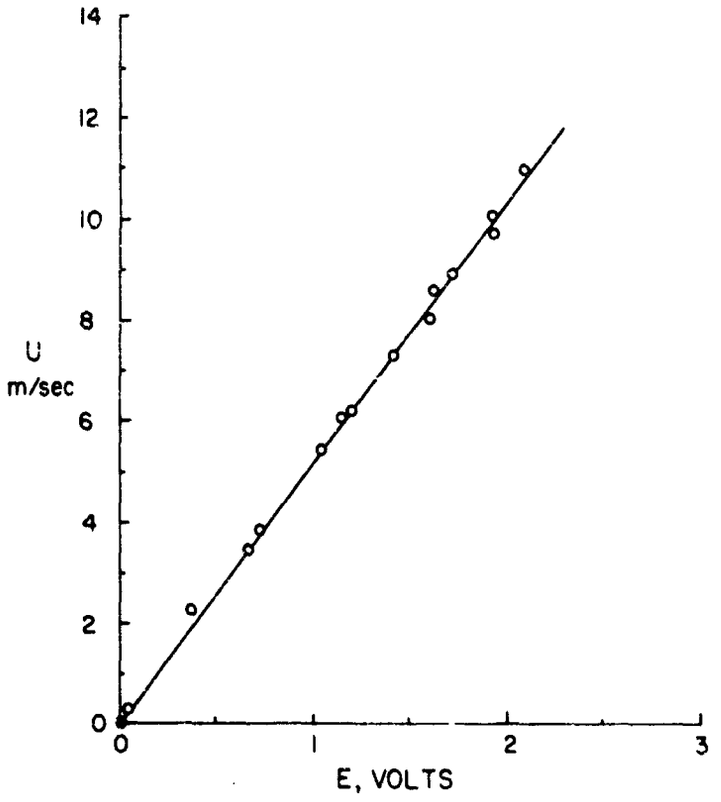

Figure 3 Calibration curve for linearized hot wire anemometer measured after sea tests.

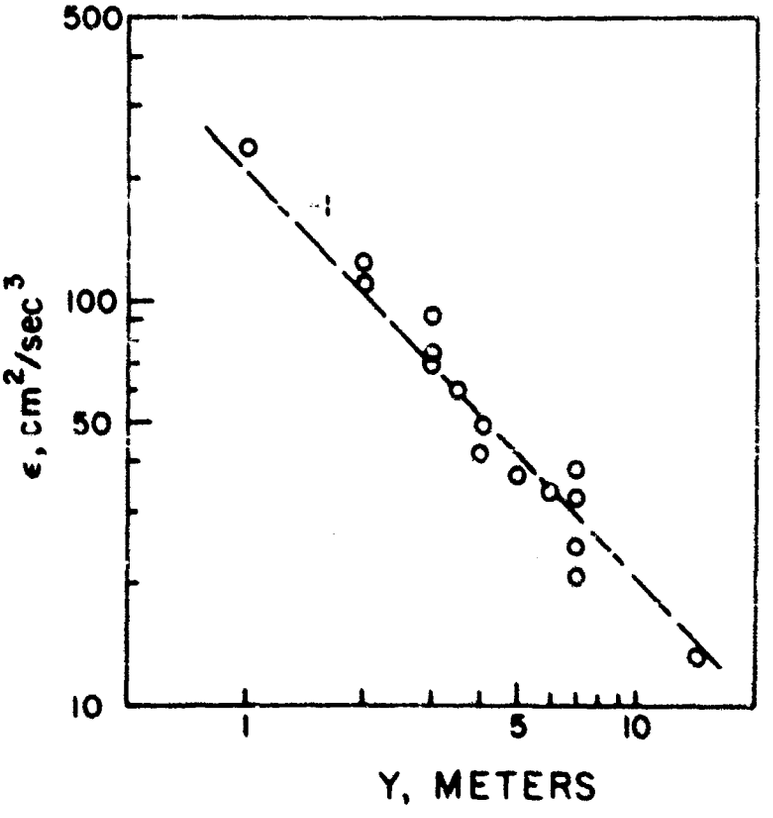

Figure 4 Viscous dissipation rate versus height above mean sea level.

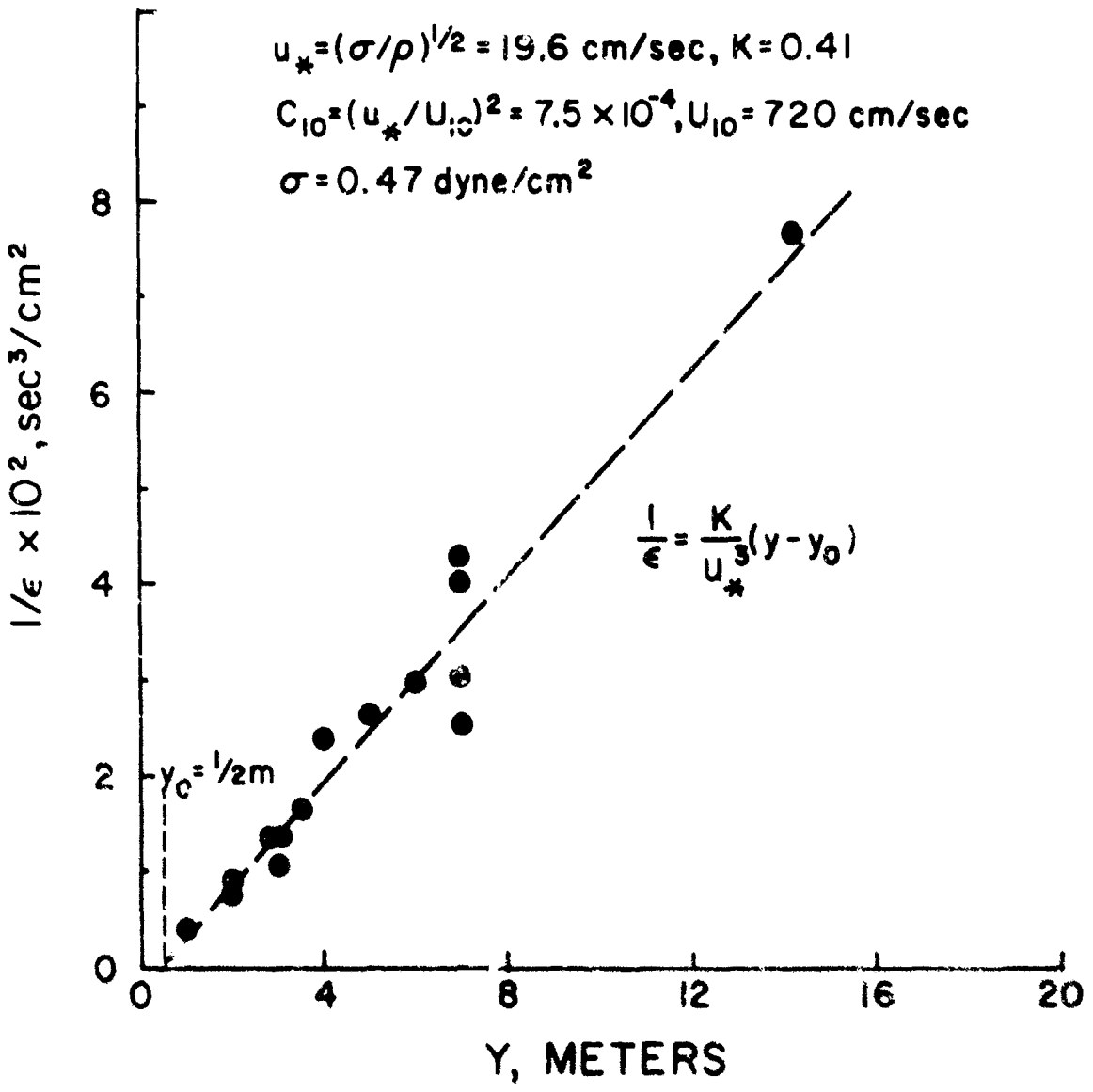

Figure 5 Calculation of y_o, u_*, σ, C_{10}

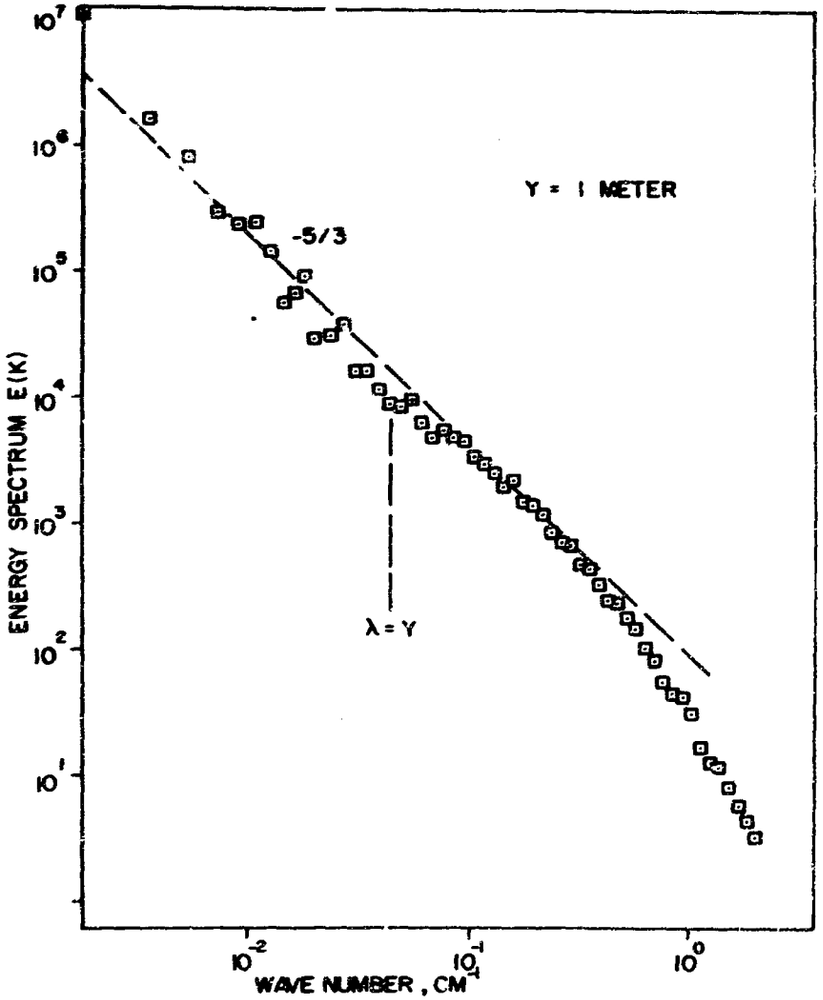

Figure 6a Velocity spectrum at 1 meter.

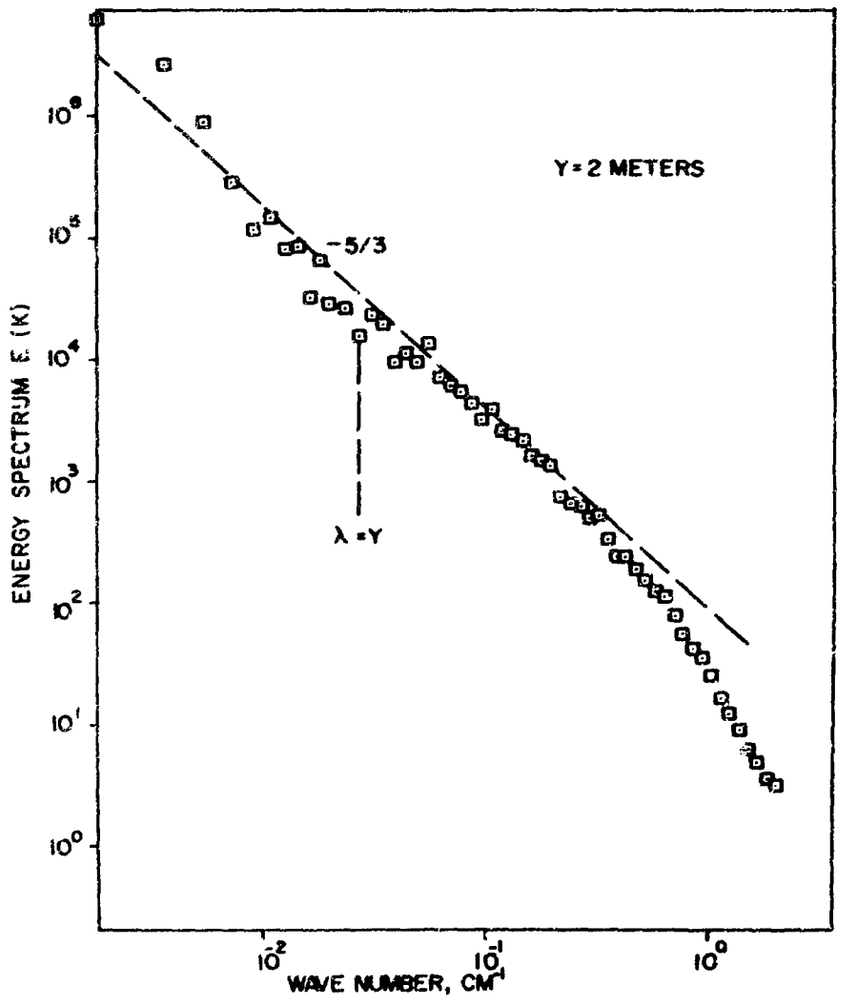

Figure 6b Velocity spectrum at 2 meters.

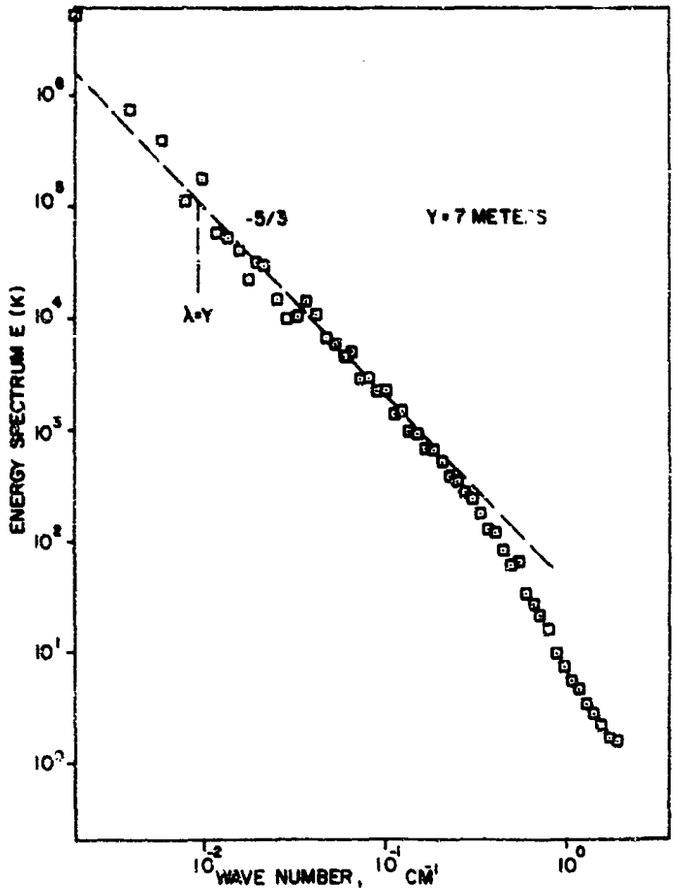

Figure 6c Velocity spectrum at 7 meters.

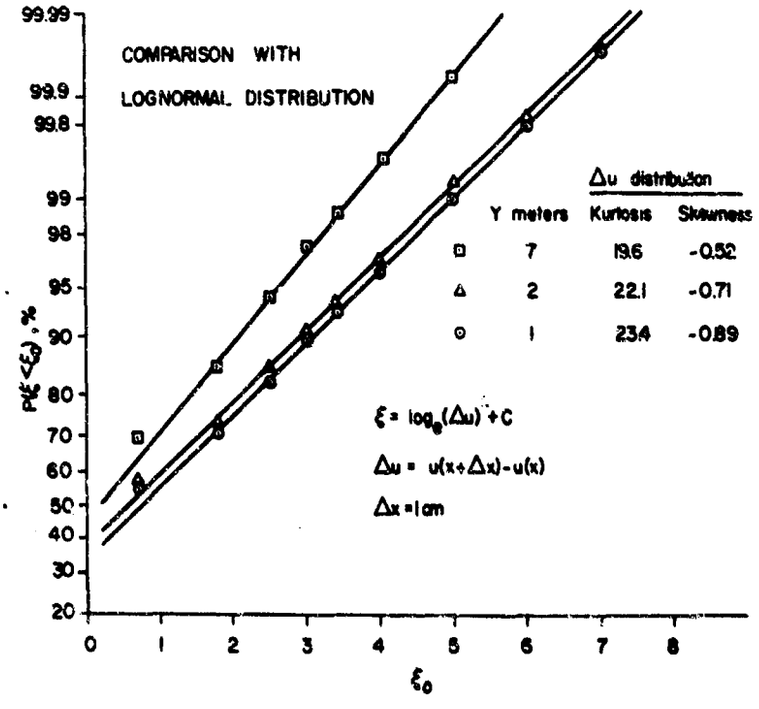

Figure 7 Distribution functions for velocity differences.

LONGITUDINAL AND LATERAL SPECTRA OF TURBULENCE IN THE ATMOSPHERIC BOUNDARY LAYER

by

George H. Fichtl*
Aerospace Environment Division, Aero-Astrodynamics Laboratory
NASA - George C. Marshall Space Flight Center
Marshall Space Flight Center, Alabama

and

George E. McVehil**
Cornell Aeronautical Laboratory, Inc.
Buffalo, New York

*Scientific Assistant.

**Head, Dynamic Meteorology Section.

SUMMARY

An engineering spectral model of turbulence is developed with horizontal wind observations obtained at the NASA 150-meter meteorological tower at Cape Kennedy, Florida. Spectra, measured at six levels, are collapsed at each level with $(nS(n)/u_{*o}^2, f)$-coordinates, where $S(n)$ is the longitudinal or lateral spectral energy density at frequency n(Hz), u_{*o} is the surface friction velocity, and f equals $nz/\bar{u}$, $\bar{u}$ being the mean wind speed at height z. A vertical collapse of the dimensionless spectra is produced by assuming they are shape invariant in the vertical.

An analysis of the logarithmic spectrum in the inertial subrange, at the 18-meter level, implies that the local mechanical and buoyant production rates of turbulent kinetic energy are balanced by the local dissipation and energy flux divergence, respectively.

I. INTRODUCTION

To determine the response of space vehicles, aircraft, tall structures, etc., to atmospheric turbulence, the engineer requires specific information about the spectral nature of atmospheric turbulence because the equations of motion of these vehicles or structures are linear and are solved with Fourier transform techniques. Thus, the environmental forcing functions must be represented in terms of spectra. Motivated by this requirement, we have developed a model for the longitudinal and horizontal lateral spectra of turbulence for the Kennedy Space Center area. The longitudinal and lateral components of turbulence are the wind fluctuations parallel and normal to the mean wind vector (see Figure 1).

II. THE NASA 150-METER METEOROLOGICAL TOWER

To obtain micrometeorological data representative of the Cape Kennedy area, especially in the vicinity of the Apollo/Saturn V launch pads, a 150-meter meteorological tower was constructed on Merritt Island at KSC. The tower facility, discussed in detail in a report by Kaufman and Keene [1], is only briefly described here.

Terrain Features

Figure 2 shows the location of the facility with respect to the Saturn V space vehicle launch complex 39. Located about three miles from the Atlantic Ocean, the tower is situated in a well-exposed area free of near-by structures which could interfere with the air flow.

The aerial photograph (Figure 3) of the terrain surrounding the tower (point T) was taken at 3500 feet above mean sea level. In the quadrant from approximately 300 degrees north azimuth with respect to the tower, clockwise around to 90 degrees, the terrain is homogeneous and is covered with vegetation about one-half to one and one-half meters high. Another homogeneous fetch with the same type of vegetation occurs in the 135- to 160-degree quadrant. The areas A (230-300 degrees), B (90-135 degrees), and C (160-180 degrees) are covered with trees from about 10 to 15 meters tall. The fetch from the tower to areas A or C is about 200 meters, and the fetch to area B is about 450 meters. The height of the vegetation over these fetches ranges from one-half to one and one-half meters, as in the area to the north of the tower. To the south-southwest in the 180- to 230-degree quadrant 225 meters from the tower, there is a body of water called Happy Creek.

Instrumentation

The complete tower facility comprises two towers, one 18 meters and the other 150 meters high (see Figure 4). The levels on both towers are instrumented with Climet (Model C1-14) wind sensors. Temperature sensors, Climet (Model -016) aspirated thermocouples, are located at the 3- and 18-meter levels on the small tower and at the 30-, 60-, 120-, and 150-meter levels on the large tower. Foxboro (Model F-2711AG) dewpoint temperature sensors are located at the 60- and 150-meter levels on the large tower and at the 3-meter level on the 18-meter tower. Wind speed and direction data can be recorded on both paper strip charts and analog magnetic tapes with an Ampex FR-1200 fourteen-channel magnetic tape recorder which uses a 14-inch reel. The temperature and dewpoint data are recorded on paper strip charts. To avoid tower interference of the flow, the large tower is instrumented with two banks of wind sensors. The details of how and when one switches from one bank of instrumentation to the other bank is discussed by Kaufman and Keene [1]. During a test in which the wind data are stored on magnetic tape, only one bank of instrumentation is used to avoid interruption of the wind data signals within any magnetic tape recording period, and thus to avoid data processing difficulties when converting analog tapes to digital tapes.

Surface Roughness Length (z_0)

In an earlier report, Fichtl [2] discussed the surface roughness length configuration associated with the NASA meteorological tower. This analysis was based upon wind profile laws that are consistent with the Monin-Obukhov similarity hypothesis. The calculations of z_0 were based on wind data obtained at the 18- and 30-meter levels and on temperature data obtained at the 18- and 60-meter levels. Most of the measurements were obtained during the hours of 0700 and 1600 EST; the gradient Richardson numbers at 23 meters (geometric height between 18 and 30 meters) for the thirty-nine cases ranged between -5.82 and +0.079. The results of these calculations (see Figure 5) show the effect the terrain features have upon the surface roughness. Later, it will be shown, through an analysis of the energy budget at 18 meters, that these roughness lengths are too large.

III. COMPUTATIONS AND INITIAL SCALING

To establish a spectral model of turbulence for the Kennedy Space Center, approximately fifty cases of turbulence were analyzed. The procedure used to calculate the longitudinal and lateral components of turbulence consisted of (1) converting the digitized wind speeds and directions (10 data points per second) into the associated north-south and east-west components and averaging these components over the duration time of each test, (2) calculating the mean wind speed and direction with the averaged components, (3) projecting the original digitized data onto the mean wind

vector and subtracting the mean wind speed to yield the longitudinal components of turbulence, and (4) projecting the original digitized data onto a normal-to-the-mean-wind vector to obtain the lateral components of turbulence. Trends contained within the data were removed by fitting the longitudinal and lateral components of turbulence to second order polynomials and, in turn, subtracting these polynomials from the component time histories. To reduce computation time, the data, with trend removed, were block-averaged over half-second intervals. The longitudinal and lateral spectra were calculated by using the standard correlation Fourier transform methods given by Blackman and Tukey [3]. These spectra were corrected for the half-second block-averaging operation with the procedure given by Pasquill [4] and for the response properties of the instrumentation.

To combine the spectra for each level on the tower, it was assumed that the similarity theory of Monin [5] for the vertical velocity spectrum could be applied to the longitudinal and lateral spectra, so that

$$\frac{nS(n)}{u_{*o}^2} = F(f,Ri), \tag{1}$$

where $nS(n)$ is the logarithmic longitudinal or lateral spectrum associated with frequency n(H and u_{*o} is the surface friction velocity, or rather, the square root of the tangential eddy stress per unit mass. F is tentatively a universal function of the dimensionless wave number f and the gradient Richardson number Ri. The dimensionless wave number is given by

$$f = \frac{nz}{\bar{u}(z)} . \tag{2}$$

Since the tower did not have the capability to measure vertical velocity fluctuations, the Reynolds stress, and hence u_*^2, cannot be calculated with first principles; viz., $u_*^2 = \overline{-u'w'}$, where u' and w' are the longitudinal and vertical velocity fluctuations and the overbar denotes a time-averaging operator. However, an estimate of the surface friction velocity can be calculated from mean wind and temperature profile data.

According to Lumley and Panofsky [6], the mean wind profile in approximately the first 30 meters of the atmosphere is given by

$$\bar{u}(z) = \frac{u_{*o}}{k_1}\left\{\ln\frac{z}{z_,} - \psi(z/L')\right\}, \tag{3}$$

where k_1 is von Karman's constant with numerical value approximately equal to 0.4, and ψ is a universal function of z/L'. L' is a stability length given by

$$L' = \frac{u_{*o}\dfrac{d\bar{u}}{dz}\bar{T}}{k_1 g\dfrac{d\bar{\theta}}{dz}}, \tag{4}$$

where $\bar{T}$ and $\bar{\theta}$ are the Kelvin and potential temperatures associated with the mean flow. The quantity z/L' is related to the gradient Richardson number

$$Ri = \frac{\dfrac{g}{\bar{\theta}}\dfrac{d\bar{\theta}}{dz}}{(d\bar{u}/dz)^2} \tag{5}$$

through the relationships

$$z/L' = \frac{Ri}{(1 - 18Ri)^{1/4}} \qquad (Ri < -0.01), \tag{6}$$

$$z/L' = Ri \qquad (-0.01 \leq Ri \leq 0.01), \tag{7}$$

and

$$z/L' = \frac{Ri}{1 - 7Ri} \qquad (0.01 \geq Ri > 0.01). \tag{8}$$

Equation (6) is a form of the KEYPS [6] equation. The functions $\psi(z/L')$ associated with (7) and (8) are given by

$$\psi(z/L') = -4.5\,\frac{z}{L'} \qquad (0.01 \leq Ri \leq 0.01) \tag{9}$$

and

$$\psi(z/L') = -7\,\frac{z}{L'} \qquad (0.1 \geq Ri > 0.01). \tag{10}$$

Lumley and Panofsky [6] have graphically indicated the function $\psi(z/L')$ for $Ri < -0.01$ and the function

$$\psi(z/L') = 0.044\left(\frac{-z/L'}{0.01}\right)^{1.0674-0.679\,\ln(-z/L'/0.01)} \qquad (Ri < -0.01) \tag{11}$$

faithfully reproduces their curve.

The calculation of u_* was based upon the wind data measured at the 18- and 30-meter levels and the temperature data measured at the 18- and 60-meter levels. Temperatures at the 30-meter level were estimated by logarithmically interpolating between the 18- and 60-meter levels. An estimate of the gradient Richardson number (5) at the 23-meter level (geometric mean height between the 18- and 30-meter levels) was determined by assuming that the mean wind speed and temperature are logarithmically distributed between these levels. The gradient Richardson number estimated in this manner is given by

$$Ri(z_g) = \frac{g}{\bar{T}(z_g)}\left\{\frac{\bar{T}(z_2) - \bar{T}(z_1)}{z_g\,\ln(z_2/z_1)} + \frac{g}{C_p}\right\}\left\{\frac{\bar{u}(z_2) - \bar{u}(z_1)}{z_g\,\ln z_2/z_1}\right\}^{-2}, \tag{12}$$

where $\bar{T}(z)$ is the mean temperature at height z; z_1 and z_2 denote 18 and 30 meters; and $z_g = \sqrt{z_1 z_2}$.

To calculate u_{*o}, z_g/L was evaluated for each case by means of one of the three equations (6) through (8), corresponding to the appropriate Richardson number class. L' was then assumed to be invariant with height, and $\psi(18/L')$ was estimated by equations (9) through (11). Equation (3) was then evaluated at the 18-meter level and solved to yield u_{*o}. The values of z_o used for this calculation are given in Figure 5.

IV. THE INERTIAL SUBRANGE AND REVISED VALUES OF THE SURFACE ROUGHNESS LENGTHS

In the inertial subrange the longitudinal spectrum is given by

$$\frac{nS_u(n)}{u_{*o}^2} = \alpha k_1^{-2/3}\,\beta_\epsilon^{2/3}\,f^{-2/3}, \tag{13}$$

where α is Kolmogorov's constant with a numerical value equal to 0.146 according to Record and Cramer [7]. The quantity β_ϵ is the dimensionless dissipation rate of turbulent kinetic energy per unit mass given by

$$\beta_\epsilon = \frac{k_1 z \epsilon}{u_{*o}^3}, \tag{14}$$

where ϵ is the rate of dissipation of turbulent energy. Below 30 meters, where we should expect the Monin and Obukhov similarity hypothesis for the wind profile to be valid, β_ϵ is a function of Ri only.

Inferences concerning the dependence of β_ϵ on Ri can be made with the aid of the eddy energy equation. For homogeneous terrain, this equation is given by

$$\frac{d\bar{E}}{dt} = u_*^2 \frac{d\bar{u}}{dz} + \frac{H}{C_p \rho} \frac{g}{\bar{T}} - \epsilon - \frac{d}{dz}\left(\frac{\overline{p'w'}}{\rho} + \overline{w'E'}\right) \tag{15}$$

where $H/C_p\rho$ is the eddy heat flux $\overline{\theta'w'}$, ρ is the mean density, E' the turbulent kinetic energy per unit mass, p' and w' denote the turbulent fluctuations of pressure and vertical velocity, and u_* is the local friction velocity ($u_* = u_{*o}$ in the Monin layer). Following Busch and Panofsky [8], we write (15) in dimensionless form, so that

$$\frac{k_1 z}{u_{*o}^3} \frac{d\bar{E}}{dt} = (u_*/u_{*o})^2 \phi - \frac{z}{L} - \phi_\epsilon - \phi_D. \tag{16}$$

The terms in this expression are in one-to-one correspondence with those of (15) and L is the Monin-Obukhov stability length

$$L = - \frac{u_{*o}^3 \, C_p \bar{T}}{k_1 \, g H}. \tag{17}$$

Near the ground a majority of meteorological conditions are characterized, at least approximately, by horizontal homogeneity, steady mean wind with no change of wind direction with height, and steady heating from below. In most cases, it is reasonable to make these assumptions with regard to the KSC tower site. Thus, to a reasonable degree of approximation, we have $d\bar{E}/dt = 0$, and equation (16) implies that in the Monin layer

$$\phi - \frac{z}{L} - \phi_\epsilon - \phi_D = 0. \tag{18}$$

Various authors have hypothesized various schemes to balance the left-hand side (18). Lumley and Panofsky [6] suggest that the local mechanical energy production is balanced by the local viscous dissipation, so that

$$\phi_\epsilon = \phi, \tag{19}$$

and thus the buoyant energy production is balanced by the energy flux divergence term, making

$$\phi_D = -z/L. \tag{20}$$

Busch and Panofsky [8] suggest that the flux divergence term is negligible and the local viscous dissipation is balanced by both the local mechanical and buoyant energy productions, so that

$$\phi_\epsilon = \phi - z/L. \tag{21}$$

We shall call (19) and (21) hypotheses I and II.

According to Lumley and Panofsky,

$$\phi = (1 - 18Ri)^{-1/4} \tag{22}$$

in the unstable Monin layer. This form of the dimensionless shear is consistent with (6). Upon combining (13), (19), and (22), the spectrum in the Kolmogorov subrange for hypothesis I takes the form

$$\left[\frac{nS_u(n)}{u_{*o}^2}\right]_I = \alpha k_1^{-2/3} (1 - 18Ri)^{-1/6} f^{-2/3}. \tag{23}$$

Combining (6), (13), (17), (21), and (22) yields

$$\left[\frac{nS_u(n)}{u_{*o}^2}\right]_{II} = \alpha k_1^{-2/3} \left\{\frac{1 - Ri\, K_m/K_h}{(1 - 18Ri)^{1/2}}\right\}^{2/3} f^{-2/3} \tag{24}$$

for hypothesis II, where K_m and K_h are the eddy viscosity and heat conduction coefficients given by

$$K_m = \frac{u_*^2}{\frac{du}{dz}} \tag{25}$$

and

$$K_h = -\frac{H}{c_p \rho \frac{d\theta}{dz}} . \tag{26}$$

Figure 6 illustrates $[nS_u(n)/u_{*o}^2]_I$ and $[nS_u(n)/u_{*o}^2]_{II}$ as functions -Ri for f = 1.0 and $K_h/K_m = 1.3$. As -Ri approaches infinity, $[nS_u(n)/u_{*o}^2]_I$ converges to zero and $[nS_u(n)/u_{*o}^2]_{II}$ diverges. As -Ri approaches zero, $[nS_u(n)/u_{*o}^2]_I$ asymptotically approaches $[nS_u(n)/u_{*o}^2]_{II}$. The difference between $[S_u]_I$ and $[S_u]_{II}$ is small (within the noise level of the data) for Ri > -1.0, and thus it is difficult to reject one hypothesis in favor of the other for sufficiently small -Ri.

The 18-meter level, longitudinal spectra were used to test hypotheses I and II. At 18 meters the cut-off value of f was approximately 2.0 in most of the cases. Actually, the Kolmogorov subrange occurs at much greater dimensionless wave numbers; however, the -5/3 power law behavior extends down to values of f on the order of unity for the longitudinal spectrum, while this is not true for the lateral spectrum. In addition, the Monin and Obukhov similarity hypothesis for the wind profile upon which the calculation of u_{*o} is based is at most valid below 30 meters. Accordingly, the 18-meter longitudinal spectra are the only ones that could be used to test the validity of hypotheses I and II without introducing assumptions about how the eddy stress and heat flux vary with height.

In figure 6 we have plotted the experimental values of $nS_u(n)/u_{*o}^2$ for the longitudinal spectrum for f = 1.0 as a function of -Ri. The experimental results scatter about the dashed line, but they appear to favor hypothesis I more than hypothesis II, especially for Ri ≤ -3.0. If we accept hypothesis I, then we must conclude that the scaling velocities, u_{*o}, are too large and thus the roughness lengths are too large. If we reject hypothesis I, then we must accept a more complicated energy balance system. We shall invoke Ockham's razor and accept hypothesis I and correct the surface roughness lengths.

We denote the surface roughness lengths in Figure 5 with z_{oo}, and the correct ones resulting from the analysis of the longitudinal spectrum will be denoted with z_o. The corresponding friction velocities will be denoted by u_{*oo} and u_{*o}, respectively. The longitudinal spectrum in the inertial subrange, scaled in terms of u_{*oo}, is given by

$$\frac{nS_u(n)}{u_{*oo}^2} = \left\{ \frac{\ln \frac{z}{z_{oo}} - \psi(Ri)}{\ln \frac{z}{z_o} - \psi(Ri)} \right\}^2 \alpha k_1^{-2/3} (1 - 18Ri)^{-1/6} f^{-2/3}. \tag{27}$$

The data points in Figure 6 correspond to $nS_u(n)/u_{*oo}^2$, not $nS_u(n)/u_{*o}^2$. At neutral stability (Ri = 0), we have $\psi(0) = 0$, and (27) reduces to

$$\left[\frac{\ln \frac{z}{z_{oo}}}{\ln \frac{z}{z_o}} \right]^2 = \frac{nS_u(n)\, k_1^{2/3}}{u_{*oo}^2 \alpha} \tag{28}$$

for f = 1.0. Denoting the right-hand side of (28) by X^{-2} and solving for z_o, we find

$$z_o = z^{1-X} z_{oo}^{X}. \tag{29}$$

Upon extrapolating the data in Figure 6 to Ri = 0 at f = 1, we find $nS_u(n)/u_{*oo}^2 = 0.24$, so that X = 1.059. The new values of z_o for this value of X and z = 18 m are shown in Figure 7. Substitution of (29) into (27) yields

$$\frac{nS_u(n)}{u_{*oo}^2} = \left\{ \frac{X^{-1} \ln \frac{z}{z_o} - \psi(Ri)}{\ln \frac{z}{z_o} - \psi(Ri)} \right\}^2 \alpha k_1^{-2/3} (1 - 18Ri)^{-1/6} f^{-2/3}. \tag{30}$$

The dashed curve in Figure 6 represents $nS_u(n)/u_{*oo}^2$ as a function of Ri according to (30) for $\chi = 1.059$ and $z_o = 0.18$ m ($z_{oo} = 0.23$ m), and it appears to fit the data reasonably well. The function $[nS_u(n)/u_{*o}^2]_{f=1.0}$ for the range of variation of z_o illustrated in Figure 7 departs from the dashed curve by only a few tenths of one percent. This means a spectral model of the longitudinal and lateral components of turbulence can be developed in terms of u_{*oo}, and the final results can be corrected by applying a multiplicative factor which is a function of the Richardson number and a nominal roughness length for the site.

V. EXTRAPOLATION TO NEUTRAL WIND CONDITIONS (Ri = 0)

The meteorological conditions of particular engineering interest are those associated with mean wind speeds at the 18-meter level greater than approximately 10 m sec^{-1}. During these flow conditions, the boundary layer is well mixed so that vertical gradients of the mean flow entropy and thus potential temperature are small and the wind shears are large. Thus, the Richardson number vanishes or at least becomes very small. Accordingly, the neutral longitudinal and lateral spectra are of particular interest in the design and operation of space vehicles. The neutral spectra were determined by extrapolating the data to Ri = 0 by the procedure developed by Berman [9]. Scaled spectra $nS(n)/u_{*oo}^2$ were plotted against Ri for various values of f, and curves were drawn by eye. Of course, the data points scattered about this line. The values of $nS(n)/u_{*oo}^2$ at Ri = 0 were then read off and corrected by multiplying the results by χ^2 to yield the neutral spectra $nS(n)/u_{*o}^2$ for the various levels on the tower. The results of this graphical process are shown in Figures 8 and 9 where the positions of the maxima shift toward higher values of f as the height increases. This means that Monin coordinates $(nS(n)/u_{*o}^2, f)$ fail to collapse the spectra in the vertical so that F(f, Ri) is not a universal function, and thus an added height dependence should be included in the analysis. Busch and Panofsky [8] have obtained similar results from analyses of tower data from Round Hill. The failure of the Monin coordinates to collapse the spectra in the vertical can be attributed to vertical variations in both the Reynolds stress and the length scale used to scale the wave number $n/\Omega(z)$.

Above the Monin layer ($z < 30$ m) in the Ekman layer ($z > 30$ m), the tangential Reynolds stress decreases with height. In addition, the variances of the longitudinal and lateral components of turbulence are decreasing functions of z. Thus, if u_* is the correct scaling velocity, scaling the spectra with the surface value of the friction velocity will cause the scaled spectra at the upper levels to fall below the 18-meter spectra.

By scaling the wave number with z, we have assumed that the integral scales of the longitudinal and lateral components of turbulence are proportional to z. One might suspect from the behavior of eddy coefficients [10] that, if the local integral scales have vertical variations, then they should increase at a rate slower than z. In addition, we have no knowledge that the integral scales of the longitudinal and lateral spectra should have the same vertical variation. However, the analysis showed that Monin coordinates will collapse spectra associated with various turbulence intensities at any particular level in the vertical.

To produce a vertical collapse of the data, it was assumed, for engineering purposes, that the spectra in Monin coordinates are shape-invariant in the vertical. This hypothesis appears to be reasonable and permits a practical approach to developing an engineering spectral model of turbulence.

The Longitudinal Spectrum

The vertical variation of the dimensionless wave number f_{mu} associated with the peak of the logarithmic spectrum scaled in Monin coordinates is given in Figure 10. A least-squares analysis of the data in this figure yields the result

$$f_{mu} = 0.03(z/18), \tag{31}$$

where z is in meters. A plot of $nS_u(n)/u_{*o}^2$ versus f/f_{mu} will shift the spectra at the various levels so that all the peaks of the logarithmic longitudinal spectra are located at $f/f_{mu} = 1$. Values of f_{mu} from other tower sites are indicated in Figure 10.

The average ratio β_u of the shifted spectrum at level z and the 18-meter spectrum, $(S_u(f/f_{mu}, z)/S_u(f/f_{mu}, 18))$, is shown in Figure 11. A least-squares analysis of these data yielded the result

$$\beta_u = (z/18)^{-0.44}, \tag{32}$$

where z is in meters. A plot $nS_u(n)/\beta_u u_{*o}^2$ versus f/f_{mu} will collapse the longitudinal spectra. The collapsed longitudinal data are plotted as a function of $0.03\ f/f_{mu}$ in Figure 12.

The function

$$\frac{nS_u(n)}{\beta_u u_{*o}^2} = \frac{C_u f/f_{mu}}{[1 + 1.5(f/f_{mu})^{r_u}]^{5/3r_u}} \tag{33}$$

was selected to represent the longitudinal spectrum, where C_u and r_u are positive constants, determined by a least-squares analysis. For sufficiently small values of f, $nS_u(n)/\beta_u u_{*o}^2$ asymptotically behaves like f/f_{mu} which is the correct behavior for a one-dimensional spectrum. At large values of f, $nS_u(n)/\beta_u u_{*o}^2$ asymptotically behaves like $(f/f_{mu})^{-2/3}$, consistent with the concept of the inertial subrange. The maximum value of (33) occurs at $f = f_{mu}$. Various authors have suggested formulas like (33) to represent the longitudinal spectrum. However, most of the representations have only one adjustable parameter available, while (33) has two: C_u and r_u. In this light (33) appears to be superior. C_u controls the magnitude of the peak, r_u controls the peakedness, and f_{mu} determines the position of the peak of $nS_u(n)/u_{*o}^2$. Upon setting $r_u = 5/3$, we obtain the form of the longitudinal spectrum suggested by Panofsky [6] to represent the strong wind spectra of Davenport [11]. Von Karman's longitudinal spectrum [12] can be obtained by setting $r_u = 2$. A least-squares analysis of the longitudinal data in Figure 12 revealed that $C_u = 6.198$ and $r_u = 0.843$.

The Lateral Spectrum

The lateral spectra S_v can be collapsed with a procedure like the one used for the longitudinal spectra. However, to determine an analytical expression for the lateral spectrum, special attention must be paid to the inertial subrange to guarantee that $S_u/S_v = 3/4$ [13]. This requirement can be derived from the mass continuity equation for incompressible flow subject to the condition that the eddies are isotropic in the inertial subrange. The experimental values of f_{mv} and β_v are given in Figures 10 and 11. These data show that f_{mv} and β_v can be represented as power laws as for the longitudinal spectra. The function

$$\frac{nS_v(n)}{\beta_v u_{*o}^2} = \frac{C_v f/f_{mv}}{[1 + 1.5(f/f_{mv})^{r_v}]^{5/3r_v}} \tag{34}$$

was used to represent the scaled spectra, where C_v and r_v are positive constants. This function behaves like the one chosen for the longitudinal spectrum.

For sufficiently large values of f, the asymptotic behavior of the ratio between (33) and (34) is given by

$$\frac{S_u}{S_v} \sim \frac{C_u}{C_v}\frac{\beta_u}{\beta_v}\left(\frac{f_{mv}}{f_{mu}}\right)^{2/3}\left(\frac{3}{2}\right)^{\frac{5}{3}\left(\frac{1}{r_v}-\frac{1}{r_u}\right)}. \tag{35}$$

In the inertial subrange we must have $S_u/S_v = 3/4$, so that upon substituting this ratio into (35), we obtain a relationship that can be used as a constraint in the determination of values of C_v and r_v and functions to represent β_v and f_{mv}. The values $C_v = 3.954$ and $r_v = 0.781$, and the functions

$$f_{mv} = 0.1(z/18)^{0.88} \tag{36}$$

and

$$\beta_v = (z/18)^{-0.38} \tag{37}$$

along with the longitudinal parameters will satisfy condition (35) and simultaneously give a good fit to the data (z is in meters). The collapsed lateral spectra and the functions given by (33) and (34) are shown in Figure 12.

VI. UNSTABLE SPECTRA

To develop an engineering model for unstable conditions, the unstable spectra were averaged and then corrected by multiplication with

$$\left\{\frac{\ln \frac{z}{z_o} - \psi(Ri)}{\chi^{-1} \ln \frac{z}{z_o} - \psi(Ri)}\right\}^2$$

for $z = 18$ m. $z_o = 0.18$ m, and $Ri = -0.3$. The longitudinal and lateral spectra for the mean unstable conditions are shown in Figures 13 and 14. The unstable spectra were collapsed by using the procedures for the neutral boundary layer and the functions (33) and (34) appear to be equally valid for the unstable case. The functions f_{mu}, f_{mv}, β_u and β_v are depicted in Figures 15 and 16, and the functions $nS_u(n)/\beta_u u_{*o}^2$ and $nS_v(n)/\beta_v u_{*o}^2$ are given in Figure 17. Table I summarizes the spectral properties of turbulence for unstable and neutral conditions.

Table I. Summary of the Spectral Properties of Turbulence for Neutral and Unstable Conditions

$$\frac{nS(n)}{\beta u_{*o}^2} = \frac{C\, f/f_m}{(1 + 1.5(f/f_m)^r)^{5/3r}}$$

	Neutral	Unstable
C_u	6.198	2.905
C_v	3.954	4.599
r_u	0.845	1.235
r_v	0.781	1.144
f_{mu}	$0.03(z/18)$	$0.04(z/18)^{0.87}$
f_{mv}	$0.1(z/18)^{0.68}$	$0.033(z/18)^{0.72}$
β_u	$(z/18)^{-0.63}$	$(z/18)^{-0.14}$
β_v	$(z/18)^{-0.35}$	$(z/18)^{-0.04}$

VII. THE LONGITUDINAL AND LATERAL CORRELATION FUNCTIONS

The normalized correlation function $R(x)$ at space lag x is related to the spectrum through the Fourier integral

$$\sigma^2 R(x) = \bar{u} \int_0^\infty S(\bar{u}\kappa) \cos(2\pi\kappa x)\, d\kappa, \tag{38}$$

where $\bar{u}S(\bar{u}\kappa)$ is the spectrum at wave number κ (cycles m^{-1}) and σ is the standard deviation of the turbulence. The wave number is related to the frequency through Taylor's hypothesis ($\kappa = n/\bar{u}$). Substitution of (33) or (34) into (38) yields

$$\frac{\sigma^2 R(\xi)}{\beta u_{*o}^2} = C \int_0^\infty \frac{\cos(2\pi \xi\zeta)\, d\zeta}{(1 + 1.5\, \zeta^r)^{5/3r}}, \tag{39}$$

where

$$\left.\begin{aligned} \zeta &= \frac{f}{f_m} \\ \xi &= \frac{x f_m}{z} \end{aligned}\right\}. \tag{40}$$

The quantity ξ is the dimensionless space lag at height z and the integral in (39) is a function of ξ only. Integration of (39) for neutral and unstable conditions with Simpson's rule yielded the results shown in Figures 18 and 19.

The dimensionless standard deviation $\sigma/\beta^{1/2}u_{*o}$ can be obtained from (39) by setting $\xi = 0$ and then taking the positive square root of the resulting expression, so that

$$\frac{\sigma}{\beta^{1/2}u_{*o}} = \left\{C\int_0^\infty \frac{d\zeta}{(1+1.5\,\zeta^2)^{5/3r}}\right\}^{1/2}. \tag{41}$$

The right-hand side of (41) is a pure number, values for which can be found in Table II.

Table II. Table of Properties of the Correlation Functions for Neutral and Unstable Conditions

	Neutral	Unstable
$\sigma_u/\beta_u^{1/2}u_{*o}$	2.227	1.897
$\sigma_v/\beta_v^{1/2}u_{*o}$	1.677	2.302
$L_u^* f_{mu}/z$	0.282	0.188
$L_v^* f_{mv}/z$	0.332	0.199

The function

$$\frac{\sigma^2 R(\xi)}{\beta u_{*o}^2} = \frac{\sigma^2}{\beta u_{*o}^2}\left\{1 + \frac{6.815}{\delta}\,\frac{C}{(1.5)^{5/3r}}\,\frac{\beta u_{*o}^2}{\sigma^2}\,\xi^{2/3}\right\}^{-\delta} \tag{42}$$

was selected to represent the results of the numerical integrations for the neutral case. The parameter δ is determined by least-squares methods. For sufficiently small values of ξ, this function behaves like

$$R(\xi) = 1 - 6.815\,\frac{C}{(1.5)^{5/3r}}\,\frac{\beta u_{*o}^2}{\sigma^2}\,\xi^{2/3}. \tag{43}$$

Now the theory of isotropic homogeneous turbulence predicts that in the inertial subrange

$$\frac{R_v(x) - 1}{R_u(x) - 1} = \frac{4}{3}, \tag{44}$$

and (43) predicts that

$$\frac{R_v(x) - 1}{R_u(x) - 1} \to \left\{\frac{C_v}{C_u}\,\frac{\beta_v}{\beta_u}\left(\frac{f_{mv}}{f_{mu}}\right)^{2/3}\left(\frac{3}{2}\right)^{\frac{5}{3}\left(\frac{1}{r_u}-\frac{1}{r_v}\right)}\right\}\left(\frac{\sigma_u}{\sigma_v}\right)^2 \tag{45}$$

as $\xi \to 0$. The quantity within the braces on the right-hand side of (45) is equal to 4/3, according to (35), and $\sigma_u/\sigma_v \neq 1$. The apparent inconsistency between (44) and (45) results because (44) is based upon the entire flow being isotropic, while (45) is based on spectra associated with turbulent flows which are only locally isotropic in wave number space for sufficiently large wave numbers. Thus, upon producing the Fourier integral, equation (39), we obtained contributions to $R(\xi)$ from both the isotropic and anisotropic portions of the turbulent flow. The quantities

$$\delta_u = 4.758$$

and

$$\delta_v = 3.399$$

and the function (42) reproduce the results of the numerical integrations of (39), for the neutral case, to within a few percent.

In the unstable case, the function (42) does not reproduce the results of the numerical integrations at large values of ξ for all values δ. To remedy this, an exponential factor was introduced into the expression, and the function

$$\frac{\sigma^2 R(\xi)}{\beta u_{*o}^2} = \frac{\sigma^2}{\beta u_{*o}^2}\left\{1 + 6.815\,\frac{C}{(1.5)^{5/3r}}\,\frac{\beta u_{*o}^2}{\sigma^2}\,\xi^{2/3}\right\}^{-1} e^{-\lambda\xi^{\gamma}} \tag{46}$$

was selected to represent the results of numerical integrations for the unstable case. The quantities λ and γ are determined by least-squares methods. It appears that $\gamma = 0.9$ can be used for both the longitudinal and lateral spectra, and

$$\lambda_u = 2.22$$

$$\lambda_v = 2.02.$$

The function (46) yields a good fit near $\xi = 0$; however, it departs from the results of the numerical integrations by approximately 10 percent at $\xi = 1$. Near the origin, (46) behaves like (43), consistent with hypothesis of the inertial subrange.

Let us now turn our attention to the longitudinal and lateral integral scales of turbulence which are defined by the expression

$$L^* = \int_0^{\infty} R(x)\,dx. \tag{47}$$

The integral scale defined in terms of the dimensionless space lag is given by

$$\frac{L^* f_m}{z} = \int_0^{\infty} R(\xi)\,d\xi. \tag{48}$$

This integral is a pure number, and upon substituting the expressions given by (42) and (46) for $R(\xi)$ and employing Simpson's integration rule, we obtain the results in Table II.

Pasquill [4] has represented the correlation functions of atmospheric turbulence with the expression

$$R(x) = e^{-x/L^*}. \tag{49}$$

The logarithmic spectrum associated with this expression is given by

$$\frac{nS(n)}{u_{*o}^2} = \frac{2}{\pi}\,\frac{\sigma^2}{u_{*o}^2}\,\frac{2\pi\, fL^*/z}{(2\pi\, fL^*/z)^2 + 1}. \tag{50}$$

This function has a maximum value at

$$\frac{L^* f_m}{z} = \frac{1}{2\pi} = 0.159. \tag{51}$$

This value of the dimensionless integral scale is significantly less (approximately 45 percent) than the ones in Table II for the neutral case. However, for the unstable case, the integral scales given by (51) depart from the ones in Table II by only approximately 20 percent.

In the neutral case, f_{mu} and f_{mv} are proportional to z and $z^{0.58}$, so that L_u^* is a constant and L_v^* is proportional to $z^{0.42}$. The former is consistant with the results of Davenport's [11] analysis

of high wind speed spectra. In unstable air, f_{mu} and f_{mv} are proportional to $z^{0.67}$ and $z^{0.72}$ and thus L_u^* and L_v^* are proportional to $z^{0.13}$ and $z^{0.28}$

VIII. THE DISSIPATION RATE OF TURBULENCE

It is possible to estimate the dissipation rate of turbulence by examining the asymptote of the dimensionless logarithmic spectrum for large f values. According to (33), the longitudinal spectrum, for sufficiently large values of f, is asymptotically given by

$$\frac{nS_u(n)}{u_{*o}^2} \sim \beta_u \frac{C_u}{(1.5)^{5/3r_u}} (f/f_{mu})^{-2/3}. \tag{52}$$

Equating the right-hand sides of (13) and (52), we obtain

$$\phi_\epsilon = \frac{k_1}{(1.5)^{5/2r_u}} (C_u/\alpha)^{3/2} \beta_u^{3/2} f_{mu}. \tag{53}$$

According to the information given in Table I and (53), ϕ_ϵ in neutral air is given by

$$\phi_\epsilon = (z/18)^{0.055}, \tag{54}$$

while in unstable air, we have

$$\phi_\epsilon = 0.63(z/18)^{0.66}. \tag{55}$$

One should keep in mind that (55) was derived from a spectral model which is an average of the unstable data, so that (55) is probably valid for conditions associated with values of Ri on the order of -0.3.

At $z/L = 0$ we have $\phi(0) = 1$, so that according to either hypothesis I or II (see (19) or (21)), we must have $\phi_\epsilon(0) = 1$. However, (54) predicts that $\phi_\epsilon(0) < 1$ below $z = 18$ m for the neutral case and at $z = 0$ we have $\phi_\epsilon(0) = 0$. Actually, the layer of air in the domain $0 < z \leq 18$ m is in the Monin layer, and we should have $\phi_\epsilon = 1$ throughout this layer during neutral conditions. If we accept a 10 percent error in ϕ_ϵ as a measure of the validity of the spectral representations given by (33) and (34), then it follows from (54) that the model can be extrapolated down to the three-meter level in the neutral case.

To understand the behavior of ϕ_ϵ in the unstable case, we write the eddy energy equation for the steady state boundary layer in the form

$$(u_*/u_{*o})^2\phi - \frac{z}{L} - \phi_\epsilon - \phi_D = 0, \tag{56}$$

as we did in Section IV. Let us now assume that the heat flux is height invariant, so that L is a constant. At the surface of the earth z/L vanishes, $(u_*/u_{*o})^2\phi(0) = 1$, and $\phi_D(0) = 0$ according to both hypotheses I and II; thus $\phi_\epsilon(0) = 1$. As we proceed away from the earth into the unstable Monin layer, ϕ_D is balanced by z/L and ϕ_ϵ is balanced by ϕ according to hypothesis I (in the Monin layer $u_* = u_{*o}$). Because ϕ is a decreasing function of -z/L, it follows that ϕ_ϵ is a decreasing function of z below 18 m. However, based upon an analysis of a sample of Cape Kennedy data, Panofsky suggests that ϕ_D is unimportant in unstable air at 30 m and above. This conclusion may not be strictly true for the entire layer above 30 m, but it is reasonable to suppose ϕ_D becomes negligibly small or vanishes somewhere above 30 m. In addition, for sufficiently large z, the dimensionless shear ϕ is small compared to -z/L and $(u_*/u_{*o})^2 < 1$, so that, according to (56), ϕ_ϵ can be estimated as -z/L. Thus, at sufficiently large heights, ϕ_ϵ is an increasing function of z. Therefore, ϕ_ϵ must experience a minimum in the lower levels. Since equation (55) implies that ϕ_ϵ is an increasing function of z in the unstable boundary layer (Ri(18 m) $\sim$ -0.3), the minimum in ϕ_ϵ must occur at the 18-meter level if we accept hypothesis I. The minimum in ϕ_ϵ probably occurs somewhere between the 18- and 30-meter levels, if the implications of hypothesis I are correct. If this minimum in ϕ_ϵ exists, it was not detected because of the wide spacing between the instrumentation levels on the tower.

The level above 30 m at which ϕ_D vanishes in the unstable model can be estimated with (56). Following Panofsky, we assume $(u_*/u_{*o})^2\phi$ is small compared to -z/L, set $\phi_D = 0$ in (56), and combine the resulting relationship with (55) to yield

$$-\frac{z^*}{L} = 0.63(z^*/18)^{0.88}, \qquad (57)$$

where z^* is the level at which ϕ_D vanishes. The 18-meter level Richardson number for the mean unstable model is on the order of -0.3. Therefore, according to (6), $18/L' = -0.19$. Now, $L = K_m L'/K_h$ and $K_h/K_m \simeq 1.3$, so that $L = -73$ m. Substituting this value of L into (57) yields $z^* = 283$ m. Above this level, ϕ and ϕ_D are small, and $\phi_\epsilon \sim -z/L$. This should be compared with (55) which predicts ϕ_ϵ increases as $z^{0.88}$.

The proposed energy budget scheme for the unstable boundary layer is summarized in Figure 20. In the lowest layer, the Monin layer, the energy budget is given by hypothesis I (see (19)). Above this layer, there is a transition region, between approximately the 18- and 30-meter levels, in which the energy budget transforms from a type I to a type III budget. A type III budget is one in which the mechanical and buoyant energy production terms and the energy flux divergence term all contribute to ϕ_ϵ to varying degrees. From the base of the transition layer to a level on the order of 300 m, ϕ and ϕ_D tend toward zero as z increases. Finally, above this level we have a region in which the buoyant energy production is balanced by the dissipation. In order for this scheme to work, the various functions in the energy equation must be functions of z/L and z must be scaled with a length scale other than L. The additional length scale should be a function of the external synoptic- and meso-scale conditions which force the turbulent flow in the boundary layer.

IX. CONCLUDING COMMENTS

It is concluded that models of spectral forcing functions for the design of space vehicles and aircraft based upon sound scientific principles can be developed. However, much work remains with regard to modeling the third and higher order moments and the associated spectra. This information could shed some light on the structure of atmospheric turbulence.

ACKNOWLEDGEMENTS

The authors are grateful to Prof. Hans A. Panofsky for the discussions and suggestions during the course of this research. The authors wish to thank Mr. Archie Jackson and Mrs. Ella M. McAllister of the Marshall Space Flight Center Computation Laboratory for performing the programming and necessary computations, and Mrs. Margaret B. Alexander of the Atmospheric Dynamics Branch, Aerospace Environment Division, Aero-Astrodynamics Laboratory, Marshall Space Flight Center, for her assistance in completing this paper.

REFERENCES

1. Kaufman, J. W. and L. F. Keene, "NASA's 150-Meter Meteorological Tower Located at Cape Kennedy, Florida," NASA TM X-53259, NASA - George C. Marshall Space Flight Center, Huntsville, Alabama, May 12, 1965.

2. Fichtl, G. H., "An Analysis of the Roughness Length Associated with the NASA 150-Meter Meteorological Tower," NASA TM X-53690, George C. Marshall Space Flight Center, Huntsville, Alabama, January 3, 1968.

3. Blackman, R. B. and J. W. Tukey, The Measurement of Power Spectra, Dover, New York, 1958.

4. Pasquill, F., Atmospheric Diffusion, D. van Nostrand Company, Ltd., New York, 1962.

5. Monin, A. S., "On the Similarity of Turbulence in the Presence of a Mean Vertical Temperature Gradient," J. Geophys. Res., Vol. 64, 1959, pp. 2196-2197.

6. Lumley, J. L. and H. A. Panofsky, The Structure of Atmospheric Turbulence, John Wiley & Sons, 1964.

7. Record, F. A. and H. E. Cramer, 1966, "Turbulent Energy Dissipation Rates and Exchange Processes Above a Non-homogeneous Surface," Quart. J. Roy. Meteor. Soc., 92, pp. 519-561.

8. Busch, N. E. and H. A. Panofsky, "Recent Spectra of Atmospheric Turbulence," Quart. J. Roy. Meteor. Soc. 94, 1968, pp. 132-148.

9. Berman, S., "Estimating the Longitudinal Wind Spectrum Near the Ground," Quart. J. Roy. Meteor. Soc., 91, 1965, pp. 302-317.

10. Blackadar, A. K. et al., "Flux of Heat and Momentum in the Planetary Boundary Layer of the Atmosphere," The Pennsylvania State University Mineral Industries Experiment Station, Dept. of Meteorology, Rept. under AFCRL Contract No. AF9604-6641, 1965.

11. Davenport, A. G., "The Spectrum of Horizontal Gustiness Near the Ground in High Winds," Quart. J. Roy. Meteor. Soc., Vol. 87, 1961, pp. 194-211.

12. Pritchard, F. E., C. W. Westerbrook, and G. E. McVehil, "Spectral and Exceedance Probability Models of Atmospheric Turbulence for Use in Aircraft Design," TR AFFDL-TR-65-122, Air Force Flight Dynamics Laboratory, Research and Technology Division, Air Force Systems Command, Wright-Patterson AFB, Ohio, 1965.

13. Batchelor, G. K., The Theory of Homogeneous Turbulence, Cambridge University Press, New York, 1953.

LIST OF FIGURES

Figure 1. The relationship between the quasi-steady and the instantaneous wind vectors and the longitudinal and lateral components of turbulence.

Figure 2. NASA Launch Complex 39, Kennedy Space Center, Florida.

Figure 3. Aerial plane view of the terrain surrounding the NASA 150-meter meteorological tower

Figure 4. Schematic diagram of the location of instrumentation on the NASA 150-meter meteorological tower at Kennedy Space Center, Florida.

Figure 5. Tentative azimuthal distribution of the surface roughness length at the NASA 150-meter meteorological tower site.

Figure 6. The dimensionless logarithmic longitudinal spectrum at f = 1.0 and z = 18 m as a function of -Ri. The variations of $[nS_u(n)/u_{*o}^2]_{f=1.0}$ for hypotheses I and II are indicated. The dashed curve corresponds to $[nS_u(n)/u_{*oo}^2]_{f=1.0}$ with z_o = 0.18 m and z_{oo} = 0.23 m for a type I energy budget.

Figure 7. Revised azimuthal distribution of the surface roughness length based upon energy budget considerations at z = 18 m.

Figure 8. Dimensionless logarithmic longitudinal spectra for neutral wind conditions.

Figure 9. Dimensionless logarithmic lateral spectra for neutral wind conditions.

Figure 10. Vertical distributions of the dimensionless frequencies f_{mu} and f_{mv} associated with the peaks of the logarithmic longitudinal and lateral spectra for neutral stability conditions.

Figure 11. Vertical distributions of the collapsing factors β_u and β_v for neutral stability conditions.

Figure 12. Dimensionless logarithmic longitudinal and lateral spectra as functions of 0.03 f/f_{mu} and 0.1 f/f_{mv} for neutral stability conditions.

Figure 13. Dimensionless logarithmic longitudinal spectra for unstable wind conditions.

Figure 14. Dimensionless logarithmic lateral spectra for unstable wind conditions.

Figure 15. Vertical distributions of the dimensionless frequencies f_{mu} and f_{mv} associated with the peaks of the logarithmic longitudinal and lateral spectra for unstable wind conditions.

Figure 16. Vertical distributions of the collapsing factors β_u and β_v for unstable wind conditions.

Figure 17. Dimensionless logarithmic longitudinal and lateral spectra as functions of 0.04 f/f_{mu} and 0.033 f/f_{mv} for unstable wind conditions.

Figure 18. Scaled correlation functions for the longitudinal and lateral components of turbulence as functions of the dimensionless space lag ξ for neutral wind conditions.

Figure 19. Scaled correlation functions for the longitudinal and lateral components of turbulence as functions of the dimensionless space lag ξ for unstable wind conditions.

Figure 20. Hypothesized scheme of the budget of turbulent energy in the unstable boundary layer for Ri(18 m) $\simeq$ -0.3.

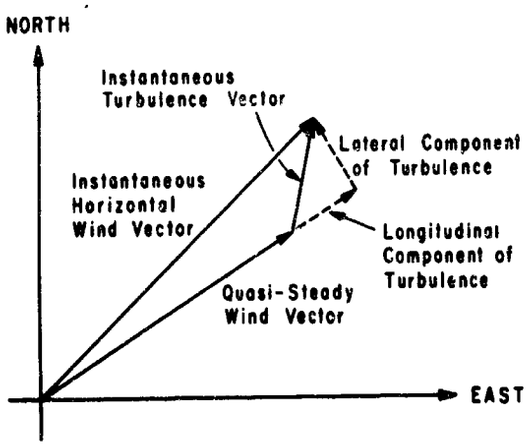

Figure 1

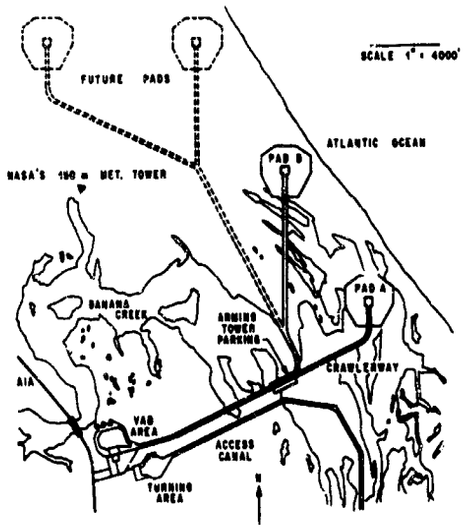

Figure 2

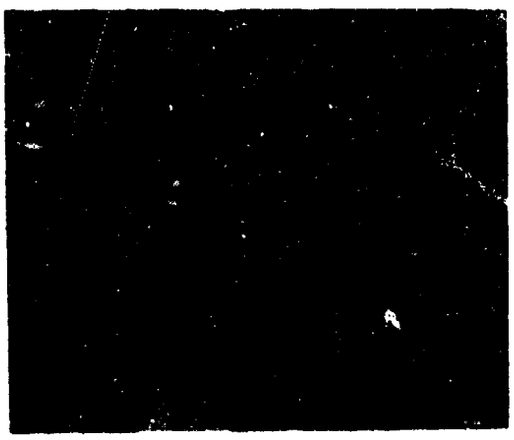

Figure 3

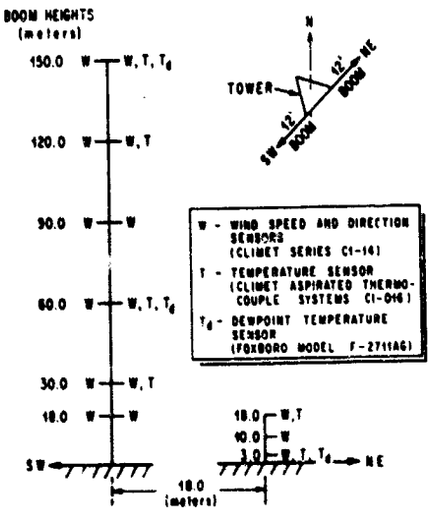

Figure 4

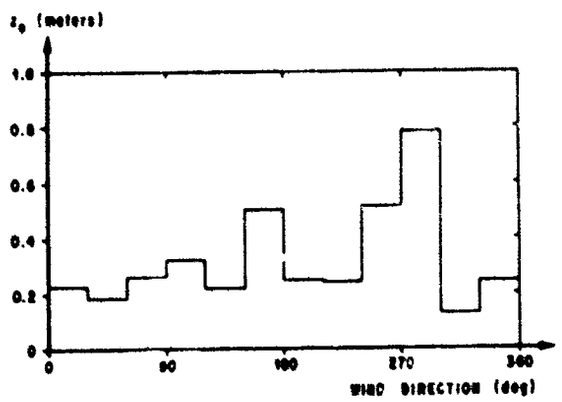

Figure 5

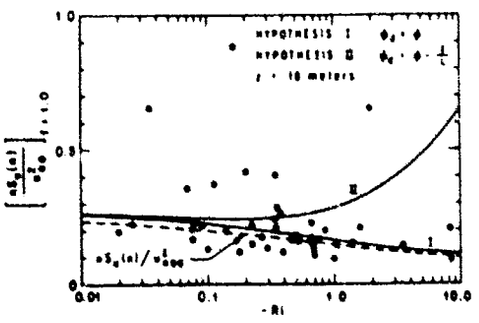

Figure 6

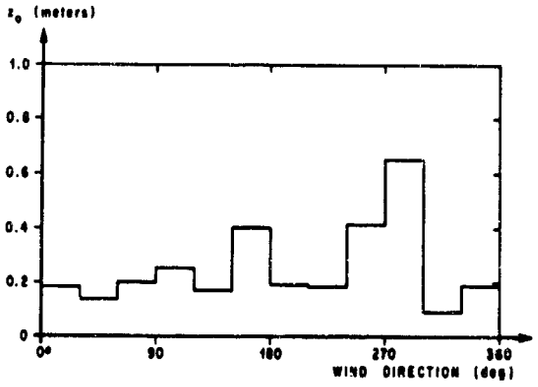

Figure 7

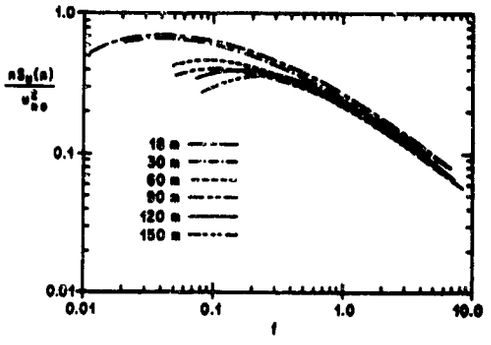

Figure 8

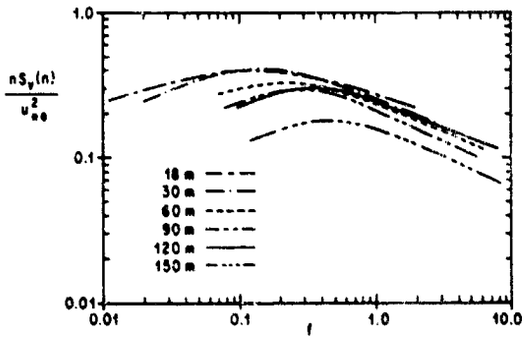

Figure 9

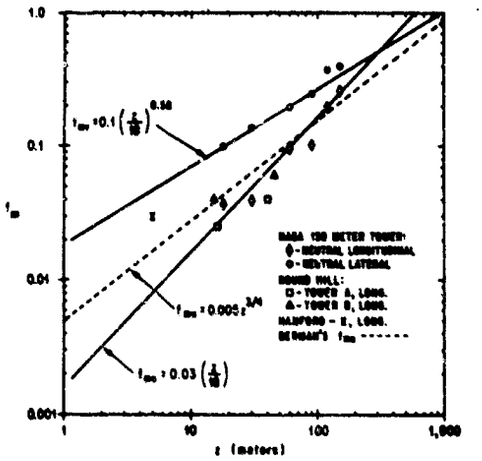

Figure 10

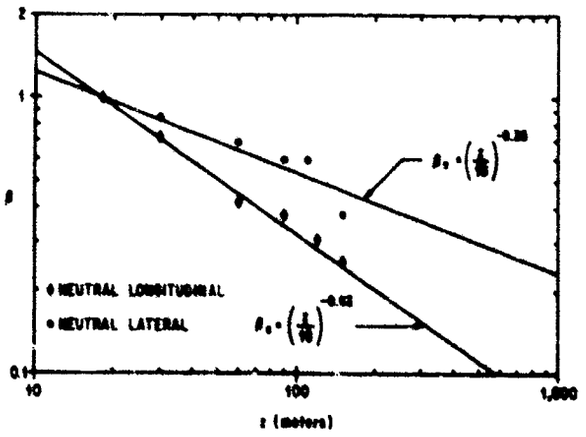

Figure 11

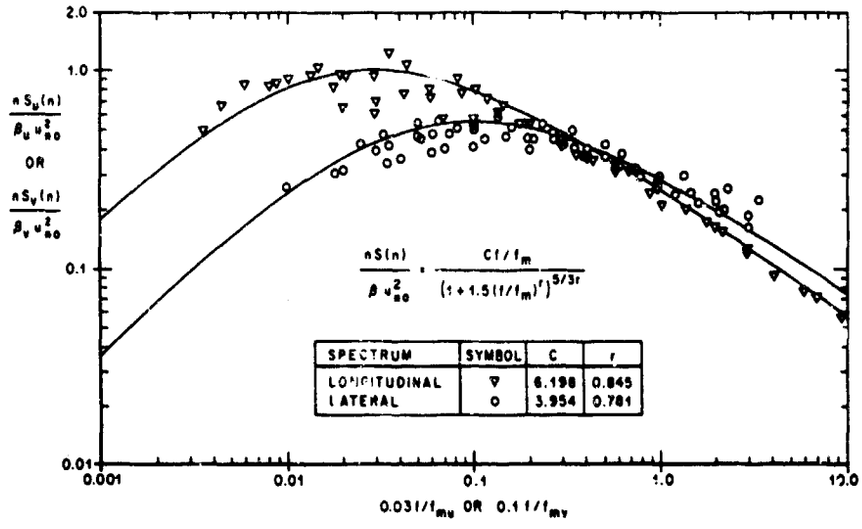

Figure 12

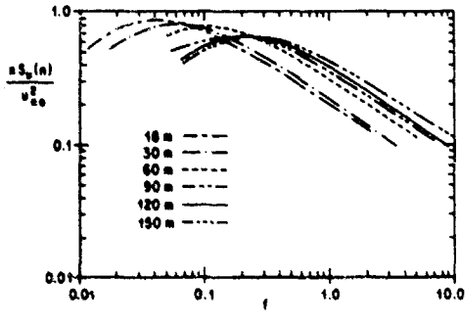

Figure 13

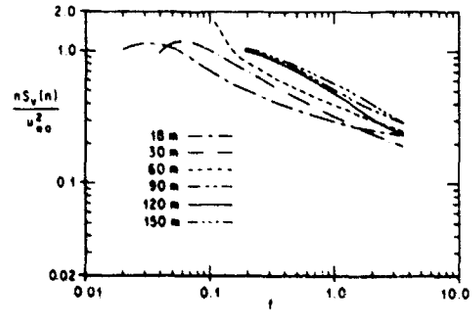

Figure 14

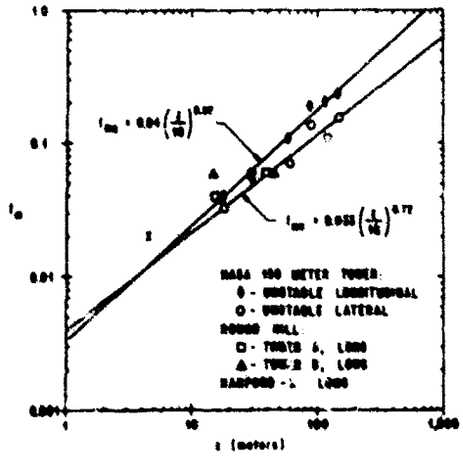

Figure 15

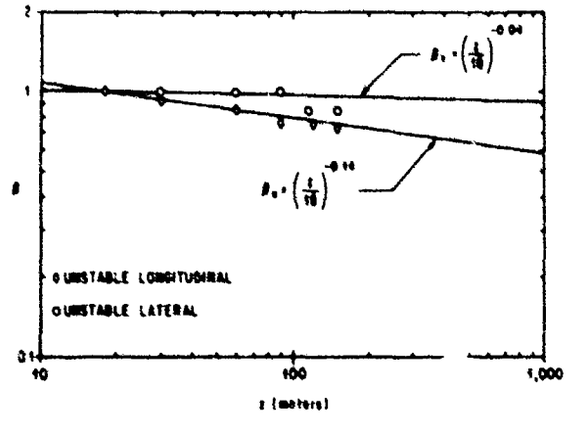

Figure 16

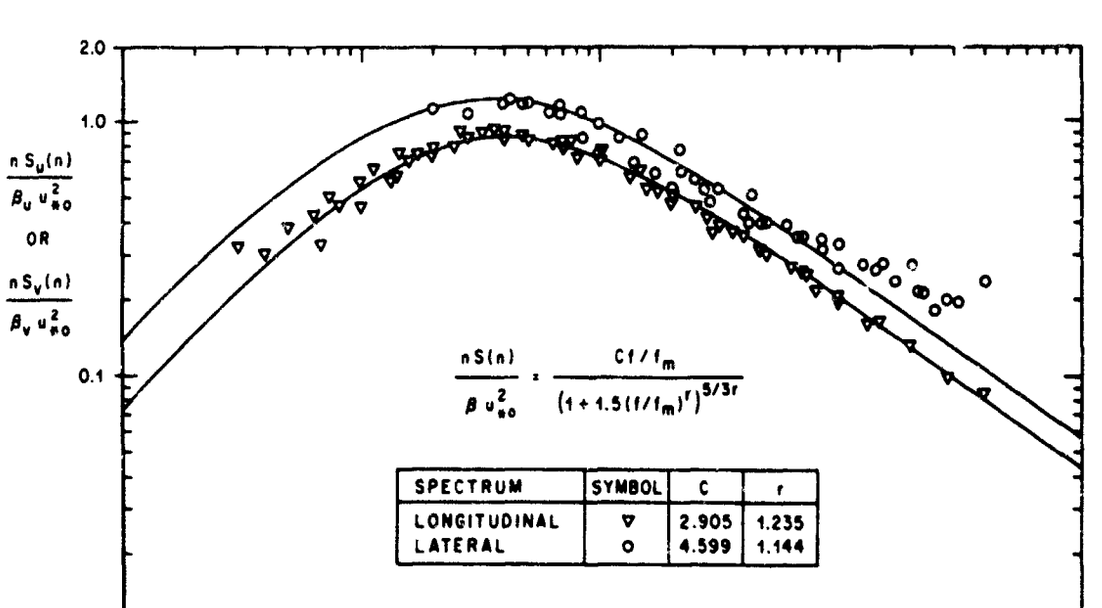

Figure 17

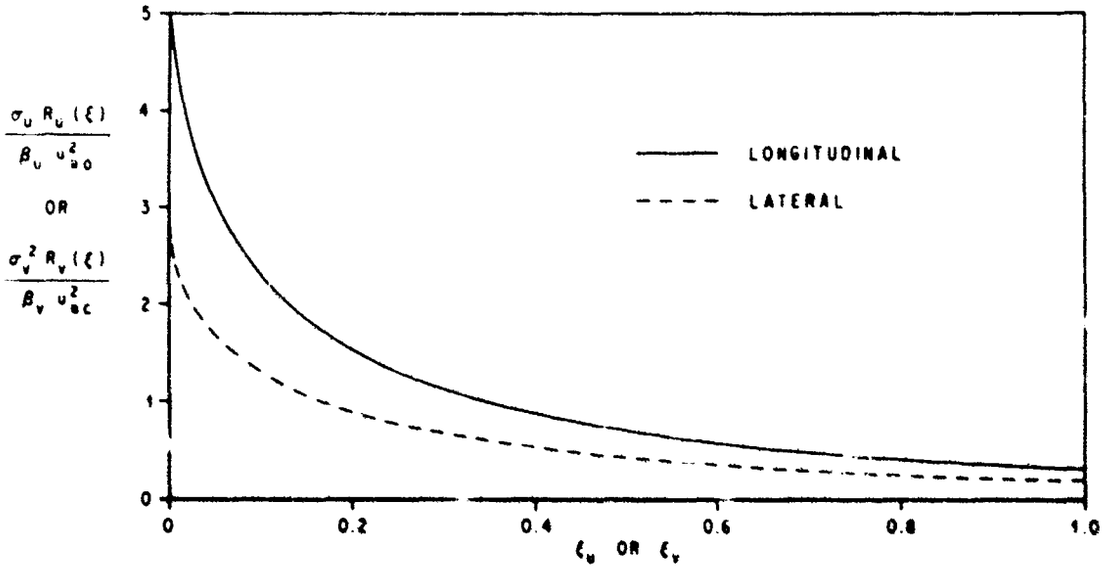

Figure 18

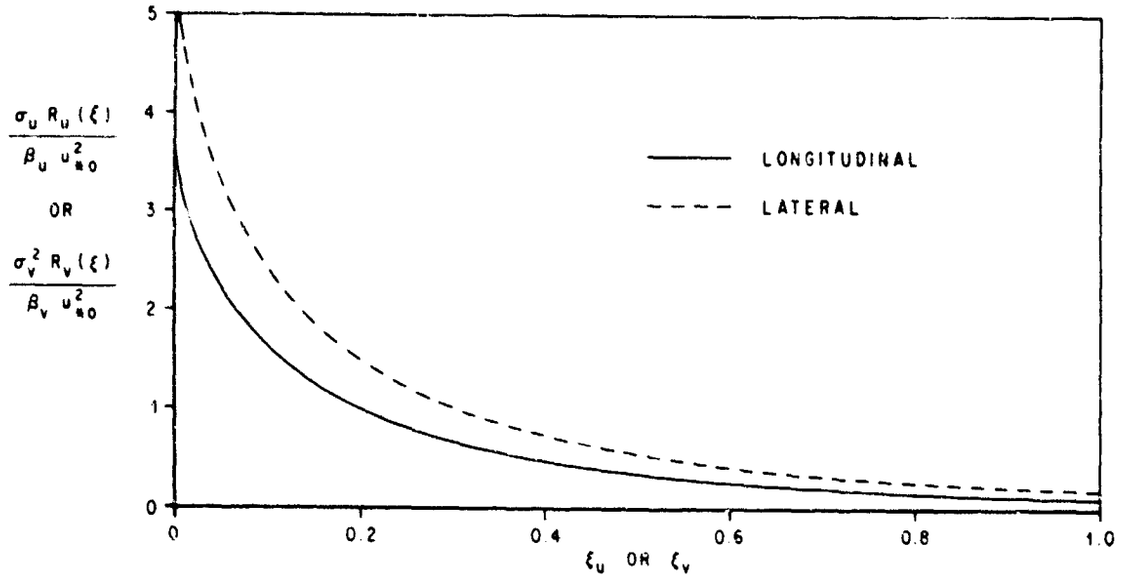

Figure 19

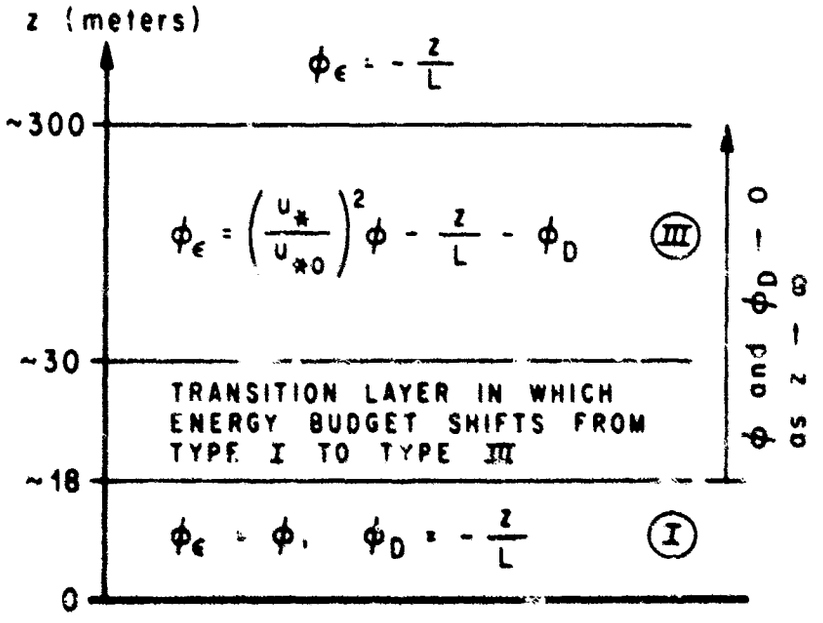

Figure 20

TURBULENCE STRUCTURE IN FLOW REGIMES OF VANISHING MEAN SHEAR

by

Heinz H. Lettau

Professor of Meteorology
The University of Wisconsin at Madison

SUMMARY

Classical models of turbulence assume eddy stress to be proportional to mean strain; they fail to predict eddy flux in fully developed regimes where mean shear and mean gradients vanish. Such cases occur commonly in jet-like flows for which the failure of classical models has caused literature statements on "negative diffusivity" or other "puzzling discrepancies."

Derived from basic fluid dynamics equations, an improved model assumes coupling between macro and micro eddy sizes of the turbulence spectrum. This permits consideration of "conservation-and-adaption" of fluid property along eddying trajectories, not only "conservation" as in classical models. Three-dimensional structure of turbulence can now be predicted without, as well with existing mean shear, and "countergradient" flux can be a legitimate consequence of eddy structure. The new model is applied to selected flow cases, for which the classical theory was unsatisfactory, including the global jet-stream as well as smaller-scale circulations and also similar experimental flow, in a rectangular conduit with controlled lateral heat flux.

1. Introduction

In environmental sciences a need exists for mathematical models which permit us to calculate mean transports and eddy diffusion of air admixtures in the always turbulent atmospheric circulations of various horizontal scales. Transport and eddy diffusion phenomena belong mostly to the class of boundary-value problems rather than initial value problems, since quasi-steady inputs, or outputs (of mass, momentum, and energy) at the atmosphere's lower and upper boundary and subsequent balance requirements are the dominant features.

Essentially, the problem may be summarized as follows. Given characteristics of the mean fields of atmospheric motion ($\bar{\underline{V}} = \underline{i}\bar{u} + \underline{j}\bar{v} + \underline{k}\bar{w}$), admixtures (a scalar $\bar{s}$, per unit of mass, like a mixing ratio), and temperature ($\bar{T}$), what are the eddy variances and covariances which constitute the symmetric tensor:

$$\begin{vmatrix} \overline{u'u'} & \overline{u'v'} & \overline{u'w'} & \overline{u's'} & \overline{u'T'} \\ \& & \overline{v'v'} & \overline{v'w'} & \overline{v's'} & \overline{v'T'} \\ \& & \& & \overline{w'w'} & \overline{w's'} & \overline{w'T'} \\ \& & \& & \& & \overline{s's'} & \overline{s'T'} \\ \& & \& & \& & \& & \overline{T'T'} \end{vmatrix} = ?$$

(As conventional, the overbar indicates a "Reynolds average" and the prime an eddy fluctuation, or turbulent departure value.)

The problem involves the basic need to understand the coupling or feedback (between mean fields $\bar{\underline{V}}$, $\bar{s}$ and $\bar{T}$, and variances and co-variances) imposed by the balance requirements. It is, of course, prohibitive with regard to cost of equipment and logistics to attempt a solution of the problem by the direct measurement of all eddy terms at any point in the atmosphere.

A more rational approach is to utilize theoretical models of the coupling. However, the classical or "phenomenological" theory assumes proportionality between mean stress and strain, and predicts eddy fluxes (for instance, $\overline{w's'}$, or $\overline{v'T'}$) with some degree of reliability only when respective mean gradients (in the above instance, $\bar{s}_z$ and $\bar{T}_y$) are finite. Note that a partial derivative with respect to a spatial coordinate is denoted by the respective subscript (x, y or z); for example, $\nabla \cdot \underline{V} = u_x + v_y + w_z$.

In Section 2, flows with substantial regions of vanishing mean gradients and strain are documented for which the "classical model" fails to explain observational facts. Developments in Section 3 show the reason for the failure and produce an improved model in which not only "conservation" but also "propagation" of fluid properties along eddying trajectories is duly considered. Applications of the theory to the observational facts documented in Section 2 are summarized in Section 4.

2. Documentation of Flow Types with Zones of Vanishing Mean Gradients

2.1 Examples of Atmospheric Flows. Orders of magnitude will be given in full, half, and even quarter powers of ten if this improves the representativeness of derived quantities. For instance, if the order of a velocity-squared is 10^7, the order of the representative velocity will be $10^{3.5}$. Atmospheric flows with vanishing mean strain show, usually, levels of wind maxima; this explains the terminology "atmospheric jet-streams" although such flows are quasi-geostrophic and dynamically different from true jets (discharged by a nozzle into quiet ambient fluid regions).

Most widely known is the jet-like structure of the tropospheric westerlies, a ring-circulation (at temperate latitudes) of about $10^{9.5}$ cm circumference, a meridional and vertical width of about 10^8 cm and 10^6 cm, respectively. If zonally averaged, the core of the jet is found near 35 to 45 deg latitudes, at sub-tropopause pressure levels between 300 and 200 millibar. Its mean state can be described by

$$(1) \qquad \bar{\underline{V}} = \underline{i}\bar{u}; \quad \nabla \cdot \bar{\underline{V}} = 0; \quad \nabla \times \bar{\underline{V}} = \underline{k}\bar{\zeta}; \quad \nabla \bar{T} = \underline{j}\bar{T}_y \ .$$

Characteristic of the mean field are the following orders of magnitude,

$$(2) \qquad \bar{u} = 10^{3.5} \text{ cm sec}^{-1}; \quad \bar{\zeta} = 10^{-5} \text{ sec}^{-1}; \quad -\bar{T}_y/\bar{T} = 10^{-10} \text{ cm}^{-1}.$$

In spite of $\overline{u_y} = \bar{v} = 0$ there is mean vertical vorticity and the order of $\bar{\zeta}$ follows as $2\bar{u}/r^*$ where

$2\pi r^* \approx 10^{9.5}$ cm = circumference of the closed x-trajectory. Evaluations of world-wide conventional aerological soundings (see Obasi (1963) or, for summary references, Lorenz (1967)) suggest the following

$$(3)\quad \begin{cases} \overline{v'v'} \approx \overline{u'u'} \approx 10^{6}, \text{ but } \overline{w'w'} = 10^{0};\ -\overline{u'v'} = 10^{5.5}, \text{ all in cm}^2\ \text{sec}^{-2}; \\ \overline{T'T'}/(\bar{T})^2 = 10^{-3};\quad \overline{v'T'}/(\bar{T}) = 10^{1}\ \text{cm sec}^{-1} \end{cases}$$

The classical theory fails inasmuch as for finite $\overline{u'v'}$ the ratio $-\overline{u'v'}/\bar{u}_y$ is infinite while $-\overline{T'v'}/\bar{T}_y = 10^{11}$ cm^2 sec^{-1} is considered a realistic value for the eddy diffusivity of this large-scale. Consideration of angular instead of relative linear momentum enhances the dilemma since it produces a pronounced counter-gradient flux. Lorenz (1967) discusses "negative" eddy viscosity but concludes that we are dealing with a phenomenon quite different from classical turbulence.

Atmospheric examples of progressively smaller scales include the low-level jet (of 10^2 to 10^3 km fetch), or other thermo-tidal motions over extended terrain slopes (down to 10^1 km fetch along topographical contour lines), and katabatic winds (air drainage along 10^{-1} to 10^0 km fetch along fall lines). Exceptional data on low-level jets were obtained during the U.S. Air Force sponsored "Great Plains Turbulence Field Program." See Lettau and Davidson (1957). The problem of interest here is downward eddy diffusion of heat and momentum across the level of wind maximum at night-time, and upward eddy diffusion of heat at day-time across a level of minimum potential temperature (at about 50m above the ground). A counter-gradient flux is documented by data in Table 1 (extracted from Tables 7.5.1 and 7.5.2 in Lettau and Davidson (1957)), showing that eddy heat flux under "extreme" lapse conditions, while independently known to be upwards directed at all levels listed, is accompanied by lapse rate and negative Richardson number only in the lowest layers. At 100m and above, classical turbulence theory fails; furthermore, the local Richardson number loses evidently any significance as a turbulence parameter, because it is always in excess of "plus unity" and larger for day-time surface heating than for night-time cooling.

TABLE 1. Vertical Profile of Local Richardson Numbers (Ri) Calculated from Observations of Vectorial Vertical Windshear and Vertical Gradients of Potential Temperature in the Lowest 800m above Prairie Ground in Nebraska. Averages for Cases of Extreme Lapse and Inversion Conditions in the Surface Layer.

m above ground :	0.8	1.6	8	100	200	400	800
Ri, extr. lapse :	-0.02	-0.04	-0.14	0.7	1.3	5.3	12.6
Ri, extr. invers.:	0.07	0.09	0.18	3.9	3.1	4.0	1.0

The smallest scale atmospheric jet-like flows are favored by persistent inversion conditions over extended, gentle and uniform terrain slopes. This explains that the U.S. Army (Quartermaster)-sponsored antarctic research program in micrometeorology has produced extraordinary documentations of such flows. Time restrictions prohibit discussion of detail, but it can be said that tower data from Plateau Station (about 80 deg S latitude) show with exceptional clarity the feature of thermo-tidal winds (for an explanation of the term, see Lettau (1967a)). Both wind speeds and mean rate of veering (in excess of an "unbelievable" rate of 1 deg/m) increase with increasing inversional temperature gradient in the lowest 32m. For references on katabatic flow, as observed at the South Pole by P. Dalrymple, reference is made to Lettau (1966a). In this flow, the Richardson number goes to infinity at levels as low as 2m, while eddy flux of heat remains "normal" but cannot be calculated if "classical" similarity concepts of eddy fluxes in the lower atmosphere are to be used.

2.2 Examples of Laboratory Simulation of Atmospheric Jet-like Flows. The common feature of atmospheric "jets" is their shallow, sheet-like structure with insignificant changes along the mean trajectory. Although there is only one solid boundary (the lower one) quasi-geostrophic conditions aloft suggest a hypothetical upper lid. Hence, laboratory simulation with pressure gradient flow between two parallel horizontal walls is more relevant than, for instance, boundary layer development in flow past one plane wall. One-dimensional pressure gradient flow (made "sheet-like" by suitable aspect ratio of the conduit) where the mean shear is essentially unidirectional ($\bar{u}_z$), can readily be subjected to controlled heat flux by maintaining the two walls at different but horizontally uniform temperatures. Outstanding examples of such experiments are those reported by Page et al. (1952) and Corcoran et al. (1952) containing detailed profiles of eddy diffusivities of u-momentum (K_u) and heat (K_T), for test Reynolds numbers between about 6,000 to 53,000. The potential of their results as model studies for sheet-like atmospheric flows has, to the best of my knowledge, not yet been exploited. One reason could be that the classical turbulence model fails here (as well as in the atmosphere) to predict

the observational profiles of K_u and K_T. Furthermore, the empirical dependancy of K_u/K_T-ratios near the conduit center appear to disagree with independent laboratory observations reported by Ludwieg (1956).

The literature includes also studies of the variance profiles in rectangular conduits; outstanding are experiments by Laufer (1950), and Reichardt (1938) as reproduced in Schlichting (1968). Due to restrictions in space, only highlights of the experimental results may be summarized.

Ludwieg (1956) derived K_T/K_u quasi-directly, utilizing frictional heating in flow at Mach numbers of about 0.7 at rather high Reynolds numbers (> 300,000). As documented in more detail in Schlichting (1968, Fig. 23.2), asymptotic values are, for these Reynolds numbers

$$(4) \qquad (K_T/K_u)_{wall} = 1.0; \quad \text{and} \quad (K_T/K_u)_{center} \approx 3/2.$$

Page et al. (1952) derived K_T and K_u separately, with some uncertainty in K_u near the center due to $-\overline{u'v'}$ as well as $\overline{u_z}$ getting small. While K_T/K_u again tends to unity towards the wall, a center value of 3/2 appears to be approached only for their tests at small Reynolds numbers. At about 0.1 relative distance off the center, their K_T/K_u decreases from about 1.4 for $\underline{Re} \approx 9,000$ to about 1.1 for $Re \approx 50,000$. Ludwieg extrapolates this to imply 1.0 for $\underline{Re} > 300,000$ and speaks of a puzzling discrepancy to (4), not explainable by theory.

For the zone of vanishing mean shear, variance measurements in rectangular conduits evidence the same departure from isotropy as in two-dimensional free jets; for references, see Lettau (1967b). Findings by Laufer (1950), in agreement with Reichardt (1938), may be summarized as follows,

$$(5) \qquad (\overline{u'u'}/\overline{v'v'})_{center} = (\overline{u'u'}/\overline{w'w'})_{center} \approx 3/2$$

When normalized by center speed, Laufer's results correspond to

$$(6) \qquad (\overline{u'u'})^{1/2}_{center}/\bar{u}_{max} = 0.027$$

For fluid region near the wall, Lumley and Panofsky (1963) have established good agreement with micrometeorological measurements, suggesting that

$$(7) \qquad (\overline{u'u'}/-\overline{u'w'})^{1/2}_{wall} = 2.4 \pm 0.2; \quad \text{and} \quad (\overline{w'w'}/-\overline{u'w'})^{1/2}_{wall} = 1.3 \pm 0.1.$$

No successful normalization of the third variance, $\overline{v'v'}$, has yet been reported.

3. Basic Theory

3.1 Mean and Departure forms of the Basic Equations. Employing conventional notation (g = gravity, $\alpha = 1/\rho$ = specific volume, ν = kinematic viscosity, S = internal source strength of s-property, ν_s = molecular diffusion coefficient) the Navier-Stokes equation, and the diffusion equation for the scalar property, s, per unit mass of fluid, are

$$(8) \qquad D\underline{V}/Dt = \partial\underline{V}/\partial t + \underline{V}\cdot\nabla\underline{V} = -\underline{k}g - \alpha\nabla p + \nu\nabla^2\underline{V},$$

$$(9) \qquad Ds/Dt = \partial s/\partial t + \underline{V}\cdot\nabla s = S + \nu_s\nabla^2 s.$$

We separate mean states from turbulent departures,

$$(10) \qquad \underline{V} = \bar{\underline{V}} + \underline{V}'; \quad s = \bar{s} + s',$$

and consider the Reynolds rules (as summarized in Schlichting (1968), page 526), including the following two (exemplified here only for s)

$$(11) \qquad (i): \ \overline{(\bar{s})} = \bar{s}; \quad \text{and} \quad (ii): \ \overline{(s - \bar{s})} = \overline{s'} = 0.$$

We define a time-derivative, following the mean motion, which is commutative with the Reynolds average,

$$d(x)/dt = \partial(x)/\partial t + \bar{\underline{V}}\cdot\nabla(x); \qquad \overline{(d(x)/dt)} = d(\bar{x})/dt,$$

whereupon the system (8), (9) yields two average equations,

(12) $d\underset{\sim}{\bar{V}}/dt = -\overline{\underset{\sim}{V}' \cdot \nabla \underset{\sim}{V}'} - \overline{\alpha \nabla p} - \underset{\sim}{k} g + \nu \nabla^2 \underset{\sim}{\bar{V}}$,

(13) $d\bar{s}/dt = -\overline{\underset{\sim}{V}' \cdot \nabla s'} + S + \nu_s \nabla^2 \bar{s}$,

and two departure equations,

(14) $d\underset{\sim}{V}'/dt = (\overline{\underset{\sim}{V}' \cdot \nabla \underset{\sim}{V}'} - \underset{\sim}{V}' \cdot \nabla \underset{\sim}{V}') - \underset{\sim}{V}' \cdot \nabla \underset{\sim}{\bar{V}} + (\overline{\alpha \nabla p} - \alpha \nabla p) + \nu \nabla^2 \underset{\sim}{V}'$,

(15) $ds'/dt = (\overline{\underset{\sim}{V}' \cdot \nabla s'} - \underset{\sim}{V}' \cdot \nabla s') - \underset{\sim}{V}' \cdot \nabla \bar{s} - (\bar{S} - S) + \nu_s \nabla^2 s'$.

These exact equations satisfy the Reynolds rules (10) and (11); namely addition of (12) and (14) reproduces (8), addition of (13) and (15) reproduces (9). Averaging all members once more leaves (12) and (13) unchanged, while in (14) and (15) all terms vanish.

Since each member of the scalar equation (15) has a counterpart in the vector equation (14), we quote for simplicity only from (15) when introducing the following names: "coupling" terms $= \overline{\underset{\sim}{V}' \cdot \nabla s'}$ (because it appears with the opposite sign in both, mean and departure equation), "gradient" (or inertia) term $= \underset{\sim}{V}' \cdot \nabla \bar{s}$, and "viscous" term (or curvature term) $= \nu_s \nabla^2 s'$ (because the Laplacian is a measure of spatial curvature of a function).

In elementary cases of fully developed turbulence, the mean equation reduces to two terms (or even one term) only, one of which must be the coupling term. The departure equation has still several members so that further partitioning is feasible and shall be based on some universal characteristics of the spectrum of turbulence.

3.2 Macro and Micro Size Eddies of the Turbulence Spectrum. Assume, for brevity, that a horizontal steady mean flow (of characteristic speed U) in a conduit (of diameter D) is maintained by a constant external force per unit mass (acceleration A, cm sec^{-2}, normally given by $\overline{\alpha p_x}$). For sufficiently large Reynolds number ($Re = UD/\nu >> Re_{crit} \approx 10^3$) the viscous term in (12) will be negligible. The acceleration (A) will essentially balance the coupling term which may reduce to a height derivative of the Reynolds stress or $(\overline{u'w'})_z$. In equilibrium, cross-sectional averages of work performed by the external force (A. U, per unit mass) must balance energy dissipated (ε, per unit mass), by viscous action in the departure flow, corresponding to $\underset{\sim}{V}' \cdot (\nu \nabla^2 \underset{\sim}{V}')$. In his classical approach, G. I. Taylor related the dissipation rate (ε) uniquely to viscosity (ν) and the characteristic diameter (λ, cm) of eddies of micro-size

(16) $\lambda \sim \nu^{3/4} \varepsilon^{-1/4}$; or, numerically, $\lambda = 15 \nu^{3/4} \varepsilon^{-1/4}$.

Although micro-size eddies possess significant curvature of the $\underset{\sim}{V}'$-field, their contribution to the total variance $(\overline{\underset{\sim}{V}' \cdot \underset{\sim}{V}'})$ will be minor. In the continuous spectrum (spectral contribution to total variances by specified eddy wavenumber bands, as a function of eddy wavenumber) λ corresponds to the region at and beyond the high wavenumber end of the intertial subrange. Let Λ cm denote an eddy size characteristic of the region near the low wavenumber end of the inertial subrange. As a supplement to Taylor's argument, let Λ be independent of viscosity but uniquely determined by ε and A. Dimensional reasoning yields

(17) $\Lambda \sim \varepsilon^2 A^{-3}$; or, numerically, $\Lambda = N^{-1} \varepsilon^2 A^{-3}$.

The numerical factor N must be determined from flow conditions since a natural requirement is that $\Lambda < D$; a more significant criterion is:

(18) Turbulence if : $\Lambda > \lambda$; correspondingly, "No Turbulence" if: $\Lambda < \lambda$.

It shall be demonstrated that (18) is an alternate version of the Reynolds criterion. Namely, with the aid of (16) and (17), the equilibrium condition $\varepsilon = A.U$, yields for the "No Turbulence" statement in (18),

(19) $\varepsilon^{9/4} A^{-3} \nu^{-3/4} < 15N$; or, $\varepsilon^3 A^{-4} \nu^{-1} = U^3 A^{-1} \nu^{-1} < (15N)^{4/3}$.

Relationships between A and U depend on flow structure. For instance, for Hagen-Poisseuille flow, in a round straight duct, $A/U = 32 \nu/D^2$, whereupon the "No Turbulence" statement in (18), with the aid of (19), yields,

(20) $(UD/\nu)^2 < 32(15N)^{4/3}$; or, $UD/\nu < 32^{1/2}(15N)^{2/3} \approx 35N^{2/3}$,

which is the classical criterion and may serve to determine the N-value when Re_{crit} is given. For practical order-of-magnitude estimates, it is convenient to take $N \approx 10^{3/2} \approx 31$. Four representative

cases of turbulent air flows—partly corresponding to types discussed in Section 2—are summarized in Table 2. Typically, micro eddies tend to show rather uniform size, while macro eddies vary from 3 km to 3 cm, with a correspondingly strong variation in the time-interval $\delta t = \Lambda/U$, as well as in "width" of the inertial subrange if measured by the ratio Λ/λ.

TABLE 2. Magnitudes of Macro and Micro Eddy Sizes (Λ and λ) for Selected Airflows ($\nu = 0.14$ $cm^2 sec^{-1}$), Estimated on the Basis of Characteristic Speed U, and Generating Force per Unit Mass (Acceleration A).

	Atmospheric Flows		Experimental Flows	
	Mean Wind	Katabatic	Wind Tunnel	Conduit
A, given by	$\lvert\overline{p_x/\rho}\rvert$	$\lvert g\Delta T/\bar{T}\rvert$	$\lvert\overline{u_x u}\rvert$	$\lvert\overline{p_x/\rho}\rvert$
A, typical cm sec^{-2}	10^{-1}	10^{1}	$10^{2.5}$	10^{2}
U, typical cm sec^{-1}	10^{3}	10^{2}	$10^{2.5}$	10^{2}
$\varepsilon = A.U$, $cm^2\ sec^{-3}$	10^{2}	10^{3}	10^{5}	10^{4}
$\lambda = 15\nu^{3/4}\varepsilon^{-1/4}$, cm	10^{0}	$10^{-0.25}$	$10^{-0.75}$	$10^{-0.}$
$\Lambda = 10^{-1.5}\varepsilon^{2}A^{-3}$, cm	$10^{5.5}$	$10^{1.5}$	10^{1}	$10^{0.5}$
Λ/λ, -	$10^{5.5}$	$10^{1.75}$	$10^{1.75}$	10^{1}
$\delta t = \Lambda/U$, sec	$10^{2.5}$	$10^{-0.5}$	$10^{-1.5}$	$10^{-1.5}$

If Reynolds averages are time means between t and $t + \Delta t$, this Δt must be large in comparison with D/U and even larger in comparison with $\delta t = \Lambda/U$; see Table 2. On the other hand, δt is large in comparison with the time-scale of micro eddies, λ/U. Hence, to filter out the contributions of micro-size eddies, we integrate (14) and (15) between t and $t + \delta t$ which produces fluctuating quantities $\underset{\sim}{V}''$ and s'', defined by

$$(21)\qquad \int_t^{t+\delta t} (d\underset{\sim}{V}'/dt)dt = \underset{\sim}{V}'' = \int_t^{t+\delta t} (d\underset{\sim}{V}'/dt)_{macro}dt; \qquad \overline{\underset{\sim}{V}''} = \overline{\underset{\sim}{V}'} = 0,$$

$$(22)\qquad \int_t^{t+\delta t} (ds'/dt)dt = s'' = \int_t^{t+\delta t} (ds'/dt)_{macro}dt; \qquad \overline{s''} = \overline{s'} = 0.$$

In the inertial subrange the spectral densities decrease significantly with increasing wavenumber. Thus, the larger the ratio Λ/λ the closer will total variances and covariances $(\overline{u'u'}, \overline{u'v'}, \ldots, \overline{s'w'})$ be approximated by $(\overline{u''u''}, \overline{u''v''}, \ldots, \overline{s''w''})$. This justifies another integration of (21) between t and $t + \delta t$, to generate a fluctuating length,

$$(23)\qquad \int_t^{t+\delta t} \underset{\sim}{V}''dt = \underset{\sim}{r}' = \underset{\sim}{i}x' + \underset{\sim}{j}y' + \underset{\sim}{k}z'; \qquad \overline{\underset{\sim}{r}'} = 0.$$

which is a redefinition of the "eddy displacement vector" introduced and employed by Lettau (1964, 1966b, 1967b, 1968). Total variances and covariances $(\overline{x'x'}, \ldots, \overline{x'z'}, \ldots, \overline{z'z'})$ characterize the trajectory structure of those eddies that are most efficient for fluxes and total variance of fluid properties, including momentum components.

3.3 Coupling Between Macro and Micro Eddies. Let subscripts denote the two broad classes of eddy sizes

$$(24)\qquad d\underset{\sim}{V}'/dt = (d\underset{\sim}{V}'/dt)_{macro} + (d\underset{\sim}{V}'/dt)_{micro},$$

$$(25)\qquad ds'/dt = (ds'/dt)_{macro} + (ds'/dt)_{micro}.$$

This partitioning must take into account all members of the right-hand sides of (14) and (15). Due to their physical nature, the gradient terms will dominate the macrostructure, and the viscous terms the

microstructure. The role of the other members can remain unspecified because exact equations for the two separated derivatives in (24) and (25) require the introduction of two additional coupling terms. They are to be determined later and shall be denoted by $\underline{F}'$ (a function of $\underline{V}$ and $\underline{V}'$) and f' (a function of $\overline{s - s_0}$ and $\underline{V}'$, where $\overline{s_0}$ is a reference value or boundary constant of s-property). With $\overline{\underline{F}'} = \overline{f'} = 0$, defining equations are

$$(26) \qquad (d\underline{V}'/dt)_{macro} = + \underline{F}' - \underline{V}' \cdot \nabla \underline{\bar{V}} ,$$

$$(27) \qquad (d\underline{V}'/dt)_{micro} = - \underline{F}' + \nu \nabla^2 \underline{V}' + (\overline{\underline{V}' \cdot \nabla \underline{V}'} - \underline{V}' \cdot \nabla \underline{V}') + (\overline{\alpha \nabla p} - \alpha \nabla p),$$

$$(28) \qquad (ds'/dt)_{macro} = + f' - \underline{V}' \cdot \nabla \bar{s},$$

$$(29) \qquad (ds'/dt)_{micro} = - f' + \nu_s \nabla^2 s' + (\overline{\underline{V}' \cdot \nabla s'} - \underline{V}' \cdot \nabla s') - (\bar{S} - S).$$

As must be true for genuine coupling $\underline{F}'$ and f' appear with the opposite sign in pairs of equations so that (26) added to (27) reproduces exactly (14) via (24), while (28) plus (29) reproduces (15) via (25).

Would there be no coupling between eddy sizes, then $F' = f' = 0$, whereupon the integrations prescribed by (21) to (23) would yield in (26) and (28):

$$(30) \qquad s' \approx s'' = - \underline{r}' \cdot \nabla \bar{s}; \quad \text{or,} \quad s' = - z' \overline{s_z} \quad (\text{if } \nabla \bar{s} = \underline{k} \overline{s_z}),$$

$$(31) \qquad V' \approx \underline{V}'' = - \underline{r}' \cdot \nabla \underline{\bar{V}} ; \quad \text{or,} \quad u' = - z' \overline{u_z} \quad (\text{if } \overline{u_z} \neq 0, \text{ only}).$$

The specialized cases above refer to perfectly realistic flow (one-dimensional with unidirectional mean gradient and shear). It can be concluded that (30) and (31) are the basis of "classical" theory, or Prandtl's mixing length. But the oversimplified nature of (30) and (31) is evident, too, because, for $\bar{w} = \bar{w}_x = 0$, (31) yields $w' = 0$, so that there could be neither vertical eddy flux nor Reynolds stress, contrary to fact. See Lettau (1964).

Forms like $\underline{r}' \cdot \nabla \bar{s}$ in (30) and (31) result from the gradient or inertia terms in (14) and (15); they indicate "conservation" of an initial value of fluid property along the trajectory of an individual eddy. It is logical to assume that the coupling terms indicate "adaption" since they oppose the gradient terms in (26) and (28). "Adaption" implies entrainment of environmental fluid (along the trajectory of an individual eddy) brought about by microstructure and viscous action, as evidenced by the fact that the coupling terms are also part of the micro structures (27) and (29).

The problem remains to specify the coupling functions $\underline{F}'$ and f' explicitly. Previous inductive reasonings in Lettau (1964, 1966b, 1967b) may be summarized and rationalized by due consideration of (21) to (23) and postulating that

$$(32) \qquad f' = - \underline{V}'' \cdot \nabla \bar{s} + \nabla \cdot (\overline{(s - s_0) \underline{V}''}) = \overline{(s - s_0)} \nabla \cdot \underline{V}'' ,$$

$$(33) \qquad \underline{F}' = - \underline{V}'' \cdot \nabla \underline{\bar{V}} + \nabla (\underline{\bar{V}} \cdot \underline{V}'') + \nabla \times [\underline{\bar{V}} \times \underline{V}'']$$

$$= + \underline{V}'' \cdot \nabla \underline{\bar{V}} + \underline{V}'' \times [\nabla \times \underline{\bar{V}}] + \underline{\bar{V}} \times [\nabla \times \underline{V}''] + \underline{\bar{V}} (\nabla \cdot \underline{V}'') - \underline{V}'' (\nabla \cdot \underline{\bar{V}}).$$

Transformations in (32) and (33) correspond to universal identities of vector-calculus. While $\nabla \cdot \underline{\bar{V}} = \nabla \cdot \underline{V}' = 0$ in nearly all turbulent flows, it must be concluded that $\nabla \cdot \underline{V}'' \gtrless 0$ because this is a prerequisite for $f' \lesseqgtr 0$ in (32). This fact reconfirms the dual role of f' as the measure of adaption (by "diverging" macro eddy motion $\underline{V}''$), but expressing also viscous coupling between macro and micro structures. Similar reasonings, although naturally more involved due to vector relations, hold true for explaining the role of $\underline{F}'$.

With the aid of (32) and (33) we rewrite (26) and (28) as follows,

$$(34) \qquad (d\underline{V}'/dt)_{macro} = (\underline{V}'' - \underline{V}') \cdot \nabla \underline{\bar{V}} + \underline{V}'' \times [\nabla \times \underline{\bar{V}}] + \underline{\bar{V}} \times [\nabla \times \underline{V}''] + \underline{\bar{V}} (\nabla \cdot \underline{V}''),$$

$$(35) \qquad (ds'/dt)_{macro} = - \underline{V}' \cdot \nabla \bar{s} + \overline{(s - s_0)} \nabla \cdot \underline{V}''.$$

To calculate total variances and covariances after integration (23) is performed, let us assume that $\underline{V}'' \approx \underline{V}'$ as well as $s'' \approx s'$ which will be tolerable if turbulence spectra have a sufficiently large ratio Λ/λ; see Section 3.2. Then, after introducing (34) and (35) into (21) to (23),

(36) $\underset{\sim}{v}' \approx \underset{\sim}{r}' \times [\nabla \times \bar{\underset{\sim}{v}}] + \bar{\underset{\sim}{v}} \times [\nabla \times \underset{\sim}{r}'] + \bar{\underset{\sim}{v}}(\nabla \cdot \underset{\sim}{r}')$,

(37) $s' \approx -\underset{\sim}{r}' \cdot \nabla \bar{s} + \overline{(s - s_0)}(\nabla \cdot \underset{\sim}{r}')$

The system (36) and (37) can be considered the endphase of stepwise developments starting in 1964. Forms corresponding to (36) and (37) appeared first in Lettau (1966b, 1967b) with some departure in sign. This difference, however, had no consequence for the previous discussion.

The important feature of the new model is that fluctuating values of all four important scalers (u', v', w', s' or T') are completely determined even for the simplest special type of mean flow (unidirectional with one-dimensional gradients), including levels of vanishing mean shear or $\bar{s}$-gradient. This establishes the significant improvement in comparison with the "classical" model which relates fluctuating values exclusively to mean gradients.

4. Applications of the New Model

4.1 General Features of Turbulent Lengthscales. The components of the eddy displacement vector (23) serve to define longitudinal lengthscales (or, variances $X^2 \equiv \overline{x'x'}$, $Y^2 \equiv \overline{y'y'}$, $Z^2 \equiv \overline{z'z'}$) as well as lateral length scales (or covariances, $f^2 \equiv \overline{x'z'}$, $f_{1,2}^2 \equiv \overline{x'y'}$, $f_{2,3}^2 \equiv \overline{y'z'}$). According to Lettau (1966b, 1967b) free turbulence satisfies perfect isotropy requirements (X = Y = Z, and zero for all covariances). The number X_X has been related to the downwind spreading of the jet, and represents a universal characteristic named the Reichardt constant. In wall turbulence—as defined by Hinze (1959)—at least one of the covariances is significant and a first universal characteristic is the Karman constant, k, for which a new covariance definition was found,

(38) $k^2 \equiv \lim_{z \to 0} [\overline{(-u'w')}\,(\overline{u_{zz}})^2/(\overline{u_z})^4] \equiv \lim_{z \to 0} (\overline{x'_z z'_z}) = 0.18$;

see for more detail Lettau (1966b, 1967b, 1968).

Variances of space derivatives of eddy displacement components define another number ($\varkappa$) because for all types of turbulence,

(39) $\overline{(\nabla \cdot \underset{\sim}{r}')^2} = 3\varkappa^2$; $\overline{(\underset{\sim}{i} \cdot \nabla \times \underset{\sim}{r}')^2} = \overline{(\underset{\sim}{j} \cdot \nabla \times \underset{\sim}{r}')^2} = \overline{(\underset{\sim}{k} \cdot \nabla \times \underset{\sim}{r}')^2} = 2\varkappa^2$.

Note that the average mixed product in (38) does not appear among the mixed products which vanish under averaged according to (39). It can be anticipated that the ratio 3/2 which appears in (5) of Section 2 finds its explanation by the two numerical factors in (39). This corresponds to the explanation of the same ratio for velocity variances in the core region of a free jet (in other words, anisotropy of velocity components, in spite of isotropy of eddy displacement components). See Lettau (1967b).

4.2 Turbulence of One-dimensional Shearflow. For the simple case of $\bar{\underset{\sim}{v}} = \underset{\sim}{i}\bar{u}$, $\bar{u}_X = 0$, and $\nabla \times \bar{\underset{\sim}{v}} = \underset{\sim}{k}\,\bar{u}_z$, equation (36) yields

(40) $\underset{\sim}{v}' = \underset{\sim}{i}[-z'\overline{u_z} + (x'_x + y'_y + z'_z)\bar{u}] + \underset{\sim}{j}(x'_y - y'_x)\bar{u} + \underset{\sim}{k}[x'\overline{u_z} + (x'_z - z'_x)\bar{u}]$.

All three components (u', v', w') are determined and remain specified even though $\bar{u}_z$ may go to zero. It can be seen readily that in view of (39) and (40), the empirical result (5) is confirmed, while (6) offers the basis for the numerical evaluation of $\varkappa = 0.027/\sqrt{3} = 0.016$; Lettau (1968) proposed to name $\varkappa$ the "Laufer constant"; its significance for the center region is comparable with that of the Karman constant for the wall region.

Near the wall, the mean shear is large, and (40) yields, after calculation of variances and covariances and neglecting of terms which do not contain $\overline{u_z}$,

(41) $(\overline{u'u'}/\overline{-u'w'})^{1/2} \approx (\overline{z'z'}/\overline{x'z'})^{1/2} = Z/l = 1/k$,

(42) $(\overline{v'v'}/\overline{-u'w'})^{1/2} \approx (\overline{x'x'}/\overline{x'z'})^{1/2} = X/l = (1-k)/k$.

The last steps in the above developments are postulates; the results agree with Lumley and Panofsky's findings (7) since a 0.428-value for the Karman constant corresponds to $1/k = 2.34$; and $(1-k)/k = 1.34$. Equation (40) also shows that $\overline{v'v'}$ does not depend on $\bar{u}_z$ and thus cannot be normalized with the aid of $\overline{-u'w'}$, in marked contrast to $\overline{u'u'}$ and $\overline{w'w'}$.

4.3 Eddy Diffusivities in One-Dimensional Shearflow. With T instead of s, and $\nabla\bar{T} = \underset{\sim}{k}\bar{T}_z$, it follows from (37) for mean flow as defined in Section 4.2, after forming covariances $\overline{u'w'}$ and $\overline{T'w'}$, that

$$(43) \qquad K_u = \ell^2 \bar{u}_z + (\overline{x'_z z'} - \overline{z'_z x'})\bar{u} ,$$

$$(44) \qquad K_T = K_u + \overline{z'_z x'}[\bar{u} - (\bar{T} - T_0)\bar{u}_z/\bar{T}_z] .$$

It is evident from (44) that possible differences between eddy diffusivities can have two distinct causes: (i) differences in boundary conditions which may produce dissimilar mean states, or $\bar{u}_z/\bar{u} \neq \bar{T}_z/\overline{T-T_0}$, and (ii) structure of eddy displacement covariances. Specifically, this statement refers to the difference in the two terms which constitute the z-derivative of the lateral lengthscale ℓ,

$$(45) \qquad \ell^2 \equiv \overline{x'z'}; \text{ hence, } 2\ell_z \ell = \overline{x'_z z'} + \overline{z'_z x'} .$$

At the center of the conduit or when $\bar{u}_z = 0$, it follows that both diffusivities are finite and dependent only on eddy displacement structure

$$(46) \qquad (K_u)_{center} = \bar{u}_{max}(\overline{x'_z z'} - \overline{z'_z x'})_{center}$$

$$(47) \qquad (K_T)_{center} = \bar{u}_{max}(\overline{x'_z z'})_{center} = \frac{3}{2}(K_u)_{center} ; \text{ if } (\overline{x'_z z'} = 3\overline{z'_z x'})_{center} .$$

The rate at which K_T/K_u departs from 3/2 (with increasing distance from the center) depends on the mean flow conditions. Indications are that the new model can explain the observational results (4); and, in view of different boundary conditions also the discrepancies between Ludwieg's and Page's results discussed in Section 2.2; but clarification of detail must be left to future work.

It is significant that in flow where the only nonzero mean derivatives are $\bar{u}_z$ and $\bar{T}_z$, the covariances $\overline{v'w'}$, $\overline{v'u'}$, and $\overline{v'T'}$ equal zero when calculated with the aid of (36) and (37). The exception is the covariance $\overline{u'T'}$ which depends on the longitudinal scale Z and other characteristics of eddy displacement statistics.

4.4 Countergradient Fluxes, and Eddy Stress in Vanishing Mean Shear. For the application of the new model to atmospheric flows, it is important to consider two-dimensional horizontal mean motion (for horizontally uniform mean states) and bi-directional mean shear. When

$$\bar{\underset{\sim}{V}} = \underset{\sim}{i}\bar{u} + \underset{\sim}{j}\bar{v}; \quad \nabla\cdot\bar{\underset{\sim}{V}} = 0; \quad \nabla\times\bar{\underset{\sim}{V}} = -\underset{\sim}{i}\bar{v}_z + \underset{\sim}{j}\bar{u}_z ; \text{ and } \nabla\bar{s} = \underset{\sim}{k}\bar{s}_z ,$$

(36) and (37) yield,

$$(48) \quad \begin{cases} u' = -z'\bar{u}_z + \bar{v}(y'_x - x'_y) + \bar{u}(x'_x + \cdot_y + z'_z) , \\ v' = -z'\bar{v}_z - \bar{u}(y'_x - x'_y) + \bar{v}(x'_x + y'_y + z'_z) , \\ w' = x'\bar{u}_z + y'\bar{v}_z + \bar{u}(x'_z - z'_x) - \bar{v}(z'_y - y'_z) , \\ s' = -z'\bar{s}_z + (\overline{s - s_0})(x'_x + y'_y + z'_z) . \end{cases}$$

The vertical eddy flux of s-property, even for $\bar{v} = \bar{v}_z = 0$ and zero values for all covariances of eddy displacement components if they involve derivatives with respect to x or y, can easily be countergredient; namely, if $\nabla = 0$,

$$(49) \qquad \overline{w's'} = -\ell^2 \bar{u}_z \bar{s}_z + (\overline{s - s_0})\cdot(\overline{z'_z x'}\,\bar{u}_z + \overline{z'_z z'_z}\,\bar{u}) .$$

In regions where $\bar{u}_z$ is small, (49) shows that $\overline{w's'}$ will be independent of $\bar{s}_z$, and dominated by $\overline{s - s_0}$ and the covariance $\overline{z'_z z'_z}$. Possibly such relationships, together with effects of wind veerings can explain observational facts discussed as in Section 2.1 (see Table 1), in connection with low-level jets and thermo-tidal winds. Extreme rate of directional shear(as observed in the lowest 32m above antarctic snow fields) is compatible with (48) and the condition of $\overline{u'v'} = 0$ while $\overline{u'w'} \neq 0$ and $\overline{v'w'} \neq 0$. Detail must be left for future discussion.

Finally, we turn to the largest circulation discussed in Section 2—namely the global jet stream at the sub-tropopause. Observational facts summarized in (1) yield, in combination with (36) and (37),

$$(50)\qquad \begin{cases} u' = -y'\bar{\zeta} + (x'_x + y'_y + z'_z)\bar{u}\,, \\ v' = -x'\bar{\zeta} - (y'_x - x'_y)\bar{u}\,, \\ w' = (x'_z - z'_x)\bar{u}\,, \\ T' = -y'\bar{T}_y + \overline{(T-T_0)}(x'_x + y'_y + z'_z)\,. \end{cases}$$

Note again that the new model produces explicitly all four fluctuating quantities, in spite of locally vanishing mean shear. Variances and covariances can readily be computed, but independent information on eddy displacement structure in this flow regime is needed. Such information is provided by the meandering trajectories of the "GHOST" (Global Horizontal Sounding Technique) balloon (see Bulletin of the American Meteorological Society, Vol. 49, page 1182, December 1968). A pronounced lack of isotropy is evident in the following estimates: $\overline{x'x'} = \overline{y'y'} = 10^{16}$, $\overline{x'y'} = -10^{15.5}$, and $\overline{z'z'} = 10^{10}$, all in cm^2; furthermore, $\overline{x'_x x'_x} = \overline{y'_y y'_y} = 10^{-0.5}$, but $\overline{z'_x z'_x} = \overline{x'_z x'_z} = 10^{-7}$. Along the jet axis, all covariances with derivatives as factors are assumed to be zero.

The above structure values, when combined in variances and covariances formed from (50) with the observational facts listed in (2), agree by order-of-magnitude with the direct data evaluations listed under (3). Notably, the mean meridional-lateral stress $-\overline{u'v'}$ is explained as $-\overline{x'y'}(\bar{\zeta})^2 = 10^{15.5} \times 10^{-10} = 10^{5.5}\ cm^2/sec^2$, the same as the directly evaluated magnitude quoted in (3). Where the classical turbulence model failed, the new model, due to its more realistic consideration of eddy displacement structure, has yielded acceptable results.

Literature References

Corcoran, W. H., F. Page, W. G. Schlinger, and B. H. Sage (1952): Temperature gradients in turbulent gas streams. Industr. Eng. Chem., Vol. 44, pp. 410-419.

Hinze, J. O. (1959): Turbulence, 585 pages, McGraw-Hill Book Co., New York.

Laufer, J. (1950): Investigation of turbulent flow in a two-dimensional channel. Nat. Adv. Counc. Aeronaut., Tech. Note 2133, Washington, D.C.

Lettau, H., and B. Davidson (1957): Exploring the atmosphere's first mile, Vol. 1, 376 pages, Pergamon Press, New York.

Lettau, H. (1964): A new vorticity-transfer hypothesis of turbulence theory. Jour. Atmosph. Sciences, Vol. 21, pp. 453-456.

Lettau, H. (1966a): A case study of katabatic flow on the south polar plateau, Antarctic Research Series, Vol. 9, pp. 1-11. American Geophysical Union, Washington, D.C.

Lettau, H. (1966b): Longitudinal versus lateral eddy length-scale. Jour. Atmosph. Sciences, Vol. 23, pp. 151-158.

Lettau, H. (1967a): Small to largescale features of boundary layer structure over mountain slopes. Proceedings of the Symposium on Mountain Meteorology (ed. E. Reiter and J. L. Rasmussen). Atmosph. Science Paper No. 122, pp. 1-73, Fort Collins, Colorado.

Lettau, H. (1967b): New hypothesis for the relationship between eddy and mean states. Physics of Fluids (Supplement 1967), pp. S79-S83.

Lettau, H. (1968): Three-dimensional turbulence in unidirectional mean flow. ECOM 66-G24-A, Technical Report 1966-67. Grant No. DA-AMC-28-043-66-G24, pp. 127-156, Univ. of Wisconsin, Madison, Wis.

Lorenz, E. N. (1967): The nature and theory of the general circulation. 161 pages. World Meteorol. Organ. Monograph. Geneva, Switzerland.

Ludwieg, H. (1956): Bestimmung des verhaeltnisses der austausch koeffizienten fuer waerme und impuls. Z. f. Flugwiss., Vol. 4, pp. 73-81.

Lumley, J. L., and H. A. Panofsky (1964): The structure of atmospheric turbulence, 239 pp. Interscience Monographs, Vol. 12, John Wiley and Sons, New York.

Obasi, G. O. (1963): Poleward flux of atmospheric angular momentum in the southern hemisphere. Jour. Atmosph. Sciences, Vol. 20, pp. 517-28.

Page, F., W. G. Schlinger, D. K. Breaux, and B. H. Sage (1952): Point values of eddy conductivity and viscosity in uniform flow between parallel plates. Industr. Eng. Chem., Vol. 44, pp. 424-430.

Reichardt, H. (1938): Messungen turbulenter schwankungen. Naturwiss., Vol. 26, pp. 404-405.

Schlichting, H. (1968): Boundary Layer Theory, 747 pp. (6th edition), McGraw-Hill Book Co., New York.

ACKNOWLEDGMENT: The research reported has been in part sponsored by the United States Army Electronics Command, Atmospheric Sciences Laboratory, Fort Huachuca, Arizona, under Grant DA-AMC-28-043-66-G24, which was terminated in September, 1968.

DETERMINATION OF VERTICAL TRANSPORTS OF MOMENTUM AND HEAT AND RELATED SPECTRA OF ATMOSPHERIC TURBULENCE IN THE MARITIME BOUNDARY LAYER

by

L. Hasse*, M. Dunckel† and D. Schriever†

*Meteorolcgisches Institut de Universität Hamburg

†Institut für Radiometeorologie und Maritime Meteorologie
an der Universität Hamburg

Summary

The fluctuations of temperature and of the horizontal and vertical component of wind have been measured by platinum wire and hot wire anemometer at 3.5 m height above the water. From this, the vertical fluxes of heat and momentum are calculated as well as spectra and cospectra. The vertical heat flux can be shown to be nearly proportional to the product of mean wind speed and temperaturedifference air-sea with a transport coefficient near 1×10^{-3} and an uncertainty of 5 mcal/cm^{2}min.

The parametrization of the vertical flux of momentum is usually done with aid of a drag coefficient. For mean conditions a value of 1.2×10^{-3} is appropriate. The dependence of the drag coefficient on the stability of density stratification is shown. Additionally, the dependence of spectra and cospectra on the stability is demonstrated.

Capitions of figures

Fig. 1. Drag coefficients versus wind speed. Reference height is 10 m. Results of our direct measurements at the fixed mast (o ●) and the buoy (▽ ▼) under stable (full symbols) and unstable (open symbols) conditions. Direct measurements of Weiler and Burling (x-wires) and of Smith (thrust - anemometer) are shown by broken lines. Drag coefficients calculated by Brocks from profiles under strictly neutral conditions are shown by full line.

Fig. 2. Drag coefficients versus stability. L_v is Monin-Obukhov-length, including influence of humidity stratification.

Fig. 3. Cospectra of the vertical and horizontal downwind velocity component, normalized with $\overline{u}^2$, for different stabilities.

Fig. 4. Spectra of the horizontal downwind (u) and vertical (w) wind velocity components, normalized with $\overline{u}^2$, for different stabilities.

Fig. 5. Heat flux from direct measurements versus $\overline{u}\Delta\Theta$. Full line is regression of H on $\overline{u}\Delta\Theta$, broken line is regression of $\overline{u}\Delta\Theta$ on H.

Determination of vertical transports of momentum and heat and related spectra of atmospheric turbulence in the maritime boundary layer

L. Hasse

Meteorologisches Institut der Universität Hamburg

M. Dunckel and D. Schriever

Institut für Radiometeorologie und Maritime Meteorologie
an der Universität Hamburg

Direct determination of the vertical fluxes of momentum and heat is possible by the eddy correlation technique. For this purpose, the fluctuations of temperature, of horizontal wind speed and of inclination of the wind against the horizontal were measured at sea together with determinations of waves and subsidiary data. Measurements have been done with platinum wires of 15 µ diameter and about 20 mm length, operated as hot wires in constant current mode. The sensors were exposed in the undisturbed air flow at a buoy 300 m windward of a research ship. The necessary upright positioning of the sensors at the buoy in the moving sea surface was maintained by a servostabilisation with reference to a gyro. This system has been used at the Baltic, the North Sea and the Atlantic.

Additionally, in the Baltic a fixed mast was available which stood in waters of 14 m depth. Sensor height in both cases was typically 3,5 m above the water. The site of most of the measurements reported herein was in the Kieler Bucht with a fetch of at least 16 km. Records of 20 or 40 minutes length were used. A greater number of sensors was applied in order to minimize effects of change of calibration due to contamination and aging. For example, the 24 measurements which underly Fig. 1 and 2 are from six days using 10 different sensors. A continous check on calibration of the velocity components is possible by aid of fast response cup anemometer and the assumption that the vertical velocity is zero in the mean over a period of say 10 minutes.

The vertical fluxes of momentum (τ) and heat (H) are calculated from the fluctations of horizontal downwind component (u') and vertical component (w') of wind and of temperature (T') by

$$\tau = -\rho \overline{u'w'} \qquad (1)$$

$$H = c_p \rho \overline{w'T'} \qquad (2)$$

where the overbar denotes averaging over the period of the record, ρ density of the air, c_p specific heat. As it is well known that in the atmospheric boundary layer the stress (τ) increases approximately as the square of the mean wind speed it is customary to define a drag coefficient ($\varkappa$) by

$$\tau = \rho \varkappa_{10} \overline{u_{10}}^2 \qquad (3)$$

the subscript 10 indicating reference to windspeed measured at 10 m height.

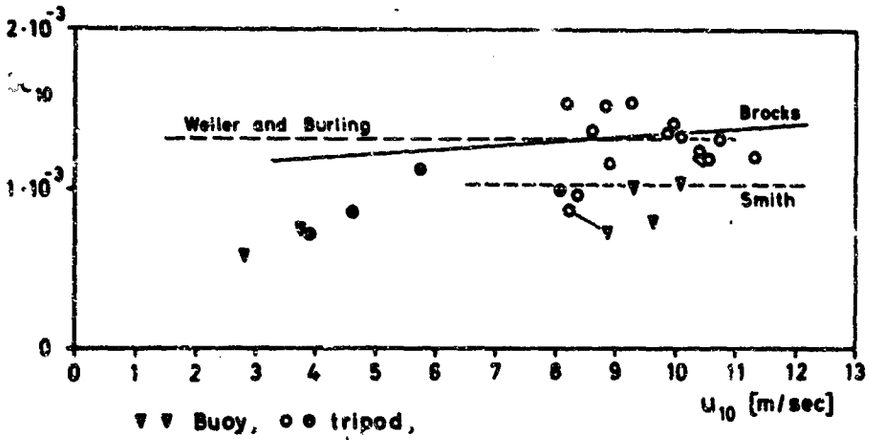

▼ ▼ Buoy, ○ ● tripod,
full symbols indicate stable, open unstable conditions.

8 Hasse Dunckel Schriever Fig.1

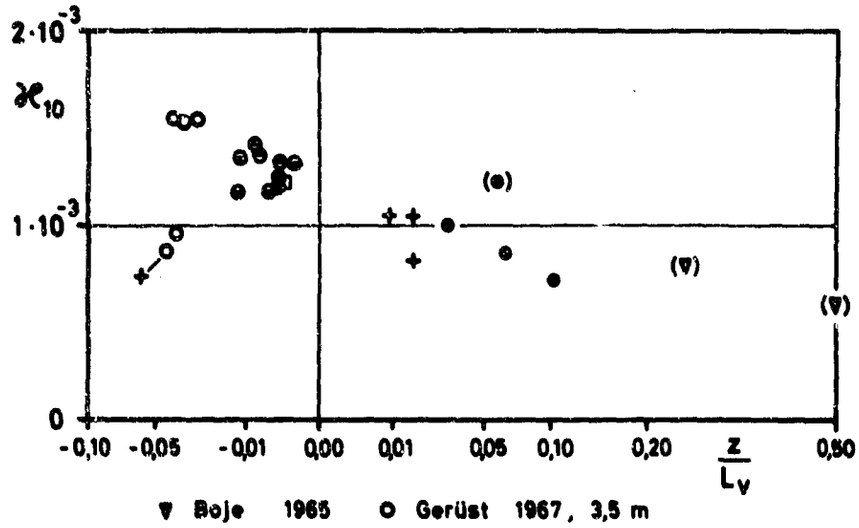

▼ Boje 1965 ○ Gerüst 1967, 3,5 m
✦ Boje 1967 ● Gerüst 1967, 2,9 m
● Gerüst 1965 ⊖ Gerüst 1967, 5,5 m

8 Hasse Dunckel Schriever Fig.2

Fig. 1 shows drag coefficients versus mean wind speed. Results of our direct measurementsare shown with different symbols (open symbols denote unstable, full - stable conditions, circles - measurements at the fixed mast, triangles - at the buoy). Results of other direct measurements over water (Smith 1967, Weiler and Burling 1967) are indicated by broken lines. The full line represents drag coefficients computed from wind profiles obtained by Brocks (personal communication) in the North Sea and Baltic with aid of a buoy (Brocks 1959). Only profils under conditions of strictly neutral density stratification (as determined from simultaneously measured profils of temperature and humidity) have been considered.

From Fig. 1 it is evident that the results of our direct determinations scatter somewhat. This scatter is in part caused by experimental errors and the natural variation of the stress. Yet it is suggested that at least a part of the scatter is due to the variation of the stability of density stratification.

This is borne out by Fig. 2, where the same drag coefficients are shown versus stability as given by z/L_v. The Monin-Obukhov length L_v was calculated from simultaneous direct determinations of heat and momentum flux, corrected for the effect of humidity stratification. For three observations (shown in brackets) the Monin-Obukhov length had to be estimated from indirect determinations of the heat flux using relation (5). Fig. 2 shows that within the obvious scatter [1]) there is a marked tendency for greater drag coefficients under unstable and smaller drag coefficients under stable conditions. Without going into details it may be mentioned here that the same result would be obtained if an increase of the drag coefficient with wind speed - e.g. as has been obtained by Brocks from profile measurements - was taken into account.

The increase of the drag with increasing instability is mainly due to an increase of spectral energy at low frequencies. To demonstrate this, six observations were selected to represent different conditions of stability (see Tab. 1). Selection has been made to obtain a broad variation in stability without prior knowledge of the spectra and care has been taken to have indepedent observations. As usual, the spectra are shown with frequency (f) as abszissa and frequency times spectral energy (Φ_{uu}, Φ_{ww}, Φ_{uw}) as ordinate so that the area under the curve is proportional to the spectral energy in the considered frequency range. The spectral energies have been normalized by division with the square of the mean wind speed. The normalized cospectrum of the horizontal and vertical velocity component may be thought of as spectral decomposition of the drag coefficient.

---

[1]) There are three observations from one day under unstable conditions with somewhat small values of $\varkappa$. As two of them have been made simultaneously on the buoy and the fixed mast with two independent instruments of the same type, it is thought that they may not be due to experimental errors but rather represent some unusual conditions.

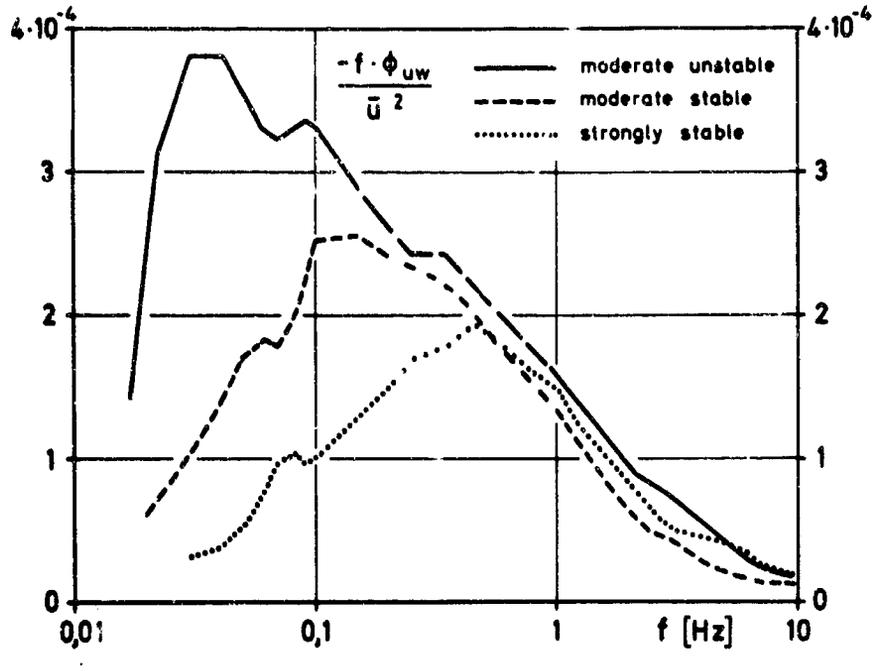

8 Hasse Dunckel Schriever Fig.3

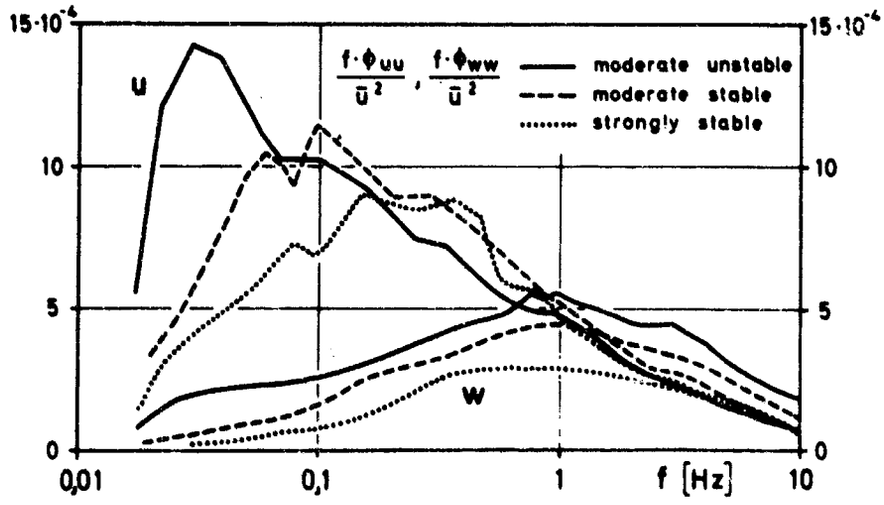

8 Hasse Dunckel Schriever Fig.4

Tab. 1 Parameter of the spectra used.

run	year	site	$\bar{u}$ m/s	ΔT C	z/L_v	density stratification
12/11	- 65	buoy B	2.66	+ 1.8	+ .53 [1]	strongly stable
11/ 9	- 65	mast B	5.59	+ 1.2	+ .10	
12/16	- 65	mast B	7.32	+ 1.4	+ .03	moderate stable
7/ 3	- 68	buoy N	6.05	+ 1.1	+ .06	
25/ 8	- 67	mast B	7.94	- 2.4	- .03	moderate unstable
11/ 2	- 68	buoy N	9.29	- 2.7	- .05	

[1] no temperature fluctuations, heat flux estimated from $\bar{u}\Delta\theta$

B Baltic N North Sea

The marked increase of low frequency cospectral energy with increasing instability (Fig. 3) may be explained as follows. With increasing instability vertical movements increase in general without appreciable change of the shape of the w spectrum (Fig. 4). A stronger increase of the spectral energy of the vertical component at low frequencies seems to be inhibited by the presence of the boundary. As the spectral correlation coefficient

$$R_{uw}(f) = \frac{\Phi_{uw}}{\sqrt{\Phi_{uu}}\sqrt{\Phi_{ww}}} \qquad (4)$$

is increasing from about .2 at higher frequencies to about .6 at lower frequencies, a uniform increase in spectral energy of the w component adds most at the low frequency part of the u,w cospectrum and the peak shifts to lower frequencies. This argument is valid even if the low frequency energy of the u component would not increase. The change in shape of the u,w cospectrum with changing stability therefore seems to be a significant feature near the surface.

From the w spectra of Fig. 4 we may draw another conclusion. On several occasions at international meetings the direct measurements of stress have been questioned with the argument that the necessary exact vertical positioning of the sensors is not achievable under field conditions. Every inclination of the sensor will give a marked deviation of w from zero especially at the very low frequencies. We therefore assume that w equals zero in the mean over the length of a record. This is justified from the observed w spectra as the spectral energy is practically zero at .01 Hz. It may be mentioned that the high pass filter which is imposed by $\bar{w} = 0$ for a record length of 20 minutes has a cut off frequency of $.8 \times 10^{-3}$ Hz and therefore cannot be responsible for the drop of the w component.

There is evidence from the spectra that the depedence of the drag coefficient on stability is real though the experimental material which we can present today

is still small. This is of some bearing as the parametrisation of the vertical fluxes becomes more and more urgent for the numerical experiments of the circulation of the atmosphere and for weather prediction. It will be possible to calculate the momentum flux by aid of formula (3) using the mean wind speed at 10 m and - at least for windspeeds up to 12 m/s - a constant drag coefficient of 1.2×10^{-3} with an accuracy of 20 or 25 %. If we take stability into consideration, an accuracy of 15 % should be achievable.
From our direct measurements the vertical flux of sensible heat may be calculated too. In Fig. 5 the heat flux (H) is given versus $\bar{u}_{10} \Delta\theta$, where is the mean difference between the potential temperature of the air (at 4 m height) and the water surface. The figure shows that the heat flux may be fairly well etimated from

$$H = -c_p \rho c_H u_{10} \Delta\theta \qquad (5)$$

with $c_H \sim 1 \times 10^{-3}$ and an uncertainity of H of 5 mcal/cm^{2}min. From the theoretical point of view it would be desirable to have the coefficient c_H given as a function of the mean wind speed and some measure of stability, but perhaps this is not even necessary for practical purposes.

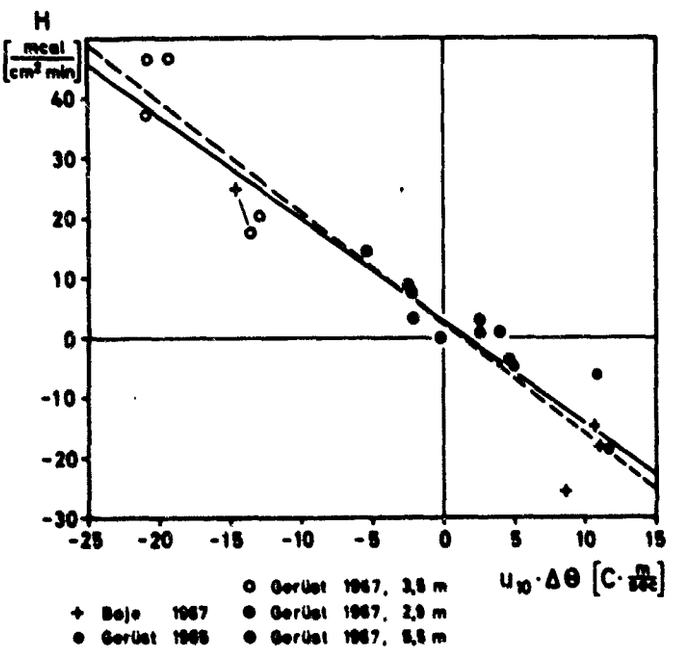

8 Hasse Dunckel Schriever Fig 5

Acknowledgement

The research reported herein was sponsored by the Deutsche Forschungsgemeinschaft and the Fraunhofer - Gesellschaft. Thanks are due to Prof. K. Brocks for his support of this work. The figures 1, 2 and 5 have been taken from Hamburger Geophysikalische Einzelschriften 11. Figures 3 and 4 are based on material presented at the IUGG/URSI Colloquium on Spectra of Meteorological Variables, Stockholm, 9. - 19. June 1969.

References

Brocks, K. 1959 : Ein neues Gerät für störungsfreie meteorologische Messungen auf dem Meer. Archiv Met. Geoph. Biokl. A 11 227-239.

Brocks, K. und L. Hasse, 1969 : Eine neigungsstabilisierte Boje zur Messung der turbulenten Vertikalflüsse über dem Meer. Archiv Met. Geoph. Biokl. A 18 (in press)

Busch, N.E. and H.A. Panofsky, 1968 : Recent spectra of atmospheric turbulence. Qu.J.R.Met.Soc. 94 132-148

Hasse, L., K. Brocks, M. Dunckel and U. Görner, 1966 : Eddy flux measurements at sea. Beitr. Phys.Atmos. 39 254-257

Hasse, L., 1968 : Zur Bestimmung der vertikalen Transporte von Impuls und fühlbarer Wärme über See. Hamburger Geophys. Einzelschr. 11 70 p.

Panofsky, H.A. and E. Mares, 1968 : Recent measurements of cospectra for heat flux and stress. Qu.J.R.Met.Soc. 94 581-585

Smith, S.D., 1967 : Thrust-anemometer measurements of windvelocity spectra and of Reynolds stress over a costal inlet. J. Marine Res. 25 239-262

Weiler, H.S. and R.W. Burling, 1967 : Direct measurements of stress and spectra of turbulence in the boundary layer over the sea. J. Atmos.Sci. 24 653-664.

MEAN WIND-PROFILE AND TURBULENCE CONSIDERATION OF A SIMPLE MODEL

by

Rainer Roth

Meteorologisches Institut der Universität München

This paper is based on studies done by the author during a one years visit to "CSIRO-Division of Meteorological Physics, Aspendale, Australia".

Summary

A model is described, by which the mean vertical wind-profil and turbulence spectra at different heights are calculated for a turbulent boundary layer without thermal stratification. The model makes use of Heisenberg's formula for the transfer of turbulent energy and is based on the assumption of a constant shearing stress in that boundary layer. As a result a logarithmic wind profile follows with 0.39 as the value of von Karman's constant, which is - in this model - strongly related to the inertial subrange of the turbulent energy spectra and therefore to the Kolmogoroff constant.

Mean Wind-Profile and Turbulence Considerations of a Simple Model. *)

Rainer Roth

Meteorologisches Institut der Universität München

Building a model means to construct a set of equations showing a similar behaviour as a special physical experiment. But even a model constructed to describe a rather complicated physical problem must solve simpler problems of the same kind. Therefore only the very simple problem of a turbulent boundary layer with horisontal homogenity and no thermal stratification near a rough wall is discussed in this paper.

If there is a gradient of the mean windspeed - here $\partial u/\partial z \neq 0$ assumed - it is known from hydrodynamics that the dissipation of energy per unit of time and mass ε is given by

$$\varepsilon = \frac{\tau}{\rho} \frac{\partial u}{\partial z} \tag{1}$$

or

$$\varepsilon = K \cdot \left(\frac{\partial u}{\partial z}\right)^2 , \tag{2}$$

where τ is the shearing stress, ρ the density and K the eddy diffusivity. From Equ. 1 and 2 follows immediatly

$$\tau = \rho K \frac{\partial u}{\partial z} \tag{3}$$

If the assumption is made that there is no divergence of the vertical flux of turbulent energy and no advection of turbulent energy in the mass under consideration than the amount of energy ε is transfered from the kinetic energy of the mean flow into kinetic energy of turbulence and from there into heat.

It is known that turbulence cascades the energy from smaller to larger wavenumbers and later at higher wavenumbers the dissipation into heat takes place. This hand over of energy between different wavenumbers is one of the main problems of turbulence theory and this problem is unsolved up to now. Among empirical formulas describing this cascading of turbulent energy is that one given 1948 by W. Heisenberg [2], which will be used here furtheron in the form

$$\frac{\partial F(\kappa)}{\partial t} = -\left(\nu + C\int_{\kappa}^{\infty}\sqrt{\frac{F(\kappa)}{\kappa^3}}\,d\kappa'\right)\cdot 2\kappa^2 F(\kappa) + C\sqrt{\frac{F(\kappa)}{\kappa^3}}\cdot\int_0^{\kappa} 2\cdot\kappa''^2 F(\kappa'')\,d\kappa'' , \tag{4}$$

where $F(\kappa)$ is the spectral density of turbulent energy per unit of mass, κ the wavenumber in rad/length, and C is a numerical constant, which will be discussed later. ν is the kinematic viscosity.

The solution of Equ. 4 for a given ratio of dissipation ε is [1]

$$F(\kappa) = \left(\frac{8\cdot\varepsilon}{9\cdot C}\right)^{4/3}\kappa^{-5/3}\cdot\left[1 + \frac{8\nu^3}{3\cdot C^2\cdot\varepsilon}\cdot\kappa^4\right]^{-4/3} \tag{5}$$

---

*) This paper is based on studies done by the author during a one years visit to "CSIRO-Division of Meteorological Physics, Aspendale, Australia".

and if

$$\kappa \ll \left(\frac{3 \cdot C^2 \cdot \varepsilon}{8 \nu^3}\right)^{1/4}$$

the solution reduces to

$$F(\kappa) = \left(\frac{8}{9 \cdot C}\right)^{2/3} \varepsilon^{2/3} \kappa^{-5/3} \qquad (6)$$

and for

$$\kappa \gg \left(\frac{3 \cdot C^2 \cdot \varepsilon}{8 \nu^3}\right)^{1/4}$$

the approximation is

$$F(\kappa) = \left(\frac{C \cdot \varepsilon}{2 \cdot \nu^2}\right)^2 \kappa^{-7} \qquad (7)$$

Both approximations, Equ. 6 and 7, intersect at

$$\kappa = \left(\frac{3 \cdot C^2 \cdot \varepsilon}{8 \cdot \nu^2}\right)^{1/4} \qquad (8)$$

It may be noticed that if Kolmogoroff - 5/3 law for the inertial subrange is given by

$$F(\kappa) = \alpha \varepsilon^{2/3} \kappa^{-5/3} \qquad (9)$$

than α and C are related by

$$\alpha = \left(\frac{8}{9 \cdot C}\right)^{2/3} \qquad (10)$$

Now assumptions have to be made to apply these formulas to the problem of a turbulent boundary layer. At last those eddies with axis parallel to the surface of the wall are strongly influenced by the presence of the surface and it seems to be reasonable to consider the wavenumber

$$\kappa_{min} = \frac{1}{z} \frac{\text{rad}}{\text{length}} = \frac{0.16}{z} \frac{\text{cycles}}{\text{length}} \qquad (11)$$

as a limiting wavenumber for those eddies. Besides this the value of κ_{min} goes fairly well with that wavenumber where the maximum occurs in measured energy spectra of the vertical component of the windspeed. For simplicity in the model is assumed

$$F(\kappa) = 0 \qquad \text{for} \quad \kappa < \kappa_{min}$$

and

$F(\kappa)$ given by Equ. 4 for $\kappa > \kappa_{min}$

In addition the assumption of isotropy is made for $\kappa_{min} \leq \kappa \leq \infty$.

The main problem now is that in the second right hand term in Equ. 4 the integral is running from zero. This integral represents the square of the vorticity in that wavenumber interval given by the boundaries of the integral, and because there is in the here described model no vorticity of turbulent motions in the interval $0 \leq \kappa \leq \kappa_{min}$, the only vorticity which remains in that interval is that one of the mean wind-profi'3. This changes Equ. 4 in

$$\frac{\partial F(\kappa)}{\partial t} = -\left(\nu + C\int_{\kappa}^{\infty}\sqrt{\frac{F(\kappa')}{\kappa'^3}}\,d\kappa'\right)\cdot 2\cdot\kappa^2 F(\kappa) + C\sqrt{\frac{F(\kappa)}{\kappa^3}}\cdot\left(\frac{1}{\sqrt{3}}\left(\frac{\partial u}{\partial z}\right)^2 + \int_{\kappa_{min}}^{\kappa} 2\cdot\kappa'^2 F(\kappa')\,d\kappa'\right) \qquad (12)$$

where a factor of $1/\sqrt{3}$ has tc be introduced because only 1/3 of $F(\kappa)$ - that is the vertical component of the turbulent motions-interacts with the mean wind-profile. Then the integral

$$\int_{\kappa_{min}}^{\infty} C/\sqrt{3}\cdot\sqrt{\frac{F(\kappa)}{\kappa^3}}\left(\frac{\partial u}{\partial z}\right)^2\cdot d\kappa$$

represents the energy which is per unit of time and mass transfered from the mean flow into turbulence and by comparison with Equ. 2 follows

$$K(z) = \int_{1/z}^{\infty} C/\sqrt{3}\sqrt{\frac{F(\kappa)}{\kappa^3}}\,d\kappa \qquad (13)$$

With the assumptions

$$u = 0 \quad \text{at} \quad z = z_0 \qquad (14)$$

$$u = u_{max} \quad \text{at} \quad z = z_{max} \qquad (15)$$

and

$$u_* = \sqrt{\frac{\tau}{\rho}} \qquad (16)$$

where u_* is constant with heigh but unknown it is possible to calculate the mean wind-profile between z_0 and z_{max} by an iteration prozess. This iteration starts with randomly choosen spectra $F(\kappa)$ for each height and makes use of the general form of the windprofil

$$\left(\frac{\partial u}{\partial z}\right)_z = \frac{u_*^2}{K(z)} \qquad (17)$$

which is equivalent to Equ. 3.

In a short form this iteration may be described as follows:

1 calculate for all heights

$$K(z) = \int_{1/z}^{\infty} C/\sqrt{3}\sqrt{\frac{F(\kappa)}{\kappa^3}}\,d\kappa$$

2 calculate u_* by

$$u_*^2 = \frac{\int_{z_0}^{z_{max}} \frac{dz}{K(z)}}{u_{max}}$$

(integrated form of Equ. 17.)

3 calculate

$$\left(\frac{\partial u}{\partial z}\right)_z = \frac{u_*^2}{K_{(z)}}$$

4 calculate for all heights and wavenumbers $F(k)$ by use of Equ. 12.

5 Go to 1

This iteration converges against a logarithmic wind-profile and reasonable spectra.

Due to the simplicity of that model one main result follows analytically if Equ. 13 is integrated by using Equ. 6 instead of Equ. 5. This gives an error in $K_{(z)}$ of the order of ν and the result is

$$K_{(z)} = \frac{1}{\sqrt{3}\cdot 2}\,(3\cdot C^2)^{1/3}\,\varepsilon^{1/3}\,z^{4/3} \qquad (18)$$

Together with Equ. 2, Equ. 17 and Equ. 10

$$\frac{\partial u}{\partial z} = \frac{u_*}{\left(\frac{(3\cdot C^2)^{1/3}}{\sqrt{3}\cdot 2}\right)^{3/4}\cdot z} = \frac{u_*}{\left(\frac{2}{\sqrt{3}\cdot 3\cdot \alpha}\right)^{3/4}\cdot z} = \frac{u_*}{k\cdot z} \qquad (19)$$

and

$$K = u_*\cdot k\cdot z \qquad (20)$$

follows, where k is used for abbreviation instead of the numerical term which should go with von Karman's constant.

As T.H. Ellison [2] gives as the best value for α

$$\alpha = 1.34 \pm 0.04$$

the consequence is

$$k = 0.39 \pm 0.03\ .$$

Furtheron this value of α is related with a value for C very close to

$$C \simeq \frac{1}{\sqrt{3}}$$

and as it is possible to give a simple model going with Heisenberg's formula which leads to the same value for C, it may be mentioned that the value of k than is

$$k \simeq (\sqrt{3}\cdot 2)^{-3/4} = 0.395\ .$$

To discuss the main result, the relation between von Karman's constant and Kolmogoroff's constant, it is reasonable to look for another hint wether it is possible that von Karman's constant depends on the inertial subrange. For simplicity $1/\sqrt{3}$ is used as the value of C and the spectrum is thought to consist of the $-5/3$ and -7 part only.

In the discussed model the condition for the existence of a -5/3 part of the spectrum at a height z is

$$\frac{1}{z} < \left(\frac{\varepsilon}{8 \cdot \nu^3}\right)^{1/4} \tag{21}$$

and by using Equ. 2, Equ. 19, and Equ. 20 this may be written as

$$\frac{u_* z}{\nu} > 1.46 \tag{22}$$

The left hand term in Equ. 22 is a wellknown quantity for the discussion of windtunnel measurements. Here measurements of I. Nikuradse are refered as quoted in [4], who found as condition for full develloped rough flow

$$\frac{u_* d}{\nu} > 70 \tag{23}$$

where d is the so called sandgrainroughnes and for those measurements d was related to z_0 by

$$d \simeq 30 \cdot z_0 \tag{24}$$

and therefore Equ. 23 may be interpreted as

$$\frac{u_* z_0}{\nu} > 2.5 \tag{25}$$

This shows that even at the height of z_0 there must be a -5/3 part of the spectrum as condition for full develloped rough flow.

If $\frac{u_* z_0}{\nu}$ is smaller than 2.5, there is no full develloped rough flow and then von Karman's constant does not appear in the formulation of the wind-profile close to the wall.

The main purpose this model was built for was to investigate more complex problems but first of all it must describe simple problems as well and this was shown in this paper.

References

[1] Batchelor, G.K. : The theory of homogeneous turbulence. Cambridge University Press 1960.

[2] Ellison, T.H. : The universal small-scale spectrum of turbulence at high Reynolds number. Mechanique de la turbulence: Colloque international. Marseilles 1961.

[3] Heisenberg, W. : Zur statistischen Theorie der Turbulenz. Z.Phys. 124, 628, 1948.

[4] Schlichting, H. : Grenzschichttheorie. Karlsruhe 1951.

ON THE DEVELOPMENT OF CYCLONES IN A STATIONARY LONG-WAVE BASIC STATE

J.Egger

Institut für theoretische Meteorologie
Universität München

Summary

In a twodimensional, quasigeostrophic twolayer-model short-wave perturbations are superimposed to a long-wave, stationary basic state. The shear of the basic flow is depending on x. On the western side and in the centre of the longwave trough and on the eastern side of the ridge strong developments are taking place. The western side of the ridge is a zone of damping. The influence of meridional and zonal vorticity-advection, temperature-advection and vertical velocity on the tendency of the short-wave perturbations are being examined.

On the Development of Cyclones in a Stationary Long-Wave Basic State

J. Egger

Institut für theoretische Meteorologie
Universität München

1. Introduction

In the upper air charts for the middle latitudes there is usually a long-wave field, in which short waves are spreading. The long waves are mostly stationary, whereas the short ones move quickly. By transversing the fields, the short waves are liable to experience considerable changes of their amplitudes [2].
The behaviour and the stability of short-wave disturbances in a stationary baroclinic zonal flow have often been examined (e.g. [1]). In this case the shear of the zonal flow is not depending on x. It does not make any difference for the development of the disturbances at which x-coordinate they are. Emanating, however, from a long-wave basic flow, as recommended by the synoptic findings, the shear depends on x. Cold troughs and warm ridges follow in succession. For the development of a, say, low-pressure disturbance it will then be of importance whether it is in front of a long-wave ridge or in its rear. To examine this influence of the stationary long-wave basic flow on the disturbances is the aim of the subject investigation.

2. Equations

The thermodynamic equation

$$\frac{\partial^2 \psi}{\partial t \partial p} + v_g \cdot \nabla \frac{\partial \psi}{\partial p} = -\frac{\sigma}{f} \omega \tag{2;1}$$

and the vorticity equation

$$\frac{\partial}{\partial t} \nabla^2 \psi + v_g \cdot \nabla (\nabla^2 \psi) + \beta \frac{\partial \psi}{\partial x} = f \frac{\partial \omega}{\partial p} \tag{2;2}$$

had been applied as initial equations - both quasigeostrophic approximated - whereby ψ is the streamfunctin, v_g the vector of the geostrophic wind, f the Coriolis-parameter, β the Rossby-parameter, σ for the hydrostatic stability and ω the vertical velocity in the p-system. σ is constant.
Vertical boundary condition: $\omega = 0$ for $p = 0$ mb and for $p = 1000$ mb.
The atmosphere is divided - in the known manner - into two layers. The indizes $i = 1, 2, 3$ are detailed to the three p-surfaces for $p = 250$, 500 and 750 mb, respectively. Equation (2;1) is applied for surface (2), (2;2) for the surfaces (1) and (3). Thereby $\pm \omega_2 / Dp$ replaces the quantity $\frac{\partial \omega}{\partial p}$ in (2;2), taking into consideration the boundary condition $\omega = 0$ ($Dp = 500$ mb). Thus, it results in

$$\left(\frac{\partial}{\partial t} + v_{g_1} \cdot \nabla \right) \nabla^2 \psi_1 + \beta \frac{\partial \psi_1}{\partial x} = f \omega_2 / Dp \tag{2;3}$$

$$\left(\frac{\partial}{\partial t} + \frac{1}{2} (v_{g_1} + v_{g_3}) \cdot \nabla \right) (\psi_3 - \psi_1) = -\sigma \omega_2 Dp / f \tag{2;4}$$

$$\left(\frac{\partial}{\partial t} + v_{g_3} \cdot \nabla \right) \nabla^2 \psi_3 + \beta \frac{\partial \psi_3}{\partial x} = -f \omega_2 / Dp \tag{2;5}$$

thereby v_{g_1} is replaced by $(v_{g_1} + v_{g_3})/2$. For this system of equations, a long-wave stationary basic state $\overline{\psi_i}$ has now to be found, to which short-wave perturbations are to be superimposed.
The equations for this stationary basic state read then as follows:

$$-\frac{\partial \overline{\psi}_{1,3}}{\partial y} \frac{\partial}{\partial x} \nabla^2 \overline{\psi}_{1,3} + \frac{\partial \overline{\psi}_{1,3}}{\partial x} \left(\frac{\partial}{\partial y} \nabla^2 \overline{\psi}_{1,3} + \beta \right) = \pm f \overline{\omega}_2 / Dp \tag{2;6}$$

$$-\frac{\partial}{\partial y} (\overline{\psi}_1 + \overline{\psi}_3) \frac{\partial}{\partial x} (\overline{\psi}_3 - \overline{\psi}_1) + \frac{\partial}{\partial x} (\overline{\psi}_1 + \overline{\psi}_3) \frac{\partial}{\partial y} (\overline{\psi}_3 - \overline{\psi}_1) = -2 \sigma \overline{\omega}_2 Dp / f \tag{2;7}$$

The "+" on the right side of (2;6) counts for $i = 1$, the "-" for $i = 3$. Having found a solution $\overline{\psi}_i$ for (2;6)-(2;7), one then superimposes a perturbation ψ_i'

to the basic state, i.e.

$$\Psi_i = \overline{\Psi_i} + \Psi_i^* \tag{2;8}$$

Applying this assumption to (2;3)-(2;5) you receive for the perturbation the system of equations

$$\frac{\partial}{\partial t}\nabla^2\Psi^*_{i,3} + \overline{v}_{g_{i,3}}\cdot\nabla(\nabla^2\Psi^*_{i,3}) + v^*_{g_{i,3}}\cdot\nabla(\nabla^2(\overline{\Psi}_{i,3}+\Psi^*_{i,3})) + \beta\frac{\partial\Psi^*_{i,3}}{\partial x} = \pm f\omega_2^*/Dp \tag{2;9}$$

$$\frac{\partial}{\partial t}(\Psi^*_3-\Psi^*_1) + \frac{1}{2}(\overline{v}_{g_1}+\overline{v}_{g_3})\cdot\nabla(\Psi^*_3-\Psi^*_1) + \frac{1}{2}(v^*_{g_1}+v^*_{g_3})\cdot\nabla(\overline{\Psi}_3+\Psi^*_3-\overline{\Psi}_1-\Psi^*_1) = -\sigma\omega_2^*Dp/f \tag{2;10}$$

This system of nonlinear equations for Ψ_i^* and Ψ_2^* is to be solved. At the time $t = 0$ a disturbance Ψ_i^* is assumed, $\overline{\Psi_i}$ being known. The behaviour of Ψ_i^* during the course of time is to be computed. As solving of (2;9) - (2;10) is the result of using numerical methods, applying of linearising can be refrained from.

3. Basic State

The equations (2;6) - (2;7) are to be solved. As the basic state is to have the shape of a wave, the assumption is obvious

$$\overline{\Psi_i} = -y(u_i + A_i\sin kx) \tag{3;1}$$

$i = 1, 3$; U_i, A_i constant, $k = 2\pi/L$; $y > 0$. L is the wave-length of the basic state. You insert (3;1) in (2;6) - (2;7), eliminate $\overline{\omega_2}$ and receive

$$u_1 = \frac{\beta(k^2 - F(A+1))}{k^2(k^2 - F(A+1/A))} \tag{3;2}$$

$$u_3 = \frac{\beta(k^2 - F(1+1/A))}{k^2(k^2 - F(A+1/A))} \tag{3;3}$$

with $F = f^2/\sigma Dp^2$ and $A = A_1/A_3$. Knowing the quotient $A = A_1/A_3$, U_1 and U_3 can be determined. Table 1 shows for several values of A and for $L = 10^4$ km the corresponding U_1 and U_3. Hereby, the same as in the following, the datas are applied:

$\sigma = 0.028\ m^2mb^{-2}sec^{-2}$; $f = 10^{-4}sec^{-1}$; $\beta = 16.2\ m^{-1}sec^{-1}$.

A	U_1 msec^{-1}	U_3 msec^{-1}
1	41	41
2	49	22
3	50	14

Table 1. U_1 and U_3 for various values of the quotient $A = A_1/A_3$.

If you choose $A > 1$ and $0 < A_1 < U_1$, $A_3 < U_3$, (3;1) can be considered as the stream-function of a significant basic state. The zonal component of the geostrophic wind is always positive and decreases when pressure increases. From Fig.1 it is evident that between longwave trough and ridge the meridional component of the geostrophic wind is directed to the North and that there ascending movement of air is predominating ($\overline{\omega_2} < 0$). Just the opposite exists, namely North wind and descending movement of air, between the ridge and trough. In the trough the shear is stronger and the air colder than in the ridge.

4. Solution of the equations for the perturbation

Starting with an assumed perturbation Ψ_i^* at the time $t = 0$ the system (2;9) - (2;10) is to be solved as a initial value problem. The quantities of the basic state are being determined as per Cap.3.

One now assumes that the disturbance Ψ_i^* as well as $\overline{\Psi_i}$ is a linear function of y, thus $\Psi_i^* = y\Phi_i$, whereby Φ_i depends only from x and t.

Substituting this assumption to (2;9) - (2;10), this shows that the problem is now twodimensional. Only the superimposing of waves in a x,p-plane has to be examined.

Elimination of ω_2^* and using (3;1) transforms (2;9)-(2;10) into

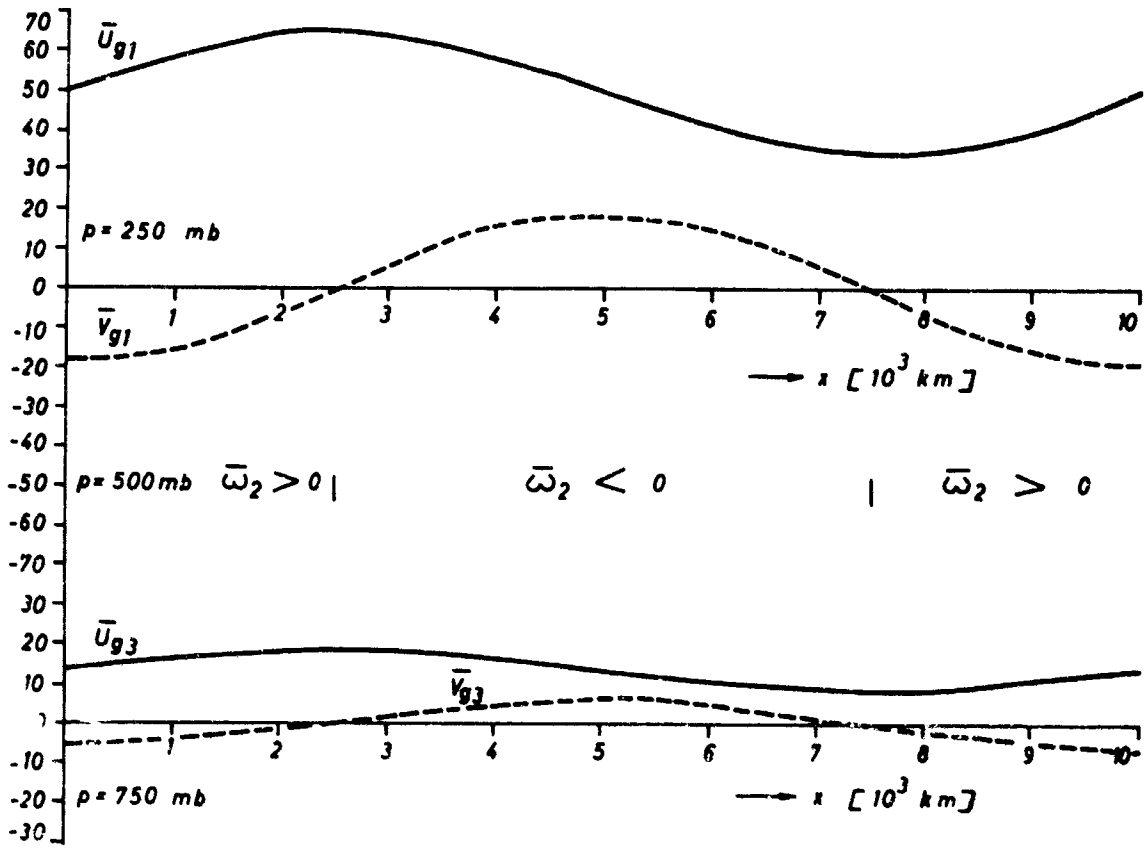

Fig.1. $\bar{u}_g$, $\bar{v}_g$ ($msec^{-1}$) corresponding to (3;1) in both of the pressure surfaces with p = 250 mb and p = 750 mb. $U_1 = 50$, $U_3 = 14$, $A_1 = 15$, $A_3 = 5$ msec^{-1}; L = 10^4 km ; y = $2\,10^3$ km.

$$\frac{\partial}{\partial t}\left(\frac{\partial^2 \Phi_{1,3}}{\partial x^2} \pm F(\Phi_3 - \Phi_1)\right) = -\left[(U_{1,3} + A_{1,3}\sin kx)\frac{\partial}{\partial x} - k A_{1,3}\cos kx - \Phi_{1,3}\frac{\partial}{\partial x} + \frac{\partial \Phi_{1,3}}{\partial x}\right]\frac{\partial^2 \Phi_{1,3}}{\partial x^2}$$

$$+ \Phi_{1,3} k^2 A_{1,3}\cos kx - \frac{\partial \Phi_{1,3}}{\partial y}(\beta + k^2 A_{1,3}\sin kx) \mp F\left[\left((U_2 + A_2\sin kx)\frac{\partial}{\partial x} - k A_2\cos kx - \frac{1}{a}(\Phi_1 + \Phi_3)\frac{\partial}{\partial x}\right.\right. \quad (4;1)$$

$$\left.\left. + \frac{1}{a}\frac{\partial}{\partial x}(\Phi_1 + \Phi_3)\right)(\Phi_3 - \Phi_1) + \frac{1}{2}(A_3 - A_1)(\Phi_1 + \Phi_3)\, k\cos kx - \frac{1}{a}\frac{\partial}{\partial x}(\Phi_1 + \Phi_3)(U_3 - U_1 + (A_3 - A_1)\sin kx)\right]$$

The x-derivations are replaced by the simplest difference-quotients. This transforms (4;1) to a system of linear equations for the 2N quantities $\Phi_{i,n}$.

$$(\Phi_{i,n-1} - 2\Phi_{i,n} + \Phi_{i,n+1})/D_x^2 \pm F(\Phi_{3,n} - \Phi_{1,n}) = RS_{i,n} \quad (4;2)$$

i = 1,3; n = 1,2,.....,N; N number of gridpoints in the x-direction; $D_x = L/N$. $\Phi_{i,n}$, $\Phi_{i,n}$ describes Φ, $\frac{\partial \Phi}{\partial t}$ at the gridpoint (n,i). The quantities $RS_{i,n}$ in (4;2) result from the right sides of (4;1) by applying the difference operators. For the point of time t = 0 one assumes a suitable with L periodic disturbance - i. e. $\Phi_{i,0} = \Phi_{i,N}$, $\Phi_{i,N+1} = \Phi_{i,1}$ - and determines the corresponding $RS_{i,n}$. Now $\Phi_{i,n}$ must result from (4;2).

Certain difficulties arise, however, by the boundary condition in the x-direction The solution is to be periodic with the interval L. Therefore one has to demand

$$\Phi_{i,0} = \Phi_{i,N};\ \Phi_{i,N+1} = \Phi_{i,1} \quad (4;3)$$

At such prescriptions the determinant of the system (4;2) is 0. This arises from taking into account of (4;3) the solution of (4;2) is determined except for one constant only.

In order to define unique the solution, the additional condition

$$\sum_{n=1}^{N}(\Phi_{3,n} + \Phi_{1,n}) = 0 \quad (4;4)$$

will be introduced [5]. One now omits in (4;2) an equation, perhaps the one for i = 3, n = N and replaces same with (4;4). It can then easily be shown that the solution of the newly developed system

$$(\Phi_{i,n-1} - 2\Phi_{in} + \Phi_{i,n+1})/Dx^2 \pm F(\Phi_{i2n} - \Phi_{i1n}) = RS_{in};\ (i,n) \neq (3,N)$$
$$\sum_{n=1}^{N} (\Phi_{i1n} + \Phi_{i3n}) = 0 \qquad (4;5)$$

is unique under consideration of (4;3) and solves (4;2) at all points [3]. Φ_{in} can now be obtained from (4;5) by inversion of the matrix.
For computing of Φ_{in} at the next point of time, $\frac{\partial \Phi}{\partial t}$ for t = 0 is being replaced by a forward, otherwise by a centered difference quotient. The time-step amounted to one hour. For the first three steps the values 1/8 h, 1/4 h, 1/2 h had been chosen.
The right-hand side of (4;5) can be split into three parts, case i = 3, n = N of course excluded,

$$RS_{in} = RSZ_{in} + RSM_{in} + RST_{in} \qquad (4;6)$$

Thereby RSZ_{in} be the part determined by the zonal vorticity-advection, RSM_{in} derives from the meridional vorticity-advection, and RST_{in} from the thermodynamic equation, thus from the temperature-advection. Therefore:

$$RSZ_{in} \approx RS_{in} = -\left[(u_i + A_i \sin kx)\frac{\partial}{\partial x} - \Phi_i \frac{\partial}{\partial x}\right]\frac{\partial^2 \Phi_i}{\partial x^2} + \Phi_i k^3 A_i \cos kx \qquad (4;7)$$

$$RSM_{in} \approx RSM_i = \left(k A_i \cos kx - \frac{\partial \Phi_i}{\partial x}\right)\frac{\partial^2 \Phi_i}{\partial x^2} - \frac{\partial \Phi_i}{\partial x}(\beta + k^2 A_i \sin kx) \qquad (4;8)$$

$$RST_{in} \approx RST_i = \mp F\Big[\Big((u_2 + A_2 \sin kx)\frac{\partial}{\partial x} - k A_2 \cos kx - \frac{1}{2}(\Phi_1 + \Phi_3)\frac{\partial}{\partial x} + \frac{1}{2}\frac{\partial}{\partial x}(\Phi_1 + \Phi_3)\Big)(\Phi_3 - \Phi_1)$$
$$+ \frac{1}{2}(\Phi_1 + \Phi_3)(A_3 - A_1)k \cos kx - \frac{1}{2}\frac{\partial}{\partial x}(\Phi_1 + \Phi_3)\left(U_3 - U_1 + (A_3 + A_1)\sin kx\right)\Big] \qquad (4;9)$$

For reasons of clearness the right-hand sides have been written in a non-discretised form.
As (4;5) is linear in Φ_{in}, the contribution added to the solution by each summand of (4;6) can be determined; accordingly the solution is composed by three parts.

$$\Phi_{in} = \Phi_{zin} + \Phi_{min} + \Phi_{rin} \qquad (4;10)$$

Thereby Φ_{zin} solves the equations

$$(\Phi_{z,i,n-1} - 2\Phi_{zin} + \Phi_{z,i,n+1})/Dx^2 \pm F(\Phi_{z,3,n} - \Phi_{z,1,n}) = RSZ_{in};\ (i,n) \neq (3,N) \qquad (4;11)$$
$$\sum_{n=1}^{N} (\Phi_{z,1,n} + \Phi_{z,3,n}) = 0$$

Analogical Φ_{min} and Φ_{rin}. Such splitting can be carried out at various points of time. It gives an idea of the coordination of the various advections and of the mechanism of the development of the cyclones.

5. Results

The process of development of a constellation is to be discussed closer, i.e. for a basic flow with the data $A_1 = 9$, $A_3 = 3$, $U_1 = 50$, $U_3 = 14$ msec^{-1}, $L = 10^4$ km, N = 20 and for a disturbance

$$\Phi_i = S \sin 2kx \qquad (5;1)$$

with $S = 5\ m^2 sec^{-1}$ for t = 0. S does not depend on p, thus the disturbance initially corresponds to a barotropic wave.
At the time t = 0 we have the stream-function

$$\psi_i = -y(u_i + A_i \sin kx - S \sin 2kx) \qquad (5;2)$$

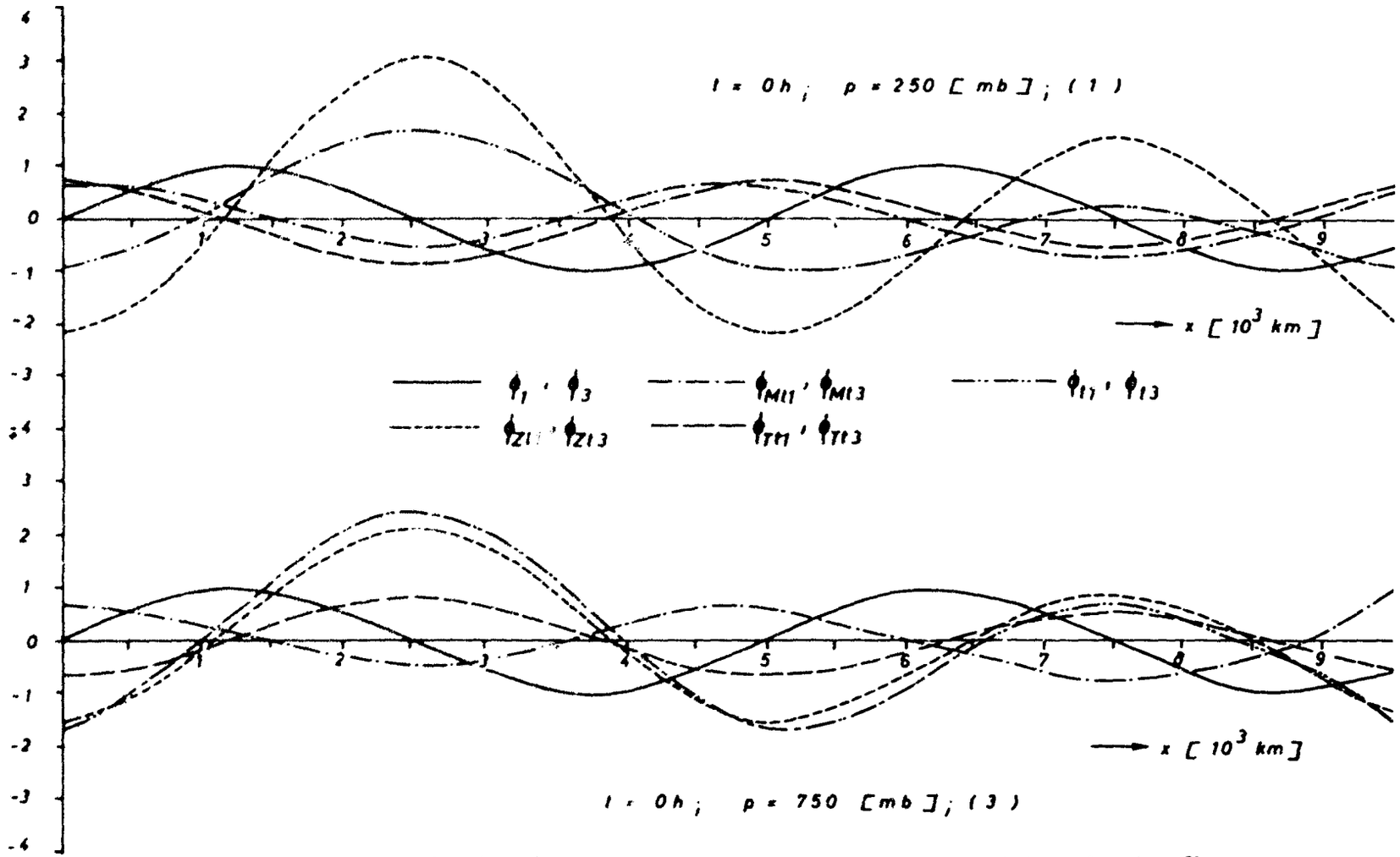

Fig.2. Φ , Φ_h , Φ_w , Φ_{Tr} , Φ_{Tt} in both of the pressure surfaces at the time t = 0h. The Φ-wave is related to a initial value 1. The other waves have an arbitrary scale.

[illegible] the [illegible] the [illegible] the [

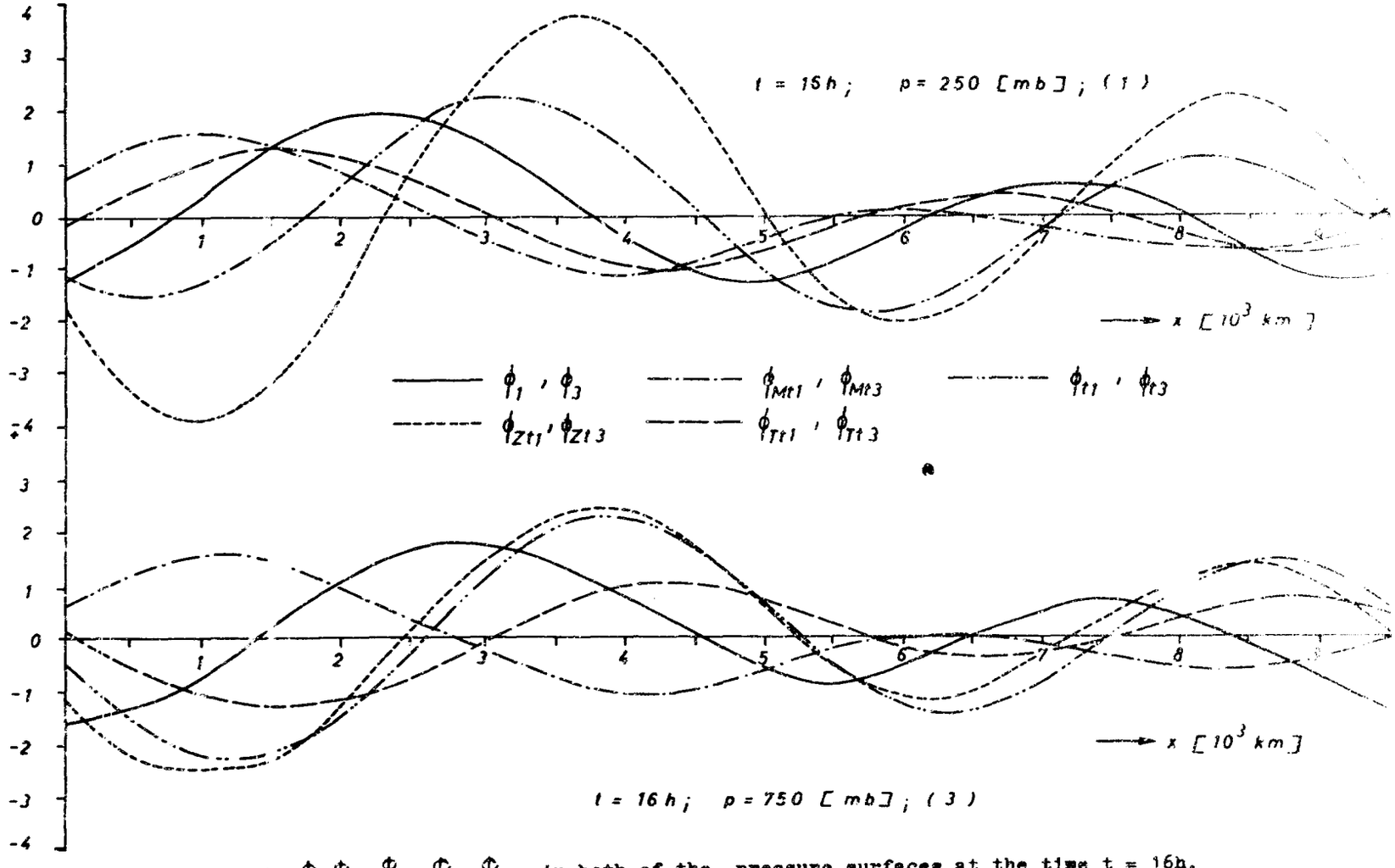

Fig.3. Φ , Φ_t , Φ_{Zt} , Φ_{Mt} , Φ_{Tt} in both of the pressure surfaces at the time t = 16h. The Φ -wave is related to a initialvalue 1. The other waves have an arbitrary scale.

4													
5	5	49	22										
6	5	49	22	15	5	1.9	1.7	-0.9	-0.6	0.5	0.6	-1.6	-1.7
7	5	β/k^2	β/k^2	5	5	1.5	1.3	-0.7	-0.7	0.7	0.7	-1.3	-1.3
8	5	β/k^2	β/k^2	15	15	1.9	1.9	0.0	0.0	0.4	0.4	-2.0	-2.0
9	1	50	14	15	5	2.8	2.4	-1.1	-0.4	-0.1	0.2	-2.0	-2.1
10	10	50	14	15	5	2.2	2.0	-1.5	-0.9	0.5	0.5	-1.4	-1.7
11	5	50	14	15	5	3.6	2.9	-2.5	-1.7	0.2	0.2	-1.7	-1.8
12	5	50	14	15	5	1.4	1.4	-0.2	0.1	0.2	0.6	-1.3	-1.7
13	-5	50	14	15	5	-3.7	-3.0	0.9	1.0	0.6	0.1	2.7	2.7
14	-10	50	14	15	5	-4.8	-4.0	---	---	---	---	3.8	3.4
15	5	50	11	15	5	1.9	1.7	-0.7	-0.3	0.1	0.4	-1.4	-1.7 (2δ)
16	5	49	15	15	5	3.0	2.6	-1.8	-1.3	0.3	0.3	-1.9	-2.0 (δ/2)
17	5	52	8	15	5	2.1	2.0	-0.8	-0.3	-0.1	0.3	-1.6	-1.9 L = 8
18	5	71	21	15	5	3.0	2.4	-1.8	-1.4	0.6	0.6	-2.0	-2.0 L = 12

Tab.2. Amplitudes of the short-wave perturbations after 16 hrs in surfaces (1) and (3) referring to an initial value of 1.0 , L - 10^4km.

The term $\pm F(\Phi_{zc_{(3)}} - \Phi_{zc_{(1)}})$ in the system of equations (4;11) for Φ_{zc} is responsible for these phase shifts. It represents the influence of divergence and vertical motion. [3]

It is particularly striking, that Φ_{Mc} is exclusively negative between $x = 3 \cdot 10^3$ and $x = 9 \cdot 10^3$. Therefore the meridional vorticity-advection in this section is continuously positive.

Summing-up the following is the normal behaviour of the various waves in the pressure-centers:

Because of its phase lead the Φ_{zc} -wave gives in (1) always a minor development-contribution than in (3) or damps stronger. It is just the opposite with Φ_{Mc} . Φ_{Tc} favours always in (1) and permanently hinders in (3).

H_1 certifies this scheme. Carriers of development in (1) are Φ_{Mc} and Φ_{Tc} . Φ_{zc} is not contributing. In (1) the contributions of Φ_{Mc} and Φ_{Tc} are largely cancelled, and Φ_c nearly coincides with Φ_{zc} . A similar distribution is being ascertained in T_1 ; however, the contribution of Φ_{zc} in (3) is, the same as before, rather slight, although negative, and in (1) always still positive. Striking is the change of sign of Φ_{Mc} since $t = 0$, which enables a deepening in both layers.

The positive meridional vorticity-advection in the section $3 < x < 9\ 10^3$ effects in particular H_2. Whilst Φ_{zc} is showing approximately the same position as at H_1 in relation to the pressure-centers, even though with by far a petty amount, and Φ_{Tc} having influence only in (1), Φ_{Mc} is damping in both surfaces, and is thus responsible for the permanent decrease of H_2 . T_2 again shows the normal distribution.

Altogether the following results:

H_1 in the trough, which is a zone of high baroclinicity, develops quickly. T_1 drifting out of this zone, is initially being filled up and deepens only after tilting of the axis has been carried out. H_2 in the ridge - an area of minor baroclinicity - is being decreased, mainly due to strong positive meridional vorticity-advection. T_2 experiences a fast deepening.

It is left to examine whether and how these models of behaviour change at the variation of several parameters. Results can be read from Tab.2.

If one enlarges A_1 and A_3, whereby U_1 and A_1/A_3 are remaining constant (Nos.1-4), H_1 and T_2 are becoming strengthened, H_2 is being quicker decreased. T_1, however, shows little impression. According to (5;3) and (1;4) this behaviour of H_1, H_2, T_2, can already be explained by a barotropic model: Increase of A_1 leads in the 500-mb-surface to a corresponding strengthened tendency. The Nos.7-8 are proving this.

The gradual deepening of T_1 is, however, not explainable by the initial situation. In pure barotropic basic states ($U_1 = \beta/k^2$) T_1 is being filled up (Nos.7-8). Nos.1-6 do not allow a distinguishing of a clear connection between the parameters and the behaviour of T_1.

Tilting forward the axes at $t = 0$ damps (No.12) compared with No.3, tilting backwards furthers all disturbances (No.11) with the exception of H_2. The influence of the nonlinear terms in the equations (3;3) can be studied at the Nos.3,9,10,13, and 14. Because of a change of the amplitude or a change of the sign at the initial perturbation, can only take effect via the nonlinear terms. The nonlinear interactions obviously support the formation of a strong low in the long-wave trough and

[illegible] ... [illegible] ... [illegible] ... [

MODELE AERO (HYDRO) DYNAMIQUE

POUR LE CALCUL DU REGIME DES ONDES DE RELIEF

par

Radyadour ZEYTOUNIAN

O.N.E.R.A. (92 - CHATILLON - France)

*Ingénieur de Recherches à la Direction de l'Aérodynamique.
Docteur ès-Sciences.

S O M M A I R E

Partant des équations simplifiées de la théorie de la convection (BOUSSINESQ) , on construit différents modèles théoriques susceptibles d'être employés pour l'étude de certaines des particularités des phénomènes dus à l'action dynamique du relief dans une atmosphère barocline en dehors de tout effet de couches limites. Certains résultats des calculs sont exposés : en particulier en théorie non linéaire, les calculs montrent qu'il s'établit en aval des obstacles, un régime de rotors (lignes de courant fermées) qui conduit dans bien des cas à une configuration analogue à celle de l'allée tourbillonnaire de von KARMAN. Ce régime de rotors étant caractérisé par une forte turbulence est responsable dans une grande mesure du phénomène de turbulence en ciel clair.

S U M M A R Y

AERO (HYDRO)DYNAMIC MODEL FOR CALCULATING RELIEF WAVES

Based on the simplified equations of the convection theory (BOUSSINESQ), various theoretical models are built that may be used for studying some peculiarities of the phenomena due to the dynamic action of the relief in a barocline atmosphere, any boundary layer effect being ignored. Some results of the calculation are presented : in particular in non-linear theory, the calculations show that dowstream of obstacles a vortex regime (closed streamlines) is established, which leads in many cases to a configuration similar to that of the von KARMAN vortex street. This vortex regime, characterized by a strong turbulence, is responsible, for a great part, for the clear-air turbulence phenomenon.

L'objet de cette étude est de montrer comment l'on peut, à partir des équations de la Mécanique des Fluides, construire des modèles mathématiques reflétant, pour des conditions aux limites adéquates, les principales particularités des phénomènes d'ondes dus à l'action d'un obstacle dans un écoulement stratifié.

L'écoulement étant stationnaire et le fluide non visqueux nous nous intéresserons uniquement à l'étude de l'action dynamique de l'obstacle sur l'écoulement en dehors de tout effet de couches limites. On expose tout d'abord une méthode effective de calcul de l'écoulement plan non linéaire au-dessus et en aval d'un obstacle placé dans un canal de hauteur H. Ensuite, on étudie l'action dynamique d'un obstacle (relief), dans l'espace à trois dimensions sur une masse d'air stratifiée, dans le cadre d'une théorie linéaire. Certains résultats des calculs effectués sont exposés à la fin de cette étude.

On trouvera une synthèse des développements théoriques sur les ondes de relief dans les Mémoires de J.W. MILES [1], R. QUENEY et al. [2], I.A. KIBEL [3] ainsi que dans notre Etude [4] ; on pourra aussi consulter le Mémoire [5] consacré à la prévision à l'échelle locale. Enfin, on trouvera une abondante documentation sur les problèmes de l'écoulement des fluides stratifiés (principalement celle concernant les études faites en Union Soviétique) dans notre cours de l'Ecole de la Météorologie de PARIS [6].

GENERALITES

Les phénomènes de frottement et d'échanges de chaleur sont négligés, mais la force répartie agissant sur le fluide et provenant de l'action de la pesanteur d'intensité g est prise en compte. Le vecteur unitaire $\vec{k}$ étant vertical ascendant et le fluide incompressible* mais stratifié, les équations du mouvement quand on néglige la force de CORIOLIS s'écrivant, pour un écoulement stationnaire

$$(1)\qquad \begin{cases} \nabla \dfrac{V^2}{2} - \vec{V} \wedge (\nabla \wedge \vec{V}) = -\dfrac{1}{\rho} \nabla p - g\vec{k} \ ; \\ \vec{V} \cdot \nabla \rho = 0 \iff \nabla \vec{V} = 0 \ , \end{cases}$$

avec

$$\nabla = \frac{\partial}{\partial x}\vec{\imath} + \frac{\partial}{\partial y}\vec{\jmath} + \frac{\partial}{\partial z}\vec{k} \ , \quad \vec{V} = u\vec{\imath} + v\vec{\jmath} + w\vec{k} \ ;$$

on satisfait l'équation de continuité en posant

$$(2)\qquad \vec{V} = \nabla\psi \wedge \nabla\chi \ ,$$

les deux fonctions de courant ψ et χ constituant la généralisation de la fonction de courant plan de STOKES.

Alors

$$\vec{V} \cdot \nabla \rho = 0 \implies \rho = \rho(\psi, \chi)$$

et l'une des intégrales de l'équation du mouvement est l'équation de BERNOULLI

$$(3)\qquad \frac{V^2}{2} + \frac{p}{\rho} + gz = J(\psi, \chi) \ ,$$

les fonctions $\rho(\psi,\chi)$ et $J(\psi,\chi)$ étant conservative le long de chaque ligne de courant.

---

* Les équations (1) peuvent être interprétées comme les équations d'un mouvement incompressible pour lequel $\nabla \vec{V} = 0$ mais $\rho \neq$ cte ; l'incompressibilité du mouvement étant une conséquence des propriétés cinématiques du mouvement et non pas des propriétés physiques du fluide.

Les deux autres intégrales premières du système d'Helmholtz se mettent sous la forme suivante [4] :

$$(4)\qquad \begin{cases} (\nabla\wedge\vec{V})\cdot\nabla\psi = \dfrac{\partial J}{\partial\chi} + \dfrac{P}{\rho^2}\dfrac{\partial\rho}{\partial\chi}\,; \\ (\nabla\wedge\vec{V})\cdot\nabla\chi = -\dfrac{\partial J}{\partial\psi} - \dfrac{P}{\rho^2}\dfrac{\partial\rho}{\partial\psi}\,. \end{cases}$$

soit

$$z = h(x,y)$$

l'équation de la paroi de l'obstacle (relief) ; nous ferons par la suite deux hypothèses :

1° - les conditions aux limites par rapport à Z seront prises sous la forme :

$$(5)\qquad \begin{cases} w = u\dfrac{\partial h}{\partial x} + v\dfrac{\partial h}{\partial y}\,, & \text{pour} \quad z = h(x,y) \\ w = 0\,, & \text{pour} \quad z = H = C^{te} \end{cases}$$

2° - à l'infini amont, loin de l'obstacle, l'écoulement non perturbé est bidimensionnel (dans le plan des x , z) et fonction uniquement de l'altitude : notée z_∞ à l'infini amont ; soit $\vec{u}_\infty = U_\infty(z_\infty)\vec{\imath}$ la vitesse loin en amont de l'obstacle, nous écrirons que

$$(6)\qquad u = U_\infty(z_\infty),\ v = w = h = 0, \qquad \text{pour} \quad x \to -\infty\,.$$

Sous ces hypothèses on obtient à partir des relations (4) le système d'équations

$$(7)\qquad \begin{cases} \nabla\wedge(\nabla\psi\wedge\nabla\chi)\cdot\nabla\psi = 0\,; \\ \nabla\wedge(\nabla\cdot\vec{r}\wedge\nabla\chi)\cdot\nabla\chi = \dfrac{1}{\rho}\dfrac{d\rho}{d\psi}\,\dfrac{(\nabla\psi\wedge\nabla\chi)^2}{2} \\ \qquad\qquad - U_\infty\dfrac{dU_\infty}{d\psi} - \dfrac{1}{\rho}\dfrac{d\rho}{d\psi}\left[\dfrac{U_\infty^2}{2} + g(z - z_\infty)\right], \\ \rho = \rho(\psi)\,. \end{cases}$$

Le système d'équations (7) généralise au cas des écoulements tridimensionnels l'équation, devenue classique de LONG, obtenue pour la fonction de courant plan d'un écoulement bidimensionnel [7] . Notons que DRAKIN dans l'étude [8] a obtenu une généralisation de l'équation de LONG au cas tridimensionnel sans faire intervenir les fonctions de courant spatiales.

Maintenant si on fait l'approximation de BOUSSINESQ, qui consiste à négliger les dérivées de $\rho(\psi)$ sauf lorsqu'elles interviennent dans le calcul de la force d'Archimède, on pourra énoncer la Proposition suivante :

<u>L'INFLUENCE DYNAMIQUE D'UN OBSTACLE, PLACE DANS UN CANAL DE HAUTEUR H, SUR UN ECOULEMENT DE VITESSE UNIFORME $U_\infty = C^{te}$, STRATIFIE SELON UNE LOI EXPONENTIELLE DECROISSANTE</u>

$$\rho(z_\infty) = \rho_0 \exp(-\beta z_\infty)$$

À L'ORDRE ZÉRO, PEUT ÊTRE CONVENABLEMENT REPRÉSENTÉE EN PREMIÈRE APPROXIMATION PAR LES ÉQUATIONS *

$$\nabla \wedge (\nabla \psi \wedge \nabla \chi) \cdot \nabla \psi = 0$$

$$\nabla \wedge (\nabla \psi \wedge \nabla \chi) \cdot \nabla \chi + \mathcal{D}(\psi + \zeta) = 0 \qquad (8)$$

LES DEUX FONCTIONS ψ ET χ ÉTANT LIÉES AVEC LA VITESSE DE L'ÉCOULEMENT PERTURBÉ PAR LA RELATION (2).

L'une des conditions aux limites pour le système (8) sera

$$\psi = 0 \quad ; \quad \text{pour} \quad \zeta = \bar{h}(\xi,\eta) \equiv \frac{h(\xi'',\eta'')}{H} \qquad (9\,a)$$

et une autre

$$\psi + 1 = 0 \quad , \quad \text{pour} \quad \zeta = 1 \qquad (9\,b)$$

ECOULEMENT PLAN

Dans ce cas le problème se ramène à la recherche d'une solution pour la fonction de courant $\psi_p(\xi,\zeta)$ satisfaisant à l'équation d'HELMOUTZ * (qui découle du système (8) en posant $\psi \equiv \psi_p$ et $\chi \equiv y$).

$$\left(\frac{\partial^2}{\partial \xi^2} + \frac{\partial^2}{\partial \zeta^2} + \mathcal{D} \right) \psi_p = -\mathcal{D}\zeta \qquad (9)$$

et aux conditions aux limites :

$$\begin{cases} \psi_p = 0 \ , \ \text{pour} \ \zeta = \bar{h}_p(\xi) ; \ \psi_p + 1 = 0 , \quad \zeta = 1 ; \\ \psi_p \to -\zeta , \ \text{pour} \ \xi \to -\infty \ ; \\ \psi_p \ : \ \text{uniformément bornée pour} \ \xi \to +\infty . \end{cases} \qquad (10)$$

---

* Ces équations sont écrites sous forme adimensionnelles, pour $\psi / U_0 H$ χ/H ; $\xi = \frac{x}{H}$; $\eta = \frac{y}{H}$, $\zeta = \frac{z}{H}$; $\nabla = \partial/\partial\xi\, \vec{\imath} + \partial/\partial\eta\, \vec{\jmath} + \partial/\partial\zeta\, \vec{k}$; $\mathcal{D} = \beta H^2 g/(U_0)^2$. Les équations (8) sont obtenues à partir des équations (7) en faisant un développement asymptotique par rapport au paramètre $\lambda = H\beta/\alpha$ et en négligeant les termes d'ordres supérieurs.

** Le paramètre $\mathcal{D}$ est lié au nombre de FROUDE : $FR = \frac{U_0}{\sqrt{gH}}$ par la relation $\mathcal{D} = \frac{\lambda}{FR^2}$.

Pour résoudre ce problème [4] on introduit la nouvelle variable

$$(11) \qquad S = \frac{\zeta - \delta(\xi)}{1 - \delta(\xi)} \qquad \text{avec} \qquad \delta(\xi) \equiv \overline{h}_p(\xi)$$

et on obtient à partir de l'équation (9), pour la fonction

$$\overline{\psi}(\xi, S) = -\psi_p\{\xi, \delta + (1-\delta)S\}$$

une équation aux dérivées partielles que l'on écrit sous forme de divergence ; cette équation étant résolue avec des conditions aux limites homogènes écrites en $S = 0$ et $S = 1$. Pour résoudre ce nouveau problème, pour la fonction $\overline{\psi}(\xi,S)$, on applique la méthode des relations intégrales de DORODNITSYN [9] ; un critère relativement simple permet ensuite de filtrer avec une bonne exactitude les solutions parasites du problème provenant de la transformation des conditions asymptotiques en ξ (pour $-\infty$ et $+\infty$) en conditions aux limites classiques en deux points (en ξ_0 et ξ_N, se trouvant respectivement suffisamment loin en amont et en aval de l'obstacle) [10]. La méthode de calcul élaborée permet alors d'obtenir pour un profil plan donné arbitraire la configuration de l'écoulement dans le canal de hauteur H au-dessus et en aval de l'obstacle en fonction du paramètre $\mathcal{F}$.

Certains résultats des calculs effectués sont exposés sur les figures 1 - 3. La figure 1 nous donne l'écoulement au-dessus et en aval d'un obstacle isolé type, calculé théoriquement pour $\mathcal{F} = 25$; on obtient comme on le voit en aval de cet obstacle un régime de rotore pendant lequel des remous tourbillonnaires sont lachés périodiquement par la crête de l'obstacle, ce qui conduit à une configuration analogue à celle de l'allée tourbillonnaire de von KARMAN. La figure 2 représente l'écoulement en aval d'un obstacle asymétrique ; nous avons mis en rapport le résultat obtenu par nous même b) avec celui de LONG obtenu analytiquement en [7]. On voit sur cet exemple que déjà le modèle avec un seul niveau intermédiaire (pendant le calcul selon la méthode des relations intégrales) donne une approximation satisfaisante de la solution exacte de LONG obtenue à partir d'une solution linéaire écrite pour un autre obstacle (qui,lui, est symétrique et n'a rien de commun avec l'obstacle de la figure 2).

Enfin, sur les figures 3 nous avons représenté le calcul a) b) c) des ondes de relief se formant au-dessus de la SIERRA-NEVADA pour différentes valeurs du paramètre $\mathcal{F}$ et aussi, en vue de les comparer avec des écoulements réels, des écoulements d) et e) construit à partir des données d'observations [11]. On remarquera que les valeurs de $\mathcal{F}$ dans les écoulements correspondants sont différents ; cela est dû, en partie aux différences de profil de vitesse à l'infini amont et aussi au fait que nos modèles théoriques délimitent l'écoulement par une surface plane solide.

ECOULEMENTS TRIDIMENSIONNELS LINEAIRES

Comme le montrent les calculs précédents, la description des ondes de relief engendrées par des chaînes de montagnes telles que la SIERRA-NEVADA peut-être faite d'une manière satisfaisante par un modèle bidimensionnel. Cependant ces modèles deviennent insuffisants si l'on veut étudier les ondes de relief créées par des montagnes isolées ; dans ce cas le facteur prédominant qui intervient dans un modèle tridimensionnel est dû au fait que le fluide a la possibilité de contourner et non plus uniquement de franchir la montagne, cette possibilité de contournement étant dans certains cas plus significative.

Le système (8) est non linéaire, pour linéariser ce système introduisons les perturbations des fonctions de courant : ψ' et χ' . Remarquons tout d'abord qu'à l'infini amont nous n'avons que

$$(12) \qquad \psi_\infty = z \qquad , \chi_\infty = V_\infty x - U_\infty y$$

le mouvement non perturbé à l'infini amont ayant une vitesse

$$\vec{V}_\infty(z) = U_\infty \vec{\imath} + V_\infty \vec{\jmath}$$

Donc nous écrivons,

$$(13) \qquad \psi = z + \psi' \qquad , \chi = V_\infty x - U_\infty y + \chi'$$

Il ne reste plus qu'à linéariser les équations (8) ; des deux équations obtenues, linéaires en ψ' et χ' on construit facilement une seule équation pour ψ' et la relation

$$w' = -U_\infty \frac{\partial \psi'}{\partial x} - V_\infty \frac{\partial \psi'}{\partial y} \tag{14}$$

qui découle de (2), après linéarisation, nous donne une équation pour $\omega = w'/U_\infty^0$ où U_∞^0 une vitesse constante caractéristique pour notre écoulement ; cette équation s'écrit sous la forme [4] :

$$\begin{aligned} &\left(U_\infty \frac{\partial}{\partial \xi} + V_\infty \frac{\partial}{\partial \eta}\right)^2 \left[\frac{\partial^2 \omega}{\partial \xi^2} + \frac{\partial^2 \omega}{\partial \eta^2} + \frac{\partial^2 \omega}{\partial \zeta^2}\right] \\ &\quad + \mathcal{D}\left(\frac{\partial^2 \omega}{\partial \xi^2} + \frac{\partial^2 \omega}{\partial \eta^2}\right) \\ &\quad - \left(U_\infty \frac{\partial}{\partial \xi} + V_\infty \frac{\partial}{\partial \eta}\right)\left[\frac{d^2 U_\infty}{d\zeta^2} \frac{\partial \omega}{\partial \xi} + \frac{d^2 V_\infty}{d\zeta^2} \frac{\partial \omega}{\partial \eta}\right] = 0 \end{aligned} \tag{15}$$

Une fois que l'on a calculé ω, c'est-à-dire w' il est facile de déterminer ψ' puis χ'.

En supposant $h = h'$ comme étant petit (théorie linéaire) on écrit les conditions aux limites, associées, à l'équation (15), sous la forme :

$$\begin{cases} \zeta = 0 \ , & \omega = U_\infty \dfrac{\partial h'}{\partial \xi} + V_\infty \dfrac{\partial h'}{\partial \eta} \ ; \\ \zeta = 1 \ , & \omega = 0 \ ; \\ \xi = -\infty \text{ et } \eta \text{ quelconque} & \Longrightarrow \omega = \dfrac{\partial \omega}{\partial \xi} = \dfrac{\partial^2 \omega}{\partial \xi^2} = \dfrac{\partial^3 \omega}{\partial \xi^3} = 0. \end{cases} \tag{16 a}$$

Par rapport à η, les conditions aux limites seront prises de telle façon que certaines conditions de convergence soient satisfaites ; par exemple si on représente la solution sous la forme d'une intégrale de FOURRIER

$$\omega(\xi, \eta, \zeta) = \int_{-\infty}^{+\infty} \omega^m(\xi, \zeta) \exp(im\eta)\, dm$$

alors on devra prendre que

$$|\eta| \to \infty \ , \quad \omega = \frac{\partial \omega}{\partial \eta} \to 0 \ . \tag{16 b}$$

Dans le cas le plus général les solutions de l'équation (15) avec les conditions aux limites (16 a) sont fonction du paramètre $\mathcal{D}$ et des deux paramètres [4] :

$$\begin{cases} \mathcal{A}(\zeta) = \left(\dfrac{d\alpha_\infty}{d\zeta}\right)^2 - \dfrac{1}{G_\infty} \dfrac{d^2 G_\infty}{d\zeta} \ , \\ \mathcal{B}(\zeta) = \dfrac{d^2 \alpha_\infty}{d\zeta^2} + 2 \dfrac{1}{G_\infty} \dfrac{dG_\infty}{d\zeta} \dfrac{d\alpha_\infty}{d\zeta} \ , \end{cases} \tag{17}$$

où

$$G_\infty(\zeta) = U_\infty^0 \sqrt{U_\infty^2 + V_\infty^2} \ , \quad \operatorname{tg} \alpha_\infty(\zeta) = \frac{V_\infty}{U_\infty} \ .$$

Dans un cas simple, quand $U_p = U_p^0$ et $V_p \simeq 0$ on écrit une solution explicite facile à mettre en oeuvre. Il est préférable d'appliquer tout abord cette solution pour un obstacle simple, puis en les combinant d'une manière judicieuse (rappelons que nous traitons ici un problème linéaire) obtenir la solution plus générale pour un relief plus complexe. Nous exposons ici certains calculs, effectués dernièrement par M. TROCHU*, qui avait pour but de calculer le champ des vitesses verticales, dans des plans ζ = const, au dessus du Bassin d'ARCACHON et de la région du CANTAL (MASSIF CENTRAL).

Pour le calcul des zones de précipitations (qui sont, en général, en bonne corrélation avec les zones où $w' > 0$) au-dessus du Bassin d'ARCACHON, figures 4 - 6, nous avons représenté la côte sous forme d'une somme algébrique de relief simple type en paraboloïde de révolution ; notons que la côte, qui sépare la mer de la terre, joue le rôle d'un obstacle du fait de la différence de rugosité de la terre par rapport à celle de la mer (cela est équivalent à l'introduction d'obstacle ayant une hauteur fictive, liée aux effets de couches limites). Une fois la côte représentée par une telle somme, nous avons calculé l'influence de chaque paraboloïde en chaque point du Bassin d'ARCACHON et avons fait la somme de ces influences ; ce calcul a été fait pour δ moyen = δ positif et négatif (en fonction de la stratification de masse d'air à l'infini amont), mais pour une même direction du vent de base $(\alpha_p)_{moyen} = 240°$ (voir les figures 4 et 5) ; sur la figure 6 on a mis en évidence l'influence de la direction du vent de base sur la répartition des zones pluvieuses ($\alpha = 270°$ et $\delta > 0$).

Dans le cas du calcul sur le CANTAL (figure 7) le relief de la région a été représenté au moyen de relief simple avec des hauteurs et des étendues variables, de telle façon que la nature du relief sur cette région soit représentée le mieux possible ; une analyse fine a permis de constater que ces calculs reflétaient d'une manière satisfaisante la mésostructure des précipitations sur cette région.

CONCLUSION

D'une manière générale les résultats obtenus sont encourageants et montrent que les modèles hydrodynamiques qui sont à leur base sont, dans beaucoup de cas, valables du point de vue physique ; en particulier, on reste convaincu de la valeur physique des ondes transversales au courant de base (voir figures 4 et 7) mises en évidence quand $\delta > 0$ soit dans le cas avec orographie, soit dans le cas du littoral par l'introduction d'une convection artificielle due au contraste de rugosité. Quand $\delta < 0$, le facteur relief seul perd de son intérêt dans le cas de l'instabilité vis-à-vis des facteurs thermiques qui conditionnent alors l'ampleur de la convection.

Enfin, notons que, en adoptant, ici, dès le départ un point de vue assez général, nous avons la possibilité d'unifier dans un seul et même formalisme la plupart des cas particuliers qui peuvent se présenter dans les problèmes d'ondes de gravité internes.

REFERENCES

[1] J.W. MILES

Synthèse des développements théoriques sur les ondes de reliefs.

Conférence générale, 12ème Congrès International de Mécanique Appliquée.
STANFORD, California U.S.A., août 1968

[2] P. QUENEY et al.

The airflow over mountains, GENEVA, World Meteorological organisation.

Techn. Note 34 - 1960.

[3] I.A. KIBEL

Short-range weather forecasting as a hydrodynamic problem.

Proc. of the XI Intern. Cong. of Appl. Mech. MUNICH (Germany) 1964
Ed. H. GORTLER Springer Verlag BERLIN pp. 779-89 (1966).

---

* Au cours de son stage d'Elève-Ingénieur à l'Ecole de la Météorologie de PARIS (années 1966 - 1967)

[4] R. Kh. ZEYTOUNIAN

Etude des problèmes d'ondes dans les écoulements stationnaires d'un fluide stratifié non visqueux.

Publication O.N.E.R.A. n° 126 - 1969.

[5] J. BLANCHET, C. FONS et R. Kh. ZEYTOUNIAN

La prévision à l'échelle locale.

La Météorologie n° 1 - 3, 1967.

[6] R. Kh. ZEYTOUNIAN

Etude hydrodynamique des phénomènes mésométéorologiques.

Ecole de la Météorologie, Ed. de la Direction de la Météorologie Nationale de PARIS, 1968, 163 pages et 51 figures.

[7] R. LONG

Some aspects of the flow of stratified fluids.

III - Continuous density gradients.

Tellu, 7, N° 3 (1955).

[8] P.G. DRAZIN

On the steady of a fluid of variable density past an obstacle.

Tellus V, 13, n° 2, 1961.

[9] A.A. DORODNITSYN

On a method of numerical solution of certain non linear problem in aero-hydrodynamics.

Proceed. 3 rd All. Union Math. Congr. MOSCOU, 1956 - PART. III pp. 447-53. Akad. Nauk SSSR (1958)

[10] R. Kh. ZEYTOUNIAN

On a criterion for filtering parasite solutions in a numerical computation.

Com. to the Intern. Symps. on High-Speed computing in fluid dynamics, MONTEREY, California, 19 - 24 August 1968.

[11] R.R. LONG

A Laboratory Model of airflow over the SIERRA NEVADA mountains.

The Rossby Memorial Volume, ROCKEFELLER, Institute Press. - NEW-YORK, 1959

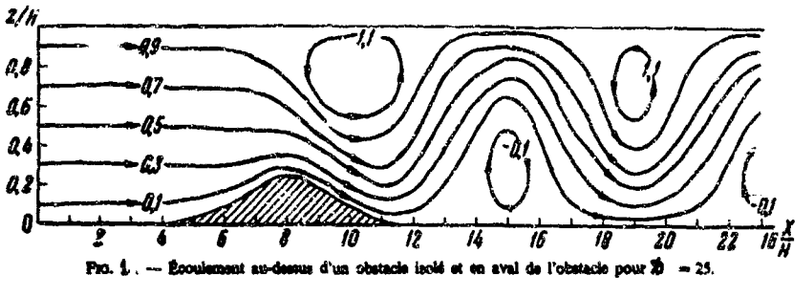

Fig. 1. — Écoulement au-dessus d'un obstacle isolé et en aval de l'obstacle pour D = 25.

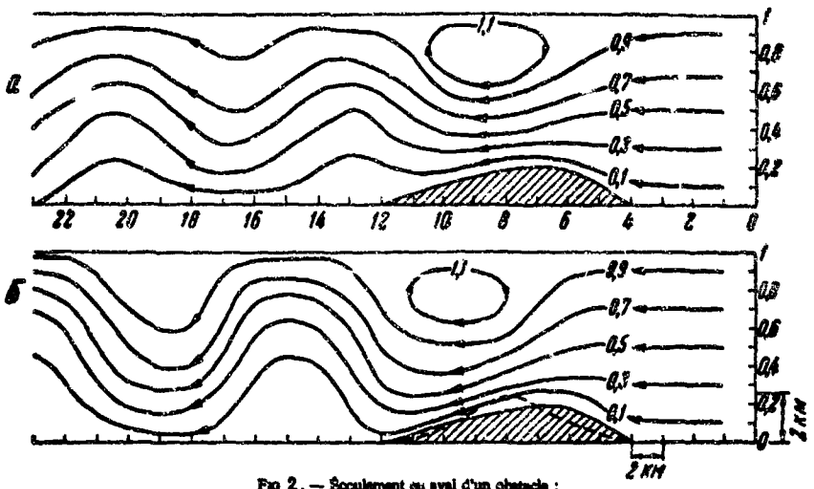

Fig. 2. — Écoulement au aval d'un obstacle :
a) d'après l'étude (de Long R. D = 24); *b*) d'après le modèle de cette étude(D = 24).

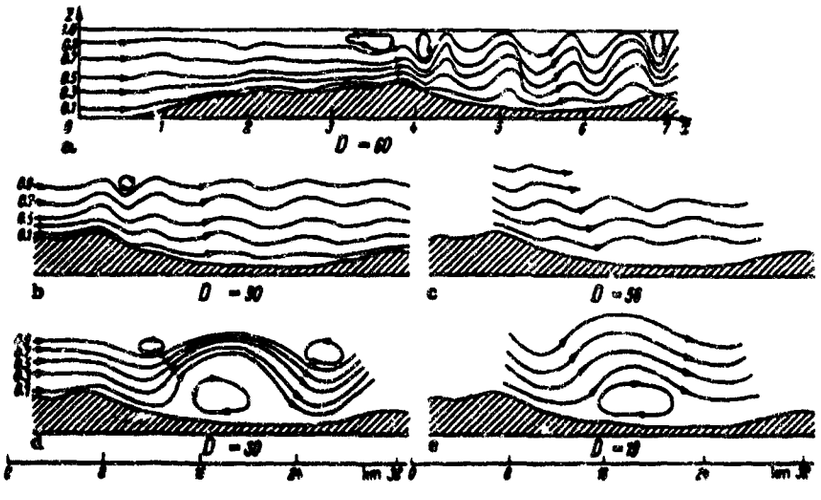

Fig. 3. — Écoulements au-dessus de la Sierra-Nevada
a) Calcul pour D = 60.
b) Calcul pour D = 90.
c) D'après les observations quand D = 56.
d) Calcul pour D = 30.
e) D'après les observations quand D = 19.

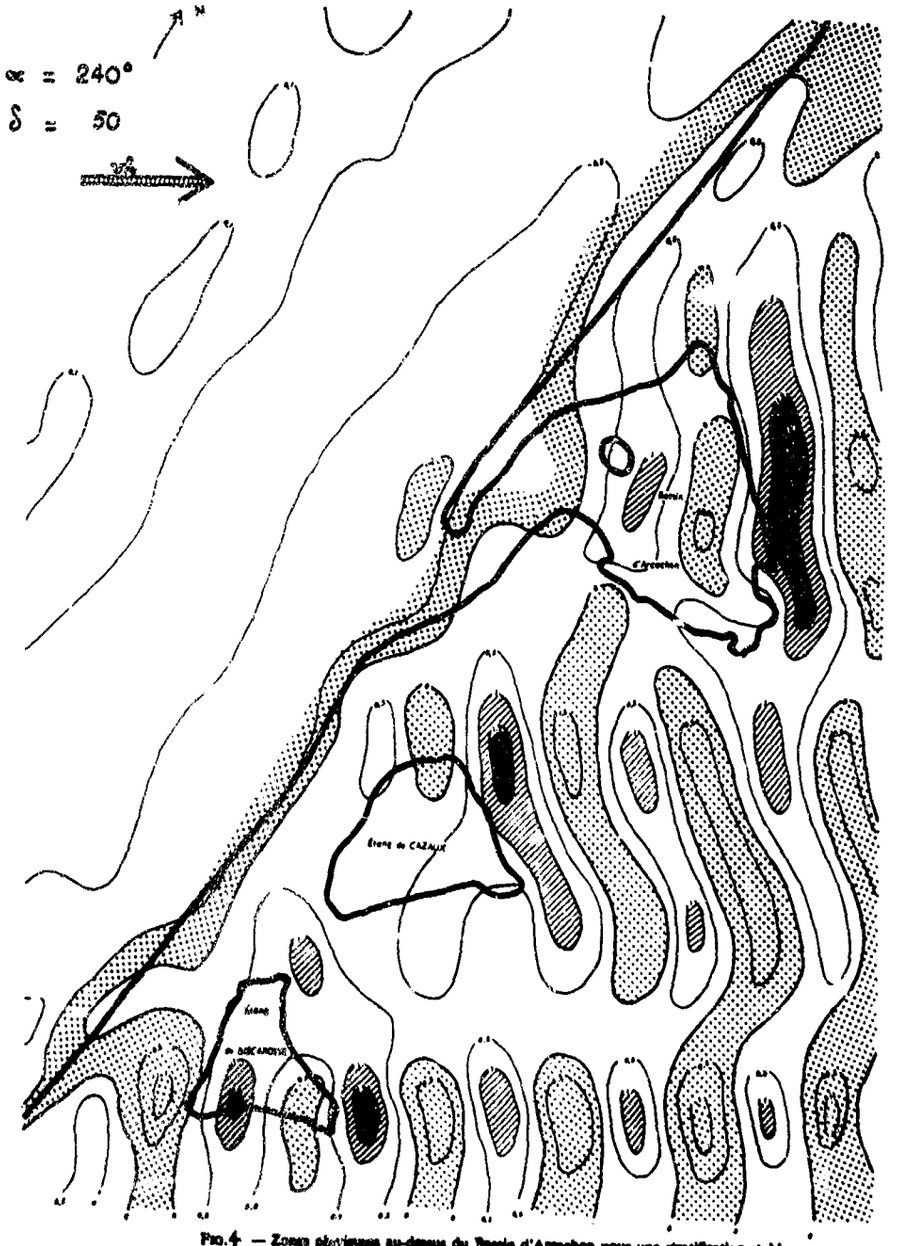

FIG. 4 — Zones pluvieuses au-dessus du Bassin d'Arcachon pour une stratification stable (négatif : en pointillé; positif : en hachures).

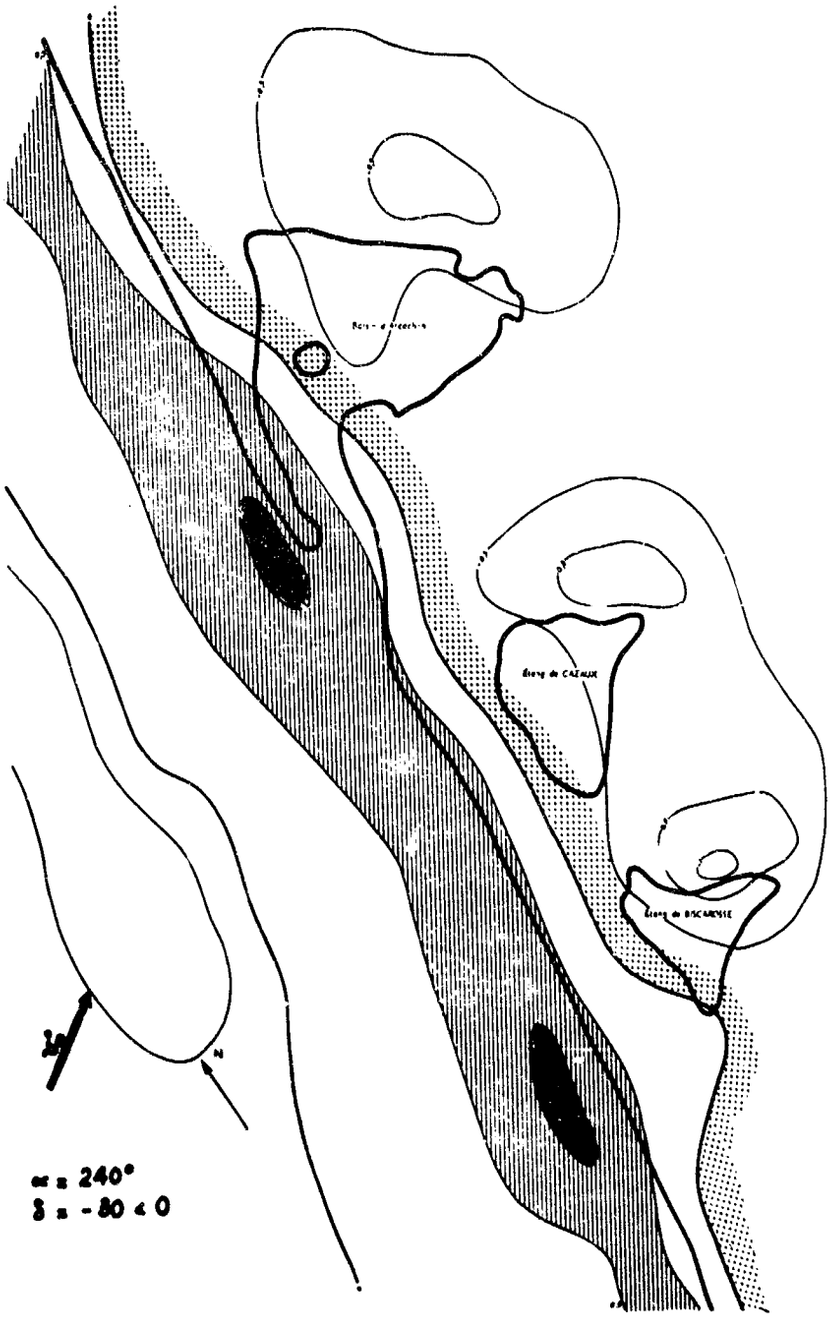

FIG. 5 — Zones pluvieuses au-dessus du Bassin d'Arcachon pour une stratification instable (on remarquera deux maxima de pluie près de la côte).

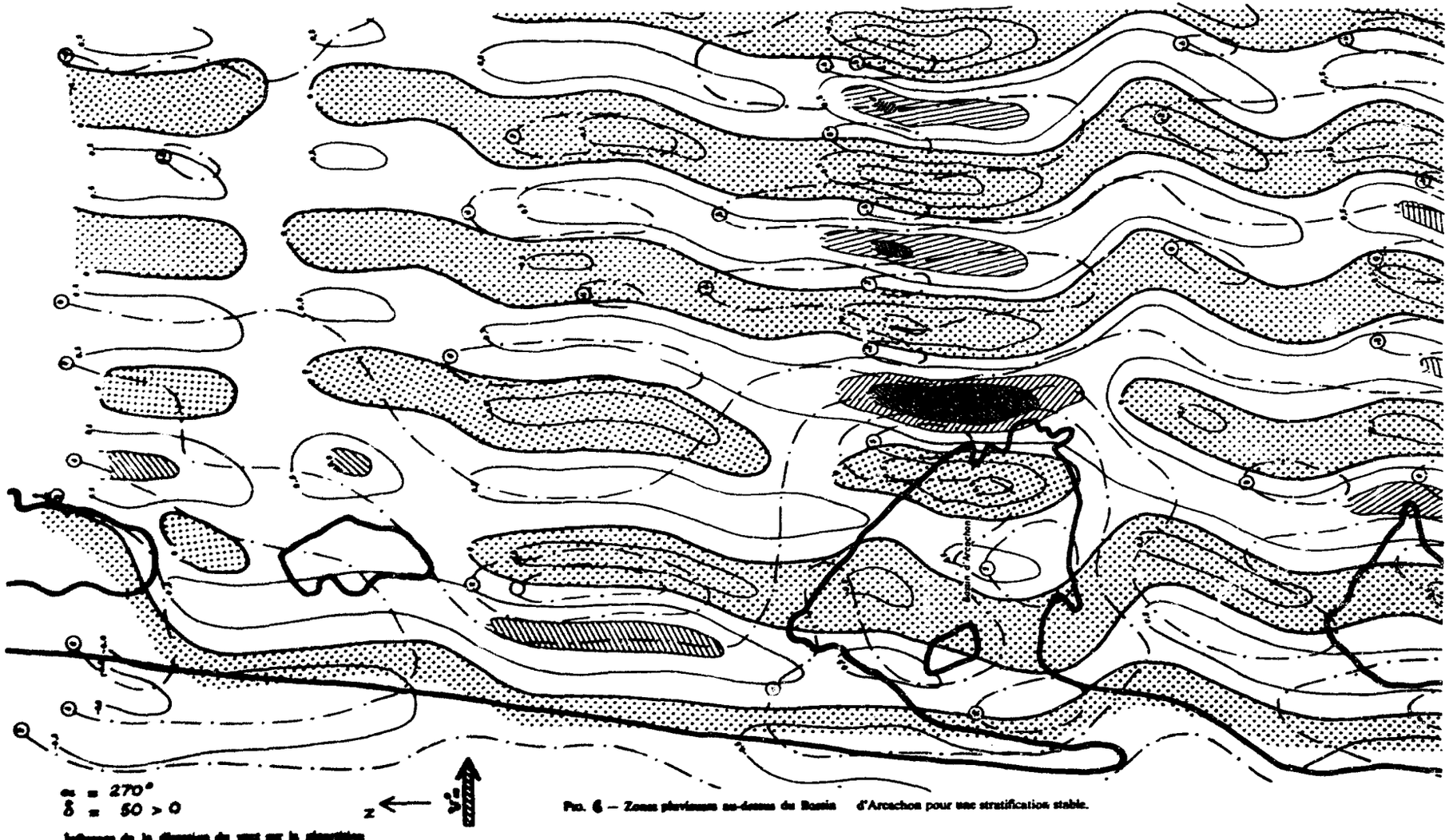

Fig. 6 – Zones pluvieuses au-dessus du Bassin d'Arcachon pour une stratification stable.

Influence de la direction du vent sur la répartition des zones pluvieuses v (voir la fig.12pour comparaison).

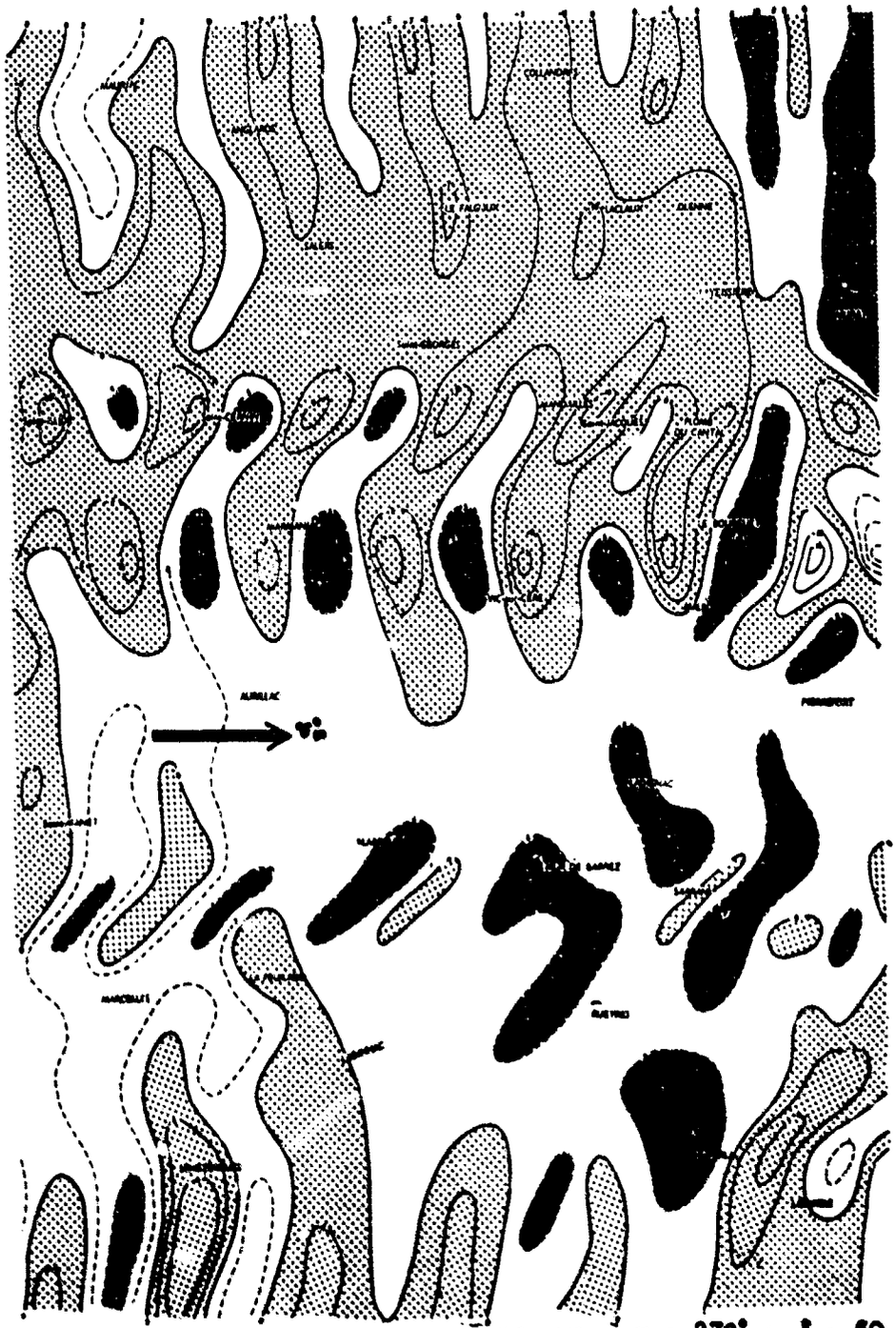

Fig. 7. — Zones pluvieuses sur une partie du Massif Central (Combi) $\alpha = 270°$; $\delta = 60$

PROBLEMS OF ATMOSPHERIC SHEAR FLOWS AND THEIR LABORATORY SIMULATION

by

J. E. Cermak and S. P. S. Arya

Fluid Mechanics Program, College of Engineering,
Colorado State University,
Fort Collins, Colorado

ABSTRACT

Shear flows generated by movement of the atmosphere near the earth's surface are accompanied by complexities not ordinarily encountered in the treatment of turbulent boundary layers. Problems arising from the following physical features are considered:

1. Thermal stratification
2. Surface roughness in the form of forests and cities
3. Non-uniformity of surface roughness and/or temperature (leading to 3-dimensional turbulent boundary layers)
4. Surface irregularities in the form of hilly and mountainous topography

The complex nature of atmospheric shear flows has stimulated efforts to study their characteristics in the laboratory under controlled conditions. Accordingly, questions of similarity between the laboratory and the atmospheric flows for both mean and turbulent quantities arise. Similarity criteria, or appropriate scaling relationships, are discussed.

Wind tunnels designed for investigations related to atmospheric shear flows are described. These facilities are shown to have a capability for simulat'ng such flows for a wide range of the physical features listed above.

PROBLEMS OF ATMOSPHERIC SHEAR FLOWS AND THEIR LABORATORY SIMULATION

by
J. E. Cermak* and S. P. S. Arya*

1. INTRODUCTION

Shear flows generated by the atmospheric flow near the earth's surface are accompanied by complexities not ordinarily encountered in turbulent boundary layers that have been studied in great detail by aerodynamists. The atmospheric boundary layer does not have a well-defined outer edge separating the laminar and turbulent flows in the ordinary sense of a flat-plate boundary layer. The horizontal and vertical accelerations of the flow are caused by forces developed through simultaneous action of surface friction, buoyancy, earth's rotation and pressure variations.

We will limit ourselves to the lowest layer of the atmosphere -- the surface layer -- in which Coriolis effects usually can be neglected. Problems arising from the following features are considered in this review:

1. thermal stratification
2. large roughness due to forests and cities
3. non-uniformity of surface roughness and/or temperature leading to three-dimensional boundary layers
4. surface irregularities in the form of mountainous topography

The effects of these features on atmospheric shear flows have not been amenable to theoretical treatment in a satisfactory way. Much time and effort has been expended in expensive field studies; however, considerable savings can be achieved through laboratory simulation of such flows. Several feasibility studies[1,2,3] have been conducted in recent years which conclude that many of the characteristics of the surface layer can be closely simulated by wind-tunnel flows. These studies have also brought out the similitude criteria and appropriate scaling relationships.

Atmospheric modeling is important not only from the point of view of its applications in predicting wind loads on structures, diffusion of heat and mass for various environmental situations, etc., but also for attainment of a basic understanding of atmospheric shear flows. Once a particular flow type has been simulated, the flow conditions in the laboratory can be systematically varied and precise measurements can be made under controlled conditions for checking existing theoretical models and developing new ones. Specially designed wind tunnels capable of generating thick and well-developed turbulent boundary layers are required for this purpose. Some of the existing facilities are described and some recommendations are made for improved designs.

2. STUDIES OF ATMOSPHERIC-SHEAR-FLOW PROBLEMS

Much work has been done by meteorologists and fluid dynamists in an effort to better understand flow phenomena in the atmospheric surface layer. A comprehensive review is given elsewhere[4,5]. In this section we will discuss some of the problems of current interest and the progress that has been made toward understanding them. Mean flow in the atmospheric surface layer has been treated as a two-dimensional motion by most investigators; however, in Sec. 2.4 the need for considering three-dimensional motion is discussed.

2.1 Thermal Stratification

The temperature inhomogeneities in the atmosphere give rise to buoyancy forces which greatly affect the mean flow and turbulence structure. On rather rare occasions of neutral stability and on plane and homogeneous terrain the mean velocity distribution in the surface layer is well represented by the logarithmic law of the form

$$U = \frac{u_*}{k} \ln \frac{z}{z_o} \qquad (1)$$

in which U is the velocity at height z, u_* the friction velocity, z_o the roughness parameter and k is Kármán's constant. The effect of buoyancy has been observed to increase the profile curvature in case of unstable stratification and to decrease it in stable conditions. This is reflected in the value of β in the following empirical power-law relationship first proposed by Deacon[6].

$$U = \frac{u_*}{k(1-\beta)} \left[\left(\frac{z}{z_o} \right)^{1-\beta} - 1 \right] \qquad (2)$$

The value of β has been observed to vary with stability and also with height, which somewhat limits the usefulness of Eq. (2). Several theoretical models based on mixing length concepts have been proposed for the thermally stratified surface layer from which theoretical mean velocity and temperature profiles have been derived[7,8]. But, most atmospheric data to date have been more conveniently represented by the similarity theory of Monin and Obukhov[5,9].

The basic assumptions of the similarity theory are that the flow is plane-homogeneous, the vertical fluxes remain constant with height and that the only pertinent variables are height z, the density ρ, the wall shear stress τ_o the wall heat flux H_o and the stability parameter g/T_a.

*Fluid Mechanics Program, College of Engineering, Colorado State University, Fort Collins, Colorado

Then, the velocity, temperature and length scales are given by

$$u_* = (\tau_o/\rho)^{1/2} \tag{3}$$

$$T_* = - H_o/(\rho C_p k u_*) \tag{4}$$

$$L = - u_*^3/(k \frac{g}{T_a} \frac{H_o}{\rho C_p}) \tag{5}$$

These lead to the following similarity relationships for mean velocity and temperature distributions

$$\frac{kz}{u_*} \frac{\partial U}{\partial z} = \phi_u(z/L) \tag{6}$$

$$\frac{z}{T_*} \frac{\partial T}{\partial z} = \phi_t(z/L) \tag{7}$$

in which ϕ_u and ϕ_t are universal functions of z/L. For small departures from neutral conditions the relation

$$\phi_u = 1 + \beta_u(z/L) \tag{8}$$

has been proposed[9] which leads to the logarithmic-linear law of the velocity distribution. Experiments[10,11,12] indicate that for stable stratification, $\beta_u \simeq 10$, and the range of applicability of the log-linear law is fairly wide ($0 < z/L < 0.5$). In unstable stratification, $\beta_u \simeq 1.5$ and the range of applicability of the log-linear law is very narrow[4,11] ($-z/L < 0.05$). The so-called KEYPS relationship is found to give a better fit to the observed data. This is given by

$$\phi_u^4 - \frac{\gamma z}{L} \phi_u^3 = 1 \tag{9}$$

in which γ is an empirical constant. For extremely unstable conditions, i.e., as $z/L \to -\infty$, the flow regime approaches that of free convection and the mean temperature and velocity profiles are defined by[4]

$$\frac{\partial T}{\partial z} = - C(\frac{H_o}{\rho C_p})^{2/3} (\frac{g}{T_a})^{-1/3} z^{-4/3} \tag{10}$$

$$\frac{\partial U}{\partial z} = \frac{K_H}{K_M} u_*^2 (\frac{g H_o}{T_a \rho C_p})^{-1/3} z^{-4/3} \tag{11}$$

in which C is an empirical constant, and K_H and K_M are eddy diffusivities of heat and momentum. The ratio K_H/K_M has been observed to be close to unity in the near-neutral conditions, but it decreases in more stable and increases in more unstable stratifications. Values close to zero for extremely stable situations and up to 3 for free convection regime have been observed[4]. The often-made assumption that $K_H = K_M$ is very poor except in near-neutral conditions.

In its present form, Monin and Obukhov's similarity hypothesis has been applied[5] to many statistical characteristics of turbulence such as variances and spectra of velocity and temperature fluctuations, co-spectra of shear stress and heat flux, energy dissipation, etc. Detailed measurements of atmospheric turbulence in the last few years[13,14,15] show that the variance and spectra of vertical velocity and co-spectra of shear stress and heat flux obey the similarity theory. But, variances and spectra of longitudinal velocity and temperature fluctuations non-dimensionalized by the similarity theory scales show a definite height dependency. The same was observed by Arya and Plate[12] in wind tunnel measurements. These limitations of the similarity theory have been discussed in much detail by Calder[16].

Other theoretical models for thermally stratified fluids have been proposed[17,18], these are based on dynamical equations in which diffusion and transport terms have been neglected. Though very useful in giving further insight into the turbulent transfer process, these theories are based on assumptions and hypotheses of doubtful validity which are not fully supported by experimental data[19].

2.2 Large Roughness

In the preceding section, the surface layer is assumed to be affected by only small surface irregularities. For the flow over tall crops, forests, urban areas, etc., this is no longer true. But, the simple model of the previous section can still be applied to flow above the roughness elements with slight modifications. The modified wind profile under neutral conditions is given for $z > h$,

$$U = \frac{u_*}{k} \ln (\frac{z-d}{z_o}) = \frac{u_*}{k} \ln \frac{z'}{z_o} \tag{12}$$

where h is the height of the surface irregularities and d is the zero-plane displacement. All other equations of section 2.2 would be applicable if z is replaced by z'. Equation (12) has been verified for atmospheric flows over tall crops[20] and forest canopies. The same is found true for wind-tunnel boundary layer flows over model crops[21] and model forests[22].

Sometimes, the flow in and around roughness elements is of main interest e.g., in air pollution studies and in determining the aerodynamical loading of individual buildings within a city. Here, size, shape and mutual arrangement of roughness elements will greatly affect the flow characteristics. Empirical similarity relationships have been found to correlate the mean wind profiles fairly well in city complexes -- a dependency on height $U \alpha z^{0.4}$ has been found to represent both field and laboratory data[24].

2.3 Non-uniformity of Surface Conditions

We have so far assumed that the ground surface is uniform as to its roughness and temperature and that the flow has attained a state of equilibrium with respect to these surface conditions. In reality, such an equilibrium is rarely reached and mean wind and temperature profiles are in some state of transition from one surface condition to another most of the time. Whenever there is a change in surface conditions, the wind and temperature profiles reflect the effect of local surface only up to a certain height above which the profiles remain unaltered and are representative of surface conditions upstream from the change. For analytical convenience an internal boundary layer is assumed to develop from the edge of the surface discontinuity. In an actual situation, several such internal boundary layers may be developing at the same time and divide the flow into different zones each representative of an upstream surface condition.

Several theories have been proposed for predicting modified wind profiles following a sudden change in surface roughness[23,25,26,27]. An internal boundary layer has been defined in various ways and the pressure changes occurring in the neighborhood of the surface discontinuity have been ignored. There is no agreement on the maximum height to fetch ratio for which upstream discontinuities no longer have appreciable affect on the local flow characteristics -- values ranging from 1/200 to 1/10 have been indicated. However, differences in the predicted wind profiles by various theories are not large. Only limited observations of profile adjustment have been made in the atmosphere[28,29]. These experiments indicate that surface shear adjustment occurs rather rapidly following the change in surface roughness. Velocity profiles are found to agree well with the theory of Panofsky and Townsend[25] when the flow is from smooth to rough, but not so well in the opposite case. The observed height to fetch ratio of 1/200 is much different from their predicted value of the order of 1/10. But a much closer agreement is obtained if the proposed modification to this theory by Blom and Warteena[30] is considered.

Townsend[31] has investigated theoretically the change in mean velocity and temperature profiles following a step change in surface heat flux and a line source of heat at the ground level. The effects of the thermal stratification are also considered. The results are shown to compare well with the observations of Rider et al.[32]. Only a few profile adjustment experiments have been performed in wind tunnels.

When air moves from land surface to a body of water or vice-versa, diabatic effects are involved following changes in temperature and moisture. Wind profile adjustments differ greatly under lapse as opposed to inversion conditions[27]. More experimental and theoretical work is required if such effects are to be predicted accurately.

2.4 Three-Dimensionality of the Mean Flow

In nature, non-uniformities of surface conditions lateral to the dominant mean flow direction are as common as changes in the longitudinal direction. Air flow over alternate strips of cultivated and uncultivated lands, along the edges of a forest or a city, parallel to the shore line and over an isolated hill are examples where the changes in surface roughness, temperature or elevation introduce cross flows. Some studies[34] have recently been made on three-dimensional turbulent boundary layers of aerodynamic type. Currently, an extensive experimental program is underway at Colorado State University to study three-dimensional effects which would be more relevant to environmental problems, such as area changes of surface roughness or temperature and mountain-like surface irregularities. Specially designed meteorological wind tunnels shown in Fig. 1 having large cross sections and long test sections are suitable for such studies.

The presence of a roughness patch or island in the way of an otherwise two-dimensional boundary layer flow causes a general retardation of the flow over the island. This produces strong edge effects which give rise to new shearing stresses and longitudinal vorticity. Such effects are likely to persist far downstream of the roughness until a new equilibrium is established. The study of flow over a hemisphere by Hawthorne and Martin[35] reveals the existence of longitudinal vorticies.

Equally important phenomenon in the meteorology of urban areas is that of the heat island effect. Interactions of a metropolitan area as a heat source on wind patterns over and around it are very important in air pollution problems. Some studies have been made[36,37] of flow of a stable atmosphere over the heated islands of Puerto Rico and Nantucket and simple numerical models have been developed for these cases.

Of much interest are the shear flows over three-dimensional mountain-like features. Theoretical treatment of such flows is extremely difficult. Some model experiments have been made, which

will be discussed in the next section. Very few field studies of such flows are available[38]. When the winds are light and stably stratified, mountain lee-waves are observed. Lee-waves have been the subject of intensive theoretical and experimental studies, an excellent review of which is given by Queney[39] et al and in the Proceedings of the Symposium on Mountain Meteorology[40].

3. SIMILARITY ANALYSIS AND MODELING CRITERIA

In the preceding section many interesting shear-flow problems of the atmospheric surface layer have been pointed out which remain far from being solved. Some of these can be better studied on a smaller scale in the laboratory. The feasibility of atmospheric modeling has now been demonstrated for a wide range of situations and modeling criteria based on similarity analysis have been laid down[1,3]. Furthermore, simulation in which some of the criteria are realized only in an approximate sense have been found to be very useful.

3.1 Neutral Boundary Layer

The simplest type of flow that is easily simulated by a boundary layer developing over a rough plate in the wind tunnel is that of a neutral atmosphere over plane and uniformly rough ground. In both cases the velocity distribution is given by Eq. (1). Provided that the requirements of an aerodynamically rough regime are satisfied, wind speed and roughness can be chosen somewhat arbitrarily. When the roughness height is large -- air flow over tall crops -- the velocity distribution is given by Eq. (12). This kind of flow has been successfully simulated by using arrays of flexible plastic strips and wooden pegs[21]. Flow structure within the plant cover is highly complex, but indications are that the velocity profiles can be represented by empirical similarity relationships which hold both in the field and the laboratory. Extensive simulation studies of flow in forest canopies have been made[22,41]. In addition to similarity of the general character of the mean flow patterns it has been observed that the turbulent intensity, spectra of velocity fluctuations and eddy diffusion coefficients in the model behave in a manner similar to that of field. Some comparisons with field data are given in Figs. 2 and 3. However, turning of the mean velocity vector with height due to combined action of Coriolis acceleration and pressure gradient observed in prototype studies is not found in the non-rotating wind tunnel.

Simulation of two-dimensional flow over a terrain representing one or more step changes in surface roughness poses no new problems provided sufficient test-section length is available to scale down the desired area. Width of the tunnel is a limiting factor if three-dimensional effects due to lateral changes in roughness are to be reproduced. However, some exaggeration of vertical scale may be necessary to accommodate large city models if the model buildings are not to be submerged in the zone of viscous flow near the wall. A systematic study of how distortion of this type can produce flow characteristics similar to flow over a rough surface is needed.

Much progress in atmospheric studies for the purpose of investigating the aerodynamic characteristics of building and tall structures has been made. Much of the work done in this area is referred to in Ref. 42. Jensen[43] was first to point out that in order to simulate static wind loads on a structure, the model must be entirely immersed in the wind-tunnel boundary layer and the scaling must be done so that the ratio h/z_o is the same in the model and the prototype. This was apparantly ignored in earlier model studies. The effect of various meteorological parameters on wind loading of structures has been discussed by Davenport[44].

3.2 Thermally Stratified Boundary Layers

Similarity criteria for thermally stratified boundary layers have been discussed in great detail[1,2,3,45]. Batchelor[47] was first to point out that under certain restrictions, a Richardson number is the sole parameter governing the flow. This Richardson number must be chosen to represent the gross features of the velocity and temperature field.

The similarity theory of Monin and Obukhov[5] has been shown to be generally valid for the stratified atmospheric surface layer. Thermally stratified boundary layers have also been studied[12,19,48,49] in the U. S. Army Meteorological Wind Tunnel at Colorado State University; the results indicate that the similarity theory is also valid for the wind-tunnel flow. It has been pointed out by Arya and Plate[12] that only the lowest 15% of the total wind-tunnel boundary layer thickness can be taken to correspond to the surface layer of the atmosphere. The form of the various normalized functions of similarity theory is found to be the same for the laboratory and the field data as shown in Figs. 4, 5, 6, and 7. This greatly enhances the credibility of the similarity theory and at the same time, indicates that the Monin-Obukhov length can be used for scaling heights. Proceeding in a more general manner using the differential equations of motion, McVehil et al[3] also arrived at the same criterion viz., the ratio z/L evaluated at some reference height should be made equal in the model and the field. It has been pointed out that this simple criterion is subject to the conditions: that the fractional changes in the potential temperature are small, and the ratio K_H/K_M is constant and independent of both height and stability. With regard to the second condition we note that similarity criterion would not change even if K_H/K_M varies as indeed it does, with stability, provided that it is a unique function of z/L. Experimental data of Fig. 6 indicates that such a unique function exists.

Because of the difficulties in measuring fluxes, it is not always possible to determine the scaling length L. A Richardson number defined in terms of the gradients of mean velocity and temperature is the most conveniently measured stability parameter. But, since it depends on height it cannot be used as a modeling parameter. According to the similarity theory, however, Ri is a

universal function of z/L -- Fig. 7. The use of Ri as a stability parameter is equivalent to that of z/L. For modeling purposes a gross Richardson number defined as follows can also be used:

$$Ri_h = \frac{gh}{T_a} \frac{(T_h - T_o)}{U_h^2} \tag{13}$$

in which h is the thickness of the surface layer (or equivalent layer in the wind tunnel), U_h and T_h are the values of velocity and temperature at the upper edge of this layer. T_o is the surface temperature and T_a is the average temperature of the layer in absolute scale. Then, equivalence of Ri_h for the model and prototype flows will yield the scaling relationship

$$\frac{(h)_m}{(h)_p} = \frac{(U_h^2)_m}{(U_h^2)_p} \left[\frac{(\Delta T_h / T_a)_p}{(\Delta T_h / T_a)_m} \right] \tag{14}$$

in which $\Delta T_h = T_h - T_o$.

3.3 Similitude Criteria for Turbulence Structure

Turbulence by its definition is stochastic in nature and complete similarity of turbulence structure is impossible to achieve as it would imply equivalence of all statistical functions. We are often interested in simulating only those properties of turbulence which are important in transporting momentum, heat and mass. In certain cases, simulation of turbulent energy in a particular narrow eddy range would be required. For this, equivalence of normalized turbulent intensities and energy spectra in the prescribed wave number range may be considered as sufficient criteria for simulation. While the turbulent intensities are comparatively easy to match, matching of turbulence spectra requires thick boundary layers and high wind speeds.

According to Kolmogorov's hypothesis[50] the structure of small scale eddies can be considered to be isotropic which leads to a universal spectrum form in the high wave number range - the so called equilibrium range which is further subdivided into a dissipation subrange and an inertial subrange. Similarity of the spectrum in the high wave number range is demonstrated by Fig. 9 in which data are taken from a variety of flows in nature and the laboratory. Kolmogorov's theory gives the length scale, $(\nu^3/\varepsilon)^{\frac{1}{4}}$ and velocity scale, $(\nu\delta)^{\frac{1}{4}}$ for scaling the data.

When the energy spectra for two flows are nearly similar, Cermak[46] has shown that the length scales $(L_d)_m$ and $(L_d)_p$ for small scale motion in the model and the prototype respectively, are related by

$$\frac{(L_d)_m}{(L_d)_p} = \left[\frac{(\varepsilon/\overline{u'^2}\nu)_p}{(\varepsilon/\overline{u'^2}\nu)_m} \right]^{\frac{1}{4}} \tag{15}$$

this criteria should be useful in comparing gross characteristics of phenomena associated with turbulent diffusion such as the width of diffusion plumes. However, a critical test of the relationship has not been made.

Following a different approach, McVehil et al[3] states that in general the non-dimensional turbulence intensities must be equal in addition to the similarity requirement of eq. 15. For thermally stratified flows, equality of non-dimensional temperature fluctuations is also required. These authors have also argued that their criterion is essentially the same as stated earlier by Cermak provided the energy spectra are nearly similar for two flows.

The above mentioned criteria of similarity of turbulence structure are necessary. These are sufficient only if the wind-tunnel boundary layer develops naturally and any artificial turbulence introduced is far upstream of the region of interest. On the other hand, if a thick boundary layer having some desired velocity profile is generated by artificial means over a comparatively short length of the tunnel, additional criteria may arise from different initial and boundary conditions prevailing in the model and prototype flows.

For thermally stratified boundary layers, the similarity theory of Monin and Obukhov has been found to be generally valid for many of the turbulence characteristics[12,14,15] including spectra outside of the dissipation range. Therefore, this theory provides a good basis for wind tunnel modeling of these characteristics.

3.4 Similarity of Motion over Topographical Features

Cermak et al[1] and Nemoto[51] have examined in detail the conditions for similarity of mean flow patterns and turbulence structure in topographical modeling. The non-dimensional parameters that are required to be matched are the Euler number, the Froude or Richardson number and the Reynolds number. Matching of the Euler number only requires geometrical similarity of gross wind directions and the distribution of vortices and eddies.

It is not possible to match the Reynolds number and the Froude number (or Richardson number) at the same time if the model fluid is also air. The Froude number is the governing parameter when some special flow phenomena occurring in light winds and strong stratification such as mountain lee-waves are of interest. Different techniques have been used for simulation of mountain lee-waves. Perhaps the earliest experiments were performed by Abe[52,53] who simulated in a wind tunnel the cloud forms caused by Mount Fujiyama using a geometrically similar 1:50,000 scale model. In this type of modeling Reynolds number similarity is indicated if the turbulent Reynolds number based on the eddy viscosity is matched with the ordinary Reynolds number of the laminar flow in the model. The flow patterns over the model revealed by the use of incense smoke were found to be in good qualitative agreement. Long[54] has simulated lee-waves over Sierra Nevada Mountain by towing the model in a tank of stratified saline water. The main features of mountain lee-waves have also been reproduced in a wind tunnel[55] using the flow of strongly stratified air under stable conditions over model mountains.

The laminar flow technique has also been successfully used in simulation studies of flows over Point Arguello[56], San Nicolas Island[57], and San Bruno Mountain[58], in California. Simulation of only gross mean flow patterns can be expected in such models. A comparison of model and prototype flows is given in Fig. 10 for the Point Arguello[56] model study which was accomplished on a scale of 1:12,000 at a gross Richardson number of approximately 0.2. Figure 11 compares the rate of decay of ground level concentrations from an upwind source in the model and prototype. In this case, where transport of the source material is primarily due to convective transport, the agreement is excellent.

When flow patterns in strong winds are of interest, Froude number can be ignored. It is not possible to obtain in wind tunnels, the Reynolds numbers of the order found in the atmosphere. If the topographical features are fairly sharp, however, mean flow patterns are independent of the Reynolds number provided that it exceeds a lower limit which will depend on the sharpness of the topographical features. The studies of winds around the Rock of Gilbralter[60], Candlestick Ball Park, Calif.[60] and the mountains near Manchester, Vermont[61], are successful examples of this kind of modeling. Better results are obtained if the model surface is artificially roughened to help minimize the depth of the viscous zone. In the modeling of large areas with comparatively smooth topography, one may have by necessity to exaggerate the vertical scale. Some experiments[51] on distorted scale models indicate that good similarity of flow pattern is not obtained, particularly close to the surface.

4. SIMULATION TECHNIQUES AND WIND-TUNNEL FACILITIES

In order to satisfy even approximately the various criteria of similarity between atmospheric shear flows and simulated flows in wind tunnels thick turbulent boundary layers with large turbulence intensities are required. Various techniques which have been employed to generate such flows can be divided into two broad categories, viz., (1) in which turbulent boundary layers are developed naturally over a long and artificially roughened surface and (2) in which thick turbulent intensities distribution at some section is developed artificially by the use of devices such as grids of rods or flat plates, curved screens, vortex generators, etc.. The latter are economical in that shorter tunnels can be used. However, the turbulence dissipates and its structure changes in the downstream direction.

For good similarity, large tunnels of the types built at Colorado State University[62] and at the University of Western Ontario[63] are required. The meteorological wind tunnel shown in Fig. 1 is of the recirculating type with a test section approximately 30 m long and 1.8 x 1.8 m in cross section. Part of the floor can be heated or cooled to any desired temperature between -5 and 200°C. An air-conditioning system allows for the ambient air temperature to be maintained between 5 and 65°C. Ambient wind speeds range between 0.5 and 40 m/sec. At a wind speed of about 6 m/sec, a boundary-layer thickness between 70 and 120 cm/sec can be obtained as the floor is varied.

An environmental wind-tunnel facility is also shown in Fig. 1. This facility has a test section of approximately 17 m long, 4 m wide and of variable height between 2 and 3 m. The wide section has been specifically designed for studying three-dimensional boundary layer flows and for conducting model studies of flow over urban areas related to air pollution and structural aerodynamic problems.

The university of Western Ontario tunnel[63] has a test section approximately 26 m long, 2.6 m wide and variable in height from 1.8 m at the entrance to 2.5 m at the end. A 30 cm high grid of horizontal graded round bars is used at the entrance to help thicken the boundary layer.

In the second category of wind-tunnel facilities, the test section lengths are usually small, (characteristic of many aeronautical wind tunnels), but devices are used to produce artificially thickened turbulent boundaries or, in some cases, desired velocity and temperature gradients. For example, shear and heating grids have been used to generate turbulent shear flows with linear wind and temperature profiles[64]. These grids may not be suitable for atmospheric simulation since turbulence levels cannot be adjusted. Armit[65] proposed a system of barriers and vortex generators. Vortex generators have been used in conjunction with a grid of plates by Lloyd[66] at University of Bristol. By these techniques thick boundary layers are obtained in which the velocity and turbulent intensity profiles are reasonably non-developing. However, the shear stress changes rapidly in the longitudinal as well as the vertical direction. Recently, the effectiveness of curved screens in generating shear in stratified flows has been demonstrated[67]. This approach shows much promise for extending fundamental studies of stratified flows.

5. CONCLUSIONS

Flow of the atmosphere over the earth's surface is affected by factors which are not included in the treatment of classical two-dimensional turbulent boundary layers. Major effects are produced on the low-speed flows by thermal stratification, large surface roughness (forests, cities, crops), non-uniformity of surface roughness and temperature, topographical features, and rotation of the earth. Excepting for the effects of rotation, the influence of these factors on mean and fluctuating quantities in the atmospheric surface layer (approximately the lower 15% of the turbulent boundary layer where vertical fluxes are sensibly constant) have been studied successfully in the laboratory.

Comparisons of data taken from the atmosphere and from the laboratory in the "constant-stress layer" have confirmed that similarity of these flows can be attained. This simulation capability should continue to be developed for the purpose of studying the basic nature of these complex flows which defy analysis and to provide improved modeling techniques. Past experience has revealed that simulated atmospheric shear flows are an invaluable aid in the study of applied problems associated with air pollution, structural aerodynamics, modification of local environments, etc.

The use of laminar stably-stratified flow over small-scale models of complex topography to study convective dispersion in a turbulent stably-stratified atmosphere has been proven to be a valuable simulation technique. Reynolds number similarity based on a Reynolds number for the atmosphere formed with an eddy viscosity and a Reynolds number for the model formed with the molecular viscosity should be considered for other problems of atmospheric motion.

Several problems may be listed whose study can lead to significant advances in our understanding and in our ability to simulate atmospheric shear flows in the laboratory. Those that appear to be the most important at this time are the following:

1. How does model distortion produced by exaggeration of the vertical scale affect similarity of two flow fields? An answer to this question is essential if flow over city complexes modeled on a scale of 1:10,000 or smaller is to be simulated with a high degree of confidence.

2. What is the effect of three dimensionality of mean flow on turbulence characteristics? As pointed out by Bradshaw[68], not even the direction of mean turbulent shear stress relative to the mean velocity vector is known when strong crossflow exists.

3. How can thick turbulent boundary layers with appropriate turbulence structure and thermal stratification be generated without the use of excessively long wind-tunnel test sections? The combined use of upstream grids, screens and vortex generators in conjunction with moderately long test sections (20-30 meters) appears to be the most promising approach.

References

1. Cermak, J. E., V. A. Sandborn, E. J. Plate, G. H. Binder, H. Chuang, R. N. Meroney and S. Ito, "Simulation of atmospheric motion by wind-tunnel flows," Fluid Mechanics Program, Colorado State University, CER66JEC-VAS-EJP-GJB-HC-RNM-SI17, May 1966.

2. Hidy, G. M., "On atmospheric simulation: a colloquium," NCAR Tech. Note NCAR-TN-22, Nov. 1966.

3. McVehil, G. E., G. R. Ludwig, and T. R. Sundaram, "On the feasibility of modeling small scale atmospheric motions," Cornell Aeronautical Laboratory Report No. ZB-2328-P-1, April 1967.

4. Lumley, J. L. and H. A. Panofsky, "The structure of atmospheric turbulence," John Wiley & Sons, Inc., New York, 1964.

5. Monin, A. S. and A. M. Yaglom, "Statistical hydromechanics, Part I: The mechanics of turbulence," Nauka Press, Moscow, 1965 (English translation by Joint Publications Research Service, U. S. Department of Commerce).

6. Deacon, E. L., "Vertical diffusion in the lowest layers of the atmosphere," Quart. Jour. Roy. Met. Soc., Vol. 75, pp. 89-103, 1949.

7. Businger, J. A., "On the structure of atmospheric surface layer," Jour. of Meteorology, Vol 12, pp. 553-561, 1955.

8. Kao, S. K., "Turbulence transfer in the boundary layer of a stratified fluid," Jour. of Meteorology, Vol. 16, pp. 497-503, 1959.

9. Monin, A. S. and A. M. Obukhov, "Basic regularity in turbulent mixing in the surface layer of the atmosphere," Trans. of the Geophys. Inst. Acad. Sci. USSR, No. 24, 1954.

10. McVehil, G. E., "Wind and temperature profiles near the ground in stable stratification," Quart. Jour. Roy. Met. Soc., Vol. 90, pp. 136-146, 1964.

11. Zilitinkevich, S. S. and D. V. Chalikov, "Determining the universal wind-velocity and temperature profiles in the atmospheric boundary layer," Izv. Atmospheric and Oceanic Physics, Vol. 4, No. 3, pp. 165-169 (English Translation) 1968.

12. Arya, S. P. S. and E. J. Plate, "Modeling of the stably stratified atmospheric boundary layer," to appear in Journal of the Atmospheric Sciences, July 1969.

13. Cramer, H. E., "Turbulent transfer processes for quasi-homogeneous flows within the atmospheric surface layer," Physics of Fluids, Vol. 10, Supplement, pp. S240-S246, 1967.

14. Busch, N. E. and H. A. Panofsky, "Recent spectra of atmospheric turbulence," Quart. Jour. Roy. Met. Soc., Vol. , pp. 132-148, 1968.

15. Panofsky, H. A. and E. Mares, "Recent measurements of spectra of heat-flux and stress," Quart. Jour. Roy. Met. Soc., Vol. , pp. 581-585, 1968.

16. Calder, K. L., "Concerning the similarity theory of A. S. Monin and A. M. Obukhov for the turbulence structure of thermally stratified surface layer of the atmosphere," Quart. Jour. Roy. Met. Soc., Vol. 92, pp. 141-146, 1966.

17. Ellison, T. H., "Turbulent transport of heat and momentum from an infinite rough plane," Jour. Fluid Mech., Vol. 2, pp. 456-466, 1957.

18. Townsend, A. A., "Turbulent transport in a stably stratified atmosphere," Jour. Fluid Mech., Vol. 5, pp. 361-372, 1958.

19. Arya, S. P. S., "Structure of stably stratified turbulent boundary layer," Ph.D. dissertation, also available as Technical Report No. CER68-69SPSA10, Fluid Mechanics Program, Colorado State University, 1968.

20. Cowan, I. R., "Mass, heat and momentum exchange between stands of plants and their atmospheric environment," Quart. Jour. Roy. Met. Soc., Vol. 94, pp. 523-544, 1968.

21. Plate, E. J. and A. A. Quraishi, "Modeling of velocity distributions inside and above tall crops," Jour. Appl. Met., Vol. 4, No. 3, pp. 400-408, 1965.

22. Kawatani, T. and R. N. Meroney, "The structure of canopy flow field," Tech. Report No. CER67-68TK66, Fluid Mechanics Program, Colorado State University, 1968.

23. Elliot, W. P., "The growth of the atmospheric internal boundary layer," Trans. Amer. Geophys. Union, Vol. 39, pp. 1048-1054.

24. Cermak, J. E., N. Z. Sadeh and G. Hsi, "Fluctuating moments on tall buildings produced by wind loading," Paper presented at Technical Meeting on Wind Loads on Buildings and Structures, National Bureau of Standards, Gaithersburg, Maryland, January 1969.

25. Panofsky, H. A. and A. A. Townsend, "Change of terrain roughness and the wind profile," Quart. Jour. Roy. Met. Soc., Vol. 90, pp. 147-155, 1964.

26. Townsend, A. A., "The flow in a turbulent boundary layer after a change in surface roughness," Jour. Fluid Mech., Vol. 26, Part 2, pp. 255-266, 1966.

27. Lettau, H. M., C. R. Stearns, W. F. Dabberdt and J. Zabransky, "Studies of effects of boundary modification in problems of small area meteorology," Research and Development Technical Report ECOM 66-G24-A, Department of Meteorology, University of Wisconsin, pp. 57-79, Feb. 1968.

28. Stearn, C. R. and H. Lettau, "Report on two wind profile modification experiments in air flow over ice of Lake Mendota," Annual Report, Contract DA-36-039-AMC-00878, Univ. of Wisconsin, pp. 115-138, 1963.

29. Bradley, E. F., "A micrometeorological study of velocity profiles and surface drag in the region modified by a change in surface roughness," Quart. Jour. Roy. Met. Soc. Vol. , pp. 361-379, 1968.

30. Blom, J. and L. Wartena, "The influence of changes in surface roughness on the development of turbulent boundary layer in the lower layers of the atmosphere," Jour. of the Atmos. Sci., Vol. 26, pp. 255-265, 1969.

31. Townsend, A. A., "The response of a turbulent boundary layer to abrupt changes in surface conditions," Jour. Fluid Mech., Vol. 22, part 4, pp. 799-822, 1965.

32. Rider, N. E., J. R. Philip and E. F. Bradley, "The horizontal transport of heat and moisture," Quart. Jour. Roy. Met. Soc., Vol. 89, pp. 507- , 1963.

33. Plate, E. J. and C. W. Lin, "The velocity field downstream from a two-dimensional model hill," Report No. CER65EJP14,1965.

34. Pierce, F. J. and Kromminhoek, D. H., "Wall shear stress diagnostic in three-dimensional turbulent boundary layers," Tech. Rept. No. 2, Contract DAHC0467c0008, Department of Mechanical Engineering, Virginia Polytechnic Institute, September 1968.

35. Hawthorne, W. R. and M. E. Martin, "The effect of density gradient and shear on the flow over a hemisphere," Proc. Roy. Soc. A., Vol. 232, 1955.

36. Malkus, J. S. and M. E. Stern, "The flow of a stable atmosphere over a heated island, Part I and Part II," Quart. Jour. Roy. Met. Soc., Vol. 10, pp. 30-41, and pp. 105-120, 1953.

37. Malkus, J. S., "The effects of a large island upon the trade wind air stream," Quart. Jour. Roy. Met. Soc., Vol. 81, pp. 539-550, 1955.

38. Davidson, B., "Some turbulence and wind variability observations in the lee of mountain ridges," Jour. Appl. Met., Vol. 2, No. 4, pp. 463-472, 1963.

39. Queney P., G. A. Corby, N. Gerbier, H. Koschmieder and J. Zierep, "The air flow over mountains," World Meteorological Organization, Technical Note No. 34, 1960.

40. Reiter, E. R. and J. L. Rasmussen (eds.), "Proceedings of the symposium on mountain meteorology," Atmospheric Science Paper No. 122, Colorado State University, June 1967.

41. Meroney, R. N., D. Kesic and T. Yamada, "Gaseous plume diffusion characteristics within model peg canopies," Technical Report ECOM C-0423-1, Fluid Mechanics Program, Colorado State University, Sept. 1968.

42. "Wind effects on buildings and structures," Proceedings of the International Research Seminar held at National Research Council, Ottawa, Canada on September 11-15, 1967, Vols. 1 and 2, University of Toronto Press.

43. Jensen, M., "The model-law for phenomena in natural wind," Ingenioren-International Edition, Vol. 2, No. 4, pp. 121-128.

44. Davenport, A. G., "The dependence of wind loads on meteorological parameters," Wind Effects on Buildings and Structures, Vol. 2, pp. 19-82, University of Toronto Press, 1967.

45. Cermak, J. E. and H. Chuang, "Vertical-velocity fluctuations in thermally stratified shear flows," Proc. International Colloquium on Atmospheric Turbulence and Radio Wave Propagation, Publishing House "Nauka", Moscow, pp. 93-104, June 1965.

46. Cermak, J. E., "Laboratory simulation of atmospheric motions in the lowest one hundred meters," Presented at the Meeting on Ground Wind Load Problems in Relation to Launch Vehicles," NASA Langley Research Center, June 7-8, 1966.

47. Batchelor, G. K. "The conditions for dynamic similarities of motions of a frictionless perfect-gas atmosphere," Quart. Jour. Roy. Met. Soc., Vol. 79, pp. 224-235, 1953.

48. Plate, E. J. and C. W. Lin, "Investigations of the thermally stratified boundary layer," Fluid Mechanics Paper No. 5, Fluid Dynamics and Diffusion Laboratory, Colorado State University, 1966.

49. Chuang, H. and J. E. Cermak, "Similarity of thermally stratified shear flows in the laboratory and atmosphere," The Physics of Fluids Supplement, pp. S255-S258, 1967.

50. Kolmogorov, A. N., "The local structure of turbulence in an incompressible fluid for very large wave numbers, C. R. Acad. Sci., USSR, Vol. 30, pp. 301-305, 1941.

51. Nemoto, S., "Similarity between natural load wind in the atmosphere and model wind in a wind tunnel," Papers in Meteorology and Geophysics, Vol. XIX, No. 2, pp. 131-227, 1968.

52. Abe, M., "The formation of cloud by the obstruction of Mount Fuji," Geophys. Mag., Tokyo, Vol. 6, pp. 1-10, 1932.

53. Abe, M., "Mountain clouds, their forms and connected air currents, Part II," Bull. Central Met. Observatory of Japan, VII, Vol. 3, pp. 93-145, 1941.

54. Long, R. R., "A laboratory model of air flow over the Sierra Nevada Mountains," The Rossby Memorial Volume, pp. 372-380, 1959.

55. Lin, J. T. and G. J. Binder, "Simulation of mountain lee-waves in a wind tunnel," Tech. Report No. CER67-68JTL-GJB24, Fluid Mechanics Program, Colorado State University, 1967.

56. Cermak, J. E. and J. Peterka, "Simulation of wind field over Point Arguello, California, by wind-tunnel flow over a topographical model," Report No. CER65JEC-JAP64, Fluid Mechanics Program, Colorado State University, 1966.

57. Meroney, R. N. and J. E. Cermak, "Wind tunnel modeling of flow and diffusion over San Nicholas Island, California," Tech. Report No. CER66-67RNM-JEC44, Fluid Mechanics Program, Colorado State University, 1967.

58. Garrison, J. A. and J. E. Cermak, "San Bruno Mountain wind investigation-a wind tunnel model study," Report No. CER67-68JEC-JAG58, 1968.

59. Field, J. M. and R. Warden, "A survey of air currents in the Bay of Gibralter," Geophysical Memo's No. 59 (R and M 1563), Published by Her Majesty's Stationery Office, 1929-1930.

60. Cermak, J. E., R. C. Maholtra and E. J. Plate, "Investigations of the Candlestick Park wind problem, Vol. II: Wind tunnel model study," Report CER63JEC-RCM-EJP27, Fluid Dynamics and Diffusion Laboratory, Colorado State University, 1963.

61. Halitsky, J., G. A. Magony and P. Halpern, "Turbulence due to topographical effects," Department of Meteorology and Oceanography, Geophysical Sciences Lab. Report Nos. TR65-2 and TR-66-5, New York University, 1964-1965.

62. Plate, E. J. and J. E. Cermak, "Micro-meteorological wind tunnel facility: description and characteristics," Report No. CER63EJP-JEC9, Fluid Dynamics and Diffusion Laboratory, Colorado State University, 1963.

63. Davenport, A. G. and N. Isyumov, "The application of the boundary layer wind tunnel to the prediction of wind loading," Wind Effects on Buildings and Structures, Vol. 1, University of Toronto Press, pp. 201-230, 1967.

64. Webster, C. A. G., "An experimental study of turbulence in a density-stratified shear flow," Jour. of Fluid Mech., Vol. 19, pp. 221-245, 1964.

65. Armitt, J., "The simulation of the atmospheric boundary layer in a wind tunnel," Central Electricity Research Laboratories, Lab. Note No. RD/L/N83/66, 1966.

66. Lloyd, A., "The generation of shear flow in a wind tunnel," Quart. Jour. Roy. Met. Soc., Vol. 93, pp. 79-96, 1967.

67. Lau, Y. L. and W. D. Baines, "Flow of stratified fluid through curved screens," Jour. of Fluid Mech., Vol. 33, Pt. 4, pp. 721-738, 1968.

68. Bradshaw, P., "Boundary-layer problems of 1966," National Physical Lab. Aero. Rept. 1203, ARC 28 191, July 1966.

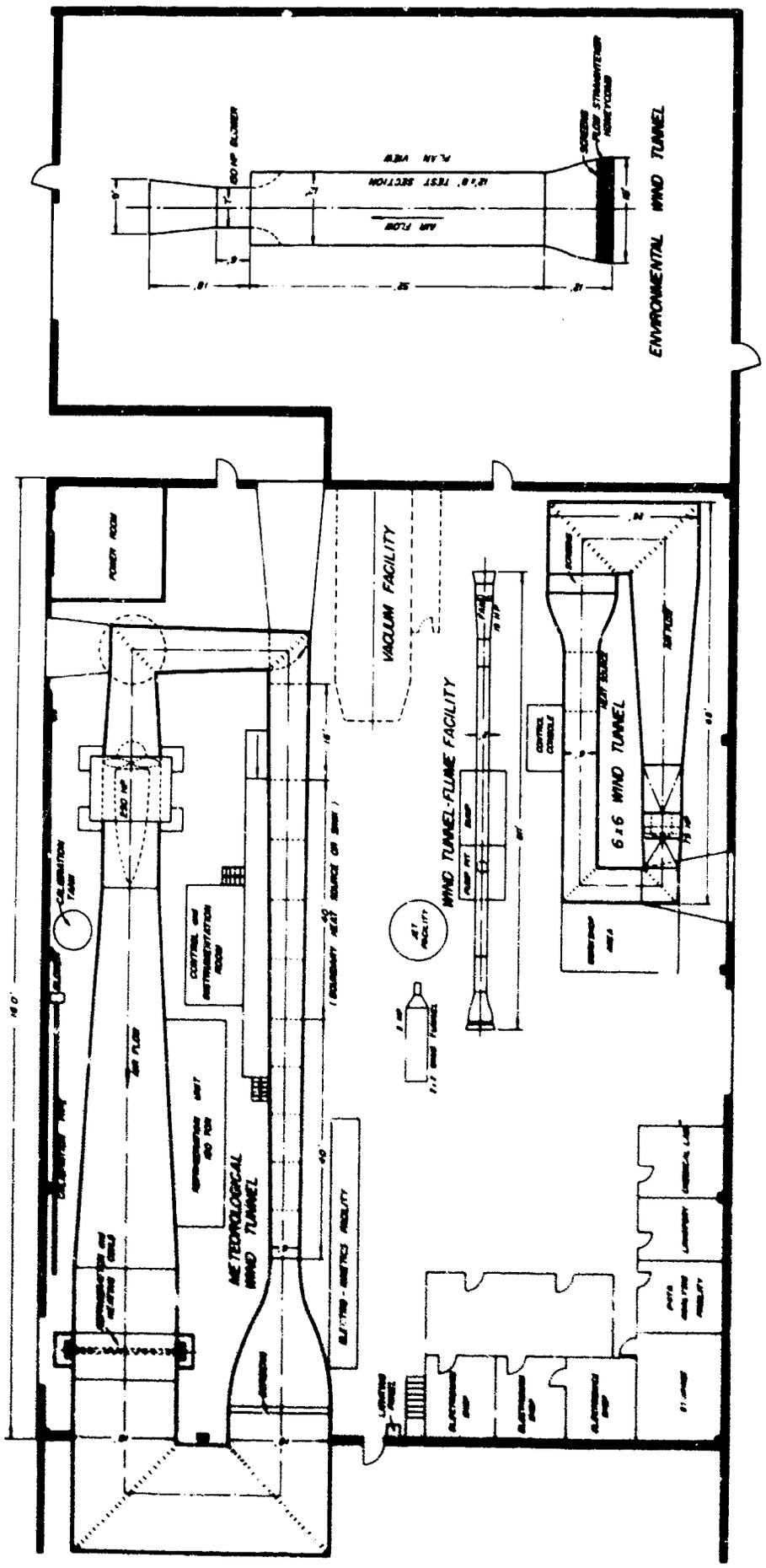

Fig. 1 Plan of Fluid Dynamics and Diffusion Laboratory

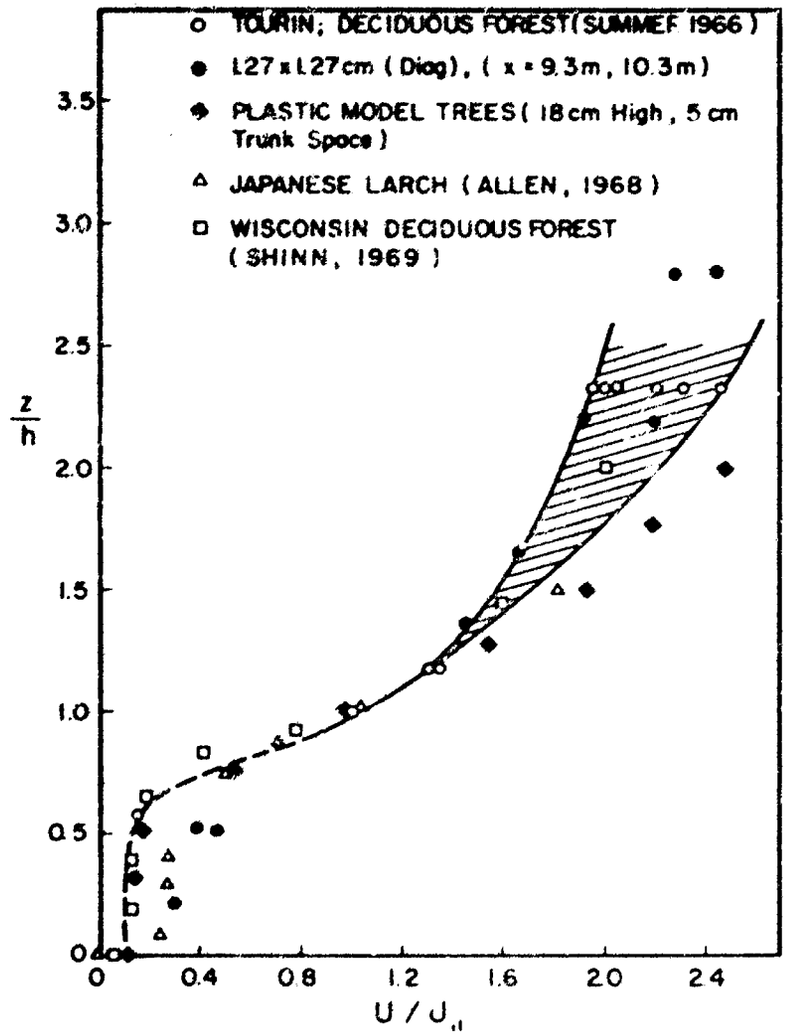

Fig.2 Comparison of Velocity Distributions in and above Model and Prototype Forest Canopies (Ref.39)

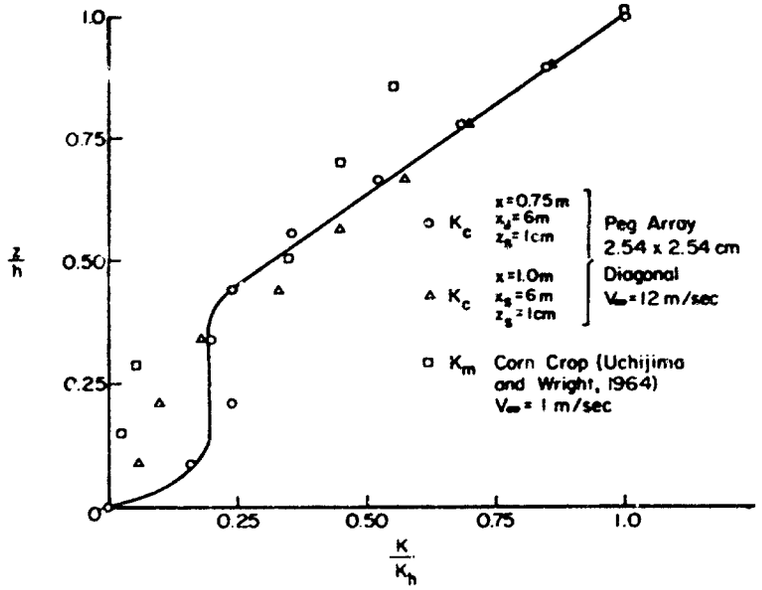

Fig.3 Comparison of the Dimensionless Eddy Diffusion Coefficient in Model and Prototype Canopies (Ref.41)

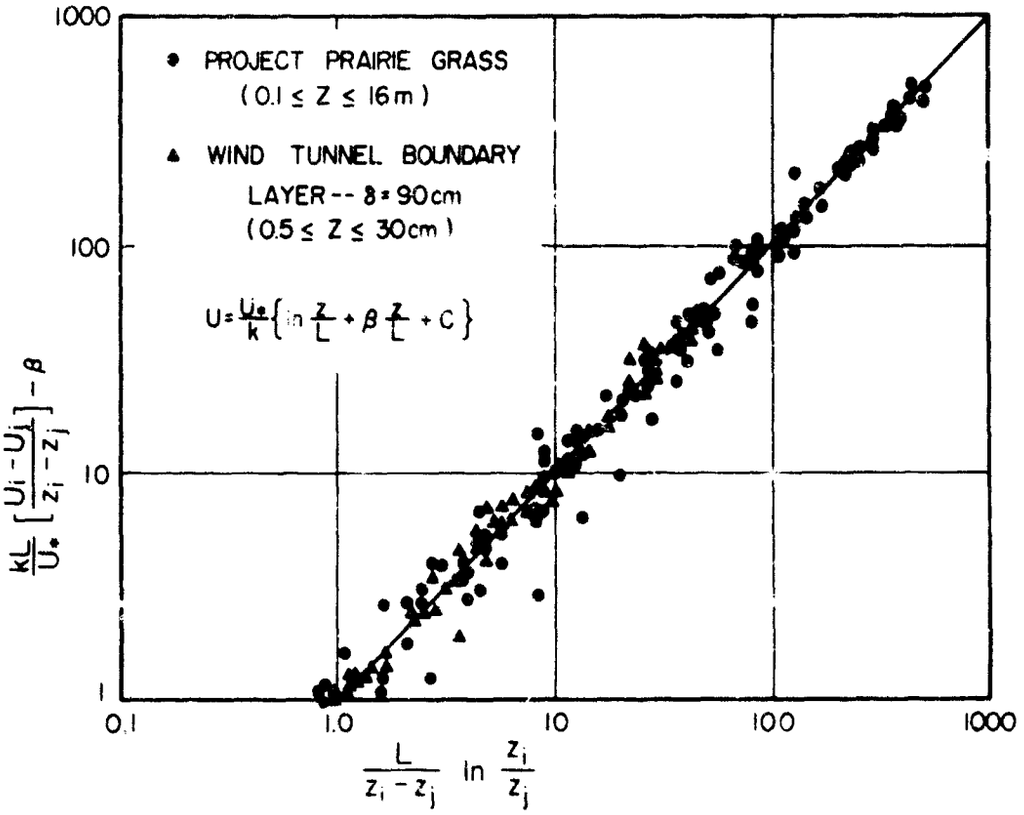

Fig.4 Comparison of Dimensionless Mean Velocity and Temperature in the Wind Tunnel and the Atmosphere (Ref.49)

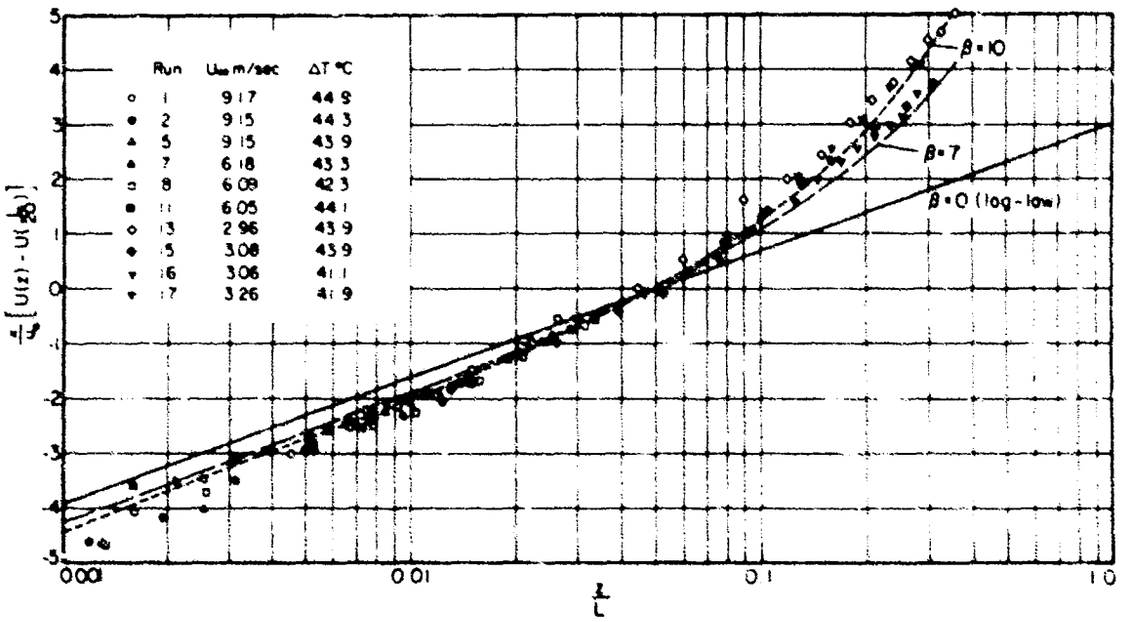

Fig.5 Mean Velocity Distribution in the Wind Tunnel in Relation to the Log-Linear Law (Ref.12)

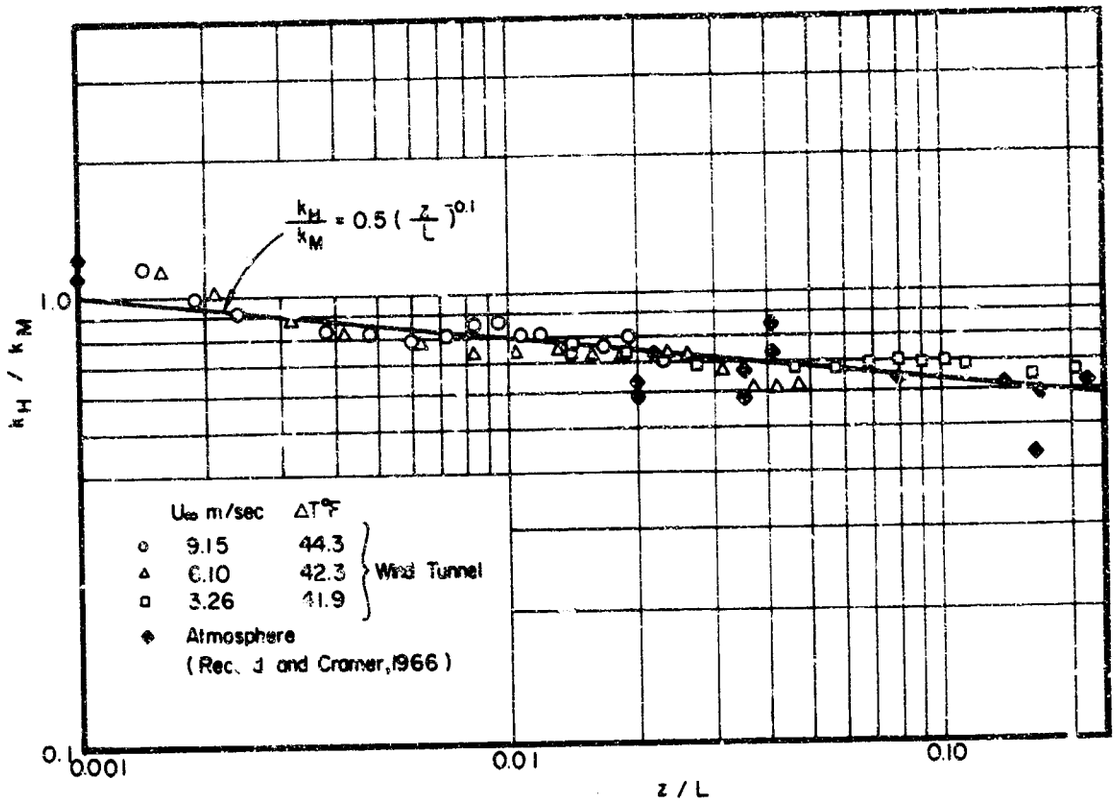

Fig.6 Variation of K_H/K_M with z/L in the Wind Tunnel and the Atmosphere (Ref.12)

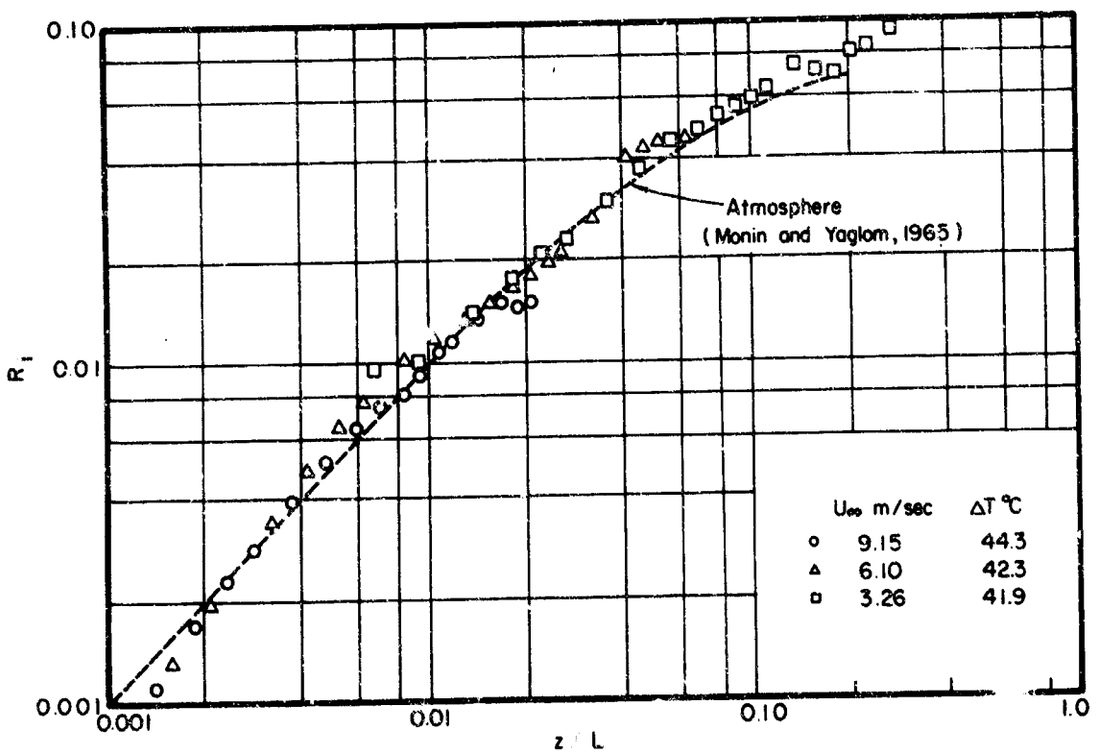

Fig.7 Richardson Number as a Function of z/L for the Stratified Flow in the Wind Tunnel and the Atmosphere (Ref.12)

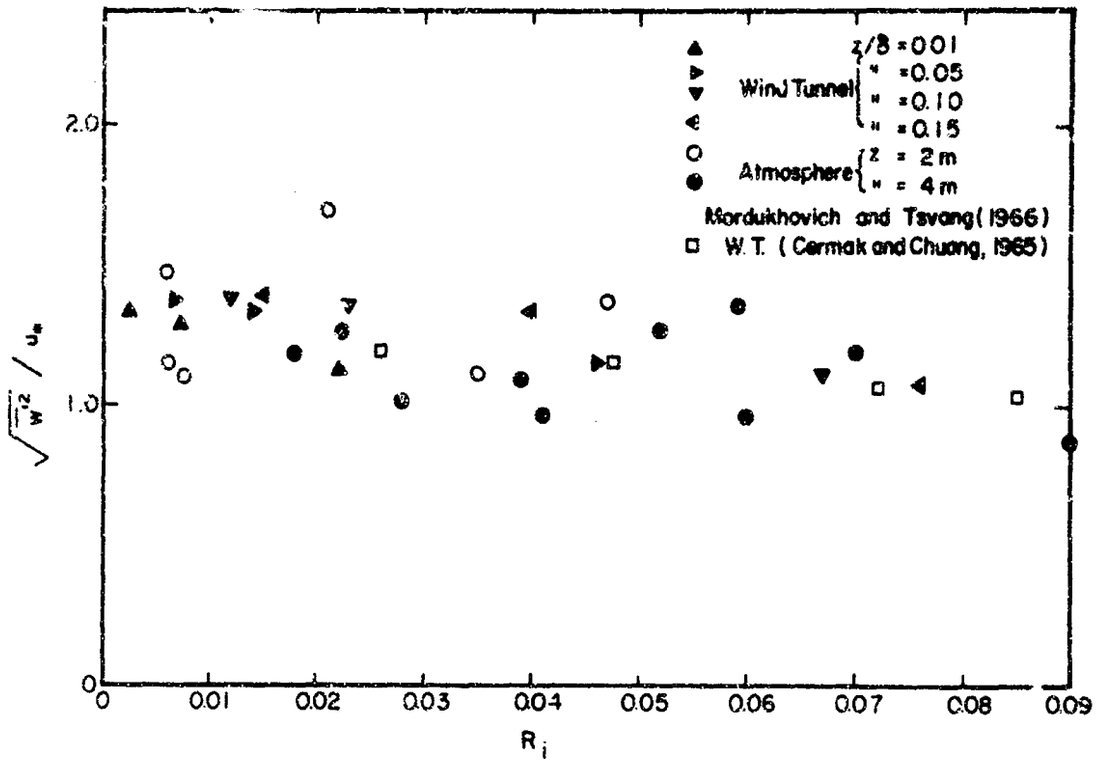

Fig.8 $(\overline{w'^2})^{1/2}/u_*$ vs. z/L : Comparison of Wind Tunnel and Atmospheric Data (Ref.12)

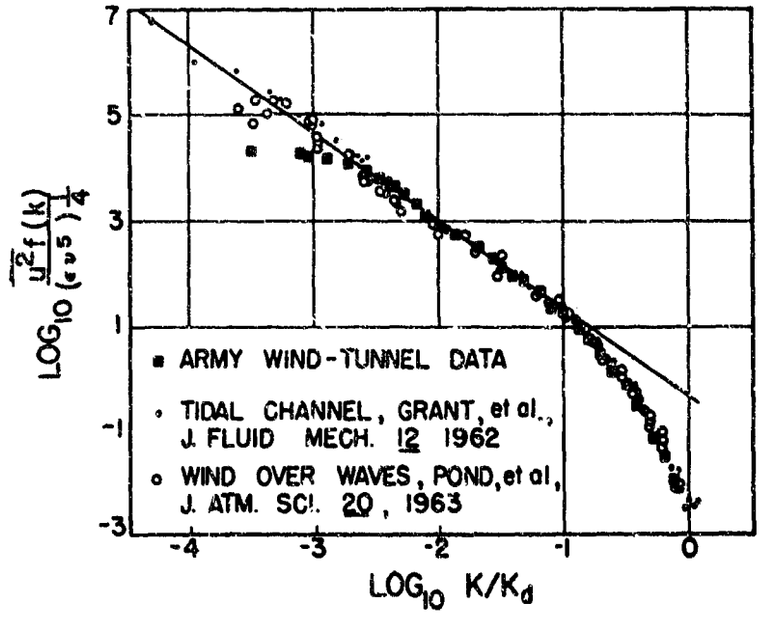

Fig.9 Comparison of Spectra Measured in the Wind Tunnel and Field (Ref.52)

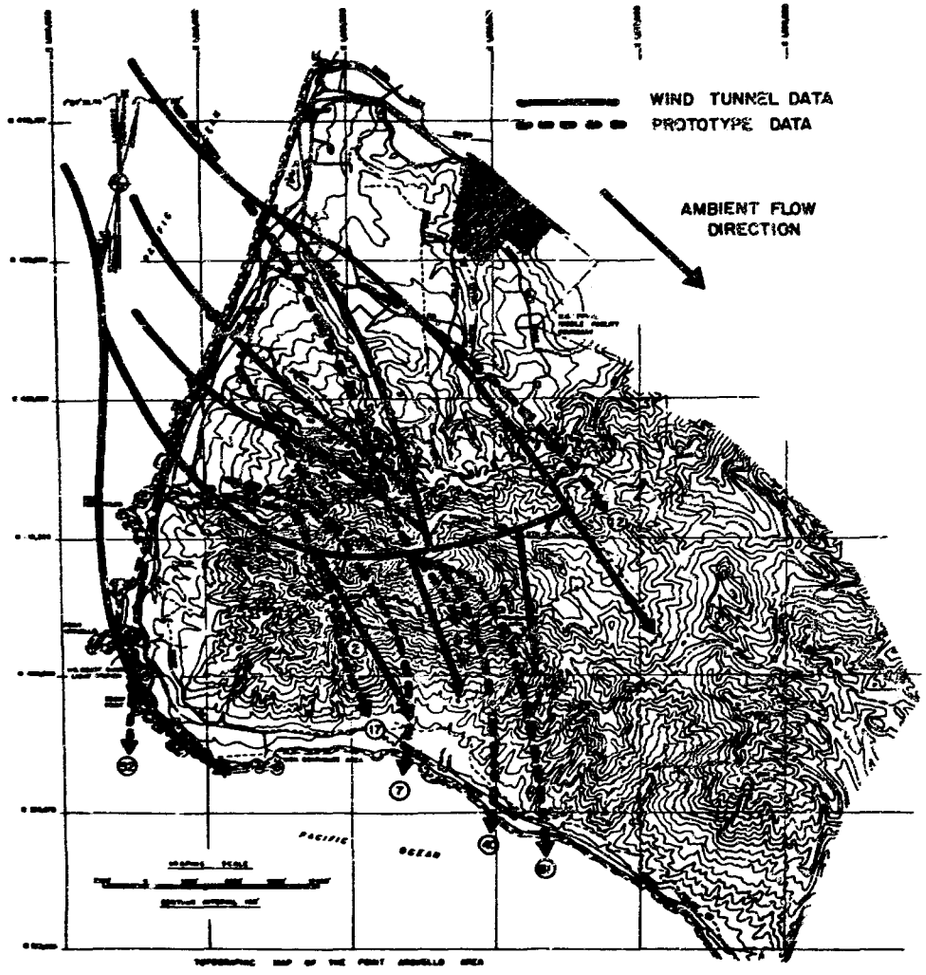

Fig.10 Comparison of Point Arguello Model and Prototype Flow Patterns for Inversion Conditions (Ref.58)

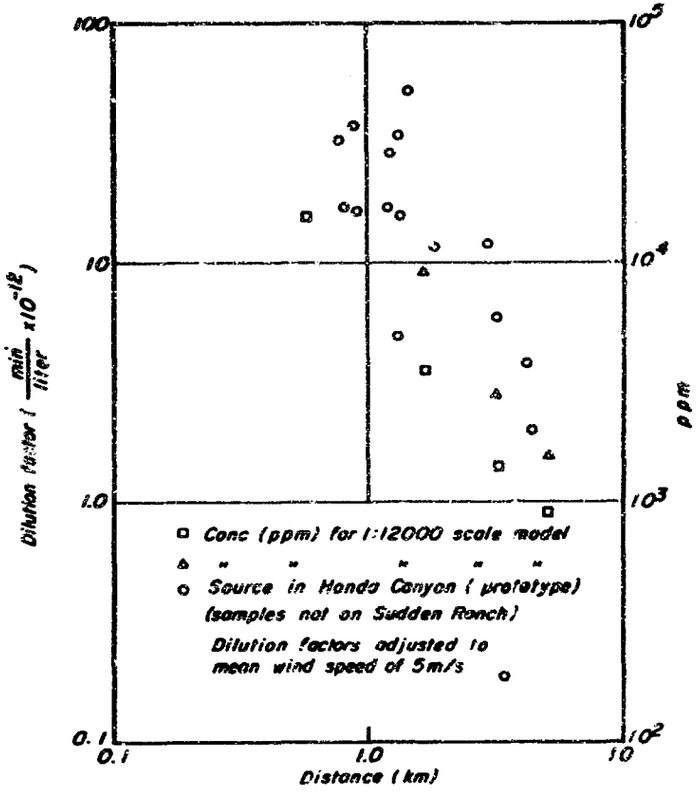

Fig.11 Downwind Variation of Dilution and Concentration in Model and Prototype Flows over Point Arguello (Ref.58)

METHODS AND CONSEQUENCES OF ATMOSPHERIC BOUNDARY LAYER SIMULATION

by David J.Cockrell* and Brian E.Lee**

*University of Leicester

**Shell Research Ltd.

Summary

When wind-tunnel testing model situations representative of flow in the atmospheric boundary layer mean velocity profiles must be simulated accurately. It is also desirable to reproduce the corresponding turbulence structure faithfully in all respects. Such reproduction calls for complete representation of the terrain upstream of the model situation. But blockage effects demand wind tunnels of large cross-sectional area for this class of work, thus full representation of the mean and turbulent flow velocity is seldom practicable and compromises are necessary. The implications of such compromises are considered.

Two basic methods of mean flow profile production are examined. These are using parallel cylinder grids having varying spacing and wedge-shaped flow-mixing devices. The extensive literature is reviewed so as to provide a guide to mean flow production for the practising aerodynamicist.

An experimental programme is also surveyed in which the mean profiles produced by both methods in a rectangular-section duct at a Reynolds number of 3.0×10^5 are compared with those generated naturally in the same duct.

Though a given mean velocity profile can be generated by more than one basic method the corresponding turbulence distributions will be very different. In particular the resulting Reynolds stress distributions can be very significant since these will cause modifications to the mean velocity profile.

13. METHODS AND CONSEQUENCES OF ATMOSPHERIC BOUNDARY LAYER SIMULATION

by David J. Cockrell (University of Leicester)
and Brian E. Lee (Shell Research Ltd.)*

Notation

$C_F = \frac{1}{\frac{1}{2}\rho u_{max}^2 x} \int_0^x \tau_w dx$	total skin friction coefficient
d	diameter of rods used in grid
h	wind tunnel or duct width
$K = K(y) = \Delta P/\frac{1}{2}\rho V^2$	non-dimensional pressure drop across grid
$K_1 = (p_o - p_d)/\frac{1}{2}\rho \overline{U}^2$	non-dimensional pressure drop of entire grid system
L	axial length measured down the wind tunnel
ℓ	centreline spacing of rods used in grid
n	parameter in power law exponent
P	total pressure in the stream
ΔP	total pressure loss along a streamline
$p = p(x)$	pressure at some streamwise section of the wind tunnel or duct
$p_d = p(y)$	pressure measured downstream of graded drag-producing device (grid)
p_o	pressure at the datum section of the wind tunnel or duct
$\overline{q^2} = \overline{u'^2} + \overline{v'^2} + \overline{w'^2}$	mean turbulence energy
$s = d/\ell$	(for cylindrical rods), solidity ratio
$U = U(x)$	maximum axial temporal mean velocity at some streamwise ordinate x
$\overline{U}$	spatial mean velocity (ratio discharge/cross-sectional area) established in a duct or wind tunnel of width h.
$u = u(x,y)$	axial temporal mean velocity
$u' = u'(x,y)$	fluctuating component of velocity in x-direction
u_{max}	axial mean velocity corresponding to y = h at section AB
$V = V(y)$	axial velocity at the grid
V_1	axial velocity far upstream or far downstream of the grid
v, v_1, v_2	disturbance axial velocities produced by the grid
$V' = V'(x,y)$	fluctuating component of velocity in y-direction
w'	(three-dimensional flow) fluctuating component of velocity in z-direction
x	streamwise ordinate
y	transverse ordinate measured from the wall
α	stream refraction coefficient
δ	boundary layer physical thickness
ν	kinematic viscosity of fluid
ρ	density of fluid
τ	boundary layer shear stress
τ_w	wall shear stress

* Work performed in the University of Leicester Engineering Department

Introduction

There is nothing novel in using wind tunnels to simulate aerodynamic situations. Experiments involving the atmospheric boundary layer may present new problems however. Prominent amongst these is the determination of flow round high-rise buildings, for in such problems the atmospheric shear flow profile is a significant ingredient[1]. The atmospheric environment, however, equally important in modelling problems concerned with vehicle performance estimation or with the dynamics of flow around bridges and similar structures.

The problems of satisfactory modelling flow round high structures in the atmospheric boundary layer are immense. If separation bubbles are to be faithfully scaled the Reynolds number of the model test must be of the order of that for full scale. Since compressibility effects should not be introduced a limit is set on the tolerable model size; for example, it must be one-tenth full scale, or larger. Blockage effects then dictate very large cross-sectional area wind tunnels, e.g. if a 150m high, 15m wide tower is to be modelled in a wind tunnel working section in which no more than 10% blockage area is tolerable the wind tunnel would need to have a working section of 50m x 5m. But even if by suitable compromises or modelling in a medium having a low kinematic viscosity this problem is overcome the question of adequate simulation of the atmospheric boundary layer remains. Is simulation of the temporal mean velocity sufficient or should turbulence characteristics be represented as well? If it is decided to attempt simulation of the latter then to achieve compatibility there is no end to the degree to which one might proceed. Ultimately compatibility implies that the instantaneous model turbulence has a one-to-one correspondence with that for full scale; it is a necessary but not a sufficient condition that root mean square values of turbulence at every point in the model field correspond to those in the full-scale field.

It is one question to say what conditions must be complied with if satisfactory results are to be achieved from a model test, but it is another matter to design the facilities required to produce them. Since it is unlikely that all can be simultaneously reproduced compromises are necessary here too. But good compromises cannot be effected without first considering which are the primary and which the secondary parameters in any problem.

It is generally considered desirable to carry out wind tunnel testing of high-rise buildings in large wind tunnels with a minimum of blockage (10% might be considered a minimum) at as high a Reynolds number as possible. Most tests are in fact conducted at a full scale to model Reynolds number ratio of more than 10:1. Some care is taken to produce a power law mean velocity profile representative of the full scale conditions. Additionally some workers seek to reproduce the root mean square turbulence components (and even the power spectral density of the turbulence component) as faithfully as possible. The purpose of this paper is to explain ways of achieving shear flow simulation and the consequences resulting from the necessary compromises.

The Atmospheric Boundary Layer

Although the atmospheric boundary layer is very complex, certain features have been idealised into commonly accepted relationships.

The mean velocity distribution can be represented by a power law having a variable exponent which is dependent on the terrain to be modelled, i.e.

$$\frac{u}{U} = \left(\frac{y}{\delta}\right)^{1/n},$$

where u is the mean velocity at a height y from the ground and U is the free stream velocity outside a boundary layer of thickness δ. Here n might vary from 2.5 to 10.0, a typical value for open European countryside being about 6.0[2].

In practice U and δ are completely arbitrary. Since $u_1/U = (y_1/\delta)^{1/n}$ where u_1 and y_1 are any related velocity and distance within the boundary layer, then $\frac{u}{u_1} = \left(\frac{y}{y_1}\right)^{1/n}$, for example $\frac{u}{u_{10}} = \left(\frac{y}{10}\right)^{1/n}$ where u_{10} is the velocity 10m from the ground[2]. Thus the profile can be modelled without the boundary layer thickness δ being known.

This is as well, for it is not easy to say in general terms how the boundary layer thickness will vary. The atmospheric velocity field is more like a vortex with its axis perpendicular to the earth than it is like linear flow through a duct. Consequently we should not anticipate a gradual increase in δ with distance. Prandtl[3] discusses the physics of a related problem, that of laminar flow generated in a fluid otherwise at rest by the rotation of a disc about an axis through its centre, and shows that the fluid flows outwards, the surface shear force being less than the necessary centripetal force so that an increase in momentum flux occurs as the fluid moves. He shows that for laminar flow over such a disc the boundary layer thickness is constant. This result was confirmed experimentally by

Gregory, Stuart and Walker[4] who also examined theoretical work by von Karman and Goldstein on the corresponding behaviour of turbulent flow. Though they found less agreement than in the laminar case it would appear that the boundary layer thickness increases with radius. Also surface roughness would appear to influence the nature of the flow as it does for other turbulent flow problems. More recent theoretical and experimental work on this problem confirming these general conclusions, is reported by Cham and Head[5].

What experimental data exists for the nature of the atmospheric boundary layer (e.g. that of Harris[6]) leads us to anticipate characteristic distributions of r.m.s. turbulence components, with peaks close to the surface and a tendency to isotropy as the free stream is approached. The shear stress distribution would be an approximately linear function of distance from the ground decreasing from the surface value τ_w at $y = 0$ to zero at $y = \delta$. Assuming that the degree of immersion of a building in the boundary layer will be considered as a significant parameter (Leutheusser and Baines[7]) the surface roughness height can be non-dimensionalised in terms of the building height. In this way it can be compared with surface finish in other experimental shear flow studies. Where the roughness height is large the surface shear stress and the shear stress (τ) at any ordinate y will also be correspondingly large. Accepting Bradshaw's[8] relationship, $\rho\overline{q^2}a_1 = \tau$ where a_1 is a dimensionless constant (0.15) and $\overline{q^2}$ is the mean turbulence energy $\overline{u'^2} + \overline{v'^2} + \overline{w'^2}$, the r.m.s. turbulence components will also be correspondingly large. There is some evidence (e.g. that of Armitt[9]) that the turbulence energy is a significant flow parameter.

Modelling the Atmospheric Boundary Layer

The aerodynamicist wishes to produce in his wind tunnel a power law mean velocity profile having an exponent which he can vary. The turbulence parameters accompanying this profile have the characteristics of fully-developed duct flow. However we have already established that the ideal tunnel has as large a working section cross-sectional area as possible and if a boundary layer is permitted to develop naturally down the entrance length, such a settling length would be of inordinate dimensions. He therefore looks for other means of achieving his end.

In the system shown in figure 1 a uniform incompressible, two-dimensional stream enters at AD with velocity $\overline{U}$ a duct of width h. Either naturally or as a consequence of some constraint situated within the area ABCD, a mean velocity profile $u = u(y)$ is established at BC. The pressure at AD is denoted by p_o, whilst that at BC is denoted by p, both independent of y. Then the problem satisfies the following requirements:

Continuity

$$\overline{U}h = \int_o^h u\,dy$$

Momentum

$\Sigma F_x = (p_o - p)h$ + thrust developed on walls and constraint

$$= \rho\left[\int_{BC}^{h} u^2\,dy - \overline{U}^2 h\right]$$

Equilibrium

When the mean velocity profile is in equilibrium the total axial force acting on the fluid, $\Sigma F_x = 0$.

Energy

Since the shear force developed on AB does no work, application of the energy equation along the streamline AB gives,

$$p_o + \tfrac{1}{2}\rho\overline{U}^2 = p + \tfrac{1}{2}\rho u_{max}^2 + \Delta P_{AB}$$

where u_{max} is the mean velocity at the section BC corresponding to $y = h$ and ΔP_{AB} is the loss in total pressure along the streamline AB.

Since the mean profile at BC is assumed to be given by

$$\frac{u}{u_{max}} = \left(\frac{y}{h}\right)^{1/n},$$

then by continuity,

$$u_{max} = \left(\frac{n+1}{n}\right)\overline{U};$$

and by momentum principles in the absence of any other constraint

$$(p_o - p)h - \int_o^x \tau_w\,dx = \frac{\rho\,\overline{U}^2 h}{n(n+2)},$$

where τ_w is the shear stress developed on the lower wall CD. (It should be noted that the shear stress developed on the wall AB is assumed to be negligible compared with that on CD, otherwise the profile could not be formed.) The right hand side is the momentum flux surplus,

$$\frac{\rho\bar{U}^2h}{n(n+2)} = \rho u_{max}^2 h \frac{n}{(n+1)^2(n+2)} ,$$

which is not equal to the normally accepted momentum thickness of a boundary layer,

$$\rho u_{max}^2 h \frac{n}{(n+1)(n+2)}$$

for in the present problem the flow is constrained by the upper wall AB.

Assuming ΔP_{AB} is negligible in the energy equation, $(p_o-p)h$ is given by

$$\tfrac{1}{2}\rho(u_{max}^2 - \bar{U}^2)h = \tfrac{1}{2}\rho\bar{U}^2h \frac{(2n+1)}{n^2} .$$

Inserting this value into the momentum equation gives

$$\int_o^x \tau_w dx = \rho \bar{U}^2h \left[\frac{2n^2+3n+2}{2n^2(n+2)}\right] = \rho u_{max}^2 h\left[\frac{2n^2+3n+2}{2(n+1)^2(n+2)}\right] .$$

Thus the drag produced on the lower wall is related to the required power law profile.

How can this drag be produced? The condition that the wall CD is smooth is artificial in view of the assumption made concerning the wall AB, unless AB be considered the centre streamline in a duct of total width 2h. In this case, (using an expression for the surface friction relevant to zero pressure gradient and n=7, that

$$C_F = \frac{1}{\tfrac{1}{2}\rho\bar{U}^2x} \int_o^x \tau_w dx = 0.074 \left(\frac{\bar{U}x}{\nu}\right)^{-1/5} , \text{ we have}$$

$$\int_o^x \tau_w dx = \tfrac{1}{2}\rho\bar{U}^2x \;\; 0.074 \left(\frac{\bar{U}x}{\nu}\right)^{-1/5} , \text{ i.e.}$$

$$\frac{x}{h} = \left(\frac{\bar{U}h}{\nu}\right)^{\frac{1}{4}} \left[\frac{2n^2+3n+2}{0.074\, n^2(n+2)}\right]$$

e.g. at a Reynolds number $\bar{U}.2h/\nu$ of 3.0×10^5 to achieve a 1/7th-power law profile in a smooth-walled duct $x/2h = 50$. Raising the Reynolds number to 2.0×10^5 increases this figure to 81.

Typically, the effect of wall roughening might be to increase the drag 1.5 times at a Reynolds number of 2.0×10^6. Such roughening would reduce the duct length required to produce a 1/7th-power law profile to 45 duct heights.

Further reduction in length is possible by still further increasing the drag. A step might well be used for this purpose.

In all these cases the normal turbulent mixing processes ensure the development of the characteristic power-law profile shape consisting of a near constant axial mean velocity except in the region extremely close to the wall. But since diffusion by turbulent mixing occurs comparatively slowly it may be necessary to use vortex generating devices downstream of the step to hasten the mixing processes. On grounds that will be developed later in the paper it is important to ensure that the shear stress profile is well represented. Vortex generating devices introduce considerable turbulence into the stream and modelling of the resulting turbulence parameters is an important though largely ad hoc process (see for example ref.10).

The figures derived in the foregoing analysis illustrate the principle of one method of profile production. The most questionable assumption made is that for the surface friction as the boundary layer develops down the duct. For flow in a favourable pressure gradient the surface friction will be greater than the value assumed and hence the values obtained for the length of duct required to achieve the required profile would be conservative. If a discrete

constraint (such as a step) is employed the analysis develops an expression for its drag but it gives no guidance on the duct length required for the profile to develop beyond indicating that it would be short compared with that required by the smooth-walled duct.

An alternative simulation technique is to use a graded drag-producing mechanism (or grid) across the wind tunnel working section. Such a technique enables the required shear flow mean velocity profile to be satisfactorily simulated but the corresponding turbulence parameters are less well represented. An important implication of this state of affa'rs, that the mean profile is not in equilibrium in the wind tunnel, is discussed later.

In forming a mathematical model for the design of a grid the characteristic argument is to neglect the production of shear stresses, assuming no further change will occur in the profile once it has been produced. Thus the flow can be regarded as potential both upstream and downstream of the grid.

Over the last 30 years there have been a number of approaches to the problem of the design of graded drag-producing mechanisms. Using Weighardt's relationship[11] the non-dimensional pressure drop, K, across the grid is related to its geometry and may be expressed as

$$K = \Delta P/\tfrac{1}{2}\rho V^2 = \Delta p/\tfrac{1}{2}\rho V^2 = ks/(1-s)^2.$$

where ΔP is the total pressure loss caused by the grid through which flow occurs with velocity V, hence $\Delta P = \Delta p$, and s the solidity ratio of the grid (which for cylindrical rods of diameter d and centreline spacing ℓ) is equal to d/ℓ. K is a slowly varying function of Reynolds number.

In order to design the grid it is necessary to establish an expression for K(y) in terms of the given upstream velocity profile and the required downstream velocity profile. Collar[12] established a method of analysis based on Rankine-Froude actuator disc theory. Assuming the total head to be conserved both upstream and downstream of the grid he used momentum and energy principles to establish the expression for K in terms of upstream and downstream axial velocities. The problem of grid design differs from actuator disc theory however in that the pressure far from the grid is not the same upstream as it is downstream and in developing the relationship Collar had to consider the evaluation of this overall pressure difference. There are additional problems associated with satisfying continuity for flow constrained by a duct and the method adopted was criticised by Taylor and Batchelor[13]. They (and others since) introduce disturbance velocities having some simple structure into the flow. Using the constancy of total head postulation both upstream and downstream of the grid they obtain the relationship

$$\frac{v_2}{v_1} = \frac{1 + a - aK}{1 + a + K}$$

Where v_1 is the velocity increment produced by the disturbance velocity at an upstream station and v_2 is the corresponding increment at a downstream station, both being constant across the section. a is a coefficient which accounts for the refraction of the stream at the grid introduced by the lateral flow. Using this equation K is given from the known velocity distribution $V + v_1$ and the required distribution $V + v_2$ once a is known. An empirical relationship for a suggested by Taylor and Batchelor is

$$a = 1.1(1 + K)^{-\frac{1}{2}}$$

Owen and Zienkiewicz[14] developed the method to permit linear shear profiles to be produced. Later Elder[15] produced a very general extension, enabling arbitrarily-shaped and positioned gauzes to be used, which is complex and difficult to follow. Recently Turner[16] has made the method much more amenable to treatment by considering numerical methods of solution, suitable for digital computation, of Elder's equations.

McCarthy[17] greatly simplified the presentation of the problem of producing highly sheared flows. Using the concept of constancy of total head in the axial direction, both upstream and downstream of the grid he further argues that since vorticity is constant along streamlines (to the first order of small quantities) the lateral total head gradient is given by

$$\frac{dP}{dy} = \rho V \left(\frac{dV_1}{dy}\right)$$

where V is the local axial velocity at the grid and V_1 is the axial velocity either a long way upstream or downstream of the grid according to which field of flow is under consideration.

Hence

$$\tfrac{1}{2}V\frac{dK}{dy} + K\frac{dV}{dy} + \frac{d}{dy}(V_{1u} - V_{1d}) = 0$$

where subscripts u and d imply upstream and downstream evaluations respectively and K is written as $\Delta H/\frac{1}{2}\rho V^2$. Whilst permitting the design of varyingly-graded grids for the production of shear flow in a duct, McCarthy's equation reduces to Taylor and Batchelor's for uniformly-graded grids.

Not only has the mathematics of grid design now become formidable, but (as Cowdrey[18] comments on the present authors simplifications of Elders method[19]) in order to get solutions at all from such sophisticated approaches linearising techniques, which are invalid in regions of high shear close to the wall, have to be adopted.

Cowdrey's approach is based on the idea of using simple concepts which mould the physics but which may well be only an approximate representation of the system. These are to consider that since the grid of rods has a major influence by blockage on the flow ahead of it, its entire influence is on the upstream flow, all lateral flow taking place before the grid. He also defines a system pressure drop coefficient K based on the static pressure difference from far upstream to far downstream of the grid.

Since the flow downstream of the grid is assumed to be unaffected by it then

$$\tfrac{1}{2}\rho\bar{U}^2K_1 = p_o - p_d = \tfrac{1}{2}\rho(V^2 - \bar{U}^2) + \tfrac{1}{2}\rho V^2K$$

where the subscripts o and d refer to upstream (datum) and downstream conditions respectively, the upstream velocity $\bar{U}$ is considered independent of y whilst the velocity at the grid V and the non-dimensional pressure drop across the grid K are both y-dependent. Writing $u^* = V/\bar{U}$ gives

$$(u^*)^2 = (1 + K_1)/(1 + K)$$

K_1 is first determined arbitrarily and its successive use is on the basis of experience. The larger the value chosen the fewer the number of rods which will be required in the resulting grid. Thus design of grids having different values of K_1 may give some measure of control over the accompanying turbulence structure. u^* is established by the shape of the velocity profile that is required, e.g. for a linear shear profile in which

$$\bar{U}\delta = \int_o^\delta u\,dy$$

then

$$u^* = 2y/\delta$$

Note that u^* is not the non-dimensional velocity ratio in the required profile: in the illustration chosen the maximum velocity is shown by continuity to be $2\bar{U}$ and not $\bar{U}$.

Thus K is determined in terms of known values of u^* and K_1. The solidity ratio relationship, $K = ks/(1 - s)^2$, is then invoked to give the required rod spacing.

Equilibrium boundary layers

The x-directed momentum equation applied at any transverse ordinate y in the boundary layer states that the rate of change of axial momentum is equal to the forces applied in the x-direction. If the phrase "equilibrium boundary layer" is used to imply that the temporal mean velocity profile is invariant with x, the momentum equation shows the profile will be in equilibrium when the x-directed force is zero, i.e. the pressure forces balance the total shear forces (inclusive of the Reynolds inertial forces). Hence the equilibrium condition is that

$$\frac{dp}{dx} = \frac{\partial\tau}{\partial y}$$

and since the pressure p can be considered invariant with respect to y, the shear stress will then be a linear function of y,

$$\frac{\tau}{\tau_w} = 1 - y/\delta$$

For a laminar flow, where the molecular viscosity is considered constant, this of course leads to a parabolic velocity profile. For turbulent flow it would be necessary to establish the form of the eddy viscosity relationship before the resulting mean velocity profile shape could be known.

The above elementary analysis assumes that the mean velocity profile is formed in a duct or wind tunnel. If it is allowed to grow naturally in this environment it will (eventually) be accompanied by a linear shear stress distribution and thus reach a state of equilibrium. Note (from fig. 8) that the shear stress, growing out from the wall, does not attain this linear distribution until a considerable duct length has been traversed. It is the initial deficiency in centre-line shear stress gradient which is responsible for the characteristic growth of turbulent boundary layer thickness parameters to a maximum, followed by a decrease to their equilibrium values (fig.7). However, if modelled artificially probably the shear stress will be non-linear. Vortex generating devices for example may impose large departures from the required shear stress profile, whilst graded grids produce little shear stress at all. In such cases the required mean velocity profile may be established in the wind tunnel but it will be out of equilibrium and the extent to which it will depart from its equilibrium shape is shown (by the momentum equation) to be dependent on the magnitude of the local shear stress gradient, (for the rate of change of x-directed momentum per unit mass equals $\partial\tau/\partial y - dp/dx$).

Since the velocity profile eventually attains an equilibrium state this development must be a stable process. Stability is brought about by the action of the mean velocity profile back on the shear stress distribution. Suppose for example that locally $\partial\tau/\partial y - dp/dx$ is large and positive. The accompanying force promotes flow acceleration and a local x-directed velocity in excess of that at larger values of y. Mixing length theory then indicates that the local Reynolds stress will no longer be strongly negative, that is there will be a reduction in the local value of shear stress and hence of the x-directed force per unit mass, $\partial\tau/\partial y - dp/dx$. In this way production of the equilibrium boundary layer can be seen to be a stable process.

The essence of atmospheric boundary simulation however is that non-dimensional duct length must be kept as short as possible. Hence there is little possibility for artificially formed mean velocity profiles to acquire an equilibrium state. Though the profile formed in the wind tunnel may represent the required atmospheric mean velocity profile the modelled profile is much more liable to change than its full scale counterpart.

How much does this lack of equilibrium concern us? Probably very little, for most wind tunnel studies are concerned with the effects of air flow under very localised conditions. Where whole regions may be modelled in the tunnel however it is important to consider that deviations from linearity in the shear stress distribution could result in unacceptable mean velocity variation in the working section. A simple test to determine whether the mean velocity profile is sufficiently in equilibrium to be acceptable should always be carried out. This could be done by examining the profile variation over the working section length before the model is inserted into the wind tunnel

Experimental programme

The wind tunnel used in the present investigation is shown schematically in fig. 2. Its purpose was to enable the behaviour of two-dimensional boundary layers produced by a variety of methods to be studied and the major criteria for the tunnel design were that overall length had to be less than 20m, that it was to be powered by a fan already available and that it must be produced economically. A working section velocity of 60m/s was considered desirable and power restrictions then limited the cross-sectional area of the working section to a maximum of $0.1m^2$. The working section was then manufactured in glass-fibre to internal dimensions of 12 inches x 4 inches (0.3m x 0.1m) and thus working section Reynolds number based on duct height was about 3.0×10^5. Provision to traverse pitot and static tubes as well as normal and slanting hot wire anemometer probes was provided every 0.3m throughout the working section length of 121 equivalent duct heights. Wind speed control was by means of adjustable shutter vanes mounted downstream of the fan. Turbulence information was obtained using a D.I.S.A. Constant Temperature Anemometer in association with D.I.S.A. hot-wire probes.

As well as permitting natural boundary layer growth, mean velocity profiles were simulated using grids of rods and flow-mixing devices. 0.036 inch (0.9mm) stainless steel piano wire tensioned in an angle-iron frame (fig. 3) was used for the rods and initially the spacing was determined by the modification to Elder's method described by the Authors[19]. Later Cowdrey's[18] method was used and shown to give improved results. The spacing of the wires was set accurately by running them over suitably machined notched rollers.

Following Schubauer and Spangenberg[20] a reversible flow-mixing device was designed, the basic element of which is shown in fig. 4. In one direction the element forms a plough-shape, reversed it is a ramp. The elements were attached to the floor and roof of the tunnel behind a step as shown in fig. 5.

Experimental results

Mean velocity profiles produced immediately behind the various mixing devices are shown in fig. 6. Grids designed to produce power-law mean velocity profiles are seen to be behaving successfully. The profiles produced by the step and forced-mixing devices are less immediately acceptable. Severe separation has occurred near the base of the ramp and by continuity, the result is an increase in the central-region velocity producing a jet-type of flow. With the plough-shape the converse has occurred. Flow has been directed towards the walls leading to a velocity-defect in the central region and a wake-type of flow. The length of duct required to attain an equilibrium state may be judged from fig. 7, in which the physical thickness, δ, of the boundary layer is that at which $u = 0.95u_{max}$. For duct flow it is of the order of 80 duct heights (compare a figure of 50 duct heights previously calculated). Profiles obtained by the use of wire grids are not in equilibrium until the same order of distance downstream of the grid. For the ramp however, an acceptably stable state is achieved in half this distance. The reason for the rapid attainment of equilibrium is the short distance required for the greatly increased shear stress to attain a linear distribution. Compared with the naturally developing boundary layer (fig. 8) the shear stress produced by the flow-mixing device used as ramp attains a linear distribution in one-quarter of the duct length (fig. 9).

The development of the centre-line shear stress gradient for the flows behind the simulation devices is given in fig. 10. As has been shown, equilibrium is attained when $\partial\tau/\partial y$ is constant and equal to dp/dx; this occurs when the non-dimensional shear stress gradient is equal to unity. A value different from unity implies mean flow acceleration or deceleration along the centre-line.

The centre-line shear stress gradient is much more critically susceptible to small changes in flow conditions than are bulk parameters, based on the mean velocity profile, since the former is the cause of temporal mean velocity changes and the latter the effect. It is a parameter which is most responsive to flow history because of the diffusion of turbulence which occurs outwards, from the walls and the simulation devices, to the duct centre-line.

Because of the lack of turbulent shear stresses produced by the graded grid, profiles produced by this means take the longest distance to achieve equilibrium. With the triangular plough simulator and particularly with the ramp simulator however, equilibrium is achieved very rapidly, in some 40 duct heights in the latter case.

Discussion of results

There are a large number of possible methods which could be utilised for atmospheric boundary layer simulation. Some are better than others but all of them have their drawbacks regarding the flows they produce and the practical difficulties involved in their use. The use of wall roughness often requires a prohibitive length of wind tunnel and only produces small scale turbulence. The use of grids of rods is the most practical method and is frequently used. They produce the required velocity profile almost immediately downstream of the grid but as turbulence diffuses outwards from the wall the consequent Reynolds stress distribution is such as to cause the profile to be modified. Added to this the turbulence associated with the grid is much smaller than it would be in the atmospheric environment and, for reasons stated earlier, the simulated profile may be unrepresentitive.

The main disadvantage of flow-mixing devices such as the ramp and plough-shape is that their use is much on a trial and error basis. Their advantage for atmospheric boundary layer simulation is that the turbulence structure can be adequately simulated as well as the mean velocity profile. Equilibrium mean velocity profiles form quickly with the ramp simulator; it is thus preferable to the triangular plough shape.

Extensive experimental data on the methods of simulation described in this paper is contained in ref. 21.

Conclusions

1. To simulate atmospheric boundary layers appropriately in wind tunnels it is at least necessary to be able to produce an arbitrary temporal mean velocity distribution and to reproduce the scale of turbulence. Following Bradshaw this then implies that all root mean square turbulence parameters are simulated.

2. Practicable simulation implies the use of graded grids of rods or of flow-mixing devices. If grids of rods are employed, Cowdrey's design method is recommended. Such simulation reproduces the mean velocity profile adequately but is less satisfactory for turbulence parameters. Both mean flow and turbulence can be simulated satisfactorily using flow-mixing devices but the processes are much less well understood theoretically. The ramp-type device permits simulation in a shorter axial length than any of the other mechanisms tested.

3. It is fortunate that development of an appropriate profile is a stable process. Like a novel, this means that the profile will come out all right in the end, though the axial length required and the corresponding turbulence profile are dependent on the methods employed.

4. It is unlikely that the simulated profile will be in equilibrium, immediately downstream of the production mechanism, since this requires the simultaneous generation of a linear shear stress profile. This is probably unimportant except where it is necessary to model extensive terrain or to examine flows about the model at large values of y/h.

References

1. Wise, A.F.E., Sexton, D.E. and Lillywhite, M.S.T.: "Studies of air flow round buildings", Building Research Station Current Papers, Design Series, 38, 1965.

2. Shellard, H.C.: "The estimation of design wind speeds", Wind Effects on Buildings and Structures, N.P.L. Symposium 16, 1963, H.M.S.O. 1965.

3. Prandtl, L.: "Essentials of Fluid Dynamics", (Trans.) Blackie, 1952.

4. Gregory, N., Stuart, J.T. and Walker, W.S.: "On the stability of three-dimensional boundary layers with application to the flow due to a rotating disc", N.P.L. Symposium on Boundary Layer Effects in Aerodynamics, 1955, H.M.S.O. 1955.

5. Cham, T-S. and Head, M.R.: "Turbulent boundary layer flow on a rotating disk", J. Fluid Mech., Vol.37, pp.129-147, 1969.

6. Harris, R.I.: "Measurements of wind structure at heights up to 598 ft. above ground level", Loughborough University of Technology Symposium on Wind Effects on Buildings and Structures, 1968.

7. Leutheusser, H.J. and Baines, W.D.: "Similitude problems in building aerodynamics", Proc. A.S.C.E. paper 5226, May 1967.

8. Bradshaw, P., Ferriss, D.H. and Atwell, N.P.: "Calculation of turbulent boundary layer development using the turbulent energy equation", N.P.L. Aero. Report 1182, 1968.

9. Armitt, J.: "The effect of surface roughness and free stream turbulence on the flow around a model cooling tower at critical Reynolds numbers", Loughborough University of Technology Symposium on Wind Effects on Buildings and Structures, 1968.

10. Counihan, J.: "An improved method of simulating an atmospheric boundary layer in a wind tunnel", Atmospheric Environment, Pergamon Press 1969, Vol.3, March 1969.

11. Weighardt, K.E.G.: "On the resistance of screens", Aeronautical Quarterly, Vol.4, pp.186-192, 1953.

12. Collar, A.R.: "The effect of a gauze on the velocity distribution in a uniform duct", A.R.C.R. and M. 1867, 1939.

13. Taylor, G.I. and Batchelor, G.K.: "The effect of a wire gauze on small disturbances in a uniform stream", Quart. Journ. Mech. and App. Math., Vol.2, pp. 1-29, 1949.

14. Owen, P.R. and Ziankiewicz, H.K.: "The production of uniform shear flow in a wind tunnel", J. Fluid. Mech., Vol.2, pp. 521-31, 1957.

15. Elder, J.W.: "Steady flow through non-uniform gauzes of arbitrary shape", J. Fluid Mech., Vol. 5, pp. 355-68, 1959.

16. Turner, J.T.: "A computational method for the flow through non-uniform gauzes: the general two-dimensional case", J. Fluid Mech., Vol. 36, pp.367-383, 1969.

17. McCarthy, J.H.: "Steady flow past non-uniform wire grids", J. Fluid Mech., Vol. 19, pp. 491-512, 1964.

18. Cowdrey, C.F.: "A simple method for the design of wind tunnel velocity profile grids", N.P.L. Aero. Note 1055, May 1967.

19. Cockrell, D.J. and Lee, B.E.: "Production of shear profiles in a wind tunnel by cylindrical rods placed normal to the stream", J.R. Aero. Soc., Vol. 70, pp. 724-5, 1966.

20. Schubauer, G.B. and Spandenberg, W.G.: "Forced mixing in boundary layers", J. Fluid Mech., Vol. 8, pp. 10-32, 1960.

21. Lee, B.E.: "Some effects of history on turbulent fluid flow", University of Leicester Ph.D. Thesis 1969.

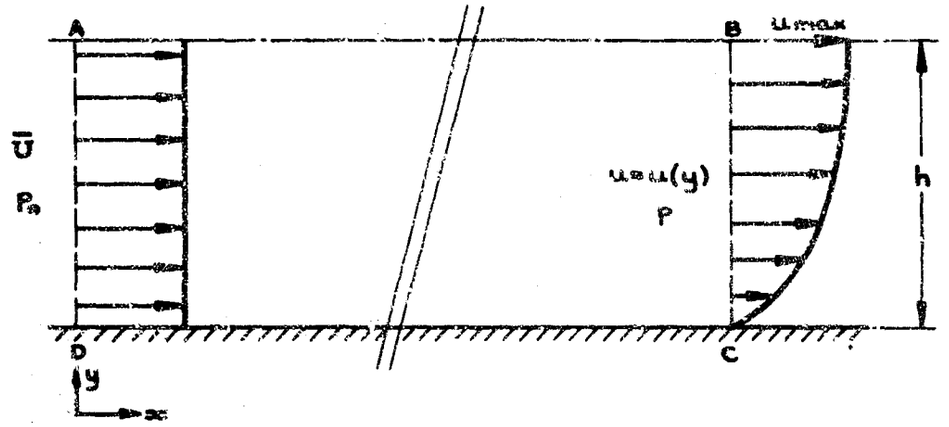

FIG. 1. MODELLING THE ATMOSPHERIC BOUNDARY LAYER

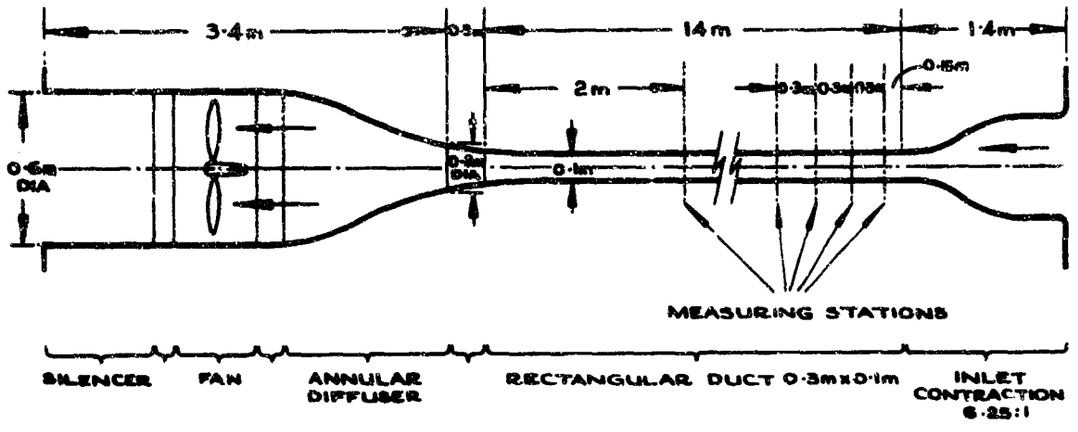

FIG. 2. EXPERIMENTAL WIND TUNNEL

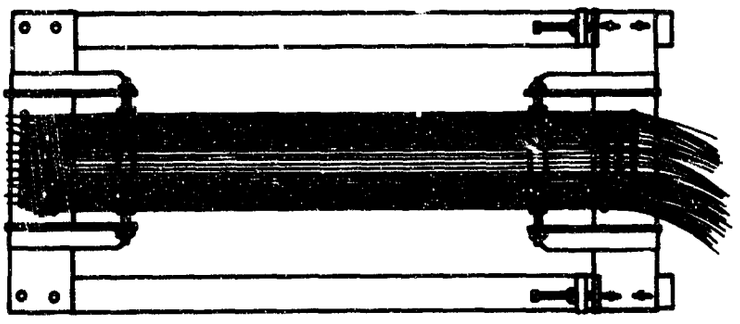

FIG. 3. PROFILE PRODUCTION BY GRADED GRID

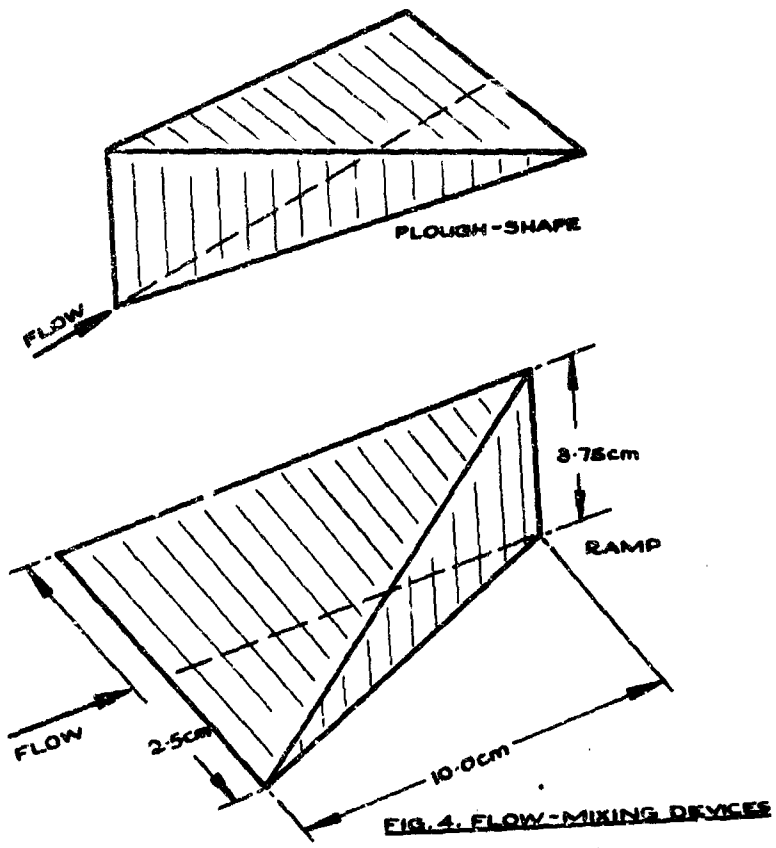

FIG. 4. FLOW-MIXING DEVICES

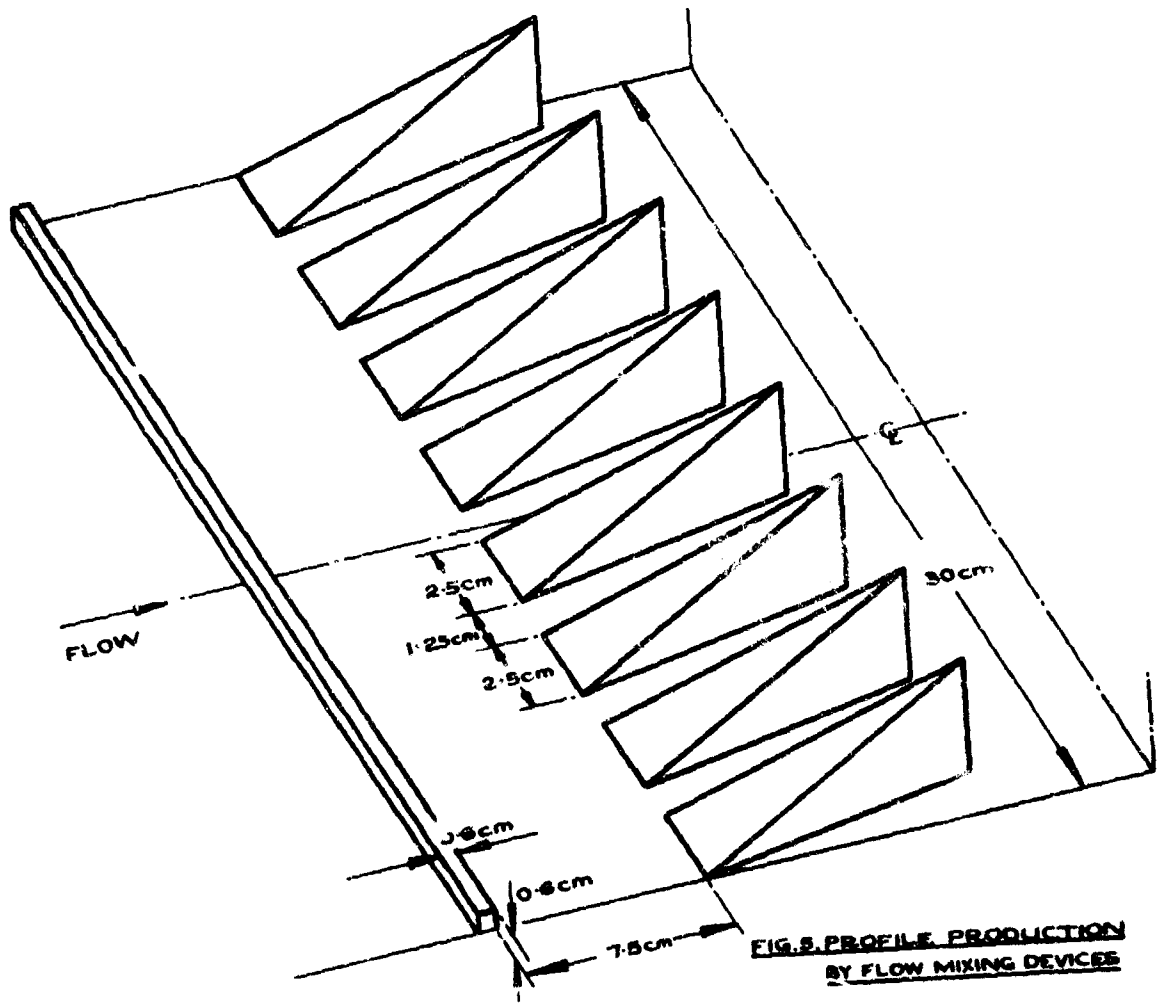

FIG. 5. PROFILE PRODUCTION BY FLOW MIXING DEVICES

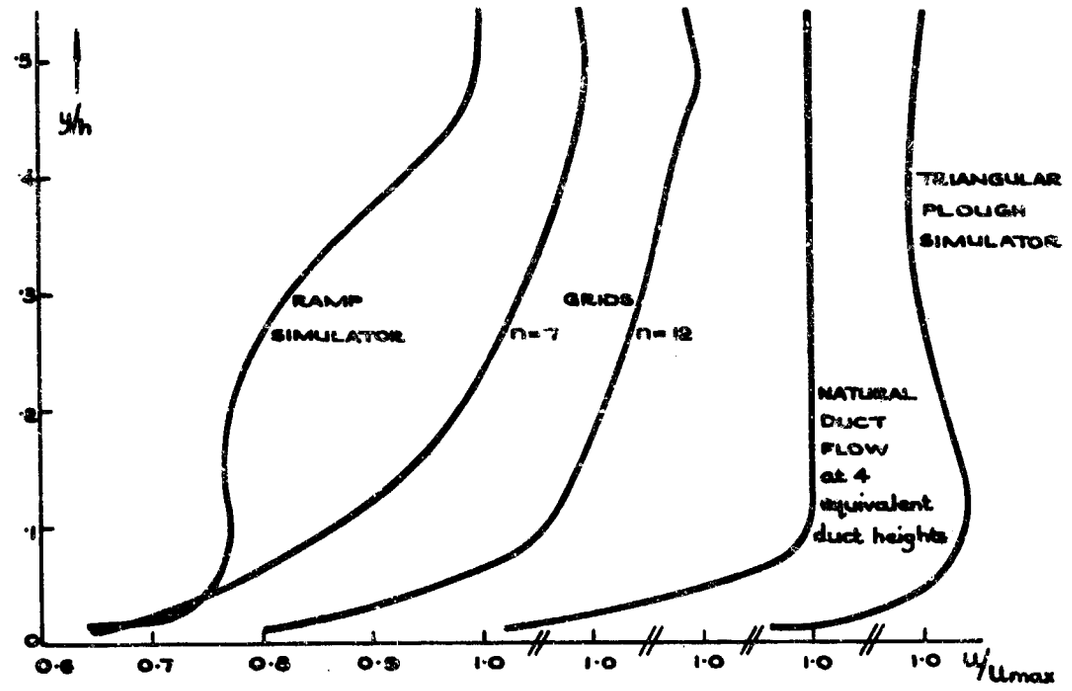

FIG. 6. VELOCITY PROFILES IMMEDIATELY BEHIND SIMULATORS

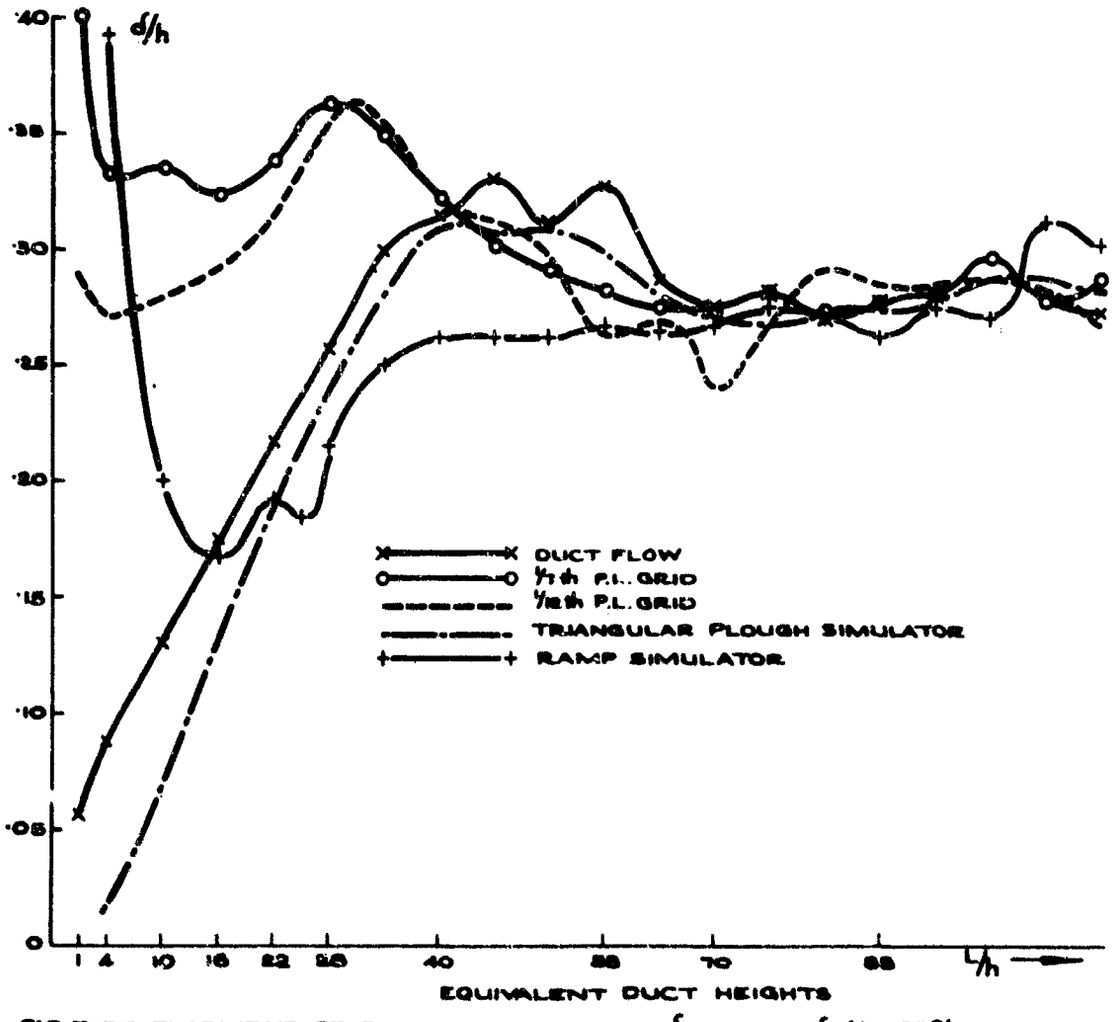

FIG. 7. DEVELOPMENT OF PHYSICAL THICKNESS δ WHEN y=δ u = 99% u max

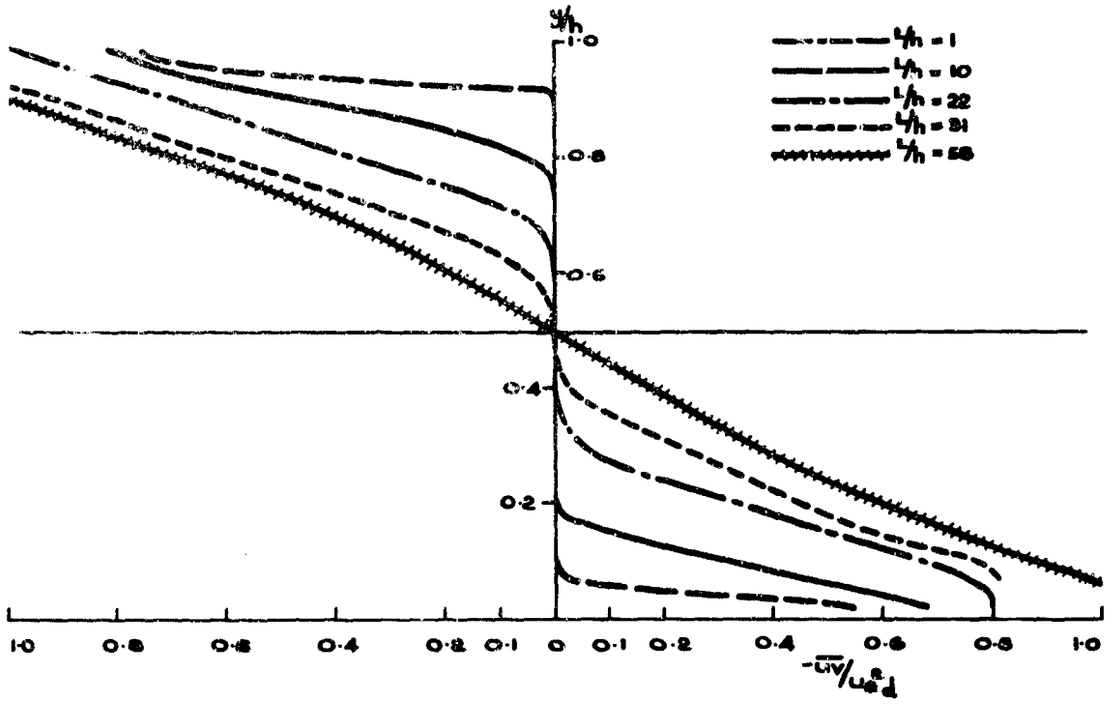

FIG. 8. TURBULENT SHEAR STRESS DISTRIBUTION IN DUCT FLOW

u_{τ_d} is the friction velocity for fully-developed flow.

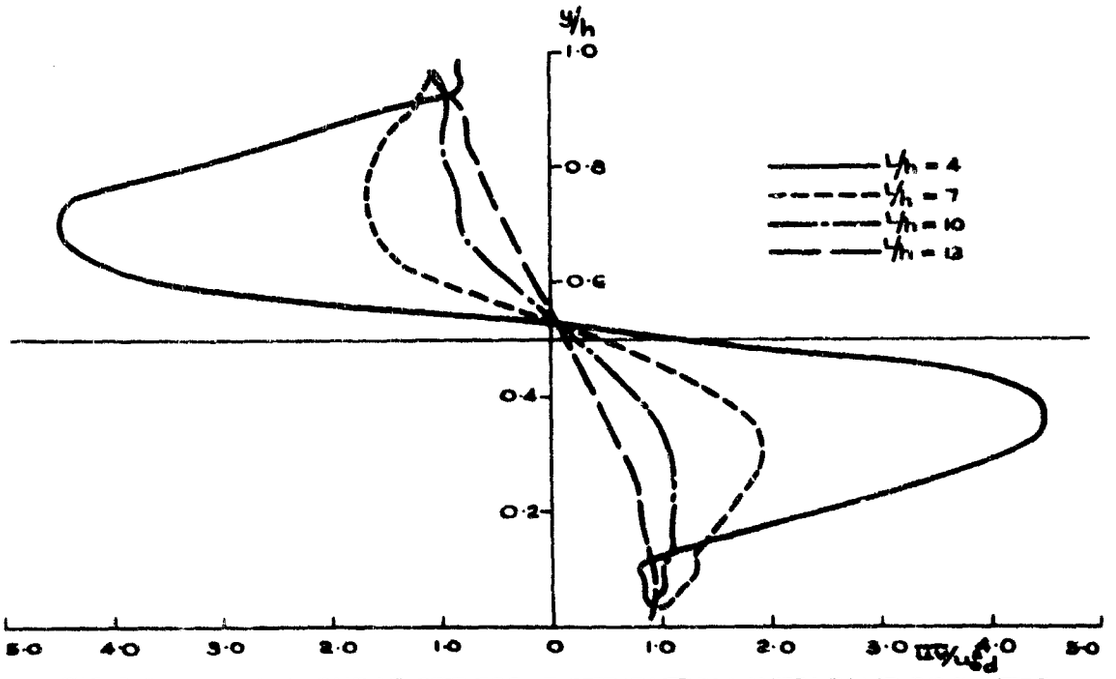

FIG. 9. TURBULENT SHEAR STRESS DISTRIBUTION WITH RAMP SIMULATOR

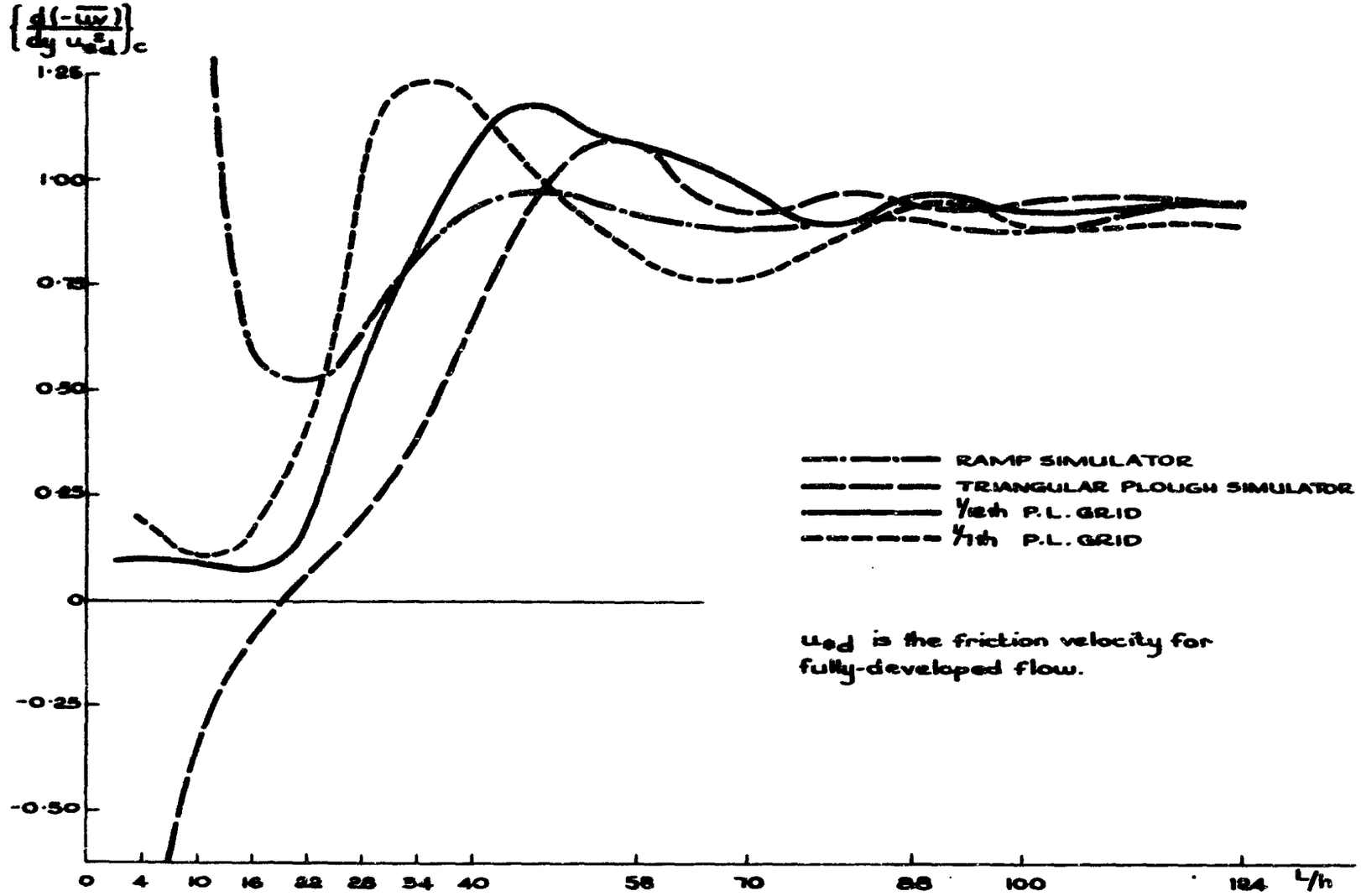

FIG. 10. TURBULENT SHEAR STRESS GRADIENT ON CENTRELINE

A METHOD OF SIMULATING A NEUTRAL ATMOSPHERIC BOUNDARY LAYER IN A WIND TUNNEL

by

J. Counihan*
Central Electricity Research Laboratories, Kelvin Avenue, Leatherhead, Surrey.

* Research Officer, Engineering Sciences Division

SUMMARY

A method is described by which a neutral atmospheric boundary layer can be simulated in a wind tunnel. An accelerated rate of boundary layer growth is obtained by the use of vorticity generators in combination with a castellated barrier and surface roughness elements. The characteristics appropriate to rough wall boundary layer flow are apparent in the simulated flow at a distance of three boundary layer heights from the generator trailing edges: at a distance of four and a half boundary layer heights the flow is acceptably representative of true rough wall boundary layer flow.

Extensive measurements have been made in order to establish that the flow produced is reasonably uniform across the span of the wind tunnel and that it does not change appreciably in the streamwise direction. The variations with height of the simulated boundary layer properties have been compared with data from natural and atmospheric boundary layers. The measured integral length scales of longitudinal turbulence have likewise been compared with similar data. In all respects satisfactory agreement is obtained between the simulated boundary layer and the natural and atmospheric boundary layers.

NOMENCLATURE

A	-	Constant
B	-	Constant
h	-	Distance from tunnel floor mm (in.)
H	-	Generator height mm (in.)
L	-	Semi-empirical length scale m (ft)
n	-	Frequency Hz (cy/sec)
r	-	Separation distance mm (in.)
$Rii(r_1,r_2,r_3)$	-	Correlation coefficient
S(n)	-	Normalised power spectral density at frequency n
U_{10}	-	Reference velocity at 10 m height m/sec (ft/sec)
U_{max}	-	Free steam velocity m/sec (ft/sec)
u(x)	-	Longitudinal velocity m/sec (ft/sec)
v(y)	-	Vertical velocity m/sec (ft/sec)
w(z)	-	Lateral velocity m/sec (ft/sec)
X	-	Non-dimensional quantity $n/\bar{U}_{10}$ L
z_o	-	Roughness length mm (in.)
δ	-	Boundary layer thickness m (ft)
γ	-	Intermittency factor

A prime denotes a fluctuating contribution and a bar denotes an average with respect to time.

1. INTRODUCTION

At one time, a uniform airflow past a building or structural model in a wind tunnel was considered adequate for the determination of mean steady surface wind loads. However, with the advent of taller buildings and larger buildings having complex external shapes it was found desirable to represent at least the velocity profile of the atmospheric boundary layer in such wind tunnel tests; that is, representation of a shear flow past the model was required. This is normally achieved by such methods as grids of rods spaced parallel to each other across the tunnel span or by gauze screens. The shape of the shear profile can easily be altered by changing the spacing and size of the rods or changing the screen resistance. Thus the effects of wind shear on the mean steady loads can be determined.

A research programme was initiated at the Central Electricity Research Laboratories (C.E.R.L.) to devise ways and means of measuring the fluctuating loads in such a way that the measurements made would be truly representative of the full scale fluctuating loading of the buildings being considered. It was subsequently found that the fluctuating component of wind loads was significant with respect to the design of cooling towers for Power Stations. To determine such loads it follows that the tests need to be conducted in an air-flow fully representative of an atmospheric or rough wall boundary layer. This in turn implies correct simulation of the intensities and scales of the turbulent quantities of these boundary layer flows.

With sufficient space available such a boundary layer can be grown naturally. In the case of the C.E.R.L. low speed wind tunnel a 1.2 metre (4 ft) high boundary layer was required in order that adequately sized test models could be used. The length of working section required to grow such a boundary layer was clearly prohibitive. Therefore an attempt was made to devise a method which would give a accelerated rate of growth and produce a fully developed boundary layer in a distance of from three to four times the required boundary layer height.

This paper describes the development of such a system at C.E.R.L. for the simulation of an atmospheric boundary layer in a wind tunnel and presents some of the more interesting results of the work.

2. OTHER METHODS OF PRODUCING SHEAR FLOW AND BOUNDARY LAYER FLOW

Adequate representation of boundary layer flow requires simulation of not only the correct turbulence intensities but also representation of the frequency power spectra of the three turbulent velocity components. In particular we require representation of the low frequency end of the spectra, that is, we require that the large, energy containing eddies should exist in the simulated flow. Eddies of comparable size, for example, to cooling towers have been measured in the atmospheric boundary layer (Harris 1968) and hence the necessity for their representation.

It is well known that shear flows can be produced adequately by the use of gauzes rods or honeycombs (Lawson 1967). These systems also produce turbulence in their wakes but this is not necessarily of the correct intensity or scale and in fact is mostly high frequency turbulence. Therefore such flows cannot be classed as boundary layer flows as defined above.

The artificial production of boundary layer flow has been attempted but the flows produced have lacked low frequency energy or the correct magnitude of turbulence intensity, or have had excessive spanwise non-uniformities. For example the system used by Lloyd (1967) does not have sufficiently large Reynolds stresses or turbulence intensities. That used more recently by Templin (1969) does not appear to have sufficient energy at low frequencies and has excessive spanwise variations in the velocity profiles.

Finally one can resort to growing a boundary layer naturally which has been done at the University of Western Ontario (Davenport and Isyumov 1967). This required a wind tunnel having a working section 24 m (80 ft) long to produce a boundary layer of about 1 m (3.5 ft) in height. Thus a boundary layer of adequate size was produced in a distance of 24 boundary layer heights, whereas the requirement at C.E.R.L. was to produce a boundary layer of similar height in three to four boundary layer heights.

3. C.E.R.L. WORK ON BOUNDARY LAYER SIMULATION

The first system used at C.E.R.L. was intended to produce an accelerated version of a model of the flow processes in a natural turbulent boundary layer as proposed by Townsend (1957). This concept implies the existence in the boundary layer of large, slow-moving, contra-rotating vortex pairs with their axes parallel to the main flow. However more recent literature has tended not to support this concept completely.

The system involved the use of a barrier, vortex generators and surface roughness elements. The generators were intended to produce Townsend's proposed vortex system and were essentially flat triangular plates set at alternate incidence across the tunnel span. It was hoped that the generated vortices would spread some of the ground level turbulence upwards in order to overcome the initial lack of turbulence in the outer section of the simulated boundary layer. However the generators produced strong, fairly concentrated vortices of a persistent nature which led to large spanwise and vertical non-uniformities of the velocity, turbulence and Reynolds stress profiles

(Armitt and Counihan 1968). Apart from this it was considered that, in using the triangular generators, some degree of asymmetry would still exist in the flow due to their alternate incidence settings.

In the second attempt to devise such a system it was proposed that the section of the boundary layer grown on the surface roughness should be left to develop freely and that the turbulence developed here should be supplemented, in sections higher up in the boundary layer, by turbulence from another source. It was hoped that eventually the two sections would blend together to form a complete boundary layer.

Since it is known what the form of the turbulence distribution in the boundary layer should be, it was assumed that a shape of generator was needed which would have in its wake a distribution of turbulence which had a maximum value near ground level and which decreased to zero at what would be the top of the boundary layer. If the correct turbulence profile is eventually produced, then whatever eddy system exists in boundary layers may be persuaded to form naturally as a consequence.

The shape chosen was a quarter ellipse in side view whose major axis is twice its minor axis. In plan view the section is wedge shaped, the wedge angle being a constant at any plan section. The apex of the wedge faces into the flow direction and hence there is no asymmetry introduced into the system. Therefore the characteristics of the elliptic wedge wake should be identical at equal distances either side of its centre-line. It was considered that a low wedge angle would be beneficial in producing a gradual vertical distribution of vorticity rather than a vortex in the wake. From this point of view a semi-wedge angle of 5 to 6° seemed reasonable. A constant wedge angle was maintained at all sections of the generator as it was felt that this was needed for the production of turbulence or vorticity over the complete generator height. Higher wedge angles than those stated above might have resulted in a section having excessive base drag. The generator has been termed an elliptic wedge vorticity generator. It does in fact produce a graded distribution of vorticity in its wake whose axes are perpendicular to the tunnel floor. This generator in combination with a castellated barrier and surface roughness has been used to produce the required boundary layer flow.

4. CHOICE OF AND OPTIMIZATION OF THE SIMULATION TECHNIQUE

The final positioning of the generators, barrier and surface roughness is shown in Fig. 1. Extensive preliminary testing had taken place in order to assess the contribution of each individual component to the flow finally produced (Counihan 1968a). All of the work was carried out in the C.E.R.L. boundary layer tunnel with the ultimate aim of producing a 152 mm (6 in.) high boundary layer in three to four times this distance. The free stream velocity was approximately 9 m/sec (30 ft/sec).

Initially the form of the longitudinal turbulence distribution in the wake of one generator was established (Fig. 2). It produces a vertical distribution of turbulence in its wake of the type postulated in Section 3, as being of the required form. The second significant characteristic of its wake is that at any given height the spanwise intensity of turbulence is sensibly constant over a good proportion of the spanwise extent of the wake. Therefore it could be deduced that it should be possible to find a generator spacing which would give very little spanwise non-uniformity. It was also decided at this stage to use the generator having the 6° semi-wedge angle since at any particular section the wake of this generator will be wider than that of the 5° generator. Therefore to obtain a similar degree of lateral uniformity the 6° generators can be spaced wider apart than the 5° generators. It was thought that this spacing should be as wide as possible to be consistent with the production of the correct form of the power spectrum of the lateral turbulent velocity component.

In deciding what the generator spacing should be it was assumed that a spanwise variation of turbulence intensity of not greater than 1% would be tolerable at any given height in the boundary layer at a distance of three boundary layer heights downstream from the trailing edges of the generators. As a result of tests to determine this spacing, a distance apart of 76 mm (3 in.) for the generators was decided on.

The dimensions and position of the barrier in the wind tunnel working section were then determined. It was thought that, if the barrier was placed at the intersection of the working section and contraction, it could influence the flow through and from the contraction. In the case of a wind tunnel in which there is no contraction before the working section the point to be considered is that there will be a relatively thick floor boundary layer and that the momentum loss due to this will have to be taken into account when deciding on the height of the barrier. As a result of some brief tests the barrier was positioned 51 mm (2 in.) from the contraction in the C.E.R.L. boundary layer wind tunnel (Fig. 1). If however the working section length of a wind tunnel is short, the barrier could be moved closer to the contraction without seriously affecting the end results. The barrier height, which was decided on in later tests, was chosen as 22 mm (0.875 in.). This was subsequently modified by the addition of 6.35 mm (0.25 in) high castellations positioned on the barrier immediately forward of the generators (Fig. 1).

From the point of view of mutual interaction, the positioning of the barrier and generators relative to each other was also of importance. This was determined by varying the position of the generators from the fixed barrier and measuring the effects of this on the

downstream turbulence intensity. These tests showed that determination of the position of the generators was to some extent arbitrary, as in the case of the barrier. In this case it was decided to position the leading edge of the generators 127 mm (5 in.) downstream of the barrier. However as in the case of the barrier, if sufficient working section length is not available the generators can be closer to it without seriously affecting the shape of the vertical distribution of turbulence measured downstream.

The surface roughness used consisted of 'Lego' baseboard, the height of the roughness elements being approximate scaled down versions of those of previous tests (Armitt and Counihan 1968).

The above barrier, generators and surface roughness were positioned as indicated for the remainder of the tests.

5. EXPERIMENTAL RESULTS

In general measurements have been made at two downstream stations, one three boundary layer heights and the other four and a half boundary layer heights downstream of the trailing edges of the generators. Mainly the measurements made at the station further downstream only are presented here. The characteristics of boundary layer flow were however adequately established three boundary layer heights downstream of the generator trailing edges.

5.1 Velocity Profiles and Reynolds Stresses

In the first instance the boundary layer to be simulated is a neutral atmospheric boundary layer appropriate to flow over rural terrain. It has been assumed that the relevant velocity profile can be approximated to by a 1/7th Power Law profile for present purposes. It can be seen from Fig. 3 that the mean of the measured profiles is very close to the curve for this power law. The flow has adequate spanwise uniformity as indicated by the difference between the curves measured at positions corresponding to the generator centre-line and the generator span centre-line. The difference between the curves represents the maximum spanwise non-uniformity in the velocity profiles.

Also shown on the curve is the profile suggested from analysis of full-scale measurements (Harris 1968) for flow of the atmospheric boundary layer over rural terrain. The agreement is reasonable bearing in mind that the surface roughness of both tests may not be exactly comparable. A theoretical assessment has previously been made (Counihan 1969a) of the extent to which the simulated boundary layer compares with a naturally grown boundary layer of similar height and roughness. The comparison was made using the velocity defect law

$$\frac{U_{max} - \bar{U}}{U_\tau} = A + B \log_{10} (\delta/Z)$$

(where $A = 2.80$ and $B = 5.60$)

in conjunction with some of the measurements made in a natural rough wall boundary layer grown on the 'Lego' baseboard. The estimated velocity ratios at various heights in the boundary layer have been tabulated:

Z/δ	Natural 24 mm (0.95 in.) thick boundary layer	Predicted 152 mm (6 in.) thick boundary layer	Simulated 152 mm (6 in.) thick boundary layer
0.40	0.815	0.860	0.875
0.30	0.740	0.800	0.840
0.20	0.650	0.730	0.805
0.10	0.515	0.620	0.730

Comparison between the predicted and simulated boundary layers seems reasonable. The discrepancies could be due to the fact that neither the natural nor simulated boundary layers seem to have reached a complete state of equilibrium. Such conditions are acceptable since it can be assumed that the atmospheric boundary layer, being constantly subjected to changes in terrain roughness, does not always have sufficient length in which to reach a state of equilibrium appropriate to a particular roughness.

The measured variation of the Reynolds stress with height is also shown on Fig. 3. The form of the distribution is very similar to that obtained in natural boundary layer flow. The theoretical Reynolds stress at ground level has been estimated on the same basis as the theoretical velocity profiles and predicts a value of 0.0024 in comparison to the value of 0.0023 measured in the simulated boundary layer. Reference can also be made to Davenports (1963) paper where results are summarised for pipe flow and natural wind experiments. The summarised data give a power law exponent of 1/7 th for a surface shear stress coefficient of 0.0025 which is in agreement with the simulated boundary layer results.

5.2 Turbulence Intensity Profiles

The longitudinal, lateral and vertical turbulence intensity distributions measured in the simulated boundary layer are shown in Fig. 4. The spread of the experimental points represents the degree of spanwise non-uniformity in the flow and, as can be seen, this can be regarded as negligible. The shapes of the distributions also approximate closely to those obtained in natural boundary layers, and the turbulence intensities of the three components are of the right order of magnitude relative to each other.

The intensity of longitudinal turbulence, based on both free stream and local velocity has been compared with the atmospheric boundary layer data (Harris 1968) in Fig. 5.. As previously stated, this data is appropriate to flow over rural terrain where the boundary layer thickness is usually taken as being of the order of 300 m (1000 ft). However the thickness in this case has been taken to be 600 m (2000 ft) (See Section 6.3), in comparing the turbulence data. The comparison of the measurements based on local velocities is probably the more realistic comparison to make, and on this basis the forms of the distribution compare reasonably well although the turbulence intensities are higher in the simulated boundary layer. The discrepancy at the lower section of the boundary layer is greater since the velocity gradient of the simulated boundary layer is greater than that of the atmospheric boundary layer in this region.

5.3 The Turbulence Spectra

Extensive spectral measurements were made in order to establish that the spectra were reasonably invariant in spanwise and axial directions and to establish the form of their variation with height (Counihan 1969b). The spectra of the three components of turbulence shown in Fig. 6 are typical of those measured. The presence of energy at the lower frequencies implies the existence of large scale turbulence which is one of the requirements specified in Section 2. In general there do not appear to be any irregularities in the forms of any of the spectra.

Theoretical forms of the longitudinal turbulence spectrum have been proposed by Davenport (1963a) and Harris (1968) which are as follows:

$$n\,S(n) \propto \frac{X^2}{(1+X^2)^{4/3}} \qquad \text{- Davenport}$$

and

$$n\,S(n) \propto \frac{X}{(2+X^2)^{5/6}} \qquad \text{- Harris}$$

where

$$X = n/\bar{U}_{10}\,L$$

and L is a length scale of magnitude 1200 m (4000 ft) derived semi-empirically by Davenport. Assuming that the height of the relevant atmospheric boundary layer is 600 m (2000 ft) then the scale of the simulated to atmospheric boundary layers is 4000:1. On this basis the theoretical spectra were calculated for comparison with that measured (Fig. 6). The agreement between the curves is quite satisfactory. At the low frequency end of the spectra the measured spectrum falls between the two proposed theoretical curves. The values of the maximum energy per octave do not agree exactly but this is not considered to be particularly significant since the assumption of a slightly different scale between the simulated and atmospheric boundary layers or a larger length L can adequately off-set this discrepancy. For instance Harris (1968) suggests that the length L could possibly be increased to a value of 1800 m (6000 ft). On this basis the agreement between the simulated and theoretical spectra was taken as satisfactory.

5.4 The Intermittency Factors

The intermittency factors of the three components of turbulence were measured and are presented in Fig. 7. This factor is defined as the proportion of time that high frequency turbulence is present in the velocity signal at a given height in the boundary layer. For example it should have a value of unity in the lower section of the boundary layer and should be approximately zero at the top of the boundary layer, assuming that there is no background turbulence. As can be seen the spanwise variations of the factors are not excessive and in all respects the forms of the distributions for the various turbulent components are very similar. The measured intermittency factors of the longitudinal turbulence are compared with similar measurements by Jorgen and Fistler (1954) in a natural boundary layer also in Fig. 7. The agreement between the measurements has been taken as satisfactory.

6. THE STRUCTURE OF THE SIMULATED BOUNDARY LAYER FLOW

Having shown that the general characteristics of the simulated flow were adequately representative of boundary layer flow it was decided to look at the structure of the flow in some detail. This was done by measuring some of the space correlations of the fluctuating velocities. The correlation is defined as:-

$$\overline{U'_P\,U'_Q} \Big/ \sqrt{\bar{U'}_P^{\,2}}\ \sqrt{\bar{U'}_Q^{\,2}}$$

where: U'_P is the turbulent velocity at a fixed point P and

U'_Q is the turbulent velocity at a point Q distance r from P

For brevity this can be written as:

$$\underline{Rij\ (r_1,r_2,r_3)}$$

where: r_1,r_2,r_3 are separations on the x, y and z axes respectively.

In these tests the measurements were confined to cases where i = j hence the correlation is now

$$\underline{Rii\ (r_1,r_2,r_3)}$$

For example the correlation coefficient of the variation of the longitudinal turbulent velocity for vertical separations is simply,

$$\underline{Ruu\ (o,r,o)}$$

i.e. x is the streamwise axis

the y axis is normal to the tunnel floor and

the z axis is horizontal or across the stream.

Extensive measurements were made of the correlation coefficients (Counihan 1969b) with a view to not only establishing the integral length scales of turbulence in the boundary layer but also to possibly gaining some insight into how the system that produces the simulated boundary layer works. A more detailed investigation into how the system works would require measurements of many more correlations than those obtained in these tests. The measurements also established the invariance of the correlation in axial and spanwise directions.

6.1 Measurements of Ruu (o,r,o) and Ruu (o,o,r)

Typical measurements of these correlations at various parts of the boundary layer are presented in Fig. 8, 9 and 10. As can be seen in Fig. 8 and 9 the vertical turbulent length scales increase with increase of h/H upto 0.25 for positive separations. Above this height the trend tends to reverse but the effect is not very pronounced and the mean length scale can be taken as being reasonably constant.

The correlations on Fig. 9 clearly indicate a peculiarity of the flow which was not measurable from fixed points lower down in the boundary layer (Fig. 8). This is taken to indicate that there is a secondary eddy or length scale in the simulated flow, which can be explained as follows. If it can be assumed that there is some inward flow to the base of the generator near the top which increases the local velocity, then these measurements can be associated with a generator 'tip effect'. Reference to Fig. 3 shows that there is a sudden increase in the velocity gradient (du/dy) near the top of the boundary layer at the generator centre-line and a measurable increase of shear stress (τ) in the same region. Since the production of turbulence is a function of the product of these quantities (τ du/dy) it can be assumed that the 'hump' in the correlation measurements is associated with this effect. The irregularity decreases with increase of downstream distance and clearly tends to lead to an apparent extension of the length scale and is less distinguishable as a secondary eddy. It was assumed that this effect did not seriously influence the main flow in the simulated boundary layer.

In the measurements at the span centre-line there was a tendency for the correlations to go slightly negative at large positive separations (Counihan 1969b). It was initially thought that this might be due to some interaction of the main flow with the tunnel roof boundary layer. However since the effect decreases with increase of distance downstream this does not appear likely It seems more probable that it is associated in some way with the barrier and it can be assumed that the motion is not a dominant one.

Typical measurements of the correlation of the longitudinal turbulent velocity for lateral separations are shown in Fig. 10. The results indicate an increase of length scale with height which, lower down in the boundary layer, is far more pronounced than that shown for the vertical separations. This trend is persistent up to a height of h/H = 0.40. The correlation also show a clearly defined trend in going negative at large separations. It is possible that some degree of periodicity exists in the lower sections of the boundary layer where mixing caused by the barrier would be less vigorous than that higher up. This periodicity would be due to rows of vortices being shed at any given height in the x-z plane by the row of generators.

It appears from the correlation measurements that the turbulence length scales are an approximate function of the generator spacing since Ruu (o,r,o) → 0 at a separation corresponding to the generator span and Ruu (o,o,r) → 0 generally at a separation of half a span.

6.2 Comparison of Correlations with Natural Boundary Layer Data

In order to establish whether in fact the measured correlations were typical of those found in boundary layers, the results were compared with similar measurements by Grant (1958) in a natural boundary layer. A natural boundary layer being that grown on a flat plate under laboratory conditions. The comparison of the correlations for vertical separation is shown in Fig. 11. Clearly the correlations are of a similar form and the scales a similar size to those measured by Grant. The only discrepancy is that higher up in the boundary layer Grants length scales tend to be slightly larger. The same conclusions can be drawn from Fig. 12 where the correlations for lateral separations are presented. It can therefore be assumed that the flow in the simulated boundary layer is representative of natural boundary layer flow regarding the integral length scales of the longitudinal turbulence and the characteristic shapes of the different correlation distributions.

6.3 Comparison of the Correlations with Atmospheric Boundary Layer Data

Since the similarity of the simulated and natural boundary layer flows has been established, the measurements can now be compared with the corresponding correlation measurements of Harris (1968) in an atmospheric boundary layer over rural terrain.

As can be noted, the correlations are plotted against the non-dimensional distance r/H, where H is equivalent to δ the boundary layer height. Therefore some height must be adopted for the atmospheric boundary layer appropriate to the relevant conditions in order to compare the data. In accordance with Davenports paper (1963) regarding the dependence of the atmospheric boundary layer height on the surface roughness length (Z_o), it was initially assumed that the height appropriate to the terrain of Harris's measurements was of the order of 300 m (1000 ft). However a comparison of the full scale results with those in the simulated boundary layer, on this assumption, showed that the atmospheric boundary layer length scales were approximately twice those of the simulated boundary layer. Therefore on the basis of the conclusions already stated in Section 6.2 regarding the similarity of the flow in the simulated and natural boundary layers it was decided to assume a height of 600 m (2000 ft) for the atmospheric boundary layer. All of the comparisons with fullscale data presented in this paper have been based on this assumption of 600 m (2000 ft) for the height of the atmospheric boundary layer.

The simulated and atmospheric boundary layer correlations are shown in Fig. 13 and 14. In general the full size length scales are slightly greater than those of the simulated boundary layer. However it can be reasonably assumed that a satisfactory simulation of the turbulence length scales of an atmospheric boundary and correlation distributions of the right form have been achieved.

It was noted that Harris's fullscale auto-correlation data did not tend asymptotically to zero for large time delays. This suggested the presence of some error in the results. Approximate corrections have been derived for these by Scriven (1969) assuming that uncorrelated spurious data was added to the signal. Application of the correction results in a better agreement between simulated and atmospheric boundary layers since it reduces the full size length scales.

However it is also of interest to note that Grants measurements (1958) of the correlation of the longitudinal turbulent velocity for longitudinal separations tends to suggest that the correlation takes longer to reach zero than theoretically predicted. The indications from this are that correction of Harris's results may lead to over correction. Clearly more atmospheric boundary layer data is desirable in order to prove or disprove the argument.

Another point worth noting also arises from the preceding analysis. If the ratio of the integral length scale of turbulence to the boundary layer thickness is the same for both the atmospheric and simulated boundary layers, for the same roughness conditions, then measurement of the atmospheric length scales may provide a suitable method by which the thickness of atmospheric boundary layers could be defined.

7. DISCUSSION

In general the simulated boundary layer does not possess any significant spanwise variations of the measured parameters. It is also sensibly constant in a streamwise direction over that section of a wind tunnel which, it is anticipated, would be occupied by the model under test. The method of simulation reproduces all of the known important parameters to a degree of accuracy that makes the simulated boundary layer comparable to a naturally grown rough wall boundary layer. However it is worthwhile making some points concerning the simulation method used and the flow produced by it.

The attainment of a velocity profile approximating to the 1/7th Power Law was not the sine qua non of the simulation but was merely chosen as a convenient and useful basis on which to build the present simulation. The profile, however, is typical of that obtained over rural terrain. It is assumed that the principles of the system adopted here can be developed to include simulation of the flow over a wide range of conditions varying from built-up areas to flat open country.

The assumption of a height of 600 m (2000 ft) for atmospheric boundary layer flow over rural terrain has given satisfactory agreement regarding the length scales and spectra of longitudinal turbulence. Obviously some sources of error still remain since the boundary layer height cannot be defined as precisely as one would like and since the choice of the value of the length L seems, to some extent, to be open to doubt.

However, on the basis of the present knowledge it can be assumed that the scale of the simulation in the C.E.R.L. boundary layer tunnel to the atmospheric boundary layer is of the order of 4000:1. It is important that the correct scaling factor is used since it affects the size of models used in wind tunnel tests for measurement of both static and dynamic loads on structures. Incorrectly scaled models will give some degree of error in static load measurements because of incorrect local Reynolds numbers, and will give wrong correlations of dynamic loads due to the ratio of the eddy to building sizes being incorrect. The importance of the eddy to building size ratios has been discussed at some length in Davenport (1963b).

It is also of interest to note the effects of this change of boundary layer height, i.e. 600 m (2000 ft) instead of 300 m (1000 ft), with respect to plume dispersion tests in the simulated flow. The current height of power station smoke stacks, for example, is of the order of 180 m (600 ft). Therefore a scaled stack in a scaled 600 m (2000 ft) boundary layer should not be influenced by the secondary flow effects of the simulated boundary layer (Section 6.1). These irregularities are confined to the top of the boundary layer so that by the time the plume will have dispersed into this region it will be sufficiently far downstream for these secondary flow effects to have become negligible.

If it could be assumed that the atmospheric boundary layer in neutral conditions has a mean height of say 600 m (2000 ft), regardless of surface roughness, this would considerably simplify the design of wind tunnel models and tests for wind loading experiments. Shellard (1963) suggests that better agreement with meteorological readings is obtained by the adoption of a common height for the atmospheric boundary layer and considering the present lack of data this seems to be the more realistic approach to take. Measurement of the integral length scales of turbulence in the atmospheric boundary layer may provide a useful method of obtaining the required boundary layer height data.

8. CONCLUSIONS

It can be concluded that adequate representation of a neutral atmospheric boundary layer, regarding both general characteristics and flow structure, can be obtained in a wind tunnel using the above method. The terrain simulated is that appropriate to open country.

Although some secondary flow effects are present in the simulated boundary layer these are not considered to be particularly significant. It is suggested that measurement of the integral length scales of turbulence may provide a basis from which to define the physical atmospheric boundary layer heights.

9. REFERENCES

Armitt, J. and Counihan, J., 1968, The simulation of the atmospheric boundary layer in a wind tunnel. Atmospheric Environment 2, 49-71.

Corrsin, S. and Kistler, A.L. (1954). NACA Tech. Note 3133

Counihan, J., 1969a, An improved method of simulating an atmospheric boundary layer in a wind tunnel. Atmospheric Environment 3, 197-214.

Counihan, J., 1969b, Further measurements in a simulated boundary layer. C.E.R.L. Note RD/L/N 68/69.

Davenport, A.G., 1963a, The relationship of Wind Structure to wind loading. Paper 2, Sym. 16, Int. Conf. on Wind Effects on Buildings and Structures NPL.

Davenport, A.G., 1963b, The buffeting of structures by Gusts. Paper 9, Sym. 16, Int. Conf. On Wind Effects on Buildings and Structures NPL.

Davenport, A.G. and Isyumov, N., 1968, The application of the boundary layer wind tunnel to the prediction of wind loading. Wind Effects on Buildings and Structures, Int. Res. Seminar, NRC Ottawa.

Harris, R.I., 1968, Measurements of Wind Structure at heights up to 598 ft above ground level. Sym. of Wind Effects on Buildings and Structures. Loughborough Univ. of Tech.

Lawson, T.V., 1968, Methods of producing velocity profiles in wind tunnels. Atmospheric Environment 2, 73-76.

Lloyd, A.R., 1967, The generation of shear flow in a wind tunnel Q. Jl. R. Met. Soc. 93, 79-96.

Scriven, R.A., 1969, Assessment of E.R.A. Gust analysis, C.E.R.L. Note (Unpublished).

Shellard, H.C., 1963, Estimation of design wind speeds, Paper 2, Sym. 16, Int. Conf. on Wind Effects on Buildings and Structures NPL.

Townsend, A.A., 1957, The turbulent boundary layer. Proc. I.V.T.A.M. Symposium on boundary layer research. Springer, Berlin.

Templin, G., 1969, Interim progress note on Simulation of Earths surface winds by artificially thickened wind tunnel boundary layers. NRC Canada LTR-LA-22.

10. ACKNOWLEDGEMENTS

The work was carried out at the Central Electricity Research Laboratories, Leatherhead, Surrey, England, and the paper is published by permission of the Central Electricity Generating Board.

FIGURE NO.

1. Final layout of generators and barrier in wind tunnel.
2. Turbulence distribution in the wake of a generator.
3. Velocity and Reynolds Stress profiles in the simulated boundary layer.
4. Turbulence profiles in the simulated boundary layer.
5. Comparison of longitudinal turbulence with full-scale measurements.
6. Frequency spectra of the three components of turbulence.
7. Intermittency factors in the simulated boundary layer.
8. Correlation of longitudinal velocity for vertical separations
9. " " " " " " "
10. " " " " for lateral separations.
11. Comparison of correlations with natural boundary layer data.
12. " " " " " " " "
13. Comparison of correlations with atmospheric boundary layer data.
14. " " " " " " " "

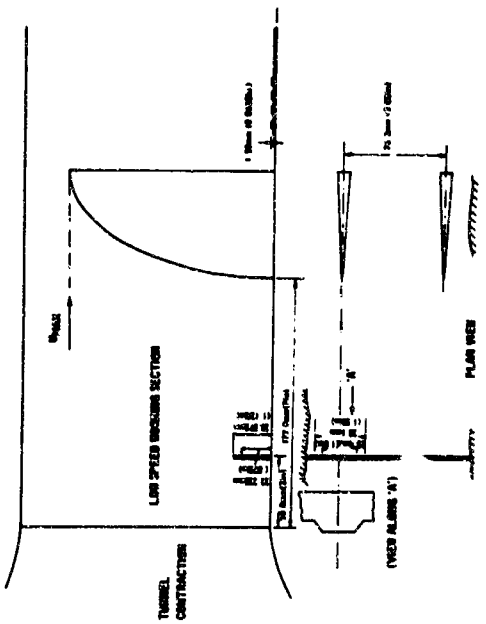

FIG. 1
FINAL LAYOUT OF GENERATORS AND BARRIER RAIL IN THE LOW SPEED SECTION OF THE WIND TUNNEL

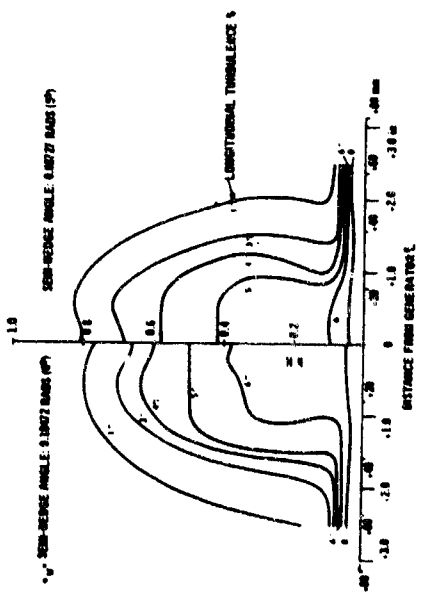

FIG. 2
CONTOURS OF CONSTANT LONGITUDINAL TURBULENCE IN THE WAKE OF AN ELLIPTIC WEDGE GENERATOR
AXIAL STN 457.2mm (18in) AFT OF GENERATOR TRAILING EDGE VIEW UPSTREAM

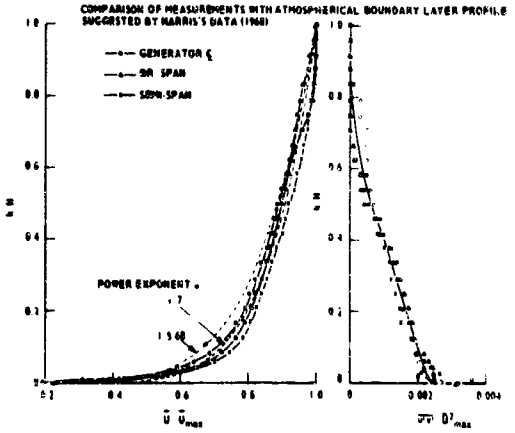

FIG 3 VELOCITY AND REYNOLDS STRESS PROFILES IN A SIMULATED BOUNDARY LAYER PLANE OF TRAVERSE 685mm (27 in) AFT OF GENERATOR TRAILING EDGES

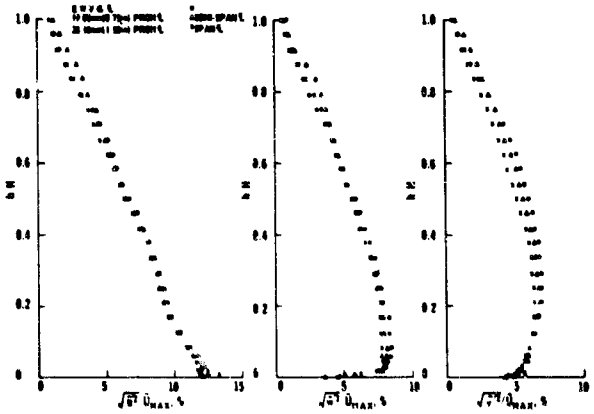

FIG 4 VARIATION OF TURBULENCE COMPONENTS WITH HEIGHT

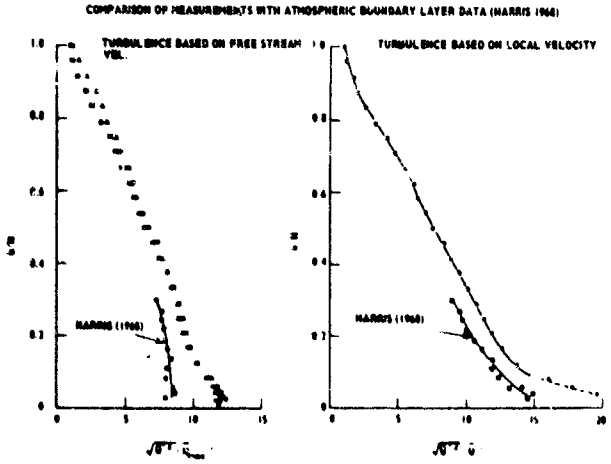

FIG 5 TURBULENCE INTENSITY PROFILES IN A SIMULATED BOUNDARY LAYER PLANE OF TRAVERSE 685mm (27 in) AFT OF GENERATOR TRAILING EDGES

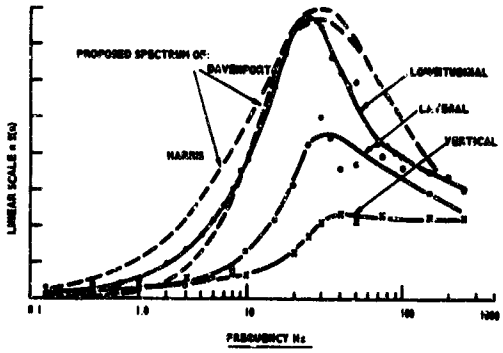

FIG. 6 POWER SPECTRA OF THE TURBULENT VELOCITIES

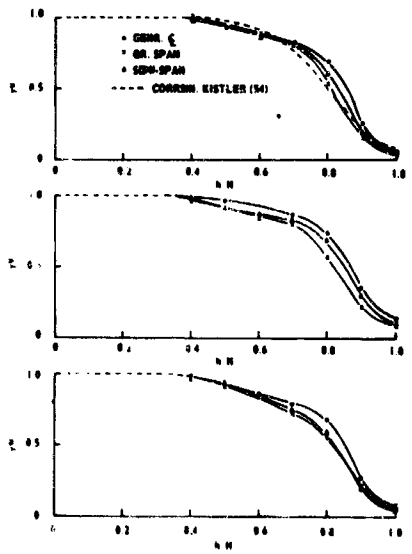

FIG. 7 INTERMITTENCY FACTOR DISTRIBUTION ACROSS THE SIMULATED BOUNDARY LAYER 685mm (27 in) AFT OF GENERATOR TRAILING EDGES

VERTICAL CORRELATION OF LONGITUDINAL VELOCITY COMPONENT

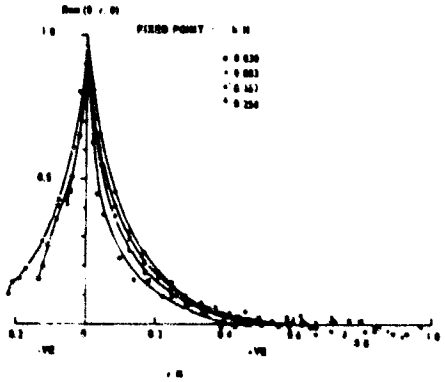

FIG. 8 CORRELATION COEFFICIENT DISTRIBUTIONS IN A SIMULATED BOUNDARY LAYER 685mm (27 in) AFT OF VORTICITY GENERATOR TRAILING EDGES
SPANWISE POSITION - GENERATOR ξ

VERTICAL CORRELATION OF LONGITUDINAL VELOCITY COMPONENT

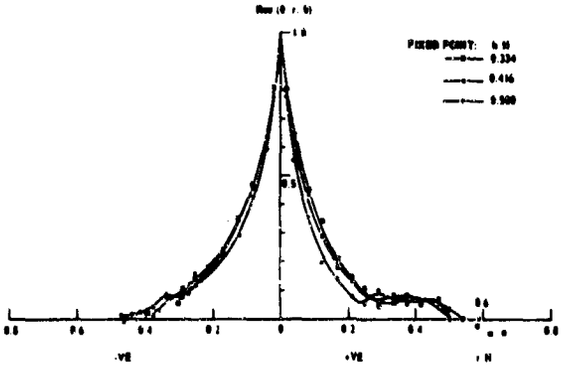

FIG 9 CORRELATION COEFFICIENT DISTRIBUTION IN A SIMULATED BOUNDARY LAYER 405mm (27 in) AFT OF VORTICITY GENERATOR TRAILING EDGES SPANWISE POSITION - GENERATOR ℄

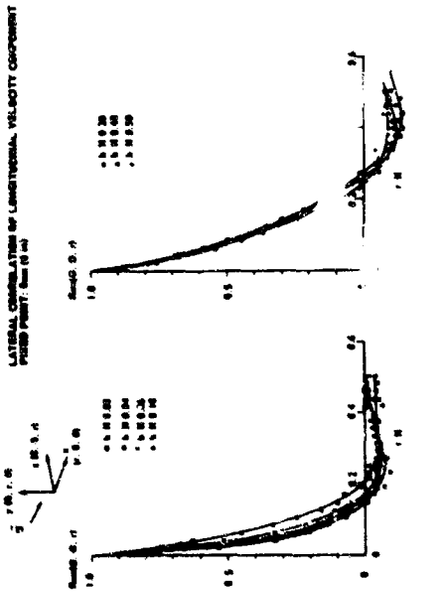

FIG 10 CORRELATION COEFFICIENT MEASUREMENTS AT VARIOUS HEIGHTS

VERTICAL CORRELATION OF LONGITUDINAL VELOCITY COMPONENT COMPARISON WITH MEASUREMENTS FROM A NATURALLY GROWN BOUNDARY LAYER

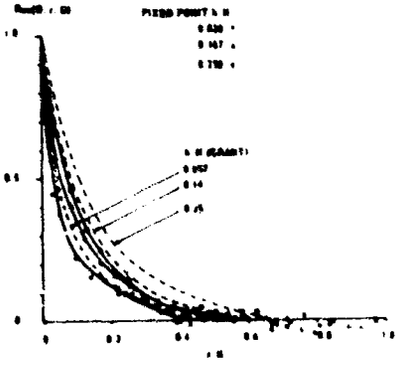

FIG 11

LATERAL CORRELATION OF LONGITUDINAL VELOCITY COMPONENT
COMPARISON WITH MEASUREMENTS FROM A NATURALLY GROWN
BOUNDARY LAYER

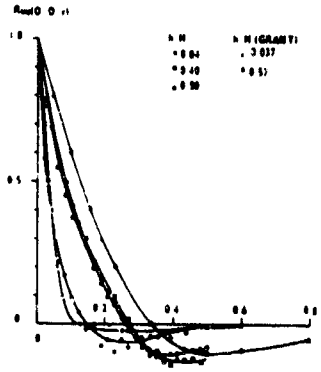

FIG. 12 COMPARISON OF CORRELATION COEFFICIENT DISTRIBUTIONS, SIMULATED
BOUNDARY PLANE OF TRAVERSE: 660mm (27 in) AFT OF GENERATORS
FIXED POINT: 0mm (0 in)

VERTICAL CORRELATION OF LONGITUDINAL VELOCITY COMPONENT

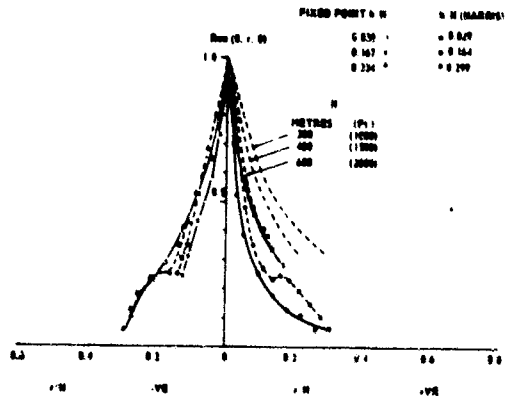

FIG. 13 COMPARISON OF CORRELATION COEFFICIENT DISTRIBUTIONS, SIMULATED
BOUNDARY LAYER PLANE OF TRAVERSE: 660mm (27 in) AFT OF GENERATORS, FIXED POINT:
1000 mm (0 in)

LATERAL CORRELATION OF LONGITUDINAL VELOCITY COMPONENT

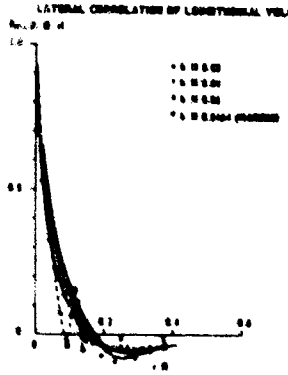

FIG. 14 COMPARISON OF CORRELATION COEFFICIENT DISTRIBUTIONS
SIMULATED BOUNDARY LAYER PLANE OF TRAVERSE: 660mm (27 in) AFT OF GENERATORS
FIXED POINT: 0mm (0 in)

LABORATORY INVESTIGATIONS OF ATMOSPHERIC SHEAR FLOWS USING AN OPEN WATER CHANNEL

by

James W. Clark*

United Aircraft Research Laboratories
East Hartford, Connecticut, U.S.A.

* Chief, Fluid and Systems Dynamics. Assisted by Richard C. Stoeffler and Paul G. Vogt.

SUMMARY

A 2-ft-wide by 6-in.-deep by 10-ft-long open non-recirculating water channel was used for investigations of stratified shear flows. This channel employs porous foam material at the inlet to shape the velocity profile and hot water nozzles to impose a temperature gradient; flexible side walls allow adjustment of the radius of curvature in the horizontal plane. Maximum flow velocity is about 1.0 ft/sec. Straight-channel results correlate with the stability theories of Drazin and others in which unstable conditions are defined in terms of dimensionless wavenumber and Richardson number. Examples are given in which the results are used in analyses of clear air turbulence encounters associated with mountain lee waves. It is concluded that the results are useful in predicting turbulence within thin, initially stable shear layers which undergo destabilizing undulations such as occur in orographic and shear-gravity waves.

This research was sponsored by the National Aeronautics and Space Administration, Washington, D.C., under Contract NASW-1582.

INTRODUCTION

There continues to be considerable interest in the nature and causes of clear air turbulence. Fundamental questions remain regarding the origins of certain types of CAT. Once these origins are determined, improved criteria for predicting the occurrence of CAT can be developed and possible methods for its detection and avoidance can be evaluated.

CAT is usually associated with flow systems having wind shear and density gradients, and sometimes with curvature of the streamlines. The UARL Open Water Channel allows laboratory-scale fluid mechanics investigations of such flows to be conducted.

Accordingly, the principal objectives of the investigations reported herein were: (1) to gain increased understanding of the nature and causes of CAT, (2) to develop improved criteria for predicting neutrally stable states in atmospheric flow systems, and (3) to compare the results of this research with available meteorological data and attempt correlations.

The paper contains three main sections --- a description of the equipment and procedures used in the fluid mechanics experiments, a discussion of an investigation of the stability of straight, stratified shear flows, and a discussion of the application of the results to atmospheric shear flows. Additional investigations in the present program which are not discussed herein included experiments with an oscillating plate to induce disturbances in a shear layer, experiments with standing shear-gravity waves, experiments with the channel walls curved, and meteorological analysis of six clear air turbulence encounters from airline, military, and NASA experience.

DESCRIPTION OF EQUIPMENT AND PROCEDURES

Figure 15-1 is a sketch of the UARL Open Water Channel indicating its major features. This facility provides a 2-ft-wide by 6-in.-deep by 10-ft-long, non-recirculating, open channel flow. The lucite side walls can be adjusted from the straight-channel position (shown by the solid lines in Fig. 15-1) to any desired curved-channel position (shown by the dashed lines) with the minimum centerline radius of curvature being about 6 ft. The flow is illuminated from beneath the glass floor using fluorescent lights.

Tapered filter beds made from a porous foam material* bonded to porous stainless steel supporting structures are used to introduce desired vertical and transverse velocity profiles at the upstream end of the channel (Fig. 15-1). Several different adjustable porous and nonporous sluices are used at the downstream end of the channel. They provide usable mean channel velocities up to about 1.0 ft/sec.

Hot-water nozzles in the plenum are used to introduce vertical and transverse temperature gradients and, hence, density stratification. Figure 15-1 shows schematically the nozzles used to create vertical gradients; twelve such nozzles are actually located in the plenum.

The coordinate system used to describe points in the flow is also indicated in Fig. 15-1. The central region of the channel away from the floor and side-wall boundary layers and away from the free surface is the region of primary interest. The gradients attainable in this central region vary with the local temperature of the water and with the shear-layer thickness. The approximate ranges in tests reported herein were:

$0.02 < V < 0.5$ ft/sec

$-3.5 < \partial V/\partial z < +3.5$ sec^{-1}

$40 < T < 100$ F

$0 < \partial T/\partial z < +135$ deg F/ft

Use was made of the curves in Fig. 15-2 (derived from tabulated data in Ref. 15-1) for calculating the Richardson number,

$$Ri = (-g/\rho)(\partial\rho/\partial T)(\partial T/\partial z)/(\partial V/\partial z)^2 \qquad (15\text{-}1)$$

for these flow conditions. The range of

---

* Scott Industrial Foam, a product of the Scott Paper Company, Foam Division, 1500 East Second Street, Chester, Pennsylvania, U.S.A.

Richardson number was from 0 (for $\partial T/\partial z = 0$) to near infinity (for $\partial V/\partial z$ approaching 0).

The Reynolds numbers per unit length in the channel vary over wide ranges due to the wide ranges of both velocity and temperature. In the present investigation, the minimum value was $Re/\ell = 1200$ per ft for V = 0.02 ft/sec and T = 40 F; the maximum was $Re/\ell = 67{,}800$ per ft for V = 0.5 ft/sec and T = 100 F.

The floor of the channel slopes downward slightly toward the sluice. Thus, some provision is made for floor boundary layer growth. Nevertheless, care must be taken to assure that observations are not influenced by this boundary layer, particularly at low channel speeds. Care must also be taken to assure that the blocking effect of the sluice under low-velocity, strong-stratification conditions does not influence the observations.

Neutrally buoyant fluorescent dye* is used to obtain qualitative information about the nature of the flow, e.g., for observing internal waves, vortices and turbulence. It can also be used to determine the wavelengths of internal waves. The dye is injected through 0.020-in.-ID stainless steel hypo tubes located immediately upstream of the tapered filter bed.

Measurements of the velocity profiles are made using the hydrogen bubble wire technique. A voltage is applied to a 0.001-in.-dia platinum wire extending from the channel floor through the surface of the water. Hydrogen bubbles are generated by electrolysis. The voltage may be pulsed to generate chains of bubbles which drift downstream with the flow. The local velocity can be determined from photographs of the chains.

A DISA Type 55D01 constant-temperature anemometer is used with Type 55A81 wedge-shaped hot-film probes for measurements of velocity fluctuations. Temperature measurements were made using a standard submersible mercury-filled thermometer.

INVESTIGATION OF THE STABILITY OF STRAIGHT, STRATIFIED SHEAR FLOWS

Introduction

The primary purpose of the fluid mechanics program was to experimentally examine the stability characteristics of straight, stratified shear flows. The end objective was to apply the results to thin, initially stable shear flows occurring in the atmosphere. Accordingly, the program was directed toward three areas: (1) answering certain questions concerning the conditions under which such flows become unstable, (2) determining the characteristics of the flow during the initial phases of breakdown, and (3) verifying one or more of the existing theoretical criteria for subsequent use in studying atmospheric shear flows.

A summary of theoretical stability criteria for straight, inviscid, stratified shear flows appears in Ref. 15-2. Of the references cited therein, the most pertinent to the present investigation are by Drazin (Ref. 15-3), Drazin and Howard (Ref. 15-4), and Miles and Howard (Ref. 15-5). Two-dimensional flow is assumed and analytic functions are used to represent the vertical profiles of velocity and density. Small, finite disturbances are introduced using a perturbation stream function. Stability criteria are derived in terms of α, d, and Ri, where α is the wavenumber of the disturbance ($\alpha = 2\pi/\lambda$ --- λ is the wavelength), d is half the shear-layer thickness ($d = (\Delta V)/2(\partial V/\partial z)_o$ --- ΔV is the velocity difference across the shear layer and $(\partial V/\partial z)_o$ is the shear), and Ri is Richardson number.

The hyperbolic tangent velocity profile assumed by Drazin (Ref. 15-3) most closely approximates the profiles that can be established in the channel by proper shaping of the tapered filter bed. Drazin derives the following equation for the neutral boundary on the αd-Ri plane:

$$\alpha d = \sqrt{\frac{1}{2} \pm \sqrt{\frac{1}{4} - Ri}} \qquad (15\text{-}2)$$

Regions of stable and unstable flow are shown in the sketch:

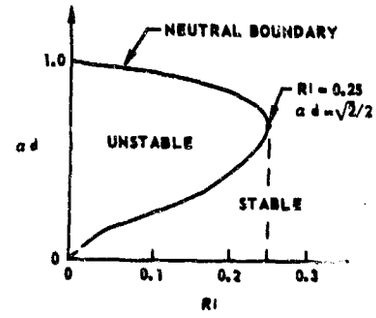

This criterion indicates that the flow would be stable for disturbances of all dimensionless wavenumbers, αd, for $Ri > 0.25$. For $Ri < 0.25$, it would be unstable for dimensionless wavenumbers which lie inside the boundary. Similar results are given by the other theories. The boundaries differ slightly for different assumed profiles, but the maximum Ri for instability is 0.25 for all profiles.

The preceding theoretical considerations formed the basis for planning the experiments. Several important features needed to be verified and/or investigated experimentally to provide information for the analyses of atmospheric shear flows. It was desired to verify the discrete wave-like nature of the initial disturbance and to obtain a method for estimating the wavelengths that occur. Next, it was desired to observe the stages through which initial distur-

* Uranine concentrate powder in water; concentrate available from Sagamore Color & Chemical Co., 82 Braintree Street, Alston Sta., Boston, Mass., U.S.A.

bances proceed to break down into turbulence; the greater the number of wavelengths that occur upstream of the turbulence, the greater the probability of detecting small waves on isentropes upstream of turbulent regions in the atmosphere. It was also desired to determine whether or not Drazin's criterion, or a similar criterion, could be broadly applied to shear flows without detailed consideration of every small "kink" in the velocity and density profiles. Finally, it was hoped that the results would provide further evidence that Ri = 0.25 should, in fact, be used as a critical Richardson number in atmospheric analyses.

Experimental Results

Profiles

Velocity, temperature, and density profiles within 5 to 10 in. downstream of the filter bed for three typical flow conditions are shown in Fig. 15-3. The corresponding velocity and density profiles in Drazin's theory are shown by the dashed lines. These profiles show the typical differences that existed between water channel velocity profiles and the corresponding ideal hyperbolic tangent profiles of Drazin. Over the central portion of the shear layer the similarity was good. The differences usually appeared near the edges of the shear layer (particularly near the low-velocity edge). Further comments on the small influence which these differences appear to have on the stability of the flow are included later in the paper.

The three velocity profiles all show positive shear, i.e., $\partial V/\partial z > 0$. Many tests were run with inverted filter beds (foam material thicker above the shear region than below it) so as to create negative shear, i.e., $\partial V/\partial z < 0$. The only effect of the change in sign of the shear was to reverse the circulation of the vortices which formed in the breakdown region.

The experimental and theoretical density profiles (Fig. 15-3) were similar over only a portion of the shear layer. The reason for this is that $\partial\rho/\partial T$ is a strong function of water temperature, particularly at low temperatures (Fig. 15-2). Control of density in the channel could be improved if provision were made to preheat all of the incoming water from its temperature in the main to perhaps 60 or 70 F.

Breakdown of Flow

Figure 15-4 illustrates the stages observed as the flow in the shear layer breaks down. There are four very distinct and repeatable stages which occur; dye traces illustrating the phenomenon are shown in the sketch and in the photographs. The photographs were taken through the lucite side wall (Fig. 15-1); the flow is from left to right. The scale appearing in the photographs was immersed in the flow close to the dye traces.

In Fig. 15-4(a), the flow appears undisturbed. Neither the dye traces nor the hydrogen bubble traces show visual evidence of any perturbation.

In Fig. 15-4(b), which is 8 in. further downstream, the center dye trace indicates the presence of a wave amplifying as it progresses downstream. The flow was approximately two-dimensional, i.e., the wave extended across the channel.

In Fig. 15-4(c), which is another 19 in. downstream, the waves have rolled up into vortices. The circulation of the vortices has the same sense as the vorticity introduced by the shear---the shear is negative in this flow condition, and all of the vortices rotated counterclockwise. These vortices grew slightly in size as they drifted downstream. Their downstream drift velocity was checked and found to be approximately V_o, the velocity upstream at the center of the shear layer. The flow was also determined to be two-dimensional at this stage. (The small kinks in the dye streamer in the lower left center of the photograph are not related to the flow pattern. These occur occasionally when a drop or two of dye that is slightly more dense than the rest comes through the probe.)

In Fig. 15-4(d), which is another 28 in. downstream --- 66 in. downstream of the filter bed --- the vortices have "burst" and the flow appears turbulent. The fluid motions were three-dimensional at this stage.

These observations are in agreement with the theoretical analysis of Michalke (Ref. 15-6). He calculated lines of constant vorticity and streaklines for a hyperbolic tangent velocity profile for Ri = 0. His results show concentrations of vorticity which superimpose a rotational motion on the basic flow. The observations are also similar to those of Freymuth (Ref. 15-7). In an experiment with a free air jet, he excited disturbances in the high-shear region using acoustic waves. His smoke traces show a similar development pattern.

Comparison with Criteria

Figure 15-5 is a summary of the results and a comparison with Drazin's theoretical criterion. Each flow condition at which waves were observed is identified by a point on the plot of αd vs Ri. The value of the wavelength used to compute α was obtained from the dye trace photographs. The different symbols in Fig. 15-5 denote different flow characteristics that were observed. The open circle symbol denotes conditions at which only waves were observed; that is, the waves extended the entire length of the channel without transitioning to vortices. The wavelengths of these waves ranged from about 3 to 6 in. The flags shown on the open circle symbols in the symbol block indicate the nature of the disturbances observed --- for example, small-amplitude waves (such as those in Fig. 15-4(b)) which persisted, waves which seemed to grow in amplitude to a certain point and then not grow further as they progressed downstream, and waves which appeared in the flow only intermittently.

The half-solid symbol denotes flow conditions at which the waves transitioned to vortices but did not transition to turbulence before reaching the downstream end of the channel. The full-solid symbol denotes flow conditions at which the full sequence of events occurred --- waves, vortices, and turbulence. The crosses with the subscript "sw" indicate conditions at which no waves of the type associated with instability occurred, but at which standing, long-wavelength (12 to 24 in.), shear-gravity waves occurred. The crosses at the bottom of the plot indicate values of Ri at which no waves of any kind were observed.

Most of the observations are in reasonably good agreement with Drazin's boundary. All cases at which full transition was observed fall in the unstable region. The four cases which fall above the boundary and at $Ri < 0.25$ can be attributed to differences between the experimental velocity profile and Drazin's hyperbolic tangent profile (this point is discussed later). The intermittent waves indicated at $Ri = 0.428$ and the steady waves at $Ri = 0.38$ are thus the only unexplainable points.

The shear, $(\partial V/\partial z)_o$, appears to be the primary factor in determining whether or not the initial waves transition to vortices and turbulence within the 120-in. length of the channel. Figure 15-6 shows the locations at which waves, vortices, and turbulence were first observed. These data are for values of Ri between 0 and 0.25 (no trend with Ri could be seen in the data). The trend indicates that the distance downstream at which waves were first discernible (Fig. 15-6(a)) varied inversely with the absolute value of the shear. This trend can be understood by considering the growth of Helmholtz waves. If it is assumed that the amplitude of the initial upstream disturbance is independent of the flow condition and that the wave must grow to some minimum amplitude before it can be observed, then the amplitude ratio at which waves will be observed will be constant. This constant amplitude ratio, according to the theory for Helmholtz waves (see Ref. 15-8), will occur at a downstream distance which varies inversely with the shear, as shown in Fig. 15-6(a).

Curves have been drawn through the data in Figs. 15-6(b) and (c) to illustrate the general trends. It is fairly certain that most of the open and half-solid symbols in Fig. 15-5 would have been solid symbols (indicating complete transition to turbulence) if the water channel had been longer. The flow conditions at which intermittent waves were observed are exceptions.

The number of wavelengths which were observed between the first discernible wave and the turbulence varied with the shear. Four or five distinct wavelengths often occurred upstream of the first vortex.

Theoretical criteria for profiles other than Drazin's are discussed in Refs. 15-2 and 15-9 (the latter criteria are based on numerical integration of the equations of motion rather than purely analytical considerations). All of these criteria indicate flow stability for $Ri > 0.25$. The neutral boundaries on the αd vs Ri plot differ somewhat, although for velocity profiles reasonably similar to those of the experiments, none predict instabilities having αd greater than about 2. An example (from Ref. 15-9) is shown in Fig. 15-7. Hazel's velocity profiles (Fig. 15-7(a)) in this example are nearly sinusoidal; they resemble the experimental profile shown in Fig. 15-3(c). His density profiles also differ from Drazin's, although most of the difference is outside of the shear layer. A comparison of Drazin's and Hazel's criteria is shown in Fig. 15-7(b). They both predict stability for $Ri > 0.25$. In addition, Hazel's criterion indicates that somewhat shorter wavelengths (larger values of αd) might be observed in unstable flows having velocity profiles which differ significantly from the hyperbolic tangent profile. The data points above the boundary in Fig. 15-5 might be in this category.

Concluding Remarks

The experiments tend to confirm the theoretical criteria of Drazin and others. The theoretical criteria of Hazel, which are for different velocity and density profiles, are different from Drazin's criterion only in that one might expect to observe somewhat shorter wavelengths in unstable shear layers. Drazin's boundary, however, would be expected to provide reasonably good estimates of the wavelengths that might occur. The experiments and all of the theories indicate that 0.25 should be used as the critical Richardson number. Finally, as many as four or five wavelengths were often observed upstream of the first discernible vortex; thus, it is reasonable to expect that several distinct waves might be observed in the isentropes when instabilities occur in atmospheric shear layers.

APPLICATION TO ATMOSPHERIC SHEAR FLOWS

Introduction

It is well known that stratified shear layers analogous to those investigated in the water channel are common in both the ocean and the atmosphere. For example, in recent papers by Woods (Refs. 15-10 and 15-11), the results of in situ studies of flows within the ocean's thermocline were reported. Woods made detailed measurements of velocity and temperature profiles in the thermocline. He found many distinct stable layers up to about 10 cm in thickness in which the shear and/or the temperature gradient were approximately constant. By releasing neutrally buoyant dye in certain of these layers, he was able to observe the flow characteristics.

In some cases, the layers underwent long-wavelength undulating motions --- wavelengths up to about 30 meters and amplitudes up to about 1.0 meter --- and the flow within the layers appeared to transition to turbulence. Wood's dye trace photographs of these transition regions are very similar to dye trace photographs of shear-layer breakdowns observed in the water channel.

Woods pointed out that these breakdowns within initially stable layers were a direct result of the long-wavelength undulating motions. He used an equation he obtained from a theoretical development in Phillips (Ref. 15-12) to show that, for certain layer and long-wave conditions, the change in shear which occurs within the layer as the flow approaches a peak or trough of the long wave can cause the local Richardson number to decrease below Ri = 0.25. Hence, the flow becomes unstable.

Woods and other investigators have recognized that similar flow conditions could exist in the atmosphere. Phillips (Ref. 15-12) and others have discussed the fundamental mechanism. Ludlam (Ref. 15-13) related certain types of billow clouds and CAT to instabilities in shear layers. Other investigators have made contributions which are indirectly related. One of the these is Haymond (Ref. 15-14); in WU-2 flights in the stratosphere, he observed a correlation between CAT and layers having strong temperature stratification. Another is Spilliane (Ref. 15-15) who also noted a correlation between stratospheric CAT over Woomera in the Australian desert and sharp, stable "kinks" in the temperature profile. A third is Hardy (Ref. 15-16) who has obtained radar returns from trains of 1.0- to 3- or 4-nmi waves with associated smaller-scale turbulence in regions where aircraft were reporting CAT. Hardy has also associated these waves with the breakdown of shear layers.

Analyses were conducted of several CAT cases in which the mechanism might have occurred. Two of these are described in this section of the paper.

Fundamentals of Flow

A schematic of the flow condition is shown in Fig. 15-8(a). At the left are shown upstream wind and temperature profiles with a stable shear layer having a thickness 2d. Within this layer, the mean wind is V_o and the mean temperature is T_o; the shear is $(\partial V/\partial z)_o$ and the environmental lapse rate is $\partial T/\partial z$.

At the right in Fig. 15-8(a) is shown a portion of a long-wavelength wave having an amplitude a (which might be 2,000 or 3,000 ft) and a wavelength λ_{LW} (which might be 10 or 20 nmi). It is assumed in this analysis that the thickness of the shear layer, the mean temperature and the lapse rate all remain constant as the flow within the shear layer experiences the undulating motion. From Phillips (Ref. 15-12), the following equation for the increase in shear that occurs at the peak (see Fig. 15-8(a)) can be derived:

$$\Delta(\partial V/\partial z) = \left[N_M^2 - n^2\right](a/V_o) \qquad (15\text{-}3)$$

For flows in the atmosphere instead of the ocean,

N_M = Brunt - Väisälä frequency = $\sqrt{\frac{g}{T}\left[(\partial T/\partial z) - (\partial T/\partial z)_{ad}\right]}$

n = wave frequency = $2\pi V_o/\lambda_{LW}$

$(\partial T/\partial z)_{ad}$ = adiabatic lapse rate, -2.98 x 10^{-3} deg C/ft*

This increase in shear is added to the initial shear. An expression for the minimum Richardson number (which occurs locally at the peak in the example given but would occur at the trough if the initial shear were negative) is

$$Ri_{MIN} = \frac{N_M^2}{\left[|(\partial V/\partial z)_o| + \Delta(\partial V/\partial z)\right]^2} \qquad (15\text{-}4)$$

Since $N_m^2 > n^2$ under all conditions of interest (this is only untrue for weakly stable lapse rates, i.e., when $\partial T/\partial z \approx (\partial T/\partial z)_{ad}$), the expression can be further simplified to

$$Ri_{MIN} \approx \frac{N_m^2}{\left[|(\partial V/\partial z)_o| + N_M^2(a/V_o)\right]^2} \qquad (15\text{-}5)$$

From Eq. (15-5) it is evident that low values of Ri_{MIN} are associated with large initial shears, $(\partial V/\partial z)_o$; with large long-wave amplitudes, a; and with low winds, V_o. The effect of $\partial T/\partial z$ on Ri_{MIN} can be seen in Fig. 15-8(b). This figure is based on typical conditions under which mountain lee waves are observed. The curves show the somewhat surprising result that the greater the initial stability (i.e., the greater $\partial T/\partial z$), the lower Ri_{MIN} will be. They also show that slightly stable layers are not likely to become unstable unless the initial shear is large.

Wavelengths of Instabilities

The experiments discussed previously tend to confirm the theoretical criteria of Drazin and others. The critical Richardson number of 0.25 and Drazin's variation of σd with Ri for neutral stability (Fig. 15-5) was used to predict wavelengths that might occur when an instability occurs in an atmospheric shear flow. These predictions are shown in Fig. 15-9. Ranges of unstable wavelengths (λ in nmi) are shown as functions of the shear-layer thickness (2d in ft) for local values of Ri between 0.25 and 0.

One can argue several different ways to reach the conclusion that, when an instability occurs,

* Note use of minus sign to denote temperature decreasing with increasing altitude.

the wavelength that will be observed will be $\lambda = (2\pi/\sqrt{2}) \cdot 2d$. One viewpoint is that if $Ri = 0.25$ at the peak of the long-wavelength wave, then the flow in the shear layer must have experienced $Ri = 0.25$ on the way up to the peak. Since instability would occur at $Ri = 0.25$, the wavelength that would be seen would therefore correspond to that for $Ri = 0.25$, or $\lambda = (2\pi/\sqrt{2}) \cdot 2d$.

All that can be said is that $\lambda = (2\pi/\sqrt{2}) \cdot 2d$ should provide a reasonable estimate of the unstable wavelengths that can be expected. As shown in Fig. 15-9, the expected wavelength for $2d = 1{,}000$ ft is 0.7 nmi, and for $2d = 5{,}000$ ft it is 3.6 nmi. Nicholls (Ref. 15-17), in analyses of his stratospheric lee-wave data over the southwestern U.S., has consistently found stable layers from 1,000 to 5,000 ft thick with internal waves (as determined from reconstructed isentropes) having wavelengths from 1.0 to 3 nmi. These observations are in very good agreement with the predictions in Fig. 15-9.

Analyses of Cases

California Lee Wave Case

During the winters of 1966-1967 and 1968-1969, Canberra and RB-57F flights were made over the southwestern U.S. to study stratospheric waves and CAT under mountain lee wave conditions. Certain of the aircraft and radiosonde data were transmitted to the author by Mr. J. M. Nicholls of the British Meteorological Office who participated in these flights (Refs. 15-17 and 15-18). All of the 1966-1967 data will be published in Ref. 15-19.

As noted previously, by reconstructing isentropes using radiosonde and aircraft temperature measurements, Nicholls has found stable layers and small-wavelength internal waves in many of his cases. CAT usually appeared in the troughs of the long-wavelength features downstream of the small internal waves.

Figure 15-10, which is based on a similar figure provided by Nicholls, shows an isentrope for a flight near the San Bernardino Mountains in Southern California at about 37,000 ft on February 3, 1967. The wind is from left to right (west to east) in this figure. According to Nicholls (Ref. 15-18):

"The major peaks of the isentrope were fixed relative to the mountains, and the inferred steticnarity implies the long-wavelength features are representative of mountain-wave airflow. The position of the wavelets and turbulence on the run and its reciprocal (which was on a parallel track 10 nmi to the north) are clearly marked. The wind direction was about 50 deg to the flight track and, assuming all peak and trough axes are normal to the wind direction, the true wavelengths would be just about one-half of those shown in the diagram, i.e., about 0.9 nmi for the wavelets, with a mountain wave separation of about 15 nmi. The turbulence and wavelets appeared to be present in the stable air brought down from 41,000 ft by the mountain wave."

Wind and temperature profiles for this case are shown in Fig. 15-11. Two very stable layers are evident at altitudes near the 37,000-ft flight level (Fig. 15-11(b)). The upper layer is approximately 2,600 ft thick; the Richardson number was calculated to be $Ri_o = 77.6$. The expected wavelength from an instability in this layer is $\lambda_{E(1)} = (2\pi/\sqrt{2}) \cdot 26{,}000 = 11{,}560$ ft, or 1.9 nmi. The shear is positive which would suggest that if an instability were to occur it would be near a peak of a lee wave instead of near a trough. The lower layer is approximately 900 ft thick and the corresponding expected wavelength is $\lambda_{E(2)} = 0.7$ nmi. The Richardson number for this layer is $Ri_o = 8.7$. The shear is negative, so that an instability would be expected near a trough of a lee wave. These and other characteristics of the expected waves that will be discussed subsequently are summarized under "California Case" in Table 15-I.

If it is assumed that the radiosonde data are representative of undisturbed conditions upstream of the mountain waves, then the minimum Richardson number that would be expected to occur in the stable layer is given by Eq. (15-4). This assumes that the shear determined from the radiosonde profile, $(\partial V/\partial z)_o$, is changed by an amount $\Delta(\partial V/\partial z)$ determined from Eq. (15-3) using the observed long-wavelength characteristics from Fig. 15-10 and the characteristics of the individual layers from Fig. 15-11. Thus, for these calculations the following were used with the appropriate dimensional units:

Layer	λ_{LW}, nmi	a, ft	T_o, deg C
1	17	3,500	-59.2
2	17	3,500	-58.9

Layer	$\partial T/\partial z$, deg C/1,000 ft	V_o, kts	$(\partial V/\partial z)_o$, kts/1,000 ft
1	2.9	34	+2.0
2	2.6	55	-5.8

The results of these calculations are shown in Table 15-I under "Ri_{MIN} --- based on $\Delta(\partial V/\partial z)$." It will be noted that the additional shear decreased the Richardson numbers greatly. Strict application of the criterion $Ri_{MIN} < 0.25$ for instability leads one to conclude that an instability would not occur and, hence, small waves would be unlikely. However, the calculated value for one of the two layers (layer 1) is very close to the critical value. A slight increase in shear - about 6% --- above that estimated using Eq. (15-3) would result in $Ri < 0.25$, in which case waves would be likely.

To obtain the minimum value of Ri_{MIN} that can reasonably be derived from a given set of temperature and velocity profiles, $2\Delta(\partial V/\partial z)$ can be used in Eq. (15-4) instead of $\Delta(\partial V/\partial z)$. The reason for this is that, at least in theory, the difference in shear between a peak and a trough is $2\Delta(\partial V/\partial z)$. In the unlikely circumstance that the radiosonde was not taken upstream in undisturbed air but instead passed upward through a trough (in the case of positive $(\partial V/\partial z)_o$), then

the change in shear would be $2\Delta(\partial V/\partial z)$.

The values of Ri_{MIN} based on $2\Delta(\partial V/\partial z)$ are also shown in Table 15-I. For both layers, Ri_{MIN} was much less than 0.25. Thus, under the specified conditions, both of the layers would be classified as unstable and waves would be expected.

The principal results of this analysis can be seen upon examination of Table 15-I and Fig. 15-10. The calculations indicate that at least one wavelength should appear ($\lambda_{E(1)}$ = 1.9 nmi) and that a second might appear ($\lambda_{E(2)}$ = 0.7 nmi). The isentropes in Fig. 15-10 show several sets of small waves having wavelengths quite close to the expected values. Moreover, $\lambda_{E(1)}$ = 1.9 nmi was expected near a peak and the longest wave observed, λ_O = 1.5 nmi, occurred downstream of a peak; similarly, $\lambda_{E(1)}$ = 0.7 was expected in a trough and waves having λ_O = 0.9, 0.95, 1.2, and 1.3 nmi were all observed in a trough. Finally, it should be mentioned that the potential temperature for layer 2 was calculated to be θ= 334 K; this is very close to θ= 333 K, which is the isentrope shown in Fig. 15-10. The small waves in this specific isentrope are evidence that layer 2 did in fact become unstable.

Nicholls has indicated that when stable layers such as those shown in the temperature profile in Fig. 15-11(b) occur, they are clearly identifiable in widely dispersed upstream soundings. He has observed the same detailed temperature structure in as many as five soundings spread out over several hundred miles. The detailed velocity structures show the same magnitude shears but with more-or-less random variations in the altitudes at which they occur.

Coloredo Lee Wave Case

A similar analysis was conducted for a case near Boulder, Colorado on February 15, 1968. This case was documented by Dr. Douglas K. Lilly of the National Center for Atmospheric Research (Ref. 15-20). Additional data for use in the present analysis were obtained from Dr. Lilly.

The isentropes are shown in Fig. 15-12. Three aircraft participated in the experiment, and the three groups of isentropes indicate the approximate ranges of altitudes in which flights were made. The wind was from west to east (left to right).

Two radiosondes were used in this analysis. One was launched at Granby (Fig. 15-13(a) and (b)) which is upstream in the mountains approximately 35 nmi west-northwest of the Marshall radar. The second was launched at Denver (Fig. 15-13(c) and (d)) which is downstream approximately 22 nmi southwest of the Marshall radar. Six highly stable layers were identified in each of the two radiosonde temperature profiles. There is considerable similarity between the two temperature profiles which were about 55 nmi apart. Only layers 4 and 7 do not seem to appear in both profiles. Layers which were subsequently found to be stable when $2\Delta(\partial V/\partial z)$ was used in computing Ri_{MIN} are denoted by an asterisk.

The characteristics of the expected and observed waves are summarized in Table 15-I under "Colorado Case." The layers have been grouped according to their altitudes. The first seven have mean altitudes between 57,725 and 67,195 ft and are associated with the upper group of isentropes; the remaining five have mean altitudes between 37,967 and 47,112 ft and are associated with the middle group of isentropes.

The principal results can be seen upon examination of Table 15-I and Fig. 15-12. Consider the upper group of isentropes first. The isentropes show a distribution of observed waves approximately as indicated in Table 15-I. Most of the waves are between about 0.8 and 2.3 nmi, with several between 4 and 5 nmi. These wavelengths agree well with the expected values except for $\lambda_{E(8)}$ = 6.3 nmi and $\lambda_{E(7)}$ = 0.4 nmi. The potential temperature for the latter layer was calculated to be θ= 483 K and, judging by the potential temperatures shown in Fig. 15-12, it is apparent that this layer did not come low enough in altitude to be in the region of the flights.

The small waves and turbulence in the isentropes appear to start near the upstream peak and to extend over at least the next two troughs and peaks. As indicated in Table 15-I, the initial shears were both positive and negative so that the small waves would be expected at peaks and also in troughs.

It is also interesting to compare the middle group of isentropes in Fig. 15-12 with the predictions. All five layers in this altitude range were predicted to remain stable even under the most pessimistic of assumptions, i.e., using $2\Delta(\partial V/\partial z)$ in computing Ri_{MIN}. No small waves are indicated in Fig. 15-12. Dr. Lilly has subsequently indicated that flights were made through this region at four levels; no small waves were observed in reducing the data, and the pilots did not report turbulence.

Concluding Remarks

The preceding results appear to confirm that very stable layers in the atmosphere can be destabilized by increases in shear caused by mountain lee waves. Moreover, it has been shown that stability criteria such as that of Drazin can be used to predict the onset of instability, the approximate wavelengths that would occur, and the locations of the small waves and turbulence.

This flow phenomenon undoubtedly occurs at all altitudes (not only in the stratosphere). As indicated previously, billow clouds of the non-convective variety are frequent evidence of the phenomenon occurring in the troposphere. It need not be associated with orgraphic disturbances. Shear-gravity waves can be created wherever a major inversion and strong wind shear occur, such as is often the case at the tropopause. These waves have wavelengths and amplitudes similar to those of mountain waves and can cause similar increases in shear within stable layers. The phenomenon can also occur when stable layers flow over the tops of large

cumulonimbus clouds.

Thus, the phenomenon could be responsible for an appreciable fraction of clear air turbulence encounters.

RESULTS AND CONCLUSIONS

1. The fluid mechanics experiments to investigate the stability of straight, stratified shear flows tended to confirm the theoretical stability criteria of Drazin and others. The experimental velocity and density profiles differed somewhat from the hyperbolic tangent velocity profile and exponential density profile assumed by Drazin. However, Drazin's theory and the experiments were in agreement in that, with few exceptions, (1) the flows were stable for Richardson numbers greater than 0.25 and (2) the wavelengths of the instabilities that were observed were in the range predicted by the theory to be unstable.

2. Four distinct stages were observed when the shear flows broke down: (1) first there was a region which appeared undisturbed; (2) downstream of this region, waves were observed; (3) these amplified and transitioned into vortices; and (4) these then burst to form turbulence. As many as four or five wavelengths were often observed upstream of the first discernible vortex. Thus, it is reasonable to expect that several distinct waves might be observed in the isentropes when instabilities occur in atmospheric shear layers.

3. The analyses of two mountain lee wave cases appear to confirm that very stable layers in the atmosphere can be destabilized by increases in shear which occur as the layers flow through the long-wavelength lee waves. The estimated wavelengths of instabilities were in good agreement with wavelengths observed in the isentropes reconstructed from aircraft and radiosonde data. Moreover, the locations of these waves and subsequent turbulence relative to the peaks and troughs of the lee waves were predicted reasonably well.

REFERENCES

15-1. Baumeister, T., ed.: Marks' Mechanical Engineers' Handbook. Sixth Edition, McGraw-Hill Book Company, Inc., New York, 1958.

15-2. Drazin, P. G. and L. N. Howard: Hydrodynamic Stability of Parallel Flow of Inviscid Fluid. Advances in Applied Mechanics, Vol. 9, published by Academic Press, New York, 1966, pp. 1-89.

15-3. Drazin, P. G.: The Stability of a Shear Layer in an Unbounded Heterogeneous Inviscid Fluid. Journal of Fluid Mechanics, Vol. 4, 1958, pp. 214-224.

15-4. Drazin, P. G. and L. N. Howard: The Instability to Long Waves of Unbounded Parallel Inviscid Flow. Journal of Fluid Mechanics, Vol. 14, 1962, pp. 257-283.

15-5. Miles, J. W. and L. N. Howard: Note on a Heterogeneous Shear Flow. Journal of Fluid Mechanics, Vol. 20, 1964, pp. 331-336.

15-6. Michalke, A.: On Spatially Growing Disturbances in an Inviscid Shear Layer. Journal of Fluid Mechanics, Vol. 23, 1965, pp. 521-544.

15-7. Freymuth, P.: On Transition in a Separated Laminar Boundary Layer. Journal of Fluid Mechanics, Vol. 25, 1966, pp. 683-704.

15-8. Huschke, R. E.: Glossary of Meteorology. American Meteorological Society, Boston, Massachusetts, 1959.

15-9. Hazel, P.: Instabilities of Stratified Shear Flow. Paper submitted for publication in Journal of Fluid Mechanics, 1968.

15-10. Woods, J. D.: Wave-Induced Shear Instability in the Summer Thermocline. Journal of Fluid Mechanics, Vol. 32, 1968, pp. 791-800.

15-11. Woods, J. D.: An Investigation of Some Physical Processes Associated with the Vertical Flow of Heat Through the Upper Ocean. Meteorological Magazine, Vol. 97, 1968, pp. 65-72.

15-12. Phillips, O. M.: The Dynamics of the Upper Ocean. Cambridge University Press, 1966.

15-13. Ludlam, F. H.: Characteristics of Billow Clouds and Their Relation to Clear Air Turbulence. Quarterly Journal of the Royal Meteorological Society, Vol. 93, 1967, pp. 419-435.

15-14. Haymond, F. B.: High Altitude Clear Air Turbulence. Technical Report No. 2, U.S.A.F. Air Weather Service, 9th Weather Squadron, Davis-Monthan AFB, Arizona, November 1967.

15-15. Spillane, K. T.: Clear Air Turbulence and Supersonic Transport. Nature, Vol. 214, No. 5085, April 15, 1967, pp. 237-239.

15-16. Hardy, K. R.: Radar Echoes from the Clear Air. Paper prepared for NATO Advanced Study Institute on the Structure of the Lower Atmosphere and Electromagnetic Wave Propagation, Aberystwyth, Wales, September 2-15, 1967.

15-17. Nicholls, J. M.: Conference at United Aircraft Research Laboratories, April 15, 1969.

15-18. Nicholls, J. M.: Meteorological Office Letter to J. W. Clark, United Aircraft Research Laboratories, May 28, 1969.

15-19. McPherson, A. and J. M. Nicholls: Results of a Series of Flights in the Stratosphere over Mountainous Terrain in the Western U.S.A. during February 1967. To be published as an R.A.E. Technical Report, 1969.

15-20. Lilly, D. K.: Lee Waves in the Colorado Rockies. Symposium on Clear Air Turbulence and Its Detection; Boeing Scientific Research Laboratories Report D1-82-0740, Seattle, Washington, August 1968.

TABLE 15-I

CHARACTERISTICS OF EXPECTED AND OBSERVED SMALL-WAVELENGTH WAVES
FOR CALIFORNIA AND COLORADO LEE WAVE CASES

Case	Stable Layer	Mean Altitude, ft	$\bar{\theta}$, °K	Thickness, Δz - ft	λ_g( ), nmi	Expected Location in Lee Waves	Ri_o	Based on $\Delta(\partial V/\partial z)$: Ri_{MIN}	Based on $\Delta(\partial V/\partial z)$: Waves Likely? ($Ri_{MIN}<0.25$?)	Based on $2\Delta(\partial V/\partial z)$: Ri_{MIN}	Based on $2\Delta(\partial V/\partial z)$: Waves Likely? ($Ri_{MIN}<0.25$?)	Waves Observed?	λ_o, nmi	Location in Lee Waves
California	1	41,900	314	2,600	1.9	peak	77.6	0.28	no(2)	0.07	yes	yes	1.9	after peak
	2	37,550	311	900	0.7	trough	8.7	0.52	no	0.17	yes		0.9-1.3	trough
Colorado(1)	1	60,718	4[illegible]	6,000	4.4	trough	5.4	0.36	no(3)	0.12	yes	yes	35%:0.8-1.2; 50%:1.2-1.8; 15%:1.8-2.3; several between 4-5	appear to start at peak and extend downstrea through at least two troughs and two peaks
	2	62,108	4[illegible]	3,200	2.4	trough	3.5	0.20	yes	0.06	yes			
	3	59,114	4[illegible]	2,800	2.0	trough	10.4	0.62	no	0.20	yes			
	7	67,195	4[illegible]	600	0.4	peak	486.7	0.20	yes	0.05	yes			
	8	59,232	4[illegible]	8,600	6.3	trough	26.5	0.61	no	0.18	yes			
	9	62,021	4[illegible]	3,000	2.2	peak	757.9	0.33	no(4)	0.08	yes			
	10	57,715	4[illegible]	5,600	4.1	trough	4.9	0.86	no	0.16	yes			
	4	47,112	3[illegible]	700	0.5	trough	1.1	0.48	no	0.27	no	no - pilots reported very little or no turbulence.		
	5	43,055	3[illegible]	1,300	1.0	trough	2.2	0.59	no	0.27	no			
	6	38,968	3[illegible]	2,600	1.9	peak	2.6	0.83	no	0.40	no			
	11	43,475	3[illegible]	1,300	1.0	trough	83.1	1.66	no	0.48	no			
	12	37,967	3[illegible]	3,500	2.0	trough	158.9	5.09	no	1.63	no			

(1) Layers 1-6 from Granby radiosonde; layers 7-12 from Denver radiosonde.
(2) Yes for 0% greater $\Delta(\partial V/\partial z)$.
(3) Yes for 2% greater $\Delta(\partial V/\partial z)$.
(4) Yes for 1% greater $\Delta(\partial V/\partial z)$.

FIG. 15-1. SKETCH OF UARL OPEN WATER CHANNEL

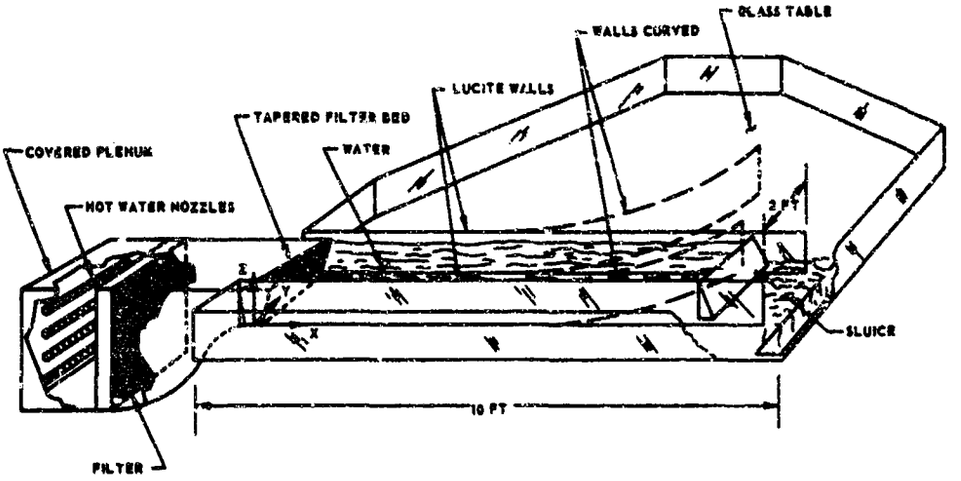

FIG. 15-2. EFFECT OF TEMPERATURE ON PROPERTIES OF WATER

DERIVED FROM DATA IN REF. 15-1

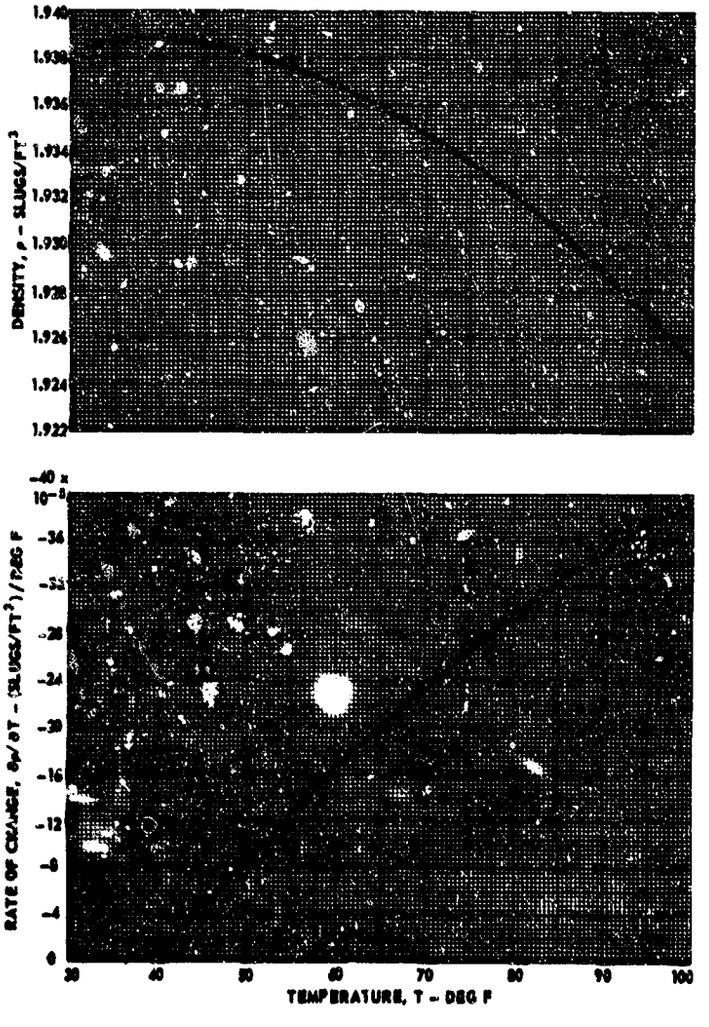

FIG. 15-3. TYPICAL VELOCITY, TEMPERATURE AND DENSITY PROFILES FOR SHEAR-LAYER EXPERIMENTS

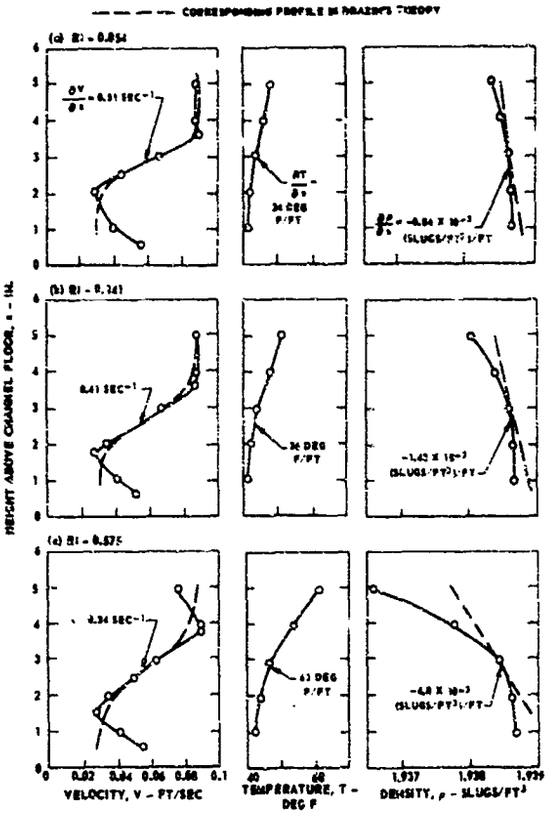

FIG. 15-4. TYPICAL STAGES OF BREAKDOWN OF FLOW IN SHEAR LAYER

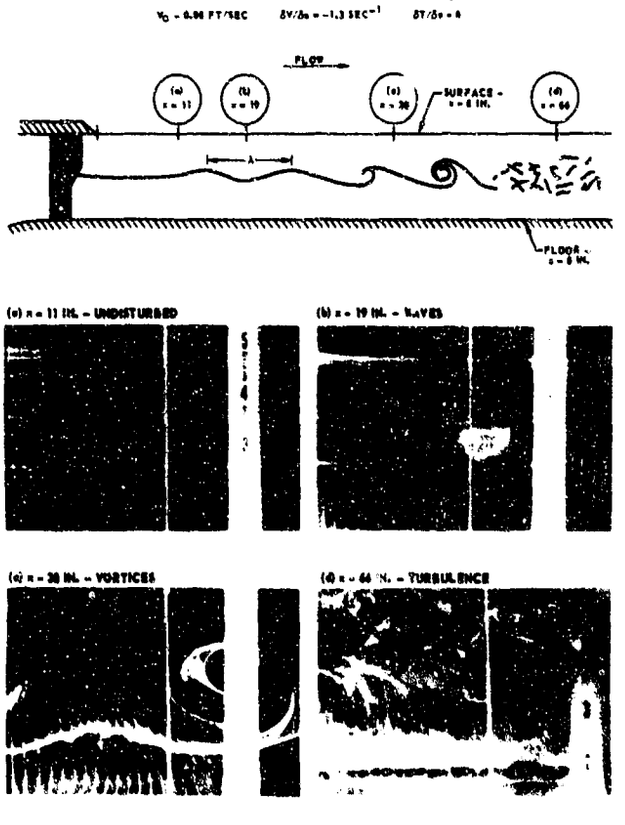

FIG. 15-5. COMPARISON OF WATER CHANNEL RESULTS WITH DRAZIN'S CRITERION FOR STABILITY

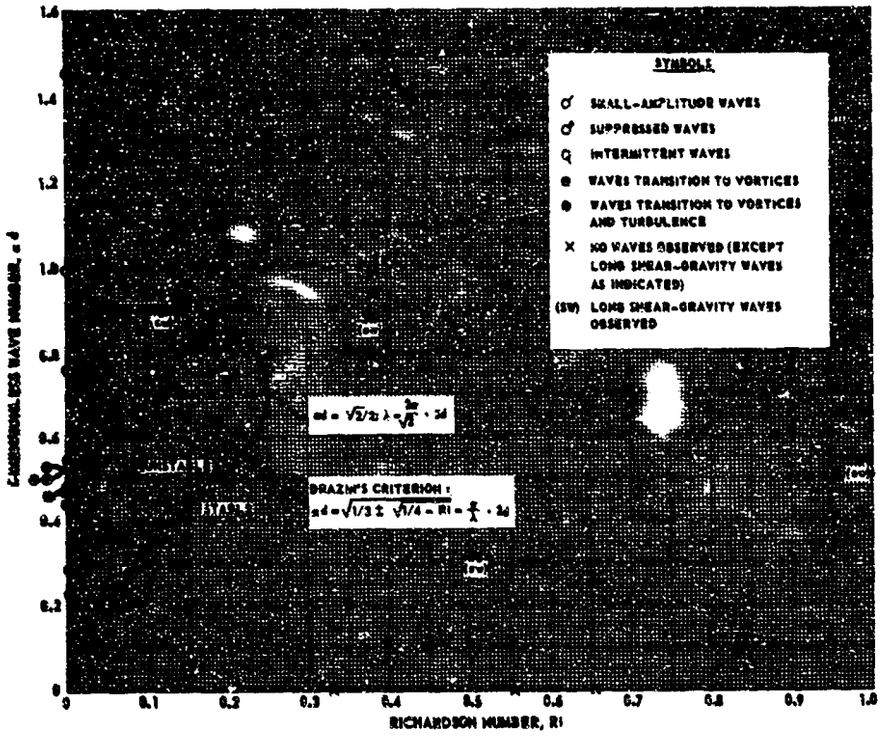

FIG. 15-6. EFFECT OF SHEAR ON DOWNSTREAM DISTANCE AT WHICH WAVES, VORTICES AND TURBULENCE WERE FIRST OBSERVED

SEE FIG. 15-4 FOR SKETCH OF TYPICAL SHEAR-LAYER BREAKDOWN
SYMBOLS SAME AS IN FIG. 15-5; $0 < Ri < 0.25$
——— ——— ———TREND IN DATA

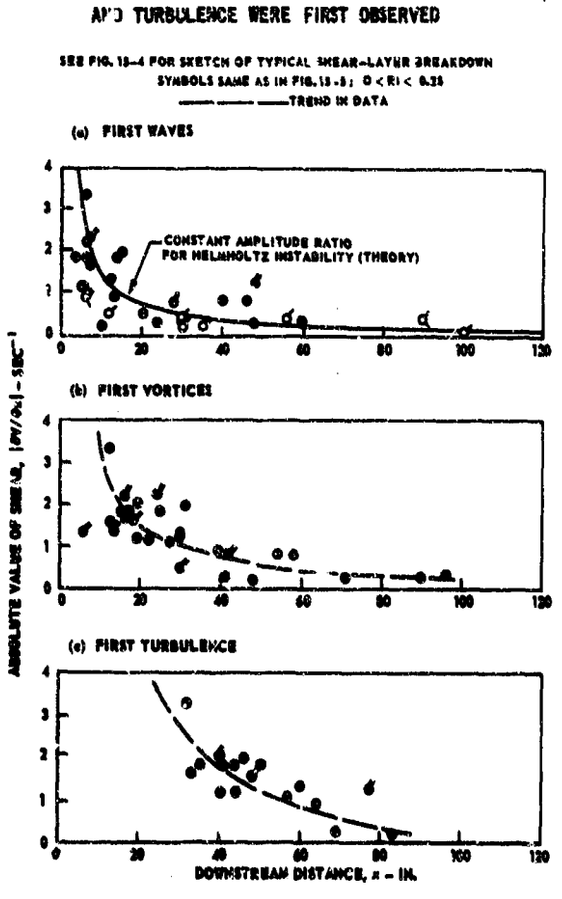

FIG. 15-7. COMPARISON OF THEORETICAL STABILITY CRITERIA FOR TWO TYPES OF VELOCITY AND DENSITY PROFILES

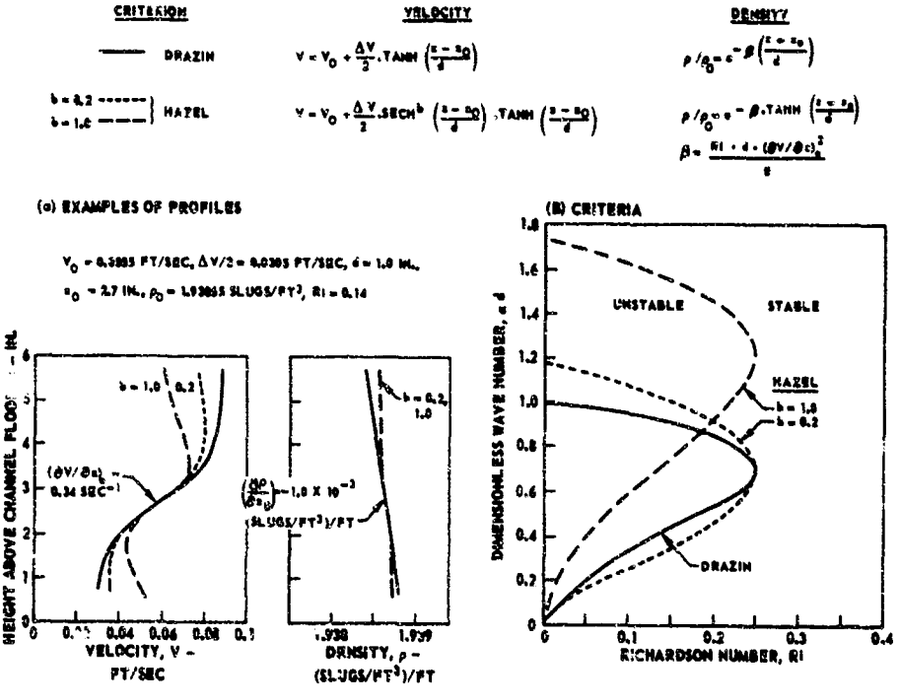

FIG. 15-8. EFFECTS OF LONG-WAVELENGTH WAVES ON STABILITY OF ATMOSPHERIC SHEAR LAYERS

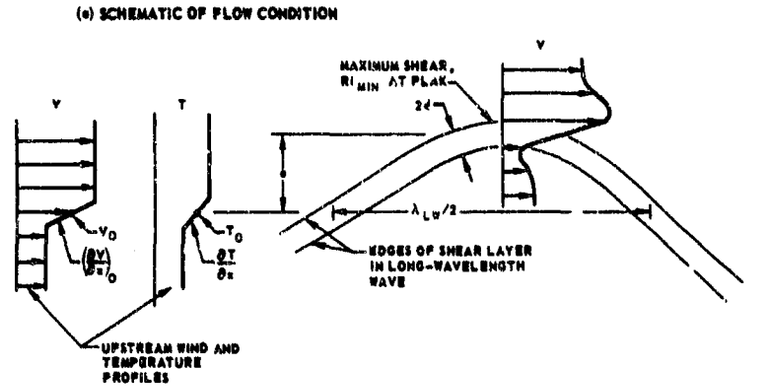

(b) EFFECT OF LAPSE RATE AND SHEAR ON Ri_{MIN} FOR TYPICAL WAVE CONDITIONS

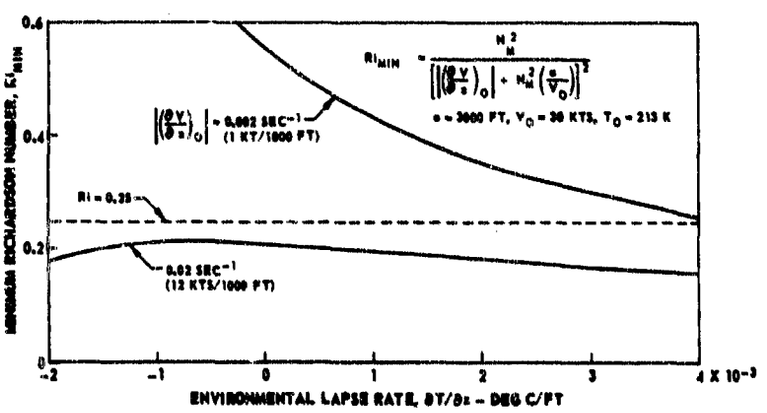

FIG. 15-9. PREDICTION OF UNSTABLE WAVELENGTHS IN ATMOSPHERIC SHEAR LAYERS USING DRAZIN'S CRITERION

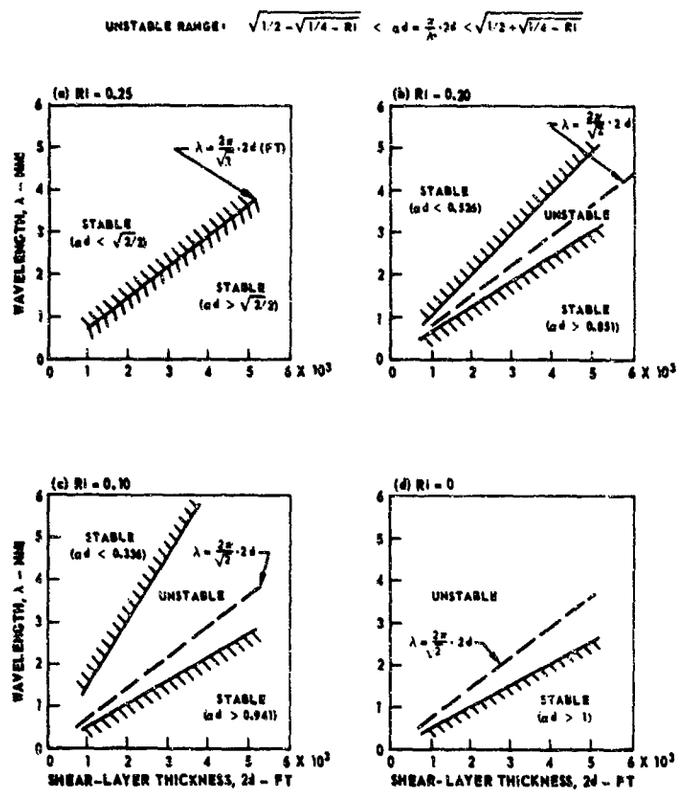

FIG. 15-10. ISENTROPES FOR CALIFORNIA LEE WAVE CASE

BASED ON DATA FROM NICHOLLS
FEBRUARY 3, 1967 - 2021-2034 GMT
AIRCRAFT FLIGHT PATHS APPROXIMATELY 50 DEG TO WIND

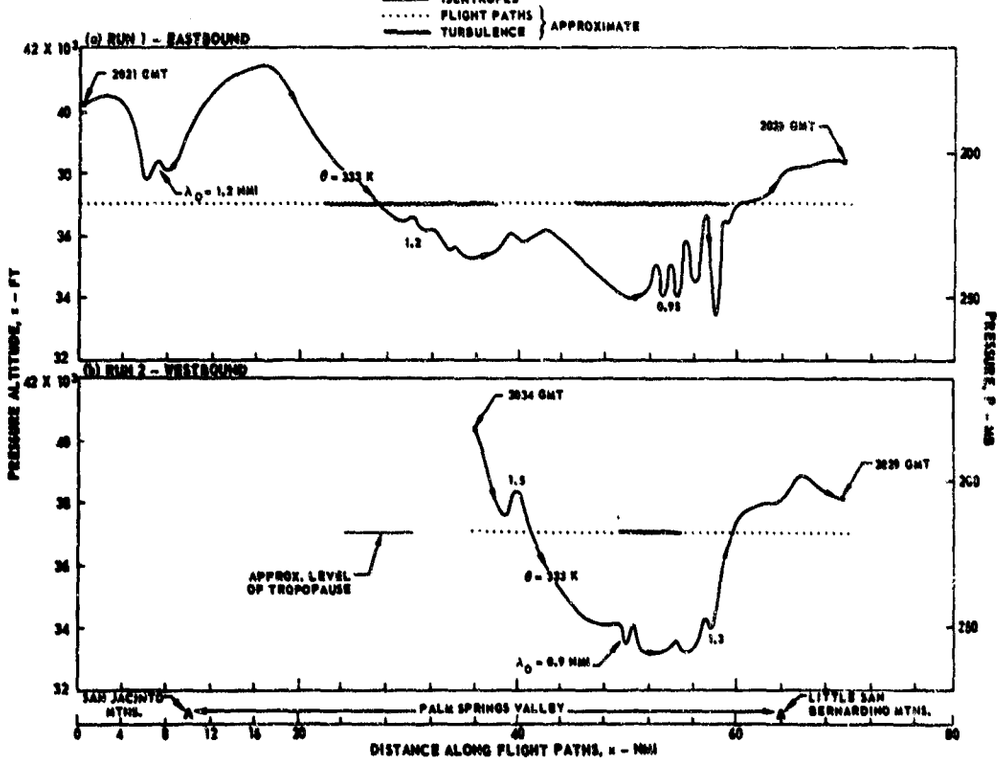

FIG. 15-11. WIND AND TEMPERATURE PROFILES FOR CALIFORNIA LEE WAVE CASE

BASED ON DATA FROM NICHOLLS
FEBRUARY 3, 1967 – 2021–2034 GMT
PROFILES ARE COMPOSITES OF AIRCRAFT AND RADIOSONDE DATA
$\lambda = (2\pi/\sqrt{\Pi}) \times d$
SEE TABLE 15–I FOR ADDITIONAL DETAILS

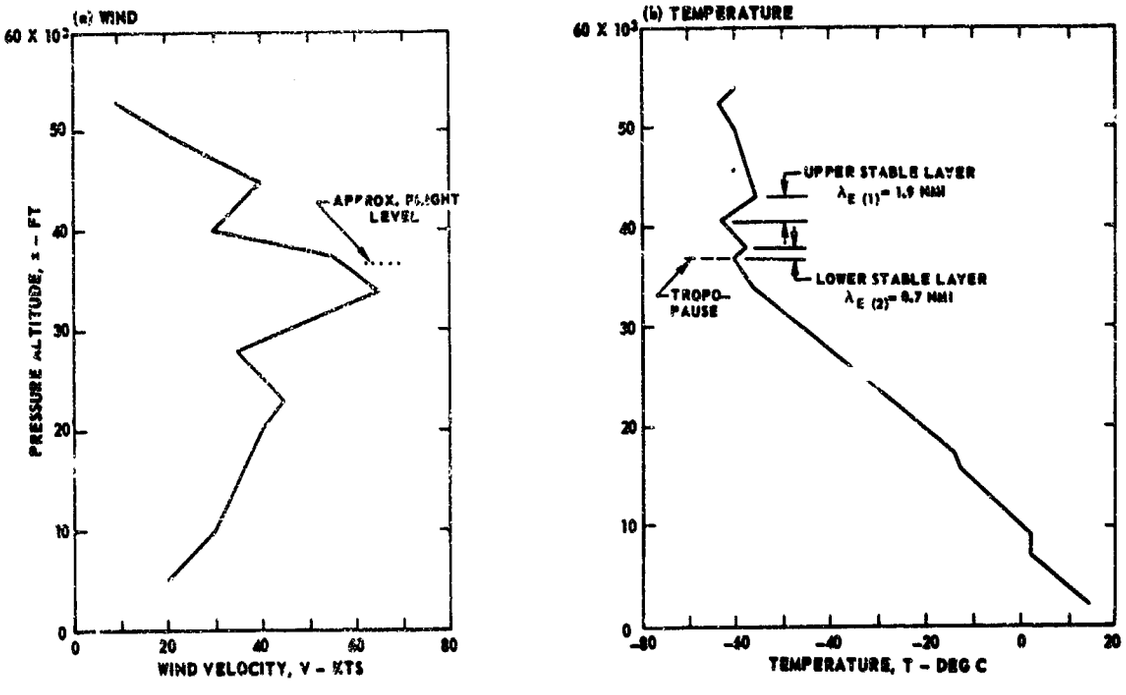

FIG. 15–12. ISENTROPES FOR COLORADO LEE WAVE CASE

BASED ON DATA FROM LILLY
FEBRUARY 15, 1968 – 2200–2400 GMT
AIRCRAFT FLIGHT PATHS APPROXIMATELY PARALLEL TO WIND
ISENTROPES
FLIGHT PATHS
TURBULENCE

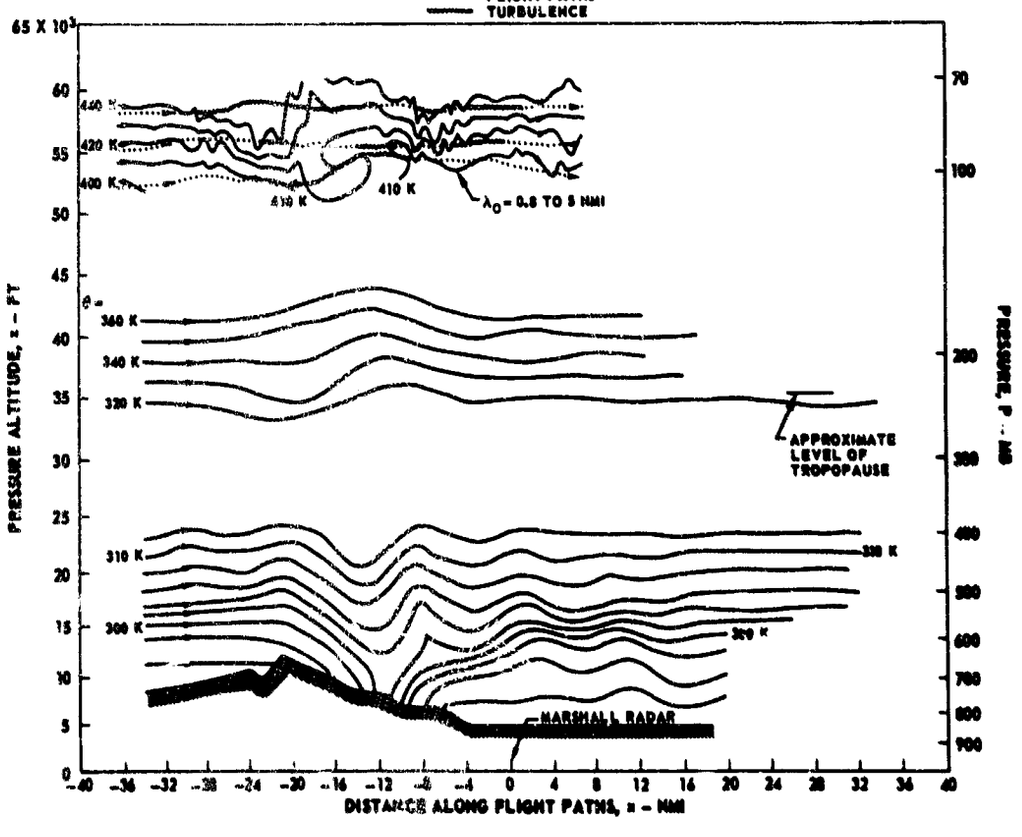

FIG. 15-13. WIND AND TEMPERATURE PROFILES FOR COLORADO LEE WAVE CASE

BASED ON DATA FROM LILLY
FEBRUARY 15, 1968 – 2200–2400 GMT
PROFILES FROM RADIOSONDE DATA
$\lambda_E = (2\pi/\sqrt{2}) \times 2d$
λ_E^* DENOTES WAVE UNLIKELY TO OCCUR
SEE TABLE 15–I FOR ADDITIONAL DETAILS

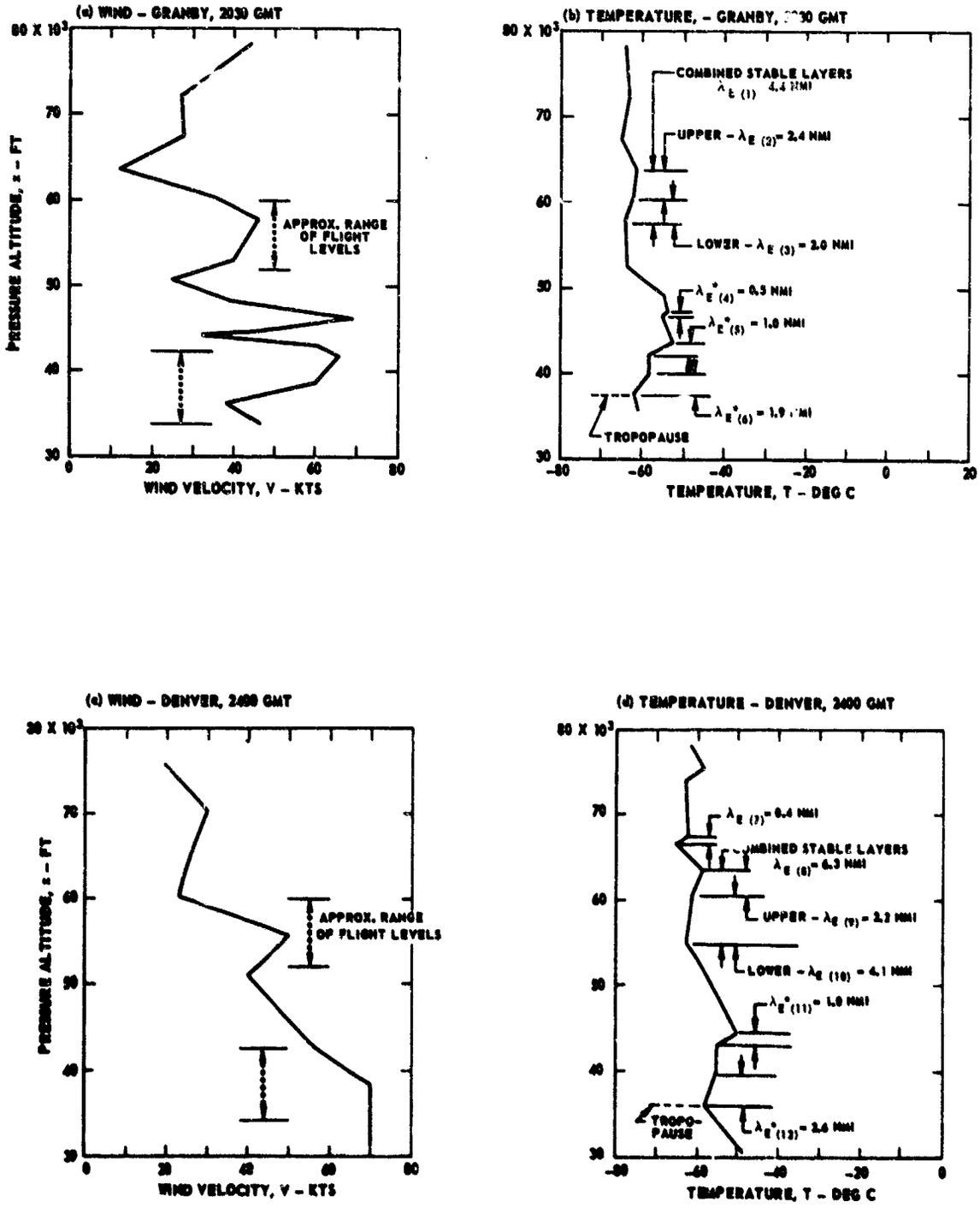

The Wake Characteristics of a Bluff Body in a Shear Flow

D.J. Maull

Cambridge University Engineering Department

Summary

A method of producing a low turbulence shear flow in a wind tunnel is described. The shear flow had an almost linear velocity profile with the velocity near the roof of the tunnel about 50% greater than that near the floor. The turbulence level was about 0.5% based on the local mean velocity.

Measurements were made of the wake of a flat plate normal to the flow direction and spanning the wind tunnel such that the velocity varied along the length of the plate. It was found that space correlations of the velocity fluctuations in the wake were significantly different when the plate was in a shear flow than when it was in a uniform stream. Spectra of the velocity fluctuations were measured at positions along the length of the plate in the shear flow and it was found that the Strouhal numbers, based on the local undisturbed free stream velocity, were approximately constant over about half the plate length.

By comparing the signals from an array of hot wires behind the plate a model of the vortex shedding is postulated.

The Wake Characteristics of a Bluff Body in a Shear Flow

by

D.J. Maull

Cambridge University Engineering Department

Introduction

The characteristics of the wind near the earth's surface may be considered as being made up of a mean velocity profile varying with height on top of which is superimposed turbulent fluctuations. Thus in studying the forces on, and the flow around, objects in the earth's boundary layer by means of models in a wind tunnel the properties of the earth's boundary layer must be correctly simulated and scaled. It has been shown by Jensen and Franck (1965) that to predict, by means of wind tunnel tests, the mean pressure distribution on a house in the earth's boundary layer, the roughness height of the wind tunnel boundary layer divided by the height of the model must be equal to the same ratio for the full scale conditions. This means that for correct simulation the wind tunnel boundary layer must grow naturally along the tunnel floor and this inevitably requires a long working section. In Jensen's tunnel the length of the working section is 7.5 m and a similar tunnel at the University of Western Ontario (Davenport (1967)) has a length of 24.4 m.

Another method of simulating the earth's boundary layer is to artificially produce a rough wall turbulent boundary layer by means of a barrier across the wind tunnel and a system of elliptic turbulence generators. This method has been described by Counihan (1969) and shows that a working section length of about five boundary layer heights is required to produce the simulated flow.

It is desirable, in attempting to interpret the results from experiments performed in a simulated atmospheric boundary layer, to differentiate between the effects of turbulence and the effects of a mean-velocity gradient. It therefore seems justifiable to carry out basic experiments on the effect of turbulence on the flow around bluff bodies and separate experiments on the effect of low turbulence shear flow around such bodies. Turbulence may be generated in a wind tunnel by means of a uniform grid and the effect of turbulence on the flow around a bluff body has been described by Bearman (1968).

There are many methods of producing a shear flow in a wind tunnel, most of which involve putting across the flow some form of non-uniform grid. An early method was that of Owen and Zienkiewicz (1957) who used a system of circular rods spanning the tunnel, the spacing of the rods being varied to produce the required velocity profile. This method was subsequently used by Gould et al (1968) to develop shear flows for the study of the flow around bluff bodies and by Wolf and Johnston (1966) to study the effect of non-uniform entry conditions on the performance of diffusers. Another method of producing a shear flow is by using honeycomb which has been cut so that it has a variable depth across the tunnel. The design of the honeycomb shape has been described by Kotansky (1966).

From the few measurements available it appears that one of the drawbacks of the method of producing a shear flow by means of non-uniformly spaced rods is that inevitably high turbulence is also produced. For instance, Gould states that in his shear flow the level of turbulence was about 6% compared with about 0.1% in a moderately well designed wind tunnel used for aeronautical research.

Another method of producing a shear flow is by using curved uniform gauzes across the flow as described by Elder (1959) and Davies (1957). This is the method reported in this paper and was used since it was thought that the turbulence levels would be significantly less than when the shear was generated by other methods. A review of other methods of producing shear flow has been given by Lawson (1968).

The production of a linear velocity profile

The method of Elder was used to design the shape of the curved gauze to produce a linear velocity profile in the tunnel. The details of the calculation are presented in the Appendix where an error Elder's analysis is corrected and a different method of solving the final equation is presented. This error has also been pointed out by Lau and Baines (1968) and Turner (1969). The axes used to define the gauze shape and the positions of the velocity traverses are shown in figure 1. The non-dimensional gauze profile is shown on figure 2, the symbols used being defined in the Appendix.

Two different gauzes were used, gauze I was 9.46 mesh/cm 29 swg and gauze II 7.88 mesh/cm and 28 swg. The gauze was placed at the beginning of the working section of an open return low speed wind tunnel, the height (ℓ) of the working section was 0.508 m and the width (b) was 0.71 m. The velocity on the centre line of the tunnel was about 15.3 m/s.

Velocity traverses were made at various places in the working section and the results for gauze I are shown on figure 3, the displacement effect of the pitot tube is small in the cases considered here and has been neglected. It may be seen that although there has been a fair amount of shear developed the velocity profile is far from linear. The gauze shape was calculated for a value of the term π^3 EB/λ (see Appendix) of 9.9 which for the gauzes used should have given a value of the velocity gradient parameter λ of 0.4. Three traverses are shown at x/ℓ and z/ℓ positions of (1.2, 0), (1.8, 0) and (1.8, 0.3), the velocity profile at (1.8, 0) is marginally better than that at (1.2, 0) and all further traverses were made at this furthest downstream position. The model described later in the paper was also mounted at this position.

Figure 4 shows results for the velocity traverse for gauze II. The results are not greatly different from those for gauze I which is understandable since for both gauzes the factor EB which occurs in the expression for the gauze shape is approximately the same. The velocity profile for gauze II, however, is rather more irregular, probably due to this gauze having a rather coarse mesh. For gauze I turbulence measurements at position (1.8, 0) are shown in figure 5 where the percentage turbulence is the root mean square of the fluctuation expressed as a percentage of the local mean velocity.

The velocity profile generated was considered to be not sufficiently linear and the gauze shape was modified, in an empirical fashion, in an attempt to increase the velocity gradient for y/ℓ greater than 0.5. A curved gauze produces a shear flow in two ways, firstly there is a drop in pressure across the gauze proportional to the square of the component of velocity normal to the gauze and secondly the velocity vector is turned, as it passes through the gauze, in a direction towards the normal to the gauze. It was therefore decided to increase the angle that the gauze made with the stream for $y/\ell > 0.5$. This was done by multiplying the coordinate of the gauze for $y/\ell > 0.5$ by a factor linear in y such that the factor was unity at $y/\ell = 0.5$ and 1.13 at $y/\ell = 1$. The modified shape is shown in figure 2.

Gauze I was fitted to this modified shape and the resulting velocity distribution is shown in figure 6. It is seen that the velocity profile is much more nearly linear and this modified gauze profile was used to generate the shear flow used in the experiments described in the next section.

The wake of a bluff body in a shear flow

Consider the prediction of the loads on a body placed near to and behind a bluff body in a stream. Whether the stream is uniform or not we may expect that the flow behind the bluff body will be unsteady and that the loads on any body downstream of it will depend upon such quantities as the correlation coefficient of the velocities in the wake of the bluff body and any dominant frequency present in the wake. The results presented here are from a preliminary investigation to show the differences between the wake of a bluff body when the oncoming flow is uniform and when it has a velocity varying along the length of the body.

The bluff body used was a flat plate, width (d) of 0.0254 m, mounted in the wind tunnel as shown in figure 1. The plate spanned the tunnel, 1.8 tunnel heights downstream of the gauze and was subject to the shear flow shown in figure 6. The flat plate is not at all representative of any practical body but it does show the important characteristic of bluff bodies, namely vortex shedding at moderate Reynolds numbers, with the advantage that the separation point is fixed at the edge of the plate. The Reynolds number for all the tests were about 2×10^4 based upon the velocity at the centre of the tunnel and the width of the plate.

Results

1. Correlation measurements

If the velocities measured at any two points are u_1 and u_2 then the correlation coefficient R is $\dfrac{\overline{u_1 u_2}}{\sqrt{\overline{u_1^2}}\ \sqrt{\overline{u_2^2}}}$. For the measurement of the correlation coefficients, two hot wires were placed in the wake of the plate, the fixed wire being 13.25 plate widths above the floor of the tunnel and at certain values of x/d and z/d. The moveable hot wire was placed at the same values of x/d and z/d but could be traversed down from the position of the fixed wire. Thus correlation coefficients were measured along lines parallel to the edges of the plate. The traverses were made just outside the edge of the wakes and the variations of the correlation coefficient with wire spacing are shown in figures 7, 8 and 9 where r is the distance apart of the probes. It is seen that when the upstream velocity is non-uniform the correlation coefficient behind the plate is much lower than when the upstream velocity is uniform. This indicates that the coherence of the vortex shedding along the plate has somehow been disrupted by the presence of shear in the upstream velocity profile.

2. Vortex shedding frequency

The frequency of vortex shedding from the plate was measured by taking the signal from a hot wire positioned just outside the wake and passing it through a narrow band frequency analyser. For the range of Reynolds numbers in the experiment the flat plate in a uniform flow gave a Strouhal number fd/u where f is the frequency and u the uniform free stream velocity, of 0.152. It was found that when the plate was in the shear flow the frequency of vortex shedding varied along the length of the plate such that the higher frequencies were measured where the free stream velocity was also high. If the local Strouhal number at a height y from the tunnel floor is defined as the ratio of the measured frequency at that height multiplied by the plate width and divided by the velocity at height y in the upstream shear flow, it was found that over a considerable length of the plate the local Strouhal number was approximately constant. This is shown in figure 10. If the shedding frequency had been constant along the length of the plate the ratio of the local Strouhal numbers at the points y/d equals 0.8 and 0.4 would have been 0.86 whereas the ratio actually measured is 0.96.

Discussion

In order to explain the change in correlation in the wake of the plate when a shear flow is upstream of the plate, the outputs from four hot-wire probes were recorded on an ultra-violet galvanometer recorder, the probes were placed just outside the wake in a line parallel to one side of the plate and about 2.5 plate widths downstream of it. In all cases probe 1 was fixed 0.45d above the tunnel floor, the spacing between the probes could be varied.

Figure 11 shows the traces from the four hot wires for the case where there is no shear present in the upstream flow. It can be seen that, whilst there is some irregularity in the individual traces, in general the four outputs are in phase leading to a fairly high correlation coefficient. This is, however, not the case when the upstream flow contains some shear. Figures 12, 13 and 14 show traces from the hot wires when shear is present and these indicate that in this case the shedding of vortices is irregular leading to low correlation coefficients.

Consider figure 12; at the beginning of section A of the record the traces from the hot wires are in phase but by the end of that section, which has occupied 0.1s, there have been 5 1/3 cycles of oscillation on trace 1 and 6 1/3 cycles of oscillation on traces 3 and 4. A disturbance is evident on trace 2 at the end of section A and this appears to propagate onto trace 3 such that at the beginning of section B there is a disturbance being simultaneously recorded on traces 2 and 3 with some distortion at the same time on trace 1. There is then in the middle of section B a period of about two cycles where the traces are fairly regular and then another period of disturbance appears on traces 1 and 2 at the beginning of section C. This is followed by a regular oscillation and at the end of section C the oscillation on all traces is approximately in phase. It therefore appears that the regular shedding of vortices is interrupted by some form of disturbance which propagates at right angles to the flow direction and that this disturbance is followed by further regular shedding along the plate bringing the signals on the hot wires back into phase.

In figure 13 the disturbance can also be seen. At the beginning of section A all four traces are in phase but due to the frequencies being different, by the end of that section we have traces 1 and 2 in phase and 3 and 4 in phase but the pairs are 180 degrees out of phase. A disturbance then appears on trace 1 and very quickly affects trace 2. It seems to move across the flow direction affecting trace 3 by the middle of section B and finally showing up on trace 4 about two thirds of the way across section B. At the beginning of section C, after the passage of the disturbance, the traces are almost in phase but by the end of the section they are once again becoming out of phase.

Some more evidence that the disturbance propagates across the flow is shown on figure 14. There is a sign of the disturbance on trace 1 at the beginning of section A and can be seen on trace 2 slightly later and progressively on trace 3 until it has reached trace 4 at the end of section A. This record also shows that the disturbance may be sometimes fairly localised. For instance in section B it only appears on trace 2 and in section C only on trace 3 with no evidence of further propagation across the flow.

An attempt was made to visualise the flow in a low speed tunnel by means of smoke injected into the flow. The shear profile was generated in this tunnel by means of shaped honeycomb and the mean velocity was about 2 m/s. The working section of the tunnel is shown in figure 15(a), at the bottom is the honeycomb with the flow vertically upwards, the highest velocity being on the right of the photograph. The model shown in figure 15 is a circular cylinder and the smoke is emitted from a slot cut in the cylinder. Figure 15(a) shows intense skewing of the vortices with the detachment point of the vortices moving along the length of the cylinder. In this figure the vortex shedding appears to be regular and hot-wire probes mounted parallel to the cylinder axis would record signals of almost the same frequency but not necessarily in phase. There is also some evidence of the vortices distorting into vortex loops or horseshoe vortices. There is also evidence of these vortex loops in figure 15(b) and here the vortex shedding is much more confused. Considering, on the left of this figure, the first fully formed vortex nearest the cylinder it appears, moving across the figure to the right, that this vortex splits into two skew vortices about a third of the way along the cylinder. There is a discontinuity in the slope of the vortex lines and this discontinuity may be the disturbance showing up in the hot wire traces of figures 12, 13 and 14.

An even more confused flow is seen in figure 15(c) where there are a large number of discontinuities in the vortices and more evidence of the vortex loops.

It seems, therefore, that in general vortex lines are formed which may join up into a single vortex line. This position of the joining up of the vortex lines moves along the plate causing the disturbance recorded on the hot wires and the lack of correlation along the length of the plate. A similar phenomena has been found by Gaster (1969) where he investigated the flow in the wake of a conical cylinder whose axis was normal to a uniform flow.

Conclusions

It has been shown that the presence of an upstream shear flow can drastically alter the wake flow of a bluff body so as to reduce the correlation coefficient in the wake. The vortex shedding from the body is altered in such a way as to make the local Strouhal number along the body constant, the dominant frequencies in the wake thus varying along the length of the body.

It is therefore clear that in investigating the flow past a complex arrangement of bluff bodies in the earth's boundary layer, where the effects of the wake of one body on the load on another body are important, the mean velocity shear characteristics of the earth's boundary layer must be correctly simulated.

References

Bearman, P.W. (1968) Some effects of turbulence on the flow around bluff bodies. Symp. Wind Effects on Buildings and Structures, Loughborough Univ. 1968.

Counihan, J. (1969) An improved method of simulating an atmospheric boundary layer in a wind tunnel. Atmospheric Environment 3, p.197.

Davenport, A.G. (1967) The application of the boundary layer wind tunnel to the prediction of wind loading. Proc. Seminar on Wind Effects on Buildings and Structures, Ottawa 1967. Univ. of Toronto Press.

Davies, G. de V. (1957) Steady non-uniform flow through wire screens. Cambridge University Ph.D. Dissertation.

Elder, J.W. (1959) Steady flow through non-uniform gauzes. J. Fluid Mech. 5, p.355.

Gaster, M. (1969) Vortex shedding from slender cones at low Reynolds numbers. To be published in J. Fluid Mech.

Gould, R., Raymer, W. and Ponsford, P. (1968) Wind tunnel tests on chimneys of circular cross section at high Reynolds numbers. Symp. Wind Effects on Buildings and Structures, Loughborough Univ. 1968.

Jensen, M. and Franck, N. (1965) Model Scale Tests in Turbulent Wind. Pt. II. The Danish Technical Press, Copenhagen.

Kotansky, D.R. (1966) The use of honeycomb for shear flow generation. AIAA Jnl., p.1490.

Lau, Y.L. and Baines, W.D. (1968) Flow of stratified fluid through curved screens. J. Fluid Mech. 33, p.721.

Lawson, T.V. (1968) Methods of producing velocity profiles in wind tunnels. Atmospheric Environment 2, p.73.

Owen, P.R. and Zienkiewicz, H.K. (1957) Production of uniform shear flow in a wind tunnel. J. Fluid Mech. 2, p.521.

Turner, J.T. (1969) A computational method for the flow through non-uniform gauzes: the general two-dimensional case. J. Fluid Mech. 36, p.369.

Wolf, S. and Johnston, J.P. (1966) Effects of non-uniform inlet velocity profiles on flow regimes and performance in two-dimensional diffusers. Stanford Univ. Dept. of Mech. Eng. Rep. PD-12.

Appendix

Starting with Elder's original equations (2.5), (2.6) and (2.7) and using his notation

$$q = u - \sum_{1}^{\infty} P_n \cos nw = u^* - \sum_{1}^{\infty} Q_n \cos nw \qquad (2.5)$$

$$BT = \sum_{1}^{\infty} \left[(1 - B)P_n + Q_n\right] \sin nw \qquad (2.6)$$

$$u - u^* = \gamma_o(q - 1) + \tfrac{1}{2}\gamma_o s \qquad (2.7)$$

and taking the case of a uniform gauze with $s = 0$ and hence $\gamma = \gamma_o$, consider the production of a linear velocity profile $u^* - 1 = (y/\ell - \tfrac{1}{2})$ where $u = 1$ (i.e upstream of the gauze the flow is uniform).

Then from equations (2.5) and (2.7)

$$(\tfrac{w}{\pi} - \tfrac{1}{2}) = \gamma \sum_{1}^{\infty} P_n \cos nw, \quad \tfrac{w}{\pi} = \frac{y}{\ell}$$

expanding $(\tfrac{w}{\pi} - \tfrac{1}{2})$ as a Fourier series

$$\tfrac{w}{\pi} - \tfrac{1}{2} = -\frac{4}{\pi^2}\left[\cos w + \frac{\cos 3w}{3^2} + \frac{\cos 5w}{5^2} + \ldots\right].$$

Therefore $P_n = \left[-\frac{4}{\gamma\pi^2}\frac{1}{n^2}\right]_{n \text{ odd}}$

from (2.5)

$$\sum_{1}^{\infty} Q_n \cos nw = \lambda(\tfrac{w}{\pi} - \tfrac{1}{2}) + \sum_{1}^{\infty} P_n \cos nw$$

$$= (1 + \gamma) \sum_{1}^{\infty} P_n \cos nw,$$

Now in (2.6)

$$BT = \sum_{1}^{\infty} (2 + \gamma - B)P_n \sin nw$$

$$= \frac{\gamma}{E} \sum_{1}^{\infty} P_n \sin nw \qquad \text{where } E = \gamma/(2 + \gamma - B).$$

Therefore

$$\frac{EB}{\gamma} x = \int_0^y \sum_{1}^{\infty} P_n \sin nw \, dy$$

$$= -\frac{\ell}{\pi}\left\{\sum_{1}^{\infty} \frac{P_n}{n} \cos nw - \sum_{\ast}^{\infty} \frac{P_n}{n}\right\}$$

substituting for P_n

$$\frac{\pi^3 EB}{\lambda}\frac{x}{\ell} = 4\left\{\sum_{m=0}^{\infty} \frac{\cos(2m + 1)w}{(2m + 1)^3} - \sum_{m=0}^{\infty} \frac{1}{(2m + 1)^3}\right\}.$$

The first twenty terms of the series have been computed and the resulting gauze shape is plotted on figure 2.

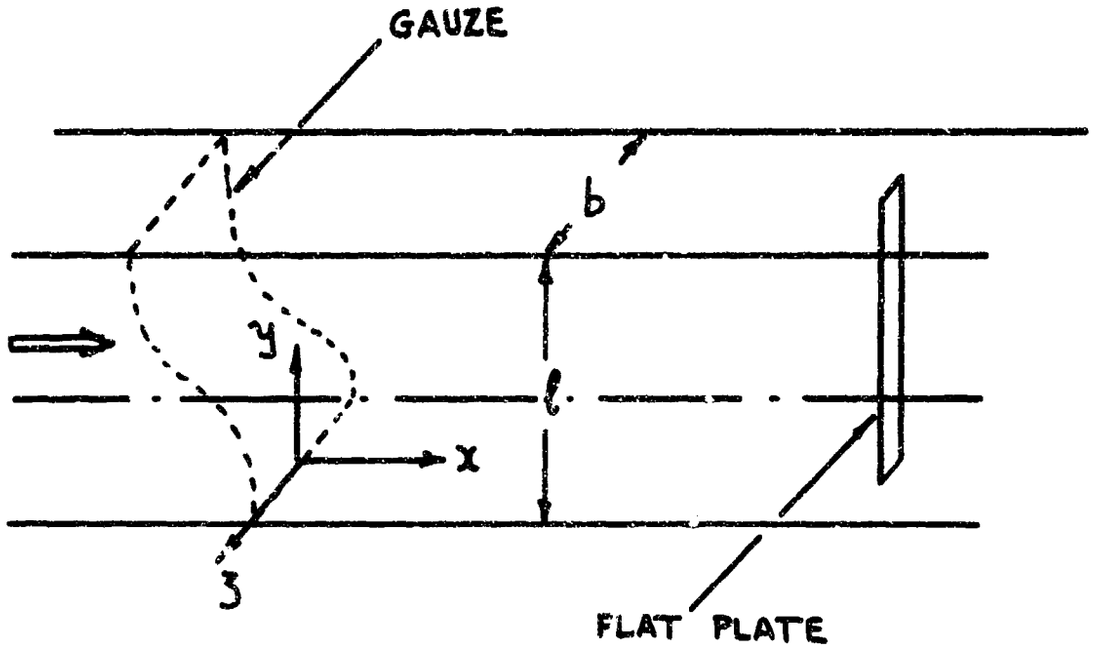

Figure 1 Experimental arrangement

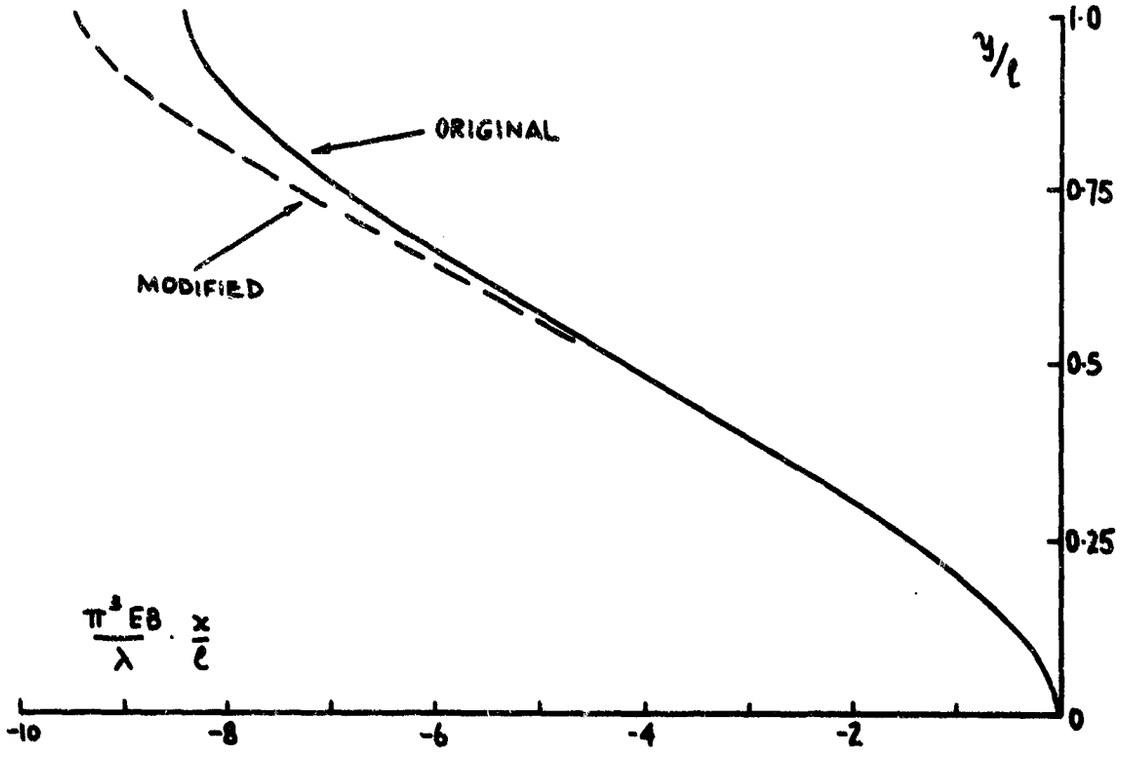

Figure 2 Original and modified gauze shapes

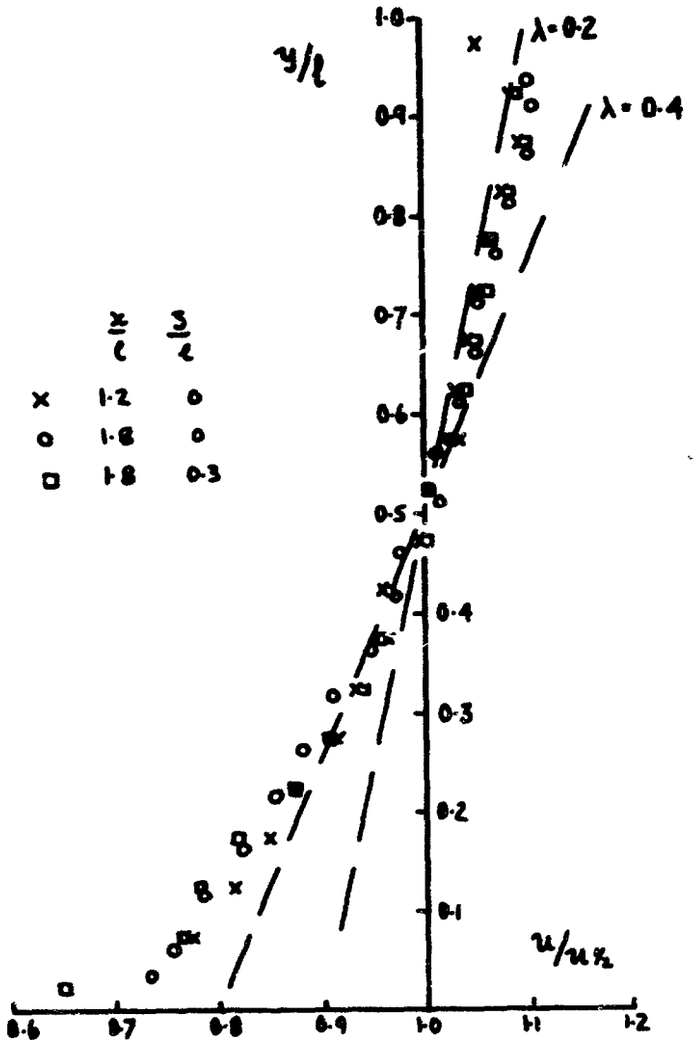

Figure 3 Velocity profile original gauze I

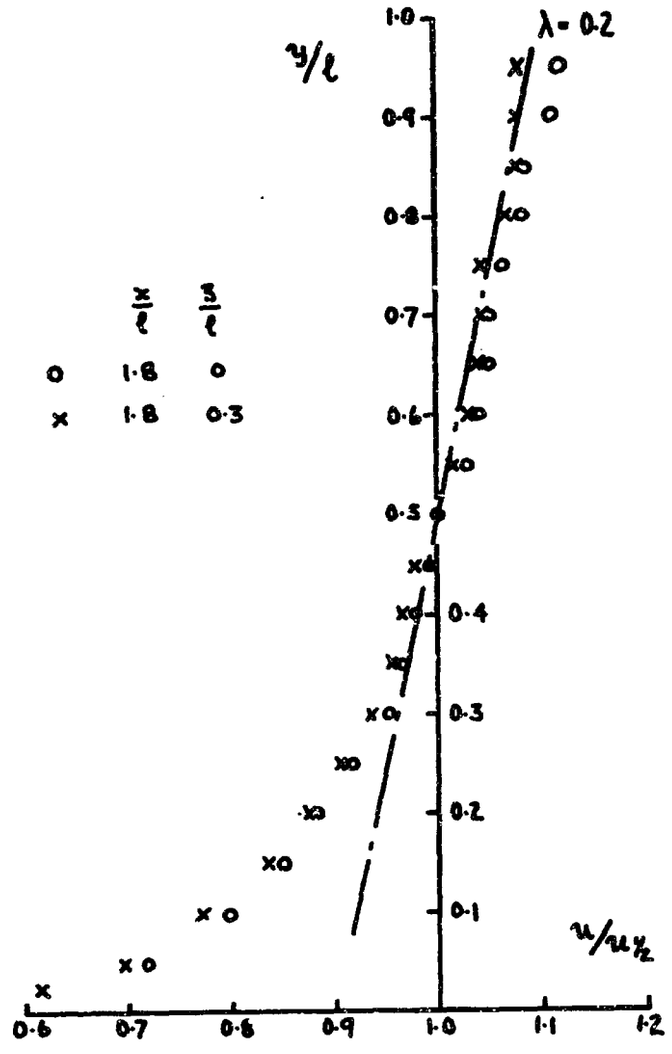

Figure 4 Velocity profile original gauze II

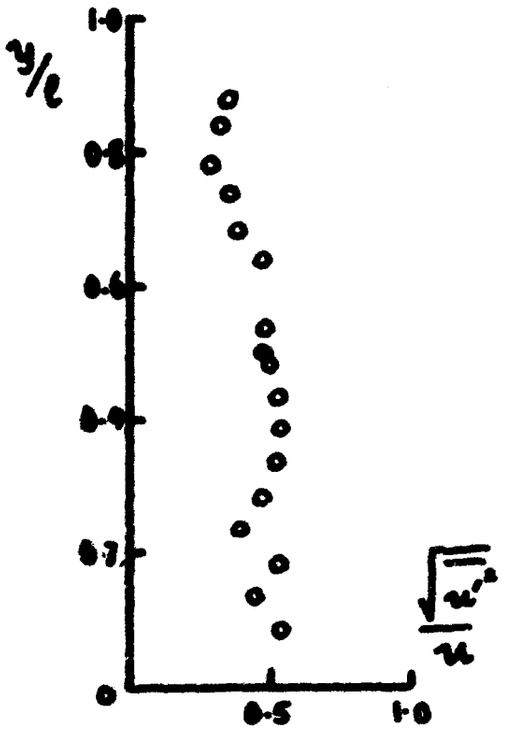

Figure 5 Turbulence level

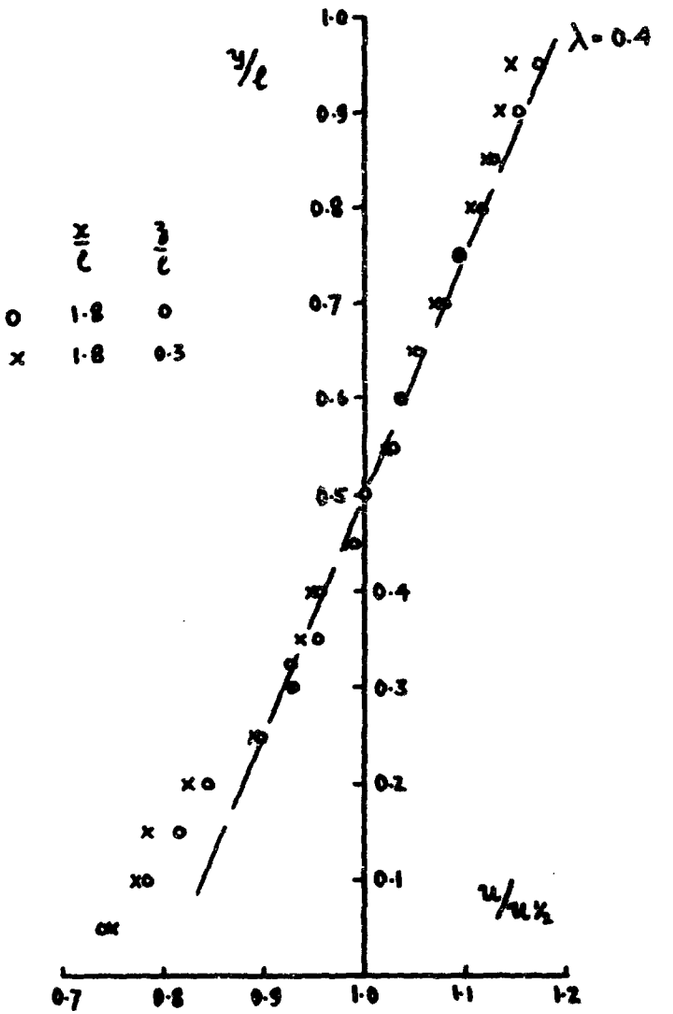

Figure 6 Velocity profile modified gauze I

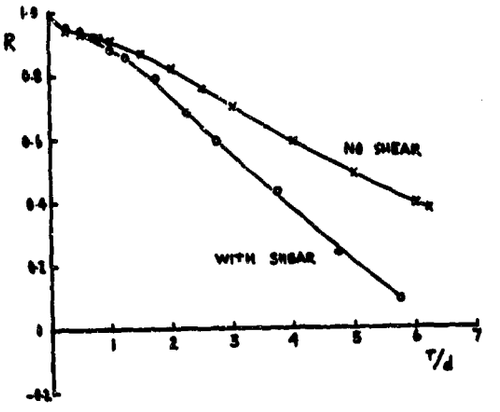

Figure 7 Correlation coefficient. Fixed probe at x/d = 2.875, y/d = 13.25, z/d = 3

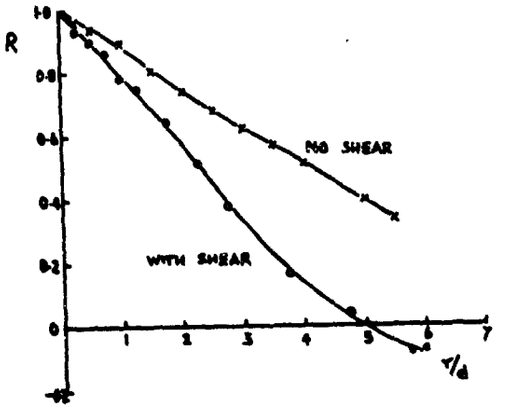

Figure 8 Correlation coefficient. Fixed probe at x/d = 5.875, y/d = 13.25, z/d = 3

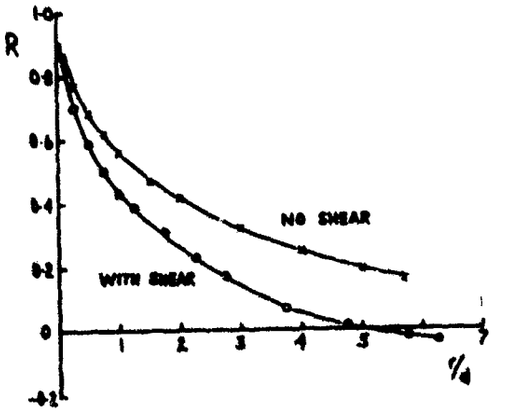

Figure 9 Correlation coefficient. Fixed probe at x/d = 9, y/d = 13.25, z/d = 3

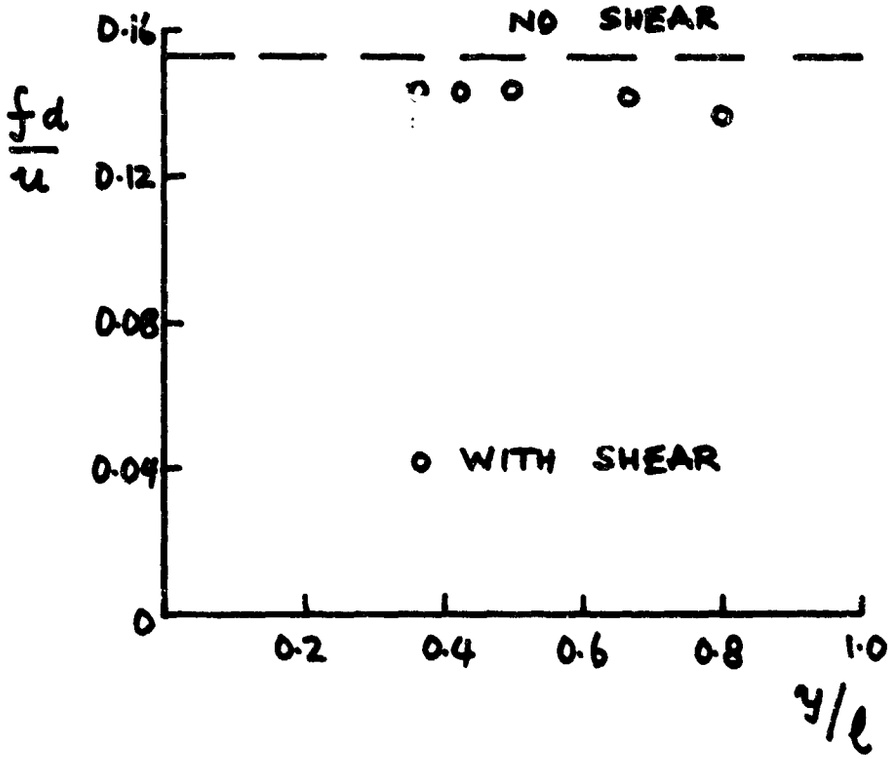

Figure 10 Strouhal number

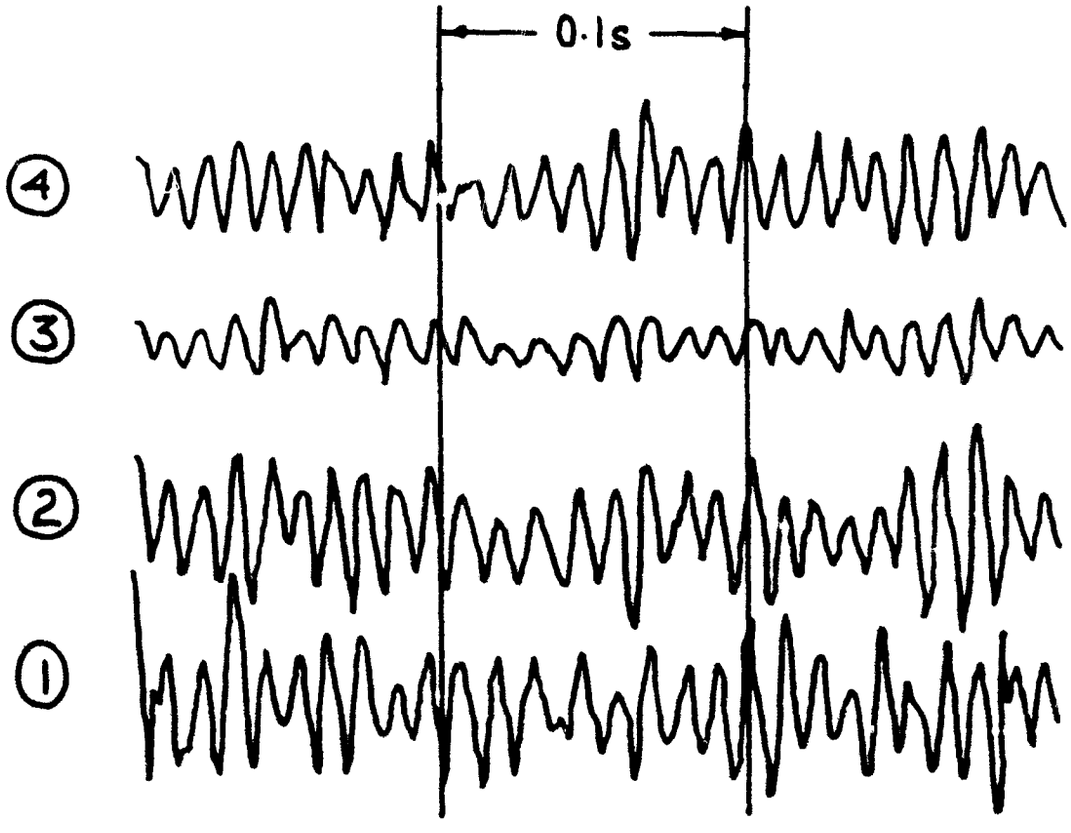

Figure 11 No shear probe separation 0.0254 m

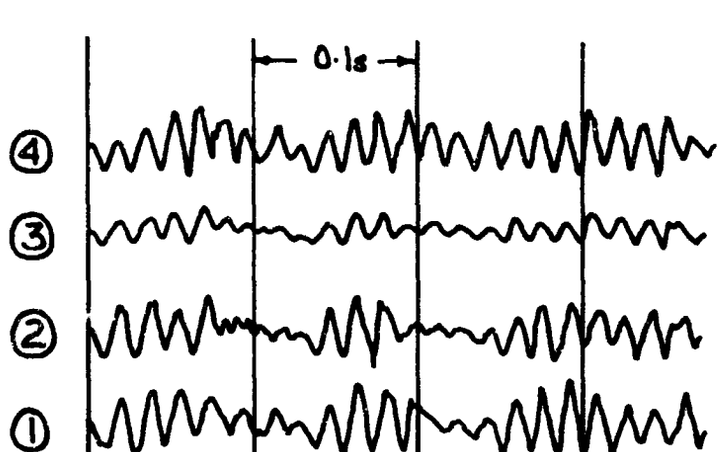

Figure 12 With shear probe separation 0.038 m

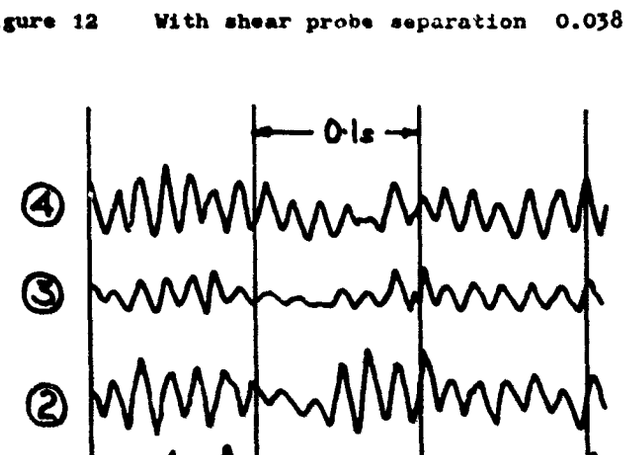

Figure 13 With shear probe separation 0.05 m

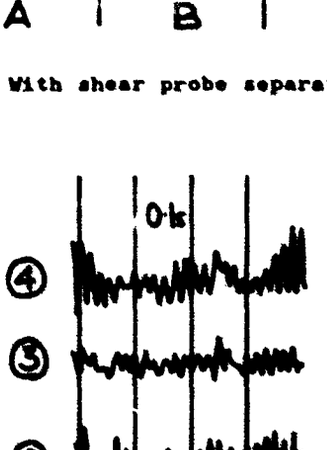

Figure 14 With shear probe separation 0.05 m

(a)

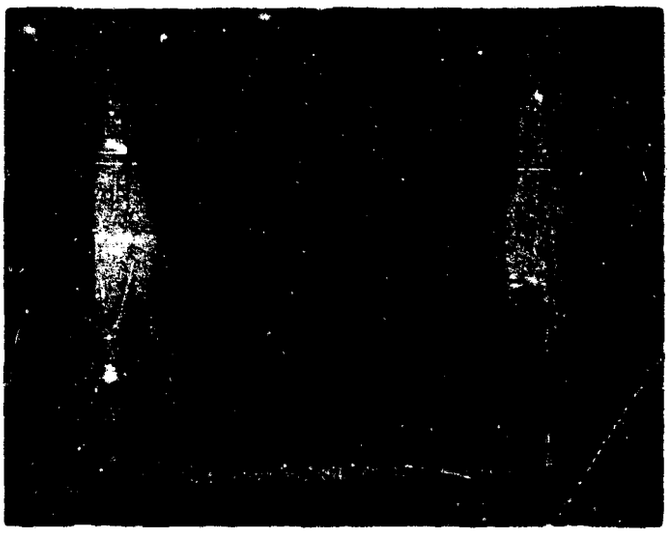

(b)

(c)

Figure 15 a, b, c. Smoke photographs with shear.

ETUDE D'UNE SOUFFLERIE POUR RECHERCHES SUR LES ECHANGES D'ENERGIE ATMOSPHERE-OCEANS

par

M. COANTIC*, P. BONNARDI**, B. FOUCHAIN**, A. FAVRE***

=:=:=:=:=:=:=

Institut de Mécanique Statistique de la Turbulence,
Laboratoire Associé du C.N.R.S., Marseille, France.

=:=:=:=:=:=:=

* Chargé de Recherches au C.N.R.S.
** Ingénieur de Recherches à l'I.M.S.T.
*** Stagiaire de Recherches au C.N.R.S.
**** Professeur à la Faculté des Sciences de Marseille, Directeur de l'I.M.S.T.

- S O M M A I R E -

Cette recherche concerne les mécanismes physiques à petite échelle des transferts de masse, de quantité de mouvement et d'énergie entre la couche de surface de l'atmosphère et les océans. L'étude des lois gouvernant ces échanges met en évidence certains facteurs dont la reproduction au laboratoire permettra une simulation partielle des phénomènes naturels.

Le dispositif projeté est une soufflerie air-eau permettant d'obtenir une couche limite turbulente d'interface de 40 m. de longueur, en contrôlant : vitesse, température et humidité de l'air ; vitesse, température et composition de l'eau ; préturbulence de vitesse et de température ; stratification ; mouvements de l'interface ; couches limites parasites dans la veine. Une maquette à l'échelle 1/5 est utilisée pour vérifier et améliorer les caractéristiques et mettre au point les techniques de mesures.

- S U M M A R Y -

DESIGN OF A TUNNEL FOR ATMOSPHERE-OCEANS INTERACTIONS RESEARCH

This research concerns the small-scale physical mechanisms of mass, momentum and energy transfers, between the atmospheric surface layer and the oceans. A critical survey of the laws governing these exchanges outlines some parameters the reproduction of which at laboratory scale will enable a partial simulation of the natural phenomena.

The equipment designed is a wind-water tunnel intended to give a 40 meters long turbulent interface boundary layer, with control of : air velocity, temperature and humidity ; water velocity, temperature and chemical composition ; preturbulence of velocity and temperature ; stratification ; interface motion ; tunnel walls boundary layers. A one fifth scale model is being used, to check and improve the performance and to test the measurement techniques.

NOTATIONS

A	production de turbulence par le travail des forces d'Archimède
c'	énergie cinétique de la turbulence
c_p, c_{pe}	chaleur spécifique à pression constante de l'air humide, de la vapeur d'eau
C/U	âge des vagues
$F = \overline{F} + f'$	humidité spécifique
g	accélération de la pesanteur
H	amplitude significative des vagues
I, I_a, I_e, I_{sa}, I_l	enthalpie, de l'air humide, de l'eau, enthalpie sensible de l'air humide, de l'eau, enthalpie latente
K , K_r	coefficient de conductibilité thermique moléculaire, radiative
L	taux de transfert d'enthalpie latente
$\mathcal{L}$	chaleur latente de vaporisation de l'eau
ΔP_v	perte de charge totale de la soufflerie
p"	fluctuation turbulente de pression
Q , Q'	flux radiatif total dans l'air, dans l'eau
q_o , q_1	flux radiatif de petite longueur d'onde, de grande longueur d'onde
R, R_a, R_h	constante de l'équation d'état pour l'air humide, pour l'air sec, pour la vapeur d'eau
R_f, R'_f	nombre de Richardson de flux usuel, généralisé
R_x	nombre de Reynolds dans la veine d'essais , $R_x = \frac{U_o X}{\nu}$
S , S'	taux de transfert d'enthalpie sensible dans l'air, dans l'eau
t	temps
U, V, W	composante horizontale, transversale, verticale de la vitesse $U = \overline{U} + U'$ $V = v'$ $W = \overline{W} + w'$
U_o	vitesse moyenne à la sortie du collecteur
OX, OY, OZ	axe horizontal, transversal, vertical
Z_o	hauteur de la veine d'essais
δ	épaisseur de couche limite
η_{ts}	coefficient manométrique de buse
ρ, ρ_a, ρ_e, ρ_h, $\tilde{\rho}$	masse spécifique de l'air humide, de l'air sec, de l'eau, de la vapeur d'eau, valeur moyenne dans la couche de surface
μ	coefficient de viscosité moléculaire
ν	coefficient de viscosité cinématique
Φ , $\overline{\varphi'}$	fonction de dissipation dans le mouvement moyen, en moyenne dans le mouvement turbulent
χ	coefficient moyen d'absorption du rayonnement de petite longueur d'onde dans l'eau
ϑ , ϑ_o , ϑ_a , ϑ_p , $\tilde{\vartheta}$	température locale, de référence, de l'eau, de paroi, valeur moyenne dans la couche de surface

$$\vartheta^* = (\vartheta - \vartheta_o)/(\vartheta_p - \vartheta_o) \qquad \vartheta^{**} = (\vartheta - \vartheta_o)/(\vartheta_a - \vartheta_o)$$

1 - INTRODUCTION.-

La connaissance du mécanisme des échanges d'énergie entre l'atmosphère et les océans est d'un intérêt majeur pour la météorologie aussi bien que pour l'océanographie. On sait en effet aujourd'hui que ces deux milieux doivent être considérés comme constituant un seul système, car l'évolution dynamique et thermodynamique de chacun d'entre eux dépend dans une large mesure des interactions qui s'exercent à travers leur frontière commune.

Bien que ce problème doive être traité à différentes échelles, l'étude de la région située à proximité de l'interface semble présenter un intérêt tout particulier. C'est en effet dans cette zone que se développent les phénomènes responsables des échanges et des transformations des diverses formes de l'énergie lorsque l'on passe d'un milieu à l'autre. La compréhension du mécanisme physique des processus à petite échelle dont les couches d'air et d'eau voisines de l'interface sont le siège, constitue donc une étape essentielle dans la solution du problème des interactions atmosphère-océans.

Les études expérimentales nécessaires présentent des difficultés certaines : il faut en effet explorer de façon détaillée, en procédant à des mesures de grandeurs moyennes et fluctuantes relativement délicates et complexes, une zone dont l'étendue verticale est de l'ordre de la hauteur des vagues ; par ailleurs, il serait souhaitable de pouvoir faire varier indépendamment les différents paramètres, afin d'en mieux séparer les effets. Or les expériences effectuées en mer supportent des contraintes d'environnement qui limitent nécessairement la finesse des mesures et sont de plus soumises aux conditions micrométéorologiques du moment qui ne sauraient être contrôlées et qui les rendent difficilement répétables. Il est donc apparu indispensable de compléter les mesures dans la nature par des expériences effectuées au laboratoire, dans des conditions bien contrôlées, de façon à pouvoir procéder à des explorations complètes, répétables et précises, des mécanismes fondamentaux des échanges au voisinage de l'interface. C'est là le programme dont l'I.M.S.T. a entrepris l'exécution en 1965, à la demande du Comité de Recherches Atmosphériques de la D.G.R.S.T., et dont nous présentons ici quelques-uns des premiers résultats.

Le premier objectif d'un tel travail est en effet la réalisation d'une installation de laboratoire où les expériences soient significatives, c'est à dire qui assure, dans une certaine mesure, une simulation des phénomènes naturels. Pour définir cette installation, il faut en premier lieu étudier les différents processus physiques responsables des interactions océans-atmosphère et préciser les équations qui les gouvernent. Ceci permet alors d'identifier les facteurs les plus importants, qu'il sera nécessaire de reproduire au laboratoire, et de déterminer les gammes de variation qu'il faudra pouvoir imposer aux principales variables pour que les paramètres caractéristiques de l'expérience possèdent des valeurs convenables. Compte tenu des contraintes pratiques, il semble possible de parvenir, sinon à une véritable similitude, du moins à une simulation partielle des échanges naturels. Nous verrons quelles sont les conditions à remplir pour atteindre ce but et présenterons les solutions techniques adoptées à cette fin. Etant donné l'importance et la nouveauté de l'installation prévue, des études sur maquette à échelle réduite ont été effectuées et ont permis d'améliorer sensiblement les performances qu'aurait eues une soufflerie correspondant au projet initial.

Ce travail a pu être effectué grâce à l'appui d'un certain nombre d'organismes, à qui nous tenons à exprimer ici notre gratitude, qui s'adresse tout particulièrement à la Délégation Générale à la Recherche Scientifique et Technique, pour les conventions de recherches N° 65 FR 133 et N° 67 00 937, et au Centre National pour l'Exploitation des Océans, pour la convention de recherches N° 69/66, et également à l'O.N.E.R.A., à la D.R.M.E., au C.N.R.S., et à plusieurs autres encore pour leur aide efficace. Nous voulons également assurer de notre reconnaissance les nombreuses personnalités scientifiques, tant françaises qu'étrangères, qui ont bien voulu nous faire bénéficer de leurs conseils, et tout spécialement Monsieur le Professeur LACOMBE, Directeur du Laboratoire d'Océanographie Physique du Muséum National d'Histoire Naturelle, pour l'aide et les encouragements qu'il nous a constamment prodigués. Nous souhaitons enfin remercier tous ceux qui ont participé à l'établissement du projet de l'installation de simulation des interactions atmosphère-océans et qui collaborent actuellement à sa construction.

2 - MECANISMES PHYSIQUES DES ECHANGES D'ENERGIE OCEAN-ATMOSPHERE.-

2.1. Les quatre processus fondamentaux :

L'essentiel des échanges d'énergie entre l'atmosphère et les océans s'effectue par le jeu des quatre processus suivants :

a) Le transfert de chaleur par rayonnement : le rayonnement de courte longueur d'onde, d'origine solaire, alimente en énergie l'ensemble du système. Traversant pratiquement sans absorption la couche atmosphérique considérée, il est en partie réfléchi à l'interface et, pour le reste, absorbé par les premiers mètres de la masse océanique. Par ailleurs, le rayonnement de grande longueur d'onde opère un transfert radiatif d'énergie entre la surface liquide, les couches supérieures de l'atmosphère et l'espace. Ce transfert entraîne en général un refroidissement localisé à l'interface et pourrait également, dans l'hypothèse d'une divergence appréciable du flux correspondant, modifier les échanges thermiques dans la couche de surface de l'atmosphère.

b) Le transfert de vapeur d'eau et d'enthalpie latente. L'humidité spécifique saturante au niveau de l'interface étant en général différente de l'humidité spécifique de l'air des basses couches, un processus d'évaporation (ou de condensation) et de transfert par convection et diffusion moléculaire et turbulente s'établit. Compte tenu de la valeur élevée de la chaleur latente de vaporisation de l'eau, ce processus entraîne un important transfert d'enthalpie entre l'océan, à qui elle est empruntée sous la forme sensible, et l'atmosphère, à qui elle est apportée sous la forme latente.

c) Le transfert d'enthalpie sensible. Les écarts de température au sein du système provoquent des transferts d'enthalpie sensible d'un point à l'autre, par convection et diffusion moléculaire et turbulente.

d) Le transfert d'énergie mécanique. Il s'effectue la plus souvent de l'atmosphère vers l'océan. A l'échelle considérée ici, il a pour effet, d'une part la formation de couches limites turbulentes dynamiques dans l'air et dans l'eau, et d'autre part la génération des vagues à la surface de la mer.

2.2. Le rôle de la turbulence :

Du point de vue des quantités d'énergie mises en jeu, le rayonnement et l'échange de vapeur d'eau apparaissent comme prépondérants, l'échange de chaleur sensible étant nettement plus faible et celui d'énergie mécanique négligeable. Il n'en faudrait pas pour autant conclure que ce dernier processus est d'un intérêt secondaire. En effet, le taux des échanges de chaleur et d'humidité entre l'océan et l'atmosphère dépend essentiellement de leurs mouvements moyens et turbulents dont la structure est elle-même gouvernée en premier lieu par les échanges mécaniques (voir PRIESTLEY (1959), LUMLEY et PANOFSKY (1964), MONIN et YAGLOM (1966)). Ainsi, la conservation de la vapeur d'eau et celle de l'enthalpie obéissent, dans la couche de surface d'une atmosphère stratifiée, aux équations moyennes suivantes (voir, par exemple, COANTIC (1968)) :

$$\overline{U}\frac{\partial \overline{F}}{\partial x}+\overline{W}\frac{\partial \overline{F}}{\partial z}=-\frac{\partial}{\partial z}\overline{f'w'}+D\frac{\partial^2 \overline{F}}{\partial z^2} \qquad (1)$$

$$\left[\overline{U}\frac{\partial}{\partial x}+\overline{W}\frac{\partial}{\partial z}\right]\left[C_p\,\overline{\Theta}+\mathcal{L}\,\overline{F}\right]=-C_p\frac{\partial}{\partial z}\overline{\theta w'}-\mathcal{L}\frac{\partial}{\partial z}\overline{f'w'}$$
$$+\frac{K}{\tilde{\rho}}\frac{\partial^2 \overline{\Theta}}{\partial z^2}+\mathcal{L}\,D\frac{\partial^2 \overline{F}}{\partial z^2}+\frac{1}{\tilde{\rho}}\frac{\partial}{\partial z}\left[k_t\frac{\partial \overline{\Theta}}{\partial z}\right]+\Phi+\overline{\varphi'}+A \qquad (2)$$

dans lesquelles les termes de transfert par la turbulence, $\overline{f'w'}$, $\overline{\theta'w'}$, sont d'une importance prépondérante. Or ces termes dépendent essentiellement du processus mécanique qui se comporte donc comme un catalyseur à l'égard de l'ensemble des échanges énergétiques dont il contrôle le niveau par le biais de la turbulence.

2.3. Les différentes formes d'énergie, et les interactions entre leurs divers modes de transfert :

Considérons seulement, pour l'instant, l'enthalpie moyenne qui constitue l'essentiel de l'énergie attachée à un élément de volume donné du système. Dans l'atmosphère, elle sera la somme de l'enthalpie sensible et de l'enthalpie latente :

$$I=I_s+I_l=\tilde{\rho}\left[C_p\left(\overline{\Theta}-273\right)+\mathcal{L}\,\overline{F}\right] \qquad (3)$$

Dans l'océan, elle n'apparaîtra au contraire que sous la forme sensible :

$$I_e=I_{se}=\rho_e\,C_{p_e}\left(\overline{\Theta}-273\right) \qquad (4)$$

Avec l'hypothèse d'un phénomène "pleinement développé", c'est à dire en négligeant les termes d'advection, l'énergie est transférée suivant la direction verticale, par le jeu des processus a), b), c), à des taux qui s'expriment comme suit :

- Pour le rayonnement dans l'atmosphère, somme des flux effectifs de petites et de grandes longueurs d'ondes :

$$Q=q_0+q_1=q_0-k_t\frac{\partial \overline{\Theta}}{\partial z} \qquad (5)$$

- Pour le rayonnement dans l'océan :

$$Q'=q_0\,e^{\chi z} \qquad (6)$$

- Pour le transfert d'enthalpie latente :

$$L=-\mathcal{L}\,D\,\tilde{\rho}\frac{\partial \overline{F}}{\partial z}+\mathcal{L}\,\tilde{\rho}\,\overline{f'w'} \qquad (7)$$

- Pour le transfert d'enthalpie sensible, dans l'atmosphère et dans l'océan :

$$S = -k \frac{\partial \overline{\theta}}{\partial z} + \tilde{\rho} C_p \overline{\theta' w'} \qquad (8)$$

$$S' = -k_e \frac{\partial \overline{\theta}}{\partial z} + \rho_e C_{p_e} \overline{\theta' w'} \qquad (9)$$

L'intégration de l'équation de conservation de l'énergie permet alors d'établir la relation globale (Cf COANTIC (1968)) :

$$S + L + Q = S' + Q' = Cte. \qquad (10)$$

Cette équation fondamentale, qu'illustre la Figure 1, traduit la conservation du flux total d'énergie transféré entre l'atmosphère et l'océan. En plus du rôle joué par la turbulence, elle met clairement en évidence le fait que les formes sous lesquelles apparaît l'énergie et les mécanismes par lesquels elle est transférée changent à la traversée de l'interface. Compte tenu du bilan global et des conditions pour les diverses variables sur la limite commune, les divers modes de transfert apparaissent donc comme intimement liés.

Si nous revenons à présent aux autres formes de l'énergie, et en particulier à l'énergie cinétique moyenne correspondant aux divers mouvements, nous voyons apparaître dans les équations, non seulement des termes de transfert, mais encore des termes de production et de dissipation qui traduisent des transformations directes, au sein de chacune des deux phases, d'une forme à une autre de l'énergie. Ainsi, pour l'énergie de la turbulence dans l'atmosphère, il vient :

$$\frac{\partial}{\partial t} \tfrac{1}{2} \tilde{\rho} \left(\overline{u'^2} + \overline{v'^2} + \overline{w'^2} \right) = 0 = -\frac{\partial}{\partial z} \left[\overline{w'c'} + \overline{w'p''} + \nu \frac{\partial}{\partial z} \left(\bar{e} + \tilde{\rho} \overline{w'^2} \right) \right]$$
$$- \tilde{\rho} \overline{u'w'} \frac{\partial \bar{u}}{\partial z} + \tilde{\rho} g \left[\frac{R_h - R_a}{R} \overline{\rho' w'} + \frac{1}{\tilde{\theta}} \overline{\theta' w'} \right] - \mu \left[\overline{\frac{\partial v_i'}{\partial x_j} \frac{\partial v_i'}{\partial x_j}} + \frac{\partial^2}{\partial z^2} \overline{w'^2} \right]$$
$$= \frac{\partial \overline{T\omega}}{\partial z} + P + A - \overline{\varphi'} \qquad (11)$$

qui montre que le niveau de turbulence dépend ici, d'une part des mécanismes classiques de production, P , à partir du mouvement moyen et de dissipation, $\overline{\varphi'}$, en chaleur, et d'autre part du travail des forces d'ARCHIMEDE, A , qui effectue une "production" positive ou négative de turbulence aux dépens de l'enthalpie sensible. C'est de la valeur du nombre de RICHARDSON généralisé :

$$R_f' = g \left[\frac{1}{\tilde{\theta}} \overline{\theta' w'} + \frac{R_h - R_a}{R} \overline{\rho' w'} \right] \Big/ \overline{u'w'} \frac{\partial \bar{u}}{\partial z} \qquad (12)$$

que dépendront le niveau et la structure des mouvements turbulents, et donc, en définitive, l'ensemble des échanges étudiés.

En conclusion, l'interaction entre les divers processus de transfert paraît constituer l'un des facteurs essentiels du problème des échanges d'énergie entre l'atmosphère et les océans, dont les divers aspects ne sauraient donc être étudiés isolément.

2.4. Les mouvements de l'interface :

La surface de l'océan est animée de mouvements complexes qui entraînent un couplage entre les processus mécaniques dans l'air et dans l'eau et modifient donc la structure turbulente de ces deux milieux et les mécanismes de transfert d'énergie dont ils sont le siège.

En particulier, suivant les valeurs relatives de la célérité de propagation des vagues et de la vitesse du vent, l'importance respective des tensions de frottement tangentielles et des forces de pression normales dans le transfert de quantité de mouvement de l'air à l'eau peut varier dans des proportions considérables. Le second mode d'échange n'ayant pas son équivalent pour l'enthalpie ou la vapeur d'eau, le degré de similitude entre les différents processus de transfert est essentiellement variable. Les théories classiques d'analogie de REYNOLDS ne pourront donc vraisemblablement pas être vérifiées au voisinage de l'interface et une étude approfondie du mécanisme dynamique dans cette région est nécessaire si l'on veut parvenir à y déterminer les taux de transfert des variables scalaires.

3 - CONDITIONS DE SIMULATION DES PHENOMENES NATURELS :

3.1. Les principaux facteurs à reproduire :

Compte-tenu du mécanisme physique des échanges naturels, les études de laboratoire prévues porteront sur la structure des couches limites turbulentes de vitesse, de température et d'humidité obtenues à l'interface d'un écoulement d'air et d'une nappe d'eau. En contrôlant la vitesse, la température et l'humidité de l'air, ainsi que la vitesse et la température de l'eau, les processus fondamentaux de transfert de quantité de mouvement, de chaleur et de masse se trouveront effectivement mis en jeu. Bien que le problème ainsi défini soit déjà d'un intérêt scientifique certain, il est clair d'après ce qui a été dit plus haut que les expériences effectuées ne seront réellement significatives vis à vis des échanges océans-atmosphère que dans la mesure où les trois facteurs particuliers que constituent la structure turbulente de l'atmosphère, les effets de la stratification et les mouvements de l'interface seront reproduits, au moins partiellement. Ceci paraît possible, à condition de réaliser une installation de dimensions suffisamment grandes et d'adopter certaines dispositions particulières.

3.2. La couche limite dynamique, et la reproduction de la structure turbulente de l'atmosphère :

La répartition des vitesses et la structure turbulente de la couche de surface de l'atmosphère présentent, comme on le sait, une étroite analogie avec celles de la région interne de la couche limite créée sur une plaque plane plus ou moins rugueuse. Ce fait est mis à profit, depuis un certain nombre d'années, pour la réalisation de soufflerles de simulation atmosphérique, ou "tunnels micrométéorologiques", destinées notamment à des études de diffusion (voir, par exemple, POCOK (1960), PLATE et CERMAK (1963), MEAY (1968)). L'écoulement atmosphérique est caractérisé, d'une part par des valeurs extrêmement élevées du nombre de Reynolds, d'autre part par des effets de stratification dépendant du nombre de Richardson. Une similitude satisfaisante ne pourra être atteinte au laboratoire que si ces paramètres conservent des valeurs convenables ; or, pour atteindre des nombres de Richardson élevés, il est nécessaire de créer des écarts de densité, et donc de température, suffisants tout en ramenant la vitesse d'écoulement à la valeur la plus faible possible ; par conséquent, pour que le nombre de Reynolds conserve malgré cela une valeur suffisamment importante et pour que les effets cumulatifs de la stratification puissent être décelés, il est nécessaire de réaliser des installations de grandes dimensions. Des conclusions analogues sont obtenues si l'on s'intéresse à la similitude des profils de vitesse en fonction des hauteurs équivalentes de rugosité ou des longueurs de MONIN-OBUKHOV, ou si l'on considère les échelles relatives que doivent posséder les gros tourbillons porteurs d'énergie et les petits tourbillons responsables de la dissipation pour que le processus de cascade d'énergie décrit par KOLMOGOROV puisse s'établir dans un domaine appréciable de nombres d'ondes (SANDBORN et MARSHALL (1965)).

La veine des soufflerias de simulation atmosphérique atteint ainsi assez couramment plusieurs dizaines de mètres de longueur, et les écarts de température qui y sont créés plusieurs dizaines de degrés, tandis que l'on s'efforce de ramener la vitesse à des valeurs de l'ordre de 1 à 2 m./s. La longueur de veine adoptée ici est de 40 mètres, les écarts maxima de température et d'humidité sont fixés à 30°C et 25.10^{-3} kg. d'eau/kg. d'air et la gamme de vitesses prévue s'étend de 1 à 14 m./s. Un calcul approché des caractéristiques de cette installation a été effectué, et certains des résultats sont présentés sur la figure 2, mettant en évidence la large gamme de variation des paramètres sans dimensions qu'il sera possible d'y couvrir.

3.3. Les couches limites de température et d'humidité, et la reproduction des transferts de chaleur et de masse :

Si la structure turbulente de l'écoulement est satisfaisante, le fait de créer un écart de température entre l'écoulement d'air et la nappe liquide provoque l'apparition d'une couche limite thermique et de transferts turbulents d'enthalpie sensible qui, dans la région interne de la couche limite, présentent une bonne similitude avec ceux que l'on rencontre dans la couche de surface de l'atmosphère. Il en est de même pour le transfert turbulent de vapeur d'eau si l'on crée un écart entre l'humidité spécifique du courant d'air et l'humidité spécifique saturante à la surface de l'eau.

Les équations gouvernant ces transferts étant linéaires vis à vis des variables température et humidité, le degré de simulation des phénomènes naturels est indépendant des écarts créés, qui peuvent donc être fixés aux valeurs convenant le mieux à l'exécution des expériences. Ceci n'est, évidemment, valable que dans la mesure où les variables scalaires peuvent être effectivement considérées comme des contaminants passifs, c'est à dire dans la mesure où le nombre de Richardson reste négligeable. Comme le montre la figure 2d, la valeur de ce dernier paramètre, calculée dans la région interne de la couche limite ($z/\delta = 0{,}25$) et pour un écart de température de 25°C entre l'air et l'eau, est une fonction fortement décroissante de la vitesse de l'air. Pour les valeurs élevées de cette dernière, les effets de stratification sont donc négligeables, et les écarts de température et d'humidité pourront être fixés, afin d'accroître la précision des mesures, aux valeurs les plus élevées autorisées par les puissances installées, soit une dizaine de degrés et de 2 à 10 gr. d'eau/Kg. d'air. Aux faibles vitesses, la stratification devient au contraire l'un des facteurs essentiels de l'expérience et ces écarts seront, soit volontairement limités afin de rester au voisinage de la stabilité neutre, soit fixés, en fonction du nombre de Richardson que l'on désire atteindre, à des valeurs pouvant être

relativement importantes : de l'ordre de 30°C et 25 gr. d'eau/kg. d'air. Les effets des échanges naturels d'énergie résultant du rayonnement paraissent pouvoir être reproduits en première approximation au laboratoire. A l'échelle considérée ici, le rayonnement d'origine solaire a pour conséquence principale un échauffement global de la masse océanique et le chauffage de la nappe liquide en constitue une simulation acceptable. Le problème du rayonnement de plus grandes longueurs d'ondes est plus complexe, en raison de la possibilité d'une divergence non négligeable du flux radiatif dans les basses couches, mais l'effet essentiel est généralement un retrait de chaleur localisé sur l'interface elle-même. Le refroidissement de cette même surface par suite de l'évaporation jouera donc un rôle analogue. Une reproduction plus directe, et indépendante, des échanges radiatifs de grandes longueurs d'ondes sera réalisée par ailleurs, en agissant sur la température de la paroi supérieure de la veine d'expériences, et donc sur l'énergie échangée par rayonnement entre cette paroi et la surface de la nappe liquide.

3.4. La reproduction des mouvements de l'interface :

L'obtention, au laboratoire, de vagues possédant des caractéristiques statistiques semblables à celles des vagues engendrées dans la nature a fait l'objet, ces dernières années, d'un nombre appréciable de travaux dont le but était, soit de parvenir à effectuer des essais techniques réellement significatifs, soit de procéder à la vérification expérimentale des théories de la génération de PHILLIPS et de MILES. Nous citerons, parmi d'autres, VERAS (1963), HIDY et PLATE (1965), GUPTA (1966), les travaux du WATERLOOPMUNDIG LABORATORIUM (1966 a,b), COLWELL (1966). Afin de parvenir à une simulation satisfaisante des vagues dissymétriques, irrégulières et tri-dimensionnelles que l'on rencontre dans la nature, il est nécessaire de réaliser des installations de dimensions importantes. Les "soufflaries à vagues de vent" atteignent assez couramment une longueur de 40 ou même 100 mètres, et une largeur de plusieurs mètres. Les parois latérales doivent être lisses et parallèles, de façon à ce que les réflexions soient équivalentes à des sources images en envergure infinie, et l'extrémité aval du canal doit être munie d'une plage possédant un coefficient d'absorption élevé.

Les caractéristiques des vagues qui seront engendrées dans l'installation prévue ont fait l'objet d'un calcul approximatif, dont certains des résultats sont présentés sur la figure 2c. Il apparaît possible d'obtenir des vagues de gravité d'amplitude appréciable, surtout pour les vitesses les plus élevées, mais elles restent dans le domaine des vagues "jeunes" dont la célérité de propagation n'est qu'une faible fraction de la vitesse du vent. Par conséquent, comme il semble nécessaire de pouvoir faire varier indépendamment de la vitesse du vent l'amplitude et surtout l'âge des vagues, un générateur artificiel de vagues, ou "batteur", doit être prévu à l'entrée du canal. La similitude avec les mouvements naturels restera en principe satisfaisante si ce générateur est commandé par des signaux aléatoires convenables et si les mesures sont effectuées suffisamment loin en aval.

3.5. Dispositions particulières :

Le but poursuivi étant la simulation des phénomènes à deux dimensions qui se développent dans le cas d'une envergure infinie, il apparaît nécessaire de réduire au minimum les effets tri-dimensionnels, et les mouvements secondaires caractéristiques des écoulements en conduites de sections non circulaires, dont les veines d'expériences de grand allongement sont souvent le siège. On peut agir, dans ce but, d'une part sur la géométrie de la veine dont le rapport de la largeur à la hauteur doit être relativement élevé (ici : 3,20 m./1,45 m.) et d'autre part sur le développement des couches limites parasites des parois latérales et supérieure, qu'il est intéressant de limiter.

Il est par ailleurs nécessaire, surtout pour les vitesses les plus basses, de déclencher et fixer la transition dès l'entrée de la veine, au moyen de "turbulateurs" convenablement disposés. On peut même envisager d'accélérer artificiellement le développement des différentes couches limites, mais ce procédé doit être employé avec prudence si l'on veut que la structure de l'écoulement reste satisfaisante.

3.6. Le type de simulation réalisable :

La reproduction complète, en similitude, du phénomène naturel au laboratoire ne semble pas pouvoir être envisagée. Par contre, il apparaît possible de réaliser des expériences où les différents processus physiques entrent effectivement en jeu et dans lesquelles les paramètres fondamentaux peuvent atteindre des valeurs significatives. Il s'agit donc là d'une simulation partielle des échanges naturels, dont le pourcentage est difficile à chiffrer, mais qui permettra de contrôler, et éventuellement d'améliorer, les hypothèses faites sur les mécanismes à petite échelle des interactions océans-atmosphère.

4.- CARACTERISTIQUES RETENUES POUR L'INSTALLATION.-

D'après ce qui précède, l'installation à réaliser correspond en fait à une soufflerie de simulation atmosphérique dont la veine surmonte un canal à vagues. La figure 3 en donne le schéma d'ensemble.

4.1. Caractéristiques aérodynamiques :

La soufflerie est du type "à retour". Ses dimensions hors-tout sont 61m x 7,50 m x 7,50m. La veine d'expériences, longue de 40 m, a une section de 3,20 m x 1,45 m. Une variation continue de la vitesse de 0,50 m/s. à 14 m/s, avec une précision relative de 2.10^{-3}, sera obtenue à l'aide d'un groupe moto-ventilateur hélicoïde de 75 CV à commande électronique. Afin d'obtenir un

fonctionnement stable aux vitesses les plus basses, la section du conduit de retour a été volontairement diminuée. La perte de charge totale délibérément accrue par l'adoption d'échangeurs thermiques à ailetage serré régularisant l'écoulement immédiatement en amont de la chambre de tranquillisation, et les diffuseurs munis de générateurs de tourbillons ou d'aubages stabilisateurs. Afin de lutter contre les inconvénients des effets tri-dimensionnels signalés en 3.5., des dispositions particulières sont prévues. On a adopté pour la section droite de la veine canal (voir figure 4) le système de quais mis au point au WATERLOOPKUNDIG LABORATORIUM (1966 b), qui délimite au centre de la veine une région peu perturbée par les couches limites latérales. Le développement de ces dernières, et de la couche limite de la paroi supérieure, doit de plus être contrôlé : des ventilateurs du type tangentiel sont prévus pour en assurer une aspiration et un soufflage uniformes à la périphérie de deux des sections de la veine (voir figure 5).

4.2. Caractéristiques hydrauliques :

Afin de permettre le contrôle de la température et de la pureté de l'eau, une circulation à faible vitesse (de 0,01 m/s à 0,10 m/s) est assurée de l'amont vers l'aval de la veine canal à l'aide d'une pompe hélice à vitesse variable de 35 CV disposée sur le conduit de retour. Les quais limitent la largeur utile du canal à 2,60 m ; sa profondeur varie de 0,75 m à 1 m. La figure 6 schématise les dispositions adoptées à l'entrée du canal pour uniformiser le débit, permettre à l'écoulement d'air d'attaquer tangentiellement la surface liquide, et engendrer des vagues au moyen d'un batteur submergé de conception nouvelle. La plage absorbante disposée à l'extrémité du canal est constituée de tubes alignés côte à côte avec une inclinaison de 7° sur l'horizontale.

4.3. Caractéristiques hygrothermiques :

Les températures de l'air et de l'eau pourront être fixées indépendamment à des valeurs comprises entre 5°C et 40°C, avec une précision de 0,1°C environ. Le degré hygrothermique de l'air à l'entrée de la veine d'expériences pourra être maintenu à des valeurs comprises entre 60 % et 100 %, avec une précision de 1 % environ. La figure 7 schématise les dispositions adoptées pour contrôler ces variables : batterie de refroidissement et de dessiccation par condensation; batterie de chauffage et injecteurs de vapeur sur le circuit d'air ; échangeurs froid et chaud sur le circuit d'eau ; générateurs thermique, frigorifique et de vapeur; circuits de régulation.

5.- ESSAIS SUR MAQUETTE.-

Une maquette complète de l'installation a été réalisée à l'échelle 1/5. La figure 8 donnera une idée de sa construction, en éléments aisément amovibles réalisés principalement à base de matériaux plastiques, le canal et les échangeurs étant métalliques.

5.1. Essais aérodynamiques :

Ils ont permis, en premier lieu, de contrôler et d'améliorer la stabilité de fonctionnement et les caractéristiques aérodynamiques de l'installation. La figure 10 permet de comparer la configuration initialement prévue au dessin amélioré auquel les essais ont permis d'aboutir. Le montage initial présentait un certain nombre de défauts : décollements dans les coudes arrondis, mauvaise alimentation du ventilateur, rotation de l'écoulement en aval de ce dernier, fonctionnement défectueux des diffuseurs, le tout se traduisant par de légères instabilités de pression et un coefficient de buse médiocre (voir figure 11 b). Le remplacement des coudes arrondis par des coudes à angle droit munis d'aubages, le déplacement du ventilateur, l'adjonction d'un nid d'abeilles dans la tubulure de retour, ont supprimé les instabilités et procuré une première amélioration de rendement. Les diffuseurs restaient toutefois le siège de décollements auxquels il a été progressivement remédié, par réduction de l'angle d'ouverture et mise en place de générateurs de tourbillons pour le diffuseur supérieur, et par adjonction de cloisons pour les diffuseurs inférieurs. La valeur du coefficient de buse a été encore améliorée. Cette configuration, ayant été jugée satisfaisante, a été adoptée pour l'installation principale, dont les caractéristiques aérodynamiques ont alors été calculées en appliquant les lois de la similitude (voir figure 11 a).

Ces essais avaient été effectués en simulant la nappe liquide par un plancher recouvert d'une paroi ondulée. Après mise en eau du canal, on a pu vérifier que le fonctionnement aérodynamique global n'était pas modifié. Une nouvelle exploration détaillée de l'écoulement dans la veine a alors été effectuée, dont les figures 12 et 13 présentent quelques résultats. Ceux-ci illustrent le développement de la couche limite sur la surface liquide en mouvement et confirment l'intérêt des dispositifs de contrôle d'écoulement dans la veine, dont la mise au point est en cours.

5.2. Essais hydrauliques :

Le principe de fonctionnement du batteur immergé, et les propriétés absorbantes de la plage ont été vérifiés sur une maquette auxiliaire. Les caractéristiques globales du circuit hydraulique ont fait l'objet d'un premier examen. D'après l'observation des vagues engendrées par le vent, dont la figure 9 donnera une idée, les dispositions adoptées pour le canal semblent satisfaisantes en ce qui concerne le contrôle des mouvements de l'interface. Des essais plus détaillés se poursuivent.

5.3. Essais hygrothermiques :

La bonne marche de l'ensemble de l'appareillage et des circuits de régulation a pu être vérifiée. Une température minimale de 5°C et une température maximale de 40°C ont été atteintes pour une vitesse de 8 m/s. Le dispositif de régulation utilisé assure la stabilité en température à ± 0,25°C près. Le contrôle du degré hygrométrique par condensation sur la batterie froide ou par

injection de vapeur a fait l'objet d'essais d'après lesquels le principe de fonctionnement retenu semble valable. Une exploration détaillée du développement des couches limites thermiques dans la veine a été entreprise et la figure 14 présente quelques-uns de profils de température mesurés.

6.- CONCLUSION.

L'examen des mécanismes physiques à petite échelle connus comme responsables des échanges d'énergie entre la couche de surface de l'atmosphère et les océans permet d'identifier les processus fondamentaux de transfert de quantité de mouvement et d'énergie mécanique, de transfert de vapeur d'eau et d'enthalpie latente, et de transfert d'enthalpie sensible, dont la reproduction est nécessaire pour l'étude au laboratoire du phénomène naturel.

Il apparaît indispensable, pour que les expériences soient significatives, de tenir compte des facteurs particuliers que constituent la structure turbulente et l'état de stratification de l'atmosphère d'une part, et les mouvements de la surface océanique d'autre part. Il en résulte que le dispositif expérimental doit être de dimensions importantes et que les conditions qui y seront établies doivent pouvoir varier dans d'assez larges proportions.

Les données obtenues ont servi de base à l'établissement du projet d'une installation de recherches, dont les caractéristiques ont pu être contrôlées par des essais détaillés effectués sur une maquette à échelle plus réduite. Cette installation est actuellement en cours de construction, et sa mise en service est prévue au cours des derniers mois de l'année 1970. Les expériences y seront effectuées dans des conditions bien définies et reproductibles, et on peut penser que les phénomènes naturels s'y trouveront simulés de façon utilisable. Les mécanismes fondamentaux par lesquels s'opèrent les échanges d'énergie entre les océans et l'atmosphère pourront donc y faire l'objet d'une étude approfondie, dans des conditions favorables.

REFERENCES :

1.- COANTIC (M.) -1968- Les interactions atmosphère-océans : les processus physiques et les équations qui les gouvernent.
Rapport I.M.S.T.(Publié dans les Cahiers Océanographiques Vol XXI -1969- N°1 pp.17-46 ; N°2 pp.105-143 ; N°3 pp.223-249).

2.- COLONELL (J.M.) -1966- Laboratory simulation of sea waves.
Technical Report N°65 -Dept. of Civil Eng. Stanford University.

3.- GUPTA (A.K.) -1966- An experimental investigation of the generation of water waves by air shear flows.
ASRL TR 116-3 -Depart. of Aeronautics and Astronautics, Massachussets Institute of Technology.

4.- HIDY (G.M.), PLATE (E.J.) -1965- Wind action on water standing in a laboratory channel.
Report P.M. 135 - NCAR, Boulder,Colorado.

5.- LUMLEY (J.L.), PANOFSKY(H.A.) -1964- The structure of atmospheric turbulence.
Interscience, New-York.

6.- MEMY (P.) -1968- Reproduction en similitude de la diffusion dans la couche limite atmosphérique.
Communication Comité Technique N°86, Sté Hydrotechnique de France,Paris.

7.- OBUKHOV (A.S.),YAGLOM (A.M.) -1966- Hydromécanique statistique.
Moscou, Moscou (Traduction américaine J.P.R.S. 37, 763).

8.- PLATE (E.J.), CERMAK (J.E.) -1963- Micrometeorological wind tunnel facility.
Fluid Dynamics and Diffusion Laboratory, Colorado State Univ.
Rep. CER 63 -EJP-JEC 9.

9.- POCOCK (P.J.) -1960- Non-aeronautical applications of low-speed wind-tunnel techniques.
AGARD Report 313.

10.- PRIESTLEY(C.H.B.) -1959- Turbulent transfer in the lower atmosphere.
University of Chicago Press, Chicago.

11.- SANDBORN (V.A.) MARSHALL (R.D.)-1965- Local isotropy in wind-tunnel turbulence.
Technical Report Fluid Dynamics and Diffusion Laboratory - Colorado State University.

12.- VERAS (M.S.)Jr. -1963- Etude expérimentale de la houle dans un canal.
Thèse Docteur d'Université, Paris (et Division d'Etudes Maritimes du C.E.E.C.).

13.- WATERLOOPKUNDIG LABORATORIUM, Delft -1966 a- Windgoot van het Laboratorium "de Voorst"
Detailmeting van de luchtstroming S.72 -I.

-1966 b- Verrgaving luchtcirculatie-systeem windgoot.
S.72 -II.

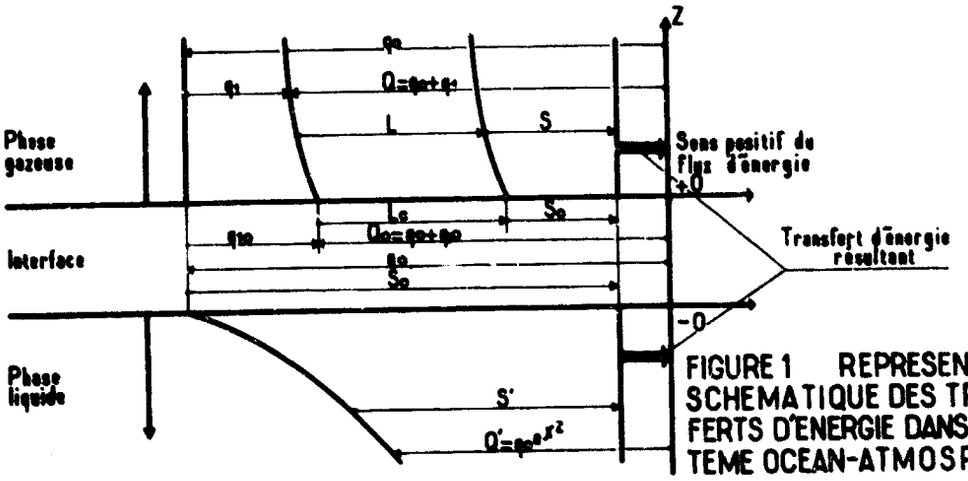

FIGURE 1 REPRESENTATION SCHEMATIQUE DES TRANSFERTS D'ENERGIE DANS LE SYSTEME OCEAN-ATMOSPHERE.

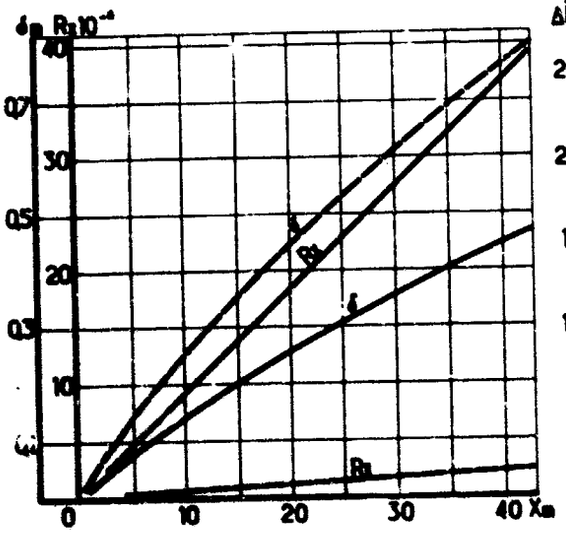

a - Nombre de Reynolds et épaisseur de couche limite

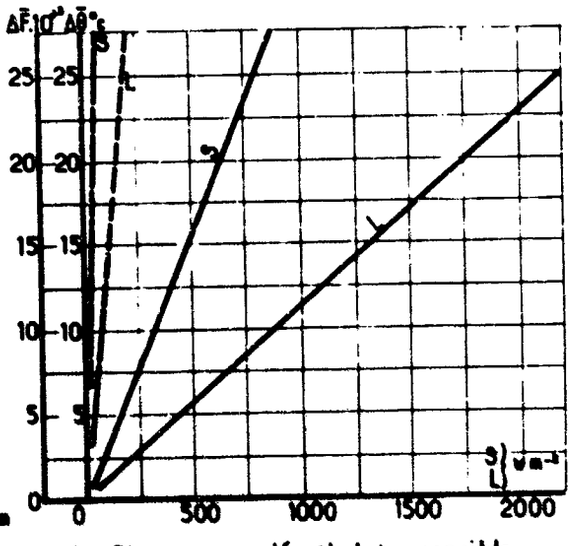

b - Flux moyens d'enthalpie sensible et latente

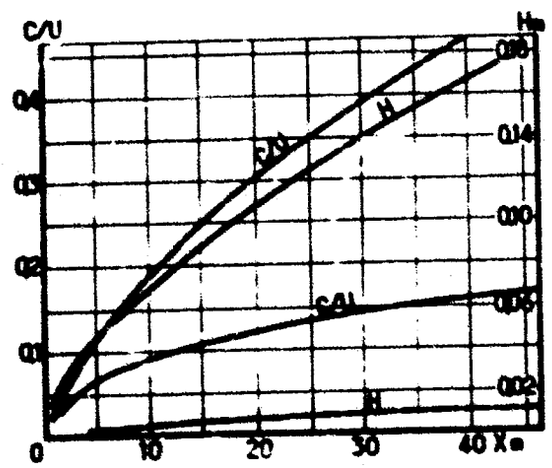

c - Age et amplitude significative des vagues de vent

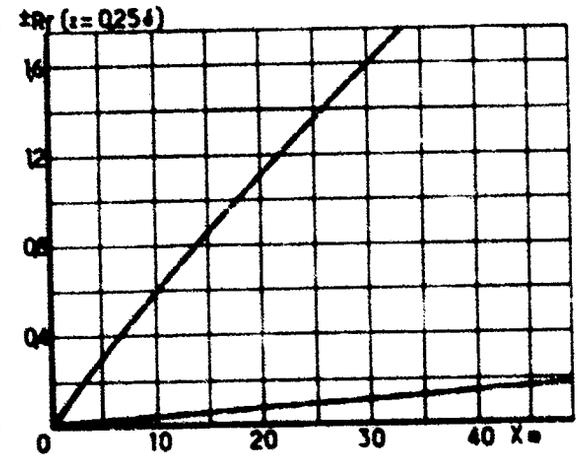

d - Nombre de Richardson

FIGURE 2 CARACTERISTIQUES CALCULEES DE L'INSTALLATION

U=1m/s
U=4m/s
U=14m/s

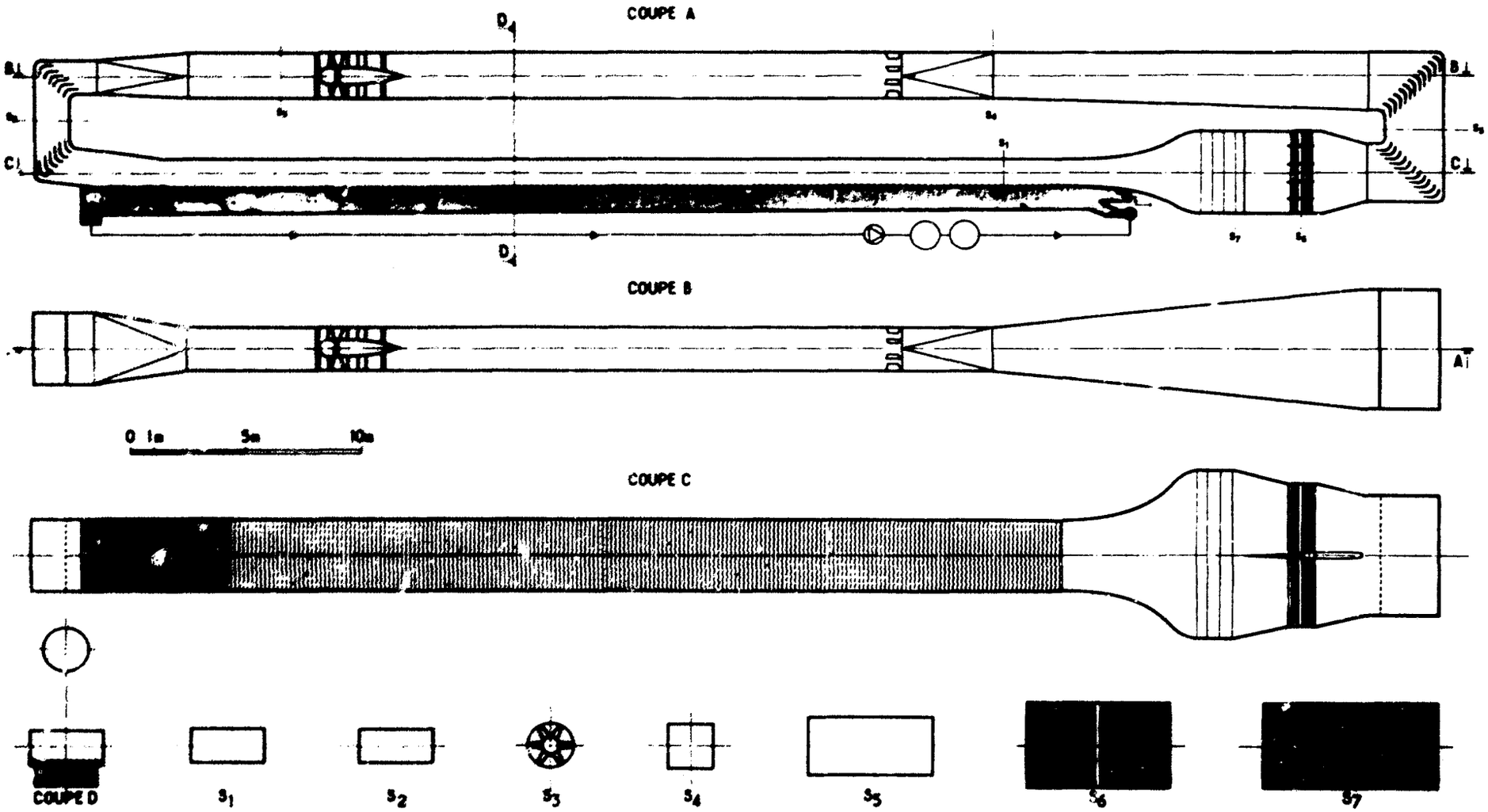

FIGURE 3 SCHEMA DE LA SOUFFLERIE

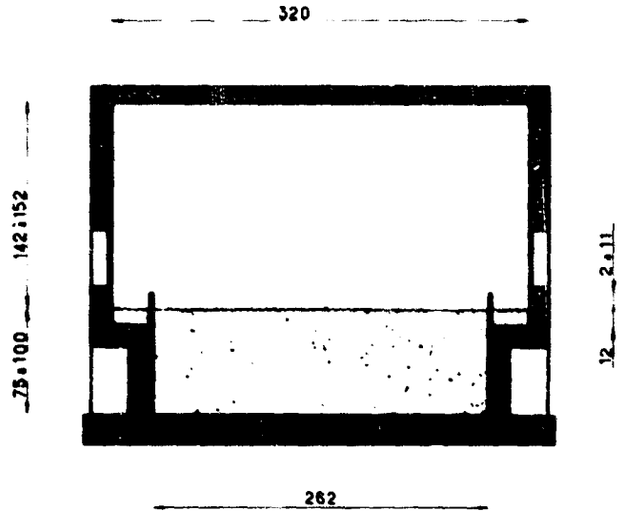

FIGURE 4 COUPE DE LA VEINE CANAL

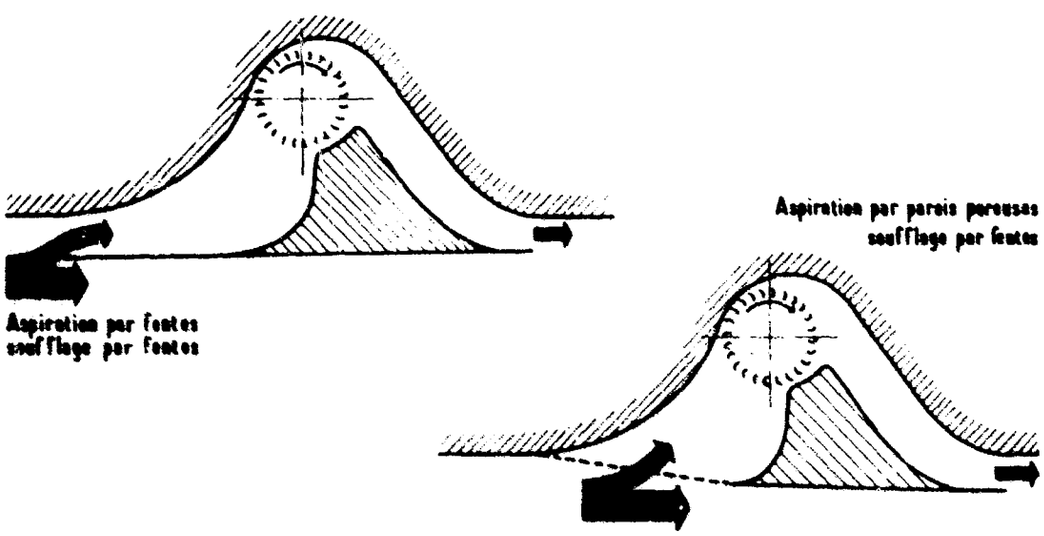

FIGURE 5 SCHEMA DE PRINCIPE DU CONTROLE DES COUCHES LIMITES

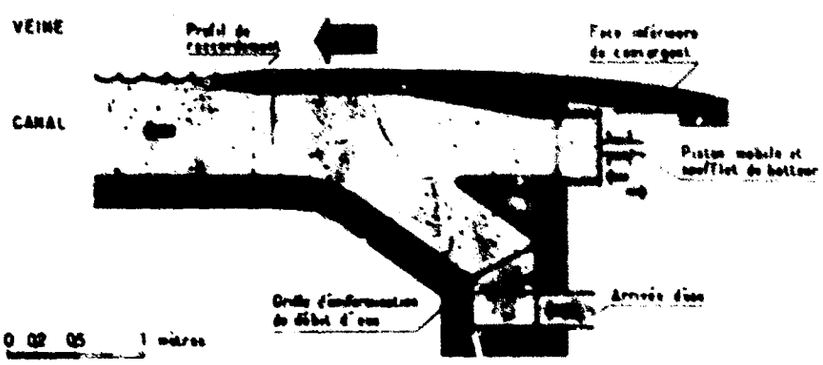

FIGURE 6 SCHEMA DU RACCORDEMENT DES CIRCUITS AIR ET EAU. DISPOSITION DU BATTEUR A VAGUES.

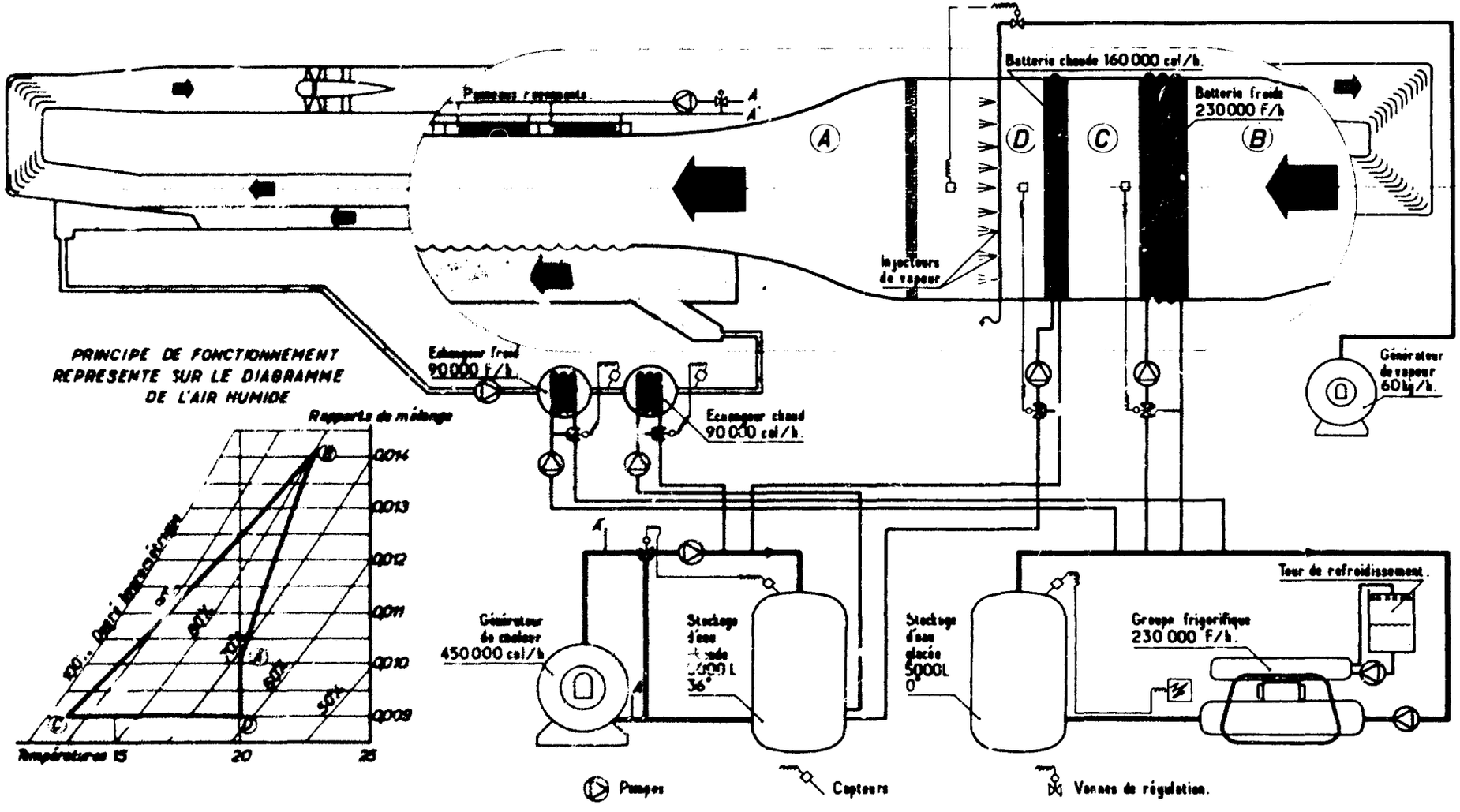

FIGURE 7 SCHEMA DU DISPOSITIF DE CONTROLE DES ECHANGES HYGROTHERMIQUES

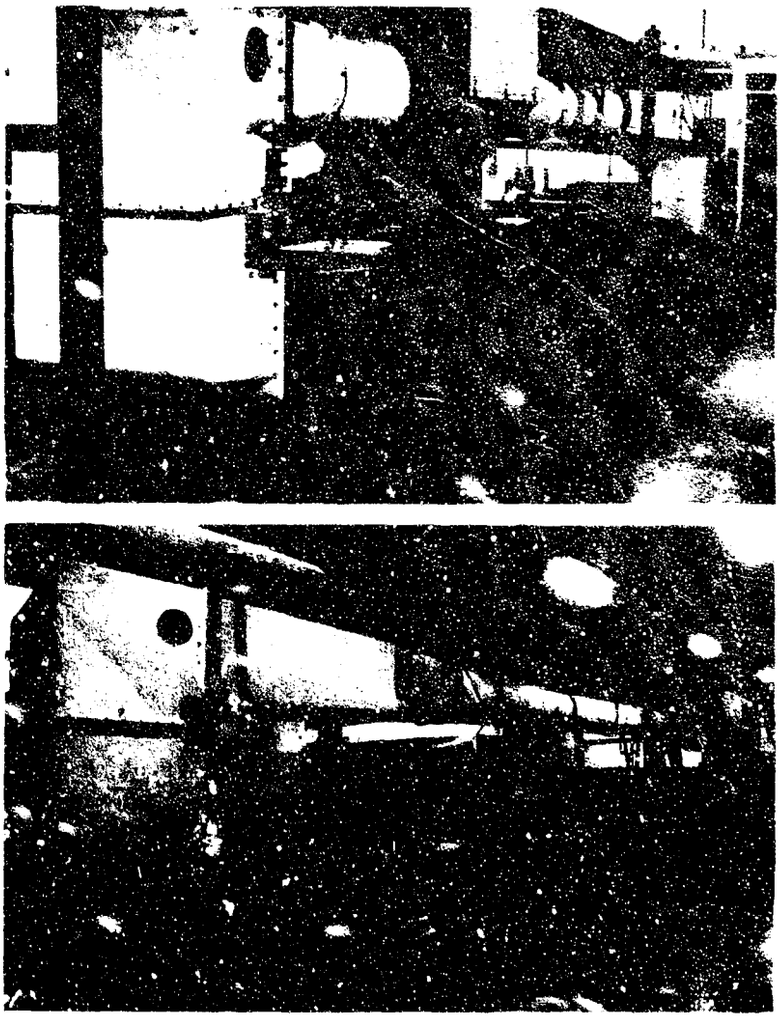

FIGURE 8 - VUES D'ENSEMBLE DE LA MAQUETTE

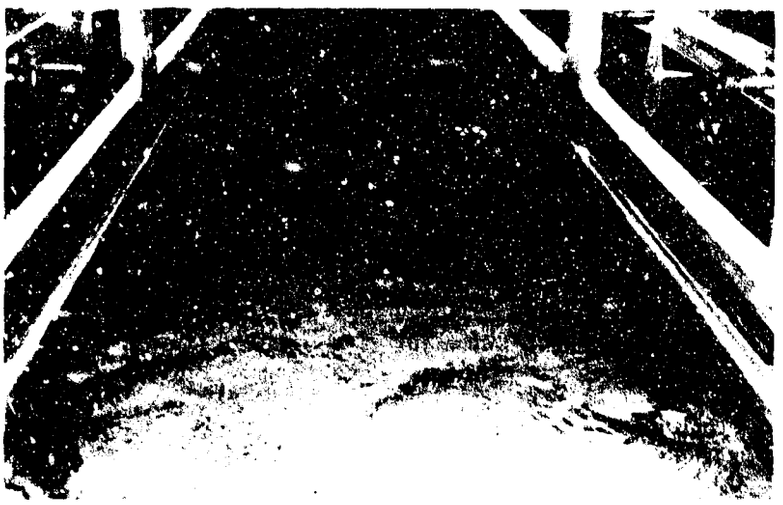

FIGURE 9 - VAGUES DE VENT OBTENUES P R UN "FETCH" DE L'ORDRE DE 4 m. A LA VITESSE DE 8 m/s.

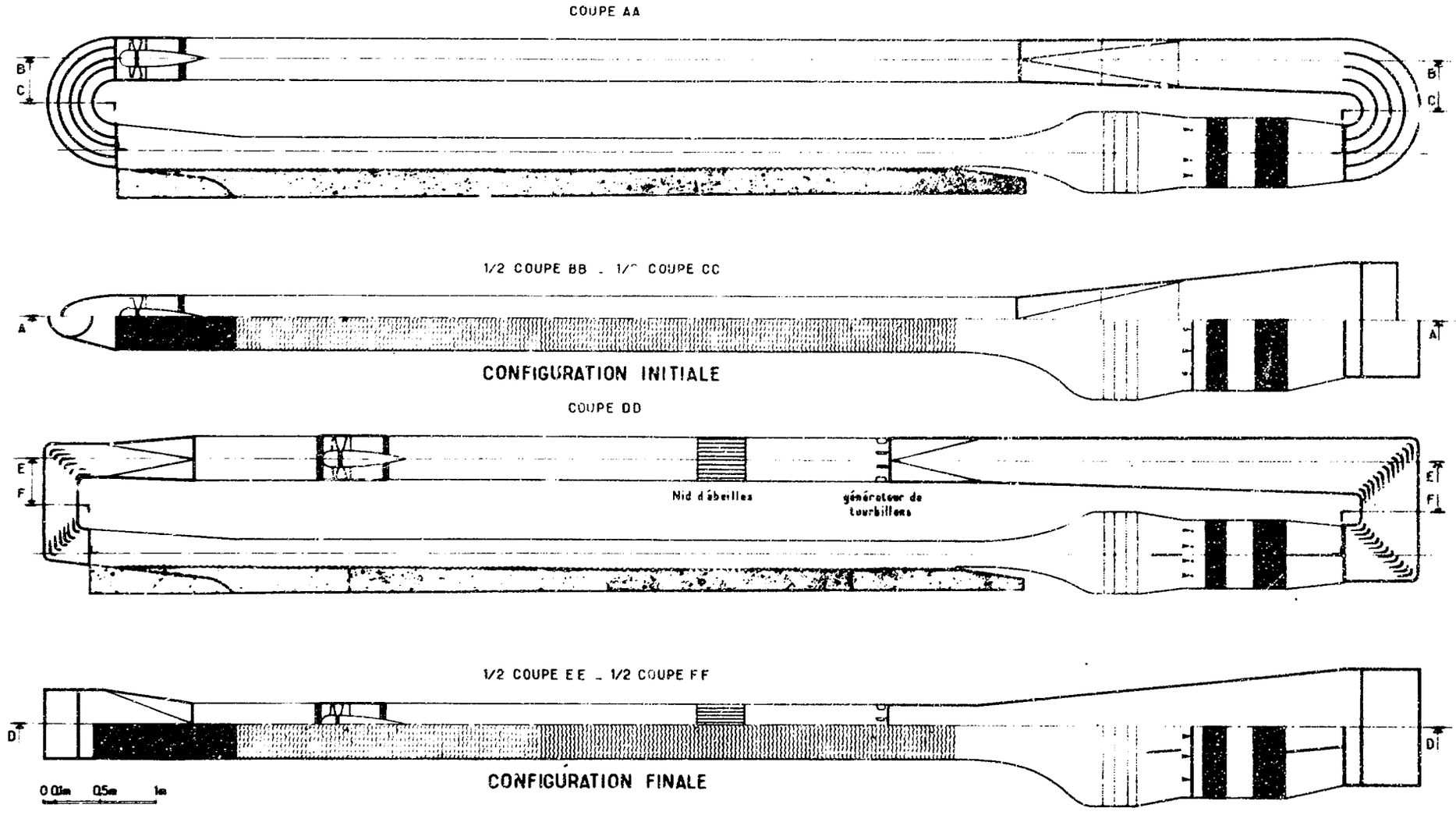

FIGURE 10 AMELIORATIONS DES CARACTERISTIQUES AERODYNAMIQUES DE LA MAQUETTE

FIGURE 11

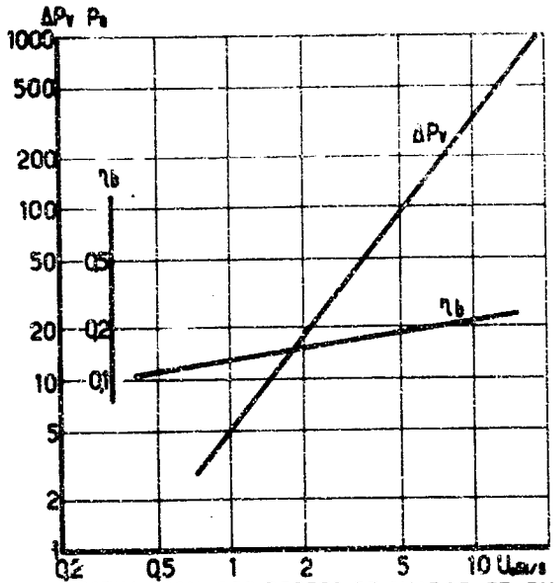

(a) ESTIMATION DES PERTES DE CHARGE ET DU COEFFICIENT DE BUSE DE LA SOUFFLERIE SE.10

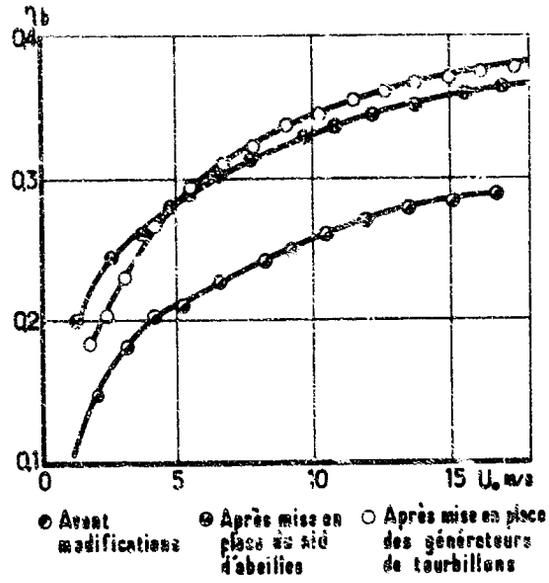

(b) COEFFICIENT MANOMETRIQUE DE BUSE DE LA MAQUETTE

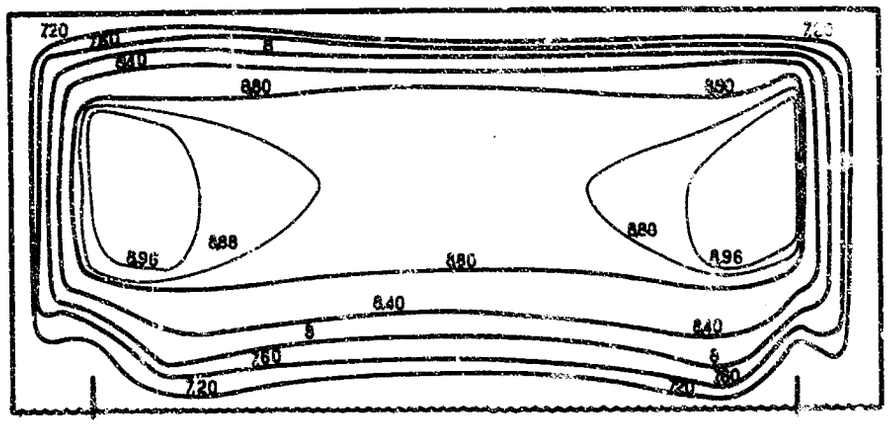

FIGURE 12 Carte des isovitesses dans la section située au 1er tiers de la veine d'expérience (Vitesses en m/s)

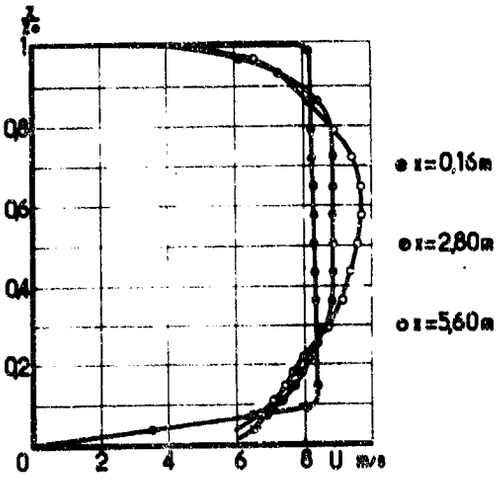

FIGURE 13 Evolution du profil de vitesse suivant l'axe de la veine d'expérience

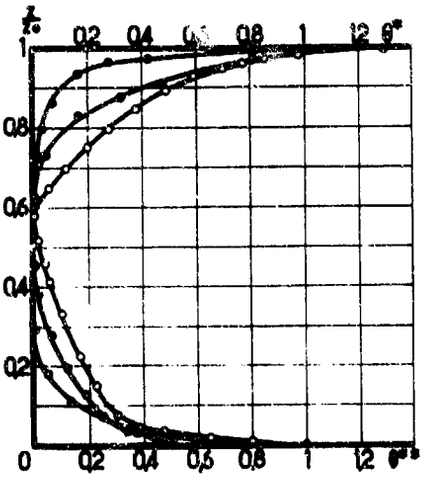

FIGURE 14 Evolution des profils thermiques suivant l'axe de la veine d'expérience.

ON THE USE OF DIFFUSING DETECTOR GASES IN THE STUDY OF ATMOSPHERIC SHEAR LAYERS WITH ADVERSE PRESSURE GRADIENTS

by

Joseph S. de Krasinski*

Department of Mechanical Engineering
The University of Calgary, (Canada)

* Associate Professor

SUMMARY

A theoretical study of the inter-relation between the velocity field in shear layers and diffusion processes is presented, adverse pressure gradients are also included. Such inter-relation is of fundamental interest in the study of shear layers and is independent of the existence of diffusion processes in natural surroundings such as air pollution. The discussion includes a variety of concentration profiles likely to be encountered. It is limited to molecular laminar processes but can be extended to turbulent ones without great difficulty.

This approach should be useful for Wind Tunnel simulation studies. Freon 12 or 21 is suggested as the diffusing agent because it can be detected in minute quantities without affecting the flow field and because the Schmidt number of these gases diffusing in air is close to unity. During the same run of the Wind Tunnel a pitot tube can measure a velocity and a concentration profile giving together information which is complementary and practically impossible to obtain by other means. Preliminary experimental results are also shown in which this method was applied to trace the dividing streamline in shear layers with an adverse pressure gradient.

NOTATION

C	mass concentration parameter
D_{1-2}, D	coefficient of diffusion of component 1 into 2
C_p	specific heat at constant pressure
H^p	the form factor
I_0, I_1, I_η	integrals defined by equation 5-3
N^∞	arbitrary big number (usually 50 or 100)
p	pressure
P	Prandtl Number
$Q(\eta_c)$	an arbitrary function of velocity of diffusion defined by 5-2
R_δ	Reynolds Number based on shear layer thickness
S	Schmidt Number = ν/D
T	Temperature (abs)
U_1	velocity at the outer edge of the viscous layer
u', v'	the x and y components of the velocity of diffusion
u, v	the x and y components of velocity
$\bar{u}$, $\bar{v}$	non-dimensional velocity components
$\bar{v}'$	mean velocity of diffusion across the shear layer
α and β	arbitrary parameters related by eq. 5-4
Γ	the concentration parameter defined as $(C_o - C)/(C_o - C_\infty)$
δ	thickness of the velocity shear layer
δ_c	thickness of the diffusion layer
δ_c^*	concentration thickness defined by eq. 4-4
ϵ	coefficient of apparent kinematic viscosity, arbitrary small number
η	relative thickness of the velocity layer
η_c	relative thickness of the concentration layer
λ	coefficient of thermal conductivity
μ	coefficient of viscosity
ν	coefficient of kinematic viscosity
ρ	density
θ_b	boundary layer momentum thickness at the edge of the step

Sub-indices

c	refers to the concentration field
i	refers to the i-th component
I	refers to the inflection point
o	refers to conditions on the line $u = 0$
T	refers to effective (total) value for a turbulent shear layer
1	refers to the outer edge of the shear layer

ON THE USE OF DIFFUSING DEFECTOR GASES IN THE STUDY OF ATMOSPHERIC SHEAR LAYERS WITH ADVERSE PRESSURE GRADIENTS

Joseph S. de Krasinski

1. INTRODUCTION

Theoretical relations have been deduced between the velocity field and concentration profiles in shear flow. Such relations might prove useful in wind tunnel simulation techniques where small quantities of a diffusing gas can be introduced and measured at will. This study is developed for laminar shear layers but might be extended, using empirical coefficients, to turbulent ones. In air pollution problems the study of the diffusing gas within the atmospheric shear layers would have a physical meaning in relation to the pollutant. Temperature gradients and gravity effects have not been included.

2. THE PHYSICAL MODEL

An atmospheric shear flow with adverse pressure gradient occurring for example in mountainous region is shown in fig. 1. A dividing streamline "d" separates the region of the circulating flow from the oncoming one and it reattaches at R. The zero velocity line u = 0 is situated below the dividing streamline and separates the positive and negative velocity regions within the circulating flow. Along this line the v velocity component is not equal zero, it changes sign at the centre of rotation "O". If a source of diffusing gas is introduced in the reverse flow below the line u = 0, say at "F", it will cross the u = 0 line and reach the dividing streamline; the extent of its crossing will depend mainly upon the coefficient of diffusion in the laminar case and upon the turbulent mixing processes in the turbulent one.

When studying such a field in the Wind Tunnel it is difficult to determine experimentally the line u = 0, the v velocity component, the centre of rotation "O", and also the position of the dividing streamline. All these data are of great importance for a physical description of the flow as well as for the theoretical formulation of the problem. As shown below such information can be more readily obtained through complementary measurements of the concentration profiles of the diffusing gas. Halogens are suggested for this purpose. They are easily detectable in minute quantities by commercially developed instruments (Halogen leak detectors); their interference with the flow is negligible and the Schmidt Number of some of them is almost unity.

3. FUNDAMENTAL EQUATIONS AND SIMILARITY CONDITIONS

It can be shown (see Ref. 1, pp. 443, 450) that for a steady shear layer with a source generating a detector gas from out-side

$$\rho \vec{U} \cdot \vec{\nabla} c_i = -\vec{\nabla} \cdot \rho \vec{U}_i c_i \tag{3-1}$$

where c_i and $\vec{U}_i$ are the mass concentration and the velocity of diffusion of the i-th component. With the usual assumptions, the last equation becomes

$$\rho \left(u \frac{\partial c_i}{\partial x} + v \frac{\partial c_i}{\partial y}\right) = - \frac{\partial}{\partial y} \left(\rho c_i v_i'\right) \tag{3-2}$$

Neglecting the term of thermal diffusion it can be also shown that

$$c_1 v_1' = -D_{1-2} \frac{\partial c_1}{\partial y} \text{ and } c_2 v_2' = -D_{2-1} \frac{\partial c_2}{\partial y} \tag{3-3}$$

where the coefficients $D_{1-2} = D_{2-1}$. Introducing the concentration parameter $\Gamma = (C_o - C)/(C_o - C_\infty)$ equations (3-3 and 3-2) become

$$(1-\Gamma) v' = D \frac{\partial \Gamma}{\partial y} \quad , \text{ where } D = D_{1-2} \tag{3-4}$$

$$\rho \left(u \frac{\partial \Gamma}{\partial x} + v \frac{\partial \Gamma}{\partial y}\right) = \frac{\partial}{\partial y} \left[\rho D \frac{\partial \Gamma}{\partial y}\right] \text{ and } v' = v_1' \tag{3-5}$$

For moderate velocities when heat generated through dissipation is negligible the momentum and energy equations for steady boundary layers or shear layers are

$$\rho\left(u\frac{\partial u}{\partial x}+v\frac{\partial u}{\partial y}\right)=-\frac{\partial p}{\partial x}+\frac{\partial}{\partial y}\left(\mu\frac{\partial u}{\partial y}\right) \tag{3-6}$$

$$\rho c_p\left(u\frac{\partial T}{\partial x}+v\frac{\partial T}{\partial y}\right)=\frac{\partial}{\partial y}\left(\lambda\frac{\partial T}{\partial y}\right)+u\frac{\partial p}{\partial x} \tag{3-7}$$

under similar initial and boundary conditions the concentration, velocity and temperature fields can be similar provided that the pressure gradient is absent and the Schmidt and Prandtl Numbers S=P=1. For turbulent mixing layers one might accept a change from D to D_T similar to the change from ν to ε, S to S_T and P to P_T, where the subscript T refers to the effective (total) Prandtl and Schmidt Numbers (see Ref. 2, footnote p. 11). There is no guarantee however that with such an interpretation strict similarity is achieved.

4. RELATIONS BETWEEN THE VELOCITY AND CONCENTRATION FIELDS IN SHEAR LAYERS

If a source of a diffusing gas is situated below the zero-velocity line one may write analogically to heat flux equation in thermal layers

$$\frac{d}{dx}\int_0^\infty \rho c u\,dy=\rho_o c_o\,(v'+v)_o \tag{4-1}$$

Putting

$$C/C_o=1-\Gamma,\quad dy=d\eta_c\delta_c, \tag{4-2}$$

equations (4-1) and (3-4) become

$$\frac{d}{dx}\delta_c\int_0^1\frac{\rho}{\rho_o}\frac{u}{u_1}(1-\Gamma)\,d\eta_c=\frac{(v'+v)_o}{u_1} \tag{4-3}$$

Introducing the concentration thickness δ_c^* defined as

$$\delta_c^*=\int_0^1\frac{\rho}{\rho_o}\frac{u}{u_1}(1-\Gamma)\,d\eta_c \tag{4-4}$$

It follows from (4-2, 4-3, 4-4) that the vertical velocity component is

$$(\bar v)_o=\left(\frac{v}{u_1}\right)=\frac{d}{dx}(\delta_c^*)-\frac{D_o}{u_1\delta_c}\left(\frac{\partial\Gamma}{\partial\eta_c}\right)_o \tag{4-5}$$

When $u=0$ at points 0 and R

$$\frac{d}{dx}(\delta_c^*)=\frac{D_o}{u_1\delta_c}\left(\frac{\partial\Gamma}{\partial\eta_c}\right)_o \tag{4-6}$$

As mentioned above there are considerable experimental difficulties in the measurement of the v component. Expression (4-5) could be used for this purpose as it contains an integral parameter δ_c^* less liable to experimental error and the gradient Γ which does not require the inversion of the pitot tube across u = 0 line as in case of velocity measurements. The most difficult of all is the measurement of the curvature expressed by $(\partial^2u/\partial y^2)_o$. All this data along the u = 0 line is important in the theoretical formulation of the problem. Using two bars for the non-dimensional velocity component u and combining (4-5) with (3-6) and (3-5), with μ and $D\rho$ constant across u = 0 line the curvature becomes

$$\left(\frac{\partial^2\bar u}{\partial\eta^2}\right)_o=\frac{u_1\delta}{\nu_o}\left(\frac{\partial\bar u}{\partial\eta}\right)_o\cdot\left[\frac{d}{dx}(\delta_c^*)-\frac{D_o}{u_1\delta_c}\left(\frac{\partial\Gamma}{\partial\eta_c}\right)_o\right]+\frac{\delta^2}{u_1\mu_o}\left(\frac{\partial p}{\partial x}\right) \tag{4-7}$$

$$\left(\frac{\partial^2\Gamma}{\partial\eta_c^2}\right)_o=\frac{u_1\delta_c}{D_o}\left(\frac{\partial\Gamma}{\partial\eta_c}\right)_o\left[\frac{d}{dx}(\delta_c^*)-\frac{D_o}{u_1\delta_c}\left(\frac{\partial\Gamma}{\partial\eta_c}\right)_o\right] \tag{4-8}$$

for the velocity and the concentrations profiles respectively. In the absence of the pressure gradients the ratio of the two curvatures is

$$\left[\left(\frac{\partial^2 \bar{u}}{\partial \eta^2}\right) : \left(\frac{\partial^2 \Gamma}{\partial \eta_c^2}\right)\right]_o = \left[\left(\frac{\partial \bar{u}}{\partial \eta}\right) : \left(\frac{\partial \Gamma}{\partial \eta_c}\right)\right]_o \cdot \frac{\delta}{\delta_c} \quad \frac{1}{S} \tag{4-9}$$

One observes that no second derivatives are present in (4-7) and (4-9) and both contain quantities which should not be hard to measure. The gradient of u across u = 0 would present the greatest difficulty which might be avoided using v. Karman's integral equation in the form

$$\frac{\mu_o}{\rho_1 u_1 \delta} \left(\frac{\partial \bar{u}}{\partial \eta}\right)_o = \frac{d\theta}{dx} + \frac{\theta}{u_1} (H+2) \frac{du_1}{dx} \tag{4-10}$$

It follows that

$$\left(\frac{\partial^2 \bar{u}}{\partial \eta^2}\right)_o = \frac{u_1 \delta^2}{\mu_o} \rho_1 \rho_o \left[\frac{d\theta}{x} + \frac{\theta}{u_1} (H+2) \frac{du_1}{dx}\right] \cdot \left[\frac{d}{dx} (\delta_c^*) - \right.$$

$$\left. - \frac{D_o}{u_1 \delta_c} \left(\frac{\partial \Gamma}{\partial \eta_c}\right)_o\right] - \frac{\delta^2 \rho_1}{\mu_o} \frac{du_1}{dx} \tag{4-11}$$

The gradients of θ and δ_c^* are easier to measure than $(\partial u/\partial y)$ at u = 0. If $\rho_1 = \rho_o$ and the pressure gradient in the X direction is negligible the last equation transforms into

$$\left(\frac{\partial^2 \bar{u}}{\partial \eta^2}\right)_o = R_\delta^2 \left(\frac{d\theta}{dx}\right) \left[\frac{d}{dx} (\delta_c^*) - \frac{D_o}{u_1 \delta_c} \left(\frac{\partial \Gamma}{\partial \eta_c}\right)_o\right] \tag{4-12}$$

The curvature of the velocity profile at u = 0 depends in general upon the pressure gradient and the v component of velocity. At points 0 and R (see fig. 1a) where u = v = 0 only the pressure gradient determines the sign of the curvature. Upstream of 0 a positive v component contributes to a positive curvature and downstream of 0 the positive pressure gradient is dominant and an inflection point is always present within the profile. The same conclusion does not apply to the curvature of the concentration profile. As seen from (4-8) the curvature follows the sign of the component v only and changes from positive to negative when crossing the point 0 along u = 0 from left to right (fig. 1b). This means that to the right of 0 the concentration profile must be a "full" one and does not contain an inflection point while to the left of point 0 the profile is not "full" and contains it. As the difference between the two gradients determines the velocity component v (eq. 4-5) and from the previous discussion the transversal gradient of Γ should increase when moving downstream one expects their mutual relation to be somewhat like in (fig. 1c). (not to scale) The strong negative v component before reattachment might reduce δ_c^* to give a negative slope of δ_c^* against X. At reattachment and at the centre 0 both must be equal.

5. THE MEAN VELOCITY OF DIFFUSION AND THE DIVIDING STREAMLINE

As mentioned in section 2 a pitot tube connected to a detecting apparatus and introduced from outside into the shear layer will not show exactly the position of the dividing streamline when the first traces of the detector gas are recorded. The penetration of the gas across the dividing streamline can be estimated by means of the mean velocity of diffusion which if assessed allows for correction needed to determine more precisely the position of this line. It follows from (3-4) that the mean velocity of diffusion

$$\bar{v}' = \frac{1}{\delta_c} \int_o^1 D \frac{\partial \Gamma}{\partial \eta_c} \left(\frac{1}{1-\Gamma}\right) d\eta_c \tag{5-1}$$

depends partially upon the variation of D across the layer and partially upon the concentration profile Γ. For turbulent shear layers D would change to D_T and also change the order of magnitude. Before more experimental data is available one may discuss the laminar case when D is constant and can be estimated (Ref 3, p.539). The concentration profiles and their slopes can be determined experimentally (see sec. 6) hence (5-1) allows the estimation of the mean velocity of diffusion and the position of the dividing streamline. Some preliminary discussion of $\Gamma(\eta_c)$ is useful before more experimental work is undertaken it allows an estimate of the order of magnitude of $\bar{v}'$ and throws more light on the diffusion processes.

Equation (3-3) indicates that an exponential decay of concentration across the shear layer, which is acceptable from physical considerations, would signify a constant velocity of diffusion across it. One may however assume this is a particular case of a more general one which could be encountered within the variety of concentration profiles discussed in the previous section. Lets assume D= constant across the layer and the remaining integrand of (5-1) some function of η_c containing two parameters in such a way that when one is equal zero the integrand is constant and so is the velocity of diffusion. The suggested function could be for example

$$Q(\eta_c) = Q = \alpha \exp\beta\eta_c \text{ (exponential)}; \quad Q = \alpha(1+\beta\eta_c) \text{ (linear)}; \quad Q = \alpha(1+$$

$$+\beta\sin \pi\eta_c) \text{ (sine)}$$

etc. The measure of success of this approach can be only assessed when comparing the results with exact solutions based on similarity. Without dealing at this stage with any particular function some general conclusions can be drawn. Taking

$$Q(\eta_c) = Q = \frac{\partial\Gamma}{\partial\eta_c} \quad \frac{1}{1-\Gamma} \tag{5-2}$$

and separating the variables

$$\ln (1-\Gamma) - \ln c = \int Q \, d\eta_c \tag{5-3}$$

with initial and boundary conditions $\eta_c = 0$, $\Gamma = 0$

$\eta_c = 1$, $\Gamma = 1-\epsilon$ where ϵ is an arbitrary small value also expressed as $1/N$ with N being an arbitrary big number depending on the definition of the limits of the concentration profile. Calling I_0 and I_1 the R.H.S. of (5-3) for $\eta = 0$ and $\eta = 1$ respectively, it follows that the integration constant C is defined either as $\ln C = I_1 + \ln c$ or $\ln C = I_0$, therefore

$$I_1 - I_0 = - \ln c = \ln N \tag{5-4}$$

This equation relates the two parameters α and β of the arbitrary function Q. It follows from (5-3) and the second definition of the integration constant that

$$\Gamma = 1 - (\exp I_0) \; (-\exp I_\eta) \tag{5-5}$$

where I_η is $\int Q \, d\eta_c$ at any value of $0<\eta_c<1$ and

$$\frac{\partial\Gamma}{\partial\eta_c} = (\exp I_0) \; Q \; (e^{\wedge} \tag{5-6}$$

therefore along the u = 0 line

$$\left(\frac{\partial\Gamma}{\partial\eta_c}\right)_0 = Q_0 = \alpha \tag{5-7}$$

and is determined by one parameter only (α or β) once the outer limits of the concentration profile have been chosen by taking an appropriate N.

The point of inflection of the profile is given by

$$\frac{\partial^2\Gamma}{\partial\eta_c^2} = 0 = (\exp I_0) \; \left[\exp (-I_\eta)\right] \; \left(\frac{\partial Q}{\partial\eta_c} - Q^2\right) \tag{5-8}$$

and from physical considerations the only condition is

$$\left(\frac{\partial Q}{\partial\eta_c}\right) = Q^2 \tag{5-9}$$

If no pressure gradient were present at the point 0 (see fig. 1a), the concentration profile there should be identical with the flat plate velocity profile provided the similarity conditions discussed in section 3 were maintained. Such a profile would have an inflection point at the origin. The choice of the arbitrary function Q could be checked at that particular point.

As a matter of illustration let assume the exponential law of velocity of diffusion i.e., $Q = \alpha \exp \beta\eta_c$. It follows from (5-4) that

$$\alpha = \frac{\beta \ln N}{\exp \beta - 1}$$

and from (5-8) the inflection point is situated at

$$(\eta_c)_I = \ln \left[\frac{\exp \beta - 1}{\ln N}\right]$$

If at origin the parameter $\beta = \ln(\ln N + 1) = \alpha$; from (5-7)

$$\left(\frac{\partial \Gamma}{\partial \eta_c}\right)_0 = \alpha = \frac{\beta \ln N}{\exp \beta - 1} = \beta$$

Finally the concentration profile obtained from (5-5) is

$$\Gamma = 1 - \exp\left[\frac{\alpha}{\beta}\left(1 - \exp \beta\eta_c\right)\right]$$

Similar procedure can be adopted for the linear and the sine law of velocity of diffusion. Fig. 2 shows three profiles with the inflection point at the origin corresponding to the three laws respectively. The arbitrary limit is determined by N=100 for all the three cases i.e., $\Gamma = 0.99$ when $\eta_c = 1$. Blasius profile is also included and is practically indistinguishable from the exponential case*. One is tempted to state that an exponential law of velocity of diffusion in the form $Q = \alpha \exp \beta\eta_c$ is associated with a concentration profile which coincides with a velocity profile when no pressure gradient is present, similarity conditions being maintained. In fig. 3 more profiles are shown for various values of the parameters α and β assuming the exponential law, and N=50 signifying the outer limit of $\eta_c = 0.98$.

Using (5-1) the mean velocity of diffusion irrespective of α and β is

$$\frac{\bar{v}' \delta_c}{D} = \ln N \qquad (5\text{-}10)$$

This approximate expression (also valid for the linear and sine law) may be useful for a more precise determination of the dividing streamline. If the limits of the concentration profile are arbitrarily extended (high value of N) so will be δ_c, hence the arbitrariness of N is only apparent.

Thermal effects, turbulence etc. will affect the concentration profile of a pollutant or detector gas. It seems useful therefore to discuss the remaining originally suggested linear and sine law velocities of diffusion besides the exponential one. If encountered in reality or in wind tunnel simulation such a discussion might be of interest.

Table I at the end of the text gives essential details of all the three profiles. Typical exponential law profiles are shown in fig. 3, letter I indicates the position of the inflection point (N=50).

6. DETAILS OF PRELIMINARY TESTS

Preliminary qualitative wind tunnel tests were made with the object of tracing the dividing streamline in a shear layer. Diluted Freon 12 was used as recommended by the

---

* The transverse gradient at the wall is about 3.5% greater than Blasius' profile.

makers of the leak detector*. This type of detector works on the principle of an increased ion emission when the working gas (Freon 12) contaminates the air surrounding an incandescent platinum cathode. The emission current is amplified and shown on an ammeter. The makers claim that partial pressures of an order of 10^{-8} mm Hg of Freon in air can be detected. The advantage of such a high sensitivity is an almost nil interference with the flow and a low degree of contamination of a closed circuit wind tunnel even after prolonged working. It also might be possible to extend such tests to real atmospheric conditions. Halogens are particularly suited for this work not only because of facility of detection but also because of their Schmidt Number (in air) which is almost independant of temperature and pressure and can be close to unity. This is important from similarity considerations. The following table gives the mean values for various cases

Halogen	Freon 11 ($C C_{\ell 3}F$)	Freon 12 ($C C_{\ell 2}F_2$)	$CC_{\ell 2}F-CC_{\ell}F_2$
Schmidt Number	1.7	1.65	1.2
Halogen	Freon 21 ($CHC_{\ell 2}F$)		
Schmidt Number	0.9		

Details of the installation are given in fig. 4. A pitot tube is connected either to a micromanometer for velocity profile measurements or to the leak detector for the freon study. The freon sensor is also connected to a vacuum pump. this ensures a constant flow through the system at each position of the pitot.

Diluted (15% by volume) Freon 12 was stored in a large, open to the atmosphere vessel and fed into a separation bubble by means of a precision needle valve. The shear layer was produced by a step, it was laminar but transition occured close to reattachment. To ensure a visual observation of the minute quantities of induced gas it was passed through detergent showing bubbles. Once equilibrium was established and the zero of the leak detector recorded, the pitot tube was lowered from the external flow into the shear layer. Micromanometer readings were taken at every station of the pitot tube. Upon reaching the first traces of Freon the leak detector showed a steady increase as the tube further lowered. On returning it decreased to zero again which showed a good capacity for making quantitative measurements of the concentration profile. The tests were so far qualitative, with the object to assess the position of the dividing streamline. Well studied model was chosen in which this position was obtained through tedious measurements of the inverted flow and its integration. Three readings were considered: the first movement of the micromanometer, a more pronounced one and a definite steady discernible movement of the indicator all three corresponding to a steadily increasing penetration of the pitot within the shear layer. The results are shown in figs. 5a and 5b. The velocity profile is given with the position of the dividing streamline obtained through flow integration. Positions a,b, and c correspond to the three detection stages of the indicator. In fig. 5a, the coincidence is very good, the shear layer was laminar and the distance behind the steps edge was 75 momentum thicknesses. Fig. 5b corresponds to the same shear layer close to reattachment after transition has occured. One observes a strong penetration of the Freon into the outer part of the layer as expected, the dividing streamline being well below. Here distance corresponds to 560 momentum thicknesses behind the step.

These results indicate that the method is promising and needs more experimental data, particularly in the turbulent shear layers.

References

1. Moore, F. — Theory of Laminar Flows, Oxford University Press, 1964.

2. Kutateladze, S.S. Leont'ev, A.I. — Turbulent Boundary Layers in Compressible Gases, Edward Arnold Publishers Ltd., 1964

3. Hirschfelder, J. Curtiss, C. Bird, R. — Molecular Theory of Gases and Liquids Wiley & Sons, N. York, 1954

* Halogen Lecksucher H-1, Catalogue IF-17 and IF-19, Balzers, Lichtenstein. Also General Electric Catalogue GEA 6817

TABLE I

Assumed velocity of diffusion	$Q = \alpha \exp \beta \eta_c$	$Q = \alpha(1+\beta\eta_c)$	$Q = \alpha(1+\beta \sin \pi \eta_c)$
Relation between α and β (eq. 5-4)	$\alpha = \frac{\beta \ln N}{(\exp\beta)-1}$	$\alpha = \frac{\ln N}{1+\beta/2}$	$\alpha = \frac{\ln N}{1+2\beta/\pi}$
Position of infl pt. (eq. 5-8)	$(\eta_c)_I = \frac{1}{\beta} \ln\left[\frac{(\exp\beta)-1}{\ln N}\right]$	$(\eta_c) = \frac{\sqrt{\beta/\alpha}-1}{\beta}$	$\beta\pi \cos \pi\eta_c = \alpha(1+\beta \sin \pi\eta_c)^2$
Condition for infl. pt. at $\eta_c=0$ (eq. 5-9)	$\alpha = \beta = \ln(\ln N+1)$	$\alpha = \beta = -1+\sqrt{1+2\ln N}$	$\alpha = \beta\pi$ $\alpha = -\frac{\pi^2}{4} + \pi\sqrt{\frac{\pi^2}{16} + \frac{1}{2}\ln N}$
Profile's eq. (eq. 5-5)	$\Gamma = 1-\exp\left[\frac{\alpha}{\beta}(1-\exp\beta\eta_c)\right]$	$\Gamma = 1-\exp\left[-\alpha(\eta_c+\frac{\beta}{2}\eta_c^2)\right]$	$\Gamma = 1-\exp\left[-\alpha(\eta_c - \frac{\beta}{\pi}\cos\pi\eta_c) - \frac{\alpha\beta}{\pi}\right]$
$\left(\frac{\partial\Gamma}{\partial\eta_c}\right)_o$ (eq. 5-7)	$\alpha = Q_o$	$\alpha = Q_o$	$\alpha = Q_o$
Mean. vel. of diffusion $\frac{\bar{\gamma}'\delta_c}{D}$ (eq. 5-1)	$\ln N$	$\ln N$	$\ln N$

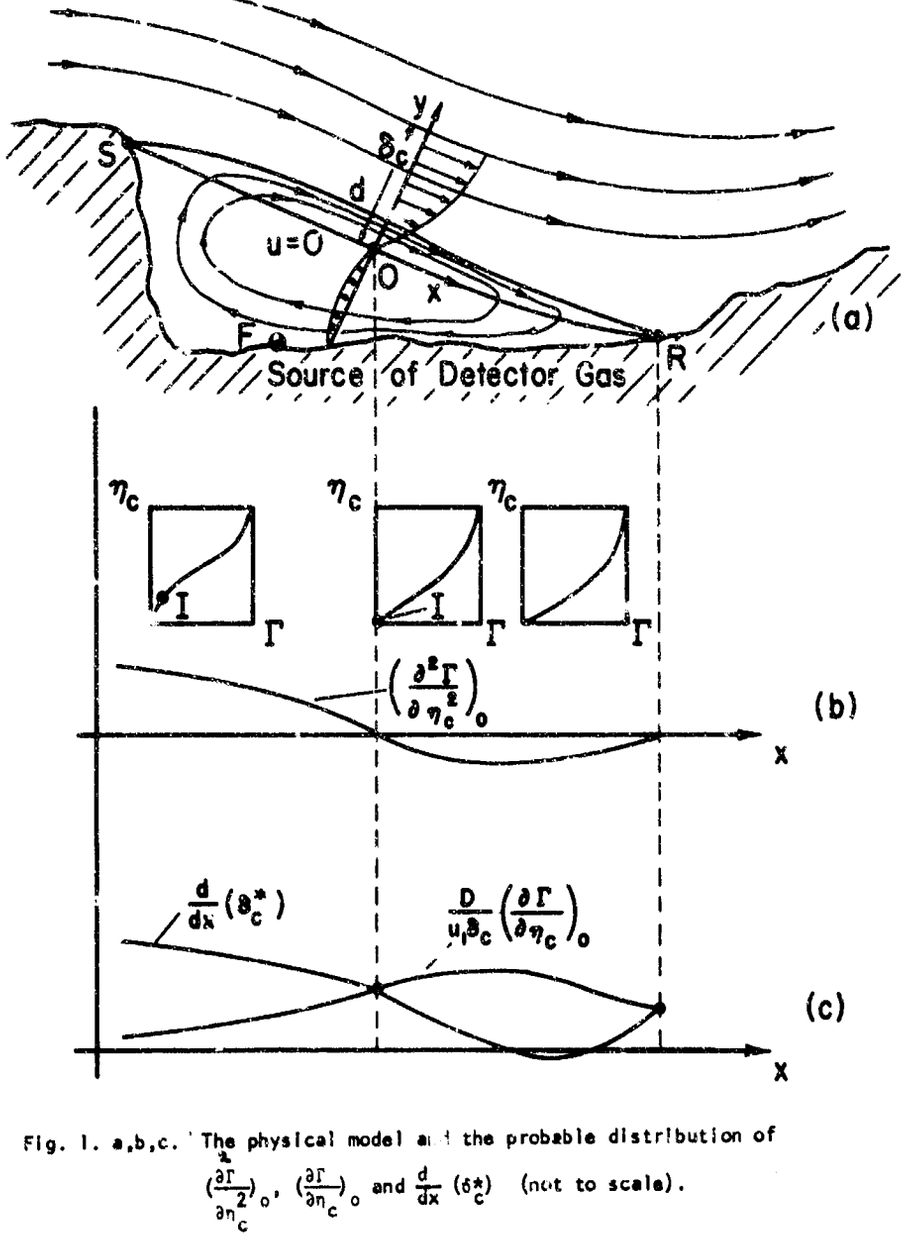

Fig. 1. a,b,c. The physical model and the probable distribution of $\left(\frac{\partial^2 \Gamma}{\partial \eta_c^2}\right)_o$, $\left(\frac{\partial \Gamma}{\partial \eta_c}\right)_o$ and $\frac{d}{dx}(\delta_c^*)$ (not to scale).

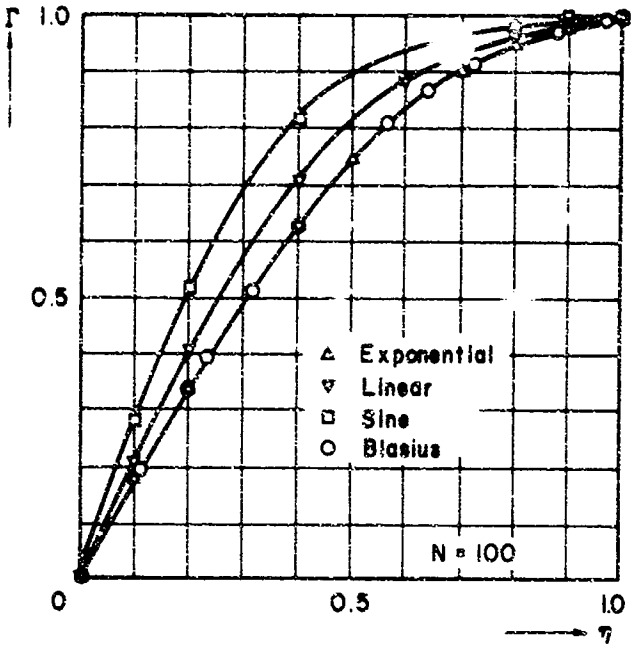

Fig. 2. Concentration profiles with an inflection point at the origin for the exponential, linear and sine laws of velocity of diffusion compared with Blasius' velocity profile (N=100).

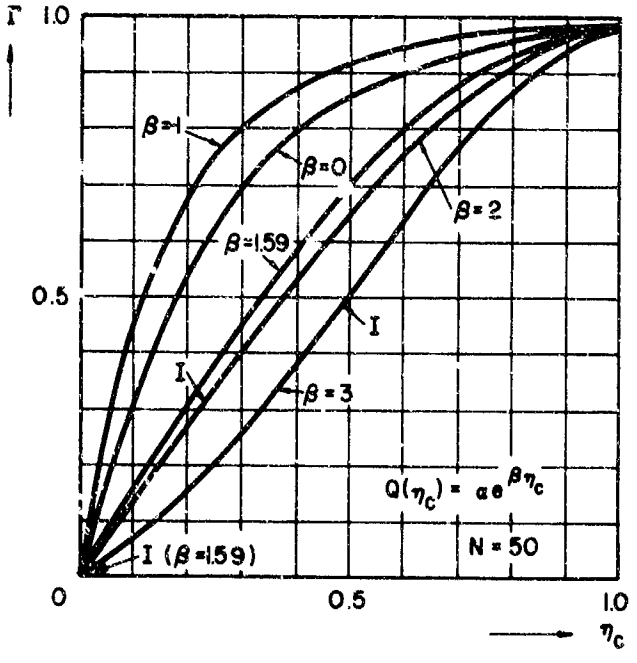

Fig. 3. Concentration profiles for the exponential law of velocity of diffusion (N=50).

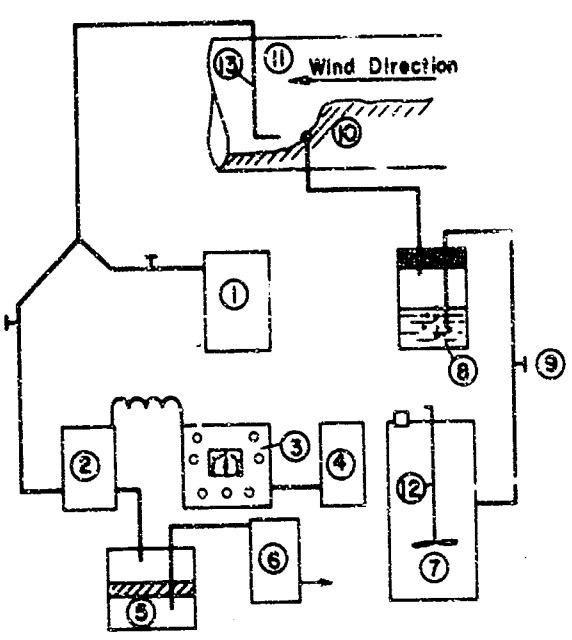

Fig. 4. The experimental layout

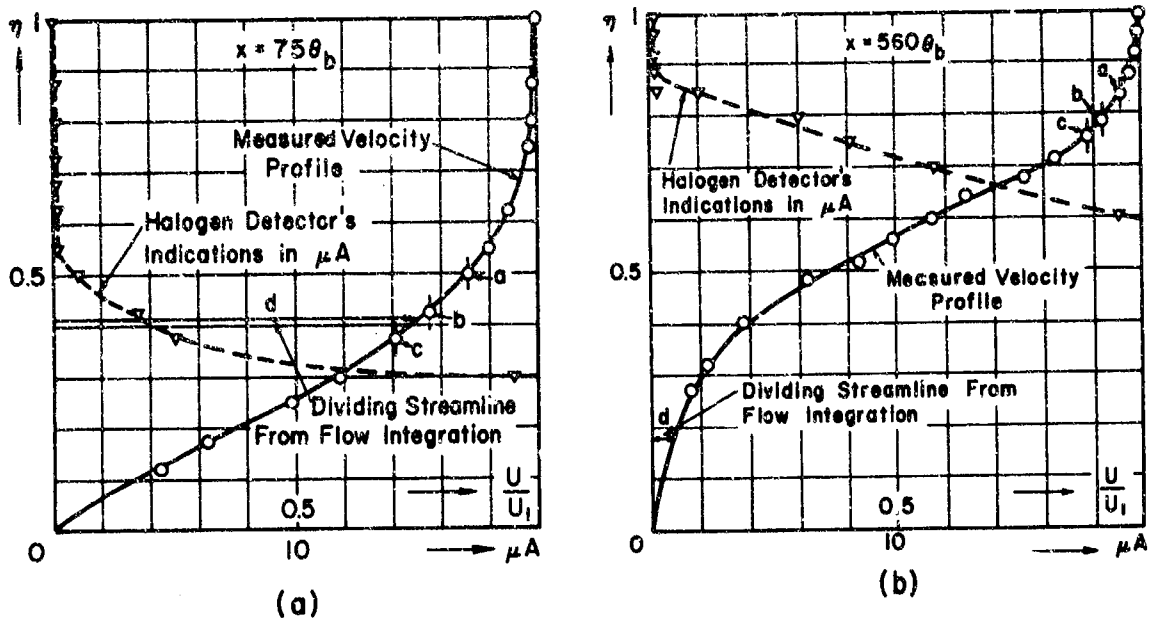

Fig. 5. The dividing streamline and leak detector's ammeter readings within a Freon contaminated shear layer. Distance behind the step a) $x = 75\theta_b$, b) $x = 560\theta_b$. (Transition upstream)

The Vertical Transfer of Momentum through the Boundary Layer

by

F. B. Smith

Meteorological Office, United Kingdom

Summary

The basic problem in analysing the wind profile and shearing stress profile in the atmospheric boundary layer is that insufficient soundly-based equations are available. This paper reviews some of the methods that have been adopted to close the solution, with particular reference to neutral stability conditions. A method, similar to one of those reviewed, is investigated in more detail. It is essentially an extension of von Karman's dimensional relationship between the diffusivity K and the wind profile applicable to the surface layers, extended to apply throughout the whole boundary layer by taking into account the turning of the wind. Solutions which bear a reasonable similarity with empirically determined profiles can be obtained if von Karman's constant is multiplied by a factor which is equivalent to reducing it by just over 10%. This change is in the right sense to correct for biases introduced in the derivatives by the finite difference scheme.

1. The significance of the atmospheric boundary layer to many meteorological processes and to other of man's interests: building structures, aircraft, the dispersal of pollutants and so on, hardly needs to be emphasised.

Unfortunately the considerable range of factors that are of importance is so great that the structure of the boundary layer, and particularly the variation of wind with height, can be extremely irregular and complex.

These factors include the varying nature of the underlying surface and the distribution of thermal stability within the layer.

It may be that we can never hope to specify in every detail the character of the boundary layer in these complicated circumstances, but at least a greater understanding than is available at present must be our continuing aim.

The first step is clearly to try to understand and predict the variation of wind velocity and shearing stress with height in horizontally uniform conditions, when the geostrophic wind is constant with height and when the stability is either neutral or simply specified by some kind of buoyancy parameter (e.g. the heat flux or the Monin-Obukhov length L). This is no new problem, of course, and solutions involving assumptions of one kind or another have been available from the time of Ekman onwards.

The surface layer in which by definition the turning of the wind (and hence the Coriolis force) may be ignored, and the vertical fluxes are virtually constant with height, has received most attention. Much effort has gone into both experimental and theoretical studies to determine the relation between the fluxes and the respective vertical gradients. Fairly definite values of $\varphi_s(z/L)$ in the relation:

$$F_s = \rho u_* k z \frac{\partial s}{\partial z} \Big/ \varphi_s\left(\frac{z}{L}\right) \qquad (1)$$

have been given by, amongst others, Dyer (1968), in both neutral ($\varphi_s = 1$) and unstably stratified conditions, for heat, water vapour and momentum (although there remain some doubts about the latter due to uncertainties in the u_* measurements).

Above the surface boundary layer is the Ekman layer where the wind gradually turns from its surface direction to the direction of the frictionless wind (sometimes the geostrophic wind) which exists outside the boundary layer. It is in this region that most research is now centred. Perhaps the most immediately relevant information can be obtained fairly simply, namely how the shearing stress at the surface is related to the geostrophic wind and the surface roughness. The form of the relation is obtained by a dimensional analysis of the internal and external parameters that define the boundary layer structure except that certain universal 'constants' dependent only on stability have to be determined empirically. The external parameters are f, the Coriolis parameter; G, the geostrophic or frictionless wind; z_0, the roughness parameter; $\delta\theta$, the potential temperature difference through the boundary layer, and similar parameters for water vapour. The internal parameters are u_*, the surface friction velocity; α, the angle between the surface wind and the isobars; H, the heat flux; h, the height of the boundary layer defined in some sense or other; L, the Monin-Obukhov length; and T_* defined by $u_* T_* \equiv \overline{w'\theta'}$. Not all these parameters are independent of each other and it can be assumed on dimensional grounds that

$$\frac{u_*}{G} = F\left[\frac{f z_0}{u_*}, \frac{z_0}{L}\right] \qquad (2)$$

and

$$\frac{u}{u_*} = F\left[\frac{z}{z_0}, \frac{z_0}{L}, \frac{f z_0}{u_*}\right] \qquad (3)$$

Following Blackadar (1967), we may expand this latter equation with respect to the very small surface Rossby number $f z_0 / u_*$, the expansion being valid for z not too large, and the complementary equation for $(G-u)/u_*$ also in terms of powers of $(f z_0 / u_*)$, valid provided z is not too small. It is argued that the two regions of validity overlap because the Rossby number is sufficiently small, and in this overlap region, retaining only the dominant terms in each expansion, the u-profiles must be identical.

Universal identity is achieved provided

$$\frac{G}{u_*}\cos\alpha = \frac{1}{k}\left[\ln\frac{u_*}{f z_0} - A\left(\frac{z}{L}\right)\right] \qquad (4)$$

$$\frac{G}{u_*}\sin\alpha = -\frac{1}{k}B\left(\frac{k}{fz_0}\right) \qquad (5)$$

These relations are reasonably well supported by experimental data in neutral stability conditions. Figure 1 shows u_*/G plotted against $\log_{10}(G/fz_0)$ and a line of best-fit subjectively drawn through the scatter of points. The data come from Blackadar (1962).

Figure 2 gives $\sin\alpha$ as a function of u_*/G. These points come from Monin and Zilitinkevich (1967).

Best fit lines drawn on these figures are then used to obtain the points in Figures 3 and 4 in order to test equations (4) and (5). and it can be seen that if $A/k = 3$ and $B/k = 8.75$ then reasonable consistency is achieved. Figure 4 suggests that $(G/u_*)\sin\alpha$ may vary slowly with (u_*/G) but this is not very significant over the range from $(u_*/G) = 0.02$, appropriate to ice or mud flats, to $(u_*/G) = 0.05$, for rough terrain.

It is only fair to say that others who have examined this kind of data have given values of A ranging from 1.2 to 4 and of B from 2 to 8 and these discrepancies may have arisen because, as Monin and Zilitinkevich (1967) have shown, A and B vary quite rapidly with stability. However, since A appears to be only about 10% of $\ln(u_*/fz_0)$ these uncertainties may not be too serious.

In non-neutral conditions more data are required to clarify the relation between the temperature scale T_* and the average lapse rate in the boundary, so that such empirical and theoretical relations which are available for the heat input may be objectively examined.

So, at the surface we can make fairly reasonable predictions of the friction velocity u_* in simple, perhaps rather idealistic, circumstances. An understanding of what is going on in the interior of the layer is harder to obtain. There is the experimental problem of obtaining ideal profiles due to upstream effects. Then there is the theoretical problem that insufficient soundly-based equations exist to complete the set required for solution. Even in stationary, horizontally homogeneous, neutral conditions there are essentially five independent unknowns, the two components of velocity, the two components of shearing stress and a parameter describing the turbulence (which might be the length-scale l, or the diffusivity K or some other parameter). To solve this set five independent equations are needed. The two momentum equations are available, and linear in the ideal conditions and there are two flux-gradient relationships of type (1) which are generally considered acceptable in spite of certain theoretical objections.

Various choices exist for the final fifth equation. All these are empirical or semi-empirical in nature. The first method starts from the basic equations of motion. The Friedmann-Keller equations which express the time rates of change of u'^2, v'^2, T'^2, $u'T'$, etc, are derived from these basic equations. Simplification is then made in a variety of ways until the number of unknowns equals the number of equations so that a solution is, in theory at least, possible. These simplifications, although often fairly drastic, are not without some justification; for example terms involving the coriolis parameter f are neglected on the grounds that f effects the mean wind profile most directly and only implicitly the turbulent fluctuation terms.

Even after all these simplifications, a solution is very difficult to obtain and although the method is not without its interest and rewards, for most purposes it seems much too cumbersome for general use. Most of this work has been carried out by Monin and is described in a series of papers (1965 (a), (b), and (c)).

A rather more practical method involves the use of the semi-empirical energy equation:

$$K_m\left[\left(\frac{du}{dz}\right)^2+\left(\frac{dv}{dz}\right)^2\right] - K_H\frac{g}{\theta}\frac{d\theta}{dz} + \frac{d}{dz}\left[K_b\frac{db}{dz}\right] = \varepsilon \qquad (6)$$

where θ = potential temperature, b = turbulent energy, ε = energy dissipation and K_m, K_H and K_b are the diffusivities for momentum, heat and energy respectively. The first term represents the production of turbulent energy by wind shear, the second the work done against buoyancy forces and the third the effect of diffusion of energy from other heights. Together with the energy equation of a series of dimensional relationships are involved, based on the so-called hypothesis of approximate similarity:

$$K_m = \sqrt{b}\,l, \quad K_H = a_\theta K_m, \quad K_b = a_b K_m \text{ and } \quad \varepsilon = ab^{3/2}/l \qquad (7)$$

where a_θ, a_b and a are taken as universal constants. As can be seen, an extra parameter is added here, namely the turbulent length-scale l. So in neutral conditions, when the buoyancy term is zero, equation (6) and (7) represent three new equations with the addition of three new variables b, ε and l (assuming a and a_b are known), and therefore we are still in the situation of having one more variable than equation.

One apparently satisfactory solution to the problem is to relate the turbulent energy b to the local friction velocity $[\tau_x^2 + \tau_y^2]^{1/4}/\sqrt{\rho}$. This assumption has been made by, amongst others, E. Peterson (1969) in a rather different context, with results that appear quite satisfactory.

Alternatively one may specify in some way or other the variation of the length-scale l with height. The simplest of these is to use a purely empirical relationship $l = l(z)$. Another way is to assume that $l(z)$ is itself determined by, or reflects, the vertical variation of wind shear or energy dissipation. We may visualise this in the following way. The instability of the vertical wind shear gives rise to a certain field of turbulence. This process is, in part, represented in mathematical form by the flux-gradient relationships. But we can go further. The transfer of momentum which results due to the existence of the turbulence sets out to modify the wind profile until some sort of equilibrium is established between the turbulent length-scale and the local curvature of the wind profile. In non-neutral conditions buoyancy forces almost certainly complicate the picture further, but in neutral conditions the argument recalls Karman's relation applicable to the surface layer:

$$l = -k \frac{du}{dz} \Big/ \frac{d^2u}{dz^2} \tag{8}$$

But in the present study l can be much more general than this. This of course raises questions of uniqueness and these remain to be answered, but since (8) satisfies the well-known relations in the constant-flux surface layer any more general formula has to conform to (8) at small z.

The most common way of generalising (8) is to write

$$l = -k \Psi \Big/ \frac{d\Psi}{dz} \tag{9}$$

where Ψ may be the wind shear $[(\frac{du}{dz})^2 + (\frac{dv}{dz})^2]$ or ε/K_m as obtained from some or all of the terms on the lefthand side of equation (6).

A series of papers investigating the solution of this set of equations with varying degrees of complexity and applicable to neutral and non-neutral stability conditions have appeared, starting with Monin (1950) and carrying on with Rusin (1975), Zilitinkevich and Laiktman (1965), Zobyleva, Zilitinkevich and Laiktman (1965). We cannot go into details here, but the general conclusion appears to be that the solutions fit the data reasonably well in the lower parts of the layer, except that u_g tends to be overestimated in some cases, but that the predicted depth of the boundary layer is much too big. For example in the last paper K_m increases up to a maximum at around 3 km in the neutral case, about ten times the expected height.

One may speculate about the reasons for this, and when the work described in the next section was begun it was thought possible that the precise form of (9) may be the cause. If Ψ is in fact the wind shear, i.e. the scalar modulus of the wind shear, then it seems rather questionable to place in the denominator the derivative of the scalar modulus rather than the modulus of the derivative of the shear vector. The latter certainly avoids one practical potential pitfall, namely that $(d\Psi/dz)$ may become zero at some height, and it also seem physically more reasonable.

In the neutral case, at least, the set of equations we need to work with may be reduced with consequent simplification of the problem. It is sufficient to retain the two equations of momentum, the two flux-gradient equations and equation (9) above or its equivalent. Historically this was the first set and problem to be investigated with the exception of the simple case when either l(z) or K(z) was specified.

As we have seen the results were not too promising. Because of this and because of the need to include the effects of buoyancy in a more direct way, the more complicated systems we have discussed above were investigated.

However since equation (9) may not be the optimum generalisation of (8) and in view of the comparative simplicity of the method, it was felt desirable to study the system yet again for neutral conditions. Monin states in one of his papers that Rusin (1963) has looked at the problem in a way which is similar to that discussed and analysed below, but to the present author's knowledge no results have been published.

2. A Simple model of the boundary layer

The very simplest and idealistic conditions are assumed, namely horizontal homogeneity of all variables except pressure, which is assumed to have a constant gradient, and a geostrophic wind which is constant with height. Conditions are assumed steady in time. Vertical velocities are ignored.

Axes are chosen so that the x-direction has components of velocity, shearing stress, friction

velocity, and geostrophic velocity equal to u, τ_x, u_* and G respectively, whereas in the y-direction the respective components are v, τ_y, v_* and 0.

The eddy diffusivity K is assumed identical in the x and y directions and has no off-diagonal components K_{xy}.

The momentum equations are

$$\rho f [u - G] = \frac{\partial}{\partial z}(\rho v_*^2) , \qquad \rho f v = -\frac{\partial}{\partial z}(\rho u_*^2) \tag{10}$$

and the flux gradient relations:

$$\tau_x = \rho u_*^2 = \rho K \frac{\partial u}{\partial z} , \qquad \tau_y = \rho v_*^2 = \rho K \frac{\partial v}{\partial z} \tag{11}$$

Defining $r(z) = \rho(z) / \rho(o)$ the following non-dimensional quantities can be formed:

$$u' = \frac{u}{G} , \quad v' = \frac{v}{G} , \quad X = r\frac{u_*^2}{G^2} , \quad Y = r\frac{v_*^2}{G^2} , \quad S = \frac{r^2 f^2 K}{G^2} \tag{12}$$

and $$\Delta z' = \frac{rf}{G} \Delta z$$

Equations (10) and (11) become

$$u' - 1 = \frac{\partial}{\partial z'} Y , \qquad v' = -\frac{\partial}{\partial z'} X \tag{10a}$$

$$X = S \frac{\partial u'}{\partial z'} , \qquad Y = S \frac{\partial v'}{\partial z'} \tag{11a}$$

The final and fifth equation, which represents our extension of equation (8) is

$$S = k^2 \frac{\left[\left(\frac{\partial u'}{\partial z'}\right)^2 + \left(\frac{\partial v'}{\partial z'}\right)^2 \right]^{3/2}}{\left[\left(\frac{\partial^2 u'}{\partial z'^2}\right)^2 + \left(\frac{\partial^2 v'}{\partial z'^2}\right)^2 \right]} \tag{13}$$

The primes will now be omitted.

Due to the presence of r in its definition (equation (12)), Δz is really proportional to an increment of pressure. Thus (13) is only equivalent to von Karman's relationship at small s provided either the variation of density (and hence r) through the surface layer can be ignored, or the long-wind profile in the surface layer really should be expressed in terms of pressure rather than in terms of height. This is probably not an issue of much importance and it suffices to state that in the surface layer, equation (13) is consistent with

$$K = k u_* z$$

where here u_* is the full friction velocity, provided r = 1.

The major problem in the solution of equations (10a), (11a) and (12) is the boundary conditions, required to define the solution, say something about the solution's nature both at the ground and at the top of the boundary layer. Short of finding an analytic solution this makes a numerical integration rather difficult to perform.

The boundary conditions are as follows:

At the ground -

(i) the shear vector (X,Y) is parallel to the limiting direction of the wind vector (u,v) as $z \to z_o$.

(ii) u and v are both zero at some specified height z_o.

At the top of the boundary layer (whose height is not a priori specified) -

(iii) $u \to G$, $v \to 0$, $X \to 0$, $Y \to 0$.

The method that has been employed is to integrate up from the surface assuming a direction and a magnitude of the surface shear vector which hopefully are consistent with a specified roughness z_0 and a geostrophic wind G. Since the earlier estimates of these properties of the shear are probably in error the solutions do not fit the upper boundary conditions and so have to be modified until a satisfactory convergence takes place.

Most of the equations are used in their integral form, being in terms of finite differences:

$$v(z+\Delta z) = v(z) + \left[Y(z+\Delta z) + Y(z)\right]\Delta z/2\, s(z+\tfrac{1}{2}\Delta z) \qquad (14)$$

$$Y(z+\Delta z) = Y(z) - \Delta z + \left[u(z+\Delta z) + u(z)\right]\Delta z/2 \qquad (15)$$

$$X(z+\Delta z) = X(z) - \left[v(z+\Delta z) + v(z)\right]\Delta z/2 \qquad (16)$$

The one equation used in differential form is:

$$s(z+\tfrac{1}{2}\Delta z) = \left[X(z+\Delta z) + X(z)\right]\Delta z/2\left[u(z+\Delta z) - u(z)\right] \qquad (17)$$

Equation (13) uses v calculated at $z-\Delta z$, z and $z+\Delta z$, u calculated at $z-\Delta z$ and z, together with a value of $s(z)$ extrapolated from $s(z-\frac{1}{2}\Delta z)$ and lower values, in order to calculate $u(z+\Delta z)$. This appears to be a very good way of finding $u(z+\Delta z)$ even if there are minor errors in the estimate of $s(z)$. But to be doubly sure when $s(z+\frac{1}{2}\Delta z)$ is determined from equation (17), a better interpolated value of $s(z)$ is found and the process repeated cyclically until convergent values of $s(z)$ and $u(z+\Delta z)$ are arrived at.

Calculations have been made with the following values:

$$G = 10\ \text{m sec}^{-1},\ k = 0.4,\ f = 10^{-4}\ \text{sec}^{-1},\ \Delta z = 5\ \text{m.},\ z_0 = 0.04\ \text{m.}$$

In the very lowest layers the wind profile is assumed logarithmic and use of this enables the scheme above to be initiated as we integrate up from $z = 0$. Inspection of equations (10) and (11) gives a schematic idea of how the solutions should appear, as demonstrated in figure 5. Equation (13), our empirical equation, thus only affects the scale and the heights at which the variables are zero or have turning values.

The shearing stress in the y-direction is the first to become negative, the u-component then reaches and exceeds its geostrophic value. Above this, the x-component of shearing stress X becomes negative and finally v should become negative before u returns to its geostrophic value.

It is also desirable that τ, the resultant of X and Y, should fall monotonically to zero, that K should reach a maximum and then fall monotonically to zero and that the implied length-scale of turbulence should reach and maintain a constant value.

These conditions are all quite demanding and closely determine the values of X and Y at the ground.

3. The results of the model

With the values of the external parameters quoted above the following conclusions may be drawn:

(i) The u component of wind only reaches its geostrophic value provided u_*/G is greater than about 0.043. Empirical evidence suggests that with a surface Rossby number given by

$$\log_{10}\left[G/fz_0\right] \simeq 6.4$$

then $u_*/G = 0.037$, $\sin\alpha_0 = 0.32$, and the wind first becomes geostrophic when $z \sim 500$ metres.

The model therefore overestimates u_* by at least 18%.

(ii) The correct behaviour of v is even more difficult to achieve. The minimum value of v depends on Y, and if Y neither goes sufficiently negative nor remains negative long enough then v cannot be brought down to zero from its low-level maximum.

It is found that v goes negative but does not return to zero if u_*/G is 0.04 or less, whereas if u_*/G is 0.0435 then v has a real minimum which is less than zero, only in the limit as $\sin\alpha_0$ approaches zero.

Obviously this implies that $\sin\alpha_0$ is much smaller than the empirically determined value, and, as a result, the heights of the key points (e.g. where K has its maximum) are too large, since the scale height increases rapidly with decreasing α_0 .

The problem appears to be then that, with the system defined precisely as ab , u(z) fails to achieve its geostrophic value at the empirically determined values of u_g and $\sin\alpha_0$ One possible explanation may be that since finite differences are being used to represent the derivatives in equation (13), a significant error may be introduced into the solutions which may be minimised by replacing von Karman's constant by a smaller value nearer 0.34. Further numerical experiments are being carried out to arrive at an optimum empirical modification of the modified k and to see whether this modification is consistent with the expected error introduced by the finite difference scheme.

The solution for $u_g/G = 0.04$, $z_0 = 0.04$ m, $k = 0.34$, $\sin\alpha_0 = 0.3$ may be described in terms of the key points in Figure 5.

(i) A: the height where Y (and hence τ_y) is first zero is at about 200 metres.

(ii) the diffusivity s (and hence K) has its maximum at 450 metres.

(iii) B: u(z) equals the geostrophic wind and Y has its maximum at about 600 metres.

(iv) C: X (and hence τ_x) is zero and u(z) has its maximum at about 800 metres.

(v) D: v(z) becomes zero and X has its minimum value at about 1400 metres.

In so far as these heights seem quite reasonable when compared with such measurements as we have, the method can claim a certain credibility although clearly many other cases need to be worked out and the k modification requires more detailed justification. It may be noted that the heights are somewhat greater than in Lettau's reanalysis of the Leipzig wind profile (e.g. K(Leipzig) has its maximum at about 250 m) and this is consistent with the slight instability noted above the surface layer which would induce precisely this kind of effect.

In conclusion then it seems that there is a very real hope that a scheme similar to the one described is capable of describing the nature of the atmosphere's boundary layer, and if after further tests this claim is verified, a comparatively practical technique for studying more complicated processes in the boundary layer will be available.

Acknowledgments

This paper is published with the permission of the Director-General of the Meteorological Office.

References

Blackadar, A. K., 1961 J.Geophys. Res., 67, 8, p.3095
1967 Report of the GARP Study Conference

Bobylova, I. M., Kilitinkevich, S. S. and Laikhtman, D. L., 1965 Academy of Sciences of the USSR, Moscow, International Colloq. of fine-scale structure of the Atmosphere.

Dyer, A. J. 1967 Quart. J.R. Met. Soc., 93, p.501

Monin, A. S. 1950 Izvestia AN SSSR, Ser. Geofis. and Geograph., 14, 3, p.232
1965 (a) Izvestia AN SSSR, Ser. Atm. and Oceanic Phys., 1,1, p.45
1965 (b) Ibid, 1,3, p.258
1965 (c) Ibid, 1,5, p.490

Monin, A. S., and Kilitinkevich, S. S. 1967 Report of the GARP Study Conference

Petersen, E. W. 1969 Pennsylvania State Univ., Center for Air Environment Studies, Publ. No. 102-69

Monin, M. L. 1963 Trudy, All-Union Scientific Meteorological Conference, 7, Gidrometeoizdat

Kilitinkevich, S. S. and Laikhtman, D. L. 1965 Izvestia, Ser. Atm. and Oceanic Phys., 1,2, p.150

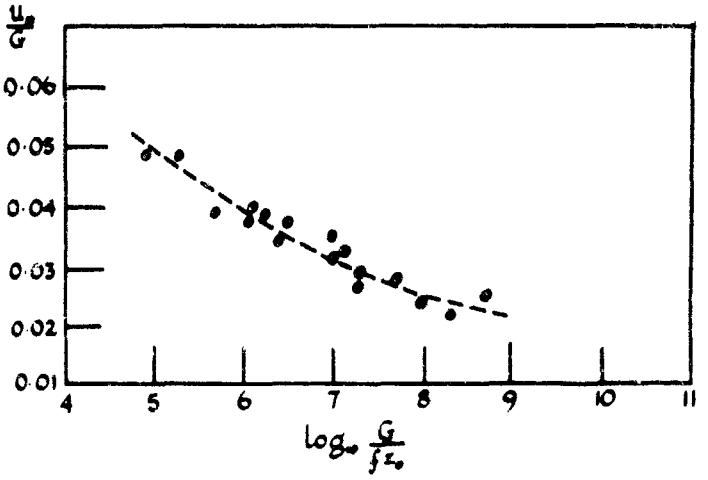

Fig. 1 The geostrophic drag coefficient

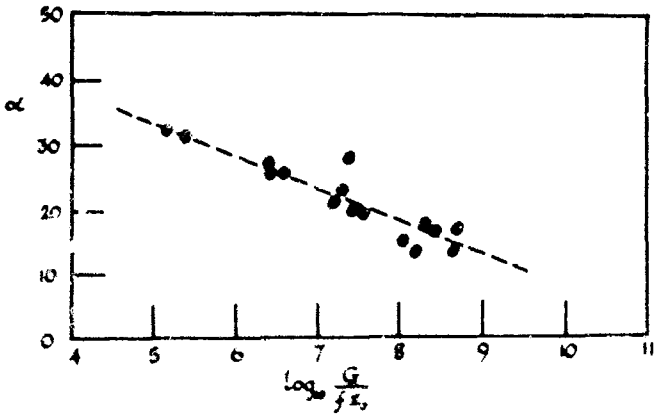

Fig. 2 Turning of surface wind, α

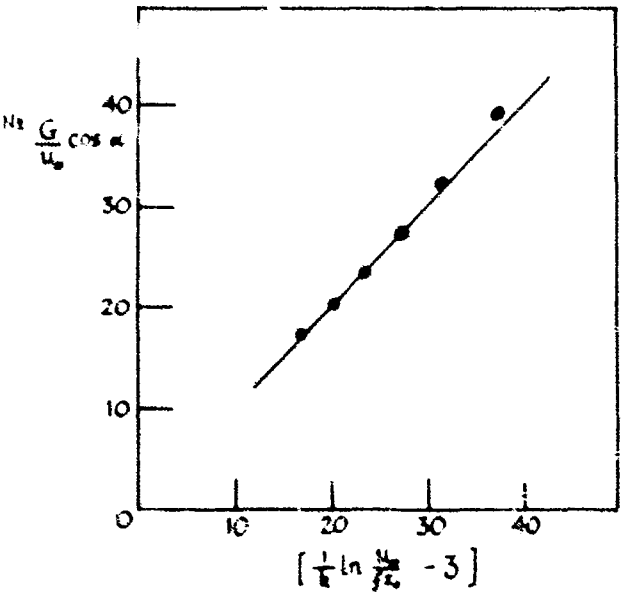

Fig 3 Test of "similarity" prediction

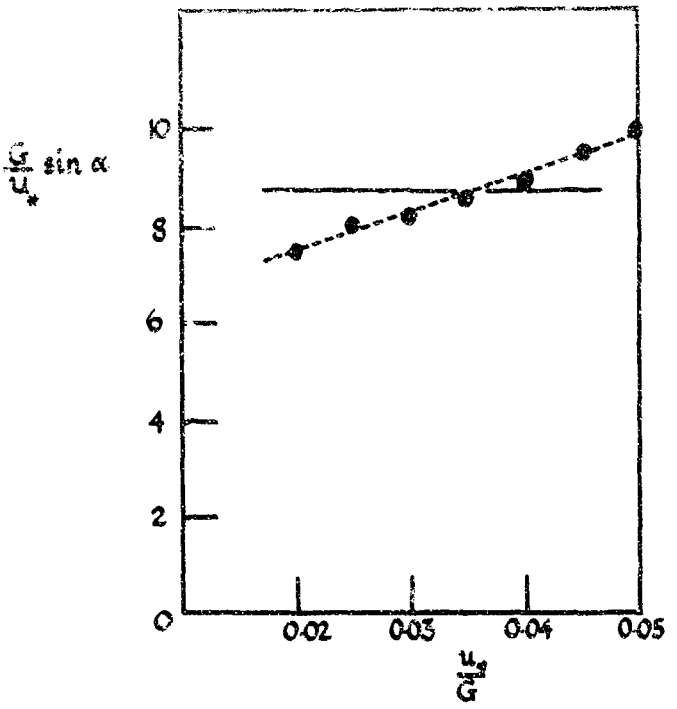

Fig.4 Second test of "similarity" prediction

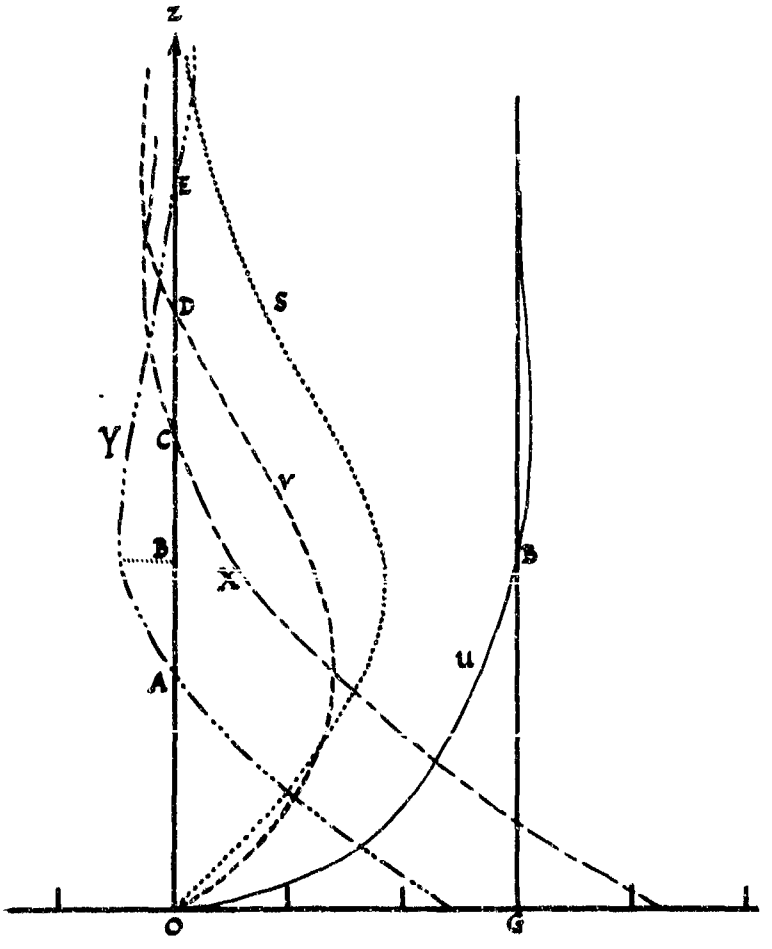

Fig.5 Schematic profiles of u, v, X, Y and s

THE ORIENTATION OF VORTICES DUE TO INSTABILITY OF THE EKMAN - BOUNDARY LAYER

F. Wippermann

Technische Hochschule Darmstadt (Germany)
Department of Meteorology

Summary

In an unstable EKMAN boundary layer vortex rolls are formed; their axes are orientated almost longitudinally, they include an angle ε of about 14° to the left with the direction of the geostrophic flow. The analogy of these vortices to the TAYLOR-GÖRTLER vortices on a concave wall and/or to the thermo-convective vortices due to a heated wall will be shown. Sometimes a superimposed second vortex system is observed whose axes are orientated in a more transversal direction. The spacing of these vortices is larger than that one or the more longitudinal vortices. The main part of this paper is concerned with deriving a formula relating the foremen-tioned angle ε to the ratio of the wavenumbers of the two vortex systems. This formula has been verified by laboratory experiments.
An application of this formula to cloud streets and seif-dunes is given; the gross-features of the last ones can be explained by vortices due to EKMAN layer instability.

I. Introduction

In recent years pictures from satellites, mainly those from Gemini and Apollo space vehicles flying in lower altitudes, have shown that clouds of the cumulus type are much more arranged in patterns of cloud rows (cloud streets) as one has thought before. Figure 1 gives such a picture of cloud streets over Georgia and South Carolina; the lateral distance of the cloud streets in this case averages to 3.2 km. They extend in the longitudinal direction for more than 150 km.

A very similar phenomenon seems to be given by the seif-dunes. These are straight and parallel chains of dunes extending often for more than 100 km in the longitudinal direction and having a lateral distance of a few kilometers too. Their height above the basis is mainly between 50 m and 100 m, they are called seif-dunes in Egypt, Yardangs in Persia, 'urqs in Arabia and alâb (sing.: elb) in Mauretania. Figure 2 shows a photograph of such dunes in the Arabian desert as seen from Gemini IV.

For a possible explanation of the formation of cloud streets or seif-dunes the vortex rolls could be used, which are caused by an instability of the atmospheric boundary layer. As a rough approximation the flow in this boundary layer may be assumed to be of the EKMAN type. In the schematic figure 3 it is shown how the formation of cloud streets and/or seif-dunes by such vortex rolls could be understood. From the observations of sea gulls WOODCOCK (1940) has concluded, that parallel stripes of upward motion exist over the open ocean under certain atmospheric conditions. Such stripes of upwind may also be explained by the vortex rolls due to EKMAN layer instability.
For instance, for the formation of seif-dunes BAGNOLD (1945), p. 224, postulates a system of wind components perpendicular to the basic flow. The wind components given by the fommentioned vortex rolls are exactly of that kind. The (doubled) diameter of such vortex rolls as obtained by theoretical investigations is in fair agreement with the observed lateral distance of cloud streets or seif-dunes.

The vortex rolls are more or less longitudinal vortices their axis is orientated almost in the direction of the basic flow. The direction of the axis and the direction of the basic flow (geostrophic wind) form an angle to the left of the wind direction varying between 13° and 16°.
In analysis of cloud patterns PLANCK (1966) found the angle ε between the direction of cloud rows and the wind in the cloud level to be 15°. ANGELL a.o. (1968) using tetroons studied the helical circulations due to such vortex rolls and found an angle ε between the axis of the helical motion and the geostrophic flow (in 500 mb) of 13°. In laboratory experiments the angle ε between the axis of the almost longitudinal vortex rolls and the basic flow has been found to be 14° by GREGORY a.o. (1955), to be 14.7° by FALLER (1963) and to be 13° 11' by HORST (1969). As a theoretical result GREGORY a.o.(1955) gives ε = 13° 10'. FALLER and KAYLOR (1965) obtained ε theoretically depending on the Reynoldsnumber; the most frequently obtained value of ε is between 14° and 16°. Similar results show the numerical integrations by LILLY (1966).

Cloud streets will be reorientated immediately when the direction of the mean wind changes, in each case it should be possible to observe the angle ε. This angle cannot be observed for seif-dunes since these are fixed and cannot be reorientated for a changed direction of the prevailing winds. Figure 4 for instance shows a case of an alâb, where the prevailing wind coming from NE forms an angle of about 25° with the direction of the chain of dunes. The direction of the prevailing wind

in this case may be seen from the direction of motion of the barchan dunes.

Sometimes a second vortex system is superimposed on the former system of "longitudinal" vortices. This is shown for example in figure 5 which gives a schematic representation of distribution of clouds in the neighbourhood of a troughline in the easterlies; the axes of vortices of the second system seem to be almost perpendicular to the axes of the more longitudinal vortices. One notices, that the wavelength in the wind direction is much larger than in the transversal direction as it should be according to one of the main results of a theoretical investigation by KUO (1963). FALLER and KAYLOR (1966) have obtained both these vortex systems in laboratory experiments; they found that the spacing of the transversal vortex rolls is two to three times that of the vortex rolls with axis in the more longitudinal direction. They also obtained cases with the two vortex systems existing simultaneously but these pictures are not very useful to measure the two spacings and the angle ε. Very recently the double system of vortices has been investigated in laboratory experiments by HORST (1969). He creates the instable boundary layer by decelerating a rotating cylindric tank. The experiments are similar to those described by STERN (1960). Figure 9 gives a photograph of one of his experiments; looking into the rotating cylinder filled with water, the two vortex systems in the boundary layer will be seen marked by sand on the ground.

The purpose of this paper is to show how the foremantioned angle ε depends on the two wavelengths in the more longitudinal and the more transversal direction.

II. The analogy of the longitudinal vortex rolls to TAYLOR-GÖRTLER vortices and to thermo-convective vortex rolls

The longitudinal vortices caused by an instability of the EKMAN boundary layer are quite analogous to the TAYLOR-GÖRTLER vortices on a wall with concave curvature or to the vortex rolls on a plane but heated wall. The analogy between the latter two has been shown by GÖRTLER (1959). The (negative) centrifugal force in the case of a concave wall and/or the buoyancy force in the case of a heated wall have to be replaced by the Coriolis force in the atmosphere. This will be shown for an assumed parallel shear flow in the atmosphere (not for an EKMAN shear flow as it should be when Coriolis forces are acting).
In a coordinate system with a concave curved x-axis, the y-axis horizontal and the z-axis in the vertical direction (as usual in meteorology) the equations of motion and the continuity equation are:

$$u_t + v u_y + w u_z - \frac{uw}{R} - fv + f^* w \cos\lambda = + K\left(u_{yy} + u_{zz} - \frac{1}{R} u_z\right) \tag{1a}$$

$$v_t + v v_y + w v_z + fu - f^* w \sin\lambda = -\frac{1}{\rho} p_y + K\left(v_{yy} + v_{zz} - \frac{1}{R} v_z\right) \tag{1b}$$

$$w_t + v w_y + w w_z + \frac{u^2}{R} + f^*(v\sin\lambda - u\cos\lambda) = g\frac{T^*}{T} - \frac{1}{\rho} p_z + K\left(w_{yy} + w_{zz}\right) \tag{1c}$$

$$v_y + w_z - \frac{w}{R} = 0 \tag{1d}$$

Herein all derivations with respect to x are put zero since the x-axis shall be the axis of symmetry for the longitudinal vortices; this means $\varepsilon = 0$ for the purpose of showing the analogy. The symbols are chosen as usual, R is the radius

of curvature of the x-axis, $f = 2\Omega \sin\varphi$ and $f^* = 2\Omega \cos\varphi$ the two Coriolis-parameters with Ω the angular velocity of the earth and φ the geographical latitude, λ is the angle between the x-axis and the west-east direction and K is the coefficient of micro-turbulent diffusion assumed to be constant. Use has been made of the BOUSSINESQ-approximation, which enables to consider the buoyancy effect due to the heated wall; T^* is the temperature deviation from the mean value in the (x,y)-plane. To close the system for the five variables u,v,w,p,T^* one needs actually a fifth equation (the energy equation). This is avoided by assuming that T^* does not depend on z.

By restricting the considerations to a flow in the layer near the wall (i.e.: $z \ll R$) one has

$$\left|\frac{u}{R}\right| \ll |u_z| \quad , \quad \left|\frac{v}{R}\right| \ll |v_z| \quad , \quad \left|\frac{w}{R}\right| \ll |w_z|$$

by which all terms containing R may be neglected, except the term $\frac{w}{R}$ in the equation for w.

Using a basic current in the x-direction ($\bar{u} = u(z)$, $\bar{v} = \bar{w} = 0$) one obtains a set of four equations for the perturbations u', v', w', p' . These perturbations are assumed to be of the form

(2a) $$f'(y,z,t) = \hat{f}(z) \exp\{ik(y-ct)\} \quad , \quad k = \frac{2\pi}{L}$$
$$\text{for } f' = u', v', w', p'$$

(2b) $$T^*(y,t) = \hat{T}^* \exp\{ik(y-ct)\} \quad ;$$

one obtains the following wavenumber equations:

(3a) $$ikc\hat{u} - \bar{u}_z\hat{w} - f\hat{v} + f^*\hat{w}\cos\lambda = K(\hat{u}_{zz} - k^2\hat{u})$$

(3b) $$ikc\hat{v} + f\hat{u} - f^*\hat{w}\sin\lambda + ik\frac{\hat{p}}{\rho} = K(\hat{v}_{zz} - k^2\hat{v})$$

(3c) $$ikc\hat{w} + \frac{2}{R}\bar{u}\hat{u} + f^*(\hat{v}\sin\lambda - \hat{u}\cos\lambda) + \frac{1}{\rho}\hat{p}_z - g\frac{\hat{T}^*}{T} = K(\hat{w}_{zz} - k^2\hat{w})$$

(3d) $$ik\hat{v} + \hat{w}_z = 0$$

After having eliminated $\hat{v}$ in (3a), (3b) and (3c) by making use of (3d) and having eliminated $\hat{p}$ by cross-derivation of (3b) and (3c) one obtains

(4a) $$\frac{K}{k^2}\hat{w}_{zzzz} - (i\frac{c}{k} + 2K)\hat{w}_{zz} + (Kk^2 + ikc)\hat{w} =$$
$$= -i\frac{f}{k}\hat{u}_z + f^*\hat{u}\cos\lambda - \frac{2}{R}\bar{u}\cdot\cdot - g\frac{\hat{T}^*}{T}$$

(4b)
$$-K\hat{u}_{zz} + (Kk^2 + ikc)\hat{u} = i\frac{f}{k}\hat{w}_z - f^*\hat{w}\cos\lambda - u_z\hat{w}$$

The system (4a), (4b) for the two variables $\hat{w}$ and $\hat{u}$ shows the effects to be studied by the three last terms of the right hand side of equ. (4a):

(5) $$f^* \hat{u} \cos\lambda - \frac{2}{R} \bar{u} \hat{u} + g \frac{\hat{T}^*}{T}$$

This shows, that the vertical component of the Coriolis force acts in the same manner as the (negative) centrifugal force or the buoyancy force. This component of the Coriolis force is different from zero as long as the perturbated horizontal motion has a component parallel to the basic current and as long as the direction of the latter one is not exactly meridional.
The horizontal component of the Coriolis force appearing in (4a) belongs to the imaginary part of the equation, the term $\frac{if}{k} \hat{u}_z$ has the effect of coupling the two equations.
This conclusion is in contradiction to that one by BARCILON (1965) that the Coriolis-force does not effect the stability at least for large Reynoldsnumbers.

For the system (4a, 4b) three essential cases can be distinguished:

(a) $f = f^* = 0$, $\hat{T}^* = 0$ — flow along a concave wall; on the right-hand side of equ. (4a) only the third term is acting, representing the centrifugal forces. In this case (4a) and (4b) give exactly the equations (2.4.1.) and (2.4.2.) investigated by GÖRTLER (1940), if the real part c_r of the phase velocity vanishes and the imaginary part is put $c_i = -\frac{\beta}{k^2}$

(b) $f = f^* = 0$, $R \to \infty$ — flow along a plane wall which is heated ($\hat{T}^* > 0$). Only the last term on the right hand side of equ. (4a) is relevant.

(c) $\hat{T}^* = 0$, $R \to \infty$ — flow along a plane and non-heated wall, Coriolis forces are acting; now the second term on the right-hand side of equ. (4a) plays an important role.

For the atmospheric boundary layer in general the conditions are those of case (c), but often (mainly over land) the buoyancy force due to the heated earth surface and the Coriolis force act together in producing longitudinal vortices in the unstable boundary layer flow. Photographs from satellites prove this in showing well developed cloud streets which are interrupted over large lakes, where thermal convection is prohibited.
For the conditions of case (b) longitudinal vortex rolls have been produced in laboratory experiments already by AVSEC (1939); it is worth while to mention that AVSEC has obtained also transversal vortex rolls, of course in separate experiments.

III. The longitudinal vortex rolls in the EKMAN boundary layer

In the EKMAN boundary layer ($|\bar{V}_g| = \bar{u}_g$, independent of height) the basic current is no longer parallel as assumed for the derivation of (4a) and (4b), but

(6a) $$\bar{u}(z) = |\bar{V}_g| \left\{ 1 - \exp\left(-\sqrt{\frac{f}{2K}}\, z\right) \cos\left(\sqrt{\frac{f}{2K}}\, z\right) \right\}$$

(6b) $$\bar{v}(z) = |\bar{V}_g| \exp\left(-\sqrt{\frac{f}{2K}}\, z\right) \sin\left(\sqrt{\frac{f}{2K}}\, z\right)$$

or in a coordinate system ($\overset{*}{x}$, $\overset{*}{y}$, z), which is rotated about an angle ε around the z-axis and whose $\overset{*}{x}$-axis forms therefore the angle ε with the direction of the geostrophic wind (x-axis)

(7a) $$\overline{\overset{*}{u}}(z) = |V_g| \left\{ \cos\varepsilon - \exp\left(-\sqrt{\frac{f}{2K}}\, z\right) \cos\left(\sqrt{\frac{f}{2K}}\, z + \varepsilon\right) \right\}$$

(7b) $$\overline{\overset{*}{v}}(z) = |V_g| \left\{ \sin\varepsilon - \exp\left(-\sqrt{\frac{f}{2K}}\, z\right) \sin\left(\sqrt{\frac{f}{2K}}\, z + \varepsilon\right) \right\}$$

In such a coordinate system, where the axis of the vortices has the direction of the $\overset{*}{x}$-axis (all the derivatives with respect to $\overset{*}{x}$ vanish) the set of wavenumber equations analogous to (4a, 4b) without regarding the effect of a curved wall and of thermo-convection is:

(8a) $$K\left\{\hat{\psi}_{zzzz} - 2k^2\hat{\psi}_{zz} + k^4\hat{\psi}\right\} - ik\left\{(\overline{\overset{*}{v}} - c)\left[\hat{\psi}_{zz} - k^2\hat{\psi}\right] - \overline{\overset{*}{v}}_{zz}\hat{\psi}\right\} = -f\hat{\overset{*}{u}}_z - ikf^*\cos\lambda\,\hat{\overset{*}{u}}$$

(8b) $$K\left\{\hat{\overset{*}{u}}_{zz} - k^2\hat{\overset{*}{u}}\right\} - ik\left\{(\overline{\overset{*}{v}} - c)\hat{\overset{*}{u}} + \overline{\overset{*}{u}}_z\hat{\psi}\right\} = f\hat{\psi}_z + ikf^*\cos\lambda\,\hat{\psi}$$

Herein ψ' is the perturbation of the streamfunction in the $(\overset{*}{y},z)$-plane, $\overset{*}{u}'$ the deviation of the velocity component in the $\overset{*}{x}$-direction; for both these quantities the form of a moving harmonic wave is assumed

(9a) $$\psi'(y,z,t) = \hat{\psi}(z)\exp\left\{ik(y-ct)\right\}$$

(9b) $$\overset{*}{u}'(y,z,t) = \hat{\overset{*}{u}}(z)\exp\left\{ik(y-ct)\right\}$$

With respect to the small scale of the vortices the variation of f and f^* with geographical latitude has been neglected ($f_y = f^*_y = 0$).

The lefthand side of (8a) is the ORR-SOMMERFELD equation for a motion in the $(\overset{*}{y},z)$-plane; the two terms on the righthand side couple the two equations (8a, 8b).

For $\overline{\overset{*}{u}}$ and $\overline{\overset{*}{v}}$ and their derivatives with respect to z in (8a, 8b) the expressions (7a) and (7b) have to be used. This has been done by LILLY (1966), who solved the equations (8a, 8b) numerically in order to find critical values of the triple (Re, k, ε) for the transition ($c_i = 0$) from stable to unstable conditions of the EKMAN boundary layer. For the Reynoldsnumber

(10) $$Re = \frac{|V_g|\, h_n}{K}$$

was used with $h_n = \sqrt{\frac{2K}{f}}$, see (6a, 6b).

LILLY's equations, of course, do not include the last term in (8a) and the last one in (8b); they are neglected as common in meteorology for large scale atmospheric motions. As shown in (4a) and (5) these terms may be important for the formation of the vortices; there is some doubt if neglection is justified in

this case.

Apart from this the numerical results show an angle $\varepsilon \neq 0$; since ε is also observed in the atmosphere and obtained in laboratory experiments, the question arises how this angle ε (between the axis of the vortex rolls and the geostrophic flow) can be understood.

IV. The angle between EKMAN-flow and the geostrophic flow

A simple explanation would be that this angle ε is determined by the direction of the actual flow averaged vertically over the total EKMAN layer. As height of the EKMAN layer one defines the height z_N , where $\bar{v}(z)$, see (6b), vanishes for the first time, i.e.:

$$z_N = \pi \sqrt{\frac{2K}{f}} = \pi h_N \quad , \tag{11}$$

see (10). If the vertical mean value is symbolized by

$$\widehat{(\cdots\cdots)} = \frac{1}{\pi h_N} \int_0^{\pi h_N} (\cdots\cdots)\, dz$$

one gets for the averaged wind direction expressed by the angle δ

$$\hat{\delta} = \operatorname{arc\,tg}\left(\frac{\hat{v}}{\hat{u}}\right) \simeq \operatorname{arc\,tg}\frac{\hat{v}}{\hat{u}} \tag{12}$$

Using (6a) and (6b) in (12) one obtains

$$\hat{u} = |V_g| \left\{ 1 - \frac{1}{2\pi}(1 + e^{-\pi}) \right\}$$

$$\hat{v} = |V_g| \frac{1}{2\pi}(1 + e^{-\pi})$$

and therefore

$$\hat{\delta} = 11^\circ 46' \tag{13a}$$

Another figure can be obtained for the angle between the geostrophic flow and the actual flow in the middle of the EKMAN layer, i.e. for $z = \pi\sqrt{\frac{K}{2f}}$. One gets

$$\delta_{(z=\pi\sqrt{\frac{K}{2f}})} = 11^\circ 42' \tag{13b}$$

These figures for ε are some what small compared with the angles obtained in laboratory experiments or observed in the atmosphere.

V. The angle between the axis of the more longitudinal vortices and the basic current

In this section it shall be shown how the angle ε is related to the wavelength of the more longitudinal vortices and also to the wavelength of a superimposed vortex system; it is assumed that the axes of the two vortex systems are orthogonal.

At least in this case of two existing (orthogonal) vortex systems it can be shown that also for a parallel shear flow ($\delta' \neq 0$) the angle $\varepsilon \neq 0$; this means ε cannot be explained by a $\bar{\zeta} \neq 0$ as tried in section IV.

In the laboratory the effect of Coriolis forces is most easily simulated by experiments with rotating dishpans. This is also the reason for using a modified cylindrical coordinate system consisting of logarithmic spirals and spirals orthogonal to them as may be seen in figure 10; such spirals should be useful to handle the vortex axes deviating from the circular basic current. The NAVIER-STOKES equation and the continuity equation will be transformed into this coordinate system (σ, η, z) starting from a system of pure cylindrical coordinates (r, ϑ, z); the transformation relations are:

(14a) $$\sigma = \left(r\, e^{-\alpha\vartheta} \right)^{\frac{1}{1+\alpha^2}}$$

(14b) $$\eta = \frac{1}{1+\alpha^2} \left(\alpha \ln r + \vartheta \right)$$

(14c) $$z = z$$

The parameter α , more clear in the inverse relations

(15a) $$r = \sigma\, e^{\alpha\eta}$$

(15b) $$\vartheta = \eta - \alpha \ln \sigma$$

gives the angle γ between the logarithmic spiral and the circle by

(16a) $$\tau_1 = \arctg \frac{1}{\alpha}$$

(16b) $$\tau_2 = \arctg \alpha$$

(16c) $$\gamma = \operatorname{arccotg} \alpha$$

see figure 6. In the following the abbreviation

(17) $$\beta \equiv \frac{e^{-\alpha\eta}}{\sqrt{1+\alpha^2}}$$

will be used where

(18a,b) $$\frac{1}{\sqrt{1+\alpha^2}} = \cos(\tau_2) \qquad \frac{\alpha}{\sqrt{1+\alpha^2}} = \sin(\tau_2)$$

From (15a), (17) and (18a) it is seen that

(19) $$\frac{\beta}{\sigma} = \frac{\cos(\tau_2)}{r}$$

With the assumption K = const, necessary for an EKMAN layer, the equations of motion and the continuity equation in the (σ, η, z)-system are:

(20a) $$u_t + \beta\left\{u u_\sigma + \frac{v}{\sigma}u_\eta - \frac{v^2}{\sigma} + \alpha\frac{uv}{\sigma} + \frac{1}{\delta}p_\sigma\right\} + w u_z - fv + f^* w\cos(\eta - \alpha\ln\sigma - \tau_2) -$$

$$- K\beta^2\left\{u_{\sigma\sigma} + \frac{1}{\sigma^2}u_{\eta\eta} + \frac{1}{\sigma}u_\sigma - (1+\alpha^2)\frac{u}{\sigma^2} + \frac{2\alpha}{\sigma}v_\eta - \frac{2}{\sigma^2}v_\eta\right\} - K u_{zz} = 0$$

(20b) $$v_t + \beta\left\{u v_\sigma + \frac{v}{\sigma}v_\eta - \alpha\frac{u^2}{\sigma} + \frac{uv}{\sigma} + \frac{1}{\delta\sigma}p_\eta\right\} + w v_z + fu - f^* w\sin(\eta - \alpha\ln\sigma - \tau_2) -$$

$$- K\beta^2\left\{v_{\sigma\sigma} + \frac{1}{\sigma^2}v_{\eta\eta} + \frac{1}{\sigma}v_\sigma - (1+\alpha^2)\frac{v}{\sigma^2} - \frac{2\alpha}{\sigma}u_\sigma + \frac{2}{\sigma^2}u_\eta\right\} - K v_{zz} = 0$$

(20c) $$w_t + \beta\left\{u w_\sigma + \frac{v}{\sigma}w_\eta\right\} + w w_z + \frac{1}{\delta}p_z + g - f^*\left\{v\sin(\eta - \alpha\ln\sigma - \tau_2) - u\cos(\eta - \alpha\ln\sigma - \tau_2)\right\} -$$

$$- K\beta^2\left\{w_{\sigma\sigma} + \frac{1}{\sigma^2}w_{\eta\eta} + \frac{1}{\sigma}w_\sigma\right\} - K w_{zz} = 0$$

(20d) $$\beta\left\{u_\sigma + \frac{u}{\sigma} + \frac{1}{\sigma}v_\eta - \frac{\alpha}{\sigma}v\right\} + w_z = 0$$

A homogeneous medium ($\varrho = \bar{\varrho}$) is considered.
The three components of the vorticity are:

(21a) $$m = i\frac{\beta}{\sigma}w_\eta - v_z$$

(21b) $$n = u_z - \beta w_\sigma$$

(21c) $$q = \frac{\beta}{\sigma}\left\{(\sigma v)_\sigma - u_\eta - \alpha u\right\}$$

where (21a) gives the component perpendicular to the (η, z)-plane and (21b) that one perpendicular to the (σ, z)-plane, see figure 10. By cross-derivation of (20c) and (20b) an equation for m is obtained, by cross derivation of (20c) and (20a) an equation for n; in both equations the pressure is eliminated. Considering averaged values and small perturbations (symbolized by bar and prime) one obtains the following linearized vorticity equations:

(22a) $$m'_t + \beta\left\{\bar{u}m'_\sigma + u'\bar{m}_\sigma + \frac{1}{\sigma}\bar{v}m'_\eta + \frac{1}{\sigma}v'\bar{m}_\eta + \frac{1}{\sigma}\bar{m}u' + \frac{1}{\sigma}m'\bar{u} + \frac{1}{\sigma}\bar{m}v'_\eta + \frac{1}{\sigma}m'\bar{v}_\eta + \right.$$

$$\left. + \frac{\alpha}{\sigma}n'\bar{v} - \frac{1}{\sigma}n'\bar{u}_\eta + \frac{\alpha}{\sigma}\bar{n}u' - \frac{1}{\sigma}\bar{n}u'_\eta - \bar{u}_z q' - u'_z\bar{q}\right\} +$$

$$+ \bar{w}m'_z + w'\bar{m}_z + \bar{m}w'_z + m'\bar{w}_z - fu'_z + f^* w'_z\sin(\eta - \alpha\ln\sigma - \tau_2) +$$

$$+ \frac{\beta}{\sigma}\left[f^* v'\sin(\eta - \alpha\ln\sigma - \tau_2) - f^* u'\cos(\eta - \alpha\ln\sigma - \tau_2)\right]_\eta -$$

$$- K\beta^2\left\{m'_{\sigma\sigma} + \frac{1}{\sigma^2}m'_{\eta\eta} - \frac{1+\alpha^2}{\sigma^2}m' + \frac{1}{\sigma}m'_\sigma + \frac{2\alpha}{\sigma}n'_\sigma - \frac{2}{\sigma^2}n'_\eta\right\} - K m'_{zz} = 0$$

(22b) $$n'_t + \beta\left\{\bar{u}n'_\sigma + u'\bar{n}_\sigma + \frac{1}{\sigma}\bar{v}n'_\eta + \frac{1}{\sigma}v'\bar{n}_\eta + \frac{\alpha}{\sigma}\bar{n}v' + \frac{\alpha}{\sigma}n'\bar{v} + \bar{n}u'_\sigma + n'\bar{u}_\sigma + \right.$$

$$\left. + \frac{1}{\sigma}m'\bar{v} - m'\bar{v}_\sigma + \frac{1}{\sigma}\bar{m}v' - \bar{m}v'_\sigma - \bar{v}_z q' - \bar{q}v'_z\right\} +$$

$$+ \bar{w}n'_z + w'\bar{n}_z + \bar{n}w'_z + n'\bar{w}_z - fv'_z + f^* w'_z\cos(\eta - \alpha\ln\sigma - \tau_2) -$$

$$- \beta\left[\cdots\cdots\right.$$

$$-\beta\left[\int^{\sigma} v' \sin(\eta - \alpha\ln\sigma - \tau_2)\,; - \int^{\sigma} u' \cos(\eta - \alpha\ln\sigma - \tau_2)\right]_{\sigma} -$$

$$-K\beta^2\left\{n'_{\sigma\sigma} + \frac{1}{\sigma^2}n'_{\eta\eta} - \frac{1+\alpha^2}{\sigma^2}n' + \frac{1}{\sigma}n'_{\sigma} - \frac{2\alpha}{\sigma}m'_{\sigma} + \frac{2}{\sigma^2}m'_{\eta}\right\} - K n'_{zz} = 0$$

For the basic current the assumption of a circular flow constant in time is made

(23a) $$\overline{v}_{(\phi)} = \overline{v}_{(\phi)}(r, z)$$

(23b) $$\overline{v}_{(r)} = \overline{v}_{(z)} = 0$$

which, of course, will not satisfy (20a) and (20b) for the mean values. One should be aware of that; the basic current (23) will be used for the sake of simplicity. Between the vector components in the two coordinate systems the following relationships are valid

(24a) $$A_{(\sigma)} = \frac{1}{\sqrt{1+\alpha^2}} A_{(r)} - \frac{\alpha}{\sqrt{1+\alpha^2}} A_{(\phi)}$$

(24b) $$A_{(\eta)} = \frac{\alpha}{\sqrt{1+\alpha^2}} A_{(r)} + \frac{1}{\sqrt{1+\alpha^2}} A_{(\phi)}$$

As a consequence here of regarding (23b) one has

(25) $$\overline{u} = -\alpha\overline{v}$$

(25) has been used to replace all the quantities $\overline{u}$, $\overline{m}$, $\overline{n}$, $\overline{q}$ and their derivatives by $\overline{v}$ or by the derivatives of $\overline{v}$. Because of (23b) $\overline{w} = 0$.

Considering the σ-spiral as the vortex axis and therefore as the axis of symmetry

(26a) $$(u'\sigma)_{\sigma} = 0$$

(26b) $$v'_{\sigma} = w'_{\sigma} = 0$$

the divergence in the (η, z)-plane will vanish

(27) $$\frac{\beta}{\sigma}\left\{v'_{\eta} - \alpha v'\right\} + w'_{z} = 0$$

and a streamfunction $\psi'(\eta, z)$ can be used

(28a) $$w' = -\frac{\beta}{\sigma}\psi'_{\eta} - \alpha\frac{\beta}{\sigma}\psi'$$

(28b) $$v' = \psi'_{z}$$

by which (21a) becomes

(28c) $$m' = -\frac{\beta^2}{\sigma^2}\psi'_{\eta\eta} + \frac{\alpha^2\beta^2}{\sigma^2}\psi' - \psi'_{zz}$$

Quite analogous expressions are obtained when the η-spiral is considered

as vortex axis. The derivations with respect to η have to vanish

(29a) $$\left(v' e^{-\alpha\eta}\right)_\eta = 0$$

(29b) $$u'_\eta = w'_\eta = 0$$

The vanishing of the divergence in the (σ,z)-plane

(30) $$\beta\left\{u'_\sigma + \frac{u'}{\sigma}\right\} + w'_\sigma = 0$$

allows for the use of a streamfunction $\varphi'(\sigma,z)$ by which

(31a) $$w' = -\beta\varphi'_\sigma + \frac{\beta}{\sigma}\varphi'$$

(31b) $$u' = -\varphi'_z$$

and according to (21b)

(31c) $$n' = -\beta^2\varphi'_{\sigma\sigma} - \frac{\beta^2}{\sigma}\varphi'_\sigma + \frac{\beta^2}{\sigma^2}\varphi' - \varphi'_{zz}$$

Making use of (28a), (28b) and (28c) in (22a) one obtains a differential equation for $\psi'(\eta,z,t)$ containing also $u'(\eta,z,t)$ as a further perturbation quantity.
In the same manner using (31a), (31b) and (31c) in (22b) a differential equation for $\varphi'(\sigma,z,t)$ is obtained which contains also $v'(\sigma,z,t)$. The two differential equations are:

(32a)
$$\frac{\beta}{\sigma}\left\{-2\bar v\left[\psi'_{\eta zz} + (1+\alpha^2)u'_z\right] + \bar v_z\left[\alpha\psi'_z - 2(1+\alpha^2)u'\right] + \bar v_{zz}\left[\psi'_\eta + \alpha\psi'\right]\right\} +$$
$$+ \frac{\beta^2}{\sigma^2}\left\{-\psi'_{\eta\eta t} + \alpha^2\psi'_t + K\left[2\psi'_{\eta\eta zz} - (1+2\alpha^2)\psi'_{zz} + 2u'_{\eta z} + 2\alpha u_z\right]\right\} +$$
$$+ \frac{\beta^3}{\sigma^3}\left\{\bar v\alpha^2\psi'_\eta - \bar v\psi'_{\eta\eta\eta}\right\} +$$
$$+ \frac{\beta^4}{\sigma^4}K\left\{\psi'_{\eta\eta\eta\eta} - 4\alpha\psi'_{\eta\eta\eta} + (1+2\alpha^2)\psi'_{\eta\eta} - 2\alpha(1-2\alpha^2)\psi'_\eta - 3\alpha^2(1+\alpha^2)\psi'\right\} -$$
$$- \psi'_{zzt} + K\psi'_{zzzz} = 0$$

(32b)
$$\frac{\beta}{\sigma}\left\{2\bar v\left[\alpha\sigma\varphi'_{\sigma zz} - (1+\alpha^2)v'_z\right] - \bar v_z\left[\alpha\varphi'_z + 2(1+\alpha^2)v'\right] - \bar v_{zz}\alpha\left[\sigma\varphi'_\sigma + \varphi'\right]\right\} +$$
$$+ \frac{\beta^2}{\sigma^2}\left\{-\sigma^2\varphi'_{\sigma\sigma t} - \sigma\varphi'_{\sigma t} + \varphi'_t + K\left[2\sigma^2\varphi'_{\sigma zzz} - (1+2\alpha^2)\varphi'_{zz} + 2\sigma\varphi'_{\sigma zz} - 2\alpha\sigma v'_{\sigma z} + 2\alpha v'_z\right]\right\} +$$
$$+ \frac{\beta^3}{\sigma^3}\alpha\bar v\left\{\sigma^3\varphi'_{\sigma\sigma\sigma} + 3\sigma^2\varphi'_{\sigma\sigma}\right\} +$$
$$+ \frac{\beta^4}{\sigma^4}K\left\{\sigma^4\varphi'_{\sigma\sigma\sigma\sigma} + 2\sigma^3\varphi'_{\sigma\sigma\sigma} - (3-\alpha^2)\sigma^2\varphi'_{\sigma\sigma} + (3-\alpha^2)\sigma\varphi'_\sigma - 3(1+\alpha^2)\varphi'\right\} -$$
$$- \varphi'_{zzt} + K\varphi'_{zzzz} = 0$$

According to (23a) the basic current has been specified as axi-symmetric; in

addition stationarity is now postulated for the basic current and for its dependence on r it is assumed

(33) $$\bar{v}_{(z)} = \mathcal{B}(z)\, r$$

corresponding to the inner part of a RANKINE vortex. From (33) with (24b) and (15a) one gets

(34) $$\bar{v}(\sigma,\eta,z) = \frac{\sigma}{\beta}\,\frac{\mathcal{B}(z)}{\lambda+\alpha^2}$$

Using the basic flow (34) in (32a) and (32b) in both these equations terms with β/σ as coefficient, terms with β^2/σ^2 and terms with β^4/σ^4 will appear but also terms which are free of β/σ. According to (19) β/σ is very small if r is very large. By the assumption of very large r (which may be in conflict with (33) valid only in the inner part of a RANKINE vortex) all the terms containing β^2/σ^2 and β^4/σ^4 may be neglected. Hereby the two equations are much simpler.

Equation (32a) contains ψ' and u', the second equation needed to close the system is eqn. (20a) in linearized form for the perturbation u'; in this equation the conditions (26a) and (26b) have to be used and also $p_\sigma = o$.
The form of a moving harmonic wave shall be assumed for the two perturbations

(35a) $$\psi'(\eta,z,t) = \Psi(z)\,\exp\{i\mu(\eta - c_1 t)\}$$

(35b) $$u'(\eta,z,t) = U(z)\,\exp\{i\mu(\eta - c_1 t)\}$$

Herewith one obtains for (32a) and the just described equation developed from (20a) the following set of two wave number equations:

(36) $$K\Psi_{zzzz} + i\mu\left(c_1 - \frac{2}{\lambda+\alpha^2}\mathcal{B}\right)\Psi_{zz} + \frac{\alpha}{\lambda+\alpha^2}\mathcal{B}_z\Psi_z + \frac{i\mu+\alpha}{\lambda+\alpha^2}\mathcal{B}_{zz}\Psi - (2\mathcal{B}+f)U_z - 2\mathcal{B}_z U = 0$$

(37) $$-KU_{zz} + \left\{\frac{\alpha+i\mu}{\lambda+\alpha^2}\mathcal{B} - i\mu c_1\right\}U + \frac{i\mu+\alpha}{\lambda+\alpha^2}\alpha\mathcal{B}_z\Psi - (2\mathcal{B}+f)\Psi_z = 0$$

On the other hand equation (32b) contains φ' and v'; here (20b) in linearized form and with regard of (29a), (29b) and $p_\eta = o$ gives the second equation needed to close the system. The form of a moving harmonic wave will also be assumed

(38a) $$\varphi'(\sigma,z,t) = -\Phi\,\exp\left\{i\nu\left(\frac{\ln\sigma}{\alpha} + c_2 t\right)\right\}$$

(38b) $$v'(\sigma,z,t) = V\,\exp\left\{i\nu\left(\frac{\ln\sigma}{\alpha} + c_2 t\right)\right\}$$

Herewith one obtains for (32b) and the forementioned equation originating from (20b) a set of the following two wavenumber equations:

(39) $$-K\Phi_{zzzz} + i\nu\left(c_2 - \frac{2}{\lambda+\alpha^2}\mathcal{B}\right)\Phi_{zz} + \frac{\alpha}{\lambda+\alpha^2}\mathcal{B}_z\Phi_z + \frac{i\nu+\alpha}{\lambda+\alpha^2}\mathcal{B}_{zz}\Phi - (2\mathcal{B}+f)V_z - 2\mathcal{B}_z V = 0$$

(40) $$K V_{zz} + \left\{ \frac{\alpha + i\nu}{1+\alpha^2} B - i\nu c_2 \right\} V + \frac{i\nu + \alpha}{1+\alpha^2} \frac{1}{\alpha} B_z \Phi - (2B + f) \Phi_z = 0$$

The two systems of wavenumber equations (36), (37) and (39), (40) are symmetric with the exception of the following deviations:

(a) The sign of the first term in (36) is opposite to the sign of the first term in (39)

(b) The sign of the first term in (37) is opposite to the sign of the first term in (40)

(c) In the third term of equation (37) appears the factor α but in the third term of (40) the factor $\frac{1}{\alpha}$

The first equations of each set namely (36) and (39) are completely symmetric in the inviscid case ($Re \to \infty$). Let us assume this for further comparison. This is justified by the argument that the terms containing Ψ_{zzzz} and/or Φ_{zzzz} are considered to be less important.
Then the amplitude functions $\Phi(z)$ and $V(z)$ obey the same differential equation as $\Psi(z)$ and $U(z)$; in both cases the transition to instability of the boundary layer depends on B , B_z , B_{zz} and f. If instability occurs vortex rolls of both systems should be formed where the wavenumber of the more longitudinal vortices is μ and of the more transversal vortex rolls is ν. For a comparison of these two wavenumbers one has to consider that ν should be counted along σ instead $\frac{\ln\sigma}{\alpha}$

(41a) $$\nu_{(\frac{\ln\sigma}{\alpha})} = \alpha \, \nu_{(\sigma)} \, \ell$$

where $$\ell = \frac{\ln\sigma \Big|_{\vartheta=2\pi}^{\vartheta=0}}{\sigma \Big|_{\vartheta=2\pi}^{\vartheta=0}} = \frac{2\pi}{\alpha \exp\left(\frac{2\pi}{\alpha}\right)}$$

obtained with (15b) for η = const. Therefore (41a) is

(41b) $$\nu_{(\sigma)} = \frac{\exp\left\{\frac{2\pi}{\alpha}\right\}}{2\pi} \nu_{(\frac{\ln\sigma}{\alpha})}$$

It has been concluded that the two wavenumbers $\mu_{(\sigma)}$ and $\nu_{(\frac{\ln\sigma}{\alpha})}$ become unstable at the same time and have to equal each other with respect to the symmetry of (36) and (39):

(42) $$\mu_{(\sigma)} = \nu_{(\frac{\ln\sigma}{\alpha})}$$

(42) with (41b) gives the ratio of the two wave numbers (each on the same measure)

(43) $$\frac{\nu}{\mu} = \frac{\exp\left\{\frac{2\pi}{\alpha}\right\}}{2\pi}$$

Since an axi-symmetric basic current has been chosen (23) one notices from figure 6, that $\gamma = \varepsilon$ and $\varepsilon = \frac{\pi}{2} - \tau_2$ or with use of (16b)

(44) $$\varepsilon = \operatorname{arc\,cotg}\, \alpha$$

Inserting (43) in (44) one gets the relationship between the angle ε and the wavenumber ratio

(45) $$\varepsilon = \operatorname{arc\,tg}\left\{\frac{\ln\left(2\pi\frac{\nu}{\mu}\right)}{2\pi}\right\}$$

The following table gives few values of the wavenumber ratio and the corresponding angle ε

$\frac{\nu}{\mu}$	α	ε
0.5	5.51	$11^\circ 10'$
0.72	4.17	$13^\circ 30'$
1.00	3.41	$16^\circ 20'$
2.00	2.48	$22^\circ 00'$

It is seen that for an observed angle $\varepsilon = 13^\circ 30'$ the wavelength in the longitudinal direction ξ is larger than that one in the transversal direction η, it is $L_\xi = 1.4\ L_\eta$. The experiments by FALLER and KAYLOR gave $2 \leq L_\xi / L_\eta < 3$ which would imply $\varepsilon \leq 11^\circ$ according to formula (45).

VI. The verification of formula (45) by laboratory experiments

Recent experiments by HORST (1969), very briefly described in section I, see fig. 9, allow to measure the angle ε as well as the simultaneous wavenumbers μ and ν. This has been done for a total of 72 runs giving ε, μ, ν for varied experimental parameters (diameter of the cylinder, height of the fluid, initial circular velocity, viscosity). Using the measured values of the wavenumbers μ and ν in equation (45) a "theoretical" angle ε_{th} has been computed and has been compared with the measured angle ε. The result is shown in figure 7 where the rather large scattering of points is overcome by comprehending them for equally spaced stripes. Indead, one notices a systematic deviation, however the mean values agree very well

$$\tilde{\varepsilon}_{EXP} = 13^\circ 11' \quad ; \quad \tilde{\varepsilon}_{THEO} = 13^\circ 19'$$

One should remember, that besides some other assumptions for the formula (45) orthogonality of the two vortex systems has been assumed; in the experiments the angle between the axes of the two vortex systems has not been measured, it is estimated to be about $60^\circ - 70^\circ$; this may be a reason for the systematic deviation. Also one should keep in mind that the assumption (23a) of an axi-symmetric basic current is inadequate for HORST's experiments where the basic current has a radial component depending on height and therefore is similar to an EKMAN boundary layer flow.

VII. The orientation of cloud streets and seif-dunes

There is no doubt that the cloud streets are formed by more or less longitudinal vortex rolls due to instability of the EKMAN layer; the helical motion, of course, will be intensified when thermal convection occurs and buoyancy forces are acting also. If both vortex systems are perceptible and the two wavenumbers are evaluable (as for instance from figure 5) the direction of the geostrophic flow can be determined; this would differ only very little from the direction of the mean wind at the cloud base.
Cloud streets will be reorientated immediately when the mean wind changes its direction.

A completely different situation exists with respect to the seif-dunes. These are probably formed also by the helical motion in vortex rolls due to Ekman layer instability. But the formation of seif-dunes takes a very long time in which climatic changes are possible including changes of the direction of the prevailing wind. Therefore the orientation of seif-dunes should give with about 14° to the right the direction of the wind averaged over the whole time of the formation of these dunes except those periods in which the boundary layer has not been unstable. Comparison of this direction with the wind direction given by climatological data of our time should allow conclusions on long term climatic changes.

Since the interior part of the seif-dunes is firm (only the sand of the outer part can be moved by wind) these dunes are fixed. When EKMAN layer instability occurs, the formation of vortex rolls does not take place over a plane earth surface as assumed in the theory of instability but over a waved topography prescribing already the angle ε and the wavenumber μ in the lateral direction, for which the amplitude of velocity perturbations will amplify. This means only the wavenumber ν in the more longitudinal direction is not prescribed directly by the topographic features but, of course, is determined by ε and μ according to (45). It should be

$$\nu = \mu \, \frac{\sup\{2\pi k_y \varepsilon\}}{2\pi} \qquad , \quad \varepsilon > 0 \tag{46}$$

Some values of the wavenumber ratio are given in the following table

ε	$\frac{\nu}{\mu}$	ε	$\frac{\nu}{\mu}$
10°	0.485	30°	5.31
15°	0.850	35°	13.0
20°	1.57	40°	31.9
25°	3.39	45°	86.6

To give an example: If $\varepsilon = 40°$ and the wavelength in the transversal direction $L_\eta = 3.5$ km, a wavelength in the direction along the dunes $L_\xi = 110$ m should occur. In figure 8, after CLOS-ARCEDUC (1968), one notices long chains of dunes showing a structure along these chains, which already have been cut to pieces. It seems possible to explain such a structure as the effect of the superimposed second vortex system having a rather high wavenumber because of a large value of ε. This would mean that the prevailing winds which had originally an almost east-west direction (from 85°, whereas the chains of dunes run 72° to 252°) would have turned to get a southerly component, say from 110° to 290° (i.e.: $\varepsilon = 38°$) and remained in that direction. The effect of the superimposed second vortex system now is supported by the basic current clearly shown by the sand blown to the right of the chain. It has been formed a "lefthand side type" of an Elb (after CLOS-ARCEDUC 1968).

The use of the logarithmic spirals for the coordinate system in the foregoing derivation excludes cases with $\varepsilon < 0$; however the reasoning is also possible for $\varepsilon < 0$ and allows also an explanation of the so-called "righthand side type" of an Elb.

If the prevailing wind would change for more than 45° from the original direction the vortices with their axis in the lateral direction and the vortices perpendicular to them would have to change their rôles. In this case ε and ν would be prescribed by the existing seif-dunes where μ would be determined by (45).

It is felt that the gross-features of seif-dunes can be explained by the two vortex systems due to an instability of the EKMAN boundary layer.

VIII Acknowledgment

The author wishes to thank Dr. H. FRANZ for his helpful assistance on the transformation of the equations into the (σ, η, z)-coordinate system.

IX. References

ANGELL, J.K. PACK, D.H. DICKSON, C.R. 1968 A Lagrangian Study of Helical Circulations in the Planetary Boundary Layer. J.Atm. Sc. 25, 707-717.

AVSEC, D. 1939 Tourbillons thermoconvectifs dans l'air, application à la météorologie. L'Académie de Paris, Thèse Dr.Sc. Serie A 1910,No.d'ordre 2777

BAGNOLD, R.A. 1945 The Physics of Blown Sand and Desert Dunes. London, Methuen and Co, pp 265.

BARCILON, V. 1965 Stability of a Non-divergent Ekman Layer. Tellus 17, 53-68.

CLOS-ARCEDUC, A. 1968 Emploi des couvertures photographiques aériennes pour la vérification des théories relatives à la formation des dunes allongées dans une direction voisine de celle du vent. XI^eCongrès International de Photogrammetrie Lausanne 8-20 Juillet 1968, pp 8.

FALLER, A.J. 1963 An Experimental Study of the Instability of the Laminar Ekman Boundary Layer. J.Fluid Mech. 15, 560-575.

FALLER, A.J. KAYLOR, R.E. 1965 A Numerical Study of the Laminar Ekman Boundary Layer. Tech.Note BN 410, July 1965, 26pp. Inst. Fluid Dyn., Univ. of Maryland.

FALLER, A.J. KAYLOR, R.E. 1966 Investigations of Stability and Transition in Rotating Boundary Layers. in: Dynamics of Fluids and Plasmas edited by S. Pai a.o., 309 - 329, ademic Press New York.

GÖRTLER, H. 1940 Über eine dreidimensionale Instabilität laminarer Grenzschichten an konkaven Wänden. Nachr.Ges.Wiss.Göttingen, Nachr.aus der Mathematik 2, 1, 26pp

GÖRTLER, H. 1959 Über eine Analogie zwischen den Instabilitäten laminarer Grenzschichtströmungen an konkaven Wänden und an erwärmten Wänden. Ing. Archiv 28, 71-78.

GREGORY, N. STUART, J.T. WALKER, W.S. 1955 On the Stability of Threedimensional Boundary Layers with Application to the Flow Due to a Rotating Disk. Phil.Trans.Roy.Soc., London, A 248, 155-199.

HORST, W. 1969 Experimentelle Untersuchungen der Wirbelstruktur in einer instabilen Ekman-Grenzschicht. Ph.Thesis, Inst.f.Meteorologie,Techn.Hochschule Darmstadt,Germ.

KUO, H.L. 1963 Perturbations of Plane Couette Flow in Stratified Fluid and Origin of Cloud Streets. Phys. of Fluids, 6, 195-211.

LILLY, D.K. 1966 On the Instability of Ekman Boundary Layer. J. Atm. Sc. 23, 481-494.

MALKUS, J.S. RONNE, C. 1960 Cloud distributions over the Tropical Oceans in Relation to Large Scale Flow Patterns. Geophys.Monogr., Am.Geophys.Union Nr. 5, 45-56.

PLANCK, V.G. 1966 Wind Conditions in Situations of Patternform and Non-patternform Cumulus Convection. Tellus 18, 1-12.

STERN, M.S. 1960 Instability of Ekman Flow at Large Taylor Numbers. Tellus 12, 399-417.

WOODCOCK, A.H. 1940 Convection and Soaring over the Open Ocean. J. Mar.Res. 3, 248-253.

Fig. 1 Cloud streets over Georgia and South Carolina as seen from an Apollo space vehicle

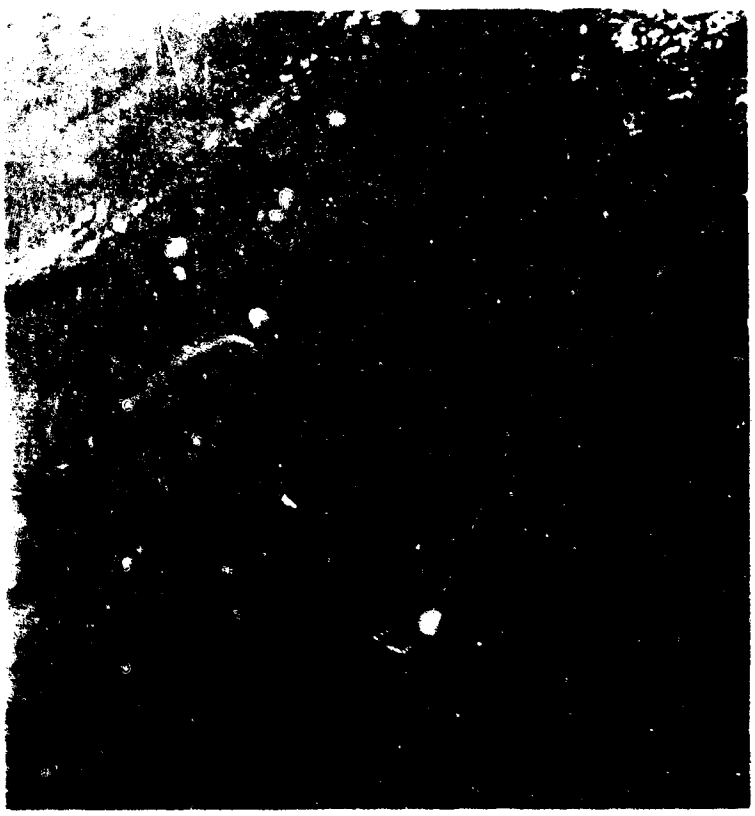

Fig. 2 Seif-dunes in the Arabian desert as seen from Gemini IV.

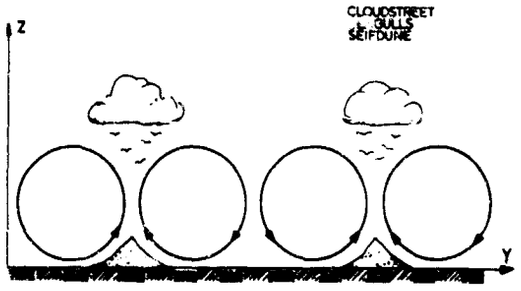

Fig.3 The formation of cloud streets and seif-dunes by longitudinal vortex rolls (schematic)

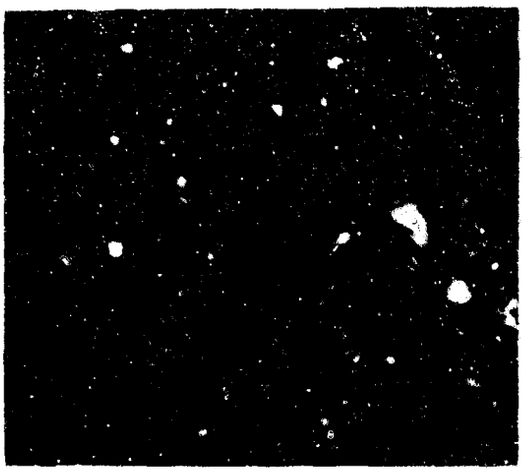

Fig.4 Isolated barchan-dunes showing an angle of about 25° between the direction of the mean wind and an elb (after CLOS-ARCEDUC 1968)

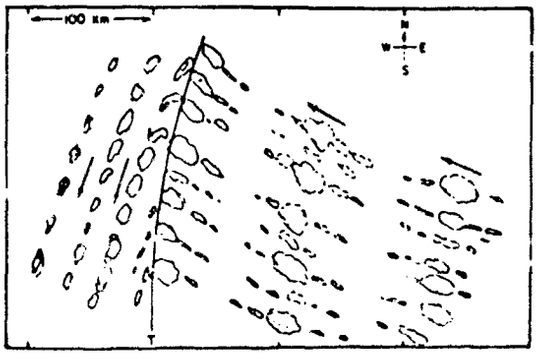

Fig.5 Cloud distribution in the neighbourhood of a trough line in the easterlies (after MALKUS and RONNE 1960)

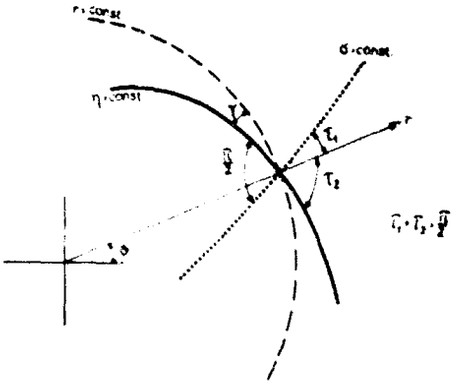

Fig.6

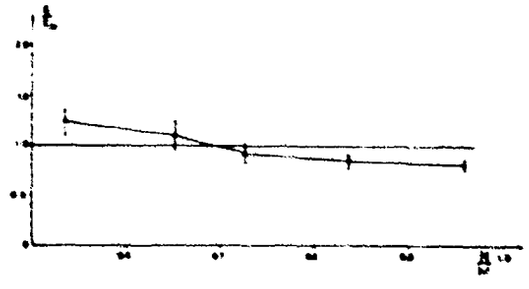

Fig.7 Verification of formula (45) by laboratory experiments (after HORST 1969); K/M in the figure means ν/μ in the text

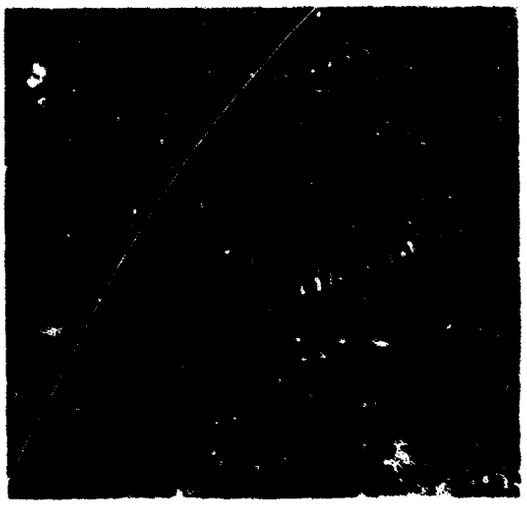

Fig.8 "Left-hand side" type of seif-dunes (after CLOS-ARCEDUC 1968)

Fig. 9 The double vortex system due to boundary layer instability as produced in laboratory experiments by HORST (1969)

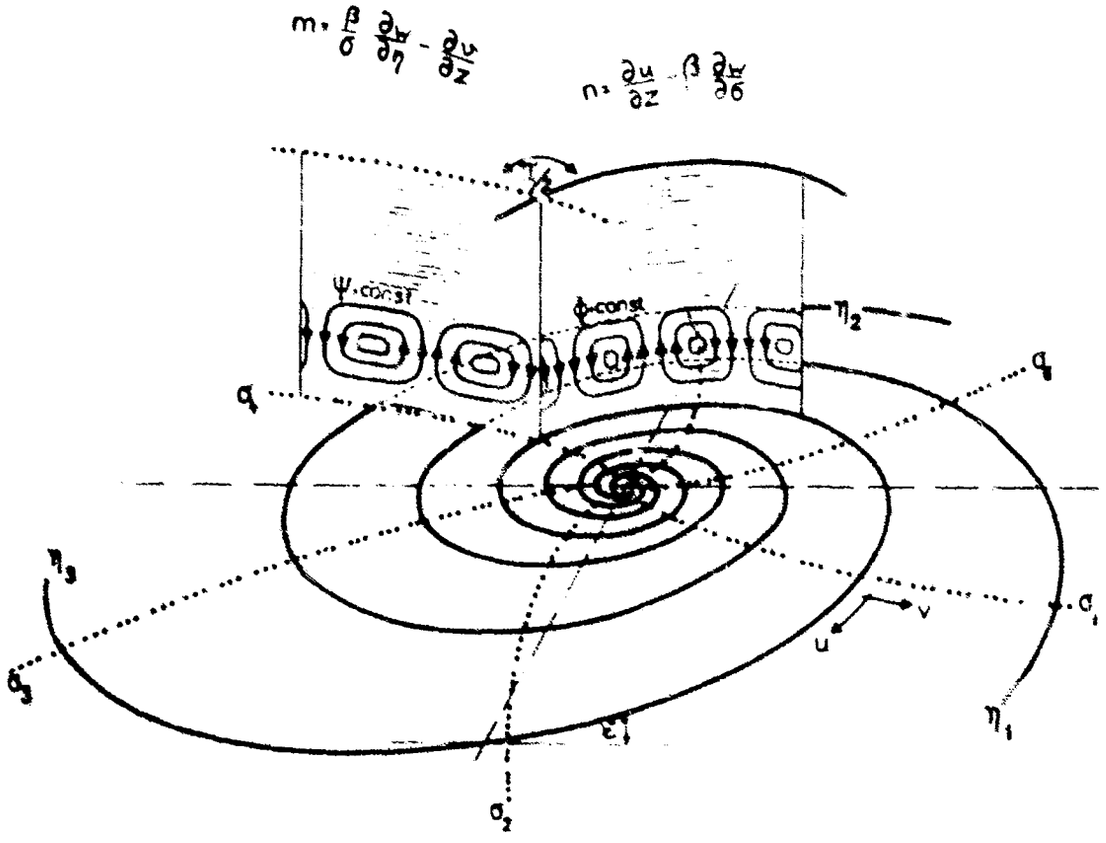

Fig. 10 Schematic representation of the (σ, η, z) -coordinate system

DIFFUSION IN THE ATMOSPHERIC SURFACE LAYER : COMPARISON OF SIMILARITY THEORY WITH OBSERVATIONS

by

W. Klug

Technische Hochschule Darmstadt
Germany*

* Most of this work was performed while the author was temporarily working at the Atmospheric Turbulence and Diffusion Laboratory, ESSA, Oak Ridge, Tenn., U.S.A. This paper was originally published in Quart. J.R.Met. Soc., 94, pp. 555-562 (1968) and is reprinted here with the permission of the Royal Meteorological Society.

SUMMARY

The diffusion model utilizing the ideas of similarity theory for the atmospheric surface layer is explained. The Surface layer is a layer adjacent to the Earth's surface in which the turbulent fluxes of momentum and sensible heat can be ... ated as constant with respect to height. The surface layer is approximately 50 m in depth. - The results of the theoretical findings are then compared with concentration measurements under known meteorological conditions. These data were obtained from Project 'Prairie Grass', where sulfur dioxide was used as tracer. The results show that good agreement between theory and experiments can be obtained only when the 'lateral turbulence level' σ_v/u_* is included through a regression equation.

I. Introduction

During the last eight years a number of papers have dealt with the application of similarity theory to turbulent diffusion in the atmospheric surface layer (Monin 1959, Batchelor 1959, 1964, Elliason 1959, Gifford 1962, Cermak 1963, Yaglom 1965, Panofsky and Prasad 1965, Pasquill 1966). None of these papers, however, compared concentrations as obtained by diffusion experiments with the predictions made by theory. Most of them considered the relative dependence on distance from the source but Pasquill (loc.cit.) compared the vertical standard deviation σ_z of concentration at a fixed distance (100 m) from diffusion experiments with similarity theory results. The aim of this paper is therefore to compare the results of diffusion experiments performed during Project 'Prairie Grass' with theoretical expectation. First, a short outline of the diffusion model utilizing the ideas of similarity theory will be given.

II. The Diffusion Model

The fundamental hypothesis of similarity of the statistical properties of turbulent flow in the atmospheric surface layer - the turbulence of which is assumed to be horizontally homogeneous - was given by Monin and Obukhov (1954). This hypothesis can be stated as follows: In a layer adjacent to the Earth's surface, which is approximately 50 m in depth, the turbulent fluxes of momentum and sensible heat can be treated as constant with respect to height. Therefore, the friction velocity $u_* = (-\overline{u'w'})^{1/2}$ and the covariance between temperature and vertical wind fluctuations $\overline{w'T'}$, which is proportional to the turbulent flux of heat, are the characteristic parameters of this layer. Together with a buoyancy parameter g/T_0 (g acceleration of gravity, T_0 mean temperature) they can be uniquely combined to a scaling length L (containing von Kármán's constant k for convenience)

$$L = -u_*^3 \Big/ \left\{ k \frac{g}{T_0} \overline{w'T'} \right\} \qquad (1)$$

which is the now well-known Monin-Obukhov stability length. The similarity hypothesis assumes that for high Reynolds numbers (which are always found in the surface layer with the exception of the very first millimetres or so above ground) all statistical properties of the flow depend only on the ratio (z/L), apart from any boundary condition which may enter.

We now consider the concentration distribution from an instantaneous source. (Since we consider the concentration only at times $t \gg d/u_*$, the source can be of small size d). The marked particles are released from this source at time t = 0 and the source is at the surface. If we denote the mean position of the particles or the centre position of the cloud by $\bar{x}$ (t), $\bar{y}$ (t) and $\bar{z}$ (t), then the concentration X_{is} at a point

with co-ordinates x, y, z and at time t, originating from a source of strength Q_{is}, will be a function of the following variables:

$$X_{is}(x,y,z,t) = f(Q_{is}, x - \bar{x}(t), y - \bar{y}(t), z - \bar{z}(t), u_*, L, t). \quad (2)$$

It should be noted here, that in accordance with similarity theory the only available length scale is L. Since we have 8 variables and 3 fundamental dimensional units, mass, length and time, 5 dimensionless ratios can be formed as follows:

$$X_{is}(x,y,z,t) \cdot L^3/Q_{is} = f_1\left\{\frac{x-\bar{x}(t)}{L}, \frac{y-\bar{y}(t)}{L}, \frac{z-\bar{z}(t)}{L}, \frac{u_* \cdot t}{L}\right\} \quad (3)$$

Referring to the similarity hypothesis again and applying dimensional reasoning, $d\bar{x}(t)/dt$ and $d\bar{z}(t)/dt$ can be obtained by the following relations:

$$\frac{d\bar{x}(t)}{dt} = \bar{u} = \frac{u_*}{k}\left\{f_2\left(\frac{\bar{z}}{L}\right) - f_2\left(\frac{z_o}{L}\right)\right\} \quad (4)$$

where z_o is the roughness length and is inherent in the boundary condition $\bar{u}(z_o) = 0$.

$$\frac{d\bar{z}}{dt} = b\,u_*\,f_3\left(\frac{\bar{z}}{L}\right) \quad (5)$$

where b is a dimensionless constant and f_3 some universal function. $\bar{y}(t)$ can be made zero without loss of generality by symmetry considerations and selection of orientation of the co-ordinate system.

By integration of Eq. (5) and dimensional reasoning we get

$$\frac{\bar{z}(t)}{L} = \left\{(b\,u_*\,t)/L\right\} \cdot f_4\left(\frac{\bar{z}(t)}{L}\right) \quad (6)$$

since $\bar{z}(0) = 0$, or

$$\frac{u_* \cdot t}{L} = f_5\left(\frac{\bar{z}(t)}{L}\right) \quad (7)$$

Using Eq.(7) in Eq.(3) we obtain

$$X_{is}(x,y,z,t) \cdot L^3/Q_{is} = f_1\left\{\frac{x-\bar{x}(t)}{L}, \frac{y}{L}, \frac{z-\bar{z}(t)}{L}, f_5\left(\frac{\bar{z}(t)}{L}\right)\right\} \quad (8)$$

$$= f_6\left\{\frac{x-\bar{x}(t)}{L}, \frac{y}{L}, \frac{z-\bar{z}(t)}{L}, \frac{\bar{z}(t)}{L}\right\} \quad (9)$$

Introducing a new function f_7, where $f_7 = (\bar{z}/L)^3 \cdot f_6$ we have

$$X_{is}(x,y,z,t) = \frac{Q_{is}}{(\bar{z}(t))^3} \cdot f_7\left\{\frac{x-\bar{x}(t)}{L}, \frac{y}{L}, \frac{z-\bar{z}(t)}{L}, \frac{\bar{z}(t)}{L}\right\} \qquad (10)$$

Since we have assumed a constant wind direction we integrate Eq. (10) with respect to time in order to obtain the concentration distribution for a continuous source and get

$$X_{cs}(x,y,z) = Q_{cs} \int_0^\infty f_7\left(\frac{x-\bar{x}(t)}{L}, \frac{y}{L}, \frac{z-\bar{z}(t)}{L}, \frac{\bar{z}(t)}{L}\right) \frac{dt}{(\bar{z}(t))^3} \qquad (11)$$

Changing the variable of integration with help of Eq. (4), Eq. (11) reads

$$X_{cs}(x,y,z) = \frac{Q_{cs}}{u_x/k} \int_{-\infty}^{+\infty} \frac{f_8\left(\frac{x-\bar{x}(t)}{L}, \frac{y}{L}, \frac{z-\bar{z}(t)}{L}, \frac{\bar{z}(t)}{L}\right)}{(\bar{z}(t))^2\left\{f_2\left(\frac{\bar{z}(t)}{L}\right) - f_2\left(\frac{z_0}{L}\right)\right\}} d\left\{\frac{x-\bar{x}(t)}{L}\right\} \qquad (12)$$

We are particularly interested in the concentration distribution at ground level downwind from the source, which we obtain by putting $y = z = 0$ in f_8. Furthermore, we notice that the distribution function f_8 gives the particle probability with respect to the centre position of the particles. This distribution function depends not only on the relative position of the particles with respect to their centroid, but also on the height of the centre above ground and therefore on time. On the other hand, the function f_8 is a sharply peaked function for values of $(x - \bar{x})$ near zero. For this range of values, $\bar{z}(t)/L$ can be treated as constant and we reach

$$X_{cs}(x = \bar{x}, 0, 0) = \frac{Q_{cs}}{u_x/k} \frac{f_9\left(\frac{\bar{z}(t)}{L}\right)}{(\bar{z}(t))^2\left\{f_2\left(\frac{\bar{z}(t)}{L}\right) - f_2\left(\frac{z_0}{L}\right)\right\}} \qquad (13)$$

using

$$f_9\left\{\frac{\bar{z}(t)}{L}\right\} = \int_{-\infty}^{+\infty} f_8\left(\frac{x-\bar{x}(t)}{L}, 0, -\frac{\bar{z}(t)}{L}, \frac{\bar{z}(t)}{L}\right) d\left(\frac{x-\bar{x}(t)}{L}\right) \qquad (14)$$

Two points remain to be investigated. The first is to express $\bar{z}(t)$ as a function of $\bar{x}(t)$ and the second is to state the function f_2 which is the

equation for the wind profile. In order to obtain the first relationship, we use Eqs.(4) and (5) and get

$$\frac{\beta \cdot k}{L} d\bar{x} = \frac{f_2\left(\frac{\bar{z}(t)}{L}\right) - f_2\left(\frac{z_o}{L}\right)}{f_3\left\{\frac{\bar{z}(t)}{L}\right\}} d\left(\frac{\bar{z}(t)}{L}\right) \tag{15}$$

III. The Wind Profile

It is assumed that the velocity of the centre of particles is equal to the mean wind velocity, and that the function $f_2(\bar{z}/L)$ can be obtained from the integrated KEYPS windprofile (Yamamoto 1959, Klug 1967). This form of the vertical wind profile under diabatic conditions is based on the same assumptions as mentioned earlier in this paper. The equation for the integrated wind profile reads

$$f_2\left(\frac{\bar{z}}{L}\right) = \gamma - 2\tan^{-1}\gamma - 2\tanh^{-1}\gamma \tag{16}$$

where γ is related to $\bar{z}/L$ by

$$(\gamma^4 - 1)/\gamma^3 = \alpha \bar{z}/L \tag{16a}$$

and α is a dimensionless constant ($\alpha = 7$).

Monin (1959) has proposed from dimensional reasoning a form for the function $f_3(\bar{z}/L)$, which is related to the wind profile. Following this proposal we write

$$f_3\left(\frac{\bar{z}}{L}\right) = \left\{1 - (f_2')^{-1}\right\}^{1/4} \tag{17}$$

with f_2' the derivative of f_2 with respect to $\alpha\bar{z}/L$. Using relationships of Eqs. (16), (16a) and (17), we obtain for Eq. (15)

$$\frac{\alpha \cdot \beta \cdot k}{L} \bar{x} = \int_{\alpha z_o/L}^{\alpha \bar{z}/L} \left\{ f_2\left(\frac{\bar{z}(t)}{L}\right) - f_2\left(\frac{z_o}{L}\right)\right\} \gamma \, d\left(\frac{\alpha \bar{z}}{L}\right) \tag{18}$$

Since $d(\alpha\bar{z}/L) = (\gamma^4 + 3)d\gamma/\gamma^4$, we have

$$\frac{\alpha \cdot \beta \cdot k}{L} \bar{x} = \int_{\gamma_o}^{\gamma} \left\{ f_2(\gamma) - f_2(\gamma_o)\right\} \frac{\gamma^4 + 3}{\gamma^5} d\gamma \tag{19}$$

Integration of Eq.(19) with Eq.(16) inserted, yields

$$\frac{\alpha \cdot b \cdot k}{L}\,\bar{x} = \left\{\frac{\xi^4+9}{3\xi} - \frac{\xi^4-2\xi^2-3}{\xi^2}\tan^{-1}\xi - \frac{\xi^4+2\xi^2-3}{\xi^2}\tanh^{-1}\xi - \right.$$

$$\left. - \frac{1}{2}\left(\xi_o - 2\tan^{-1}\xi_o - 2\tanh^{-1}\xi_o\right)\frac{\xi^4-3}{\xi^2}\right\}_{\xi_o}^{\xi} \qquad (20)$$

This function was evaluated with the help of the IBM-7090-Computer of Oak Ridge National Laboratory and the result is presented in Fig. 1.

For convenient comparison with earlier papers $X_{cs} \cdot L^2/(Q_{cs} \cdot k \cdot \alpha^2)$ is plotted in Fig. 2 as a function of $(\alpha \cdot k \cdot b \cdot \bar{x})/|L|$. The parameter of the curves is $\alpha\, z_o/L$. It should be noted here that for this purpose of comparison f_9 of Eq.(13) is put equal to one. The results obtained differ slightly from the results in Gifford's paper (1962) Figs. 2 and 3, where the diabatic wind profile was integrated numerically.

IV. Comparison with diffusion experiments

The set of diffusion data which seems to be the most suitable for comparison with theory is the one obtained by Project 'Prairie Grass' (Barad 1958). The wind profile measurements published were used to determine the stability length L and friction velocity u_* after a method which was proposed by the author in a recent paper (Klug 1967). No experiment was used in the analysis if the standard error of estimate between the observed and theoretical wind profile was > 10 cm sec^{-1}. With the procedure mentioned, values of L and u_* were obtained for each run and are listed in Table 1. The concentration data used were those of the maximum concentration on each arc after smoothing the original data.

The value of the constant b in Eq. (5) is still open to question. Several values between 0.1 and 1.0 have been proposed by different authors. We are using b = 0.4, a value which was advocated by Ellison (1959) and by Pasquill (1966).

The next step to take is to determine the function of f_9 of Eq. (13). For this purpose it was assumed that

$$f_g\left(\frac{\bar{z}}{L}\right) = G \cdot g\left(\frac{\bar{z}}{L}\right)$$

where g (0) = 1. G was then computed for those runs taken under neutral conditions

$$G = \left\{ X_{cs}(x \cong \bar{x}, 0, 0) \cdot u_* \cdot \bar{z}^2 \left\{ f_2\left(\frac{\bar{z}}{L}\right) - f_2\left(\frac{z_s}{L}\right) \right\} / (Q_{cs} \cdot k) \right\}_{ADIAB.} \qquad (21)$$

The mean values of G for all runs taken under adiabatic conditions averaged to $G_{50m} = 0.09$, $G_{100m} = 0.12$, $G_{200m} = 0.13$, $G_{400m} = 0.13$ and $G_{800m} = 0.13$. The value of G increases considerably from the 50 m to the 100 m arc, but then remains fairly constant. This behaviour can be ascribed to the fact that the source height in the diffusion experiments concerned was not at the surface (as was assumed in the model), but 46 cm above ground. As Yaglom (loc.cit.) explains, only when the travel time $t \gg h/u_*$ (where h is the source height), will the particles have 'forgotten' the source height where they started from so that the effect of a non-zero source height will be negligible. The values of G above were used to determine the function $g(\bar{z}/L)$ from the concentration values.

Table 1. Values of friction velocity u_* [cm sec^{-1}] and stability length L [m]

Run	u_* [cm sec^{-1}]	L [m]	Run	u_* [cm sec^{-1}]	L [m]
5	43·9	- 19·0	41	26·1	23·1
6	50·3	- 58·9	42	43·5	4,084·2
7	35·4	- 4·5	43	40·6	- 7·0
8	33·3	- 48·4	44	46·3	- 11·7
9	52·1	- 18·4	45	44·3	- 38·2
15	25·6	- 5·7	46	40·6	228·9
17	24·1	33·5	54	28·5	37·0
18	22·1	16·6	55	43·2	293·8
21	44·0	150·4	56	34·5	69·2
22	53·1	133·6	60	33·1	44·0
23	44.2	95·9	61	60.3	- 9.6
35	27·0	30·5	62	40·4	- 7·1
38	30·9	40·5	65	32·5	30·4

When the values of g were computed, it turned out that there was no correlation with $\bar{z}/L$. Instead, it was found that g remained effectively constant within one run (if g were a function of $\bar{z}/L$ it would vary with distance), but they varied considerably from one run to the next. Therefore other relationships were tried. A significant correlation was found between g and $\sigma_v/u_* \, m(v'^2) \; /u_*$. A plot of g in relation to σ_v/u_* is given in Fig. 3. The regression line drawn in this figure is

$$g = - 0.28 \, \sigma_v/u_* + 1{\cdot}48$$

The correlation coefficient is $r = 0.84 \pm 0{\cdot}04$.

5. Conclusions

The results indicate that the model introduced earlier does not include all pertinent variables in the dimensional analysis. This forces us to the conclusion that Eq. (2) should include σ_v in the list of independent variables and Eq. (3) should therefore read:

$$X_{ik}(x,y,z,t) \cdot L^b/Q_{ik} = f_i^* \left\{ \frac{x-\bar{x}(t)}{L}, \frac{y-\bar{y}(t)}{L}, \frac{z-\bar{z}(t)}{L}, \frac{u_* t}{L}, \frac{\sigma_v}{u_*} \right\} \qquad (22)$$

Putting it in other words, the tacit assumption which was made in setting up Eq. (2) was that all other variables which may be left out in this

relationship depend uniquely on the variables listed. In our case this would lead to assuming that $\sigma_v/u_* = f(\bar{z}/L)$ only. However, there seems to be an increasing amount of observational evidence that this is not true (see Lumley and Panofsky 1964). The foregoing results are an indirect verification of these results.

After taking into account σ_v by the empirical relationship above, th agreement between observed and calculated concentration is good. The ratio R of observed to calculated concentrations is on average over all 26 runs

$$R_{50m} = 1{\cdot}01 \pm 0{\cdot}04, \qquad R_{100m} = 1{\cdot}01 \pm 0{\cdot}04,$$

$$R_{200m} = 1{\cdot}01 \pm 0{\cdot}04, \qquad R_{400m} = 1{\cdot}04 \pm 0{\cdot}06,$$

$$R_{800m} = 1{\cdot}00 \pm 0{\cdot}08.$$

It must be recognised that this good agreement was obtained only after the empirical relationship $G{\cdot}g(\sigma_v/u_*)$ was employed. It seems doubtful whether such good results could be achieved by merely transferring these results to another set of experimental data.

There is still some discrepancy between the findings of the above analysis and the results by Pasquill (loc.cit.), who found that the standard deviation σ_z of the vertical concentration distribution at a fixed distance could not - under his assumptions - be preticted when using Eq.(5) of this paper and a value of b = 0·4. Pasquill states, however, that a 'much more statisfactory correspondence' between predicted and observed values of σ_z can be obtained by changing b from 0·4 to 1·2. A possible explanation of the discrepancy is, that by determining G in the above analysis (which has the same effect as changing b to a larger value), the same result as Pasquill's is already incorporated in the analysis.

Acknowledgments

The author is grateful for interesting and helpful discussions with Dr. F. Gifford, Dr. F. Pasquill and Dr. F.B. Smith. The smoothed concentration data were made available by Dr. D. Haugen, APCRL. A portion of this work was completed under an agreement between the Environmental Science Services Administration and the Atomic Energy Commission, U.S. Government.

References

Barad, M.L. 1958 'Project prairie grass, a field program in diffusion,' Geophys.Res.Paper, 1, 59.

Batchelor, G.K. 1959 'Some reflections on the theoretical problems raised at the symposium,' Adv.Geophys., 6, pp.449-452.

1964 'Diffusion from sources in a turbulent boundary layer,' Archiwum Mechaniki Stosowanej, 3, pp. 661-670.

Cermak, J.E. 1963 'Lagrangian similarity hypothesis applied to diffusion in turbulent shear flow,' J.Flud Mech. 15, pp. 49-63.

Ellison, T.H. 1959 'Turbulent diffusion,' Sci.Progress.. 47, pp. 495-506.

Gifford, F.A. 1962 'Diffusion in the diabatic surface layer,' J.Geophys.Res., 67, pp. 3,207-3,212.

Klug, W. 1967 'Determination of turbulent fluxes of heat and momentum from the wind profile,' Quart.J.R.Met.Soc., 93, pp.101-104.

Lumley, J.L. and Panofsky, H.A. 1964 The structure of atmospheric turbulence, J.Wiley & Son, New York.

Monin, A.S. 1959 'Smoke propagation in the surface layer of the atmosphere,' Adv.Geophys., 6, p.331.

Monin,A.S. and Obukhov, A.M. 1954 'Basic laws of turbulent mixing in the ground layer of the atmosphere,' Trudy Geophys.Inst.ANSSR No. 24 (151), pp. 163-187.

Panofsky, H.A, and Prasad, B. 1965 'Similarity theories and diffusion,' Int.J.Air Water Poll.,9,pp.419-430.

Pasquill, F. 1966 'Lagrangian similarity and vertical diffusion from a source at ground level,' Quart.J.R.Met.Soc., 92, pp. 185-195.

Yaglom, A.M. 1965 'Lagrangian properties of turbulence in a diabatic surface layer and in convective jets,' Izv.Atm.and Oceanic Phys.Ser., 1.,pp. 157-166.

Yamamoto, G. 1959 'Theory of turbulent transfer in non-neutral conditions,' J.Met.Soc. Japan, 37, pp. 60-70.

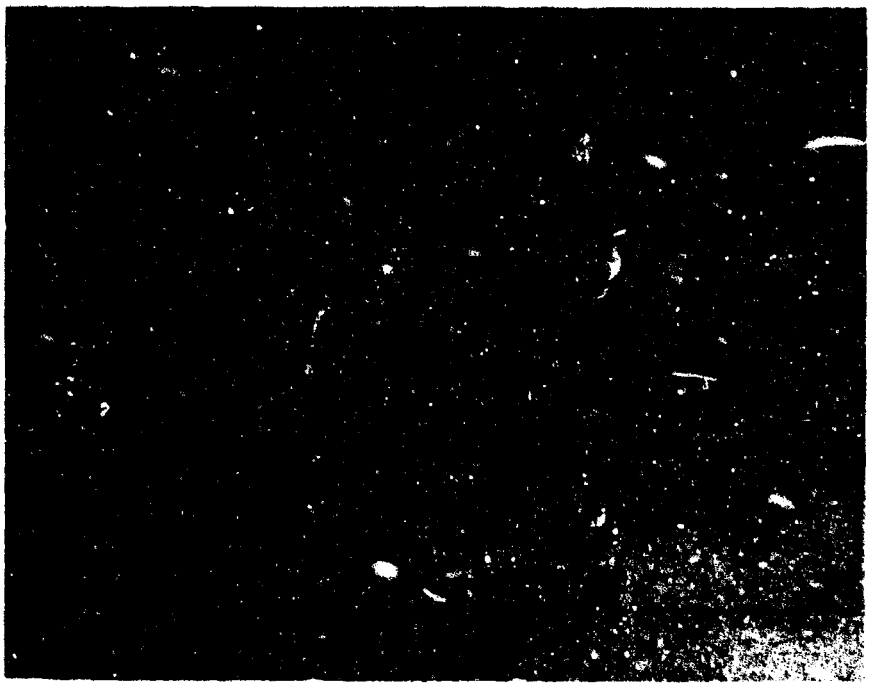

Figure 1 : Plot of dimensionless height of centre position of the cloud against dimensionless distance from source for different stabilities. Full lines unstable, broken lines stable stratification.

Figure 2 : Dimensionless axial concentration values as a function of the dimensionless downwind distance. Full lines stable, broken lines unstable stratification. Parameter values of $|\alpha s_0/L|$; f_q of Eq. (15) is put arbitrarily equal to one.

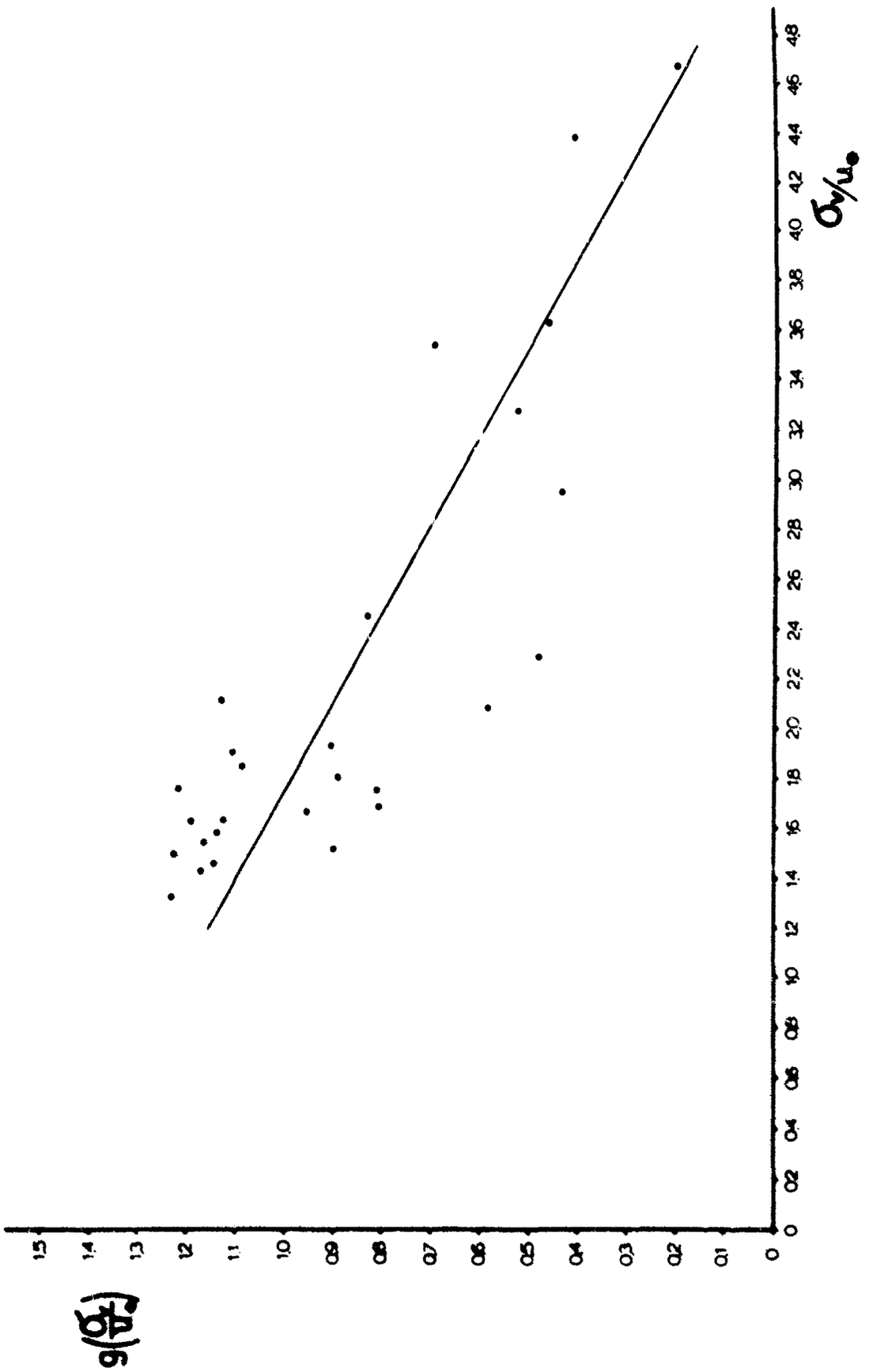

Figure 3 : Mean values of $\phi(\sigma_v)$ for each run in relation to σ_v/u_*.

SOME MEASUREMENTS OF INSTABILITIES AND TURBULENCE IN EKMAN BOUNDARY LAYERS

by

D. R. Caldwell
Oregon State University

and

C. W. Van Atta
University of California, San Diego

SUMMARY

To simulate certain features of atmospheric and oceanic shear flows, some characteristics of rotation-dominated laminar and turbulent Ekman boundary layers have been studied using hot-wire anemometry and a large rotating table. The Ekman layers are generated on two 4.3 meter diameter rotating circular plates by sucking air through the 12.7 cm wide gap between the plates into a central hub with a large blower. Beginning at Reynolds numbers (layer thickness · core speed/kinematic viscosity) of 100 or so we observe wave-like disturbances similar to Class A (also called Type II) instabilities. The spectra of these waves and their variation with height and Reynolds number are presented. Rapid increase of wave amplitude with Reynolds number was observed. As the Reynolds number is increased above 200, the general turbulence level increases until the layer becomes fully turbulent near a Reynolds number of 1000. We present observations of the mean profile in the layer and turbulence spectra. We find that the profiles are logarithmic and very similar to profiles in the classical smooth plate layer. The proper scaling parameter for the spectra appears to be the Kolmogoroff scale based on the local dissipation rate.

NOTATION

a	growth rate of disturbance divided by Ω
A	minimum detectable wave amplitude
A_c	initial wave amplitude
c_r	phase speed of disturbance divided by V
D	Ekman depth = $(\nu/\Omega)^{\frac{1}{2}}$
f	frequency, HZ
k	wave number
K	dimensionless wave number = kD
L	Kolmogoroff length = $(\nu^3/\epsilon)^{\frac{1}{4}}$
r	radial coordinate
R	outer radius of flow
R_e	Reynolds number based on V and D
R_{ec}	critical Reynolds number for onset of wave instability
R_0	Rossby number = $V/2\Omega R$
S	volume flow through blower
S_k	power spectrum of turbulence
U^*	friction velocity
u	radial velocity component in boundary layer
v	circumferential velocity component in boundary layer
V	circumferential velocity in interior flow
Z	vertical coordinate normal to rotating plates
Z_0	roughness length
δ	measured boundary layer thickness
ϵ	dissipation rate
Ω	angular velocity of rotating table
ν	kinematic viscosity
σ_0	wave frequency divided by table frequency

I. INTRODUCTION

The instabilities of the laminar Ekman boundary layer have been studied experimentally by Faller[1] and by Tatro and Mollo-Christensen[2]. The most pertinent theoretical work is by Lilly[3]. Faller was able to visualize waves which set in at a Reynolds number of 125. The Reynolds number, R_e, is defined as VD/ν where V = stream speed, D = boundary layer depth, and ν = viscosity. He called these "Type I" waves. Faller and Kaylor[4] describe a "Type II" wave which sets in at a Reynolds number of 70. The Type II waves have a longer wavelength and higher phase speed than Type I. In Greenspan's[5] review, Type I is called class B and Type II is called class A.

Lilly and Faller and Kaylor used different numerical techniques to study the problem and obtained values for the critical Reynolds number and some parameters of the waves. A compilation of experimental and theoretical results is given in Table I. According to both experimental studies the waves break up into turbulence at somewhat higher Reynolds numbers; 200 to 500 according to Faller and Kaylor, 200 to 350 according to Tatro and Mollo-Christensen. In this paper we shall present the results of an experimental study using apparatus similar to that of Tatro and Mollo-Christensen. In addition to standard analog techniques, we have used digital data recording and processing to study the waves in more detail and to look at the transition to turbulence.

The Reynolds numbers in the earlier experiments were too small to produce the fully turbulent boundary layer relevant to atmospheric shear flows. In the present experiments, we have studied mean profiles and turbulence spectra for Reynolds numbers up to 1500, well above the onset of fully developed turbulence.

II. APPARATUS

A schematic of the flow system is given in Fig. 1. Air is drawn in on top of the table, brought to the outside under plate C, made to flow to the center between plates A and B, and then blown out up the center pipe. The mass flow was monitored by a pitot-static tube placed in the blower outlet and a strain gage differential pressure gage. The table was rotated by a Graham variable speed transmission at speeds continuously variable up to 105 r.p.m. The transmission is powered by a three-phase motor which holds the speed as steady as the power line frequency.

Measurements of mean and fluctuating velocities were made with hot-wires near the bottom surface of plate B, near the top surface of plate A, and in the interior flow between the plates. The probes were inserted through one of a series of holes drilled in plate B.

A remotely operated probe traversing mechanism was used to adjust the vertical position and orientation of the hot-wire probes. The degree of rotation was indicated by a potentiometer and vertical displacements were measured by counts of a micro-switch triggered by a cam mounted on the shaft which moved the probe. Each revolution of this shaft corresponded to .0025 inches of vertical motion.

Electrical connections to the rotating apparatus were provided by two sets of slip rings. A set of copper strips dipped in mercury-filled grooves was used for both high power and low noise circuits. A set of mechanical rings was used for less critical circuits.

The hot-wire measurements were made in two ways. For mean flow measurements, the hot wire was connected to a constant resistance circuit (DISA Model 55A01). The voltage required to keep the hot wire at constant resistance was measured by a voltage-to-frequency converter and a counter. Some of the turbulence measurements were made by high passing and recording this signal. When it was desired to make multi-channel recordings, each hot wire was connected in series with two twelve-volt car batteries and a 1000 ohm resistor for a "constant current" mode of operation. The voltage across the hot wire was amplified and band-passed (band 0.1 to 20 cps) before the signal was passed through the slip rings. Signals were recorded digitally on a system composed of a Vidar scanner, Preston amplifier, Applied Development Corporation analog-to-digital converter and an incremental tape recorder. The recorder can make 500 steps per second, so with twelve-bit accuracy and one channel, for example, 250 numbers per second can be recorded.

III. THE BASIC INTERIOR FLOW

At the beginning of these experiments the apparatus was smaller than shown in Fig. 1. The geometry was the same and the plate separation was the same, but the overall diameter was only 214 cm (measured to the last entrance screen). In the interior, the flow direction was found to be nearly tangential, with the flow spiraling in at an angle of one or two degrees from tangential, depending on the speed of flow and the rate of rotation.

If the Rossby number R_0 ($= V/2r\Omega$, where Ω is the basic rotation rate) were zero and the flow of infinite horizontal extent, the circulation, $2\pi Vr$, should be independent of position. (It should be noted that V is the speed of circumferential flow relative to the rotating plates). The direction of flow in the core would be exactly tangential with transport to the center occurring only in the boundary layer on each plate. The circulation would be equal to S/D where S is the volume flow through the blower and $D = (\nu/\Omega)^{\frac{1}{2}}$, the Ekman layer depth. Near the boundaries the flow would be described by:

$$u = [\sin(z/D) \exp(-z/D) \exp(-z/D)]\, S/(2\,Dr)$$

$$v = [1-\cos(z/D) \exp(-z/D]\, S/(2\,Dr)$$

where u is the radial component and v the tangential component of velocity and z is the vertical distance from the boundary. As $z \to \infty$, $u \to 0$ and $v \to V$.

This flow, which satisfies the equation of continuity exactly and satisfies the Navier-Stokes equation in the limit of zero Rossby number, is an ideal Ekman layer bounding an exactly geostrophic core flow. This flow will not be realized in the present apparatus because: (1) The flow is not horizontally infinite but must develop from the edge of the table and (2) The Rossby number cannot be made small enough. The effects of both development and non-zero Rossby number on the circulation are as follows. Near the edge of the table the circulation (calculated in the rotating system) is very low. It increases as the flow develops inward and then decreases as the Rossby number becomes larger near the center of the table. At the lower rotation rates the outer adjustment region extends farther toward the center. Centrifugal instability seems to be the cause of this long adjustment region. The circulation of the flow in the rotating coordinate system at radius r is $2\pi r V(r)$. In the stationary system it is $2\pi r V(r) + 2\pi r \Omega^2$, which in the ideal case is equal to $S/D + 2\pi r \Omega^2$. At the outer screen, $r = R$, the fluid has not yet been accelerated faster than the basic rotation so its circulation is at most $2\pi R \Omega^2$. There must, therefore, be a region where $V(r)$ is such that the circulation decreases as we go outward. But centrifugal stability would require the circulation to increase outward, so this region must be unstable. In the adjustment region the hot wire signal shows very large oscillations indicating large eddies in the flow.

IV. BOUNDARY LAYER MEAN FLOW

An example of the measured laminar boundary layer flow profiles is shown as Fig. 2. At a given height the probe was rotated and the response as a function of direction plotted. The direction of maximum apparent speed was found, and the speed measured at that angle. The zero angle is taken as the direction of flow well away from the plate. Measurements cannot be made closer than about .02 cm from the plate because of heat losses from the hot wire to the plate. The measured boundary layer thickness δ was defined as the height z where $v/V = 0.8$, which corresponds to $z = D$ in the Ekman solution. For most measurements, the v component alone was determined by aligning the hot wire parallel to the radius for the entire traverse.

In order to investigate the variation of δ with radius, δ was measured at several blower speeds (below wave producing speeds) at several radii. There was very little variation of boundary layer thickness with either speed of flow or radius at these low Reynolds numbers, a behaviour contrary to that observed by Tatro and Mollo-Christensen, who found a significant variation of thickness with radius and Reynolds number.

At higher Reynolds numbers the boundary layer profile changes radically with increasing Reynolds number. Turbulence smooths out the profiles and eliminates the overshoot, as shown in Fig. 3. Actually, the overshoot persists to higher Reynolds number, but occurs at larger distances from the boundary than are shown in Fig. 3.

At Reynolds numbers higher than those at which the above observations were made the flow appears fully turbulent. The "waves" become lost in a smooth turbulent spectrum. The mean profiles lose their resemblance to laminar profiles, and the total turning of the direction of flow decreases.

Mean profiles of u and v are shown in Fig. 4 in the form u/V and v/V vs. $10(\Omega Z/u^*)^{.6}$. This height scaling, by $0.1\, u^*/\Omega$, reduces all the profiles at one radius for various Reynolds and Rossby numbers to one curve, but the profiles at a different radius reduce to a slightly different curve. The boundary layer characteristics at the two locations could be expected to differ somewhat because of variations in the radial pressure gradient.

The values of u^* used for the scaling were derived from the v profile by assuming the straight line section to obey the relation $u = 2.5\, u^* \log_e (Z/Z_0)$. The roughness length, Z_0, turns out to be about 0.001 cm and the drag coefficient about .003. Although these profiles cannot be fit with a smooth flow relation with only U^* as a variable parameters, the values of U^*Z_0/ν are sometimes less than 0.1, which corresponds to the smooth flow regime in the non-rotating case.

The u profiles do not collapse nearly as well to a single curve when scaled in the same way as the v profiles. They do clearly show that the maximum value of u occurs much closer to the surface than in the laminar case.

V. ONSET OF INSTABILITY

The hot-wire signal began to exhibit a wavelike character as the Reynolds number was increased. Characteristic records are shown in Figs. 5 and 6. As the Reynolds number was slowly increased, the waves appeared quite suddenly. The amplitude at first increased rapidly with increasing Reynolds number and then grew more slowly. With further increase in Reynolds number, the waves eventually were submerged in a growing turbulent spectrum.

The critical Reynolds number was found by observing the waves on an oscilloscope to find their approximate frequency, then feeding the signal from the hot-wire through a Krohn-Hite band pass filter with both cutoff frequencies set at the wave frequency. The filtered wave signal was then fed to a Hewlett-Packard voltage-to-frequency converter, which gives a pulse rate proportional to the magnitude of its input voltage, regardless of polarity. The pulse rate was then averaged by a counter for typically 100 secs. The output of the counter was plotted against Reynolds number until a sudden increase in reading showed that the waves had started. Critical Reynolds numbers measured in this way corresponded exactly with those taken from complete spectral analyses.

The critical Reynolds number for the observed waves seems to depend on Rossby number, or at least on the radius at which the observation is made. Figure 6 shows the critical Reynolds number as a function of Rossby number. Tatro and Mollo-Christensen found an apparent radial dependence which was removed when the measured boundary layer thickness and tangential velocity were used in calculating the Reynolds number instead of D and a velocity based solely on the total mass flow. Our critical Reynolds numbers, which were computed using the measured tangential flow, and the measurements of boundary layer depth shown in Table 2 [which shows no measurable deviation from $(\nu/\Omega)^{\frac{1}{2}}$] do exhibit an apparent variation of critical Reynolds number with either radius or Rossby number. This may be explainable through a remark of Faller[4] that apparent variations of critical Reynolds number with Rossby number in this type of apparatus might be due to the fact that as the disturbances grow from infinitesimal amplitude, they move into regions of higher Reynolds number. The apparent critical Reynolds number then will always be higher than the Reynolds number at which they started to grow. The increase will depend on the Rossby number, according to this relationship:

$$R_e^2 (R_e - R_{ec})(R_e^{-2} - R_{ec}^{-2}) = \frac{2 c_r}{a} R_0 \log_e (A/A_c)$$

where R_e = apparent critical Reynolds number

R_{ec} = true critical Reynolds number

R_0 = Rossby number

c_r = phase speed divided by tangential core flow

a = growth rate of waves divided by Ω

A = minimum detectable amplitude of waves

A_c = amplitude of waves when they start to grow.

When the data shown in Fig. 7 is fitted to this relationship in a least squares sense, we find the best fit with $R_{ec} = 55.7 \pm 3$ and $A/A_c = 5 \times 10^4$. It might be noted that the determinations of critical Reynolds numbers were made by increasing the blower speed with rotation rate constant until the wave appeared. This procedure increases the Reynolds number and Rossby number proportionately, so we approached the curve of apparent critical Reynolds number vs. Rossby number at an oblique angle. This may be the cause of much of the scatter in the points in Fig. 7.

VI. INSTABILITY SPECTRA

Spectra were calculated from the hot wire signals by processing the recordings made as described previously on a Control Data 3600 Computer. The techniques used to compute the transform are as described by Haubrich[5], except that the Cooly-Tukey algorithm was used to shorten the computations.

The spectrum changes radically in the Reynolds number range 100 to 200. Figure 8 shows the effect on the spectrum of increasing the Reynolds number from 124, just at onset, to 320. At $R_e = 320$ the waves no longer stand out from the general turbulent spectrum, which seems to have an onset point of its own. Figure 9 shows the variation with Reynolds number of peak energy

(energy in a band centered around the spectral maximum) in db and the energy at 6.5 cps. The waves start first and stand out well above the noise until $R_e \sim 300$ when they appear to lose energy to the turbulence.

Figure 10 shows the relative energy in the waves as a function of distance from the boundary. The shape of the curve, especially the sharp minimum between three and four Ekman depths, compares quite well with Fig. 12 of Lilly's paper. At $Z/D \sim 3$ both horizontal components of the "orbital velocity" go through minima according to Lilly. The maximum, $Z/D \sim 1$, is also consistent with Lilly's picture.

The peak widths in Fig. 8 are typical. The Q of the peak is always 4 to 5. The center frequency, f_0, seems to increase with Reynolds numbers, but not sharply. The quantity $\sigma_0 = 2f_0/\Omega$ should be dependent only on the Reynolds number $[2\pi f_0/\Omega = (2\pi/\Omega)(c_r Vk/2\pi D) = c_r K R_e$, where c_r is the dimensionless phase speed used by Lilly]. The measured values of σ_0 are plotted vs. Reynolds number in Fig. 11 and the values of frequencies for Type I and Type II waves as predicted by Lilly are plotted for comparison. It seems clear again that we are observing waves similar to Type II. Correlation of observed spectra (particularly peak frequencies) with the growth rate diagrams of Lilly (Figs 1 through 8) is very difficult because: (1) The oscillations at a given frequency are produced by waves which have many different values of vector wave number. Figure 11 shows a diagram similar to Lilly's Fig. 7 with contours of σ_0. The lines of constant frequency cross the contours of growth rate in such a way that, for example, $\sigma_0 = 10$ for waves close to both of the two maxima of growth rate. (2) The waves are observed at Reynolds numbers much above R_{ec}; they have grown by a factor of about 50,000 so one has no right to expect a linear perturbation calculation to be applicable. (3) Even if the analysis were applicable, the calculation of the growth of the waves would require following their progress through from the first Reynolds number at which they become unstable to the Reynolds number at which they are observed. The largest amplitude wave at a particular Reynolds number is not necessarily the one which has the highest growth rate for that Reynolds number, but the one which has grown the most through its entire history.

VII. TURBULENCE SPECTRA

Figure 12 shows amplitude spectra of the hot-wire signal at Reynolds number of 1340, Rossby number of 1.20, measured with a spectrum analyser. Each line represents data taken at a different height. The turbulent energy is clearly contained within the boundary layer; it decreases by a factor of over 1000 as the height is increased. When the spectra are rescaled by Kolmogoroff's first hypothesis (using length and time scales depending only on ν and ϵ, the local dissipation rate) and using the dissipation in a constant stress boundary layer ($\epsilon = U^*/(0.4\,Z)$), they collapse into one curve, shown in Fig. 13. If the Reynolds and Rossby numbers are varied, the spectra change, but the same scaling seems to work.

VIII. CONCLUSIONS

1. Despite the uncertainties involved in comparing observed spectra with growth rates calculated from perturbation theory, it is clear that we are mainly observing Type II waves because: a) The critical Reynolds number, when corrected for curvature (Rossby number) effects, is very close to previous results for Type II. b) The central frequencies of the waves are increasing with increasing Reynolds number as in Lilly's calculation for Type II, rather than decreasing toward zero as his calculation shows for Type I. c) The variation of wave intensity with distance from the boundary (Fig. 10) is consistent with the eigenfunctions shown for Type II by Lilly (his Fig. 12). However, the difference in this respect between I and II is small.

2. We are evidently seeing the waves emerge from the general level of disturbances in the flow after they have been growing for some time. At a given frequency we see waves with many different wavelengths and directions, some of which may in fact be of "Type I." The distinction becomes somewhat blurred at the higher Reynolds numbers; growth rates vary by no more than a factor of two along a line in Fig. 11 between the most unstable modes of each type. The waves observed by Tatro and Mollo-Christensen seemed to have higher Q's, as their chart recordings do not show the "modulation" characteristics of wide-band signals exhibited in our Figs. 5 and 6.

3. The vertical scale of the turbulent profiles is u_*/Ω.

4. The proper scaling factors for the spectra are Kolmogoroff length and time scales based on the local dissipation rate for the constant stress boundary layer.

ACKNOWLEDGEMENTS

This work was supported principally by NSF Grant GA 849. The authors have been partially supported by NSF Grant GK 1515 and GA 1452. The assistance of Ken Helland in this work is appreciated.

REFERENCES

1. Faller, A. J., "An Experimental Study of the Instability of the Laminar Ekman Boundary Layer," J. Fluid Mech., Vol. 15, pp. 560-576, 1966.

2. Tatro, P. R. and Mollo-Christensen, E. L. J., "Experiments on Ekman Layer Instability," J. Fluid Mech., Vol. 28, pp. 531, 1967.

3. Lilly, D. K., "On the Instability of Ekman Boundary Flow," J. Atmos. Sci, Vol. 23, pp. 481-494.

4. Faller, A. J. and Kaylor, R. E., "A Numerical Study of the Instability of the Laminar Ekman Boundary Layer," J. Atmos. Sci., Vol. 23, pp. 466-480, 1966.

5. Greenspan, H. P., The Theory of Rotating Fluids, Cambridge University Press, 1968.

6. Csanady, G. T., "On the "Resistance Law" of a Turbulent Ekman Layer," J. Atmos. Sci., Vol. 24, pp. 467-471, 1967.

7. Haubrich, R., "Earth Noise, 5 to 500 Millicycles per Second," J. Geoph. Res., Vol. 70, pp. 1415-1427, 1965.

TABLE 1

		Theory		Experiment		Present Work
		Faller and Kaylor	Lilly	Faller, Faller & Kaylor	Tatro & M-C	
	R_{ecrit}		110	125 ± 5	124.5 + 7.32 R_0	
	λ/D	11	11.9	10.9	11.8	
Type 1	ϵ^*	+12°	8°	+14.5 ± 2.0	+14.8 ± 0.8	
	V_p/V_{geo}		.094	---	3.4%	
	R_{ecrit}		55	---	56.3 ± 116.8 R_0	56.7
	λ/D		21	22 to 33	27.8 ± 2.0	(frequency)
Type 2	ϵ^*		-20°	+5° to -20°	0° to -8°	61% of that predicted by Lilly
	V_p/V_{geo}		.57	---	~16%	

* ϵ is angle between wavefront and the "Tangential" direction.

Results of calculations and observations of instabilities

TABLE 2

PER = 2.322 D = .230

Radius	RE	R_0	δ/D
cm			
97	33	.039	.997
	50	.0595	.969
	64	.076	.988
	77.5	.092	1.000
	90	.107	.965
	103	.128	1.010
	123	.146	1.035
36	52	.166	1.014
	92.5	.296	1.028
	131	.418	1.008

Boundary layer thickness

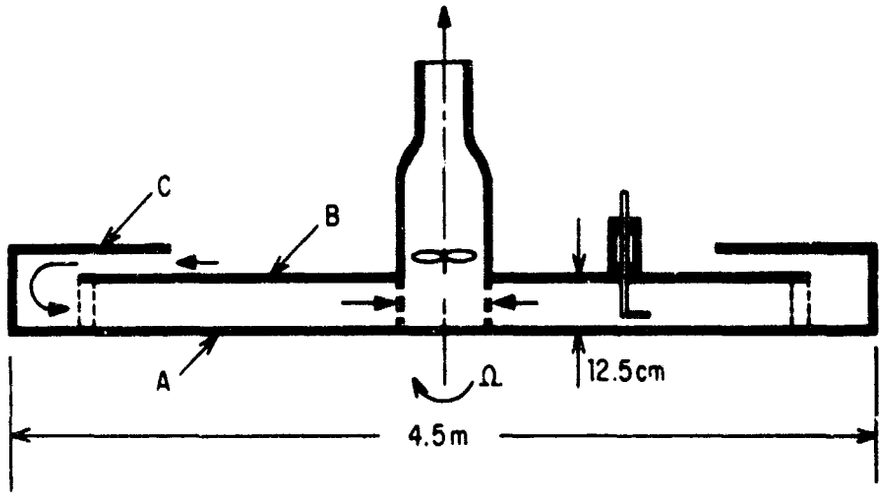

1. Schematic diagram of apparatus

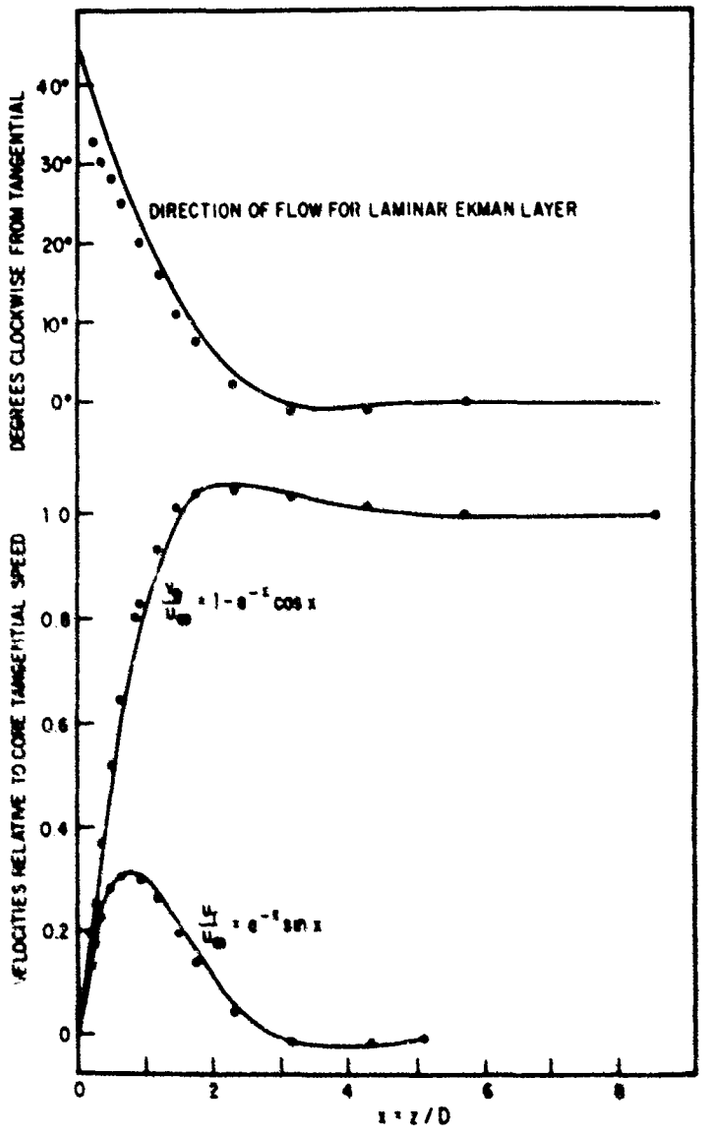

2. Velocity profiles for the laminar boundary layer

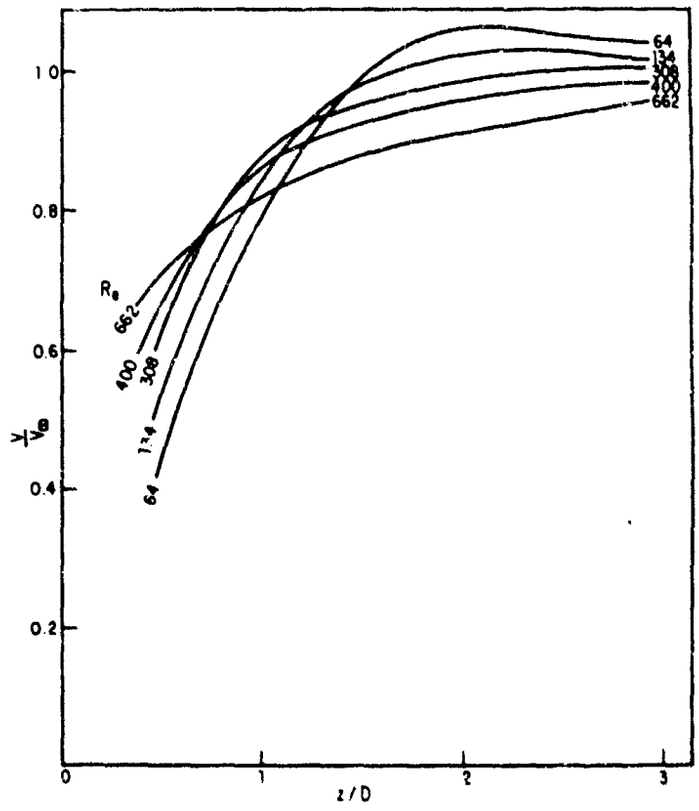

3. Mean velocity profiles, V/V vs. Z/D , for higher Reynolds numbers

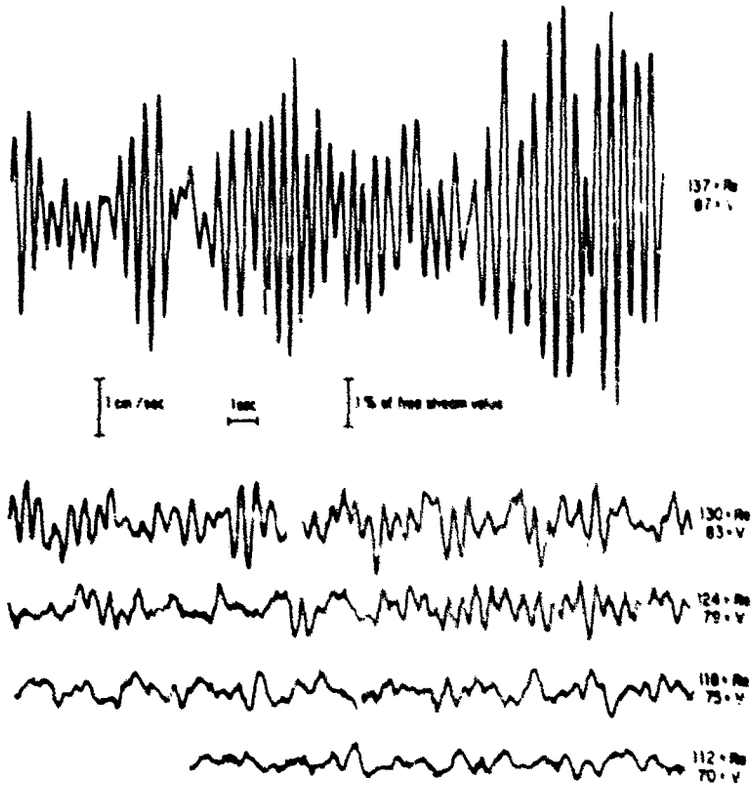

5. Instabilities near their first appearance

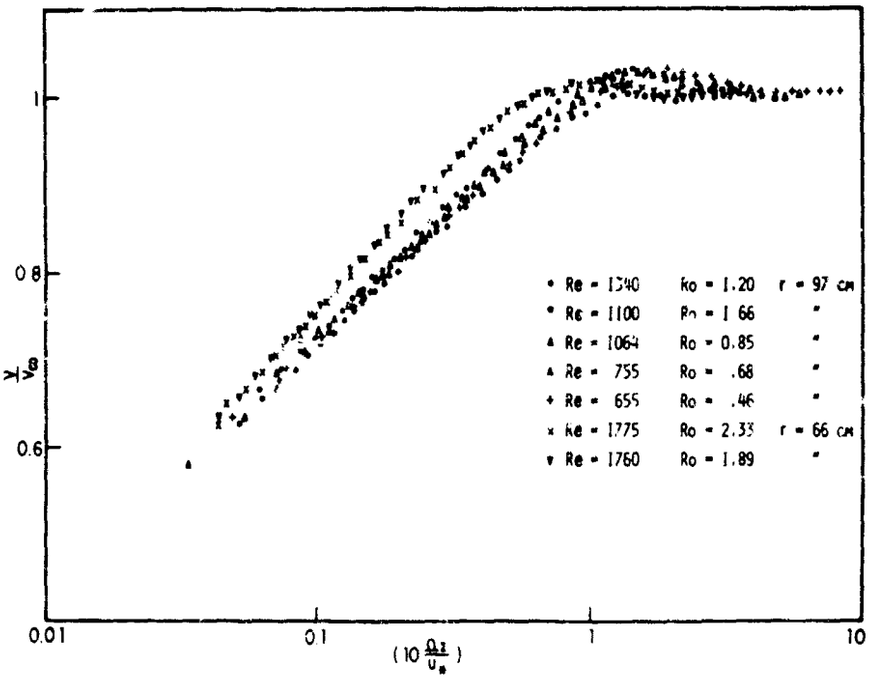

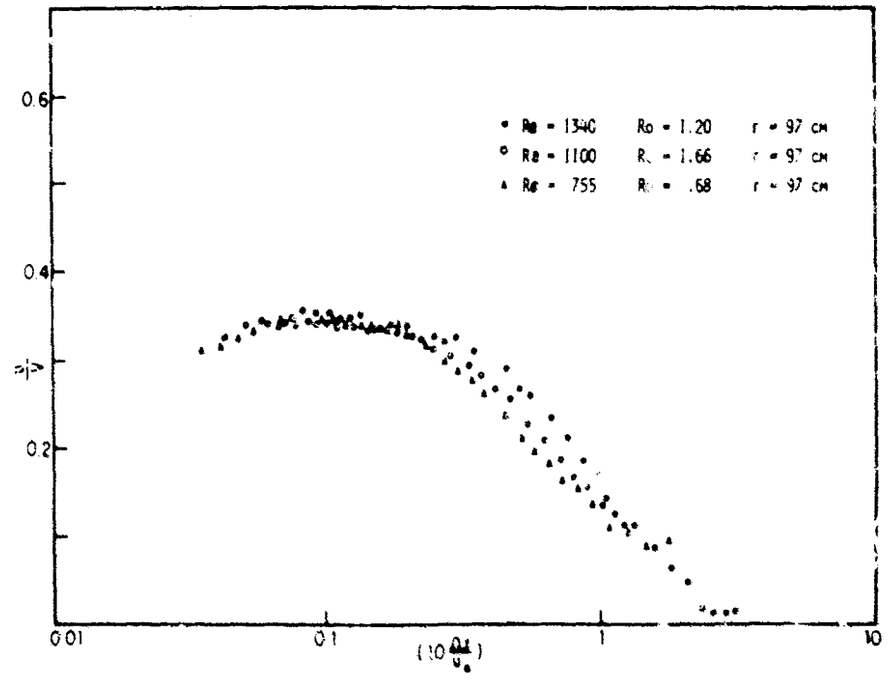

4. **Fully turbulent boundary layer profiles**

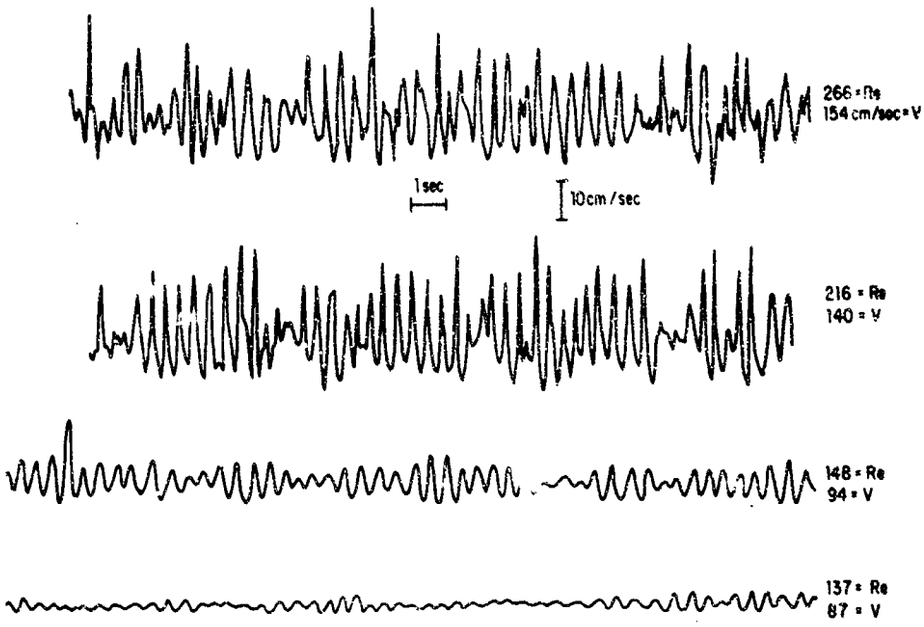

6. Growth of instabilities with increasing Reynolds number

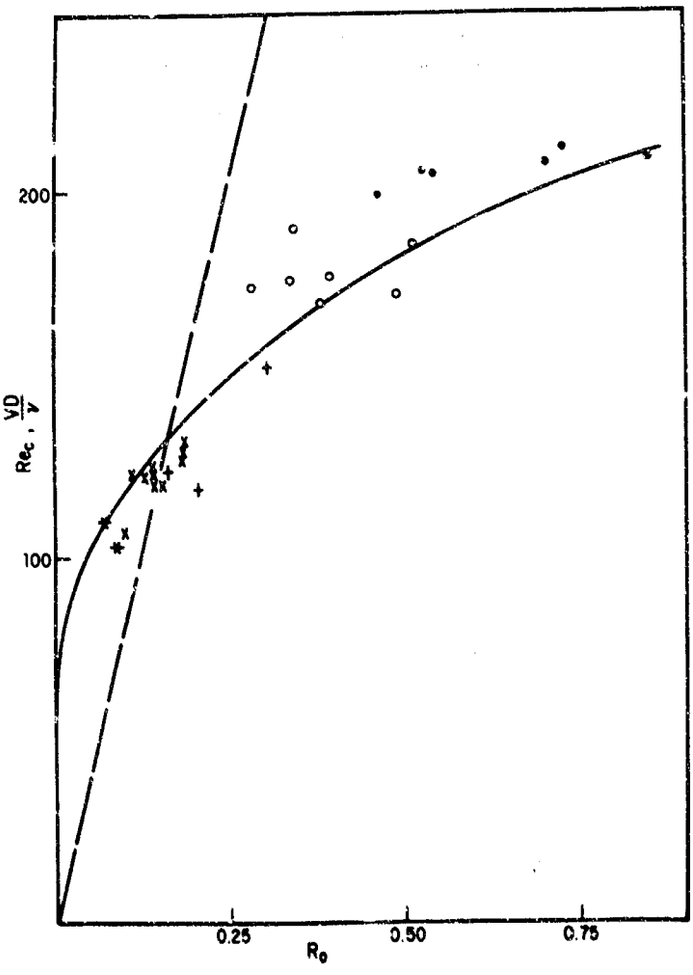

7. Apparent critical Reynolds number as a function of Rossby number

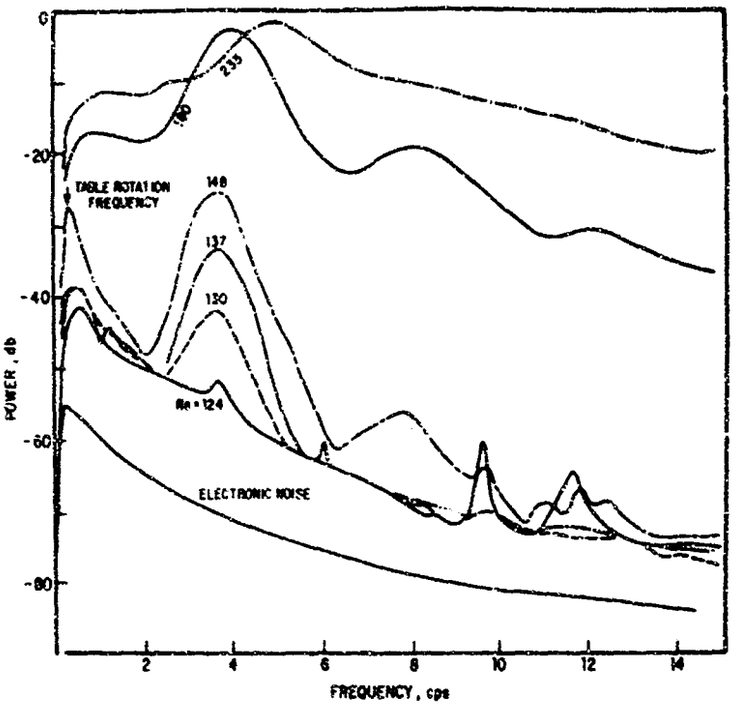

8. Power spectra of hot-wire signal at various Reynolds numbers

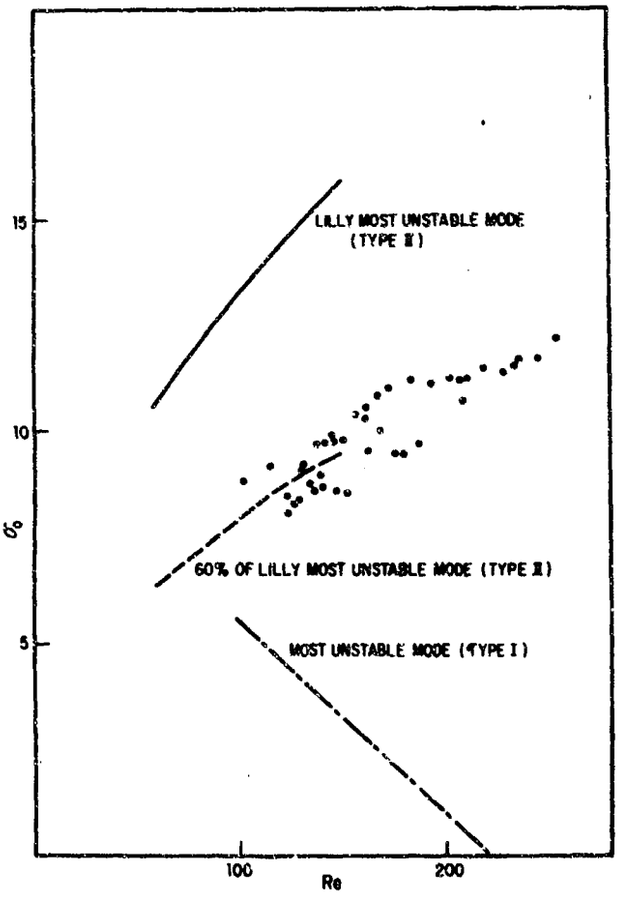

9. Frequency of spectral peak as a function of Reynolds numbers

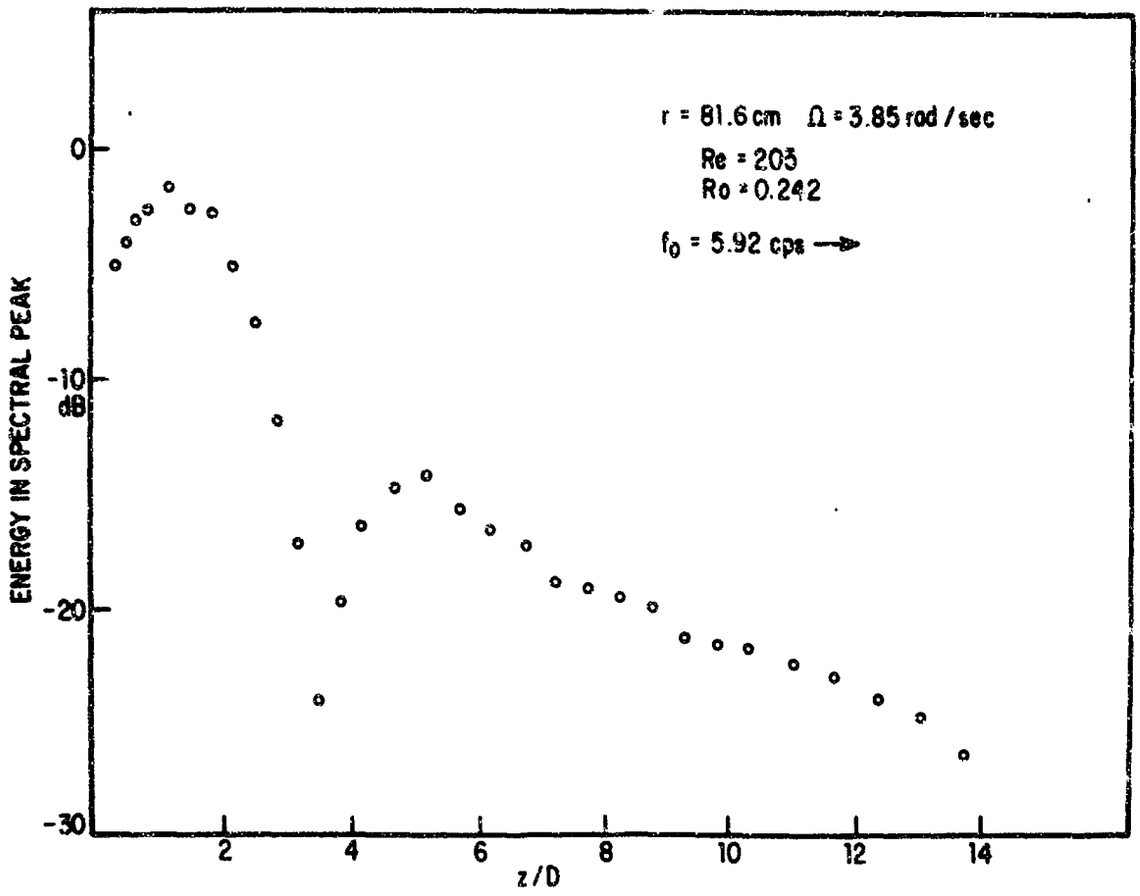

10. Energy in spectral peak vs. distance from boundary

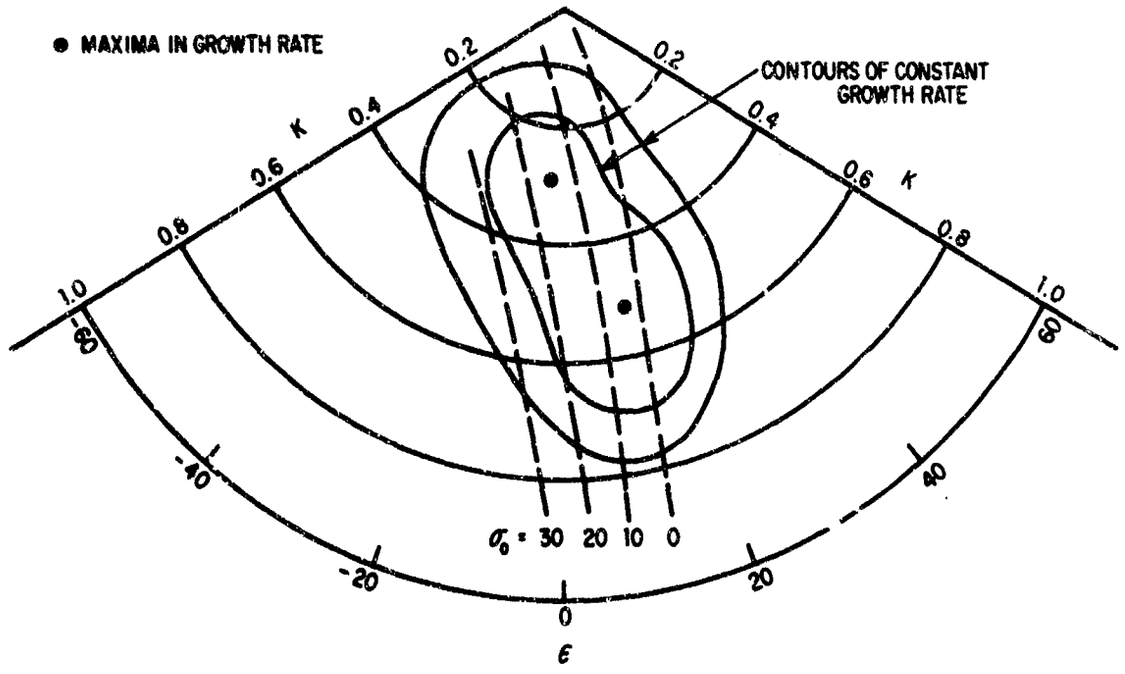

11. Theoretical predictions of growth rates and frequencies for $R_e = 150$

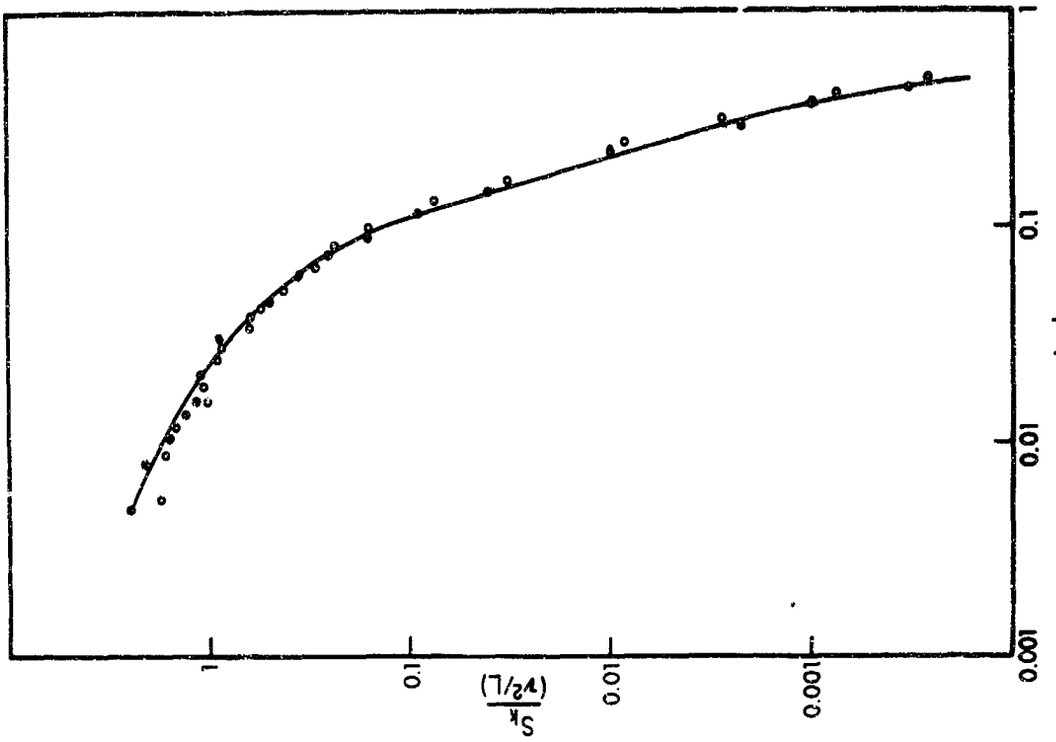

13. Non-dimensional turbulent spectra

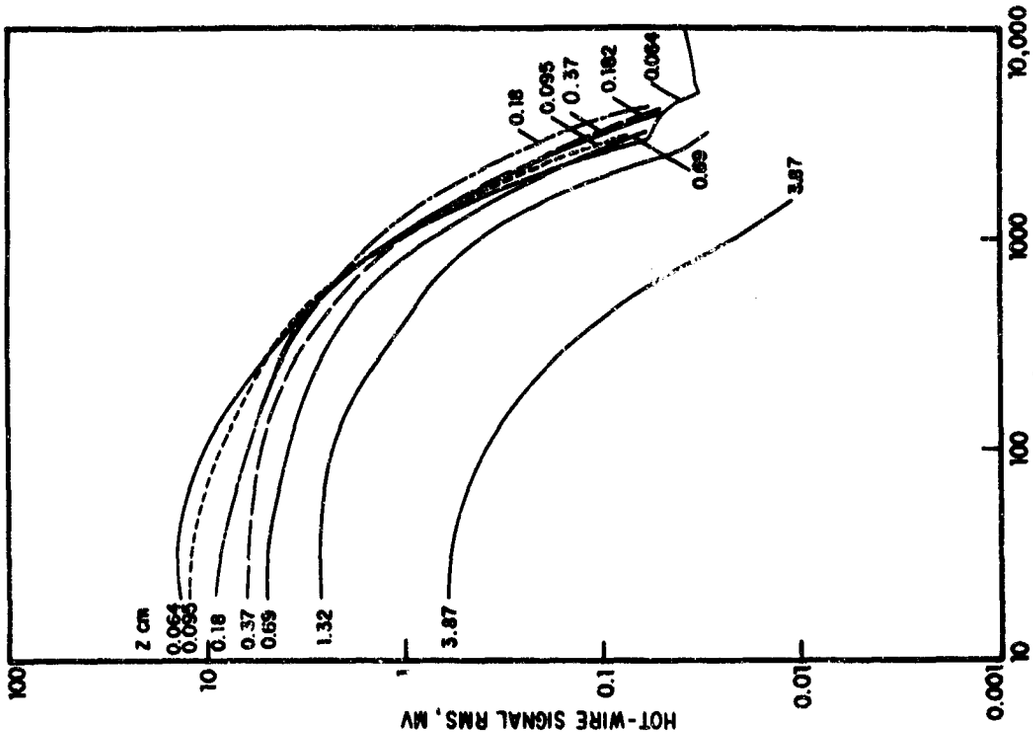

12. Turbulent spectra for various heights

A Review of Industrial Problems Related to Atmospheric Shear Flows

by

C. Scruton

National Physical Laboratory, United Kingdom.

SUMMARY

The non-aeronautical problems related to atmospheric shear flows are broadly divided into those of the effects of the airflow itself on environmental conditions and those of the effects of the airflow on structures immersed in it. The first category includes wind shelter, smoke dispersal and air pollution, and the flow of wind in and around building complexes. By far the most important problems in the second category relate to the design of structures against the loadings due to wind. For many buildings and structures consideration of the time-averaged wind loads is sufficient but with the modern tendency towards more slender and lighter structures using methods of fabrication which produce less structural damping, they have become more prone to respond to the unsteady wind loading which arises either directly from the fluctuations of wind force due to the turbulence of atmospheric shear flows or to the inherent aerodynamic instability of the structure.

The important properties of atmospheric winds in the above problems are the variation of the wind speed and direction with height, and the characteristics of the turbulence and their dependence on height. These properties vary with the terrain over which the wind flows and with the strength of the wind. Some of the effects of the speed profiles and of the turbulence of atmospheric shear flows on smoke dispersal and wind loading are briefly discussed.

1. Introduction

Inasmuch as atmospheric shear flows form a part of our climatological environment it is evident that their influence and consequently the related problems must be widespread indeed. However, in this review discussion will be limited to some of the problems relating to the building and constructional industry. These can be conveniently regarded as falling into two categories: the problems associated with the airflow itself, and those concerned with the effects of the airflow on the building or structure. In the first category are the problems of wind shelter, of smoke dispersal and air pollution, and of the wind environment around and through building complexes, town centres, etc. In the second category are the problems of wind loadings on buildings and structures. For the design of some structures the time-averaged wind loads suffice, but for others, especially for those of slender, lighter construction employing modern methods of fabrication which provide only low amounts of structural damping, the unsteady wind loads leading to an oscillatory response must enter into the design considerations. Such unsteady wind loadings may arise directly from the fluctuations of wind pressure due to the velocity fluctuations of turbulent winds, or from some source of aerodynamic instability.

Smoke dispersal, wind environment, steady and unsteady wind loadings are all influenced by the characteristics of atmospheric winds in the earth's boundary layer. These characteristics vary with the terrain over which the wind flows, and thus the response of a structure to wind and the other wind effects mentioned above will differ considerably according to the site on which it is constructed.

2. Relevant Characteristics of Atmospheric Shear Flows

The characteristics of atmospheric shear flows which are relevant to the problems of smoke dispersal, to environmental wind conditions, and to wind loading of structures are basically the wind speed (and/or wind pressure) and its temporal and spatial variations. Temperature gradient is significant only in so far as the lapse rate influences the wind speed characteristics. While meteorologists have provided much valuable information on the mean winds speeds, not enough is known about the turbulence structure in the atmospheric shear flows. However, a number of investigations have been made, or are in progress. The following resume of generally accepted characteristics of the atmospheric winds for adiabatic lapse rate conditions is largely due to the work of Davenport[1,2] and Harris[3,4]. The supporting evidence is not always very strong and modifications can be expected as more information becomes available.

(a) Wind profile

A power law expression for the variation of mean wind speed with height

$$\frac{\bar{V}_z}{\bar{V}_G} = \left(\frac{z}{z_G}\right)^{\alpha} \qquad \ldots (1)$$

($\bar{V}_z$ and $\bar{V}_G$ are the mean wind speeds at local height z and at gradient height z_G) is more convenient than the usual logarithmic profile expression in equation (1). The exponent α, and the gradient height, depend on the roughness of the terrain, as in the following Table 1.

Table 1

Type of Terrain	α	z_G metres	K
Open terrain with very few obstacles: open grass or farmland with few trees or other barriers, prairie, tundra desert, low islands, etc.	0.16	300	0.005
Terrain uniformly covered with obstacles 9-15 in high: residential suburbs, small towns, woodland scrub, etc.	0.28	430	0.015
Terrain with large and irregular objects: centres of large cities, broken country with windbreaks of tall trees etc.	0.40	560	0.050

K is the surface drag coefficient referred to a height of 10 metres. $K = \frac{\tau_0}{\rho \bar{V}_{10}^2}$ where τ_0 is the Reynolds shear stress.

The gradient height is defined as that at which the wind is free of the earth's frictional influence. Because of the drag of the earth's surface the wind direction does not remain constant well height but veers away from the centre of depression as the height increases. A theoretical analysis by Ekman suggests that for the "city centre" terrain this veer could be as much as 45 degrees but measurement suggest that the actual veer may be somewhat less than its theoretical value.

The fluctuations of windspeed due to turbulence are expressed as power spectra. For longitudinal turbulence a normalised turbulence spectrum is used which is assumed independent of height, wind speed and terrain roughness. This standard spectrum* in the form suggested by Harris[2] is

$$\frac{n\, S^u(n)}{K\, \bar{V}_{10}^2} = 4\, \frac{X}{(2+X^2)^{5/6}} \qquad \ldots (2)$$

where n is the frequency

$S^u(n)$ is the power spectral density function of the longitudinal component of turbulence u

K is the surface roughness coefficient of the terrain (see Table 1)

$\bar{V}_{10}$ is the mean windspeed at height 10 metres

and $X = \frac{n\, \ell}{\bar{V}_{10}}$, where ℓ is an arbitrary length to which Davenport assigned a value of 1200 m.

The above expression yields the variance σ^{u2} as

$$\sigma^{u2} = 6.7\, K\, \bar{V}_{10}^2 \qquad \ldots (3)$$

and combining this with the expression for the power law profile yields the profile for the turbulence intensity.

$$\sigma_z^u / \bar{V}_z = 2.58\, K^{\frac{1}{2}} \left(\frac{10}{z}\right)^{\alpha} \qquad \ldots (4)$$

and for the integral length scale of the turbulence L_x

$$[L_x]_z = 100 \left(\frac{z}{10}\right)^{\alpha} \text{ metres} \qquad \ldots (5)$$

The above data relate to the properties of the turbulence and mean windspeed at a point in space. The design analyses for structures require a knowledge of the spatial correlations of the turbulence, and particularly of the lateral and vertical correlations of the longitudinal components of turbulence (L_y^u and L_z^u). Measurements of the vertical scales of the longitudinal (L_z^u) and of the lateral (L_z^v) components of the turbulence in open country reported by Harris gaves values of $L_z^u = 60$ m and 72 m approximately at heights of 100 and 180 m respectively. The values of L_z^v at corresponding heights were 29 m and 34 m. Alternatively the spatial correlation may be expressed by the coherence, which is based on the normalised cross-correlation spectral density function for individual wave numbers. If we ignore the out-of-phase component of the cross-spectra,

$$R^u(z, z', n/\bar{V}) = \frac{S^u(z, z', n/\bar{V})}{\sqrt{S^u(z, z, n/\bar{V})\, S^u(z', n/\bar{V})}}; \qquad \ldots (6)$$

---

*The relation (2) is very similar to the form suggested by von Karman to describe isotropic turbulence.

and, assuming homogeneous turbulence,

$$S^u(z,z,n/\bar{V}) = S^u(z',z',n/\bar{V})$$

and hence

$$\sqrt{\text{coherence}} = \frac{S^u(z,z',n/\bar{V})}{S^u(z,z,n/\bar{V})} \qquad \ldots (7)$$

For the vertical correlation of the longitudinal component Davenport has given the following relations showing the dependence of the coherence on the wave number and the distance apart $\Delta z = z-z'$:-

$$\sqrt{\text{coherence}} = e^{-k\Delta z \cdot \frac{n}{\bar{V}}} \qquad \ldots (8)$$

The coefficient k depends on the reference velocity used and on the terrain. With the reference velocity at the standard height of 10 metres the available information suggests that k=6 for built up areas and k = 7.7 for open country.

3. Influence of Velocity Profile and Turbulence on the Time-averaged Wind Loads on Structures

Most design procedures for buildings and structures are based on time-averaged wind loads calculated using design wind speeds which are the maximum windspeeds averaged over a specified short period of time which are considered likely to occur at the site. This period may vary from a few seconds to several minutes but is always much shorter than the minimum of 20 minutes required for atmospheric winds to become quasi-stationary in character (so that fluctuations with time-scales less than 20 minutes can be regarded as contributions to the turbulence). The adoption of a design wind speed based on a period of less than 20 minutes therefore contains an allowance, or a "gust factor", which takes some account of the increase in mean wind speeds of short duration gusts. The design wind loading obtained is usually assumed to apply uniformly to the whole of the structure and takes no account of the incoherence of the wind speed along the length of a horizontal (or vertical) structure of length much greater than the lateral (or vertical) scale of the longitudinal components of the turbulence. This incoherence results in some reduction of the total wind loading when the design wind speed is based on a short-duration gust period. However, the turbulence also affects the wind force and pressure coefficients through changes in the mean airflow. In the following discussion of these effects the coefficient are referred to the mean wind speed averaged over a long period of time.

Bearman[5] has examined the influence of intensity $\sqrt{u^2}/\bar{V}$ and scale of turbulence L_x on the base pressures behind a series of flat plates of small aspect ratio set normal to the stream. For a range of the product $\frac{L^2_x}{A} \cdot \frac{\sqrt{u^2}}{\bar{V}}$ from 0 to 0.09 (where A is the area of the plate) the base pressure coefficients all collapsed on to one curve with a maximum increase of the base "underpressure" coefficient $[-C_{pb}]$ of about 30 percent, which represented an overall drag coefficient increase of about 10 percent.

The influence of turbulence on the base pressure coefficients on a long square section prism[7] is shown in Figure 1. The very large reduction in the value of $[-C_{pb}]$ in turbulent winds is attributed to the turbulence in the approaching stream causing the shear layers to re-attach on the side faces before separating again at the corners. The differences in $[-C_{pb}]$ at the low incidence represent reductions of about 30 percent in the drag; this reduction, however, is not maintained at the higher inclinations, when reattachment of the separated shear layers cannot occur. Accompanying the changes in C_{pb} were marked reductions in the fluctuating lift coefficient (a measure of aerodynamic excitation due to vortex shedding) and in its spanwise correlation length. Except for very slender buildings (H/B > 10) the reductions in the mean drag coefficients were not apparent in the results of tests on rectangular buildings shown in Fig. 2, the mean drag coefficients found in smooth flow for the square section blocks (H/D = 1.0) can be compared with those in turbulent flow, for which the intensity was about 10 percent and the ratios of the longitudinal and lateral scales of the longitudinal components to the width were given by $L^u_x/B = 4$ and $L^u_y/B = 1.3$ respectively. The same diagram also suggests that for the very low Reynolds numbers at which the tests were carried out, turbulence does not reduce the drag of circular cylinders.

The influence of turbulence on the airflow over a circular cylinder would be expected to be most marked near the critical Reynolds number. This is supported by the results presented in Fig. 3 in which the critical Reynolds number is shown to decrease progressively as the intensity of turbulence increases. Bearman[5] has used the results of Fig. 3 to show that the critical Reynolds number for a

two-dimensional cylinder is a function of a turbulence parameter $\frac{\sqrt{u^2}}{\bar{v}}\left(\frac{D}{L_y^u}\right)^{1/5}$ (see Fig. 4). For this purpose the critical Reynolds number was defined as the Reynolds number at which the value of C_D falls to 0.8. The evidence for assessing the influence of turbulence on three-dimensional cylinders (e.g. chimney stacks) is scanty. The results of Fig. 5 suggest that turbulence produces some reduction in the overall drag coefficient even at much higher Reynolds numbers in the transcritical range.

In addition to the turbulence properties of atmospheric winds the variation of mean wind speed with height may have a marked influence on the pressure distributions and on the overall forces due to wind. In most of the wind-tunnel investigations which have been carried out with a wind profile the profile has been produced by a grid of rods or by surface roughness. Since both of these methods also introduce turbulence it is difficult to assess the separate influences of turbulence and profile. The pressure distributions on the walls and roofs of low-rise buildings in simulated atmospheric shear flows are dependent on the flow characteristics and are often markedly different from those obtained in smooth uniform flow. In particular the very high underpressures often found on low-pitched roofs in smooth uniform flow are reduced in the atmospheric shear flow and this reduction appears to be in part due to the profile and in part due to the turbulence. For some tests on high-rise building blocks Baines[8] produced a profile using curved screens with consequent little increase in the turbulence. With this arrangement he found that the surface pressures* along the centre-line of the windward face increased with height as the square of the windspeed at the local height. The underpressure on the leeward face remained constant with height at a value determined by the pressure over the roof. The overall drag and overturning moment are, as coefficients of a building would be expected, less in gradient than in uniform winds if the reference wind speed is taken as that at the top of the building. Typical and the reductions for a rectangular building 133 m (high) by 70 m by 24 m shown below (the reference area and height are the area of the wide face and the total height)

	Wind normal to a wide face		Wind normal to a narrow face	
	C_D	C_M	C_D	C_M
Smooth Uniform flow	1.25	0.62	0.29	0.17
Turbulent shear flow	0.92	[illegible]	0.19	0.12

Measurements of the pressure distributions around cooling towers in smooth uniform flow and in turbulent shear flow show reductions in the peak underpressure at the sides and in the base underpressure in both subcritical and supercritical airflows.

The variation along the height of the ratio of the sectional drag coefficient at local height to that at mid-height shown in Fig. 5, is of some interest. It shows a reduction of the drag coefficients by about 15 percent when turbulence of about 6 percent is introduced into the stream, and also considerable non-uniformity in the distribution of drag, with a sharp peak near the top of the stack. This peak on a C_{D_z}/C_{D_m} plot is, as would be expected, much higher in the gradient than in the uniform wind.

4. The Dynamic Response of Flexible Structures to the Direct Forcing Action of Randomly Fluctuating Forces due to Turbulence

In this section we are concerned only with the direct forcing of an elastic structure by the random fluctuations of the drag forces due to turbulent winds. The response of flexible structures to any inherent aerodynamic instability mechanism will be discussed in the next section. Both of these oscillatory response problems have become increasingly important with the adoption of modern methods of fabrication which have led to lighter structures with less inherent structural damping, and also with the tendency to build taller and more slender structures than hitherto.

---

*"Pressure" in this context defines the difference between the pressure on the surface and the static pressure of the approaching wind. When this is negative it is referred to as an underpressure.

Because we are now dealing with the random properties of turbulence we are concerned with the statistical averages of both the input excitation and the output deflection response, the wind force on the structure will have a mean and a fluctuating component and the response will also be time-dependent.

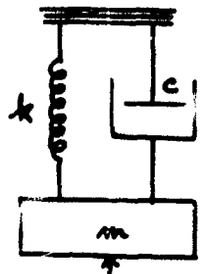

FORCE $P(t) = \bar{P} + p(t)$

DISPLACEMENT $Q(t) = \bar{q} + q(t)$

FIG. 6

For the simple linear single degree-of-freedom system shown in Fig. 6, the differential equation of notation is

$$m\ddot{Q} + c\dot{Q} + kQ = P(t) \qquad \ldots (9)$$

from where we can separate a time-average response $\bar{q} = \bar{P}/k$ and for the fluctuating component write

$$m\ddot{q} + c\dot{q} + kq = p(t) \qquad \ldots (10)$$

If $p(t)$ can be expressed in terms of a spectral density function $S^P(n)$ such that

$$\overline{p(t)^2} = \int_0^\infty S^P(n)\, dn \qquad \ldots (11)$$

the response is given in terms of another spectral density function $S^q(n)$

$$\overline{q(t)^2} = \int_0^\infty S^q(n)\, dn$$

$$= \frac{1}{k^2} \int_0^\infty |H(n)|^2 \cdot S^P(n) \cdot dn \qquad \ldots (12)$$

$$S^q(n) = \frac{1}{k^2} |H(n)|^2 S^P(n) \qquad \ldots (13)$$

where $|H(n)|^2$ is the transfer function between the power spectral density functions for $q(t)$ and $p(t)$ and is termed the structural admittance. For the system of Fig. 6

$$|H(n)|^2 = \frac{1}{\left[1 - \left(\frac{n}{n_o}\right)^2\right]^2 + 4\zeta^2 \left(\frac{n}{n_o}\right)^2} \qquad \ldots (14)$$

where $n_o = \frac{1}{2\pi}\sqrt{\frac{k}{m}}$, the natural frequency and $\zeta = \frac{c}{c_o} = \frac{c}{\sqrt{km}}$ the critical damping ratio.

An expression for the fluctuating force on a small area A is

$$P(t) = \tfrac{1}{2} \rho V(t)^2 A C_D + \rho \frac{\delta V}{\delta t} \cdot \frac{A^2}{D} \cdot C_m \qquad \ldots (15)$$

where $V(t) = \bar{V} + u(t)$. Neglecting the virtual mass term C_m and the terms in $u(t)^2$ this yields

$$\bar{P} = \tfrac{1}{2} \rho A \bar{V}^2 A C_D \qquad \ldots (16)$$

$$p(t) = \rho \bar{V} A u(t) \qquad \ldots (17)$$

and a relation between the force spectrum and the gust spectrum

$$S^p(n) = 4 \cdot \frac{\bar{P}^2}{\bar{V}^2} \cdot S^u(n) \qquad \ldots (18)$$

The expression is valid only for a "point" area where the turbulence scales are much greater than the typical dimension of the body for the more practical case where the dimensions of the structure and the turbulence scales are of the same order Davenport[9] introduces a factor $|\chi(n)|^2$ termed the "aerodynamic admittance", so that

$$S^p(n) = 4 |\chi(n)|^2 S^u(n) \cdot \frac{\bar{P}^2}{\bar{V}^2} \qquad \ldots (19)$$

$|\chi(n)|^2$ is a function of $nB/\bar{V}$ and $\frac{D}{L_x}$, where D is a linear dimension of the body, and for either n or D equal to zero $|\chi(n)|^2 = 1$. Combining equation (19) with equation (13) the power spectrum of the response becomes

$$S^q(n) = 4 |H(n)|^2 |\chi(n)|^2 \frac{\bar{P}^2}{k^2 \bar{V}^2} \cdot S^u(n) \qquad \ldots (20)$$

$$= 4 |H(n)|^2 |\chi(n)|^2 \frac{\bar{q}^2}{\bar{V}^2} \cdot S^u(n)$$

or in a normalised form

$$\frac{n S^q(n)}{\bar{q}^2} = 4 |H(n)|^2 |\chi(n)|^2 \frac{n S^u(n)}{\bar{V}^2} \qquad \ldots (21)$$

The procedure for obtaining the power spectral density function $S^q(n)$ is illustrated by Fig. 7. Then the variance of the deflection

$$\sigma^{q2} = \int_0^\infty S^q(n) \cdot dn$$

$$= \int^\infty n S^q(n) \, d \log(n) \qquad \ldots (22)$$

is given by the area under the curve of Fig. 7(e).

If the probability distribution function is known or can be assumed (e.g. a gaussian distribution is usually assumed), further statistical information of interest to structural designers can be derived, including the number of times the deflection $q(t)$ exceeds a specified value in a prescribed period of time, and the maximum value of $q(t)$ in a prescribed period of time.

A main problem in the calculation of the response by this method is that of evaluating the aerodynamic admittance $|\chi(n)|^2$. For large buildings the lateral and vertical scales of longitudinal components of the turbulence have a marked influence on the aerodynamic admittance. There is little theoretical analysis applicable, but for flat plates normal to the airstream Vickery[10] has had some success with a "lattice" model, in which it is assumed that the plate is composed of a uniform lattice grid with members of small width compared with the smallest wavelength of the velocity fluctuation of interest, and a mesh spacing large compared with the width of the members. It also assumes that the presence of the plate does not influence the velocity of the airstream approaching the individual members of the "lattice". The force on air element of the lattice in time dependent flow is written (equation 15)

$$P(t) = \tfrac{1}{2} \rho V(t)^2 A C_D + \rho \frac{\partial V(t)}{\partial t} \cdot \frac{A^2}{D} \cdot C_m \qquad \ldots (23)$$

where D is a body dimension

A is a reference area for the virtual mass and the drag coefficients, C_m and C_D, respectively.

Vickery's analysis then gives

$$|\chi|^2 = \left\{ 1 + \frac{4\pi^2 C_m}{C_D^2} \left(\frac{nD}{\bar{V}} \right)^2 \right\} \frac{1}{A^2} \iint^{AA} R^U(a,b,n)\, dA_a\, dA_b \qquad \ldots (24)$$

where dA_a and dA_b are elements of area of the plate and $R^U(a,b,n) = \frac{S^U(a,b,n)}{S^U(n)}$, the normalised cross-spectral density function of velocity. For atmospheric turbulence

$$R^U(a,b,n) = \exp\left(-7.5 \cdot \frac{n\, r_{ab}}{\bar{V}} \cos 1.4\right) \cdot \frac{n\, r_{ab}}{\bar{V}} \qquad \ldots (25)$$

where r_{ab} is the distance between two velocity measuring points. Vickery's theoretical values of $|\chi(n)|^2$ for square flat plates and their dependence on L_x/D and frequency parameter are given in Fig. 8. Measured and theoretical values of $\chi(n)$, together with the following empirical relationship, are compared in Fig. 9.

$$\chi(n) = \frac{1}{1 + \left(\frac{2m\sqrt{A}}{\bar{V}} \right)^{4/3}} \qquad \ldots (26)$$

Detailed discussion of the fluctuating forces on flat plates, and the results of more recent research at the NPL are presented by P.W. Bearman* at this meeting.

The method outlined above has been extended to apply to simple linear systems such as self-supporting lattice towers but also to sheeted-in structures (tall buildings).

For code purposes, methods for determining a dynamic "gust factor", the ratio to the mean wind-speed of the steady wind speed required to produce a static deflection equal to the maximum deflection produced by turbulent wind, have been suggested for the use of structural designers. Such gust factors take into account the nature of the terrain inasmuch as this influences the characteristics of the atmospheric shear flows, the fundamental natural frequency, the structural damping, and the size of the structure. Typically, for city building blocks of heights over 60 m and structural damping ratio $c/c_c = 0.02$ the design wind speed based on the dynamic gust factor approach mentioned above would exceed that based on a maximum 10-second gust speed using the static approach. For lesser heights the static approach gives more conservative loadings than the dynamic approach.

5. The Influence of Turbulence on the Aerodynamic Stability of Structures

There are a number of aerodynamic mechanisms which can excite oscillatory or divergent instabilities of structures. These mechanisms do not require the forcing action due to the fluctuations of wind speed of the approaching stream but can occur, and indeed are often more pronounced, in smooth airflow. Neither is coupling between two degrees of freedom, as in the classical flutter of aircraft wings, a necessary feature; oscillations can be set up in a single degree of freedom system. The practical manifestation of such instabilities is to be found in the wind-excited oscillations of suspension bridges (as, for example, those that destroyed the first Tacoma Narrows bridge), in the swaying of tall chimneys and buildings in wind, and in the galloping motions of transmission lines. Because the instabilities are present in smooth airflow most of the aerodynamic data acquired and used in the past for their prediction has been determined from investigations in wind tunnels with smooth airflow. Because the shapes are aerodynamically bluff, theoretical estimates of the exciting wind forces are not available, and the data from experimental investigations are inadequate to cover all the variations of shape, size, aspect ratio, frequency, amplitude, Reynolds number and characteristics of the shear flow, on which the excitation depends. Thus for the design of specific structures suspect to aerodynamic instabilities, the most reliable predictions of the wind-excited oscillations are made with the aid of a wind-tunnel tests of aeroelastic models in airflows of appropriate characteristics (see Scruton[11]).

The influence of turbulence on the aerodynamic stability of structures has not yet been extensively investigated but some of the effects found are mentioned below.

---

*Paper No. 24 "Fluctuating forces on bluff bodies in turbulent flow" by P.W. Bearman.

The two types of aerodynamic exciting mechanisms most commonly experienced are the vortex and the galloping excitations. The former arises from the periodic discharge of vortices alternately from each side of a bluff body which give rise to alternating cross-wind forces (frequently referred to as "lift forces") to which a flexible structure will respond by oscillating in a cross-wind direction, and the response will be particular large when the predominant frequency of vortex shedding coincides with a structural natural frequency. The galloping type excitation depends on the destabilising character of the variation of the mean (time-average) wind forces with incidence and can occur when the lift slope is negative[12]. For small amplitude oscillations the criterion for galloping type instability is

$$\frac{d\,C_L}{d\alpha} + C_D < 0 \qquad \ldots (27)$$

As for vortex-induced motions the displacements for galloping-induced oscillations are in the cross-wind direction; there is little to distinguish the oscillations arising from the two types of excitation except perhaps the greater violence of those due to the latter. When the motion is simple harmonic, the aerodynamic excitation is conveniently measured in terms of an aerodynamic damping force per unit length $K_a \dot{z}$ where z is the displacement. Alternatively for vortex-induced oscillations a fluctuating lift coefficient C_L is sometimes used to give a fluctuating force

$$F = \tfrac{1}{2} \rho V^2 D C_L \sin 2\pi Nt \qquad \ldots (28)$$

where N is the frequency of the oscillation. There is a simple relationship between the non-dimensional form of $K_a \left(k_a = \frac{K_a}{\rho N D^2} \right)$ and C_L of the form

$$C_L = -c \cdot \frac{\pi k_a \eta_0}{V_r^2} \qquad \ldots (29)$$

where the value of c depends upon the modal shape of the oscillation, η_0 is the non-dimensional amplitude z_0/D, and V_r is the reduced velocity V/ND. If the aerodynamic force per unit length is spread over a wide range of frequencies, the force is given by its power spectral density function $S^F(n)$ such that

$$\overline{F^2} = \int_0^\infty S^F(n)\, dn \qquad \ldots (30)$$

and

$$C_L = \overline{F^2} / \tfrac{1}{2} \rho V^2 D$$

The effect of turbulence and shear on the galloping type excitation will follow the changes in the steady lift and drag coefficients due to the changes in the mean flow brought about by the turbulence and shear. The influence of turbulence on the galloping oscillations of a cantilevered square-section prism have been investigated by Novak[15]. He found that for the same mean wind speed the amplitude of the galloping oscillations progressively decreased as the turbulence intensity was increased. Even with fairly high intensities of about 9 percent, however, vigorous large amplitude oscillations were maintained. In the tests the increase in intensity was associated with an increase in the scale of the turbulence.

The influence of velocity profile on vortex-shedding has not been studied systematically, and there are relatively few investigations of the influence of turbulence. Most investigators have found that the introduction of turbulence does not change the predominant frequency of vortex shedding but does decrease the spectral peak of the exciting forces found at the Strouhal frequency and in general broadens the bandwidth of the vortex shedding frequencies. An exception to this comes from the work of Bearman[13] who measured Strouhal numbers of vortex shedding from a circular cylinder in smooth and turbulent airstreams for Reynolds numbers spanning the critical Reynolds number. The results are shown in Fig. 10. The introduction of turbulence lowered the value of the critical Reynolds number. For the smooth and the turbulent airflow at sub-critical Reynolds numbers the Strouhal number $S \approx 0.2$ but at the supercritical values the Strouhal numbers differed, reaching 0.46 and 0.32 respectively. In both cases the bandwidths of the spectra of velocities in the wake of the cylinder were increased and the peak was reduced in going from sub-critical to supercritical values of the Reynolds number. In measurements of the spectra of the lift force fluctuations in turbulent flow on rectangular prisms of various aspect ratios Vickery[6] found that when the breadth/depth ratio exceeded 1 a predominant frequency of vortex shedding was evident while with the ratio less than unity the lift fluctuations corresponded more closely to the broad spectrum of the turbulence velocity.

Measurements of the excitation in turbulent airstreams show the same tende[illegible]he observations

of Strouhal number and of wake velocities. For a long square prism Vickery[7] found that the fluctuating lift coefficient C_L reduced from 1.32 in smooth flow to 0.68 in turbulent flow of 0.10 intensity and $L_x/D \approx 1$; and the correlation length reduced from 5.6D to 3.3D. The above measurements were carried out on stationary models. Oscillatory motion of the models has been shown to interact with the vortex-shedding and thus to increase the vortex-excitation. It is of interest, therefore, to examine the effects of turbulence on the response of oscillatory models. Fig. 11 gives the response amplitudes of a model stack in smooth and in turbulent flows in each case for the wind speed which yielded the maximum amplitude. These maximum amplitudes occurred at $V_r = 6.4$ and $V_r = 4.9$ in smooth and in turbulent flows respectively and, for a specific value of the structural damping, the amplitudes were greater in the turbulent winds. The result is contrary to what would have been expected from the reduction in the peak of the lift coefficient spectrum found in turbulent winds, and indicates that the motion influenced the regularity and strength of the vortex shedding. Similar increase of the cross-wind amplitudes in turbulent flow and compared with those in smooth flow have been observed in other investigations concerning circular section structures, but the changes in the reduced velocity for maximum amplitude have not always been in the same direction.

Fig. 12 shows the amplitude response of a model of a square-section building block to a smooth and turbulent airflows with no shear the cross-wind response in smooth airflow shows the peaked characteristics typical of narrow band excitation. There was negligible response in the in-wind direction. In the turbulent airflow the amplitude responses in both character and the maximum amplitude steadily increased with wind speed. The amplitude in the cross-wind direction was three to four times greater than that in the wind direction. While there is some evidence to suggest that the in-wind amplitudes could have been satisfactorily estimated by the methods outlined in the previous section, the dependence of the cross-wind excitation on the characteristics of the wake precludes successful attempts at calculation of the cross-wind amplitudes until more information of the fluctuating lateral forces on building shapes in turbulent flow is available. At present the most reliable estimates of cross-wind amplitudes are made from tests of aeroelastic models in airflows simulating the appropriate characteristic of atmospheric shear flows.

6. Dispersal of Air Pollutants

The properties of atmospheric shear flows play an essential part in the dispersion of gaseous (or particulate) pollutants in the atmosphere such as arise in the discharge of the effluent plumes from industrial smoke stacks. When the plume source is close to buildings, or in a valley, or close to an escarpment, the local airflow will dominate the dispersal of the plume, and in general recourse must be made to wind-tunnel experiment to provide estimates of the resulting local pollution. Such model experiment should reproduce geometric similarity, similarity of the wind shear and turbulence of the approaching stream, and equivalence of certain similarity parameters concerning plume buoyancy and efflux velocity.

Analytical methods exist for determining the gas concentrations arising from plumes from single stacks surrounded by flat open ground. The calculation is in two parts. The first involves the estimate of an effective height of the emission by the use of one of many plume rise formulae which have been suggested in recent years. A recommended formula, applicable to neutral or near neutral conditions is

$$\Delta h = 0.175 \frac{q_h^{\frac{1}{2}}}{\bar{V}^{3/4}} \qquad \ldots (31)$$

Δh is the plume rise to give an emission height H

$$H = h + \Delta h$$

where h is the height of the chimney

q_h is the heat emission rate in cal/s

and $\bar{V}$ is the mean wind speed in m/s

the gas concentration at a point (x,y,z) is calculated by one of the several dispersion formulae, the most widely used of which is that due to Sutton:

$$C(x,y,z) = \frac{q_m}{\pi C_y C_z \bar{V} x^{2-n}} \exp\left(-\frac{y^2}{C_y^2 x^{2-n}}\right) \times$$

$$\times \left\{ \exp\left[-\frac{z-H}{C_z^2 x^{2-n}}\right] + \exp\left[-\frac{z+H}{C_z^2 x^{2-n}}\right] \right\} \qquad \ldots (32)$$

At ground level $z = 0$ and

$$C(x,y) = \frac{2 Q_m}{\pi C_y C_z \bar{V} x^{2-n}} \exp\left[-\frac{1}{x^{2-n}}\left(\frac{y^2}{C_y^2} + \frac{H^2}{C_z^2}\right)\right] \quad \ldots (33)$$

This is a maximum when $y = 0$, $x = x_m$ where

$$x_m = \left(\frac{H^2}{C_z^2}\right)^{\frac{1}{2-n}} \quad \ldots (34)$$

and

$$C_m = \frac{2 Q_m C_z}{\pi \bar{V} e H^2 C_y} \quad \ldots (35)$$

In the above equation

C is the gas concentration, mass/unit volume

Q_m mass emission rate of the gas

x,y,z space coordinates, origin at point of emission, y cross-wind and z vertical

n a diffusion coefficient related to the wind profile exponent $\alpha = n/(2-n)$

C_y and C_z are diffusion coefficients dependent on the kinematic viscosity, the mean velocity and the intensity of turbulence of the lateral and vertical components respectively

C_y and C_z for different stability categories are available. For the calculation of the maximum concentration at ground level Reference 16 recommends for half-hour sampling times.

Stability	C_z/C_y
Moderately unstable	0.9
Neutral	0.7
Moderately stable	0.5

The formulae are not suitable for inversion or highly unstable conditions.

7. Shelter and Wind Environment

Although there is little information either from wind-tunnel investigations or from field observations of the influence of shear flows on the shelter afforded by fences, screens, hedgerows, etc. that which is available (e.g. reference 17) suggests that considerable differences in the degrees of shelter are to be found in turbulent shear flow as compared with those in a smooth uniform flow. In wind-tunnel tests of shelter effects it is therefore necessary to reproduce the characteristics of atmospheric shear flows.

Instances of the unpleasantly high and gusty wind conditions which can be produced in and near building complexes, and especially near the bases of tall rectangular building blocks, are frequently reported. Low-rise buildings often provide some measure of protection against the ambient wind but wind speed of approaching winds can be considerably increased at ground level near the windward and side faces of tall slab-like building blocks. This is due to the wind speed gradient producing a corresponding gradient of pressure on the windward face, and the downward flow which results forms a frontal vortex at the base of the windward face which swaps away round the sides of the buildings. The high wind speeds near the windward and side faces may be increased still further by the presence of near by buildings and wind speeds up to 50 percent higher than those of the approaching wind can result. This problem and the associated problems concerning the ventilation of buildings and building complexes can be investigated in wind-tunnels in which, of course, it is essential to reproduce the shear properties of the approaching winds and also the local topography and building environment. It is usually difficult to suggest curative measures; any canopy at first or second floor level to stop the downflow has to be of large area to be effective, and where presentative measures have been successful there have been complaints of airlessness and lack of ventilation on days of light winds.

8. Concluding Remarks

This paper has attempted to review briefly the present position in the study of problems concerned

with the influence of atmospheric shear flows on industrial projects. As such it has been confined to wind effects on buildings and structures and to aspects of manmade environment influenced by atmospheric winds. No discussion has been offered on the relation of atmospheric shear flows to natural phenomena which influence our environment such as water evaporation and transport of water vapour, soil erosion, and snow and sand drifting.

Much further research and investigation are needed before will be possible to predict the behaviour of a structure in wind without recourse to wind-tunnel tests. The meteorologist must provide more detailed information of the structure of the wind in the earth's boundary layer and of the effects of terrain; there is for instance an acute lack of data on wind over cities, in which most building takes place. The aerodynamicists must acquire a better understanding of the flows around the aerodynamically bluff structural shapes in turbulent winds and of the time-dependent pressures and forces which result.

References

1. Davenport A.G. — The relationship of wind structure to wind loading Paper 2. Proceedings of conference on Wind Effects on Buildings and Structures. H.M.S.O. London 1965.

2. Davenport A.G. — The spectrum of horizontal gustiness near the ground in high winds. Quart. J.R. met. Soc. vol. 87 April 1961, pp 194-211.

3. Harris R.I. — On the spectrum and autocorrelation function of gustiness in high winds. E.R.A Technical Report No. 5273.

4. Harris R.I. — Measurements of wind structure at heights up to 598 ft above ground level. Paper 1 Proc. Symp. or Wind Effects on Buildings and Structures, Loughborough, 1968.

5. Bearman P.W. — Some effects of turbulence on the flow round bluff bodies NPL Aero Report 1264, 1968 also Paper II Proc. Symp. on Wind Effects on Buildings and Structures, Loughborough 1968.

6. Vickery B.J. — Load fluctuations on bluff shapes in turbulent flow. University of Western Ontario Res. Rep. BLWT-4-67, 1967.

7. Vickery B.J. — Fluctuating lift and drag on a long cylinder of square cross-section in a smooth and in a turbulent stream. NPL Aero Report 1146, 1965 and J. Fluid Mech. (1966) Vol. 25, part 3, pp. 481-494.

8. Baines W.D. — Effects of velocity distribution on wind loads and flow patterns on buildings. Paper 6 Proceedings of conference on Wind Effects on Buildings and Structures HMSO, London 1965.

9. Davenport A.G. — The application of statistical concepts to the wind loading of structures. Proc. Instn. civ. Engrs. vol. 19 pp 449-472, August 1961.

10. Vickery B.J. — On the flow behind a coarse grid and its use as a model of atmospheric turbulence in studies related to wind loads on buildings. NPL Aero Report 1143, March 1965.

11. Scruton C. — Aerodynamics of Structures. Paper 4, Proceedings of the International Research Seminar, 1967. University of Toronto Press, 1968.

12. Scruton C. — The Use of Wind Tunnels in Industrial Aerodynamics Research AGARD Report 309, Oct. 1960.

13. Bearman P.W. — The flow around a circular cylinder in the critical Reynolds number regime. NPL Aero Report 1257 Jan. 1968.

14. Whitbread R.E. and Scruton C. — An investigation of the aerodynamic stability of a model of the proposed tower blocks for the World Trade Center, New York NPL Aero Report 1156 July 1965.

15. Novak M. — The effect of turbulence on the aeroelastic instability of a square section prism. Univ. of Western Ontario Rep. BLWT-7-68, July 1968.

16. — The calculation of atmospheric dispersion from a stack. CEGB Publication 1966.

17. Jensen M and Frandk N. — Model-scale Tests in Turbulent Wind. Part I Danish Technical Press, Copenhagen 1963.

18. Wise A.F.E. Newton A.T. and Lillywhite M.S.T. — Studies of Air Flow Round Buildings The Architects Journal, 1965 vol 141 (19th May) pp 1185-9.

19. Cowdrey C.F. — Two Topics of Interest in Experiment Industrial Aerodynamics Part II Design of velocity-profile grids Paper 29 Proc. Symp. on Wind Effects on Buildings and Structures, Loughborough, 1968.

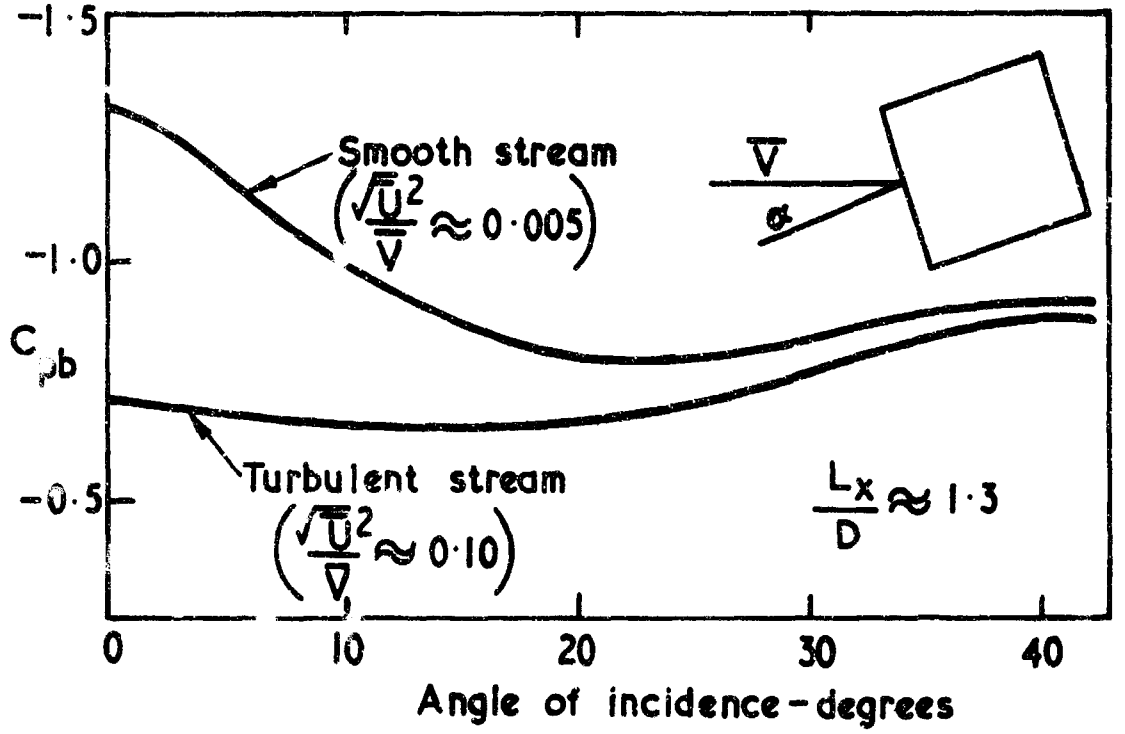

FIG. 1. Variation of base pressure coefficient on a square-section prism (AR = ∞) in a smooth and a turbulent airflow (Vickery[7]).

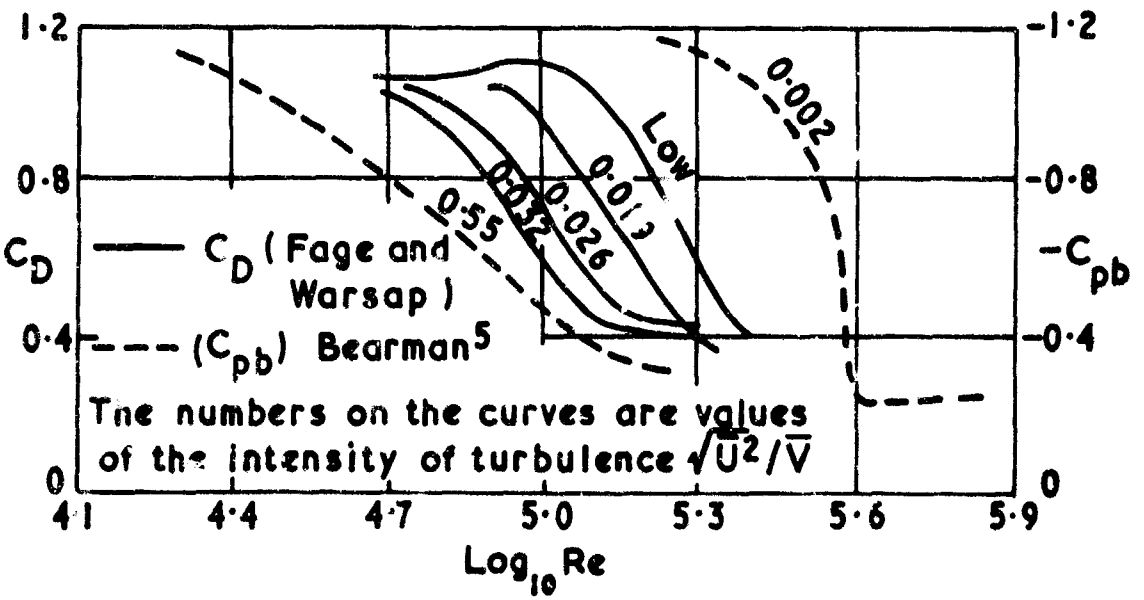

FIG. 3 Effect of turbulence on the drag (or base pressure) of a circular cylinder (AR = ∞)

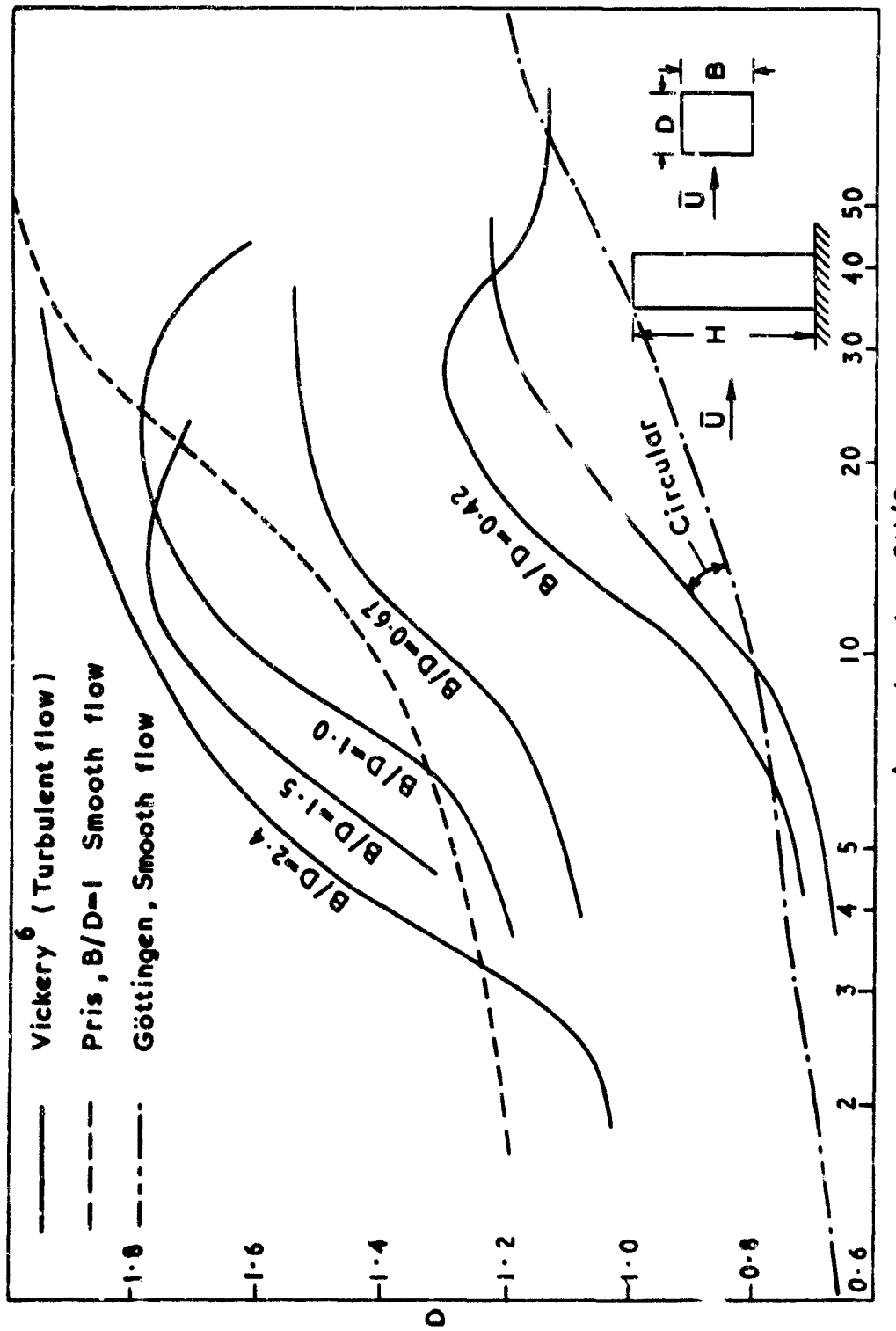

FIG.2 Influence of turbulence and aspect ratio on the drag coefficient of tower blocks of rectangular and circular section

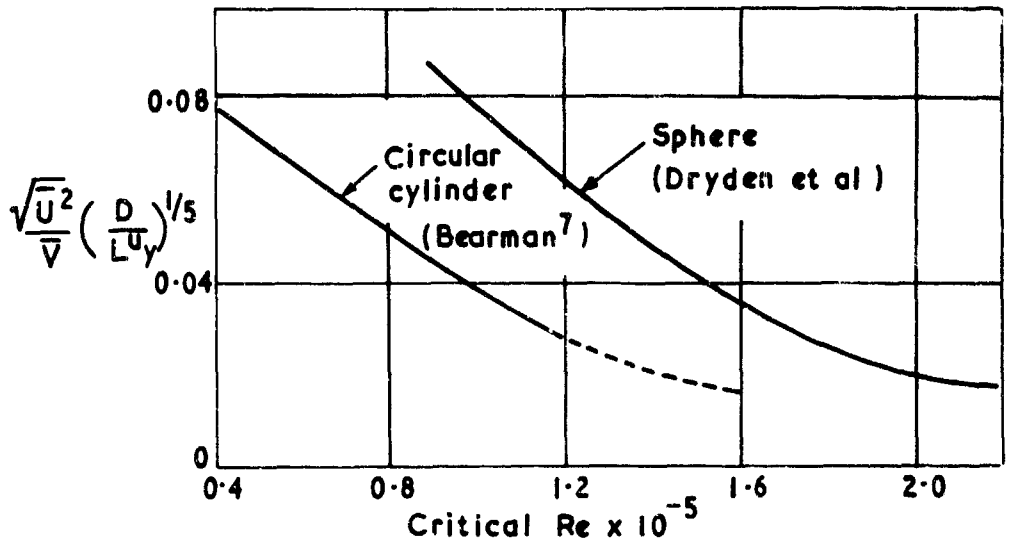

FIG.4 Critical Reynolds number for a sphere and a cylinder as a function $\frac{\sqrt{\overline{U^2}}}{\overline{V}}\left(\frac{D}{L^{u}_{y}}\right)^{1/5}$

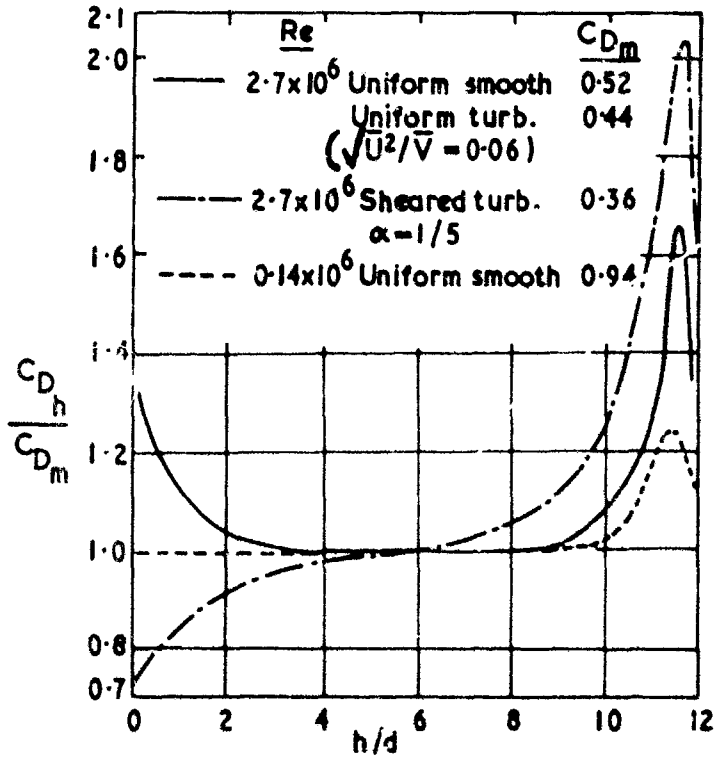

FIG. 5 Effect of Reynolds number, turbulence and velocity profile on the distribution of drag along circular-section chimney of height H = 12 d

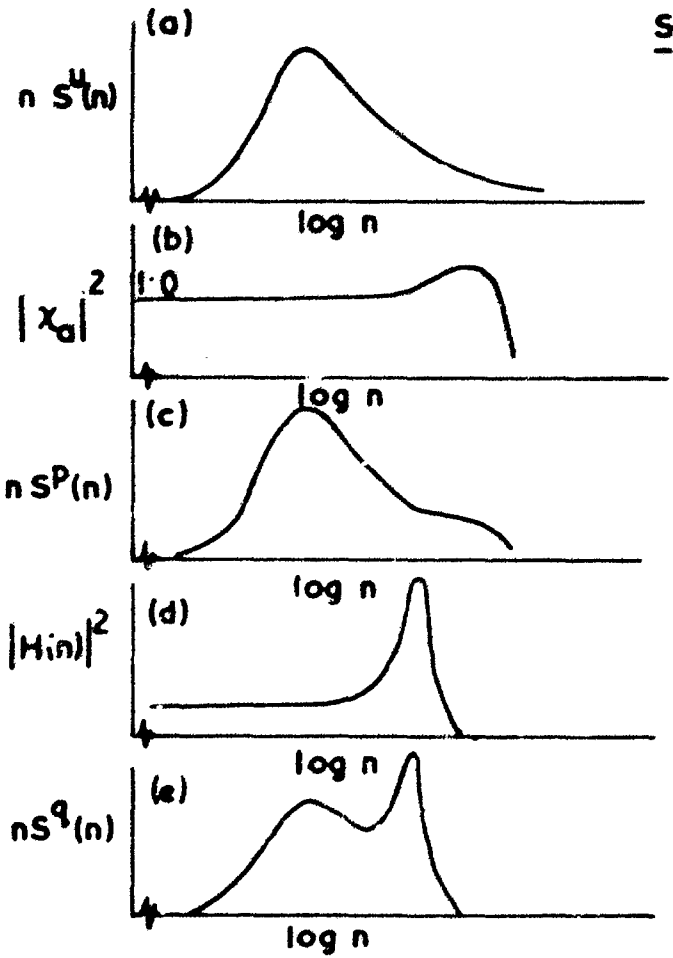

System $Q(t) = \bar{Q} + q^{(t)}$

$$m\ddot{q} + c\dot{q} + kq = p^{(t)}$$

$$nS^{p}(n) = 4\,|\chi(n)|^{2}\,\frac{\bar{p}^{2}}{\bar{v}^{2}}\,.\,nS^{u}(n)$$

$$|H(n)|^{2} = \frac{1}{\left[1-\left(\frac{n}{n_o}\right)^{2}\right]^{2} + 4\zeta^{2}\left(\frac{n}{n_o}\right)^{2}}$$

$$nS^{q}(n) = \frac{1}{k^{2}}\,|H(n)|^{2}\,S^{p}(n)$$

$$= 4\,|H(n)|^{2}\,|\chi(n)|^{2}\,.\,\frac{\bar{Q}^{2}}{\bar{v}^{2}}\,.\,nS^{u}(n)$$

FIG.7. The spectral approach to the determination of the response of a flexible structure to turbulent airflow (after Davenport).

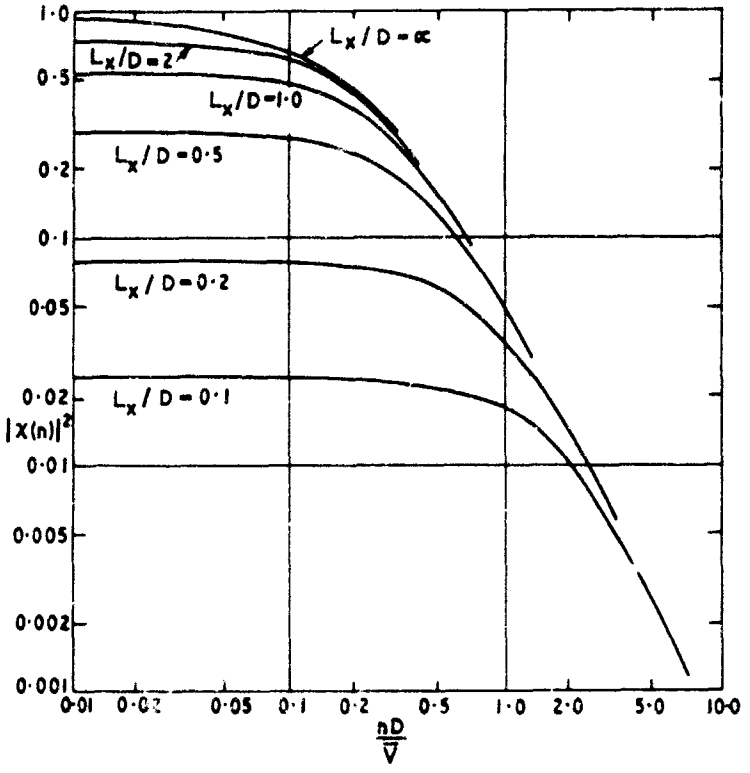

FIG.8 Theoretical values of $|X(n)|^2$ for a square D x D lattice plate

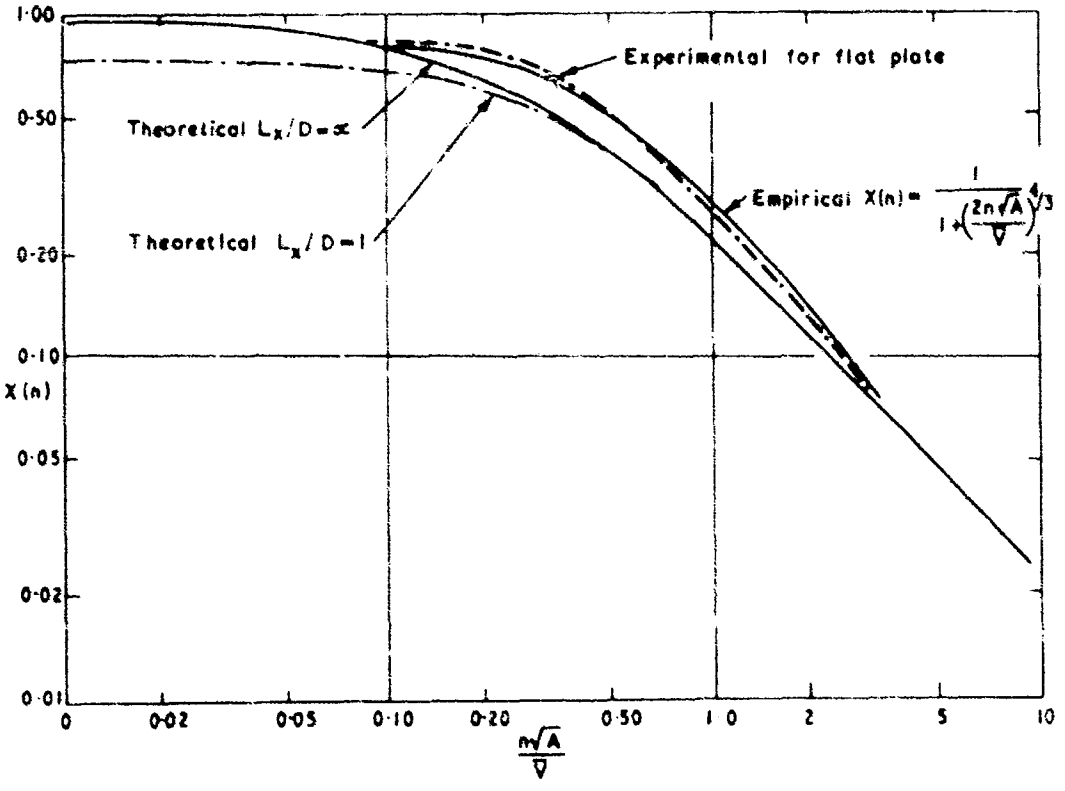

FIG. 9 Theoretical and experimental values of (n)

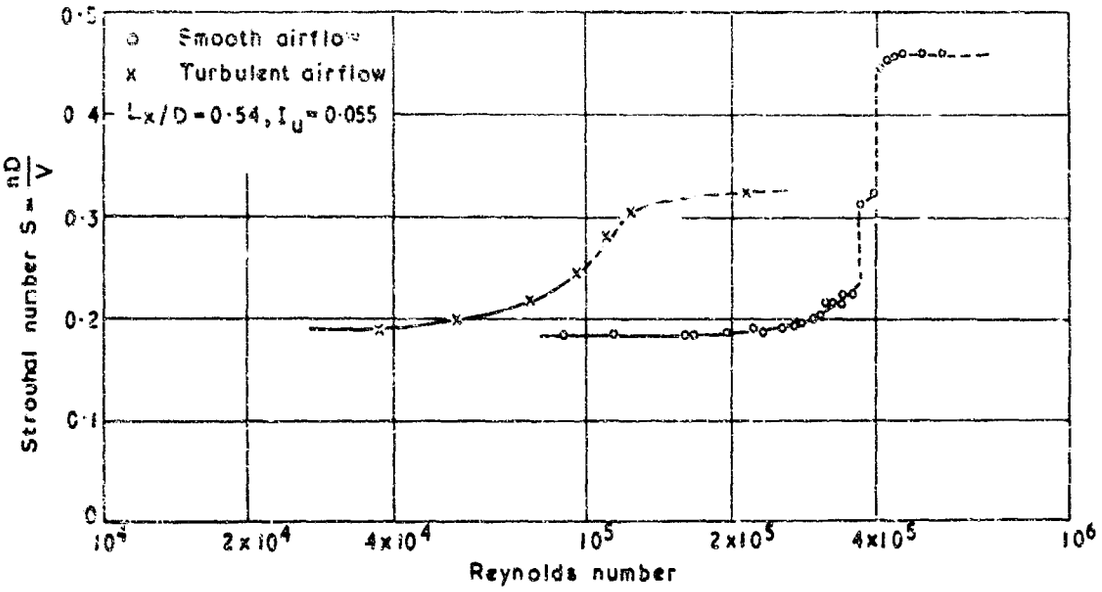

FIG.10 Variation of Strouhal number with Reynolds number for a circular cylinder in smooth and turbulent airflows

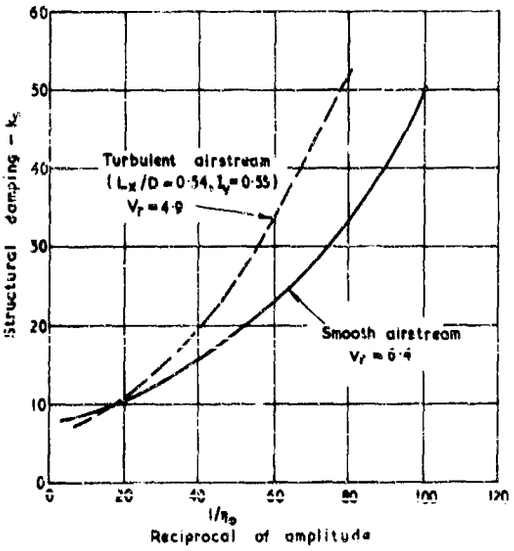

FIG.11. Variation of the muximum amplitude of oscillation of a model stack of circular cross-section in smooth and turbulent airflows.

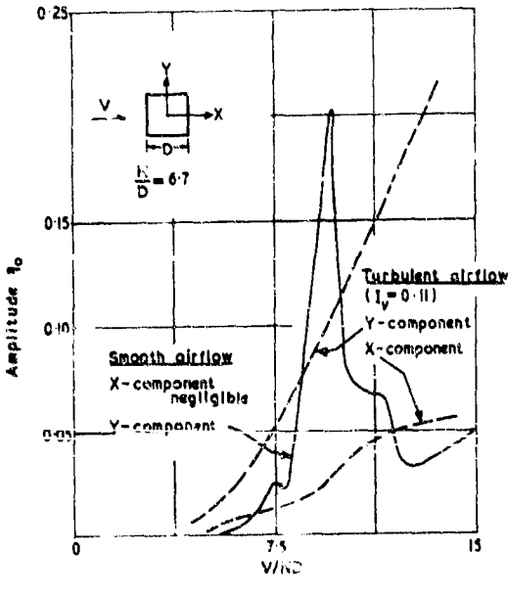

FIG.12. Amplitude response curves for a cantilever of square section in smooth and turbulent uniform airflows. $(\delta_s = 0{\cdot}07)$

FLUCTUATING FORCES ON BLUFF BODIES IN TURBULENT FLOW

by

P.W.Bearman

National Physical Laboratory,
Teddington, Middlesex, England

Summary

This paper describes an investigation into the effect of turbulence on the fluctuating drag forces experienced on a series of square plates set normal to a uniform turbulent flow. The experiments were performed as part of a research programme to examine the influence of atmospheric turbulence on the response of flexible buildings and structures. Power spectral density measurements of the fluctuating component of the drag on square plates in turbulent flow are presented. The measurements show the importance of the ratio of turbulence scale to plate size. There is shown to be a strong correlation between the fluctuating drag force and the velocity fluctuations in the approaching flow. Measurements of aerodynamic admittance are presented to show the form of this function and to show how it varies with change of the ratio of turbulence scale to plate size. Finally, the effect of the body on the turbulence is considered and there is a discussion on how the turbulence is distorted as it is swept past a plate.

Fluctuating Forces on Bluff Bodies in Turbulent Flow

by

P.W. Bearman*

National Physical Laboratory,
Teddington, Middlesex, England

1. Introduction

Under strong wind conditions the flow approaching buildings and structures is highly turbulent and a turbulent wind will induce a random exciting force which could set a flexible structure into some mode of vibration. In order to be able to determine the response, it is important that the effects of turbulence on the flow around bluff bodies should be more clearly understood. The main objects of this paper are to investigate the effect of turbulence on the fluctuating drag forces experienced on a series of square plates set normal to a uniform turbulent flow and to examine the relationship between the approaching turbulent flow and the resulting fluctuating forces.

This particular bluff body shape was chosen because it was hoped that there would be no regular vortex shedding and that the major part of the fluctuating drag force would be directly related to the approaching turbulent flow. Davenport[1] has suggested the use of a frequency-dependent transfer function, relating fluctuating force to fluctuating velocity, called aerodynamic admittance. Measurements of the aerodynamic admittance of flat plates have been reported by Wardlaw and Davenport[2] and Vickery[3] but agreement between the two sets of measurements is poor. One of the aims of the present research was to carry out a more systematic investigation of aerodynamic admittance with particular attention being paid to the importance of the ratio of turbulence scale to plate size.

In addition to the effects of the turbulence on the plates there will be some effect of the plates on the stream turbulence. Hunt[4] has proposed a theory to analyse the distortion of the turbulence in the flow past a body. Measurements of the turbulence structure ahead of a plate are discussed in the light of Hunts' findings.

2. Experimental Arrangement

The experiments were conducted in a wind tunnel with a 9ft (2.74 m) × 7ft (2.13 m) by 12ft (3.66 m) long working section. A highly turbulent flow was generated by the installation of a grid at the beginning of the working section. The grid, which is seen in figure 1, was of the bi-planar type. It was constructed from 1.5 in × 0.75 in (3.81 cm × 1.9 cm) wooden slats spanning the tunnel and the distance between slats, the mesh size M, was 7.5 in (1.9 cm).

Fluctuating drag forces, on square plates of side 2,3,4,6 and 8 in (5.08, 7.61, 10.16, 15.22 and 20.30 cm), were sensed by a semi-conductor strain-gauged balance. The plates were supported on a light, hollow, tapered sting 18 in (0.457 m) long and the sting was protected from the airflow by a shroud attached at the balance end to the earthing frame (see figure 1). Transverse oscillations of the sting and model were eliminated by placing a thin strip of foam rubber around the end of the sting, between it and the shroud. The lowest natural frequency of the balance, with the sting and a 4 in square plate attached, was about 1.5 KHz. The whole assembly was supported on a massive I-beam bolted to a concrete bed beneath the tunnel. The support system was so positioned as to place the plates at 6.33 ft (1.93 m) from the beginning of the working section (i.e. 10.1 M).

Turbulence measurements were made with a DISA linearized constant-temperature hot-wire anemometer. Fluctuating velocity and fluctuating drag signals were recorded on an AMPEX FR1300 tape recorder. These signals were later digitized and analysis was performed on a KDF-9 computer using the methods described by the author[5].

3. Experimental Results and Discussion

3.1 Flow behind the turbulence producing grid

At the plate position adopted for the fluctuating drag measurements the turbulence was investigated with a linearized hot-wire anemometer. At a mean velocity U = 60ft/sec (18.3m/sec) the intensity $\frac{\sqrt{u^2}}{U}$ = 0.083 and the longitudinal integral scale of turbulence L_x = 3 ins (i.e. L_x was of the same order as the size of the plates and simulated turbulence conditions similar to those experienced by large buildings). At the test position, over the area to be occupied by the plates, the mean velocity

---

*Senior Scientific Officer

and the intensity of turbulence were found to be uniform to within ± 0.5%. At a fixed distance from the grid the turbulence intensity decreased very slightly with increase of tunnel speed. Spectra of the 'u' component of turbulence, measured at two wind speeds, are shown in figure 2.

3.2 Measurement of Fluctuating Drag

The fluctuating drag component of the square plates was measured over a range of Reynolds number. The power spectral density estimates of all the drag signals are plotted together in figure 3. This graph shows the power spectral density estimate of the fluctuating drag coefficient $F(C_D)(n)$ at frequency n, plotted as the non-dimensional quantity $\frac{UF(C_D)(n)}{D}$ where D is plate side, against the non-dimensional frequency parameter $\frac{nD}{U}$. The measurements illustrate the importance of the parameter L_x/D, the ratio of the integral scale of turbulence to the size of the plate. For each plate size the results show little dependence on Reynolds number.

Since

$$\left(C_{Dr.m.s} \right)^2 = \int_0^\infty \frac{UF(C_D)(n)}{D} \, d\left(\frac{nD}{U} \right)$$

where $C_{Dr.m.s}$ is the root mean square value of the coefficient of the fluctuating component of drag, it is clear that the smallest plate has the largest mean square drag coefficient. This is primarily because, on the smaller plates, the correlation areas of the energy-containing eddies of the turbulence are comparatively larger. There are two possible length scales that could be used to non-dimensionalize the results shown in figure 3, plate side or turbulence scale. The data are shown non-dimensionalized by plate dimension D and, in this case, the variation of the parameter L_x/D can equally well be thought of as being due to a plate of fixed size in a turbulent stream of fixed intensity and varying scale. Increasing the scale of turbulence, while the intensity remains constant, will have the effect of increasing the power spectral density at long wavelengths and decreasing the power spectral density at short wavelengths. This effect is manifest in the spread of results for the various values of L_x/D (shown in figure 3) at low values of $\frac{nD}{U}$. An interesting feature of the spectra in figure 3 is the collapse of the data on to a single curve at high values of nD/U. Since the data are non-dimensionalized by plate dimension it suggests that, at these values of nD/U, the drag is not directly related to the approaching turbulence spectrum but is, perhaps, partly related to wake induced pressure fluctuations on the rear face.

The r.m.s. values of fluctuating drag coefficient are shown in figure 4 plotted against $1/D^2$. It can be expected that the fluctuating drag will be a function of both $\frac{\sqrt{u^2}}{U}$ and $\frac{L_x}{D}$ and, since $\frac{\sqrt{u^2}}{U}$ and L_x were constant in these experiments, it seemed most appropriate to plot drag against the inverse of plate area. As a comparison the values of $C_{Dr.m.s}$ in nominally smooth flow are shown.

3.3 Discussion of Fluctuating Drag Results

Before discussing the effect of turbulence on fluctuating drag the simpler case of the drag of a body in a stream of varying velocity will be discussed. The flow velocity $U(t)$ can be described by equation (1)

$$U(t) = U+u \tag{1}$$

where U is the time mean velocity and u the fluctuating velocity. u is directed in the same sense as the mean flow and the fluctuations are assumed to be perfectly correlated across the flow. Equation (2) (for derivation see Bearman[6]) shows the relationship between the power spectral density of the fluctuating component of the drag coefficient and the power spectral density of the velocity of the approaching unsteady flow.

$$F(C_D)(n) = \frac{4C_D^2 \, F(u)(n)}{U^2} \left[1 + \frac{C_m^2}{C_D^2} \left(\frac{2\pi nD}{U} \right)^2 \right] \tag{2}$$

where C_D is the mean drag coefficient and C_m is the coefficient of virtual mass.

In turbulent flow equation (2) will be modified in some way by the extent of the spacial correlation of the fluctuating velocity. Davenport[1] argues that, in turbulent flow, there will still be a linear relationship between drag fluctuations and the incident velocity fluctuations and he has termed the function $\chi^2(n)$ where $\chi^2(n) = \frac{U^2 F(C_D)(n)}{4C_D^2 F(u)(n)}$, aerodynamic admittance. In the simple unsteady flow considered above

$$\chi^2(n) = 1 + \frac{C_m^2}{C_D^2} \left(\frac{2\pi nD}{U} \right)^2$$

and at small values of $\frac{nL}{U}$ aerodynamic admittance will approach unity.

Wardlaw and Davenport[2] and Vickery[3] have measured the aerodynamic admittance of flat plates in turbulent flow. Following these authors, figure 5 shows $\chi^2(n)$ plotted against $\frac{nD}{U}$ for the four sizes of square plate examined in this investigation. As $\frac{nD}{U}$ tends to zero, aerodynamic admittance rises to a value less than unity. The simple unsteady theory assumed an infinite correlation length for the fluctuating velocity whereas in turbulent flow, at very long wavelengths, the correlation length will be of the same order as the integral scale. Therefore it can be argued that measured values of $\chi^2(n)$ will be less than unity. At high values of $\frac{nD}{U}$ the aerodynamic admittance drops off at a rate of about 14dB/octave. Vickery[3] suggests that, at high values of $\frac{nD}{U}$, the spacial correlation of the turbulence decreases rapidly and that this will have a much stronger effect on $\chi^2(n)$ than the increase in the drag force resulting from the virtual mass contribution.

The measurements of $\chi^2(n)$ made by Vickery[3] on a square plate in a turbulent flow of intensity 10% and with a scale approximately equal to the plate size, are also shown in figure 5 and are in agreement with the authors' results.

Vickery[3] has formulated a theory to calculate the aerodynamic admittance of a lattice plate which has individual members small compared to the correlation lengths of the velocity fluctuations of interest. The main assumptions are that the force on a member can be related directly to the local upstream velocity and that the correlation of forces is identical to the lateral correlation of upstream velocities. For a square lattice plate Vickery[3] finds

$$\chi^2(n) = \frac{1}{D^4}\int_0^D\int_0^D\int_0^D\int_0^D F(u_1,u_2)(r,n)\,dx_1\,dx_2\,dy_1\,dy_2$$

where $F(u_1,u_2)(r,n)$ is the normalised form of the lateral co-spectral density function of the longitudinal component of the oncoming turbulent flow. x_1y_1 and x_2y_2 are the co-ordinates of two points on the plate surface and $r = \sqrt{(x_2-x_1)^2+(y_2-y_1)^2}$.

Vickery further assumed that the lattice plate theory could be applied to solid plates and showed some comparisons of theory with experiment. He measured the function $F(u_1,u_2)(r,n)$ behind a grid (similar to the one used in this investigation) and fitted his results with the empirical relation.

$$F(u_1,u_2)(r,n) = e^{-7.5\left(\frac{\theta}{2\pi}\right)}\cos 1.4\pi\left(\frac{\theta}{2\pi}\right)$$

where

$$\frac{\theta}{2\pi} = \frac{r}{2\pi L_x}\left[1+\left(\frac{2\pi nL_x}{U}\right)^2\right]^{\frac{1}{2}}$$

Theoretical values of aerodynamic admittance have been computed and are presented in figure 6 for the values of L_x/D investigated in the experiments together with the experimental results for the extreme values of L_x/D. At low values of $\frac{nD}{U}$ there is fairly close agreement with experiment when $L_x/D = 1.5$ but for smaller values of L_x/D the predicted large reduction in $\chi^2(n)$ is not realised. The agreement in $\chi^2(n)$ between theory and experiment at high values of $\frac{nD}{U}$, may be partly fortuitous because the measurements of the power spectral density of drag at these values of $\frac{nD}{U}$, have suggested that the drag fluctuations are not directly related to the upstream velocity fluctuations.

3.4 Investigation into the structure of the flow ahead of the plates

The ideas discussed in the previous section are based on the assumption that there is some correlation between the longitudinal component of the upstream fluctuating velocity and the fluctuating drag. To test this assumption a hot wire was introduced into the flow at various distances, x, ahead of the 4 in square plate, along the stagnation streamline. The fluctuating velocity and fluctuating drag signals were recorded simultaneously and later digitised. The cross-correlation coefficient between velocity and drag force, $\frac{u\overline{C_D}}{\sqrt{u^2}\sqrt{C_D^2}}$ was computed at various time delays and the results are plotted in figure 7. At each position the maximum correlation occurred when the velocity led the drag force and, as expected, the time delay to maximum correlation increased with distance ahead of the plate. The maximum value of the correlation is shown plotted against position ahead of the plate in figure 8. As x/D tends to zero the correlation will also approach zero because at the plate surface the longitudinal component of the fluctuating velocity must be zero. At $x/D = 1$ the

correlation for the whole signal rose to the value 0.65 and, from the slope of the curve, appears to rise even higher further ahead of the plate. The high value of this correlation is surprising when it is remembered that for this plate $L_x/D = 0.75$ and the velocity has only been measured at points on the stagnation streamline, whereas fluctuating velocities anywhere over an area of the same order as the size of the plate could affect its drag.

In addition to the unfiltered correlations figure 8 shows maximum values of time-delayed, filtered cross-correlations for a high and low value of the frequency parameter $\frac{nD}{U}$. Although at the low value of $\frac{nD}{U}$ the measurements indicate a very strong correlation between drag and upstream velocity the simple linear theory of Vickery underestimates $\chi^2(n)$, at this value of L_x/D, by about 50%. At the high value there was small correlation and therefore these measurements also help to support the argument that at these values of $\frac{nD}{U}$ most of the drag fluctuations are wake induced.

In order to progress further with the understanding of the effect of turbulence on bodies the effect that the body has on the turbulence must be considered. Hunt[4] has formulated a theory, based on turbulence rapid distortion theory, to analyse the turbulence in a flow sweeping past a body. The principal assumption made in the theory is that, in the time it takes for the turbulence to be swept past the body, the changes in the mean flow around the body and the effect of its boundaries distort the turbulence for more than its own internal viscous and non-linear inertial forces. The turbulence will be distorted by stretching and twisting of the vortex line filaments as they are convected past the body.

The assumptions that have to be made are first, that the mean flow is irrotational, which limits analysis to that region of the flow outside the boundary layers and wake. The second assumption is that $\sqrt{u^2} \ll U$ so that the only contribution to vortex line stretching and twisting comes from changes in the mean flow. Thirdly in the time it takes for a fluid element to be swept past the body, T, the turbulent energy dissipated by viscous stress is small which leads to the condition $\frac{L_x}{D} \gg \frac{\sqrt{u^2}}{U}$. With these assumptions Hunt shows that the problem reduces to the solution of a number of linear equations in which there will be no interaction between the different wavenumbers of the turbulence.

In the experiments described in this paper $\frac{\sqrt{u^2}}{U} \ll 1$ and, since $L_x/D = O(1)$, $\frac{L_x}{D} \gg \frac{\sqrt{u^2}}{U}$ and therefore in the free stream the conditions of the theory were met. At this stage no attempt has been made to calculate the distortion of the turbulent flow ahead of the plates because, when the scale of turbulence is of the same order as the size of the body, the amount of computation required is extremely large. The theoretical ideas will be used, however, to discuss qualitatively the effects of turbulence. When the eddy sizes of the turbulence are large compared to the size of the body $\left(\frac{L_x}{D} \to \infty\right)$, the effect of the body on the turbulence will be similar to its effect on the mean flow. Therefore ahead of a plate, along the stagnation streamline, the u fluctuation will decrease while the turbulence intensity based on local velocity will remain constant. On the other hand as the eddy sizes become very small compared to the size of the body $\left(\frac{L_x}{D} \to 0\right)$ the dominant effect will be the stretching of the vortex lines by the mean flow. This gives the interesting result that, ahead of a plate u increases. When $L_x/D = O(1)$ there will be some combination of these effects.

In order to illustrate some of these features, further measurements along the stagnation line ahead of the 4 in plate are presented. Figure 9 shows measurements of mean velocity, and also the turbulence intensity, based on both local velocity U_ℓ and free stream velocity U, plotted against distance ahead of the plate, x/D. The rise in $\frac{\sqrt{u^2}}{U_\ell}$ near the plate suggests that the range of eddy sizes within the turbulence was such as to produce some stretching of the vortex lines. Near the plate, around the stagnation region, very high levels of turbulence intensity were recorded and clearly the condition $\sqrt{u^2} \ll U_\ell$ will no longer be satisfied.

The theory of Vickery, when applied to solid plates, assumes that the turbulence approaching each element of plate area behaves as if the body were in a stream where $\frac{L_x}{D} = \infty$. This suggests, from the work of Hunt, that along the stagnation streamline the power spectral density of the approaching flow $F(u)(n)_\ell$ should decrease at all wavenumbers in such a way that

$$F(u)(n)_\ell = F(u)(n) \cdot \frac{U_\ell^2}{U^2} \qquad (3)$$

where $F(u)(n)$ is the power spectral density of the fluctuating velocity for upstream. Power spectra of fluctuating velocity along the stagnation streamline at four stations ahead of the plate are shown in figure 10. $F(u)(n)_{\ell/U}$ is shown plotted against n/U and the area under each spectrum

is equal to the square of the turbulence intensity based on free stream velocity. Compared with the spectrum in the absence of the plate, the power at low wavenumbers shows a marked decrease whereas at higher wavenumbers there is little change. If $L_x/D = \infty$ and there was no stretching of vortex lines by the mean flow the level of the spectrum at all wavenumbers would be given by equation (3).

Returning to the theoretical values of aerodynamic admittance plotted in figure 6 it can be seen that as L_x/D decreases $\chi^2(n)$ becomes increasingly larger than Vickery predicts. This is in agreement with the argument that as L_x/D becomes smaller the distortion of the turbulence intensifies the longitudinal component of turbulence ahead of the body. More work is required to determine the importance of turbulence distortion and to determine whether, if L_x/D is large enough, the much simpler ideas of Vickery are sufficient to predict $\chi^2(n)$ accurately at low values of $\frac{nD}{U}$. It is interesting to note that when $L_x/D = 1.5$ the aerodynamic admittance values predicted by Vickery are only 20% too low. Another area requiring more attention is the understanding of the complex interaction between the turbulence and the wake.

4. Conclusions

Power spectral density measurements of the fluctuating drag on square plates in turbulent flow show the importance of the scale parameter L_x/D. As L_x/D increases, the correlation areas of the energy-containing eddies of the turbulence are comparatively larger and the root mean square value of the drag coefficient fluctuations increases. Correlations of the velocity signal from a hot wire, placed at various distances upstream of a plate $\left(\frac{L_x}{D} = 0.75\right)$, with the fluctuating drag signal confirmed that the majority of the drag fluctuations was linearly related to the velocity fluctuations in the approaching flow. This relationship between velocity and drag helps to justify, particularly at values of $\frac{nD}{U}$ less than 0.1, the concept of aerodynamic admittance. In the range of values of L_x/D from 1.5 to 0.375, however, the theory of Vickery at small $\frac{nD}{U}$, was found to underestimate seriously the value of aerodynamic admittance. Measurements of the structure of the turbulence ahead of a plate show that this was primarily due to the significant distortion of the turbulence by the body.

5. Acknowledgements

The author wishes to thank Mr. G.S. Smith for the design of the drag balance. This work was carried out as part of the general research programme of the National Physical Laboratory.

References

1. Davenport, A.G. — The application of statistical concepts to the wind loading of structures. Proc. Inst. Civ. Engrs., 1961, Vol. 19 paper no 6480 pp 449-472.

2. Wardlaw, R.L. and Davenport, A.G. — Some experiments on the fluctuating forces on flat plates in turbulent flow. N.R.C. of Canada Aero. rep. LR-415 Dec. 1964.

3. Vickery, B.J. — On the flow behind a coarse grid and its use as a model of atmospheric turbulence in studies related to wind loads on buildings NPL Aero. rep. 1143 (1965)

4. Hunt, J.C.R. — A theory of turbulent flow over bodies, to be published.

5. Bearman, P.W. — Digital analysis of hot-wire data, NPL Aero. rep. 1273 (1968).

6. Bearman, P.W. — An investigation of the forces on flat plates in turbulent flow. NPL Aero. rep. 1296 (1969).

BM

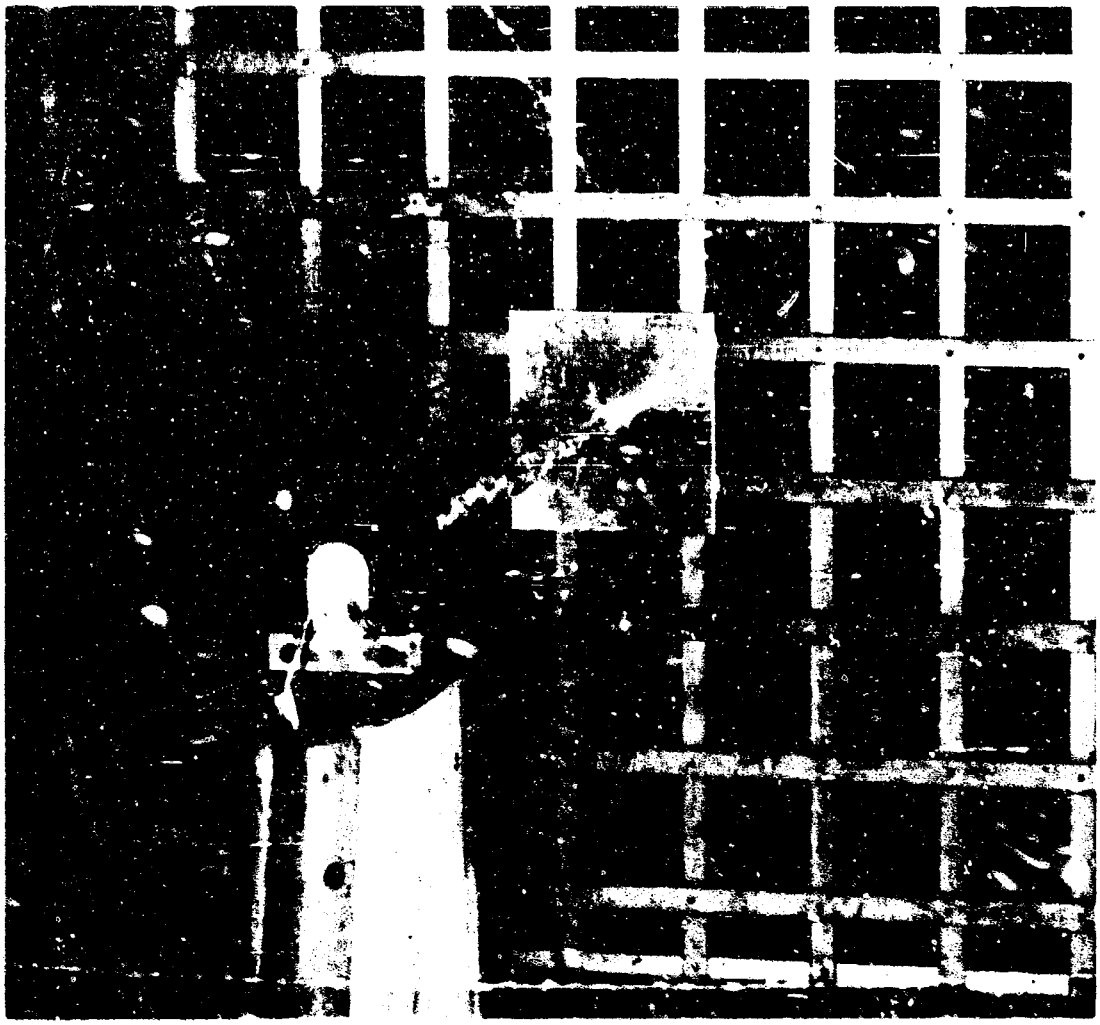

FIG. 1. Flat plate mounted behind the turbulence grid.

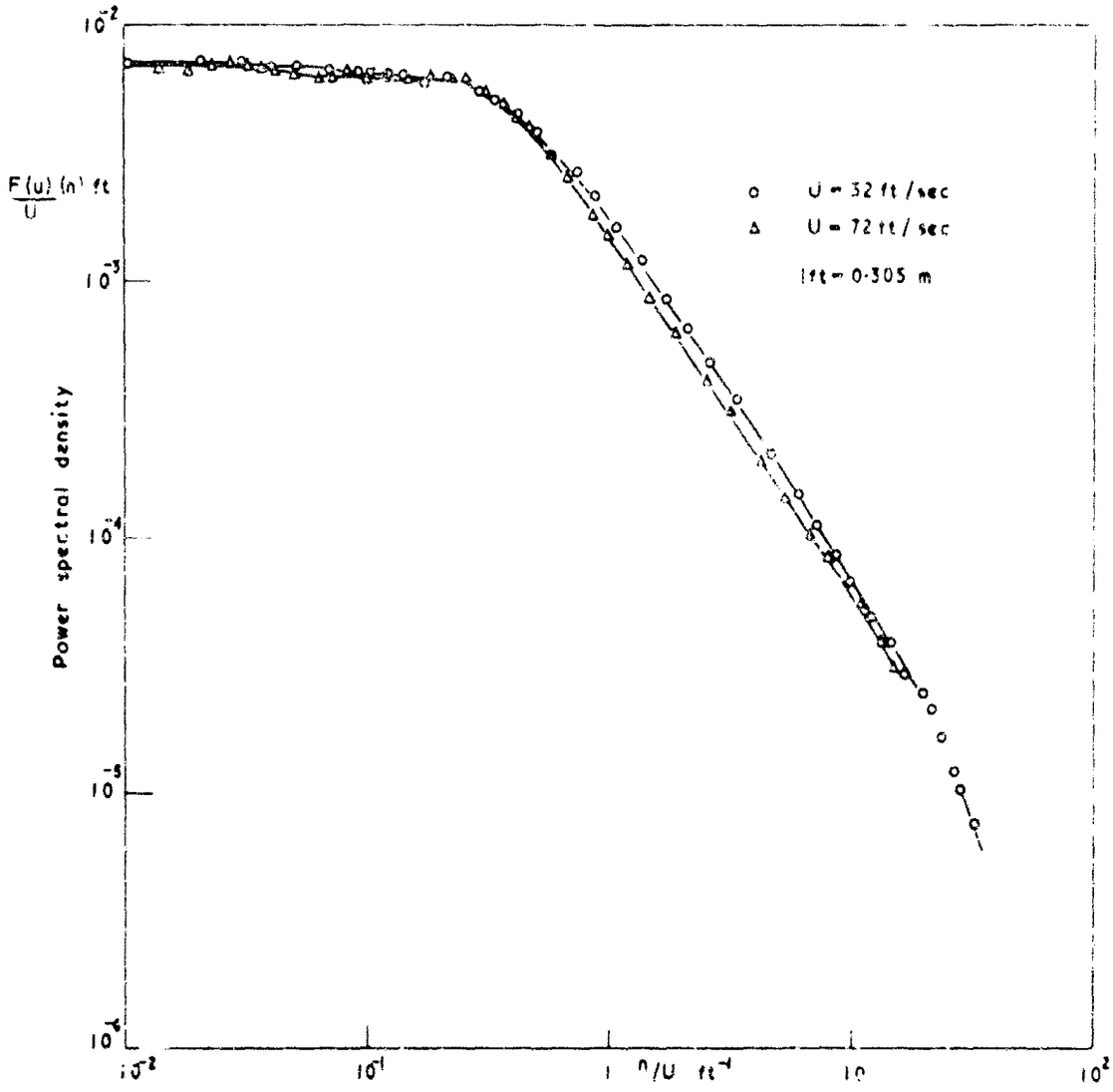

FIG. 2 Spectra of longitudinal component of turbulence at test position

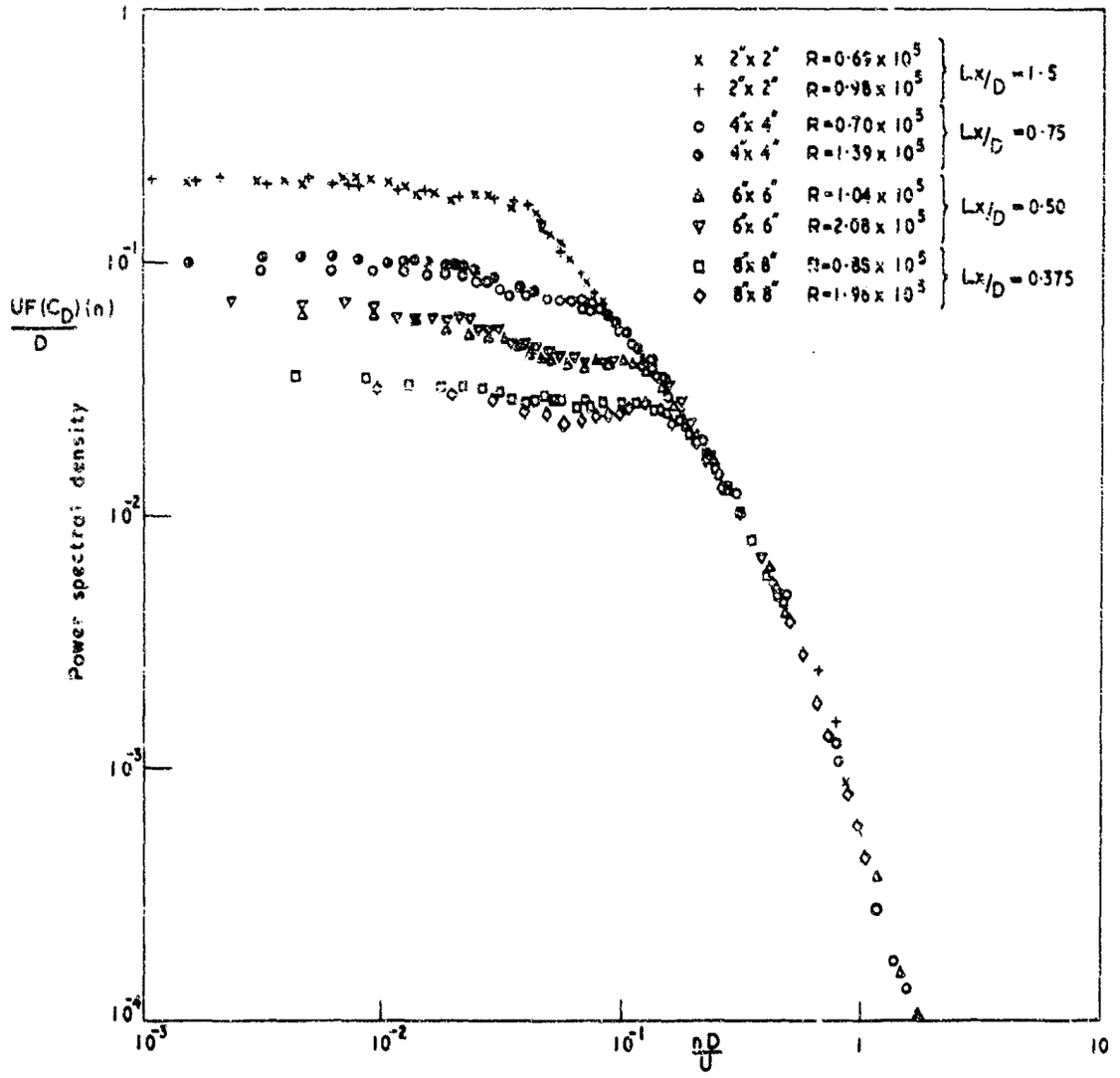

FIG.3 Spectra of the unsteady component of drag of flat plates in turbulent flow

(Lx = 3 in., $\frac{\sqrt{u^2}}{U} \approx 0.083$)

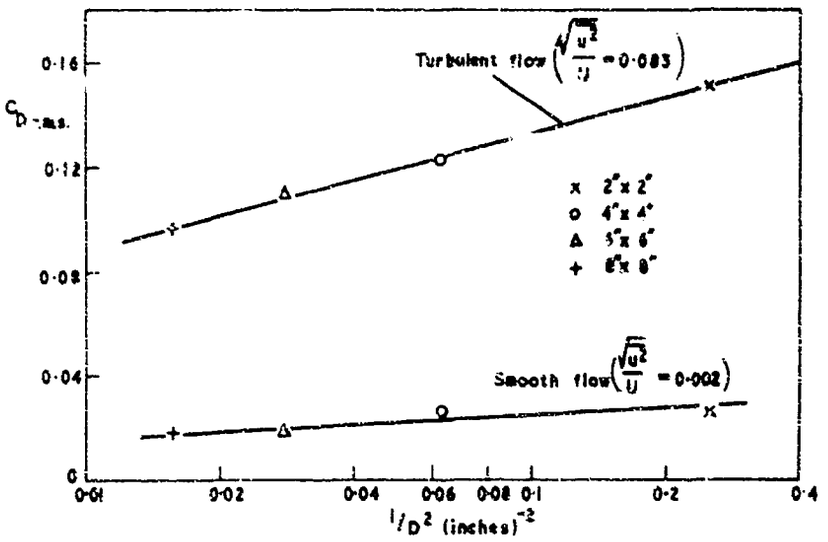

FIG.4 R.M.S. of drag coefficient fluctuations of flat plates in smooth and turbulent flow

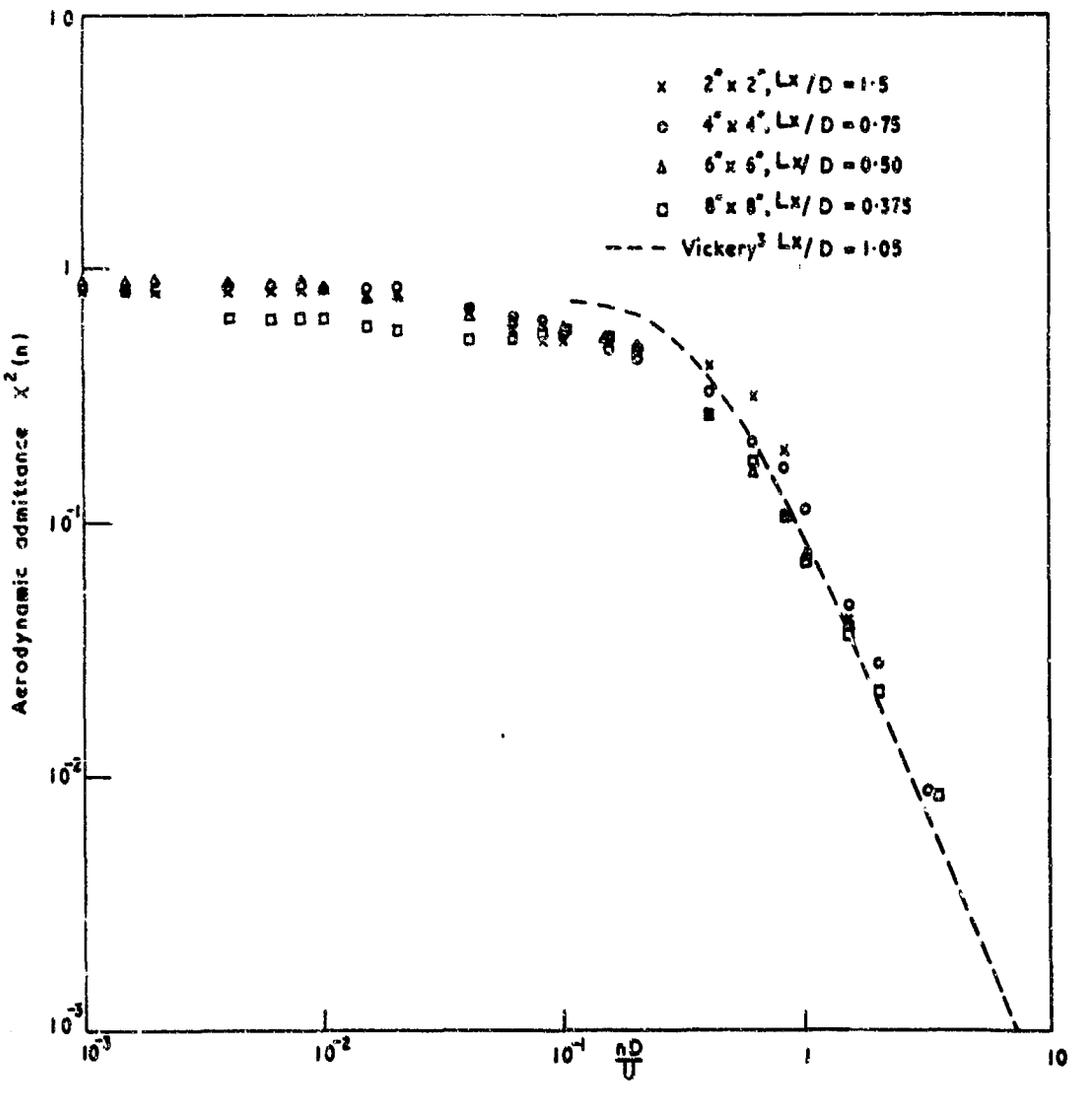

FIG.5 Aerodynamic admittance of flat plates

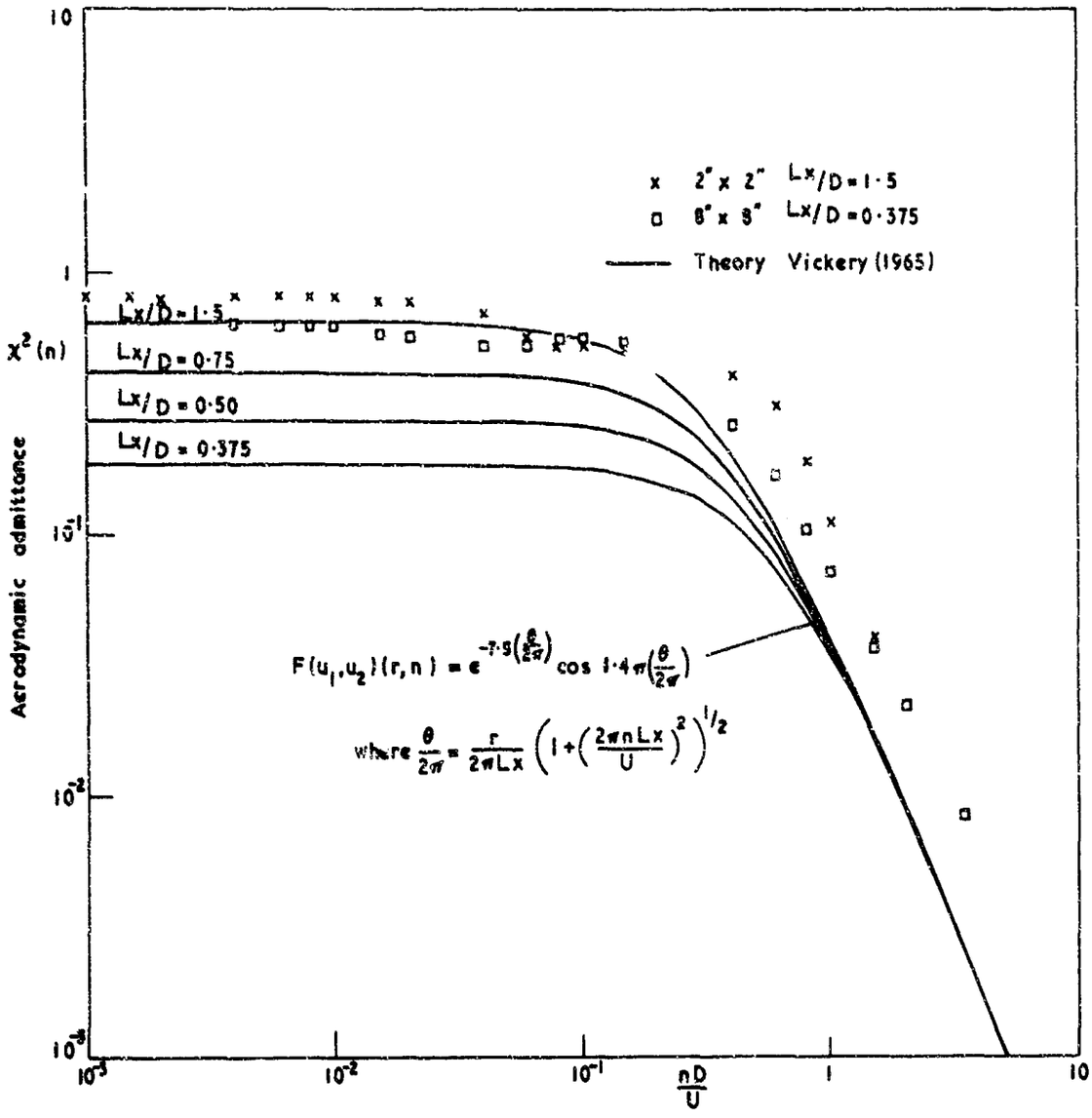

FIG.6 Theoretical values of aerodynamic admittance

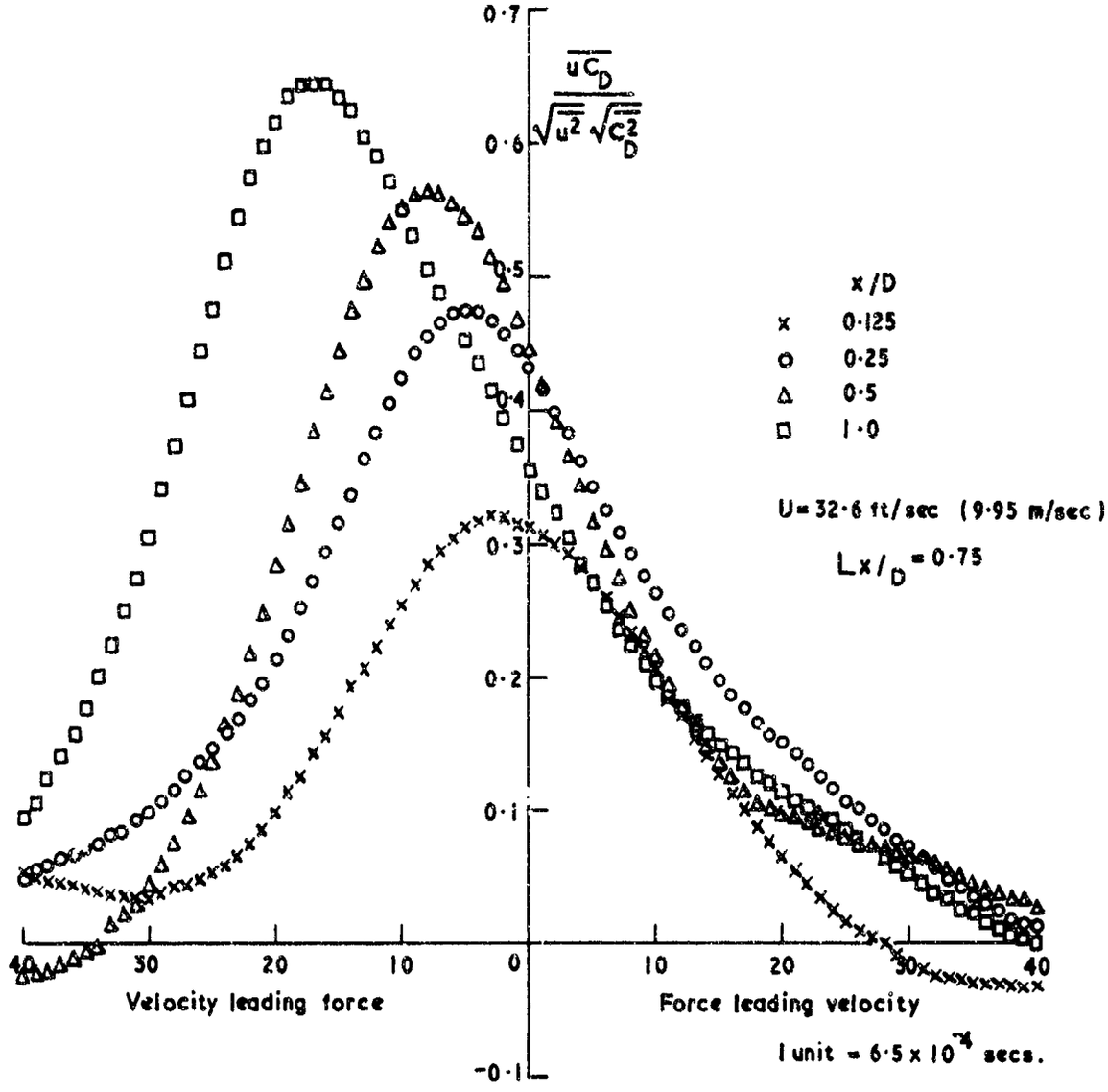

FIG.7 Time-delayed cross correlation between velocity and force

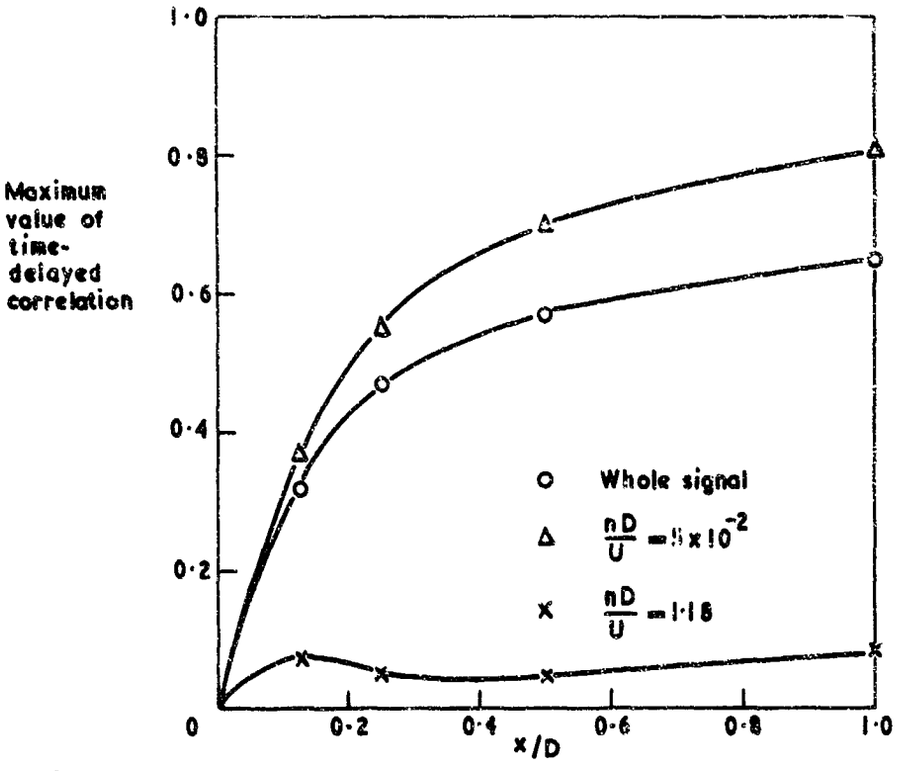

FIG.8 Variation of the maximum time-delayed correlation between velocity and drag at various distances ahead of the plate, along the mean stagnation line

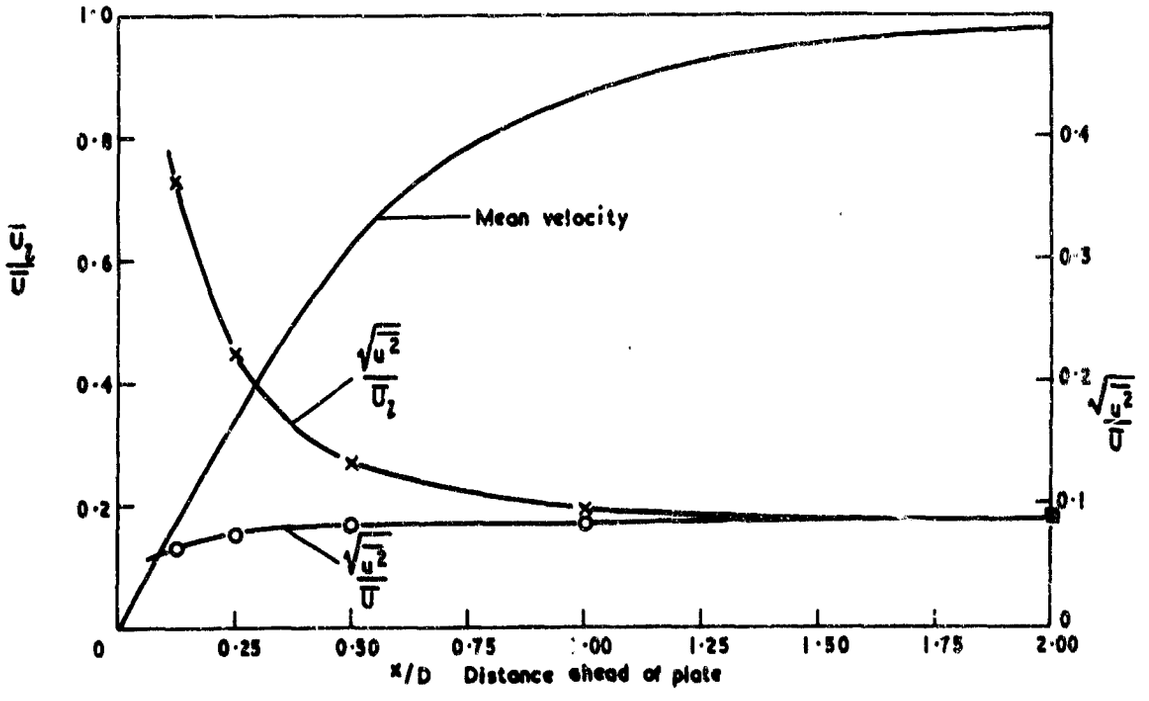

FIG.9 Stagnation line flow — flat plate, $L_x/D = 0.75$, $\frac{\sqrt{u^2}}{U} = 0.083$

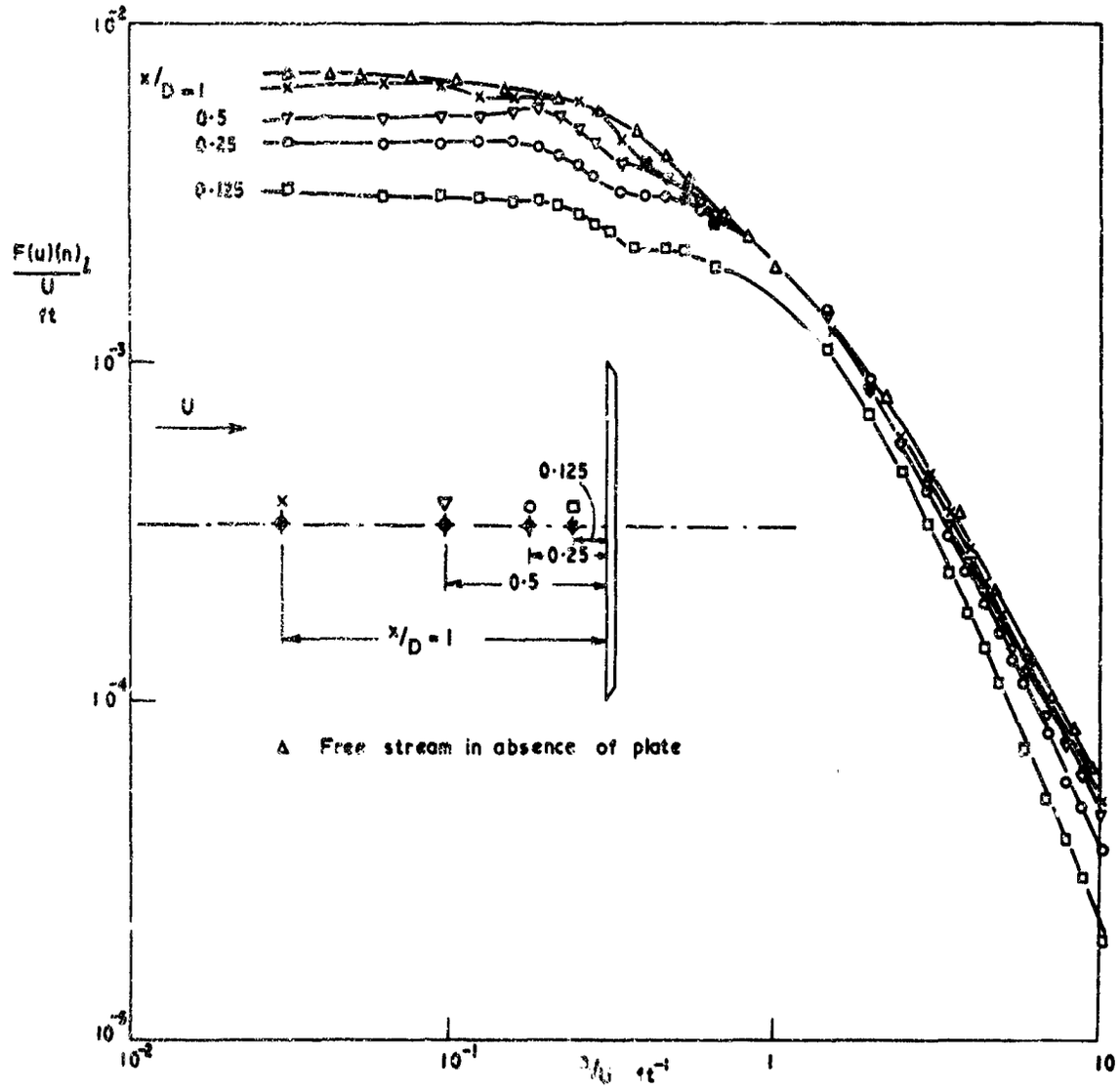

FIG. 10 Spectra along stagnation line — flat plate, $^{L_x}/_D = 0{\cdot}75$

WIND EXCITED BEHAVIOUR OF CYLINDRICAL STRUCTURES

- ITS RELEVANCE TO AEROSPACE DESIGN -

by

D.J.Johns

Department of Transport Technology, University of Technology,
Loughborough, Leicestershire.

ABSTRACT

A literature review is given of available data on the influence of ground winds on typical aerospace structures. Relevant data from non-aerospace studies are also disucssed.

The major concern of the paper is the wind induced excitation of circular, cylindrical shell structures in either the swaying (bending) or ovalling (breathing) modes and the relationships between these modal natural frequencies and the frequency spectrum of the aerodynamic input. The data on discrete vortex shedding in the sub-critical and super-critical Reynolds No. ranges is necessarily considered.

The relevant structural vibration analyses to predict the natural frequencies of the stiffened and unstiffened shells are briefly outlined and certain deductions made on the efficacy of various types of stiffening.

Consideration is also given to problems associated with complete lattice structures typical of launcher designs and with single component members of such structures.

WIND EXCITED BEHAVIOUR OF CYLINDRICAL STRUCTURES

- ITS RELEVANCE TO AEROSPACE DESIGN -

D.J. JOHNS*

1. Introduction

In recent years there has been an increasing awareness of the need to allow for the static and dynamic effects of wind on the design of civil engineering and aerospace structures and there has been a useful cross-fertilisation of ideas and information feedback between these branches of engineering. This is particularly evident in the number and scope of major symposia which have attracted meteorologists, architects, civil engineers, aerodynamicists and aerospace structural engineers.

The first major symposium on "Wind Effects on Buildings and Structures" was held as recently as 1963 at [illegible], England, and 34 papers were published (Ref. 1) including a significant review paper by Scruton.

A second similar symposium was held at Ottawa, Canada, in 1967 and the published proceedings (Ref. 2) contain 37 papers. Ref. 3 also contains 37 papers of a symposium held at Loughborough, England, in 1968.

These three meetings dealt more specifically with civil engineering applications as did Refs. 4 and 5 which only dealt in part with wind effects.

Refs. 6 and 7 dealt specifically with ground wind load problems related to launch vehicle structures and appear to have been the most significant unclassified meetings of this type to date.

In addition to the papers presented at these meetings there have been many individual papers of note and they will be referred to later. For example, Ref. 8 contains a useful survey of data on static loads due to wind, and Refs. 9 and 10 summarise the sources of data and the main considerations in selecting design winds for ta[illegible] structures.

For a particular building or other structure a study of wind effects requires a prior knowledge of the maximum wind speeds at the proposed site for the structure. Since it would be unusual for this precise knowledge to be available it is necessary to infer it from meteorological records often taken a considerable distance away. The designer must also take account of local topography, prevailing wind directions, the variation of wind speed with height, the presence of other adjacent structures, etc., and most importantly, the degree of turbulence in the wind.

Because of uncertainties in these various parameters recourse is often had to wind-tunnel tests in which these parameters, especially wind profile and turbulence, and the structural flexibility are all modelled. Significant in this field is the work of Davenport, some of which is reported in Refs. 1, 2, 7. Ref. 11 contains a useful summary of the problems of simulating the atmosphere and Refs. 12 to 14 present a general mathematical analysis to determine the effects of random turbulence as a forcing function on tall slender structures. Ref. 14 contains a useful review of wind excited response problems.

The main concern of this present paper is that class of dynamic problems resulting from excitation due to vortex shedding. Some of the vast literature now available will be discussed and it is hoped that certain definitive conclusions can be drawn as to the nature and implications of vortex shedding from circular cylindrical structures. Results will be presented from recent studies on the lateral bending and ovalling oscillations of such structures due to vortex shedding.

---

*Professor of Aeronautics; Department of Transport Technology, University of Technology, Loughborough, Leicestershire.

In passing it should be mentioned that Paper 22 of Ref. 3 contains much valuable data on the unsteady aerodynamic derivatives of various prismatic beams of open and closed section which might be considered as components of a space frame structure for civil or aerospace engineering applications. In general, the closed box profiles and the ⊢⊣ - shaped profile were the worst from an aeroelastic point of view whereas the other open-sections were all essentially stable. Considerable data on other non-circular cylindrical sections is contained in Refs. 1 to 3 and 7.

2. Vortex Shedding Phenomena - Model Tests

2.1 General

Research into vortex streets behind a circular cylinder dates from the late 15th century and in 1878 early experiments by Strouhal led to the empirical correlation of the vortex shedding frequency N, the diameter d, and the stream velocity V, through the non-dimensional Strouhal No.

$$S_N = Nd/V \qquad (1)$$

Many papers have discussed this parameter and its dependence on Reynolds No., and it appears that several distinct regions of Reynolds No. exist in which different phenomena occur. These various regions are not separated by clear boundaries but by transition zones which can be altered by individual experimental conditions. These regions are referred to in Ref. 15 and shown in Fig. 1., as symmetric, regular, irregular and supercritical defining the nature of the vortex shedding phenomena. Refs. 16 - 18 were also useful in delineating these various regions.

It is with the irregular (sub-critical) and supercritical Reynolds No. range ($R_N > 300$) that this paper is primarily concerned but the intervening transition zone around the critical Reynolds No. (i.e. $2 \times 10^5 < R_N < 2 \times 10^6$) will also be discussed. Much of the data available on the aerodynamic Strouhal No. over the above Reynolds No. range is shown in Fig. 1 as taken from Ref. 18.

2.2 Sub-critical Region

In the sub-critical Reynolds No. region ($300 < R_N < 2 \times 10^5$) the boundary layer is laminar, its separation from the surface is not appreciably affected by Reynolds No., and the Strouhal No. in equation (1) remains at an almost constant value of 0.2 for an infinite aspect ratio circular cylinder.

Experiments reported by Meier-Windhorst (Ref. 19) using water and by Scruton (Paper 24 - Ref. 1) using air and by others, have shown that one consequence of periodic vortex shedding has been the existence of a periodic force in a direction normal to the wind stream. The frequency of this force when the cylinder is stationary is given by a value of $S_N \simeq 0.2$ in eqn. (1) but it appears that for an oscillating cylinder there are certain ranges of wind speed for which the cylinder oscillations themselves control the frequency. Thus Parkinson has shown (Paper 18 - Ref. 2) that onset of oscillations can occur (if the structural damping is sufficiently small) when the Strouhal frequency equals the natural frequency of the cylinder and the instability which persists over a range of wind speed (which also depends on the structural damping) will do so with a frequency dominated by the natural frequency and <u>not</u> by the Strouhal frequency corresponding to the particular wind speed. The assumed 1 to 1 relationship between successive bending oscillations at the natural frequency and the vortex shedding is given in Fig. 2(a) but Fig. 2(b) presents alternatively a 3 to 1 relationship which could result in a lower critical wind speed. There is no experimental evidence for this known to the author although, as mentioned in (iii) below, higher harmonics of the Strouhal frequency are likely to be present which might produce an apparently lower critical wind speed than would correspond to a value of $S_N = 0.2$.

As well as lateral bending oscillations it is possible with lightly damped, plain cylindrical cantilevers for significant vibrations to develop in the direction of the flow (Ref. 20). These have been reported to occur at a frequency twice that of the lateral oscillations and this suggests that the periodic forces associated with vortex shedding can have a significant streamwise component. (Ref. 21). In other words the unsteady pressure distribution as a single vortex is shed does not in general have a resultant normal to the flow. The significance of this will be re-emphasised later in Section 3, when discussing ovalling oscillations.

From the available sub-critical data it is clear that the cylinder response to fluid dynamic forces from vortex shedding is not strictly speaking a resonance effect since the cylinder motion alters the flow field significantly. The main conclusions for sub-critical flow are summarised in Paper 37 of Ref. 2.

(i) cylinder motions increase the circulatory strength of developing vortices,

(ii) cylinder motions increase the two-dimensionality of the flow field,

(iii) the dynamic lift contains higher harmonics of the Strouhal frequency,

(iv) striking flow field modulations can occur when the ratio of cylinder frequency to Strouhal frequency is between 0.8 and 1.1 but not close to unity.

2.3 Supercritical Regime

Unfortunately most practical structures of interest operate at Reynolds Nos. upto and into the supercritical region and the data available for this region and the transition zone which precedes it have been rather inconclusive.

According to some researchers they have found a marked rise in S_N above $R_N = 2 \times 10^5$ such that a value of $S_N = 0.46$ occurred at $R_N = 1.5 \times 10^6$ whereas other researchers have shown completely contradictory results with values of $S_N < 0.2$. Typical results are given in Fig. 1 taken from Ref. 18 where it is asserted that it is questionable whether periodicity of vortex shedding still exists above $R_N = 2 \times 10^5$ and that only a wide frequency band turbulence occurs. The evidence presented in Fig. 1 certainly indicates no discrete vortex shedding for $2 \times 10^5 < R_N < 1.5 \times 10^6$ but for $1.5 \times 10^6 < R_N < 3 \times 10^6$ one might deduce that there is a progressive decrease in S_N from 0.46 to 0.2. This would mean that a structure of bending frequency w could experience a corresponding progressive increase in V_{cr} (since $V_{cr} = wd/S_N$) with V and a continual condition of resonance of increasing severity, due primarily to the consequent increase in dynamic pressure. This condition of increasing amplitude with speed and no pronounced single critical speed has been quoted elsewhere as evidence for the absence of a discrete vortex shedding frequency but from the above argument that is not necessarily proven.

It is of interest that data has been presented by Chen (Ref. 18) in Fig. 1 for a value of $S_N \triangleq 0.2$ in the supercritical region although he proceeds to discount it based on his own experimental results.

The results of Fung (Ref. 22) and Roshko (Ref. 16) for a rigid cylinder have shown no discrete frequency in the broad turbulence spectrum for the transition range of Reynolds Nos. although each spectrum in this range has a peak at a value of S_N which decreases in this range from 0.17 down to 0.05. These values imply a low effective forcing frequency in a broad frequency band and if significant vibrations are to occur as a result the dynamic pressures must be sufficiently great and the structural damping sufficiently low and the possibility referred to earlier might then apply with the effective Strouhal frequency being lower than the natural frequency (i.e. $N = j\omega$). Roshko has also shown that a discrete frequency peak can occur for $R_N > 3.5 \times 10^6$ corresponding to $S_N = 0.267$.

It is believed that the probable main causes for the disagreements between various researchers are the differences in end effects and other three-dimensional effects and the fact that many of the cylinders tested have been rigid.

The experiments of Ref. 15 for a rigid cylinder have shown the strong three-dimensional nature of the vortex pattern and in the Discussion of Ref. 17 other results were quoted showing that the distance along the cylinder over which the periodic lift forces arecorrelated decreases to about 1 diameter at transition Reynolds Nos. It is not surprising if overall oscillatory lift and drag measurements are then inconclusive.

When the cylinder is not held rigidly but can interact with the flow it would appear that the correlation length can increase markedly when the phase of the vortex shedding is locked into synchronism along the entire cylinder by the cylinder motion itself.

Some recent experiments at the N.P.L., are referred to in Ref. 21 and Paper 18 of Ref. 2 for a cylinder in the Reynolds No. range 10^5 to 3×10^6. The results showed that the presence of a free end can have significant effects as the flow is entrained over the free end of the cylinder to pass down the leeward face thereby causing a thickening of the wake and a consequent decrease in the local vortex shedding frequency. This gives a wider spectral peak to the overall oscillatory forces.

When such a flexible cylinder is heavily damped a wide band input will produce a random amplitude response function provided that the amplitude of motion is sufficiently small not to affect the aerodynamic forces and to cause locking-in

or synchronisation. The variation of amplitude with speed would then be expected to follow a quadratic law as was indicated in Ref. 23.

However, within a limited speed range ($4 < V/wd < 7$) and when the structural damping is low large amplitudes may occur when the cylinder movement causes an increase in the vortex induced forces and in the lengthwise correlation, and the cylinder and shedding frequencies coincide. In supercritical flow the results showed an amplitude peak corresponding to a Strouhal No. of 0.2 although other peaks occurred at higher velocities (S_N = 0.1 and 0.08).

Another comprehensive investigation has been reported by Cincotta et al (Paper 20 of Ref. 7). They showed that the unsteady aerodynamic lift forces varied with Reynolds No. as indicated in the Table below. The corresponding values of the "effective" Strouhal No. are also shown.

Reynolds No. Range	S_N	Nature
1.4×10^6 to 3.5×10^6	.18	Wide Band Random
3.5×10^6 to 6×10^6	.25	Narrow Band Random
6×10^6 to 18.2×10^6	?	Random plus Periodic

It was also shown that the r.m.s. aerodynamic lift coefficient increased with model motion with a maximum occurring when the model oscillating frequency coincided with the aerodynamic Strouhal frequency. An unstable (negative) aerodynamic damping component of the unsteady lift force occurred when the model frequency was less than the aerodynamic frequency otherwise a stable damping component occurred.

The relevance of these latter results to full-scale chimney stacks or aerospace vehicles is not certain as the model was two-dimensional spanning the tunnel and end effects have been shown to be very significant.

Tests relating directly to launch vehicles have been reported in Refs. 7 and 14 and in many other individual papers.

Thus Ref. 24, whilst comprehensive, has only a small amount of data for constant diameter models which may be compared with other results and the majority of the data is mainly significant in showing the effects of local geometry, surface roughness, external protuberances, etc. The results quoted for the uniform cylinder showed smaller responses compared to most of the other models with conical or hemispherical noses. Unfortunately also, the results for $V/wd \triangleq 5$ correspond to a value of Reynolds No. in the transition zone so that, not surprisingly, no pronounced peaks were experienced for the smooth cylinder. The rough cylinder did however show a peak at about $V/wd \triangleq 5$.

Further relevant references are Refs. 25, 14 and 26. Ref. 25 shows a peak reduced velocity of $V/wd = 8$ at a Reynolds No. in the range 1.5×10^6 to 2.2×10^6. However, Ref. 14 reports on tests concerned only with models of actual launch vehicles and shows that for the Saturn I-B and Saturn V models violent self-excited oscillations were experienced at Reynolds Nos. as high as 4×10^6 based on maximum diameter. For these models the peak response appeared to be a result of vortex shedding from the lower stages at a Strouhal No. of 0.2 based on the maximum diameter of these stages. When the structural damping was increased the sharp peak was eliminated and the response was characterised by a random amplitude constant frequency motion.

Ref. 26 is a review paper concerned partly with ground wind problems and in addition to overall bending oscillations it also considers the buffeting problem of localised portions of the structure. The relevance of this to the ovalling problem will be discussed later.

3. Vortex Shedding Phenomena - Full Scale

3.1 Swaying Oscillations

The wind-excited swaying vibrations observed on tall chimney stacks occur chiefly in the supercritical Reynolds No. range. As Den Hartog reported in Ref. 27 such vibrations have been observed with a value of $S_N = 0.21$ up to $R_N = 6.2 \times 10^6$ which agrees with the values indicated in Fig. 1. Other full-scale experiences are quoted in Refs. 3, 28 and 29.

In particular Paper 25 of Ref. 3 should be mentioned as it relates to a space frame structure (the Gyrotron at EXPO '67) composed of 8100 tubes each 16ft. long x 6in diameter and having one of four possible wall thicknesses. The flattened ends of the tubes were bolted to special end joint members such that the tubes were much stiffer in the flattened plane than normal to it.

Oscillations occurred in the plane of the wind at wind speeds of about 25ft/sec., in the tubes whose flattened ends were perpendicular to the plane of the wind and at 50ft/sec. transverse oscillations occurred when the flattened ends were in the plane of the wind. The streamwise vibrations are clearly caused by the streamwise component of the vortex shedding periodic force at a frequency twice the lateral component. This also supports the evidence quoted in Section 2.2.

It should be mentioned that any theoretical prediction of the natural frequency of such a tube structure should take due account of the effect of any inplane compressive load causing an effective reduction in the frequency.

3.2 Ovalling Oscillations

Ovalling oscillations have also been experienced on various chimneys as reported by Scruton (Paper 24 of Ref. 1); Johns and Allwood (Paper 28 of Ref. 3) and in Refs. 30 - 32. From these results it has been suggested in Refs. 30 and 31 that ovalling occurs at a wind speed such that a 2 to 1 relationship exists between the ovalling natural frequency and the vortex shedding frequency (see Fig. 3(a)). This assumption has been questioned in Paper 28 of Ref. 3 and Figs. 3(b) to 3(d) show possible 4 to 1, 1 to 1 or 3 to 1 relationships. If r is the value of this critical relationship and $S_N = 0.2$ the critical wind speed is given by

$$V \triangleq 5wd/r \qquad (2)$$

where $r = 1, 2, 3, 4$, etc., signifying progressively lower critical ovalling wind speeds. The lowest actual critical wind speed would depend on the structural damping present and on some parameter such as $(\rho V^2/E)$, i.e. the ratio of aerodynamic and structural stiffness. The results for the full-scale chimney described in Paper 28 of Ref. 3 indicate a value of $r = 1$ as being most likely rather than the values of $r = 2$ reported earlier. See Section 5.

Figs. 3(c) and 3(d) are based on the possibility that the axes of the ovalling mode are <u>not</u> orthogonal with the wind direction but are aligned with the axes of the resultant periodic surface pressure distribution which are not necessarily orthogonal to the wind.

Evidence for this latter possibility is given by the fact that significant streamwise swaying oscillations are possible at a frequency twice that of the lateral oscillations (Ref. 20 and Ref. 21) and by the form of the measured pressure distribution shown in Paper 28 of Ref. 3 which is seen to have a resultant close to a line 135° from the stagnation line.

The circumferential modes excited during ovalling clearly constitute a design case of significance and require detailed analysis and test to ensure a particular structure has sufficient integrity to meet this case. In many ways it is comparable to the local buffeting or forced vibration case discussed in Ref. 26 and in Section 2.3.

4. Cylindrical Shell Vibration Analyses

The following procedures can be used to study the invacuo vibration characteristics of circular cylindrical shells:

(a) Exact solutions of the shell governing differential equations

(b) Variational techniques such as the Rayleigh-Ritz and Galerkin's method

(c) Finite element or finite difference approach

Because of the uncomplicated nature of the assumed shell configurations it was decided to use the continuum approaches of (a) and (b) only.

The assumed uniform shell configurations studied have been:

(A) a shell clamped at its base and with a free or ring-stiffened upper end, i.e. a typical chimney structure, and, secondly,

(B) a shell simply supported at both ends and stiffened with intermediate rings and/or stringers.

For the first case (A) using a variational approach, three possible types of axial mode shapes have been considered viz:

(i) a two degree of freedom polynomial function as in Paper 28 of Ref. 3;

(ii) a two degree of freedom trigonometric function and

(iii) a two degree of freedom "beam function" approximation

These three types of modes have been discussed in Refs. 33 and 34 and appropriate results presented. Fig. 4 shows the envelope of the non-dimensional structural frequency parameter Δ for various values of circumferential wave number n and length/radius ratio (L/a) for a particular value of radius/thickness ratio (a/h). The shell upper end was free.

For shells of large L/a the minimum frequency will correspond to n = 1 i.e. a swaying oscillation. For smaller L/a the minimum frequency will correspond progressively to n = 2, 3, 4, etc., as L/a decreases. Should the wind excite these higher n modes the term 'ovalling' no longer seems appropriate and the term "breathing" oscillations is perhaps to be preferred.

It is to be noted that for moderate to large values of L/a the assumption of zero hoop and shear strains in the shell elastic equations leads to considerable simplifications in the analyses with no significant inaccuracy in the results. The main implication of this assumption is that the sextic frequency equation which would generally result from a full treatment of the shell equations using two generalised co-ordinates in the axial modal functions, reduces simply to a quadratic frequency equation.

It has also been shown that the addition of a single stiffening ring to the free-end of a clamped-free shell may not significantly increase the frequencies for modes of $n \geq 2$ (for n = 1 a decrease results) and results for the particular chimney described in Paper 28 of Ref. 3 show that even with an infinitely stiff ring an increase of only 20% is possible over the zero ring frequency. Since a single end ring has limited advantages in raising the ovalling natural frequencies a much more useful solution would be to add intermediate stiffening rings at fairly close spacing along the length of the shell. For reasonably stiff rings Ref. 35 based on an exact solution can be used directly to predict the frequencies of each intermediate shell section for either simply-supported or clamped end conditions. For light intermediate rings the more general method of Ref. 36 should be used which also follows an 'exact' method of solution.

Another investigation has recently been completed (Ref. 37) using a variational approach for shells stiffened by stringers and/or rings simply supported at their ends, i.e. the second case (B) referred to earlier. The main conclusions were that the in-plane (axial and circumferential) and rotary inertias can have a significant effect in lowering the breathing natural frequencies of vibration of shells, particularly for stiffened shells. Eccentricity of the stiffeners also alters the frequency spectrum considerably. Of all the possible stiffener configurations considered, internal rings yielded higher frequencies compared to other configurations and stringers when attached internally or symmetrically could yield frequencies lower than the corresponding unstiffened shell. The results for the cases analysed show that calculations treating the stringers as discrete elements have little advantage over those with the stringers treated as smeared even for sparsely spaced stringers. The results shown for n = 1(i.e. sway oscillations) in Fig. 4 from a detailed analysis using shell theory could also have been obtained with very little error from "engineers beam theory".

This latter theory has had wide application to beam-type static and vibration problems and one interesting such application is reported in Ref. 38. This shows how an 18% increase in base bending moment can occur in a typical large, liquid-fuelling booster vehicle due to the interaction of inertia (gravity) forces and lateral wind forces. Whilst this analysis dealt specifically with static loadings it should be noted that similar effects, e.g. of the inplane gravitational forces on the natural frequencies and of the additional inertia force bending moments due to lateral deformation, should be considered in dynamic wind load studies.

5. Wind Tunnel Ovalling Studies

The design of experiments to simulate ovalling in a wind tunnel requires that the normal rules of aeroelastic modelling be obeyed as far as possible. A general discussion of scaling is given in Ref. 26 and Ref. 23 discusses scaling as it applies to vortex shedding induced vibrations.

In general the main requirement is for geometric similarity, viz. the same values for model and prototype of L/a; a/h, etc.

The corresponding ovalling frequency w is then given by

$$w_a \propto \left(\frac{E}{\rho}\right)^{\frac{1}{2}} \left(\frac{h}{a}\right) \qquad (3)$$

and if, from eqn. (2)

$$V_{cr} = \frac{10wa}{r} \tag{4}$$

it is seen that,

$$V_{cr} \propto \left(\frac{E}{\sigma}\right)^{\frac{1}{2}} \left(\frac{h}{a}\right) \times \frac{1}{r} \tag{5}$$

Therefore for a geometrically scaled model of the same material one would expect the same value of V_{cr} provided r is also invariant. Unfortunately, the Reynolds No., i.e.

$$R_N = \frac{Vd}{\nu}$$

will vary from model to full scale according to the parameter $\frac{d}{\nu}$ and if ν is invariant there is a direct scaling error in R_N and possible an error in S_N. If a compressed air or other tunnel is used which can reproduce the full scale Reynolds No. whilst keeping V the same then the value of dynamic pressure will be in error so that even if the material and the damping is the same for model and full-scale the ratio of $\rho V^2/E$ will vary.

All ovalling tests to date by the present author have been made in an atmospheric wind tunnel using aluminium shells rather than steel as in the full-scale structures. This change of material did not significantly affect eqn. (3) since $(E/\sigma)^{\frac{1}{2}}$ is approximately the same for both metals. However, with V_{cr} being the same for model and full-scale the value of $\rho V^2/E$ is obviously 3 x as large with the aluminium model as for the steel full scale structure and one might anticipate that a lower V_{cr} might have been obtained as a result.

In fact the full scale structure ovalled at a speed corresponding to r = 1 in eqn. (4) whereas the model structure ovalled at a much lower speed with r = 3. This single result would indicate that V_{cr} is a function of $(E/\rho V^2)$. It should also be mentioned that photographs (e.g. Fig. 5) and film taken during these model tests show an ovalling pattern conforming to Fig. 3(c) or (d), i.e. where r = 1 or 3. These records also indicated very large amplitude oscillations of the order of 10% of the diameter and low fatigue life.

Further tests have since been made on shells of smaller L/a and as expected it was found that breathing oscillations occurred in the lowest modes corresponding to values of n = 3 and above. The evidence to date for sub-critical flow suggests that the amplitudes of oscillation likely to be experienced in the high n modes should be small as the correlation between the circumferential modal shapes and the unsteady pressure distribution (as shown in Paper 28 of Ref.3 for a rigid cylinder) should be weak. However, whether this will be so for supercritical flow or whether at any Reynolds No. 'locking in' of the flow to the breathing vibration mode can occur as for swaying oscillations remains to be determined. It is clear however that further research is needed on these topics for both civil engineering and aerospace engineering applications. Supercritical Reynolds No. ovalling tests are planned for September 1969 as are more subcritical tests with both steel and aluminium models. These will, it is hoped, give further useful information.

6. Conclusions

The nature of vortex shedding and of the associated dynamic instabilities of circular cylindrical shell structures have been discussed. Special attention has been paid to swaying and ovalling oscillations of such structures and recent experimental data considered.

The ovalling oscillations were seen to be of large amplitude sufficient to cause rapid fatigue and clearly much more research is needed into those structural design cases which involve circumferential modes of vibration.

Methods of analysis to determine these vibration modes have been outlined and the efficacy (or otherwise) of various types of stiffening discussed.

7. Acknowledgements

The work reported here forms part of a study on "Wind excited vibration of circular cylindrical shells" supported by the Ministry of Techno ogy (U.K.). Their support in the research is gratefully acknowledged.

Acknowledgement is also made to the assistance provided by Dr. C.B. Sharma, Mr. M.Procter and Mr. J. Court.

References

1. Anon — Wind Effects on Buildings and Structures Symposium No.16, N.P.L. Teddington, England (Published by H.M.S.O.), June 1963.

2. Anon — Wind Effects on Buildings and Structures, International Research Seminar, N.R.C., Ottawa, Canada (Published by Univ. of Toronto), September 1967.

3. D.J. Johns, C. Scruton, A. Ballantyne (Editors) — Wind Effects on Buildings and Structures Symposium at Loughborough, England (Published by Univ. of Loughborough), April 1968.

4. Anon — Symposium on Tower-Shaped Steel and Reinforced Concrete Structures, International Assoc. of Shell Structures (I.A.S.S.), Bratislava, Czechoslovakia, June 1966.

5. Anon — Symposium on Tower-Shaped Structures, International Assoc. of Shell Structures (I.A.S.S.), First Session: Dresden, D.D.R., May 1968; Second Session: The Hague, Holland, April 1969.

6. Anon — Proceedings of National Symposium on Winds for Aerospace Vehicle Design, U.S.A.F. Geophysics Res. Dir., A.F. Surveys in Geophysics No. 140, (AFCRL-62-273(I)), March 1962.

7. Anon — Meeting on Ground Wind Load Problems in Relation to Launch Vehicles, N.A.S.A. Langley Res. Center, NASA TM-X-57779, June 1966.

8. J.E. Uppard — A survey of reports on experimental studies of the forces exerted on model structures by the wind and by blast waves, Atomic Weapons Res. Establishment (U.K.), Rep. No. E 6/67, May 1967.

9. L.H. Blakey — Design winds for tall strctures, I.E.E.E. Trans. on Aerospace-Support Conference Procedures AS-1(2), pp. 358-361, 1963.

10. W.W. Vaughan — Considerations and philosophy of ground winds criteria foundation. In NASA Aero-Astrodynamics Res. Review (Ed. W. Murphree) No. 5, pp. 146-157, 1966.

11. J. Armitt, J. Cainihan — The simulation of the atmospheric boundary layer in a wind-tunnel. Atmospheric Environment (Pergamon Press), Vol. 2, pp. 49-71, 1968.

12. K.N. Handa — Response of tall structures to atmospheric turbulence, Univ. of Southampton, ISVR, Tech.Rep. No. 4, December 1967.

13. J.E. Bailey et al — Launch vehicle wind and turbulence response by non-stationary statistical methods, NASA CR-846, Rep. 1340, 1967.

14. W.H. Reed, III — Models for obtaining effects of ground winds on space vehicles erected on the launch pad, Published in Virginia Polytechnic Institute Engineering Extension Series Circular No. 4, Part C, The Proceedings of the Conference on The Role of Simulation in Space Technology, Paper XVIII, August 17-21, 1964.

15. J.S. Humphreys — On a circular cylinder in a steady wind at Transition Reynolds Numbers, J.Fluid Mech., Vol. 9, Pt. 4, pp. 603-612, December 1960.

16. A. Roshko — Experiments on the flow past a circular cylinder at a very high Reynolds Number, J.Fluid Mech., Vol. 10, Pt. 3, pp. 345-356, May 1961.

17. A.W. Marris — A review on vortex streets; periodic wakes and induced vibration phenomena, ASME Series D, Jnl. of Basic Engineering 86, pp. 185 - 193, Discussion 193-196, June 1964.

18. Y.N. Chen — Vibrations excited by wakes on circular cylinders at supercritical Reynolds Numbers, Sulzer Technical Review - Research Number pp. 70-77, 1966.

19. A. Meier-Windhorst — Flatterschwingungen von Zylindern un gliechmassigen Flussigkeitsstrom; Mitt. des Hydraulischen Institute der Technischen Hochschule, Munchen, Heft. 9, Münich, 1939.

20. B. Vickery, R. Watkins — Flow-induced instabilities of cylindrical structures, Proc. 1st Australasian Conf. on Hydraulics and Fluid Mech., pp. 213-241, Pergamon Press 1963.

21. R.E.D. Bishop, A.Y. Hassan — The Lift and drag forces on a circular cylinder - oscillating in a flowing fluid, Proc.Roy.Soc. Ser A, Vol. 277, pp. 50-75, 1964.

22. Y.C. Fung — Fluctuating lift and drag acting on a cylinder in a flow at supercritical Reynolds Numbers, J.Aero/Space Sci. 27 (ii) pp. 801-14, November 1960.

23. L.R. Wootton — The oscillations of model circular stacks due to vortex shedding at Reynolds Numbers from 10^5 to 3×10^6, NPL Aero Report 1267, June 1968.

24. D. Buell et al — A wind tunnelinvestigation of ground wind loads on axi-symmetric launch vehicles, NASA TN D.1893, October 1963.

25. G. McCullough, W.J. Steinmetz — A wind tunnel study of ground wind loads on launch vehicles including the effect of conduits and adjacent structures, NASA TN D-2889, July 1965.

26. H.L. Runyan et al — Use of dynamic models in launch vehicle development, AGARD Report 479, May 1964.

27. J.P. Den Hartog — Recent technical manifestations of Von Karman's vortex wake, Proc. Nat.Acad. of Sci., U.S.A., Vol. 40, No. 3, pp. 155-157, 1954.

28. W.W. Pa,on — Vibration problems in tall stacks solved by aerodynamics Engineering News Record, July 12, 1934.

29. W. Neidel — Experimentelle schwingungsuntersuchungen an hohen schornsteinen, Beton-und Stahl betonbau, pp. 263-268, 1961.

30. W. Dickey, G. Woodruff — The vibrations of steel stacks, A.S.C.E., Trans., Vol. 121, pp. 1054-1087, 1956.

31. E. Dockstader et al — Resonant vibration of steel stacks, A.S.C.E. Trans., Vol. 121, pp. 1088-1112, 1956.

32. W. Dickey — The Design of two steam electric plants, A.S.C.E., Trans., Vol. 121, pp. 253-272, 1956.

33. D. Johns et al — On wind-induced instabilities of open ended circular cylindrical shells, Paper presented to I.A.S.S. Meeting (Ref. 5), April 1969.

34. C.B. Sharma, D.J. Johns — Vibration characteristics of a clamped/free and clamped/ring-stiffened circular cylindrical shell, (To be published: Proceedings of Symposium on Structural Dynamics, Loughborough, England, April 1970).

35. K. Forsberg — Influence of boundary conditions on the modal characteristics of thin cylindrical shells, AIAA Jour., Vol. 2, (12), pp. 2150-2157, December 1964.

36. K. Forsberg — Exact solution for natural frequencies of ring-stiffened cylinders, AIAA/ASME Meeting Structures, Structural Dynamics, Materials; New Orleans, April 1969.

37. S. Parthan, D.J. Johns — Effects of inplane and rotary inertia on the frequencies of eccentrically stiffened cylindrical shells, AIAA Meeting on Structural Dynamics and Aeroelasticity, April 1969.

38. R.P. McFarland — Beam columning in ground wind load analyses, AIAA Jour., Vol. 1(9), pp. 2147-2149, September 1963.

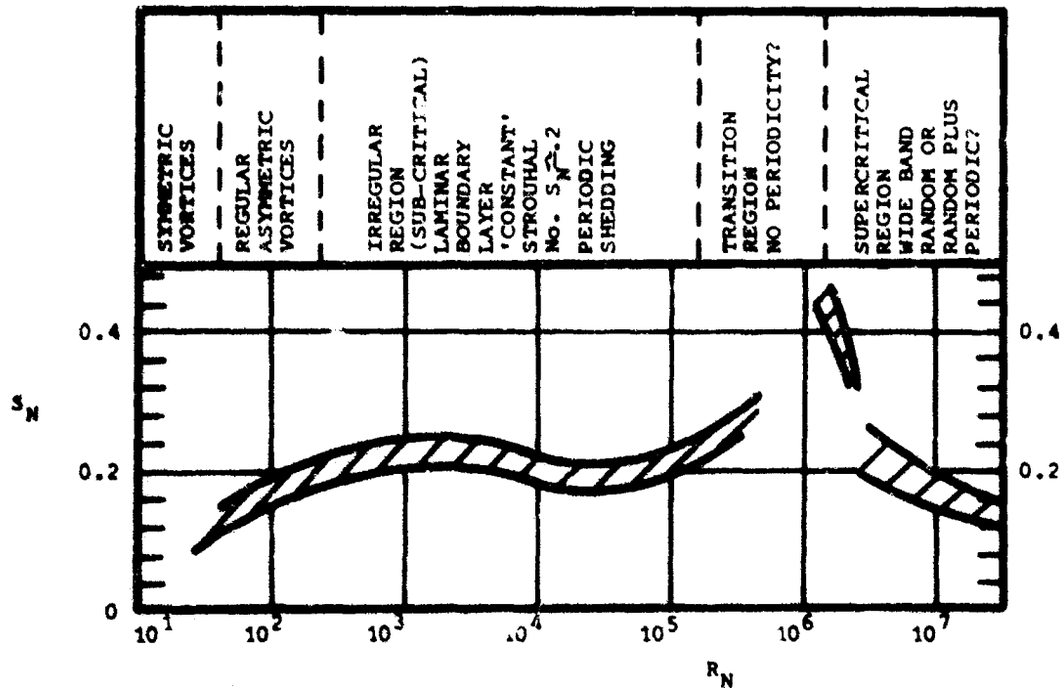

FIG 1 VORTEX SHEDDING FREQUENCIES FOR VARIOUS REYNOLDS Nos. (DATA FROM REFS 15-18)

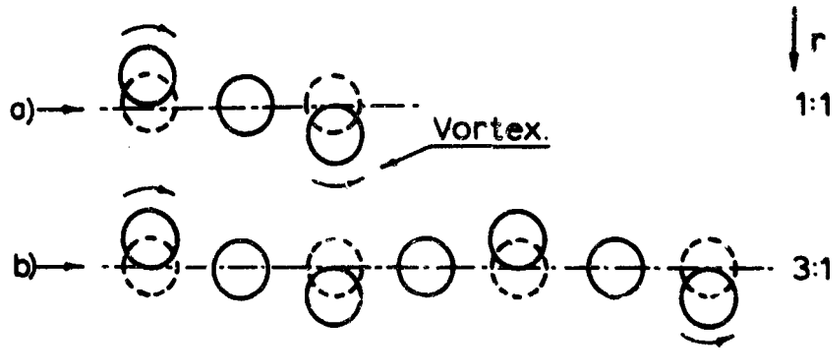

FIG.2. ALTERNATIVE RELATIONSHIPS BETWEEN BENDING OSCILLATIONS & VORTEX SHEDDING.

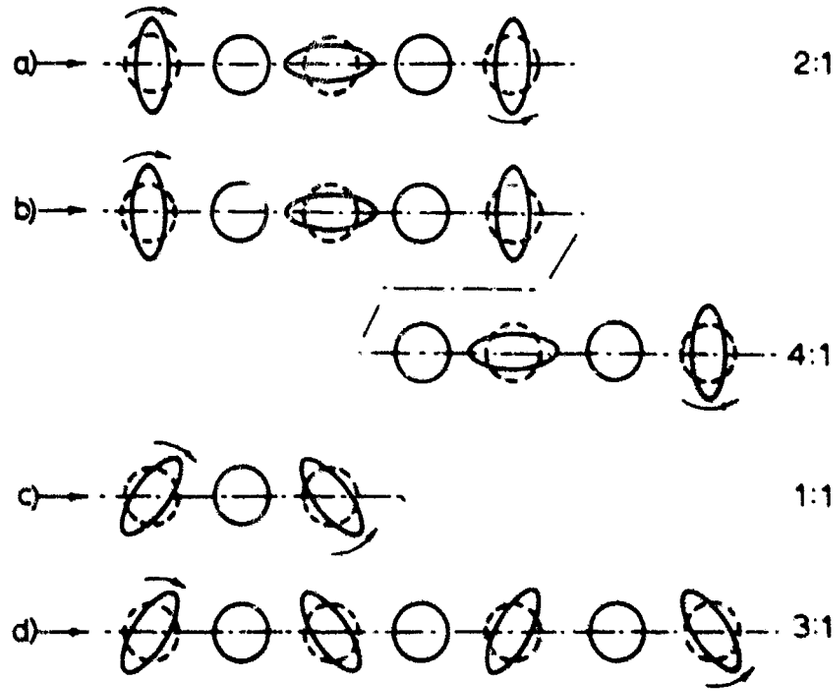

FIG.3. ALTERNATIVE RELATIONSHIPS BETWEEN OVALLING OSCILLATIONS & VORTEX SHEDDING.

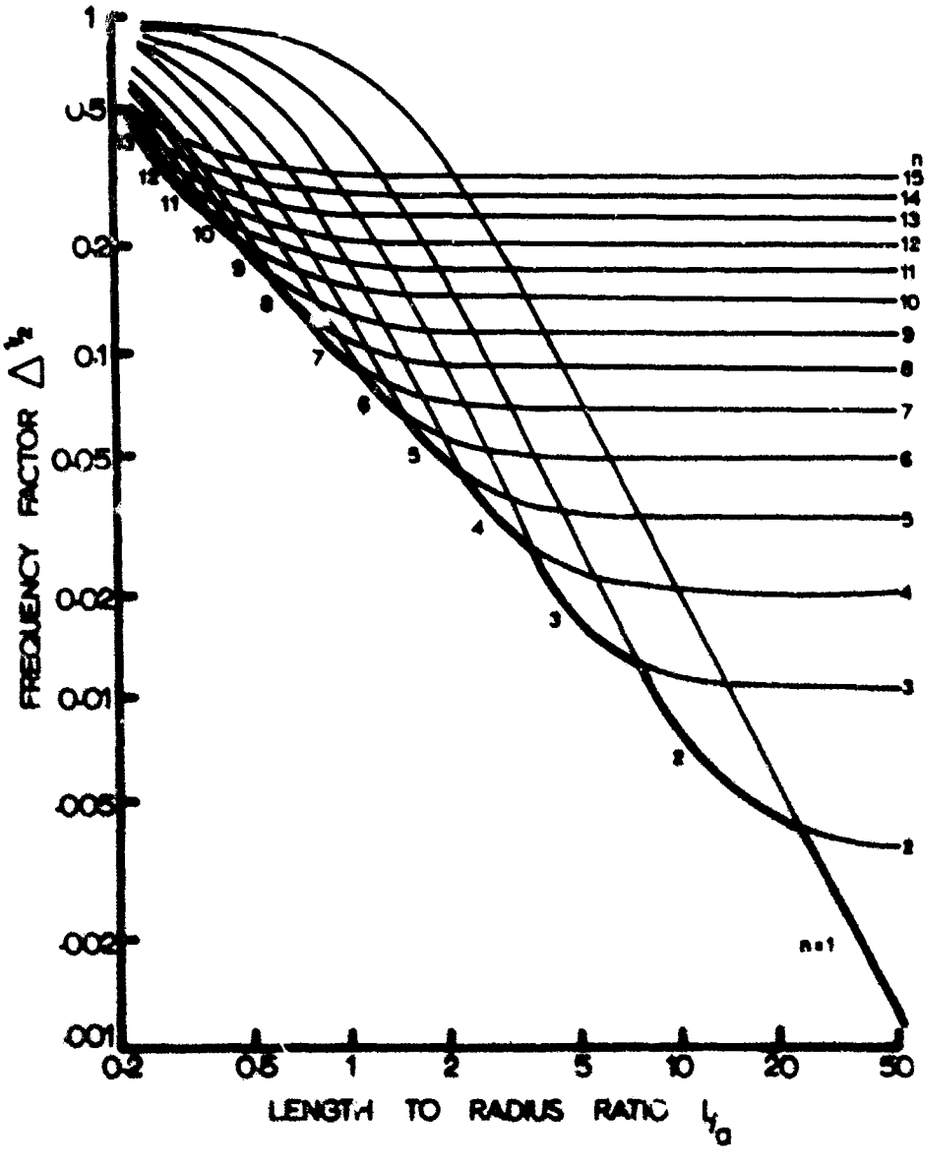

FIG.4 CLAMPED-FREE SHELL FREQUENCY ENVELOPE
($a/h = 200$, $\nu = 0.3$)

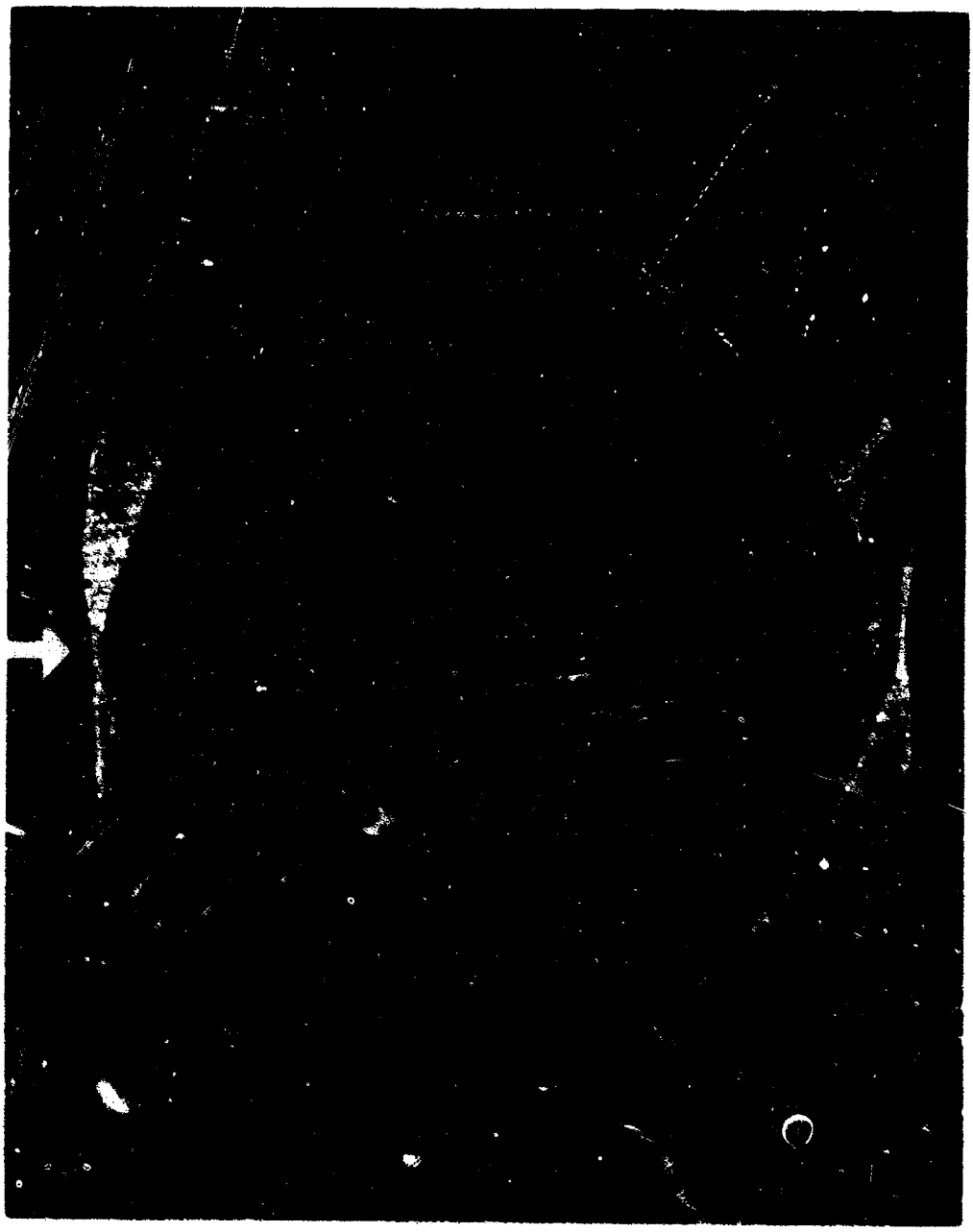

FIG 5 PHOTOGRAPH SHOWING ONE CYCLE APPROX OF CHIMNEY OVALLING OSCILLATION

Notation

a	radius of circular cylindrical shell (ft.)
d	diameter of circular cylindrical shell (ft.)
E	Young's Modulus of material (lb/in^2)
h	thickness of circular cylindrical shell (ft.)
L	length of circular cylindrical shell (ft.)
n	number of circumferential waves
N	vortex shedding frequency (hertz)
r	number in eqn. (2)
R_N	Reynolds No. = dV/ν
S_N	Strouhal No. = Nd/V
V	velocity (ft./sec.)
w	natural frequency of shell (hertz)
σ	density of shell material ($slug/ft.^3$)
ρ	density or air ($slug/ft.^3$)
ν	kinematic viscosity ($ft.^2/sec.$)
Δ	non-dimensional frequency parameter = $\sigma a^2(1-\mu^2)w^2/E$
μ	Poisson's ratio

STATISTICAL ANALYSIS OF GUST VELOCITIES FOR SPACE LAUNCHERS DESIGN

by

Dott.Ing. E.Albanese
Dott. F.Bevilacqua
Dott.Ing. E.Vallerani

FIAT - DIVISIONE AVIAZIONE - TORINO - ITALY

SUMMARY

- A dominant role in the design of launch vehicles is played by the atmospheric disturbances encountered during flight. A widely adopted philosophy to derive the aerodynamic loads induced by these atmospheric disturbances is that of considering the distribution of the atmospheric air velocity field as a quasi-steady horizontal component (wind profile) with superimposed unsteady fluctuations (gust).

- In this note the results of the studies performed by FIAT for the definition of the design gust velocity to be adopted in the calculations of the lateral dynamic loads acting on the ELDO A Vehicle during flight will be reported.

- The problem of the gust is treated from a statistical point of view, defining a gust velocity not to be exceeded during all the flight, with a given probability of occurrence; on the basis of world wide statistical data of vertical gust velocities, the probability to encounter during a given flight trajectory a gust of assigned intensity has been evaluated. The total probability is obtained through integration along an assigned trajectory of the frequency distribution components in which the turbulence has been subdivided.

- The two dimensional gust velocity frequency distribution to be adopted in the design of Space Launch Vehicles has been derived from data relative to vertical gust measured by aircraft. The intensity of the gust which has a given probability to occur during an assumed trajectory is reported in a series of charts, that may be used both for the design and the pre-launch checks procedure of Space Launchers.

STATISTICAL ANALYSIS OF GUST VELOCITIES FOR SPACE LAUNCHERS DESIGN

Dott.Ing. E.Albanese, Dott. P.Devilacqua, Dott.Ing. E.Vallerani

F I A T - Divisione Aviazione - TORINO - ITALIA

1. INTRODUCTORY REMARKS

During the ascent trajectory through the atmosphere a Satellite Launch Vehicle may be subjected to the actions of atmospheric disturbances that significantly contribute to increase the aerodynamic loads, as well as to aggravate the vehicle control problems.

The mechanism of the atmospheric disturbances is very complex due to the random nature of the air motion, that is caused by a wide number of variables; nevertheless the aerospace vehicle designers have felt, since long time, the need to schematize these phenomena in a way suitable for the evaluation of their implications on the vehicle.

The deficiencies connected with the methods usually adopted to detect the distribution of the atmospheric velocity field, methods that smooth most of the gustness since perform measurements of wind velocity averaged over a time period, have lead to the subdivision of the atmospheric disturbances into a quasi-steady mean horizontal wind component, named wind profile, to which are superimposed the unsteady fluctuations, named gusts.

A synthetic wind profile, statistically representative of a multitude of wind profiles measured in a given place during a given period in which the launch is expected to occur, ought be obtained; in absence of more circumstantial information the well known Sissiwine wind profile is usually assumed for preliminary design pourposes.

The very time dependent unsteady fluctuations in wind speed, not included in the wind profile, are taken into account through the adoption of a discrete gust that should be statistically representative of the local and temporal atmospheric conditions.

To the loads determined assuming the synthetic wind profile, are to be superimposed the loads due to the gusts; the methods adopted for adding up these loads are not yet standardized and are related to the general design philosophy adopted for each vehicle. In the present note only the magnitude of the discrete gust velocity occurring with a given probability during the entire flight, (to be adopted in the design) will be discussed and not the methods to derive the loads induced on the vehicle and the way in which these loads are combined with the other aerodynamic loads.

A different more detailed approach for dealing with the atmospheric air unsteady fluctuations is the continous turbulence approach utilized in connection with random process techniques to calculate the response of a vehicle structure in terms of the power spectra density of turbulence encountered during flight; this method, of more modern conception gives undoubted advantages of completness in the spectral description of the loads induced on the structure but requires a knowledge of the phenomena of more difficult acquisition.

In the present note a method is outlined to define, on a statistical basis, for a given trajectory the probability to meet a discrete gust with a velocity intensity V_g greater than an assigned value; or, conversely, for defining a gust velocity intensity $(V_g)_p$ not to be exceeded, during a given trajectory, with an assigned probability p % .

The use of such approach is justified in the framework of a general design philosophy based on an assumed probability of launch success; this implies the assumption of a given gust velocity value (design gust) having an assigned probability of not being exceeded during the overall flight, that meets such requirement such design gust is supposed, for conservative purposes, to occur at any time during flight in a plane perpendicular to the vehicle longitudinal axis.

2. DESIGN GUST VELOCITY ACCORDING TO PROBABILITY OF OCCURRENCE

The purpose of the present note is the evaluation of the design gust velocity, that is to say the gust velocity having an assigned probability of not being exceeded during the entire flight of a vehicle; this evaluation is accomplished on statistical basis considering the frequency distribution of gust velocities $G(Vg)$ defined as the average number of gusts per unit path lenght exceeding a given values of gust velocity Vg.

The appropriate distribution of $G(Vg)$ is greatly dependent on the atmospheric conditions; therefore is useful to separate the air turbulence distribution into several components; two main components are conventionally assumed: the "storm turbulence" an the "clear air turbulence". The former is connected with the severe conditions present in thunderstorm and later with the conditions relative to moderately rough clear air. These two types of turbulence are combined in different proportions with the non turbulence (still air) condition according to the mission and the type of vehicle under consideration; for special classes of Launch Vehicles only the clear air components must be accounted for.

Even if several parameters are expected to influence the frequency distribution of each component, such as altitude, latitude, launch site orography, season of the year, up to now no systematic dependance has been found except for the altitude. The thecnique, more widely adopted to determine that dependence of the frequency distribution of the gust velocities, is based on the measurements of the vertical accelerations experienced by an aircraft during horizontal flight; by this method therefore only the vertical components of the gust velocity distributed at random respect to all directions is ascertained.

The representation of the altitude influence on the gust velocity frequency distribution, that is derived from such type of measurements, is given by a sum of distribution components of exponential type

$$G(Vg, z) = \Sigma_i a_i B_i(z) \exp[-f_i(z) \cdot Vg] \qquad \text{Eq. 1}$$

where: a_i is the average number of gust peak per unit path lenght (1 Km) relative to the i-th component.

$B_i(z)$ is the proportion of the unit path lenght in which the i-th distribution component is expected to occur.

$f_i(z)$ is a function expressing the influence of the altitude on the i-th distribution component.

The still air condition $(i = 0)$ is obviously characterized by $a_o = 0$ and $P_o = 1 - \Sigma_i P_i$

Relatively to the schematization of the air turbulence previously reported, only two components are assumed namely: clear air turbulence $(i = 1)$ and storm turbulence $(i = 2)$.

Several problems require the knowledge of the projection of the three dimensional gust velocity frequency distribution into a plane normal to the flight path; not being readily available up to now these information, use has been made of the one dimension atmospheric turbulence data obtained from airplane operations suitably transformed.

The assumption of spatial isotropy of the atmospheric turbulence (1), (2) allows, in connection with the methods developed by Fine (3) and generalized by Bullen (4), the transformation from the vertical gust distribution to a plane distribution. According to such method if a one dimensional cumulative frequency distribution projected from a three dimensinal distribution is of exponential type:

$$G_\perp = \text{Cost} \cdot \exp[-x] = \text{Cost} \, \frac{2^{1/2}}{(-1/2)!} \, x^{1/2} \, K_{1/2}(x) \qquad \text{Eq. 2}$$

then the projected cumulative frequency distribution in two dimension is

$$G_{\perp\perp} = \text{Cost} \cdot x \cdot K_1(x) \qquad \text{Eq. 3}$$

being $K_y(X)$ the modified Bessel function of order J defined by Waston (5).

The increase in the frequency distribution in passing from a one dimensional to a two dimensional treatement may be expressed by the magnification factor

$$\Psi = \frac{G_{\Phi\Phi}}{G_{\Phi}} = x \cdot \exp\left[x\right] K_1(x) \qquad \text{Eq. 4}$$

The trend of such function computed from the tables reported in (5) is shown in Fig. 1.

Applying the above transformation to each of the distribution frequency components, the generalized two dimensional distribution, derived from the one dimensional (eq.1), turns out to be:

$$G_{\Phi\Phi}(V_g,z) = \Sigma_i\, a_i\, B_i(z) \cdot f_i(z) \cdot V_g \cdot K_1\left(f_i(z) \cdot V_g\right) \qquad \text{Eq. 5}$$

For the generalized frequency distribution the magnification factor previously introduced turns out, under the assumption of no correlation among the distribution components to be expressed by the relation:

$$\Psi(V_g,z) = \frac{G_{\Phi\Phi}(V_g,z)}{G_{\Phi}(V_g,z)} = \frac{\Sigma_i \Psi_i(V_g,z) \cdot a_i B_i(z) \cdot \exp\left[-f_i(z) \cdot V_g\right]}{\Sigma_i\, a_i B_i(z) \exp\left[-f_i(z) \cdot V_g\right]} \qquad \text{Eq. 6}$$

For any assigned gust velocity value V_g, knowing the above mentioned distribution frequency functions (Eq.1 and Eq.5), the probability to meet along an assigned flight path a gust with an intensity equal or higher than V_g, can be determined on the basis of the trajectory; such probability is obtained integrating the distribution frequency $G(V_g,Z)$ over the trajectory path:

$$P_L(V_g) = \int_L G_{\Phi}(V_g,z) \cdot dL \qquad \text{Eq. 7}$$

In general the evaluation of the above line integral (Eq.7) cannot be performed analitically due to the complessity of the integrand and, for complex trajectories, also of the path of integration; anyway its evaluation can be accomplished by means of numerical methods.

It would be desirable to have, for the launch site of interest, the collection of the information of the measurements of the vertical gust velocities, performed during a given period of the year, in order to derive frequency distribution of the gust in the form prevously discussed (Eq.1) to be utilized in the present method for the definition of the design gust velocity.

In absence of the specific information resort is usually made to the information on atmospheric turbulence relative to world wide statistics such as the one reported by Press and Steiner (6) wh. over the altitudes up to about 18 Km ($\sim$ 60 Kfeet.).

The simplified model used in ref.6 to describe the turbulence one introduced by Mc Dougal et alii (7) that considers two types of turbulence termed "storm turbulence" and "non storm or clear air turbulence"; the frequency distribution obtained by Press and Steiner for these two types of gust distribution are :

$$\text{storm} \qquad \bar{G}_1(U_{de}) = 20 \exp\left[-U_{de} / 2.2\, K_1\right] \qquad \text{Eq. 8}$$

$$\text{non storm} \qquad \bar{G}_2(U_{de}) = 15 \exp\left[-U_{de} / 5.3\, K_2\right] \qquad \text{Eq. 9}$$

The $\bar{G}_1$ and $\bar{G}_2$ distributions are frequency distributions per mile of flight defined as function of the derived gust velocity U_{de} expressed in ft/sec.; the intensity parameters K_1 and K_2, variable with altitude are reported in fig.2 of ref.6.

The overall gust distribution proposed in ref.6 is therefore given by:

$$\bar{G}(U_{de}) = 20\ B_1 \exp\left[-U_{de}/2.2\ K_1\right] + 15\ B_2 \exp\left[-U_{de}/5.3\ K_2\right] \qquad \text{Eq.10}$$

being B_1 and B_2 the appropriate proportions of flight distance flown respectively in non-storm and storm turbulence; these values, variable with altitude, are reported in fig. 4a, 4b of ref.6; the extimation of such values, expecially B_2 is, as discussed by Press and Steiner, very crude and is based on several assumptions and extrapolations that need further confirmation. In absence of more detailed data we will assume nevertheless these values for our analysis.

The distribution reported by Press and Steiner (Eq.10) falls within the general form of eq. 1; transforming the units and introducing the true air speed instead of the equivalent derived velocity, the following values to be inserted into eq. 1 are found:

$$\begin{cases} a_1 = 10.8 \\ a_2 = 8.1 \end{cases} ; \qquad f_1(Z) = \frac{3.28\sqrt{\sigma}}{2.2\ K_1} ; \qquad f_2(Z) = \frac{3.28\sqrt{\sigma}}{5.3\ K_2}$$

The variations with altitude of the parameters K_1, K_2, B_1 and B_2 to be used in connection with eq.1 and 5, obtained from ref.6, are reported in fig.2, while the computed variations of $f_1(Z)$ and $f_2(Z)$ with altitude, are reported in fig.3.

The one and two dimensional frequency distributions per Kilometer of path length $G_\theta(V_g,z)$ and $G_{\theta\theta}(V_g,z)$ of the gust velocity V_g, evaluated on the basis respectively of eq. 1 and eq. 5, assuming the two components supposted by Press and Steiner (6) are plotted as a function of velocity and altitude in figs. 4 and 5 respectively.

It can be observed from the results reported in fig 4a and 4b that for the low values of the gust velocity V_g the slope of the curves, wathever the altitude, is steeper than for the higher gust velocity values. This is connected to the fact that the frequency distributions at the low velocities are dominated by the clear air turbulence component, that having a value of the altitude function f higher than the storm component ($f_1 > f_2$ see. fig.3) more rapidly decades, so that for the higher gust velocities only the storm component influences the frequency distribution; in the range of intermediate gust velocities both the components give the same contribution to the frequency distributions. This fact determines the characteristic shape of the curves in the semi-logarithmic plane that are formed by two straight lines connected by a curve.

The higher frequency values fall in the altitude range from 7 to 11 Km. where also the Sissinwine wind profile reaches the maximum values; for all velocities at an altitude of 9 Km. a maximum is reached.

The magnification factor ψ relative to the transformation of the clear air turbulence component of the gust velocity frequency distribution passing from a one dimensional to a two dimensional treatment results, whatever the altitude and velocity, greater than the corresponding factor ψ_2 relative to the storm turbulence component.

The values of the overall magnification factor $\psi(V_g,z)$ defined by eq.6, are reported in fig. 6; from the performed computations it has been observed that for gust velocities higher than about 10 m./sec. this value is almost coincident with the ψ_2 value relative to the storm turbulence component, while at lower velocities it is influenced by both the components.

The general trend for velocities greater than 10 m./sec. is characterized by an increase of ψ for increasing velocities and a decreasing altitude; in the low velocity range the trend is complicated by the different contribution of both the frequency distribution components.

The probability P to meet a gust having a velocity higher than an assigned value Vg during a vertical path ranging from sea level up to a given altitude Z has been calculated on the basis of the one-dimensional and two-dimensional distribution functions G_* and G_{**}; the results are reported in fig. 7a and 7b respectively.

The above results can be also applied to rectilinear trajectories introducing a constant factor equal to the inverse of the cosine of the angle between the rectilinear trajectory and the vertical.

From figures 7a and 7b it can be observed that, whatever the gust velocity, the contribution to the probability P given by the frequency distribution relative to the altitudes above around 14 - 15 Km (except for the highest velocities) is quite small. The condition $P \geq 1$ correspond, by definition, to the certainty of meeting during the flight a gust velocity Vg.

These charts can be used for the choice of the design gust velocity; a given probability of occurrence is assumed and, in connection with the flight path, the associated gust velocity is found.

If the probability of 1% is selected as a design criterion and a vertical path from 0 to 20 Km is choosen, the design gust velocity Vg = 7,4 m/sec, assuming a one-dimensional frequency distribution, and Vg = 9,5 m/sec, assuming a two-dimensional frequency distribution, is found.

3. DESIGN GUST VELOCITY SELECTION FOR ELDO - A SATELLITE LAUNCH VEHICLE

FIAT Aviation Division, under request of ELDO (European Launcher Development Organization), has developed some studies to determine the Design Gust Velocity value having the 1% probability of occurrence during the entire flight of the ELDO - A Vehicle (8). The work performed for the ELDO TD/B12 has offered to the authors the opportunity to develop the more unified treatment of the design gust velocity definition reported in the present note; we briefly report hereafter the basic considerations and the results of such work done for the ELDO - A Vehicle.

In absence of gust data relative to the Woomera (Australia) launch site, the data of reference 6 relative to the frequency distributions have been adopted.

The trend of the dynamic pressure curve relative to the ELDO - A Vehicle flight trajectory and of the Sissinwine wind profile, versus altitude, have suggested the possibility to neglect the contribution brought by the low and high altitude ranges to the probability of encountering a gust of an assigned velocity.

It can be observed in fact from the curves reported in fig.8, that below about 6 Km and above about 18 Km the values of the dynamic pressure q do not exceed the 80% of qmax and the value of the wind velocity is strongly reduced with respect to its maximum. This justifies the possibility to limit to a reduced altitude range the investigation relative to the probability of meeting a gust velocity inducing critical loads on the vehicle structure.

It has been observed that the gust velocity connected with 1% probability does not vary significantly for the three altitude ranges considered in the parametric study and reported in fig.8.

The influence of a magnification factor with a value $2 < \Psi < 3$ has been analyzed to offer a parametric investigation around the value of $\Psi = 2.51$ suggested by Fine (3) in connection with straight flight paths having different slopes with respect to the vertical.

The results of this parametric investigation are reported in fig.9 for the three altitude ranges choosen and are compared with the corresponding curves deduced from the more accurate analysis reported in the previous paragraph.

The influence of the slope of the trajectory is quite small even if angles up to 45° have be nvestigated, that means that the flight path deviation from the vertical is not very significa.

The comparison reported in fig. 9 convalidates the assumption usually made of $\Psi = 2.5$; the resulting gust velocities with a probability of occurrence of the 1% in the altitude range investigated lies between 8,5 and 9 m/sec.

On the basis of these results a value of 9 m/sec has been proposed as design gust velocity for the ELDO - A Vehicle.

4. CONCLUSIONS

The method exposed in the present note enables a rapid evaluation of the gust velocity associated with an assigned probability to be adopted in the design of space launch vehicles.

Considering the scarce influence of the trajectory slope with respect to the vertical, the probability curves P_{90} (fig. 7b) relative to a vertical flight path, offer a sufficently good approximation of the probability function P associated with a general trajectory of a launch vehicle.

Assuming a one per cent probability of meeting a gust velocity along the entire trajectory, the corresponding gust velocity is about 9 m/sec.

The method is suitable for including more realistic frequency distributions provided they are given in the form of exponentials

5. ACKNOWLEDGMENT

The Authors thank the direction of FIAT Aviation Division for having authorized them to present this report.

6. REFERENCES

1. NOTESS, C.B. : A Study of the Nature of Atmospheric Turbulence Based Upon Flight Measurement of the Gust Velocity Components
WADC Tech.Rep. 57-259, ASTIA Doc.No. AD 118242, U.S. Air Force, May 1957

2. PRESS, HARRY : Atmospheric Turbulence Environment with Special Reference to Continuous Turbulence.
Rep.115 AGARD, N.A.T.O. (Paris), APR-MAY 1957

3. PINE, M. : A Random Distribution of Gust Corresponding to a Measured Frequency of Vertical Gusts.
Aeron. Quarterly, vol.IX

4. BULLEN, M.I : A Property of the Function $\frac{2^{1-n}}{(n-1)!}\left(\frac{r}{a}\right)^n K_n\left(\frac{r}{a}\right)$ Applied to Determine Gust Distributions a Plane
R.A.E. T.M. S.699 May 1967

5. WATSON : Treatise on the Theory of Bessel Functions
:Cambridge University Press.

6. PRESS,H;STEINER,R. : An Approach to the Problem of Estimating Severe and Repeated Gust Loads for Missile Operations
NACA TN - 4332

7. Mc DOUGAL,R.L.;
COLEMAN, T.L.;
SMITH, P.L. : The variation of Atmospheric Turbulence with Altitude and Its Effect on Air-plane Loads
NACA RM L53 G 15a 1953

8. ALBANESE, E;
BEVILACQUA,F. : Gust Loads. FIAT TD/B12 Report TM EF12/52.

7. SYMBOLS

α_i : the average number of gust peak per unit path length (1 Km) relative to the i-th component.

B_i : the proportion of the unit path length in which the i-th distribution component is expected to occur.

f_i : a function expressing the influence of the altitude on the i-th distribution component.

$G(V_g, Z)$: frequency distribution of gust velocities.

K_i : Modified Bessel function of order J .

L : Path of integration .

$P_L(V_g)$: Probability to meet along the path L a gust with intensity higher than Vg.

V_g : Gust velocity (m/sec).

$(V_g)_p$: Gust velocity associated to probability of occurrence P.

Z : Altitude (Km);

Ψ : Magnification factor (see Eq. 4).

σ' : Ratio of free stream density to sea level density.

Suffixes.

$*$: Conditions relative to the one - dimensional distribution.

$**$: Conditions relative to the two - dimensional distribution.

0 : Conditions relative to still air.

1 : Conditions relative to non storm (clear air) turbulence.

2 : Conditions relative to storm turbulence.

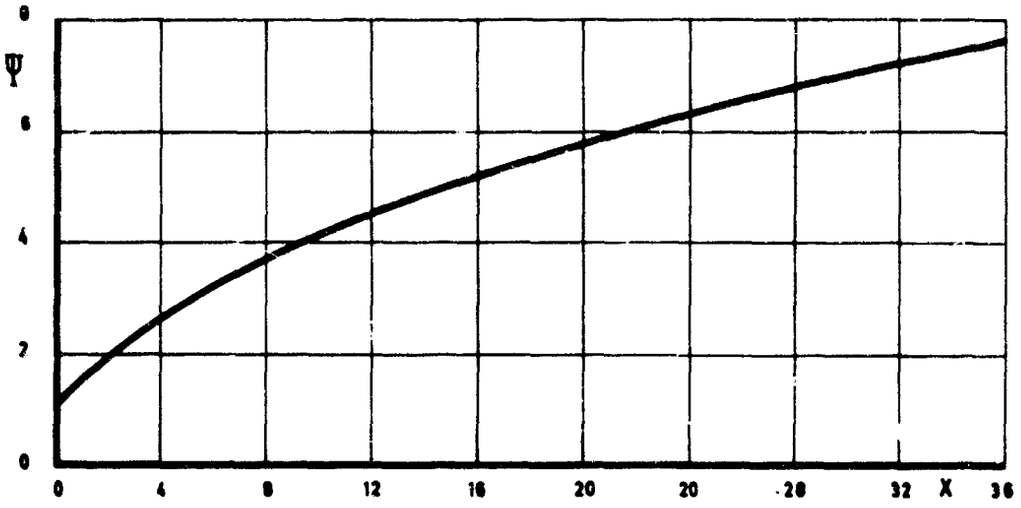

Fig. 1 - Magnification Factor: $\Psi = x \cdot \exp[x] \cdot K_1(x)$

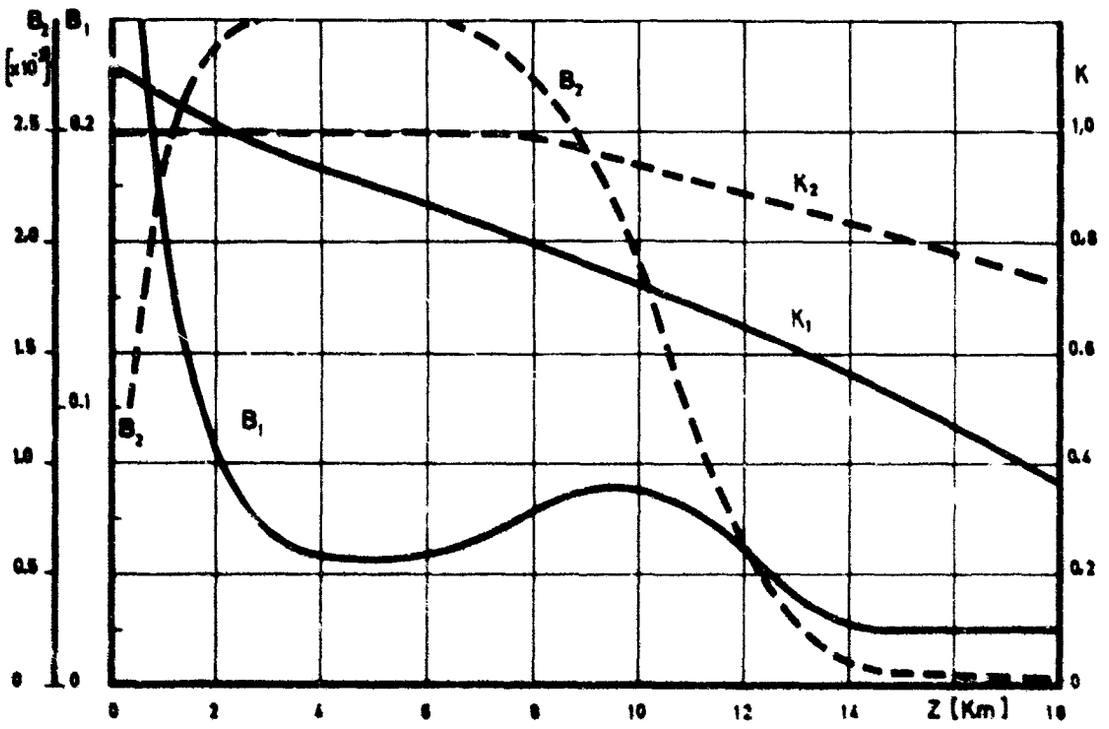

Fig. 2 - Altitude parameters (Ref. 6)

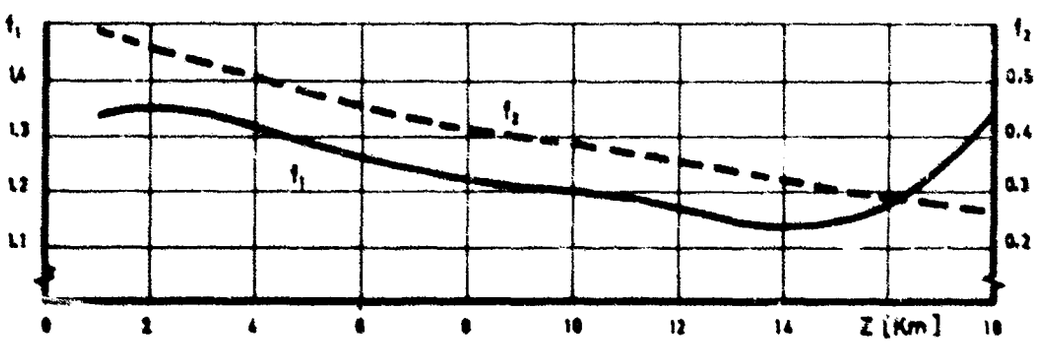

Fig. 3 - Altitude functions

GUST VELOCITY FREQUENCY DISTRIBUTION FUNCTION

Number of gusts per Km.

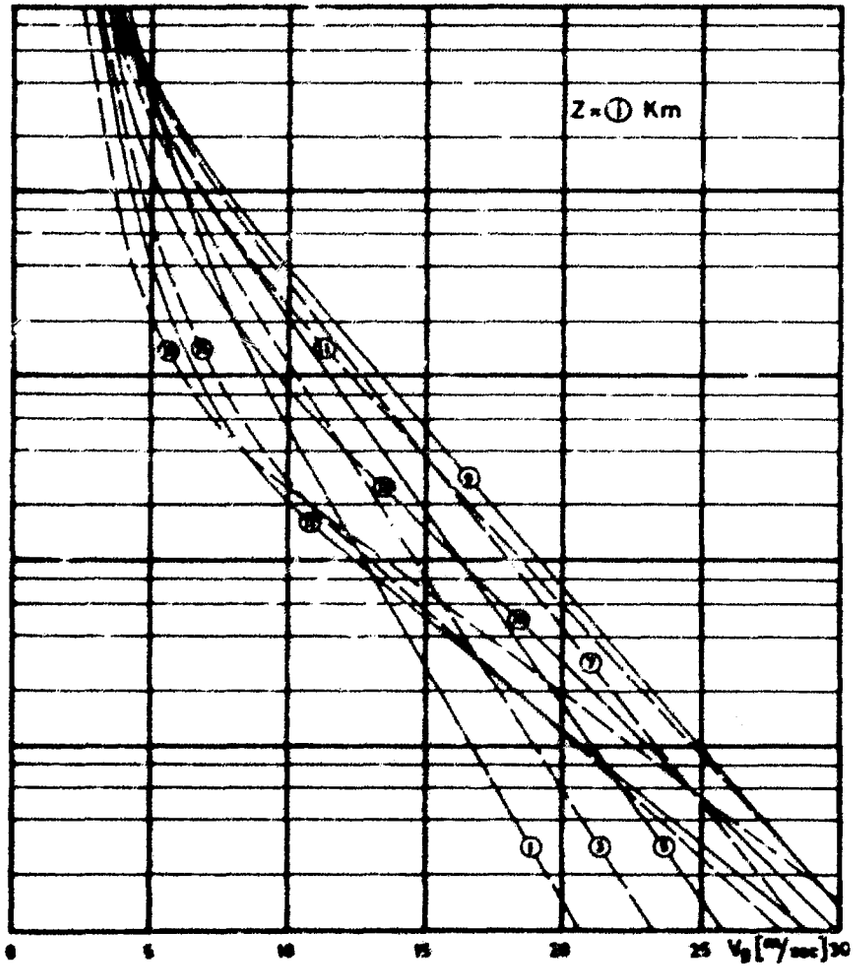

Fig. 4a - $G_g(V_g, Z)$ one dimensional distribution

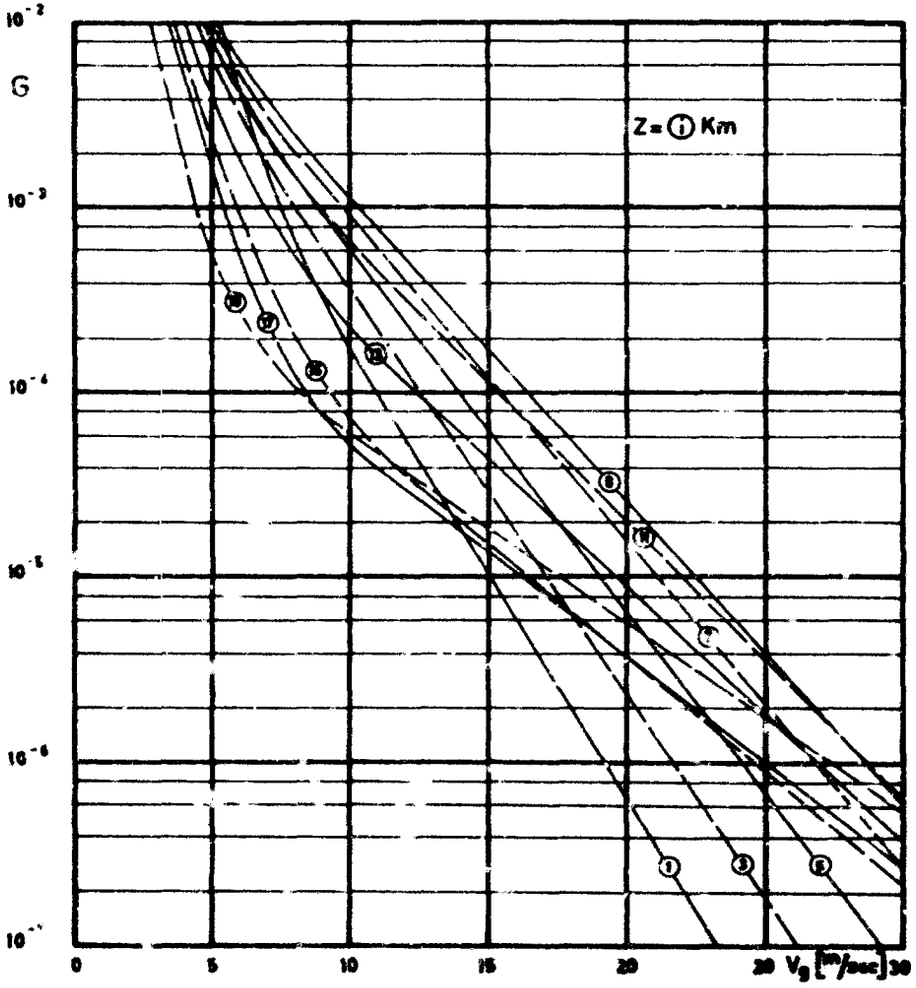

Fig. 4b - $G_{gc}(V_g, Z)$ two dimensional distribution

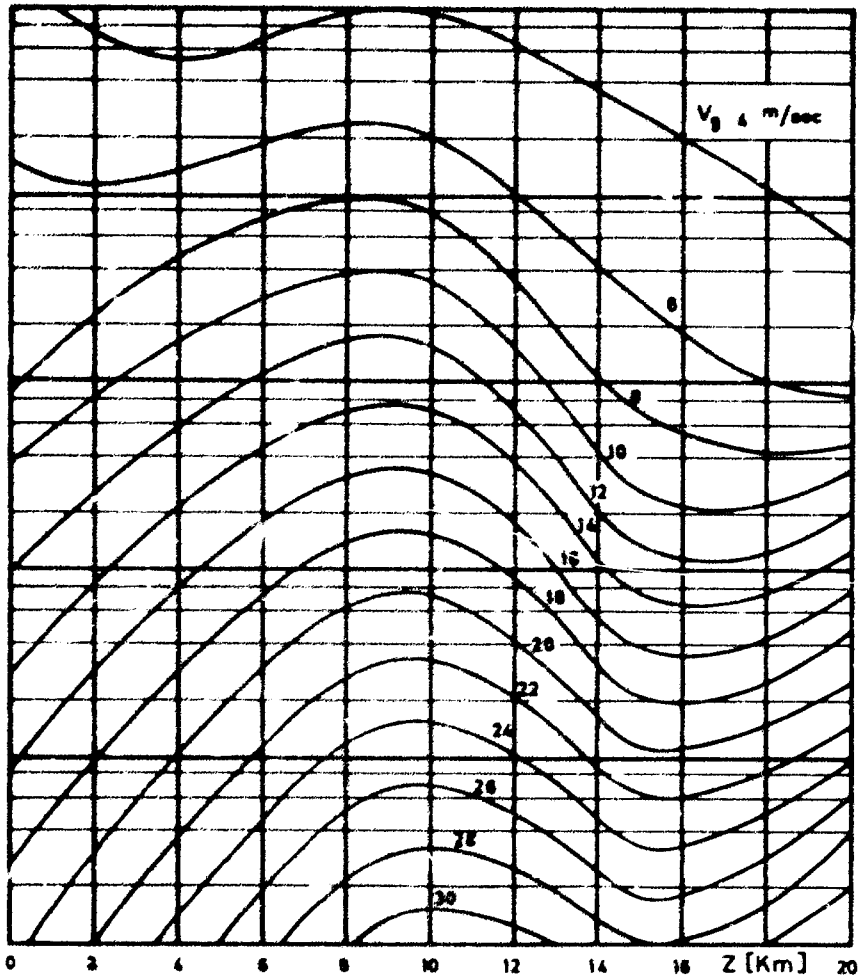

Fig. 5a - $G_e(V_g, Z)$ one - dimensional distribution

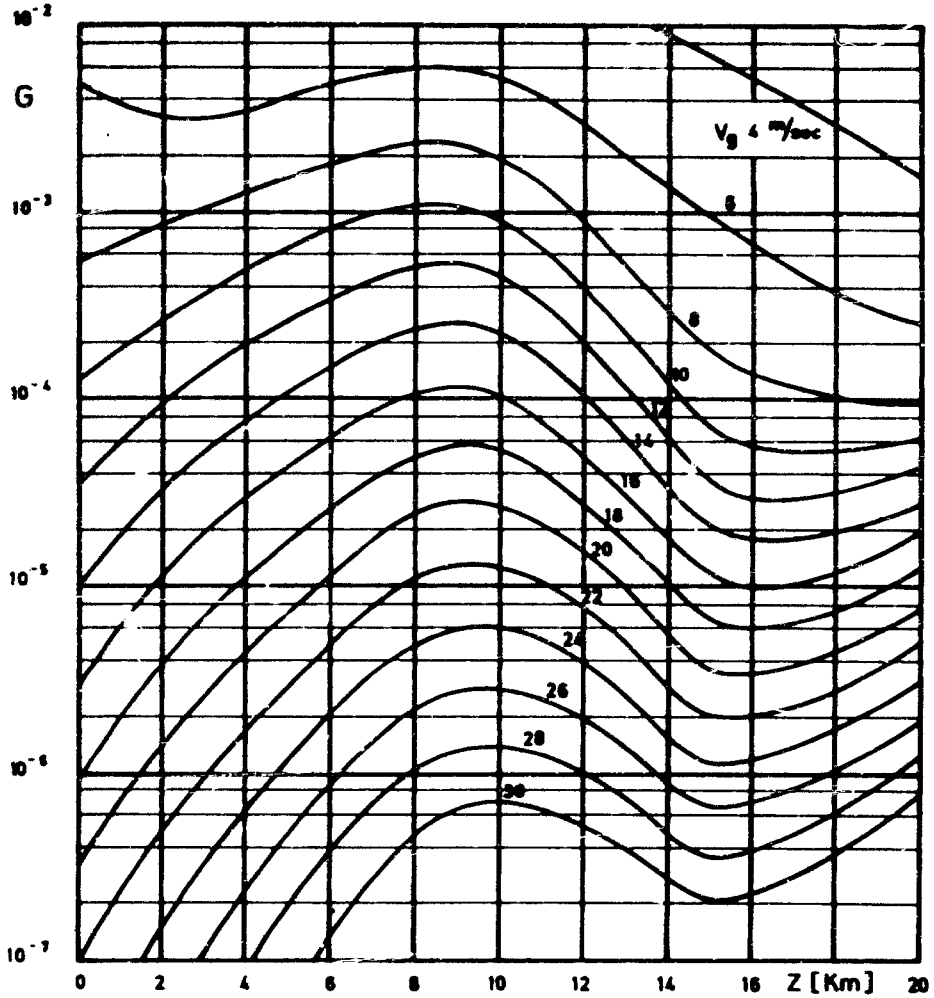

Fig. 5b - $G_{ee}(V_g, Z)$ two - dimensional distribution

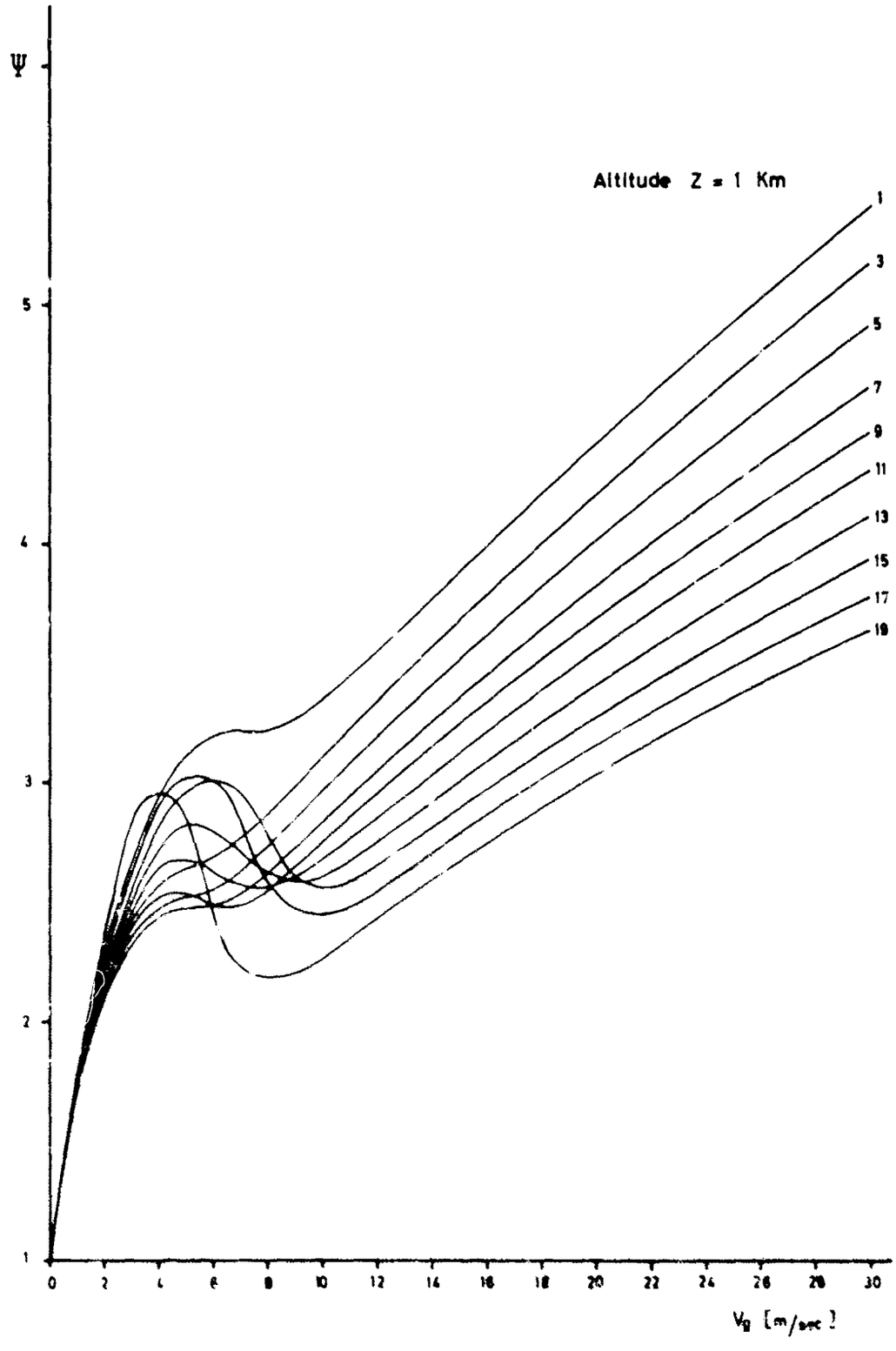

Fig. 6 - Magnification factor $\Psi = G_{z,\theta}/G_\theta$

PROBABILITY TO MEET A GUST: $V \geq V_g$ IN THE VERTICAL PATH: $0 \div Z$

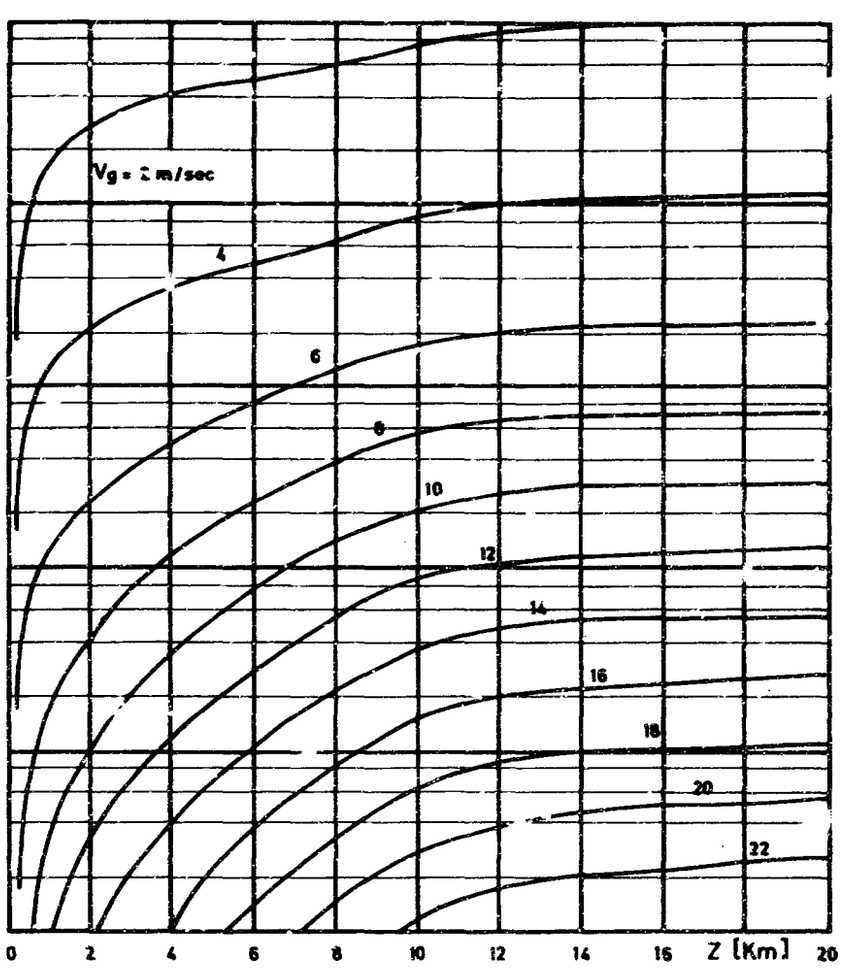

Fig. 7a – P_e associated to the one-dimensional distribution

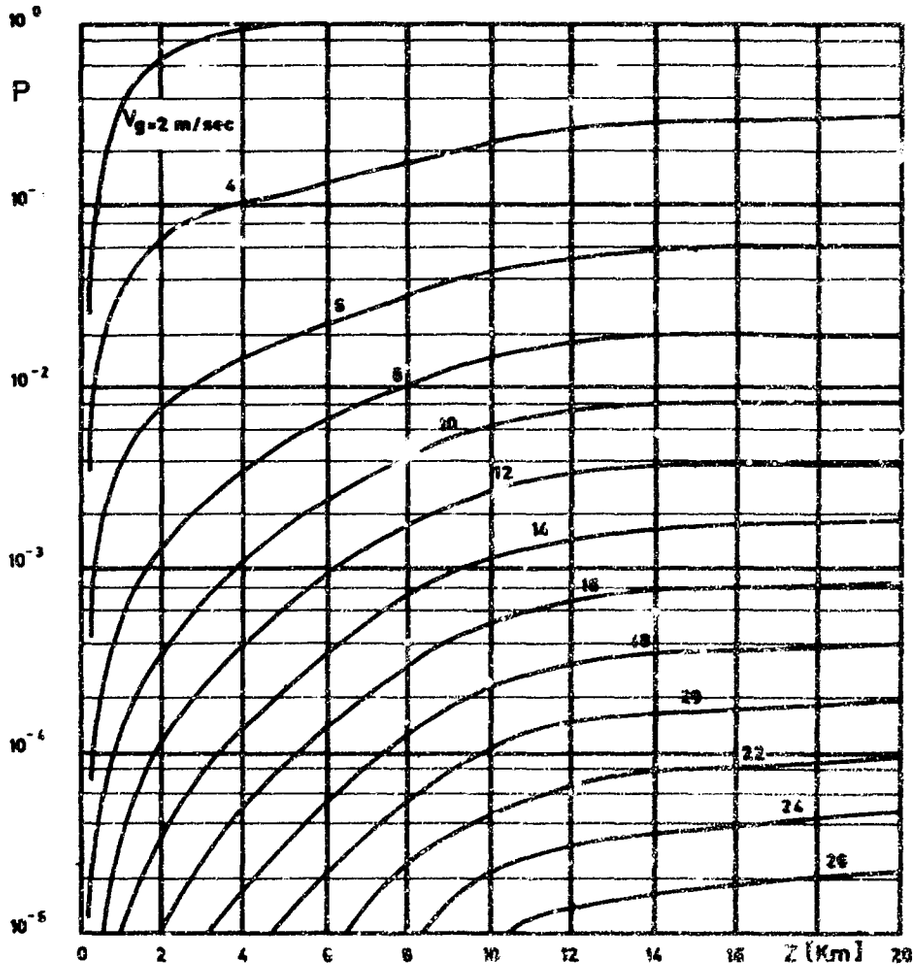

Fig. 7b – P_{e_2} associated to the two-dimensional distribution

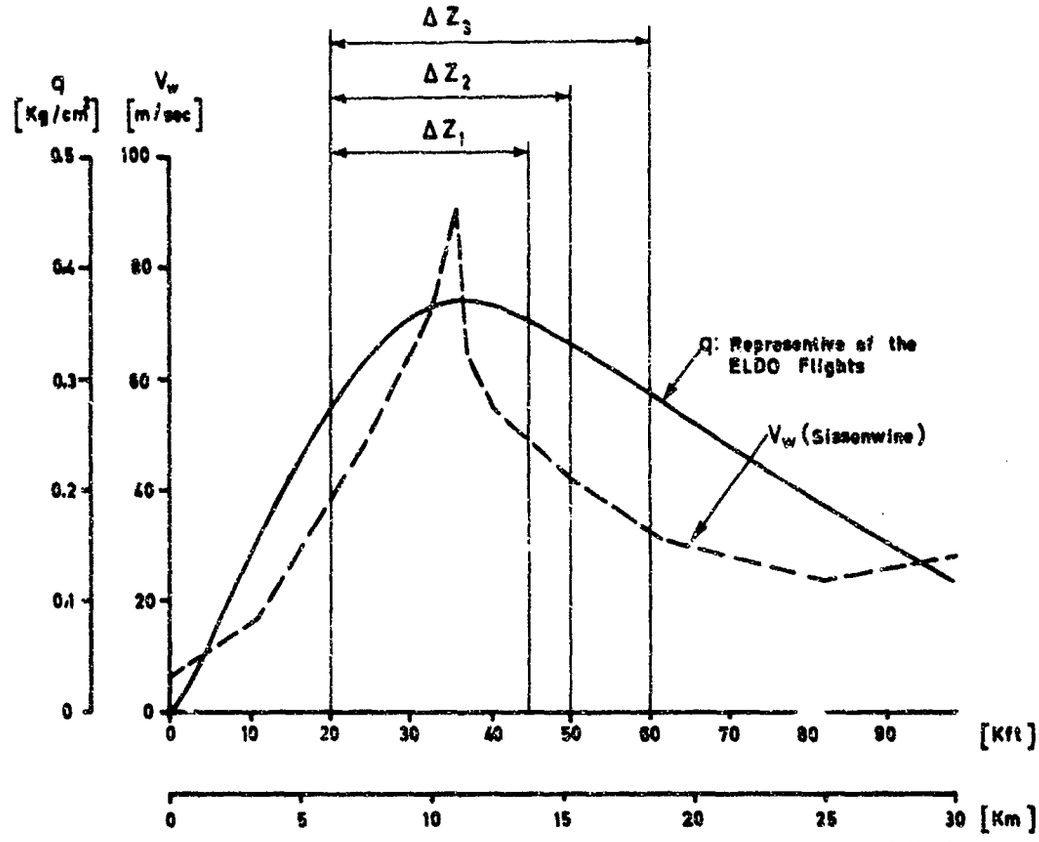

Fig. 8 - Dynamic pressure q and wind speed V_w vs altitude.

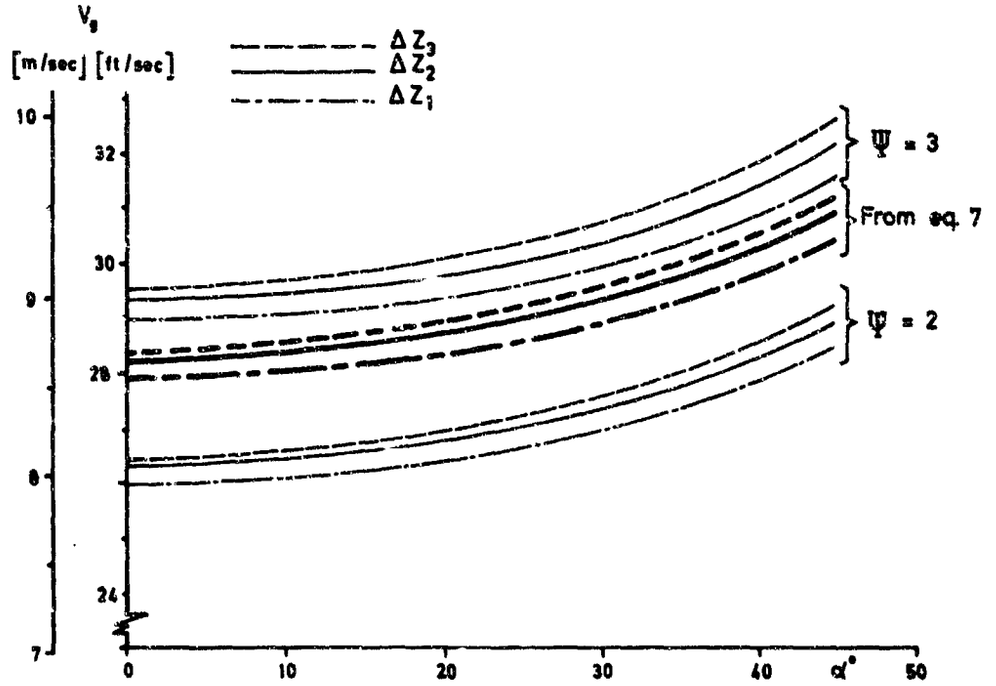

Fig. 9 - Gust Velocity $(V_g)_{1\%}$ exceeded with 1% probability over the ΔZ path - versus flight path angle α.

Aérodynamique des parois perforées; Application au projet d'écrans de protection contre le vent; Etude du fonctionement de ces écrans

par Jacques Valensi et Jean Rebont

Institut de Mécanique des Fluides de l'Université d'Aix-Marseille, France

Aérodynamique des parois perforées; Application au projet d'écrans de protection contre le vent; Etude du fonctionnement de ces écrans

par Jacques VALENSI et Jean REBONT (x)
Institut de Mécanique des Fluides de l'Université d'AIX-MARSEILLE

1. Le problème de l'aérodynamique des parois perforées se pose dans de nombreuses applications, notamment dans l'étude du projet et du comportement des parachutes ainsi que dans l'étude des écrans destinés à protéger un espace déterminé des actions du vent.

Il est rendu compte ci-après des résultats d'essais systématiques qui ont été conduits à l'Institut de Mécanique des Fluides de Marseille dès 1952 en vue de déterminer les propriétés aérodynamiques d'une bande poreuse indéfinie, exposée à un courant d'air stationnaire, de vitesse uniforme à l'infini, normale au plan de la bande (3) (4). Un calcul théorique a été exécuté, qui a permis d'atteindre l'expression du coefficient de traînée aérodynamique de la bande, par unité de longueur, en fonction de sa porosité aérodynamique et également en fonction de sa porosité géométrique (1) (2).

Ces différentes acquisitions ont reçu diverses applications, en particulier dans l'établissement du projet d'un mur pare-vent installé en 1954 dans le port de Marseille en vue de protéger des actions du vent les navires à quai et en cours d'accostage (5), ainsi que tout récemment dans l'établissement du projet d'écrans destinés à protéger des actions du vent des zones d'habitation (6).

2. Coefficient de résistance à l'avancement d'une bande poreuse indéfinie

2.1. Mesures

Les mesures ont été effectuées en soufflerie sur une bande de hauteur $h = 15$ cm, traversant la section de la veine d'essais. Dans sa partie médiane, une portion de la bande a été rendue indépendante du reste de la bande, de façon à permettre les mesures de traînée. L'écoulement sur cette portion, disposée symétriquement par rapport au plan vertical de symétrie de la veine, est bidimensionnel; autrement dit, les mesures effectuées caractérisent une bande d'allongement infini.

Ont été essayées des bandes faites de toiles métalliques à mailles carrées, de différentes porosités géométriques (rapport de la surface projetée des vides à la surface totale), et également des bandes faites de tôles minces perforées à trous ronds disposés en quinconce, de différentes porosités géométriques. Pour ces deux types de bandes poreuses et dans le domaine utilisé des vitesses (V compris entre 10 et 30 ms^{-1}), le C_x est fonction de λ et de V, mais pour un λ donné, C_x tend rapidement vers une limite lorsque V augmente. A égalité de λ et de V, le C_x d'une toile métallique est différent de celui d'une tôle perforée; pourtant, il est possible de trouver une expression très simple pour le C_x limite (fluide incompressible, nombre de Reynolds rapporté à la hauteur de la bande de l'ordre de plusieurs milliers), qui représente avec une très bonne approximation les résultats des expériences et qui est valable aussi bien pour les toiles métalliques que pour les tôles perforées. Il suffit pour cela d'introduire une nouvelle grandeur mesurable, la

---

(x) J. Valensi, Professeur à la Faculté des Sciences, Directeur de l'Institut de Mécanique des Fluides de l'Université d'Aix-Marseille
J. Rebont, Ingénieur du CNRS, Chef du Bureau d'Etudes de l'I. M. F. M.

porosité aérodynamique σ, qui est définie par le rapport du débit traversant la bande, par unité de longueur, au produit de la vitesse V de l'air à l'infini par la hauteur de la bande.

La porosité aérodynamique peut être également définie, en considérant le tube de courant qui s'appuie sur le contour de la bande, comme le rapport de la section droite à l'infini amont de ce tube de courant à la surface de la bande traversée par le courant.

De cette façon la mesure de la porosité peut être effectuée d'une manière précise en utilisant la méthode des fumées mise au point par l'un des auteurs il y a déjà de longues années.

Dans le cas présent les mesures sont effectuées dans le plan vertical de symétrie de la soufflerie et la porosité σ est égale au rapport de la hauteur du tube de courant à l'amont de la bande, là où la vitesse est pratiquement uniforme (à une distance de la bande égale à environ trois fois sa hauteur), à la hauteur de la bande. On trouve pour expression de C_x : $C_x = 2 (1 - \sigma^2)$ (fig. 4). Naturellement le σ, dans cette expression, désigne la porosité limite mesurée pour la vitesse V assurant au C_x unitaire sa valeur limite.

On remarque que cette expression de C_x est théoriquement valable dans tout le domaine de variation de σ, de 0 à 1, limites comprises. Pourtant, dans ce domaine, la configuration du sillage de la bande varie considérablement, comme le montrent les essais de visualisation effectués en utilisant deux moyens d'essais différents: la soufflerie d'une part, un tunnel plat hydrodynamique, d'autre part.

Les essais en soufflerie montrent d'ailleurs que pour V variant entre 10 ms^{-1} et 30 ms^{-1} et pour des bandes de hauteur 15 cm, le caractère général du sillage ne dépend que de la porosité aérodynamique de la bande.

2.2 Caractère du sillage à l'aval d'une bande poreuse

Pour une bande très poreuse, on observe un sillage quasi stationnaire analogue à celui admis par Oseen pour un obstacle plein et en particulier, une bande pleine. L'écoulement, irrotationnel à l'amont de la bande et autour de la bande à l'extérieur du sillage, est rotationnel dans le sillage. A l'aval de la bande et dans le sillage, les lignes de courant deviennent rectilignes et parallèles à la diraction de la vitesse à l'infini amont, sauf aux frontières où l'on observe une couche de discontinuité enroulée.

Pour des bandes de porosité décroissante le sillage se transforme en un sillage de tourbillons alternés empiétant progressivement sur la région calme immédiatement à l'aval de la bande.

La transition s'effectue pour un σ voisin de 0,63. Ces caractères sont bien mis en évidence pour $\sigma > 0,5$ par les spectres obtenus au tunnel plat hydrodynamique (fig. 1) et à la soufflerie pour $\sigma < 0,6$ (fig. 2).

La fréquence de détachement des tourbillons alternés pour une vitesse du courant non perturbé donnée, est fonction croissante de la porosité, tandis que le pas des tourbillons est une fonction décroissante de la porosité. C'est ce que montre la figure 3, qui représente la fréquence réduite des tourbillons alternés ($V = \frac{n\,h}{V}$ où n désigne la fréquence en cycles par seconde, et h la hauteur de la bande), en fonction de σ.

On peut rapprocher ces dernières observations des observations faites par B.G. de Bray (8) à l'aide de fils chauds, concernant le spectre d'énergie des fluctuations de la vitesse dans le sillage de plaques poreuses carrées. Désignant par v la composante longitudinale de fluctuation, il vient :

$$\frac{v^2}{V^2} = \int_0^\infty \nu \; F \; (\nu) \; d \; (L \nu)$$

La fonction $\nu F(\nu)$ d'après cet auteur passe par un maximum lorsque λ est inférieur à 0,4, pour $\nu \simeq 0{,}115$, quel que soit λ compris entre 0 et 0,4. En fait, cette valeur de ν correspond à la moyenne des fréquences réduites de détachement des tourbillons alternés obtenus à l'I.M.F.M., pour σ compris entre 0 et 0,67. Comme il a été dit plus haut en effet, cette fréquence réduite est fonction de σ, donc de λ.

On va voir dans les paragraphes qui suivent la relation qui existe entre λ et σ, valable quelle que soit la forme des perforations ou des mailles des bandes poreuses, pourvu que leur densité ou leur répartition soit uniforme sur toute l'étendue de la bande.

2.3 Théorie approchée de l'écoulement à travers une bande poreuse (fluide incompressible) de grande porosité et de longueur infinie normale au vent

2.3.1 Cette théorie constitue en fait une application de la théorie d'Oseen, suivant la méthode proposée par J. Pérès (7) utilisant l'équation d'Euler dans laquelle on néglige le produit $\overrightarrow{v} \wedge \overrightarrow{\text{rot}\ v}$ où v désigne la vitesse de perturbation dans le sillage.

On peut montrer que l'écoulement dans le sillage résulte de la superposition d'un écoulement dit auxiliaire, dérivant d'un potentiel, et représentant bien l'écoulement à l'extérieur du sillage, avec un courant dit de retour, parallèle à la vitesse à l'infini et de sens opposé.

Dans le cas d'une bande très poreuse, la composante de la vitesse normale à la bande peut être prise constante sur toute la hauteur de la bande, tandis qu'on peut admettre l'égalité des composantes tangentielles de la vitesse de part et d'autre de la bande. Il vient alors pour la vitesse complexe de l'écoulement auxiliaire (1), (2)

$$w = h(2-\sigma) + i\,\frac{h(1-\sigma)}{\pi}\,L\,\xi \text{ , où } \xi = \frac{1-z}{1+z} \text{ , avec } z = x + iy$$

tandis que la vitesse du courant de retour parallèle à la vitesse à l'infini portée par l'axe des x, la bande étant portée par l'axe des y, est constante. Posant cette vitesse égale à $-2H$, la porosité σ, prend la forme

$$\sigma = \frac{h - H}{h}$$

relation qui donne H fonction de σ, tandis que Δp prend la forme simple

$$\Delta p = -2\rho h^2 (1-\sigma)$$

Il vient donc pour le C_x théorique unitaire :

$$C_{x_t} = 4(1-\sigma)$$

et l'on remarquera que l'expression empirique donnée plus haut peut s'écrire :

$$C_x = 4(1-\sigma) - 2(1-\sigma)^2$$

L'expression de C_{x_t}, correspond en fait à la tangente à la courbe expérimentale pour $\sigma = 1$; elle est donc bien valable pour σ très voisin de 1.

2.3.2 Relation entre λ et σ

Elle est obtenue très simplement en supposant la vitesse uniforme à la traversée de la plaque et la pression uniforme à l'amont et à l'aval de la bande, qui dès lors, se conduit comme une surface de discontinuité de pression. Deux relations sont fournies, d'une part par le théorème de Bernoulli, appliqué entre un point à

l'infini amont et un point de la section contractée des veines d'air immédiatement à l'aval des mailles des toiles ou des orifices des tôles, d'autre part par l'équation de continuité soit

$$p + \frac{1}{2} \rho V^2 = p_1 + \frac{1}{2} \rho V_1^2$$

$$Vs = V_1 \lambda Sm$$

où l'indice 1 s'applique aux grandeurs physiques dans la section contractée et où m désigne un coefficient de contraction.

Combinant ces deux équations, il vient :

$$\sigma = \frac{\sqrt{s} \quad m \lambda}{\sqrt{1 + 2 m^2 \lambda^2}}$$

d'où, d'après l'expression de C_x fonction de σ :

$$C_x = 2 \frac{1 - m^2 \lambda^2}{1 + 2 m^2 \lambda^2}$$

La condition $\sigma = 1$ pour $\lambda = 1$ donnerait $m = 1$. La comparaison avec l'expérience montre que, dans le domaine étudié, précisé plus haut, il y a lieu de prendre pour les toiles métalliques, pour lesquelles C_x est pratiquement constant, $m = 0,85$ et pour les tôles perforées, C_x étant une fonction légèrement décroissante de Re, $0,9 < m < 0,95$ pour $1000 < Re < 3000$ (fig. 4 et 5).

Application : Mur pare-vent perforé

Les considérations précédentes ont été mises à profit pour la recherche de la configuration optimale d'un mur écran, en vue de réaliser une région calme à l'aval d'un mur dans le cas d'un vent dominant de direction parallèle à l'axe de symétrie du mur.

La figure 6 rend compte de la configuration adoptée. Pour des raisons de stabilité mécanique et aussi afin d'éviter la formation d'un sillage de tourbillons alternés, le mur est constitué de deux parois parallèles proches de porosité géométrique 0,45.

L'essai de cette configuration a été effectué en soufflerie (3,30 x 2,20 m^2, 30 ms^{-1}) sur un modèle de hauteur h = 0,450 m, posé sur une paroi plane horizontale dont la face supérieure lisse coïncide avec le plan horizontal de symétrie de la veine. Le bord d'attaque de la plaque est arrondi.

Il a été porté sur la figure 7, les courbes d'iso-vitesses réduites $\bar{u} = \frac{u}{V}$, parallèles à la vitesse du courant de la soufflerie, mesurées dans un plan parallèle au panneau central du mur et situé à 1,33 h, à l'aval de ce panneau. Il a été également représenté sur la même figure, la direction et la grandeur de la projection de la vitesse réduite de l'air sur le plan de mesure, soit $\bar{w} = \frac{w}{V}$. Les mesures ont été effectuées à l'aide d'une sonde anémométrique directionnelle.

La protection du mur s'étend sur une région dont la hauteur est égale à environ 1,5 h, sur une profondeur de l'ordre de 3 à 4 h, où la pression dynamique n'atteint que le dixième de la pression dynamique amont du mur.

La figure 8 met en évidence l'ascendance de l'écoulement à l'aval du mur ainsi que l'enroulement de la couche de discontinuité à la frontière supérieure du sillage.

Bibliographie

1. 2. R. de Possel et J. Valensi - Sur le sillage d'une plaque perméable; C.R. 236 pp 2211-13, 1953 et Publications Scientifiques de l'Université d'Alger, Série A, Vol. I, fasc. 2, 1954, pp. 267-280

3. J. Valensi et R. de Possel - Traînée d'une bande perméable de largeur constante; C.R. 238 pp 1966-68, 1954

4. J. Valensi et R. de Possel - Traînée et porosité aérodynamique d'une bande perméable; cas des tôles perforées; C.R. 239, pp. 579-80, 1954

5. J. Valensi - Etablissement d'un mur pare-vent perforé pour les navires à quai, 1ère partie - Association Technique Maritime et Aéronautique , Session 1955 (17 pages)

6. J. Valensi- Brevet C.N.R.S. , n° provisoire 175 536, 27.11.1968, repris par ANVAR (1969)

7. J. Pérès - Cours de Mécanique des Fluides, Gauthier-Villars, Paris, 1936; Sillages d'Oseen, pp. 277-305.

8. B.G. de Bray - Low speed wind tunnel tests on perforated square flat planes normal to the air stream; ARC Technical Report, C.P. n° 233, London, Her Majesty's Stationery Office, 1957.

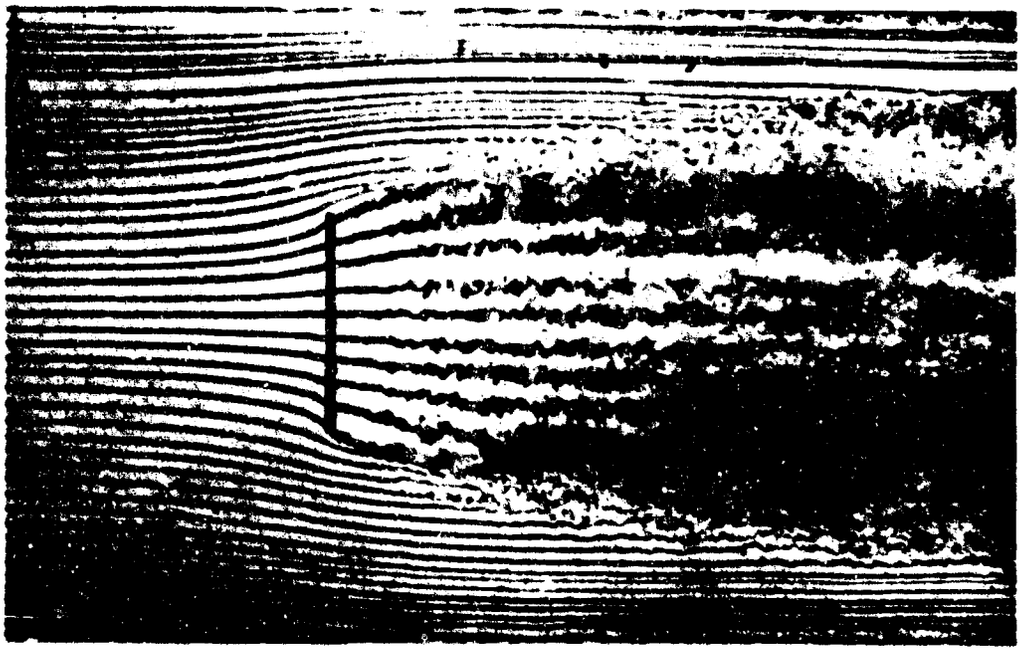

Fig. 1 a - Porosité géométrique λ = 0,45 , σ = 0,64

FIGURE NON DISPONIBLE
AU MOMENT DE TIRAGE

Fig. 1 b - Porosité géométrique λ = 0,66 , σ = 0,82

Fig. 1 - Essais au tunnel plat hydrodynamique hauteur 10 mm , largeur de la bande 100 mm. Tole métallique perforée . Sillage de la bande ; instantané 10^{-6} sec environ. V = 120 cm/s

Fig. 2a - Porosités

$\lambda = 0$

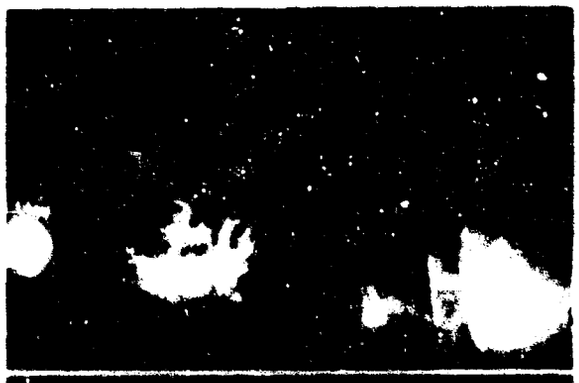

Fig. 2b - Porosités

$\lambda = 0,283 \quad \sigma = 0,45$

Fig. 2c - Porosités

$\lambda = 0,44 \quad \sigma = 0,63$

Fig. 2d - Porosités

$\lambda = 0,50 \quad \sigma = 0,67$

Fig. 2 - Essais aux fumées en [illegible], la fumée est émise en amont de la bande de tôle perforée et dans le plan médian V = 19,30 m/s instantané 10^{-6} sec.

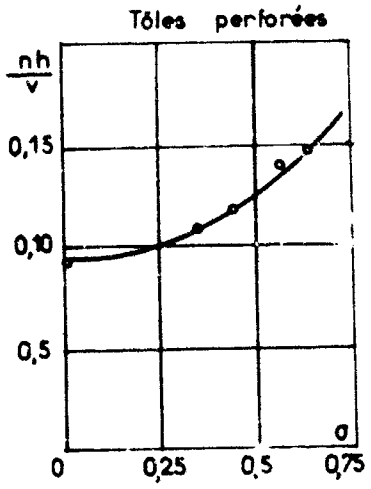

Fig. 3

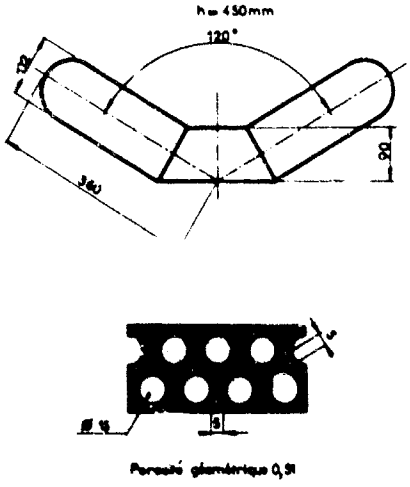

Fig. 6

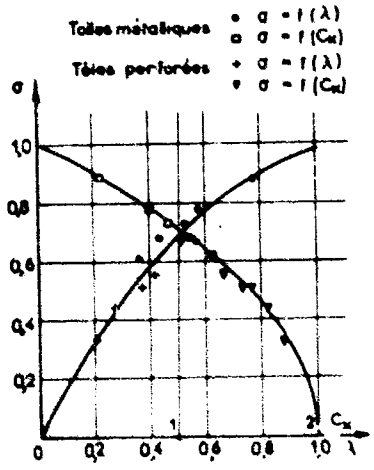

Fig. 4

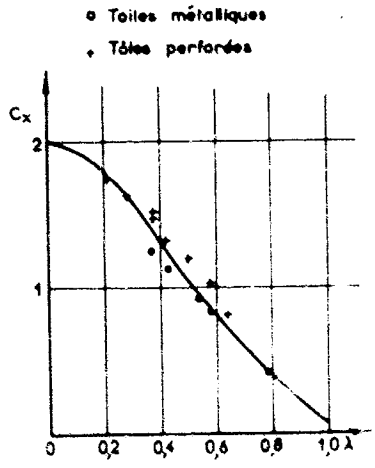

Fig. 5

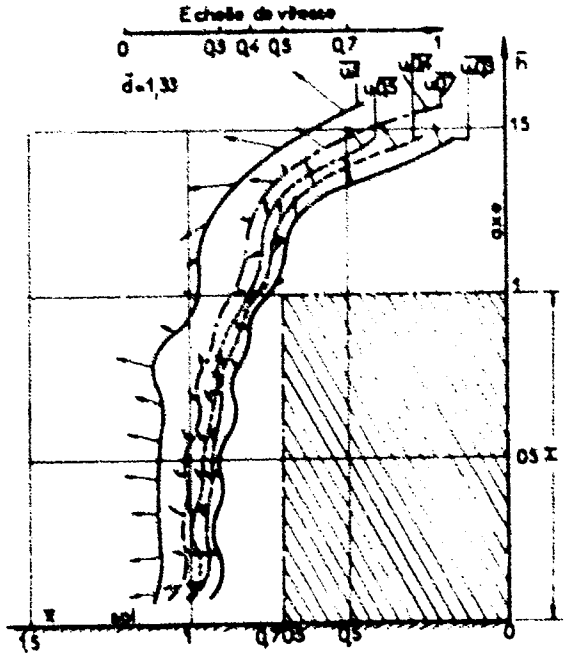

Fig. 7

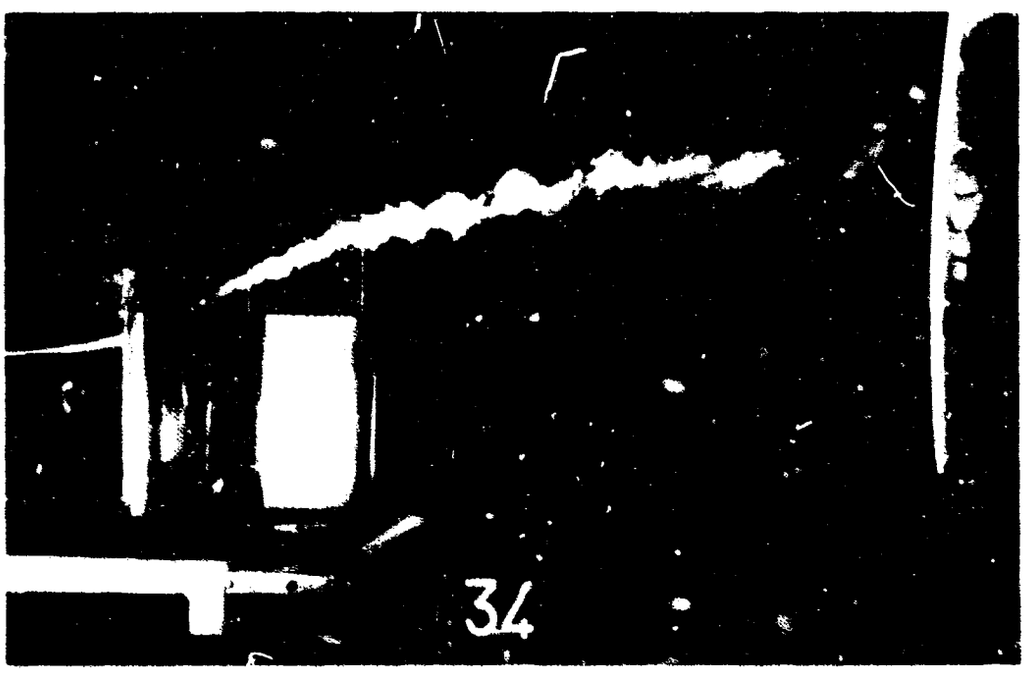

Fig. 8 - Essais aux fumées en soufflerie, la fumée est émise en amont du mur perforé dans le plan médian

hauteur du mur H = 0,450 m
largeur du mur l = 0,720
porosité géométrique A = 0,47
vitesse de la soufflerie V = 18 m/s

APPENDIX 'A'

DISCUSSIONS FOLLOWING THE PRESENTATION OF PAPERS AT THE AGARD FLUID DYNAMICS PANEL SPECIALISTS' MEETING ON "THE AERODYNAMICS OF ATMOSPHERIC SHEAR FLOWS"

Sept. 1969

Munich, Germany

APPENDIX 'A'

DISCUSSIONS

This appendix contains the discussions which followed the presentation of the papers at the Specialists' Meeting on "The Aerodynamics of Atmospheric Shear Flows" held at the Künstlerhaus, in Munich, Germany on 15-17 September, 1969.

These discussions are transcribed from forms completed by the authors and questioners during the meeting and are keyed (by reference number) to the papers contained in this Conference Proceedings.

APPENDICE 'A'

DISCUSSIONS

Le présent appendice est un recueil des discussions qui ont suivi la présentation des exposés à l'occasion de la Réunion des Experts tenue au Künstlerhaus, à Munich, Allemagne, du 15 au 17 septembre 1969 et consacrée au thème "The Aerodynamics of Atmospheric Shear Flows".

Le texte de ces discussions a été transcrit à partir de fiches remplies à cet effet par les auteurs et par ceux ayant désiré leur poser des questions. Les discussions sont numerotées suivant les numéros de références des exposés.

LIST OF SPEAKERS AND DISCUSSORS

Bearman, P.W., Dr	NPL, Teddington, Middx.	*UK*
Bevilacqua, F., Dr	Ufficio Tecnico Studi Speciali, Torino	*Italy*
Bogdonoff, S.M., Prof.	Princeton University, Princeton	*USA*
Caldwell, D.R., Prof.	Oregon State University, Corvallis	*USA*
Cermak, J.E., Prof.	Colorado State University, Fort Collins	*USA*
Clark, J.W.	United Aircraft Research Laboratory, Connecticut	*USA*
Coantic, M. Dr	CNRS, 12 Av. du Gal Leclerc, 13-Marseille	*France*
Cockrell, D.J. Dr	University of Leicester, Leicester	*UK*
Counihan, J.	Central Elect. Laboratory, Leatherhead, Surrey	*UK*
Dunckel, M.	Dipl. Phys. Meteor. Inst. der Univ. 2 Hamburg	*Germany*
Egger, J. Dr	Inst. für Theoretische Meteor. der Univ. 8 München	*Germany*
Fichtl, G.H. Dr	NASA Marshall Space Flight Center, Alab. 35812	*USA*
Gibson, C.H. Prof.	University of California, San Diego	*USA*
Hunt, J.C.R. Dr	Central Elect. Research Laboratory, Leatherhead	*UK*
Isyumov, N.	University of Western Ontario, London	*Canada*
Jones, J.L. Jr.	NASA Ames Research Center, California	*USA*
Klug, W. Dr	Technische Hochschule Inst. für Meteor., 61 Darmstadt	*Germany*
Korkegi, R.H. Dr	Wright-Patterson AFB, Ohio 45433	*USA*
de Krasinski, J. Prof.	The University of Calgary, Calgary 44	*Canada*
Kuchemann, D. Dr	Royal Aircraft Establishment, Farnborough	*UK*
Lawson, T.V.	University of Bristol, Bristol	*UK*
Legendre, R.G.	ONERA, 92 Châtillon/Bagneux	*France*
Lettau, H. Prof.	University of Wisconsin, Madison	*USA*
Libby, P.A. Prof.	University of California, San Diego	*USA*
Marschner, B.W. Prof.	Colorado State University, Fort Collins	*USA*
Maull, D.J. Dr	Cambridge University, Cambridge	*UK*
Napolitano, L.G. Prof.	University di Napoli, Viale C Augusto	*Italy*
Naumann, A. Prof. Dr	Technische Hochschule, Aachen	*Germany*
Panofsky, H.A. Prof.	Pennsylvania State University, Pennsylvania 16802	*USA*
Persen, L.N. Prof.	Norges Tekniske Høgskole, Trondheim	*Norway*
Pesaresi, R.	SACLANT, La Spezia	*Italy*
Quadflieg, H.	Technische Hochschule, Aachen	*Germany*
Roach, W.T. Dr	Meteor. Office, Bracknell	*UK*
Roth, R. Dr	University München, 8 München 13,	*Germany*
Schmidt, F.H. Prof. Dr	Koninklijk Nederlands Meteor. Inst. Utrechtseweg 297	*Netherlands*
Scorer, R.S. Prof.	Imperial College, London, S.W.7.	*UK*
Scruton, C.	University of Oxford, Oxford	*UK*
Smith, F.B. Dr	Meteorological Office Bracknell	*UK*
Valensi, J. Prof.	Univ. d'Aix-Marseille, 1 rue Honnorat, 13-Marseille	*France*
van Atta, C.W. Dr	University of California, La Jolla	*USA*
Wieringa, J.	Koninklijk Nederlands Meteor. Inst. Utrechtseweg 297	*Netherlands*
Wippermann, F.K. Prof.	Technische Hochschule, Aachen	*Germany*

A

Young, A.D. Prof.	University of London, Queen Mary College, London, E.1.	*UK*
Zeytounian, R. Dr	ONERA, 92 Châtillon/Bagneux	*France*

DISCUSSION OF PAPER 1

"THE STRUCTURE OF ATMOSPHERIC SHEAR FLOWS"

by H.Panofsky, USA

A.D.Young. (a) Is it generally the case that for large positive Richardson numbers there are no strong winds associated with velocity shears, since the presence of the latter would presumably induce turbulence independent of the Richardson numbers?

(b) Would not the presence of turbulence due to strong velocity shears result in spectra of a different character from the turbulence associated with negative Richardson numbers?

H.Panofsky. (a) In the upper air, strong winds *can* occur in regions of large positive Richardson numbers, since the hydrostatic stability is strong enough to prevent turbulence; e.g. in the "Jet Stream" we often find winds exceeding 100 km/hr, with no turbulence.

(b) I am interpreting "strong shears" as "zero Richardson numbers". The high frequency (or high wave-number) from the spectra behaves in the same way with negative and zero Richardson numbers. If wave numbers $\ll 1/Z$ (Z is height) there is much more energy with negative than with zero Richardson numbers.

L.G.Napolitano. You mentioned that the probability distribution function of meteorological variables is not always Gaussian. My question is: does the probability distribution function in these cases obey any of the several other theoretical distribution functions known from probability theory?

H.Panofsky. We have not attempted to fit any of such functions.

C.H.Gibson. There is some experimental evidence that many quantities related to the higher frequency components of turbulence at High Reynolds number, as well as scalar quantities mixed by turbulence like temperature, may be described by lognormal probability distribution functions. In particular squared derivatives of velocity and temperature appear to be lognormal. This behavior was assumed by Kolmogoroff in his third hypothesis[1].

H.Panofsky. Actually, I was talking about a different kind of non-Gaussian behavior - the variation with stability. Under neutral condition, the simple fluctuations of the vertical velocities themselves are nearly Gaussian (although, not the distribution of the derivatives). But with decreasing stability, even the vertical velocities take on skew distributions; many small downdrafts, and a few large updrafts.

L.G.Napolitano. Has anybody provided yet a physical explanation for the occurrence of skewness in the probability distribution function of the velocity components?

H. Panofsky. Only the qualitative explanation that convections near the surface consist of narrow columns of strong updrafts surrounded by large areas of slowly sinking motion.

REFERENCES

1. Kolmogoroff, A.N. J. Fluid Mech. 13, Vol.1, 1962, p.82.

DISCUSSION OF PAPER 2

"THE ORIGINS AND FORMS OF DYNAMIC INSTABILITY IN CLEAR AIR AT HIGH ALTITUDE"

by R. S. Scorer, UK

Errata

Page 2.2 - Formula (2.2) to read

$$-\tfrac{1}{2}(\eta\Delta z)^2\, Ak^2 \sin kx$$

Page 2.4 - In last line of para. 2

"unstirred" to read "stirred"

Page 2.5 - Formula (3.6) to read

$$= g\frac{\beta_0}{q_0}\delta z$$

Formula (3.8) to read

$$Ri = g\beta/(\eta_0 + \delta\eta)^2$$

$$= g\beta/\left(\eta_0 + g\frac{\beta_0}{q_0}\delta z\right)^2 \text{ by (3.6)}$$

Discussion

W. T. Roach. Prof. Scorer has discussed mechanisms by which turbulence may be initiated in a shear layer in the so-called "free" atmosphere.

In the Meteorological Office, we have been considering an approach to the problem of how turbulence might be *maintained* by large scale synoptic development processes for periods of an hour or more (as it has been observed by aircraft). This work has followed three steps.

1. Expressions for dynamical processes which change static stability wind shear and therefore Richardson number following the motion.

2. It has been assumed that the gross effect of turbulence (once it has set in) is to maintain the Richardson number at some limiting (and small) wake by counteracting the dynamical processes tending to reduce Richardson number.

3. These ideas have been given a preliminary test on the Bushy 10-level numerical forecast model and show some promise as a forecasting tool.

R. S. Scorer. The early idea about the prediction of CAT* was to find out what the critical Richardson number was by theory or observation, and then say that CAT would occur when an airstream possessed a smaller value. Dr Roach and I are both pursuing the idea that the precise value of Ri at which dynamical instability sets in is not important because one is never likely to observe an airstream in which Ri is less than this value which has

---

* CAT = Clear Air Turbulence.

not already become turbulent. Therefore we look for mechanisms which will significantly reduce Ri and if we see situations in which they will be or are operating we can probably expect the outbreak of CAT, and we hope that this way of understanding the mechanisms will be more useful in forecasting.

D. Kuchemann. A flow has been described, which appears to contain a succession of vortex cones. We have obtained, at the RAE, an asymptotic solution for such cones. For a series of such cones, one would expect a pattern of streamlines bounding the air that flows into the cones and out of them, which bears some resemblance to the "cat's eyes" pattern mentioned by Prof. Scorer. But we found that the cone flow was essentially time-dependent and that the cone-size will, in general, grow with time, if the flow is to be regarded as two-dimensional. I would like to ask, therefore, whether any such changes with time have been observed in the atmosphere.

R. S. Scorer. It is easy to watch the evolution of the vortices occurring in the atmosphere over a period of a few minutes on occasions when they are made visible by cloud, which in many common circumstances acts as a good tracer, as explained in the paper.

There is not great precision in the theory of billows, and it has been assumed always that the evolution of one vortex is not very different from that of its neighbours, although of course there may be a considerable time lag in the evolution of the billow 12 or 20 wavelengths distant.

R. Pesaresi. Does your model describe the turbulence generation due to the breaking of internal waves or can the "billows" form on the crests of the internal waves?

R. S. Scorer. In the written version of my paper (which Mr Pesaresi could not possibly have had time to read yet) I mention that my paper does not deal at all with situations in which the static stability becomes negative. These will be discussed in Paper No. 11 and I think the question of "breaking" of internal waves by increasing their amplitude should be deferred until the discussion of that paper. My paper is concerned with the billows on shear layers generated where a very stable layer is inclined away from the horizontal. The most common situation for this to happen is in mountain lee waves, but there are other, especially frontal, situations where it could just as well occur.

DISCUSSION OF PAPER 3

"MOUNTAIN WAVES IN THE STRATOSPHERE MEASURED BY AN AIRCRAFT OVER THE WESTERN U.S.A. DURING FEBRUARY 1967"

by A. McPherson, UK

R.S. Scorer. In the theoretical treatments of mountain waves from Lyra, (1943) onwards it has never been argued that a stable stratosphere would suppress disturbances due to mountains, although other people have incorrectly hinted that it would act like a rigid lid (or that the lid in their treatment would have the same effect as the stratosphere). It has been recognized for a long time that, to get waves in the troposphere best developed it is necessary to have a decrease in the stability upwards in the troposphere so that the wave amplitude has died away to almost nothing at the tropopause.

In recent work by Berkshire & Warren (Q.J.Roy.Met.Soc., in press, Oct. 1969) it is becoming evident that a situation in which lee waves are almost fully trapped in the troposphere is one in which waves would be largest in the stratosphere. This happens, evidently, because a periodic - but decreasing downstream - train of waves on the tropopause excites waves in the stratosphere more than an individually larger but single hump or trough such as occurs on the tropopause when there is no trapping of lee waves at all in the stratosphere. This new series of observations seems to provide examples of this mechanism. In the oral presentation it was implied that the situations in which the pilot lost control of the aircraft involved a very vigorous atmospheric "disturbance". It seems that the loss of control was due to flying through a discontinuity of temperature and wind which may have no turbulence (i.e. chaotic motion producing mixing) in it at all.

The 1-g experience resulted from the large speed with which the aircraft traversed the discontinuity and the only observations we can make use of are those in which the aircraft is flown so that the pilot does not lose control! Dr McPherson made some generalizations at the end of his presentation as if he was attempting to describe the climatology of CAT in mountain waves from the experience on half a dozen, or so, occasions. This is quite unjustified, and I think generalizations should only be attempted on the basis of a theory, well confirmed by observations, and not on the basis of selected experiences (selected as to terrain, at least).

A. McPherson. In describing the incident referred to by Prof. Scorer I took great care to avoid the use of the word "turbulence". There is little doubt that a disturbance existed but it may not have been turbulent. In support of the other evidence I pointed out that at the time when the speed and temperature changes were occurring there was a periodic variation in the barometric height representing a change in pressure of about 1 mb. The changes were such a frequency that they cannot have been variations in aircraft height. The remarks about piloting are offensive and should be withdrawn. I was careful to disclaim any attempt to describe climatology of turbulence. The generalizations were intended only to summarize the results of this exercise. It was hoped that the results would stimulate theoretical work.

H. Panofsky. So far, the emphasis has been on the role of waves on clear air turbulence. However, CAT sometimes does not occur with waves, but seems to require fine structure in temperature profile. This suggests a simultaneous fine structure in the wind profile; in fact, this is indicated in observations lower down. Thus an important factor in the production of CAT is the vertical wind shear. These comments are confirmed in the next paper.

A. McPherson. No comment.

DISCUSSION OF PAPER 4

"DEUX REMARQUABLES EXEMPLES DE CISAILLEMENT DANS LA STRATOSPHERE CONCERNANT LE VENT ET LA TEMPERATURE"

by G.D. Barbé, France

R.S. Scorer. Mr Barbé's soundings seem most likely to be showing standing (i.e. lee) waves because there is only a slow change in time at a fixed point, and because a horizontal wavelength typical of such waves is indicated and the vertical velocities seem to be about the right magnitude. But one cannot settle this matter with soundings from only one point. The other most probable explanation is that they are unstable growths in a geostrophic air-stream with large vertical gradient of the wind, as described in my paper on pages 2-6 and 7 These would have a much smaller vertical velocity and a much longer horizontal wavelength. The horizontal wavelength of course, can only be inferred as a result of an assumption about the inclination of the surfaces containing the wave crests to the vertical. In the case of the stratospheric waves computed by Warren and Berkshire these surfaces are very steeply inclined away from the vertical, which is very important in a case like this.

G.D. Barbé. 1. En ce qui concerne l'hypothèse du Dr Scorer que la répartition en altitude du vecteur vent entre 10 et 32 km pourrait être expliquée par l'existence d'ondes de relief stationnaires sous le vent:

(a) il est exact que, en un point donné, la variation dans le temps est faible.

(b) la longueur d'ondes horizontale de telles ondes ne peut être déterminée par nos mesures dans le cas particulier des 11 et 12 mars 1968; par contre, d'autres mesures faites simultanément en 3 points (voir en particulier WMO-No. 227. TP. 121, Technical Note No. 95, 1969, pp. 275 à 277) donnent très sensiblement la même répartition aux sommets d'un triangle équilatéral de 50 km de côté, de la température, de la direction, de la vitesse du vent avec l'altitude. D'où il semble résulter que la longueur d'onde est supérieure à 50 km.

(c) l'estimation de la vitesse verticale de l'air déduite de la variation de la vitesse verticale du ballon ne peut être faite à l'aide de nos mesures par suite de l'erreur relativement importante concernant la mesure de la vitesse verticale du ballon. Ceci résulte en particulier de la superposition des deux courbes donnant la répartition avec l'altitude de la vitesse verticale du ballon lors d'un sondage double (cf WMO précité pp. 280-282, figures 12 et 13).

2. Je ne suis pas en mesure pour le moment de commenter la deuxième hypothèse du Dr Scorer.

H. Panofsky. First, I am happy to see that Mr Barbé's paper confirms the coexistence of wind shear with temperature gradients, thus explaining the association between clear-air turbulence and vertical temperature gradients.

The large fluctuations of wind speed found in this paper are quite similar to those discovered elsewhere, for example by NASA personnel at Cape Kennedy, USA. Further, their horizontal structure has been explored by plane in Russia. Analogous structures were first observed with Meteor trains in the thermosphere; and on the basis of these observations Hines first suggested that these fluctuations are due to gravity waves.

G.D. Barbé. Je n'ai aucune observation à présenter concernant les remarques du Prof. Panofsky, sinon que celles-ci reçoivent mon accord.

DISCUSSION OF PAPER 5

"TURBULENCE STRUCTURE IN THE ATMOSPHERIC BOUNDARY LAYER OVER THE OPEN OCEAN"

by C.H.Gibson and R.B.Williams

J.C.R.Hunt. Could Prof. Gibson please elaborate on the physical implications of his complicated statistical analyses of the flow?

C.H.Gibson. Measured lognormality of $(du/dx)^2$ implies that Yaglom's[10] cascade hypothesis may be valid since it predicts lognormality. The non-Gaussian intermittent behavior of high Reynolds number turbulence illustrated by the extreme values of Kurtosis measured in this study for velocity and temperature gradients is also a characteristic of larger scale atmospheric structure as evidenced by the formation of fronts.

J.Wieringa. Calculations of the drag coefficient C_D are made for different heights by different people which makes comparison awkward. Can you - or anybody else present, like Prof. Panofsky - agree on some arbitrary but definitive choice of the C_D calculation height?

C.H.Gibson. 10 meters was used because the mean velocity was known at this position, and also to permit comparison with previous values of C_{10} reported in Phillips' recent book shown in one of the slides.

Decision Panofsky: 10 m.

R.Pesaresi. Did you find any influence of the sea surface waves on the variability of dv/dt that you have just shown?

C.H.Gibson. No. Measurements were not made under different surface wave conditions. No attempt has yet been made to relate the variability of $\partial u/\partial t$ or $\partial T/\partial t$ to wave phase, although such measurements were made during BOMEX (Barbados Oceanographic and Meteorological Experiment - with G.R.Stegen - discussed in Proceedings of BSRL Turbulence Symposium Seattle 1969 in J.Fluid Mec.) and will be reduced eventually.

DISCUSSION OF PAPER 6

"LONGITUDINAL AND LATERAL SPECTRA OF TURBULENCE IN THE ATMOSPHERIC BOUNDARY LAYER"

by G.H.Fichtl, USA

A.D.Young. (a) In Figure 6 of printed paper there are a number of points well above the curves with which you chose to fit the data. Were there any good reasons for ignoring these points?

(b) The remaining points could be fitted by a straight line independent of Richardson number which would be just as good a fit as the theoretical curve used. Why not use such a straight line?

G.H.Fichtl. (a) I cannot think of a reason for neglecting these points and they were not neglected in the analysis.

(b) Yes, one could fit the data points with a straight line. However, this would require a more complicated energy budget. We accept the type I energy budget hypothesis for the Monin layer because the data in our paper tend to agree with the theoretical calculations and the type I energy budget has been verified by other investigations.

J.C.R.Hunt. Could Prof. Fichtl answer two questions:

1. On account of the great variation of spectra from place to place is the placing of the NASA tower 5 km away from the rocket site not too far?

2. In both hypotheses I and II Prof. Fichtl assumes $dE/dt = 0$. I wonder whether this is a good approximation because of the considerable variation in roughness in the locality of the tower which produces gradients in turbulence kinetic energy. We have reason to believe this approximation may not be a very good one because, if the atmospheric boundary layer is simulated in the laboratory, the dE/dt term is of the same order as the mechanical production term.

G.H.Fichtl. 1. No. The terrain in the viscosity of Saturn V launch pads at Cape Kennedy is similar to that associated with the town site.

2. In the laboratory it is difficult to obtain conditions in which $dE/dt = 0$, while in the atmosphere it is possible to realize this condition. In order to show that $dE/dt = 0$ at our site we must construct additional towers, so that $dE/dt = 0$ is merely a hypothesis. However, micrometeorology data from other sites which are similar to the Cape Kennedy site appear to show that $dE/dt = 0$ is a reasonable hypothesis. We plan to test this hypothesis in 1970.

DISCUSSION OF PAPER 7

"TURBULENCE STRUCTURE IN FLOW REGIMES OF VANISHING MEAN SHEAR"

by H.Lettau, USA

R.S.Scorer. Does the relation $w' = x'\bar{u}_z$ have a physical justification or is it based on a desire for some sort of algebraic symmetry?

H.Lettau. The physical justification is the vorticity-transfer concept outlined and discussed in my 1964 paper in "Journal of Meteorology".

DISCUSSION OF PAPER 8

"DETERMINATION OF VERTICAL TRANSPORTS OF MOMENTUM AND HEAT AND RELATED SPECTRA OF ATMOSPHERIC TURBULENCE IN THE MARITIME BOUNDARY LAYER"

by M.Dunckel, Germany

C.Scruton. The question was: what were the sea conditions, e.g. wave heights etc. at the time of the tests, and did the sea condition influence the value of the surface drag coefficient.

D.Schriever (co-author). Wave heights during the different runs varied from about 0.2m to about 1.5m, and in this range we could detect no influence on the drag coefficient, although waves were mostly those expected from wind speed (no remarkable swell involved). Possible influences of wave generation could not be studied till now, since meteorological conditions varied rapidly during the measurements on the Baltic and the North Sea. We hope to get the necessary comparisons with steady state waves from measurements taken on the Atlantic during ATEX expedition in 1969.

F.H.Schmidt. In Equation (5) a relation is given between H and $u_{10}\Delta\theta$. There will exist a relation between u_{10} and $\Delta\theta$ also. Could Mr Dunckel say something about the influence of the latter relation on Equation (5)?

D.Schriever. We think that the dependence of u_{10} on $\Delta\theta$ is inherent in the relation as given in Equation (5). The combination of the effects of stratification (represented by $\Delta\theta$) and wind shear (represented by u_{10}) seems to give the linear relationship as demonstrated in Figure 5.

DISCUSSION OF PAPER 9

"MEAN WIND-PROFILE AND TURBULENCE-CONSIDERATIONS OF A SIMPLE MODEL"

by R.Roth, Germany

Errata

Page 9.3 Equation (17) should be read as:

$$u_*^2 = \frac{u_{max}}{\int_{z_0}^{z_{max}} \frac{\partial z}{K(z)}}$$

Discussion

H.Lettau. The defining equation for the "minimum wave number" could involve a numerical constant which you appear to assume in Equation (11) to be equal to unity. Would you please comment on this value?

R.Roth. 1. This assumption $x_{min} = 1/z$ was made as it is the simplest one. 2. This goes well with the observed maximum in w-spectra in the atmospheric boundary layer. 3. More in general it works out that the assumption of a limiting wave number x_{min} leads to a mixing-length l given by $l = (\sqrt{3.2})^{-\frac{3}{4}} x_{min}^{-1}$ if $C = 1/\sqrt{3}$ is used.

L.N.Persen. 1. I just want to clarify one point to make sure that I have understood you right. Is it so that you justify the use of Kolmogoroff's power law which to my knowledge is only valid in an isotropic homogeneous turbulence in the presented case of shear flow because you maintain that no matter what you start out with you arrive (through your iteration scheme) at a logarithmic law?

2. In that case the conclusion seems inevitable that you have found the solution to the shear flow.

3. I would then like to make a final comment. As far as I can see the proposed procedure rules out the influence of density stratification as well as the temperature variation with height. All you are then left with is an ordinary boundary layer in an incompressible fluid. Why don't you then examine the existing theories for such cases, for instance by using Dr Spalding's formulation of the law of the wall? I would like to know if the author is familiar with this procedure?

4. I am willing to accept that line of thinking.

R.Roth. 1. Yes.

2. Yes, at least I hope to contribute something to this solution.

3. No, I am not familiar with that procedure but I wanted to start with the simplest case and go step by step to the more complex problems. As it was said in the oral presentation it was possible to apply this model to the flow over a smooth wall and its transition to rough conditions. Both wind profiles and drag coefficients are in good agreement with measurements.

DISCUSSION OF PAPER 10

"ON THE DEVELOPMENT OF CYCLONES IN A STATIONARY LONG-WAVE BASIC STATE"

by J. Egger, Germany

B. W. Marschner. Is the disturbance perturbation a uniform superposition of constant magnitude and phase from 700 mb to 200 mb. If so, is this mathematical simplification physically sensible?

J. Egger. The initial disturbance has been chosen uniform in all p-surfaces for most cases. This gives no mathematical simplification but it simplifies the explanation of the developments.

L. N. Persen. I think that the comment of the Chairman is a very important one because the influence of the initial choice of the disturbance may seriously affect the result. I would therefore like to ask the author if he has verified that his results maintain their characteristics in the cases of other forms of initial disturbances.

J. Egger. In some experiments I started with disturbances, which had a tilting of axis towards the east or the north. But the character of development did not change. Only the amount of increase or decrease changed.

DISCUSSION OF PAPER 11

"MODELE AERO(HYDRO)DYNAMIQUE POUR LE CALCUL DU REGIME DES ONDES DE RELIEF"

by R. Zeytounian, France

R. S. Scorer. This is an excellent paper carrying us one stage further in the understanding of the mechanics of inviscid stratified flows. All the results are necessarily in terms of particular cases and the choice of cases is important. Long's treatment was specially significant because he showed how separation and reversed flow could occur without friction in a stratified stream. I do not regard the limitations on the way he was able to determine the boundary shape as very important because there is no special merit in any particular mountain profile; and even if we wish to model an actual mountain it is never two dimensional and we cannot model (either in a calculation or in a laboratory experiment) the on-coming air stream very accurately anyway, and no stream profile has any special merit in practice.

What we need to know is whether we have missed any important mechanism by being restricted to the solution of cases that are linear. I think the present studies show that we have not and it is satisfying to know this. It would be helpful if the author could explain why his calculations for Long's final mountain profile (Fig. 2) is not the same as Long's. It is qualitatively the same; but are the small differences due to a different

distance upstream of the mountain at which the condition that the stream is horizontal is imposed?

R. Yotsumian. Effectivement les différences dans la configuration des lignes de courant en aval de l'obstacle sur la Figure 2 par rapport à celles obtenues par R.Long sont dues aux conditions en amont mais aussi dans une plus grande part, au fait que, au cours du calcul numérique effectué nous avons simulé la variation verticale au moyen d'un modèle avec deux niveaux intermédiaires (dans les méthodes des relations intégrales).

Des calculs plus précis faits entièrement par PEKELIS en URSS au moyen d'une méthode analogue ont montré que les résultats obtenus numériquement étaient entièrement comparables avec les résultats analytiques de Long. En ce qui concerne les effets non linéaires, ils seront très importants surtout dans les problèmes réellement tridimensionnels quand *les effets de contournement* de l'obstacle sont quelquefois plus importants que les effets *d'écoulement au-dessous de l'obstacle*.

Certains résultats numériques, obtenus dernièrement en URSS, confirment cet état de choses.

DISCUSSION OF PAPER 12

"PROBLEMS OF ATMOSPHERIC SHEAR FLOWS AND THEIR LABORATORY SIMULATION"

by J.E.Cermak, USA

Errata

Page 12-1, *l*.59 H_0 should read $Ho/\rho C_p$

Page 12-6, *l*.24 $(\nu/\varepsilon)^{\frac{1}{4}}$ should read $(\nu/\varepsilon)^{\frac{1}{4}}$

Page 12-15, Figure 8. In caption z/L should read Ri

Discussion

J.C.R.Hunt. Could Prof. Cermak answer two points concerning Section 3-3 of his printed paper?

1. Although we cannot simulate all the statistical properties, do you think it is only important to simulate the extreme values of fluctuating velocity for wind-loading problems rather than diffusion and wake simulation problems (i.e. the higher moments)?

2. With regard to the comments on the effect of vorticity generators, grids, etc., it may be possible to simulate the spectra and r.m.s. values of turbulence at a section (which may be sufficient for wind-loading problems). However, in simulating diffusion and the development of wakes it is clearly important to have the right *gradients* in the stream direction of the flow. Do you have any idea about criteria as to how great or how little differences in such gradients between atmospheric and wind tunnel flow are tolerable for accurate simulation of diffusion and wake flow?

J.E.Cermak. Good simulation of wind loading on structure requires simulation of the turbulence spectra as well as the distribution of extreme values. Local pressure fluctuation on a structure are controlled by wave lengths of turbulence having the same order of magnitude and smaller than the building width; however, small overturning moment and force fluctuation are controlled primarily by scale of turbulence larger than the building dimension (particularly the extreme value of small wave number disturbance)

2. Insufficient data are available on the effects of turbulence-characteristics gradients in the mean flow direction on diffusion to be able to give criteria you seek at this time. Any forthcoming criteria will require specification of the degree of accuracy expected from the simulation effort.

DISCUSSION OF PAPER 1

"METHODS AND CONSEQUENCES OF ATMOSPHERIC BOUNDARY LAYER SIMULATION"

by D.J.Cockrell, UK

Errata

13.2 section *Introduction*, line 29 the word "minimum" in brackets at the end of the line should read "maximum".

Discussion

R.H.Korkegi. The few mixing devices - rods and vortex generators - produce a turbulent shear layer by their wakes. I wonder to what extent the local flow perturbations due to these devices are damped out at the measuring station in such an artificially produced turbulent shear layer?

D.J.Cockrell. So far as the graded-rod velocity profile producer is concerned there is good evidence (in our Reference 21 amongst other places) that the local flow perturbations are damped out rapidly by the coalescence of the wake-type flows and jet-type flows behind the rods. This is unlikely to be the case with other velocity profile generating devices.

T.V.Lawson. Few buildings or structures project from a smoothly uniformly rough surface. The environment in which they find themselves is an amalgam of their near environment, their general environment and the local topography. We have heard mainly of attempts to produce a general environment, in particular a general environment which does not decay. My question is: does the speaker know of any work which describes the relative importance of near environment and topography (both of which require detailed mapping) with general environment upon which we have concentrated. Providing there are no topographical features, how crude can the production of velocity and turbulence profiles be? If topographical features have to be mapped, how crude can general local environment be?

D.J.Cockroft. So far as the effect of near environment and topography is concerned I have nothing to add to the list of references given by Prof. Cermak. There is sufficient experimental evidence to indicate that a mean velocity profile must be provided in model tests though it may not need to be much more sophisticated than a linear profile. However, by using the methods which we have indicated it is as easy to produce a power-law profile with known exponent parameter or a log-linear profile, as it is to produce a linear mean velocity profile. As we have indicated, the Reynolds stress gradient affects the degree of equilibrium of the mean velocity profile. Whether this is significant or not depends on working section length and the degree of non-uniformity over the working section that can be afforded in the mean velocity profile.

The other way it affects the problem aerodynamically is in the degree to which the flow pattern associated with a body placed in the tunnel is changed by turbulence.

Armitt (our Reference 9) makes a contribution here, as does some initial work on the flow over a forward-facing step by Moorman*. In Paper 14 Counihan suggests that not only is the mean square turbulence significant, but also that its energy should be contained in large-scale eddies. To this degree therefore he appears to be arguing for spectral density similarity. As yet there would appear to be insufficient experimental evidence to say how significant this similarity really is, but my colleagues and I think that good reproduction of the mean square turbulence (at least) is important in studies of flow wind grips of buildings where the point of reattachment of separated regions may well be critical.

* Moorman, J. - Flow over a Forward-Facing Step. University of Leicester Engineering Dept. Internal Report 1969.

DISCUSSION OF PAPER 14

"A METHOD OF SIMULATING A NEUTRAL ATMOSPHERIC BOUNDARY LAYER IN A WIND TUNNEL"

by J.Counihan, UK

L.N.Persen. I think that you have made an excellent job in providing a flow situation in your tunnel that corresponds to the atmospheric conditions. However, I would like to know, when talking of the forces exerted on structures like slender masts or towers, if not the interaction between the flow and the structure is just as important as the reproduction of the real flow.

J.Counihan. Prof. Persen also had a second question which I replied to first concerning the statement I made that "recent work had not completely verified Townsend's proposed models of the vortex systems in boundary layers". This statement was based on the work of Tritton and a paper by Kline et al. Both papers have been published in the J.F.M. However, the point I wish to draw attention to was that if one approaches the problem of simulating a boundary layer by trying to devise a system to produce complex vortex systems, then this does not seem to be a very good approach; especially also since, as far as I am aware, the vortex systems of boundary layers have not been defined very definitely. This was why I chose the approach of first trying to reproduce the correct form of turbulence

distribution through the height of the boundary layer. The second part of the question can be commented on by Dr Hunt of C.E.R.L. who can probably give you more details concerning this point.

J.C.R.Hunt. Perhaps I can answer Prof. Persen's comment since I am working with Mr Counihan. At the Central Electricity Research Laboratories we are considering the entire problem from the simulation of atmospheric turbulence to the appropriate scaling of the elastic properties and density of the structures placed in the boundary layer. For example we have been studying the pressures on and the stresses in a model of a cooling tower made of 'DEVLON' - an epoxy resin containing small steel balls. This material has the right density and elastic properties for a proper model. We have found that the effects of movement of this body on the flow is very small, however other bodies exist in which this is not so. The forces on such bodies will be discussed tomorrow by Mr C.Scruton.

J.Counihan. I agree with Dr Hunt's comments. Our work at C.E.R.L. at the moment is mainly concerned with the measurement of cooling tower wind loadings in a turbulent boundary layer, whereas Mr Scruton of N.P.L. will consider different types of structures tomorrow.

DISCUSSION OF PAPER 15

"LABORATORY INVESTIGATIONS OF ATMOSPHERIC SHEAR FLOWS USING AN OPEN WATER CHANNEL"

by J.W.Clark, USA

S.M.Bogdonoff. In your photograph No.4, you showed dye streams and hydrogen bubbles. In your observations, did you see any three-dimensional flows (did you examine dye lines off center)?

Can you explain the relatively smooth hydrogen bubble traces in the region which the dye trace showed to be turbulent?

J.W.Clark. The waves and vortices were two-dimensional, that is, they extended completely across the channel from wall-to-wall. The turbulence appeared three-dimensional.

One must distinguish between (1) the dye streamer, which originated far upstream and hence shows the integrated effect of the flow, and (2) the bubbles, which originated where the photograph was taken and hence show the approximately instantaneous flow properties. The bubbles should not be expected to show much flow distortion in the photograph because the velocity and turbulent fluctuations are so small .... less than 0.05 ft/sec for this case.

R.S.Scorer. 1. The billows in the photograph shown at the end of the talk appeared to be rotating in the wrong direction.

2. You referred to gravity waves produced other than by mountains. These may occur but they are generally much smaller, but it was remarked to me yesterday after I had emphasized the importance of mountain waves that the sliding up slopes could occur over rather long time intervals at fronts, and that near fronts over the ocean we could expect to find billows (i.e. CAT if there are no clouds) there.

3. It has become customary to use density profiles to the velocity profiles which are matched. In your experiments, and I think in Drazin's theory, there is a concentration of velocity gradient but a uniform density gradient throughout the channel. It is probable that in the atmosphere the vorticity is concentrated because the density is concentrated. Ought one to use someone else's theory in applying it to the atmosphere?

4. It is interesting that pictures of fine billows have been in the literature for several decades; the explanation of them in terms of instability of a shear layer produced by tilting a layer of large static stability has been known to meteorologists for about ten years; yet the current interest in the subject clearly originated in Wood's observations under the surface of the Mediterranean. It seems that people did not like to be told by the cloud photographers that they could have seen it for themselves if they had kept their eyes open.

J.W.Clark. 1. Correct - I cannot tell whether the slide is mounted backwards or whether I pulled the wrong slide out of the bag.

2. Quite correct - I expect that in due time we will find the phenomenon occurring over fronts, thunderstorms, etc. I have analyzed some of the USAF Project HICAT data, and this appears to be the case indeed.

3. Offhand, I know of no such theory. Someone should look into this. I would not expect the unstable wavelengths to be much different though.

4. Yes, it was suggested some time ago by Scorer, Ludlam and others that such a phenomenon exists. Credit should also be given to McPherson and Nicholls (Paper No. 3) for their fine measurements on the Canberra flights. I believe this is the first time adequate atmospheric data are available for calculating stability and expected wavelengths. Much more analysis can be done on their data. The HICAT reports also will prove fruitful in this respect, although I have found a definite lack of RAOB data of sufficient detail to describe the fine structure of the velocity and temperature profiles for these cases.

DISCUSSION OF PAPER 16

"WAKE CHARACTERISTICS OF A BLUFF BODY IN A SHEAR FLOW"

by D.J.Maull, UK

A.D.Young. (a) Presumably there are differences in pressure with height immediately behind the gauze. Are these small enough to be ignored at least in the working section?

(b) There appears to be an interesting parallel between your results and those of Dr Gaster on a tapered cylinder in a uniform stream. How close is that parallel?

D.J.Maull. (a) The velocity profile remained constant down the tunnel after about a distance of one half tunnel height past the gauze. There was no measurable pressure gradient across the tunnel.

(b) Dr Gaster's results are very similar to mine obtaining the same type of vortex pattern.

J.C.R.Hunt. 1. Has Dr Maull measured cross-correlations with time lag to give his interpretation of the vortex mechanism on a more quantitative basis?

2. What are Dr Maull's views on uniform shear flows past finite length cylinders and cylinders which are allowed to oscillate?

D.J.Maull. 1. No

2. The finite length cylinder will be even more complicated and it is planned that we will investigate this. If the cylinder oscillates it is probable that if the oscillation frequency is near the vortex shedding frequency then the vortices may well correlate over a portion of the span.

S.M.Bogdonoff. I believe that the model spanned the stream from the wall to the free surface. Since the end effects will be important and different at each end, might you comment on these end effects and whether you believe your results are applicable to a two-dimensional body?

D.J.Maull. The model certainly spanned the wind tunnel and end effects may well be important and as has been shown by Gaster.

H.Quadflieg. Did you vary the Reynolds Number and did this show forms of branching of the smoke lines.

D.J.Maull. No. I.e. Re number has not been changed.

DISCUSSION OF PAPER 17

"ETUDE D'UNE SOUFFLERIE POUR RECHERCHES SUR LES ECHANGES D'ENERGIE ATMOSPHERE-OCEANS"

by M.Coantic, France

R.Legendre. Quel est le rôle des embruns dans le mécanisme des échanges de chaleur et de masse et quelles conditions de similitude faut-il respecter notamment en ce qui concerne la capillarité pour étudier ce rôle?

M.Coantic. Les embruns jouent certainement un rôle très importants dans les transferts lorsque la vitesse du vent est grande. Nos essais préliminaires ont montré leur apparition à partir de 12m/s environ. Il semble possible d'étudier leurs effets par les méthodes

mises au point au sujet des écoulements turbulents diphasiques. En ce qui concerne les vagues de surface proprement dites les essais prévus seront effectués dans le domaine des ondes de gravité.

DISCUSSION OF PAPER 18

"ON THE USE OF DIFFUSION DETECTOR GASES IN THE STUDY OF ATMOSPHERIC SHEAR LAYERS WITH ADVERSE PRESSURE GRADIENTS"

by J. de Krasinski, Canada

Errata

Equation 4-11 on Page 18-3, instead of:

$$\left(\frac{\partial^2 \bar{u}}{\partial \eta^2}\right)_0 = \frac{u_1 \delta^2}{\mu_0} \rho_1 \rho_0 \text{ (etc.)}$$

should be:

$$\left(\frac{\partial^2 \bar{u}}{\partial \eta^2}\right)_0 = \left(\frac{u_1}{\mu_0}\right)^2 \delta^2 \rho_1 \rho_0 \text{ (etc.)}$$

Discussion

P.A.Libby. The author has identified the boundary layer at point "0" with the Blasius solution. It is true that $u = v = 0$ at "0" and that $u = 0$ all along the line through 0 but $v \neq \infty$ upstream of 0 so that the Blasius profile cannot really apply then.

J. de Krasinski. One cannot speak in this context of exact similarity but rather a quasi-similarity. At outer boundary layer the concentration profile has the usual requirements.

DISCUSSION OF PAPER 19

"A REVIEW OF THE VERTICAL TRANSFER OF MOMENTUM THROUGH THE BOUNDARY LAYER"

by F.B.Smith, UK

R.S.Scorer. Dr Smith bases much of his argument on his extension of the equation

$$l = -k \frac{\partial u}{\partial z} \Big/ \frac{\partial^2 u}{\partial z^2} \qquad (1)$$

. for which he says the justification is that it leads to the observed logarithmic pro-
ile. But there is nothing unique about this because the same can be said about the
elation

$$l = kz \tag{2}$$

). which Prandtl justified on the grounds that the mixing length could be expected to be proportional to the length characteristic of a point, namely distance from the boundary. The physical argument for (1) seems to have been concocted to justify it as a "local version" of (2) i.e. one which depends only on local conditions and I wonder if Dr Smith would give his justification for it; noting that if $l \propto (\partial^2 u/\partial z^2)^{-1}$ enters the argument what about

$$l = -\tfrac{1}{2} k \frac{\partial^2 u}{\partial z^2} \Big/ \frac{\partial^3 u}{\partial z^3} \tag{3}$$

and so on (this is not a suggestion)? In any case all these relationships must depend on a similarity of the features at all heights, in which case, if the result to be obtained by a generalization of (1) or (2) does not possess the same kind of similarity, the transfer properties must be strictly local, and a physical argument must be given for this too.

F.B.Smith. Although Prof. Scorer's Equations (1) and (2) are mathematically equivalent in the surface layer, it is possible to think of them expressing two distinct physical relations. Prandtl has explained (2) in saying that the nearby presence of the ground-boundary impresses itself strongly on the size of the eddies and leads one to expect $l \propto z$. Equation (1) expresses, to me at least, the notion that the turbulent length-scale impresses itself on the curvature of the wind-profile, until an equilibrium is established between them. Thus, for example; where the eddies are predominantly small, the dynamical linking between different layers of the air is week and strong curvatures are permissible.

The introduction of higher derivatives, such as in Scorer's Equation (3), cannot of course be entirely ruled out, and this emphasizes the questions of uniqueness that must arise in this sort of modelling. One may only prefer (1) to (3) on the grounds that (3) is more likely to involve derivatives of (1) as well as (1) itself.

H.Lettau. Possibly, part of the difficulties encountered by Dr Smith may be caused by his assumption that l can be expressed by Kármán constant (k) and wind shear and curvature. I have found (see Equation (38) of my paper No. 7) that an expression similar to Dr Smith's is valid only as a limiting case in the approach to the boundary,

$$k^2 = \lim_{z \to 0} [u^{*2} (\bar{u}_{33})^2 / (\bar{u}_3)^4]$$

while in the surface layer only $u^* = l\bar{u}_z$.

If the expression is used with $k = \text{const.}$, throughout the Ekman layer then l is overestimated and convergence to geostrophic wind becomes too slow.

F.B.Smith. The physical dimensional arguments suggest that l, or the diffusivity k may be expressed in terms of the curvature of the wind profile, i.e. $l = A \dfrac{|\text{shear}|}{|\text{grad(shear)}|}$, where A is constant of proportionality, assumed independent of height z. Only when we equate this expression with von Kármán's relationship in the limit as $z \to 0$ do we find that $A = k$. Thus von Kármán's constant does not enter into the expression *a priori*, but only as a result of the known behaviour near $z = 0$.

In this sense I do not think my approach is inconsistent with Prof. Lettau's comment. However, it is true that before any modification to the finite difference form of Equation (13) is made, the values of l are too large but after the constant modification, the magnitudes of l seem much more reasonable and attain a nearly constant value at large z.

DISCUSSION OF PAPER 20

"THE ORIENTATION OF VORTICES DUE TO INSTABILITY OF THE EKMAN - BOUNDARY LAYER"

by F. Wippermann, Germany

R.S.Scorer. Prof. Wippermann's theory is evidently applicable to his laboratory experiments but I question the application of geophysical phenomena. In the case of dunes we have a time scale far exceeding the day, and mechanisms tending to build up dunes in arbitrary winds would seem more likely to operate. Possibly it is anabatic winds, which are probably quite strong on some days with dunes of the size mentioned. Also similar arrangements of sand occur on beaches and these are certainly not produced by Coriolis forces.

Cloud streets have a time scale of an hour or less and it is not credible that their form is due to Coriolis forces. For example in Figure 1 of Prof. Wippermann's paper the streets are forming in a wind along the streets from the sea after the air has been over the land for only a few minutes. They do not form at night and are clearly a buoyancy dominated phenomenon. The theory is questionable because it contains a uniform constant viscosity which is not applicable to the atmosphere. The circulation time for a particle is also of the order of an hour or less.

Over the sea in bursts of polar air particularly, there is a strong thermal wind and this dominates the wind profile right down to the sea and we do not have an Ekman profile; indeed sometimes the flow near the surface is outwards across the isobars towards high pressure, and in such cold air masses the buoyancy term in g is almost certainly dominant over the Coriolis term in f in the basic equations (e.g. (1-c)).

If the motions were Coriolis rather than buoyancy dominated the cloud would not appear as lines but as layers that means that cloud would exist above the downcurrents just as much as above the upcurrents. Any mechanism breaking up such a layer must necessarily be buoyancy dominated and it is not really practical to say that the motion below is Coriolis dominated because the occurrence of the streets is very dependent upon the time of day over land.

Prof. Wippermann has a beautiful theory but I am quite unconvinced that it is as universal as he suggests.

F. Wippermann. As shown in Equation (4-a) of the pre-print version both effects, the coriolis forces and the buoyancy, act in destabilising the basic flow (the beginning of Section VII is not expressed correctly and may lead to a misunderstanding). I agree with Prof. Scorer's opinion that in many cases the buoyancy dominates.

I do not see how the anabatic winds suggested by Prof. Scorer could cause such an impressive regularity of seif dunes as shown for example in Figure 2. The anabatic winds

would probably produce a very irregular field of dunes corresponding to cloud pattern caused by convection of the type of Benard cells.

However, as I stressed in the oral presentation, I think that such anabatic winds on seif dunes in the very first stage will determine the orientation, the wavelength and the phase angle of disturbances. This allows the destabilised Ekman flow to change its direction from case to case. In this respect the buoyancy plays an important role in the formation of seif dunes too.

I admit that for the formation of cloud streets in most cases buoyancy may dominate the Coriolis forces. However for cloud streets observed over the ocean in the subtropics this seems to be not true. To Prof. Scorer's last point: when vortex rolls have been built up due to Ekman layer instability (without buoyancy), the helical motion in these rolls will cause cloud streets as shown in schematic Figure 3 assuming enough moisture is available. It is difficult for me to see how in this case a cloud layer could be formed.

H. Lettau. I would like to comment on the dune problem. Desert sand is a particular medium. It is capable of moving, and the wind can pile it up but only when a threshold value of friction velocity is exceeded (about 25cm/sec, according to our experience in the Peruvian desert). Furthermore, after an initial pile-up has occurred, there will be a feedback on the wind structure. No corresponding factors apply to Ekman instability. For Barchan dunes the separation of flow at the crest-line and the resulting vortex, according to our experience, is highly significant.

F. Wippermann. The feedback mentioned by Prof. Lettau is certainly important for moving dunes of smaller size, for instance such as Barchan dunes. I agree that for these the vortex rolls due to Ekman layer instability are not relevant. However, for seif-dunes, which extend sometimes for 100 - 200 km, the vortex rolls due to Ekman layer instability provide the surface winds as needed for the formation of the dunes. It is of course true that a critical velocity must be exceeded which allows for saltation.

A. D. Young. Could we please have some idea of the magnitudes of the quantities involved in these vortex streets, for example what is the range of height in which they are found and what are the magnitudes of the lateral vortices to be expected in them?

F. Wippermann. I'm not able at the present to give you exact figures. In referring to the numerical study by Faller and Kaylor (1965) the helical motion decreases to zero at a level of about 2 to 3 times the height of the Ekman layer, i.e. roughly at about 2 to 3 km. The vertical velocity as well as the lateral velocity is in the order of few meters per sec.

F. H. Schmidt. I cannot judge Prof. Wippermann's theory at this moment. I would like to make a remark, however, with respect to Prof. Scorer's opinion that upslope motions along dunes are responsible for the origin of these dunes. These upslope winds occur only during daytime. During night-time downward motions are present.

R. S. Scorer. I think that anabatic winds would be much stronger and more turbulent, and therefore much more likely to transport sand, than katabatic winds. But I was only speculating off the cuff about dunes and remarking that there are many other possible, and probably more potent, mechanisms than the mechanism described by Prof. Wippermann. Prof. Lettau knows much more about dunes.

In answer to Prof. Young's question it can readily be said that cloud streets typically have a cloud base and top of 3000 ft and 4000-5000 ft above the ground, with the streets a mile or two apart.

The updrafts under the streets are quite adequate for gliders to soar easily and are typically 2-5 metres per sec, while the downdrafts are wider and feebler and of the order of ½-2 metres per sec. The transverse component would be about the same magnitude.

DISCUSSION OF PAPER 21

"DIFFUSION IN THE ATMOSPHERIC SURFACE LAYER: COMPARISON OF SIMILARITY THEORY WITH OBSERVATIONS"

by W.Klug, Germany

A.D.Young. I am not clear what has happened in the analysis to the diffusion coefficient of the source. Is it implicitly included in the empirical functions that you have used?

W.Klug. The diffusion coefficient of the source material is not taken into account, because it is assumed that the diffusing material follows the air movements.

T.V.Lawson. Could I ask a very naive question? The surface layer is considered to be 50 m thick. To what height of puff does the analysis presented apply?

As a supplementary question could I ask: If the source is elevated, for what distance from the source does the analysis apply?

W.Klug. The model applies only to surface or near surface sources. Here it is estimated to be valid up to distances from the source in the order of 1 km. For the case of an elevated source I cannot give you an estimation.

J.E.Cermak. In the atmospheric surface layer $\partial w/u_*$ correlates well with z/L ; however, $\partial v/u_*$ and $\partial u/u_*$ from both field and laboratory measurements do not correlate well with z/L . Do you have a physical explanation for this?

W.Klug. A possible explanation of the facts mentioned is that the longitudinal and lateral components of turbulence are also influenced by mesoscale parameters, such as terrain effects.

F.B.Smith. The concentration for a continuous source is obtained in Equation (11) by integrating the concentration for a puff (Equation (10)) with respect to time. This ignores the motion of the puff in time due to the action of the larger eddies. For a ground-based source the vertical motions of the puff may be small and therefore justifiably neglected but the lateral motions will not be small and allowance should be made. The same will be true of the vertical motions for an elevated source.

W. Klug. As was explained in the last section of the paper it was assumed in setting up Equation (2) that if any parameters (such as describing the action of larger eddies) may be left out in this relationship then these parameters depend uniquely on the variables listed. However, the conclusion reached is that the lateral motion does not depend on the mentioned variables and allowance for this was made through the use of the empirical relationship $g(\sigma v/u_*)$.

DISCUSSION OF PAPER 22

"SOME MEASUREMENTS OF INSTABILITIES AND TURBULENCE IN EKMAN BOUNDARY LAYERS"

by D.R. Caldwell, USA

N. Isyumov. I wonder if Prof. Caldwell would like to comment on the application of his experimental results and the general phenomenon of Ekman boundary layer instability to the lower layer of the atmosphere. Could this be a source of energy for atmospheric turbulence at low wave numbers?

R.S. Scorer. Buoyancy and mechanically produced eddies are far too dominant in the lowest 1000 ft for Coriolis dominated oscillations or instabilities to be observable. Even mountain lee waves with wavelengths of a few miles show no observable Coriolis effect, and one has to come to wavelengths of the order of 100 miles before Coriolis forces are important. It is quite a different matter in the ocean where inertial oscillations of a period of a pendulum day are sometimes the dominant feature of the motion.

N. Isyumov. Could Prof. Scorer suggest a mechanism or source for low frequency scale variations of atmospheric turbulence other than mechanical or thermal? Large variations in the scale of longitudinal turbulence have been observed which cannot entirely be explained by variations in mechanical surface roughness and it has been suggested that Ekman boundary layer instability may be a possible explanation.

H. Lettau. You mentioned conclusions based on the assumption of a "constant-stress boundary layer". I am wondering about the necessity of making this assumption, since the vertical change of the vector of shearing stress could be obtained by a height-integration of the geostrophic departure, if the equation of motion is considered, and measured distributions of the two velocity components are available.

C.W. van Atta. As Prof. Lettau has indicated we could estimate the stress distribution using the geostrophic departure integral method. We have not yet done this. Direct measurements of the components of the Reynolds stress would be even more desirable.

DISCUSSION OF PAPER 23

"A REVIEW OF INDUSTRIAL PROBLEMS RELATED TO ATMOSPHERIC SHEAR FLOWS"

by C. Scruton, UK

R.S. Scorer. Mr Scruton ends by saying that "the meteorologist must provide more information..." This is clear because all his formulae contain V , the wind speed. and he has told us nothing about it. But I feel bound to remark that the wind varies more from day to day than any of the other factors in his formulae. The meteorologist spends his time forecasting for tomorrow, but not for a week ahead, and collecting climatological information about the extremely variable events of the past, and the questions posed to him must be posed in this context. To emphasize that the actual weather is a sequence of events that vary enormously may I briefly mention the "Sheffield incident" when a great many roofs were blown off in one restricted section of the city one night. Evidently what happened was that the natural wavelength of standing waves in the airstream happened to be matched to the spacing of three hill ranges upwind of the city in such a way that the lee waves were of exceptionally large amplitude, and beneath the first wave trough there was a very strong and probably relatively smooth wind for an hour or two. The Professor of Geography woke to find the roof tiles arranged neatly on edge embedded in the grass lawn by the house! This incident was the kind of event which occurs once in a few decades, perhaps, but it cannot be ignored.

In Sutton's diffusion formula there are three coefficients whose values cannot be known with any precision because they vary so much from day to day, and from place to place. The apparent usefulness of the formula is destroyed by the fact that it does not really apply when there are major disturbances present such as those due to buildings, trees, and topographical features. But more important is the fact that it is not even valid for small wind speeds which are the cause of the majority of situations in which pollution reaches serious concentrations. (I would refer anyone who is not convinced of this to the pictures in my book "Air Pollution"). Consequently the problem of high pollution levels has to be approached in a different way.

In turbulent airstreams the size of the largest eddies in relation to building size can be of major importance in determining the pollution levels achieved in wakes where there is some recirculation. The levels are highest where recirculation continues for a long time before eddies are shed, if the source is within the wake or at an appropriate position on the building. Probably the typical eddy size in the kind of turbulent airstream usually studied is not large enough for this purpose, though it may be adequate for wind load purposes and it might be a good idea to have a few people walking about in the wind tunnel upstream of the model when air pollution studies are made (See "Air Pollution" page 118, para. 9).

Wind tunnels are quite inadequate for studies of the effects of topographical features because of the great nocturnal stratification of the air and these phenomena are best studied on the site of interest - and why not?

I think we need much more liaison between engineers and meteorologists with special or local knowledge, if these problems are to be satisfactorily handled.

C. Scruton. It appears that Prof. Scorer did not find the paper sufficiently specific in its definitions of the wind speed. For structural design purposes the paper defines the design wind speeds as "the maximum wind speeds averaged over a specified period of time which are considered likely to occur at the site". This implies that observations of wind speed over a sufficient number of years are required to enable statistical estimates of the probability that wind speeds of certain strength (averaged over specified durations) will be equally or exceeded in a specific period of years. In this respect the meteo-

rologist is asked to forecast probabilities, not for tomorrow but perhaps for hundred of years hence, and his forecast will become more accurate as the amount of tatistical data available to him, and the length of the period over which it is taken, are increased. Prof. Scorer implies that the winds involved in the "Sheffield incident" could not have been predicted, but at the same time he attempts a probability forecast by saying that it is the kind of event which occurs once only in a few decades. If observations of the Sheffield wind over very many decades had been available, it is to be expected that the probability of the wind involved in the incident he so graphically described would have been accurately forecast.

With regard to Prof. Scorer's remarks on the use of Sutton's diffusion formulae it was emphasized in the paper that these analytical methods could be expected to apply only for diffusion over flat open ground, and that where the plume is close to buildings, or in a valley or close to an escarpment, the local airflow will dominate the dispersal of the plume. For rough topographies, and particularly where pollution of buildings and areas close to the point of emission is of concern, the paper recommends wind-tunnel tests carried out under proper similarity conditions. Estimates of local pollution, where the air turbulence near the point of emission remains mostly of mechanical origin, are quite effectively based on wind-tunnel experiments, and for most such cases sufficiently reliable indication is given without reproducing the temperature stratification. More precise estimates are, of course, made in wind-tunnels where temperature stratification can be achieved, and this is particularly so where pollution estimates over wide areas remote from the source are required. While agreeing wholeheartedly with Prof. Scorer on the desirability of more liaison between meteorologists and engineers it is difficult to see how pollution *predictions* can necessarily be obtained by studying the phenomena at the site of interest when the buildings etc., which so seriously disturb the local airflow are not present at the site until the site development is complete!

REFERENCE

Scorer, R.S. *Air Pollution*, Pergamon Press, 1968.

DISCUSSION OF PAPER 24

"FLUCTUATING FORCES ON BLUFF BODIES IN TURBULENT FLOW"

by P.W.Bearman, UK

J.C.R.Hunt. 1. As perpetrator of some of the ideas Dr Bearman has just mentioned, I thought I might say that, with my colleagues at the Central Electricity Research Laboratories, we are studying theoretically and experimentally the turbulent flow round circular cylinders. We believe that we should aim to understand the flow before we can make much progress in calculating fluctuating pressures; if anyone here would like to find out more about our work, I would be glad to describe it to them.

2. I thought it might be worth pointing out that Mr Scruton and Mr Bearman have been concentrating on bodies which are laterally symmetric to the oncoming flow.

It would appear then that the fluctuating drag is mainly a function of the fluctuating velocity parallel to the mean flow. However, if the body is not symmetric, for example a square or rectangular block offset to the wind, then the lateral turbulent velocity will contribute as much or more fluctuating drag and lift as the line velocity component. Given the rate of change of drag and lift with orientation of a building to the wind, it is possible to obtain an estimate for the effects of these lateral components.

3. I would like to take up the comment Prof. Scorer made in the previous discussion. He stated that wind tunnel testers ought to be more concerned about the large scale wind fluctuations brought about by showers, etc. Although such phenomena are important there is no need to simulate them in the laboratory (at least for wind loading problems) because they are large scale and of low frequency. In that case it is possible to work out the loads on the building, provided we have the meteorological data. The reason for wind tunnel tests is to simulate the atmospheric turbulence at scales of the order of the body size, because at these scales the flows round the body and the pressure are most sensitive to the incident turbulence and are least understood.

P.W.Bearman. No reply.

T.V.Lawson. I would like to question the use of the principle of "Aerodynamic Admittance" especially when considering the flow around buildings which have a length in the downwind direction. The building can add to the structure what was not originally present and the term admittance is deceptive. Are we not watching Hamlet without the Prince?

P.W.Bearman. Our aim is to understand the physics of the flow in order that we can make meaningful investigations into more complicated situations. This experiment has been made as simple as possible in order to understand some of the parameters involved. It appears from the work of Davenport et al., however, that the "aero amic admittance" approach is a useful one and worth following further. It seems useful to first examine that part of the fluctuating force spectrum that results from a direct forcing by the approaching flow. When we understand this we can progress to try and understand the more complicated effects produced by the building itself.

DISCUSSION OF PAPER 25

"WIND EXCITED BEHAVIOUR OF CYLINDRICAL STRUCTURES - ITS RELEVANCE TO AEROSPACE DESIGN"

by D.J.Johns, UK

D.J.Maull. 1. Is it correct to relate the ovalling vortex shedding when you have a short aspect ratio cylinder which is open at the top and subject to large tip effects?

2. Does the Helmholtz resonance of the cylinder enter into the problem?

D.J.Johns. "Ovalling" has been noticed primarily on shells of large length to radius ratio for which the lowest structure frequency corresponds to $n = 2$ to 4. However, it is

recognized that aerodynamic tip effects do occur, e,g. there is some evidence that the local Strouhal frequency is less near to the tip of a solid cylinder due to a thickening of the wake, as mentioned in my paper. Clearly one must also anticipate some aerodynamic effects due to the open nature of the hollow shell as compared to a solid cylinder. The correlation of observed swaying oscillations with predictions is based on criteria for vortex shedding phenomena for chimney structures, so it has been assumed that the observed "ovalling" phenomena also are due to vortex shedding, particularly as similar criteria seem to apply.

Dr Maull's questions can only be definitely answered when data are obtained on the unsteady pressure distributions near to the tip of a rigid and ovalling shell. However, I do believe that vortex shedding is the explanation for the ovalling instability and not Helmholtz resonance.

J.C.R.Hunt. Firstly Dr Johns is presumably not implying that the collapse of the stubby oil tanks is attributable to vortex shedding? Secondly I was interested in his observations that the shells were oscillating in various modes before collapse. At the Central Electricity Research Laboratory we have been investigating such higher modes in aeroelastic models of cooling tower shells. We find that relative amplitude of the higher modes is dependent on the spectrum of the incident turbulence. Therefore to bring us back to the subject of atmospheric shear flows, if the modes of oscillation of shell like structures (cooling towers, oil tanks, or rockets) are to be simulated in the laboratory the correct simulation of the atmospheric shear flow is required.

D.J.Johns. In showing photographs of the collapsed oil tanks as "obvious" examples of a static instability (and I did not discuss these at all in the written paper) I was wishing to indicate that prior to the static collapse quite significant dynamic motions were evident. There was no intention to suggest that the collapse was due to vortex shedding but rather that when these dynamic motions were analysed the results showed that resonances existed at the lowest four or five natural frequencies (corresponding to typical values of n in the range 5 to 9). It was particularly satisfying that our structure theory to predict these natural frequencies agreed very well with those measured values and gave confidence in the reliability of the theory.

Regarding Dr Hunt's second point I fully agree that simulation of a full-scale situation must include the factors he has mentioned. However, in our present work we are concerned with obtaining agreement between theory and a particular measured experimental situation which does not include simulated shear or turbulence. If and when our theory appears reliable we will then attempt to apply it to special full-scale situations.

DISCUSSION OF PAPER 26

"STATISTICAL ANALYSIS OF GUST VELOCITIES FOR SPACE LAUNCHERS DESIGN"

by F. Bevilacqua, Italy

Errata

Page	*Line*			
1	15	Siasenwine	instead of	Sissiwine
2	9	the latter	instead of	later

Page	*Line*			
2	27	$\beta_0 = 1-\Sigma_1 B_i$	instead of	$P_0 = 1-\Sigma_1 P_1$
2	37	dimensional	instead of	dimensinal
3	1	Watson	instead of	Waston
3	Eq. (7)	$P_L(V_\epsilon) = \int_L G(V_\epsilon z)dL$	instead of	$P_L(V_g) = \int_L G = (V_g z)dL$
3	Eq. (8)	non storm	instead of	storm
3	Eq. (9)	storm	instead of	non storm
4	Eq. (10)	$\bar{G}_*(Ude) = \ldots$	instead of	$\bar{G}(Ude) = \ldots$
4	23	f_1	instead of	f
4	31	ψ_1	instead of	ψ
5	10	corresponds	instead of	correspond
6	13	sufficiently	instead of	sufficently

Discussion

G.H.Fichtl. The Marshall Space Flight Center at Huntsville, Alabama, have been concerned with the problem of gust velocity criteria for space vehicles for the last six years. Our criteria of a 9m/sec gust agree exactly with your criteria. However, our criteria were derived from vertical detailed wind profiles, data which are entirely different from those of Steiner and which were used in your paper.

Our wind profiles (1700) were obtained at the Kennedy Space Center, Florida, with the jimsphere wind sensor which is capable of detecting wind fluctuations with vertical wave lengths as small as 15 m. I contend that it is the fluctuations on these wind profiles which excite space vehicles. Steiner's criteria or model are only valid for horizontally flying vehicles and his criteria were derived from clear air and storm turbulence data.

F.Bevilacqua. From a practical point of view of missile design we are very pleased to learn that at the Marshall Space Flight Center a gust velocity of 9 m/sec was adopted after a very wide wind profile investigation with the jimsphere and with advanced methods of analysis.

In absence of more adequate data on the gust frequency distributions we had adopted the classical PRESS and STEINER frequency distribution data valid for horizontal flight vehicles and, on the basis of the method outlined in our paper, we have obtained information on the bi-dimensional frequency distribution of our concern assuming the mean isotropic distribution of the atmospheric turbulence.

From your remark we understand that the isotropicity condition is considered unreliable on the basis of the recent wind profiles and statistical analyses obtained by NASA.

We would therefore be extremely interested to study the NASA reports leading to the adoption of the same gust design velocity obtained in our study.

DISCUSSION OF PAPER 27

"AERODYNAMIQUE DES PAROIS PERFOREES: APPLICATION AU PROJET D'ECRANS DE PROTECTION CONTRE LE VENT; ETUDE DU FONCTIONNEMENT DE CES ECRANS"

by J.Valensi, France

Errata

Page	*Para.*	*Line*			
1	2	17	5×10^5	instead of	plusieurs milliers
2	2.2	18	ν	instead of	V
3	2.2	5	0,63	instead of	0,67
3	2.3	25	v_0	instead of	h in the equation
			i	instead of	l in the equation
3	2.3	29	v_0	instead of	h

Discussion

J. de Krasinski. What are the views of the author concerning the rather different behaviour of a three-dimensional porous body in free airstream? The case I am referring to is the drag of a porous sphere of variable density which I once tested in a low speed wind tunnel. The results quoted were independent of Reynolds number variations within the range $R_D = 0.8 \times 10^5$ to 2.2×10^5. A wire basket in the shape of a sphere was constructed and could be filled with continuous thin turnings obtained on a lathe out of high grade steel. Due to elasticity these turnings filled the basket uniformly even at higher wind speeds. Their width varied from about 0.5 mm to about 3 mm and did not affect the drag either. The relative density of the sphere was expressed as a parameter.

$$\alpha = \frac{\text{weight of the porous sphere}}{\text{weight of a solid sphere of the same material}}$$

The parameter $1-\alpha$ was to some extent a measure of the porosity.

The coefficient C_D was defined as

$$C_D = \frac{\text{Drag}}{\frac{1}{2}\rho u^2 \pi R^2}$$

R = radius of the sphere.

The results of the measurements on the porous sphere showed two interesting points might be noted: (a) The maximum drag occurred at an extremely low value of α ($\alpha = 0.015$), which I call the critical density; (b) The drag coefficient $C_D = 1.2$ was higher than the corresponding drag of a disc ($C_D = 1.0$).

It is also obvious that for $\alpha = 0$, $C_D = 0$ and for $\alpha = 1$, C_D will be that of a sphere at the corresponding Reynolds number and surface roughness ($C_D = 0.6$). These results are very much different than for the two dimensional case.

I would be interested to hear some comments of Prof. Valensi.

J.Valensi. The case raised by Prof. de Krasinski is most interesting. Unfortunately, it is difficult for me to answer straight away to h.. question as the theory and the experi-

ments of which I have given a. account are valid only for two-dimensional flow.

One can think that the wake of a very porous sphere has a section much larger than the section of the wake of a plane sphere; this could explain a large loss of momentum in the wake corresponding to the larger drag. I will ask one of my students to make some experiments to find out the configuration of the wake of a very porous sphere and will let Prof. de Krasinski have the results of these investigations.

P.W.Bearman. The author may be interested in a paper presented at AGARD Specialists' Meeting on "Separated Flows" (C.P.4) showing effect of lose bleed on the wake behind a bluff body. The flow patterns are similar to those presented here and there was also found to be an increase in Strouhal number with bleed rate. The drag on the body was reduced with increasing bleed rate and this was mainly due to a stabilization of the vortex street and a reduction of vortex street drag. Could this effect of reduced vortex drag contribution be important in determining the drag of perforated plates?

J.Valensi. The comments of Dr Bearman are most interesting as they bring up a confirmation to the results concerning the influence of the porosity on the frequency of the shedding vortices, which I have obtained more than fifteen years ago.

The effect on the drag of the frequency of the shedding vortices and, consequently, on the scale of these vortices, is shown up in my experiments by the expression of the drag: $C_x = 2(1 - \sigma^2)$.

It is important to mention again that the Benard-Kármán Vortex Street is observed in the wake of a porous plate only for σ between 0 and 0.63.

APPENDIX B

R O U N D T A B L E D I S C U S S I O N

concluding the

AGARD Fluid Dynamics Panel

Specialists' Meeting

on

"The Aerodynamics of Atmospheric Shear Flows"

Munich 15-17 September 1969

Board:	Affiliation:
Prof. B.W. Marschner	Colorado State University, U.S.A.
Mr. C. Moruto	Dept. of Eng. Science, Univ. of Oxford, U.K.
Prof. R.S. Scorer	Imperial College, London S.W. 7, U.K.
Prof. J.E. Cermak	College of Engineering, Colorado State Univ., USA
Prof. H.A. Panofsky	Pennsylvania State Univ., U.S.A.

Transcribed and edited

by

R. Friedrich

Institut für Strömungsmechanik

der Technischen Hochschule München

Prof. Mayschner: Ladies and gentlemen, I have the pleasure to open our round table discussion. The format will be relatively simple. I'll ask the members at the table to make some summarizing remarks, some perhaps provocative, some exploratory and then merely moderate the discussion between the panel and the audience and within the panel. The only thing I ask is to use your button and identify yourselves for the proceedings. The panel needs no introduction since have all been on the program. I'll call first upon Prof. Panofsky to open the discussion.

Prof. Panofsky: It is a little difficult to start something like this after three days of sitting down and enjoying oneself. Summarizing the whole meeting in five minutes is not easy. I am not very good at saying anything provocative, I am going to leave that to my neighbor on the right (Prof. Scorer). I am going to make however some random remarks, seeing this kind of a conference from the meteorologist's point of view. The name of the conference implies some problems of atmospheric shear layers and there are large amounts of shear everywhere in the atmosphere. So, really we could have talked about all of dynamic meteorology. This is too large a subject and actually the conference was a little more limited. I suppose almost all our papers dealt with layers where the shear was unusually large, so large in fact that turbulence either occured or at least could be expected; either we were dealing with the shear layer close to the ground or some elevated shear layer. Now, elevated shear layers are important in connection with clear air turbulence, but I don't want to talk about it now, it may come up during later discussions. What I would like to do is summarize some aspects of what goes on in the lowest part of the atmosphere and mainly, what are some of the practical problems which the meteorologist is asked to solve. I think that among such problems, where the meteorologist can be useful is first of all providing information which can be applied to structures. This aspect of meteorology was mostly emphasized in this conference, particularly the effect of winds on buildings, towers, standing structures and also on moving structures such as airplanes. Now in the case of standing structures, the problems are relatively simple for the meteorologists because one is normally only interested in situations of fast winds, so that one really does not have to be concerned too much about hydrostatic stability (the Richardson number being approximately zero). I think that, for such applications we have the greatest difficulty in trying to prescribe horizontal resolution whatever is needed to be known. The kind of thing one needs to know is the velocity-spectra and the wind. We have seen that here the velocity-spectra are different everywhere and people can get pretty good pictures of what the wind-speed-spectra are at one place; but they are completely different somewhere else as far as low frequencies are concerned. High frequencies on the other hand we can specify very well. As far as mean speed is concerned we have a similar problem; wherever we need it we don't have it. Very often the wind speeds are given at airports and we want to have the wind in the middle of the city. In all applications are involving information near the ground, we have the problem that there are large variations horizontally and we cannot get observations everywhere.

The second kind of applications to structures has to do with airplanes. Occasionally airplanes also fly near the ground. Most of them have to land sometimes and there again we have some meteorological problems. In that case again we need different kinds of meteorological information which we understand fairly well because in that case we deal mostly with vertical velocities which are somewhat more difficult to measure than horizontal velocities but which are more easily understood. Again we are having problems because the horizontal variations of terrain and their effects are quite complex.

The next important application of meteorological information that has been mentioned is the question of the effect of meteorological parameters on air pollution and dispersion. This has just come up only briefly and I don't want to say much about it. I would like to contradict one of the

like to contradict one of the other speakers in the way in which this is mostly now being handled. For a long time most of the work was based on formulae by Sutton. However there have been quite a few studies lately and, e.g. in the U.S.A. quite different techniques are now being used and I would like just to suggest that there is a quite good summary on the subject called "Meteorology and Atomic Energy 1968". Also Dr. Pasquill is about to revise his book on "Atmospheric Diffusion". There are still some particular problems in atmospheric dispersion and I cannot summarize them all here. I think one of the mayor ones is that we do have to take into account variations of stability of the atmosphere. Nighttime conditions with clear sky and light winds present perhaps the worst difficulties in trying to estimate dispersion of contaminants.

Other applications of low-level information which have not come up very much during this meeting have to do with the vertical flow of momentum, heat, moisture and other quantities through the lower atmosphere, and their relation to large-scale meteorological parameters. These are important in agricultural meteorology but most particularly in trying to improve the system of mathematically forecasting the behavior of the large-scale weather. There is a lot of work going on in this area at the moment and millions are being spent on trying to just estimate how these fluxes are being produced. Here again one of the mayor problems is the lack of spatial homogeneity; scientists tend to make point measurements, but what is needed is average measurements over large horizontal areas and this one topic seems to be one of our mayor problems throughout. Finally, just to complete this, I mention one more application which we have been discussing at Stockholm about three months ago and that is the question of propagation of waves. Propagation of waves is very much affected by the turbulence in the lower atmosphere, such as radar waves, sound waves, optical waves. Here again we are very much concerned with not just the wind distribution but in this case the effects of vertical stratification. But, if I want to summarize, one of the main problems in most applications is the lack of horizontal homogeneity near the ground and we cannot be everywhere at the same time.

Prof. Cermak: I wish to break my comments up into essentially three main categories. The first one is the aeronautical application of knowledge on atmospheric shear flows, the second is some of the problems associated with atmospheric shear flows in the area of basic fluid mechanics or aerodynamics and the third is a few comments on the expectation of solving some of the problems we are faced with by the use of wind tunnels. I would like to state, at least in my opinion, that an understanding of atmospheric shear flows is really an essential part of the education of an aeronautical engineer if he is going to be properly prepared to solve some of the problems he will be faced with in the design of aircraft on almost any scale of aircraft you might think of. The reason for this is that we are now confronted with basic problems associated with take-off and landing -- particularly with the problems of take-off and landing of VSTOL aircraft that are being designed and tested. We also have to bring the supersonic transports back down to earth and, as I understand it, the stability associated with the low-speed flight of these aircraft, especially under perturbed conditions of the atmospheric surface layer, is a problem at this point in time. Accordingly, stability analysis and the actual structural design of aircraft require information on atmospheric shear flows. We also have the problem associated with city-planning, of locating landing facilities in cities for VSTOL aircraft, and especially helicopters, where we must deal with the local environment produced by wind blowing over buildings. Perhaps we will have to design wind screens or some kind of shelter to protect the local landing sites.

We have another problem which is of considerable practical importance, especially as aircraft get larger. This is the prediction of dispersion rates for intense vortices shed

by aircraft at landing and take-off sites. The movement of these vortices by the ground-level winds and the dispersion of these ground-level turbulence need further study. Another problem that is rather serious is that of proper design of automatic landing systems. We know that turbulence, the turbulent fluctuations of refractive index near the surface of the earth, strongly affects the transmission of electromagnetic energy and can result in misjudgement of the height of incoming aircraft. Another problem is the dispersal of fog and smog near runways and the associated problem of visibility for pilots when landing. This can be quite a serious difficulty especially for the small private aircraft when they are descending and suddenly lose visibility because of a ground-based layer of smog. Then, of course, we have the problem of clear-air turbulence which is quite closely associated with the zones of intense shear in the atmosphere; primarily at elevations above the atmospheric surface layer.

Secondly, I would point out some of the basic problems in fluid mechanics we need to study if we are to reach a fundamental understanding of the phenomena we see in atmospheric shear flows. I believe that development of this subject is still in its infancy. Many workers have viewed the subject more or less from a deterministic point of view. However, flow phenomena in the atmospheric surface layer are better described from a probabilistic standpoint. Some re-thinking on how to describe turbulence in the boundary layer and the associated mean wind distributions from this point of view is needed. Along the same line we need to consider extreme value statistics of the wind fluctuations within the boundary layer and the atmospheric surface layer. Unfortunately, the commonly used energy spectra do not tell us what the probable extreme values will be.

Now going to more conventional types of problems we need to study the effect of time and space dependent boundary conditions. When working in the atmosphere we must face up to the fact that variable boundary conditions produce major deviations from the classical two-dimensional boundary layer. What is the rate of change of turbulent-boundary-layer characteristics when we introduce a perturbation? A few studies have been made but not enough. What are the turbulence characteristics introduced by crossflows or what are the turbulence characteristics associated with three-dimensional turbulent boundary layers? I mentioned on Tuesday that this is one of the areas where we have an abundance of ignorance concerning the basic physics. Another problem we need to study is the effect on turbulence characteristics for shear flows in rotation. Certain important aspects of this problem were pointed out by Dr. Caldwell. Laboratory facilities such as those used by Dr. Caldwell will enable signigicant studies to be undertaken. Another problem of importance is the effect of large-scale perturbations in the outer edge of the turbulent boundary layer. What is the effect of these perturbations on the actual structure of turbulence in the surface layer and what effects penetrate to the boundary? In the atmosphere we have large-scale turbulence at the outer edge of what we call the planetary boundary layer and the question that comes to mind is how are these disturbances propagated through the surface layer and how do they change turbulence in this particular layer. These are questions I believe to be important when trying to relate our classical boundary-layer theory with what we actually encounter in the atmosphere. Another problem I would like to point out is the effect and the behavior of turbulence in stagnation zones. This is particularly important for stability analysis of low-speed aircraft and VSTOL-aircraft. The "skin" loading of large structures by turbulent winds such as Dr. Bearman discussed this morning is also an important problem. These are a few of the fundamental problems which are in need of more intensive study.

Finally, I wish to comment on the applications of the wind-tunnels to help to solve these problems. I must point out two basic difficulties in modeling the atmospheric shear layer with complete similarity. One difficulty is the restriction on the lateral scale of turbulence that we can achieve in the wind tunnel. When we observe an atmospheric surface

layer with stable stratification, we see a meandering motion where the wave length may be tens of kilometers in size. These disturbances appear to be produced by mesoscale phenomena which we know little about. This results i. some uncertainty when attempting to simulate diffusion problems on a rather large scale. The outer characteristic of atmospheric shear flows we cannot simulate in the wind tunnel is that of turning of the mean wind with height near the surface of the earth. We have taken the point of view that if we can adequately simulate the turbulent diffusion in the wind tunnel then we can get a good approximation to actual conditions by superimposing the turning of the mean wind with height. These two difficulties should be studied further in both the field and the laboratory in an effort to determine how well our existing wind tunnel facilities approximate true similarity. I have been attempting to categorize problems we can successfully study in the tunnel and those we cannot. I have arrived at a tentative rule that can be used as guidance. When the scale of the flow disturbances of importance in the phenomenon we are studying is of about the same scale as the phenomenon itself modeling can be accomplished with satisfaction in the wind tunnel. This will be the situation e.g. when the fluctuating overturning moment for a large structure in the center of a city is under study. Here the major flow disturbances are created by the buildings surrounding the structure and are approximately the same size as the structure. Problems of a more basic nature in this category for which wind tunnels have contributed significant knowledge include the effects of thermal stratification and roughness on turbulence structure and diffusion in turbulent boundary layers, the effect of density stratification on stability of shear layers and the characteristics of gravity waves generated by flow of a stably stratified fluid over mountain-like geometry. Wind tunnels will probably make their greatest contribution to our knowledge of atmospheric shear flows through future systematic studies of this type. In the opposite case where the scale of the disturbances are small compared to the scale of the phenomenon under study similitude may be poor. An example of this is an effort to study the behavior of a smoke plume over an open area say ten or more kms in extent. Here the turbulence is created by the instabilities at the ground produced by the surface roughness and thermal effects on a scale small compared with the overall scale of the plume. Here the possibility for successful modeling is in doubt because the large scale disturbances which ultimately dominate the actual plume are not present in the model. Future developments in the generation and simulation of large scale turbulence in wind tunnels by use of jets, vorticity generators, moving boundaries, etc. may relax this restriction.

Prof. Scorer: In one of the early papers Dr. McPherson gave an example of the good cooperation between meteorologists and aeronautical engineers in doing research into the atmosphere. He told us that they obtained from past experience a good site to do these things where the amplitude was large and they obtained daily forecasts and expectations etc. from the forecasters. Now this kind of cooperation does not extend very far beyond the realm of aeronautical engineering. Dr. Clark was one of the very few people who took his laboratory experiments and had a theory which worked for them and applied it to the actual measurements in the atmosphere, and he obtained extremely good results. We can feel some confidence now that we understand something more about those mechanisms. These people who are working in a realm of the atmosphere where the meteorological information is relatively good are well off. We can put up soundings, can lay on aircraft and make measurements and nobody else is bothered about what goes on in that piece of the atmosphere. But, when we come to the lowest thousand feet particularly over cities we find that the measurements are very very few in far between and this is where we need now much more detail. And strangely enough it is the aviation authorities that prevent us from making a lot of these observations. We must not have towers or balloons on strings near airports. It even goes further than that. The public health people in Cincinatti built beautiful radio-controlled well-instrumented toy aircraft and were going to study the pollution in Cincinatti by measuring the atmospheric stratifi-

cation. Then the aviation people stopped the whole project. This is an example of the difficulty and there are very few places where there is good instrumentation. Some people have big towers and Central Electricity Generating Board in England are using television masts now to make soundings. There are also some nice big chimneys which they can use. But, these cases are rather exceptional and I think that it would be good if people like those assembled here could put more pressure on those who might make the observations to get them made in the area where we need them to be made and this includes valleys and cities.

When one can apply theories to cases where there are plenty of measurements the results always teach us something both when the theory does work out and when it does not. But, there is often a tendency for people (and this is very evident in a journal like the Journal of Fluid Mechanics), in the last but one paragraph, just before the author makes his acknowledgements, to think up an application to the atmosphere and gaily say that this explains something or other. Of course generally this sort of rather facile explanation doesn't come off when examined carefully, and this is partly because we have not got very good observations in the region we are concerned with and partly because people who work in laboratories and with theories do not tend to work closely with people who have a long experience of the atmosphere in order to make sure that there is genuine relevance to particular phenomena.

Excessive claims are sometimes made for the use of wind tunnels and I am not going to contradict any claims when one is concerned with forces on bodies; but it is when one is concerned with diffusion problems particularly in connection with air pollution that I think the claims can be exaggerated. Most of our diffusion problems occur when the wind speeds are low and this is when the dynamicly based diffusion formulas are not valid. It is also the case which is very difficult to model accurately because of the motion associated with large stratification in the atmosphere. The atmosphere is actually quite a good laboratory itself if we learn how to use it, if we learn how to put up smoke generators, measure tracers, observe free balloons and so on. An enormous amount can be learned there.

Prof. Panofsky asked to be provoked. So, perhaps now is the time. He mentioned some books and he is a good friend of mine, so I assume from the fact that he didn't mention my book that he didn't know about it. So I have some reason to tell you about it now. It is called "Air Pollution". I mention this because it is really a picture book. It contains about a hundred pictures of phenomena to which I think he wants the attention to be drawn. The point of mentioning this is because he did mention books and I think the list ought to be complete. Now also there is a very readable pamphlet by Dr. M. Smith. This is one in which advice is given on how to think about pollution problems with reference to the motion of the atmosphere. He doesn't tell you to use a certain formula, he says certain formulae have certain properties but ... and then the important stuff begins. This is concerned with the stratification of the atmosphere and topographical and other small scale effects. Hans Panofsky also mentioned the Stockholm conference. One of the most interesting ways of making soundings in the atmosphere, without actually going there, that came out in this conference was by beaming sound waves upwards using a sort of sonar. He exploits the fact that layers with large stratification give a measurable reflection when contorted by some sort of turbulence and this is a very cheap sort of instrument. It doesn't require a large amount of technology or maintenance. The author was A. R. Mahoney (Weapons Research Establishment, Salisbury, South Australia). It is a very useful technique which I think more people should know about.

Now there are two final points: one is that we need more liaison with practical meteorologists and I mention this because this conference is composed mostly of people in rather specialist institutions, research institutions and universities. But, the people who

actually do the job, particularly in connection with air pollution, are probably not here - public health inspectors, architects, civil engineers etc. and they have to botch things up as best as they can. I think, we ought to remember their jobs when we are pontificating and saying how things ought to be done, we ought to seek to help them in making practical decisions. It is not for us to tell them in detail what to do, and fortunately the enormous variations in the atmospheric behavior prevent us from giving them instructions. (Otherwise the world would become a terrible buresucracy). The detailed decisions ought to be made on the spot by the local man and we should give him a better idea how to do it. That is one task. The other striking thing about this conference was that there was a very great non-uniformity in the level of technical knowledge assumed by the authors, and this varied according to what aspect of the subject we were dealing with. I am not criticising anybody, I am just remarking on this fact. For example Hans Panofsky gave a very nice elementary treatment, which I hope I knew most of, but I thought that he was quite right in doing it in that way because most people here do not know this part of dynamical meteorology. On the other hand many papers started at such a high technical level that many people may have been afraid of asking questions at all about some of the basic assumptions. When I asked Dr. F.B. Smith a question somebody behind me muttered: "Schlichting page 224", as if to imply "you had better go and do your homework before asking silly questions". On the other hand I could have said "Scorer page 2" in answer of one of the other questions asked. We have a genuine difficulty here, in knowing how universal is the knowledge that we take for granted. I spend much time teaching mathematicians who are going to become experts in fluid mechanics and we have this problem of deciding how much meteorology, how much Kolmogorov, how much Monin-Obukhov and how much of all these things they ought to know. I don't think anybody can give answers here but, I think it is something we ought to think more about. A civil engineer can say something about public relations, labor relations, economics etc. But does he know any of the kind of meteorology that we have been talking about? Does he know how to use the local forecasting office when operating on a construction site? I rather suspect that there is not enough liaison between such people and that partly our education system is at fault in not teaching people those aspects which used not to be very important, but which are now evidently becoming more important.

References: "Air Pollution" by R.S. Scorer, Pergamon Press, Oxford 1968.

"Recommended Guide for the Prediction of Dispersion of Airborne Effluents" edited by Maynard Smith (Brookhaven National Laboratories). Published by the American Society of Mechanical Engineers, United Engineering Center, 345 East 4th Street, New York N.Y. 10017. U.S.A.

Mr. Scruton: As the last in the line I must be careful not to repeat what some of the previous speakers have said. My impression of this meeting is that we have had from the meteorologists some very interesting and detailed papers. But, I am not yet sure how information they give is going to fit into the standard pattern or structure of the wind which engineers want to use in structural design. Engineers really need statistical averages and probabilities of maximum winds, the speed and spectra and correlations etc. occuring over certain period of time, say e.g. the life-time of the structure. With regard to Dr. Scorer's point about the liaison between meteorologists and structural engineers it should be noted that in England about 9 or 10 years ago engineers had to set up their own research station to get the information on the wind structure which they wanted. I don't think meteorology as carried out in England by public bodies would necessarily give the information engineers want. Of course, engineers are very keen on getting this information over cities and all the difficulties which Dr. Scorer pointed out are very evident. He mentioned the sonar-radar-technique as a possibility method of making these measurements and I would like to suggest that

perhaps the Doppler-laser-technique might also provide a suitable means of obtaining wind structure over cities. As structural engineers we are concerned with the aerodynamics of bluff bodies and this is almost an open book, very little is as yet known and there is very good opportunity here for aerodynamicists to work on very important problems. We want to know the effects of turbulence and shear on the mean airflows over bluff bodies and also to be able to assess the aerodynamic admittance of bluff bodies in atmospheric shear flows. Aerodynamic stability properties are also influenced by shear and turbulence, and also by the amplitude of oscillation. Of course this requires methods in wind tunnels for representing the shear flows. Here again there is wide scope for ingenuity in research. Dr. Scorer said most of the present methods in use are not satisfactory. Well, I think there are opportunities here for producing something which is more satisfactory. The change of wind direction with height which Prof. Cermak mentioned may not be so important in regard to tall structures because most of the energy which causes the structure to oscillate comes from the top third of the structure and there probably is not very much change in wind direction with height on the top third of the tall structure. I was very interested in Prof. Cermak's remark during his talk about the possibility of simulating turbulent flows with laminar flows by equating the Reynolds number of the laminar flow using the kinematic viscosity, to that of turbulent flow using the eddy viscosity. Many years ago we used to carry out flow experiments over landscapes at very low wind velocities. We had little confidence in the results but if with the relationship suggested by Prof. Cermak we might have been doing better than we knew.

Another aspect is the provision of high Reynolds number facilities. If we are dealing with sharp-edged bodies perhaps this does not matter quite so much but with certain structures it is certainly important to have methods of reproducing flows at high Reynolds numbers. It was not mentioned at this meeting, but there is some possibility in the suggestion made by Mr. Armitt of the Central Electricity Research Laboratory in which he relates the flow over round bodies to the roughness Re-number of the surface rather than to the Re-number itself as we know it. This suggestion appears to be supported and confirmed by experiment.

Mr. Antonatos: Do any of the speakers care to comment on the ability of predicting phenomena that is a short-term prediction applicable to flying aircraft to be able to avoid certain conditions that could lead to catastrophical events? Of course you know we talked about the various shear conditions and transfer of momentum, certain approaches to stationary buildings and the buildings do have an advantage, they stay there and you can design for certain conditions but for aircraft, because there is limited structural capability, you try to avoid certain conditions that can occur and even now by looking at certain cloud formations e.g. that are set up by various wave phenomena. Can you predict to any reasonable accuracy a turbulent condition or a sheer condition that could lead to catastrophic failure in the aircraft so that the aircraft in a short time can avoid it?

Prof. Scorer: As with almost all forecasting jobs people learn and get better at it by experience and what I would say is that if you hope ever to have people who can do this kind of forecast you have got now to make people try to do it. Some are trying, and they are getting better at it and their limitations are fairly well known by airline pilots. Pilots send information and succeeding aircrafts on the same route get to know this pretty quickly, and there is pretty good liaison with aviation forecasters. But essentially this is a thing which people learn to do by trying to do it. They discover more about the gaps in their knowledge by trying. I think nobody is entitled to make any promises but, I feel pretty certain that the forecasting of this will get better in the next 10 years. As aircraft fly higher we have to learn more about the differences between the new layers that

have been frequently flown in and the old ones you know quite a lot about.

Prof. Panofsky: A couple of weeks ago at the London meeting, there was a speech by a gentleman named Lorens about predictability generally in the atmosphere, and he came out with a statement which I think can be proven: the larger the phenomenon the more predictable it is. One of the most difficult things to predict is the change of wind in the next two minutes, which is due to very small eddies. Such predictions are important for certain applications to rockets. To predict a rather small-scale effect like an individual turbulent breakdown is extremely difficult. I would have said that what we are getting pretty good at doing is to point out certain general regions in which clear air turbulence is going to be very much of a problem, and to estimate its probability. And as Dr. Scorer mentioned, if some other plane has been around before and had trouble then you probably have trouble also.

Dr. Roach: My question is mainly directed to Prof. Cermak and Prof. Scorer and it concerns laboratory simulation of free shear flows with particular reference to the study of clear air turbulence mechanisms. We have seen the elegant experiments of Dr. Clark here, and the work of Woods has also been mentioned. Now, I would like to ask the panel in what direction do they think such studies should now go?

Prof. Cermak: I believe the study of Dr. Clark has given us considerable basic information on the mechanism but, the problem still will be to predict when the conditions are right for these mechanisms to occur in the atmosphere. The basic philosophy I have in this particular area is the following: whenever we have a flow problem which we wish to relate to the atmosphere we should encourage more field studies and examination of the actual phenomena in the atmosphere. There are some studies being undertaken in Japan with instrumentation suspended from a helicopter. Very fine resolution is being obtained in the density and the velocity structure. Critical structures are observed and the resulting instabilities are being studied . I think further studies along this line would be very revealing. Studies in the laboratory along the line of Dr. Clark's work and perhaps some studies in the wind tunnel to determine the volume of turbulent fluid produced by breakdown of an unstable shear layer and the way in which the spectra of turbulence varies after breakdown would be useful.

Prof. Scorer: I think there are two points here. One is that we can say now that if the motion is strictly 2D then it will break down in the form of these overturning billows. The theoreticians should be invited to answer the question: does it break down in another manner when the motion is not strictly 2D? Is there any other way that the laminar horizontal flow can begin to break down other than by turning over in rolls in this way? I don't think there is in the free atmosphere if the flow is strictly 2D. So this is a theoretical challenge. Along with this we need to investigate more 3D problems in laboratory experiments too. Dr. Roach didn't mention the beautiful experiments of Dr. Thorpe. These are absolutely superb. They are again 2D.

Now to the other point. It seems likely that a 2D theory has really got the essentials of the mechanism, because we know that 2D motions are more unstable than 3D ones, so that in a situation where the motion is 3D, the bits which break down are likely to be like the 2D motion. But I don't know whether this is certain. The more important question is, how do we get to the state where the motion is ready to break down? With a layer of large static stability or a layer with rather large shear we know whereabouts they will break down in a mountain wave or a frontal surface which produce modifications in their structure to make it unstable. What we need now is to look one stage further back and see how we get to the previous stage. What are the mechanisms for generating layers of large static stability? What are the mechanisms for producing shear layers other than by large static stability?

There are many possible mechanisms and I think there will be several of these all feeding the billow mechanism. That is where I think the research should be directed.

Dr. Hunt: I should first like to apologize for the insulting reference to Schlichting! Secondly I should like to address a question to Prof. Cermak who put his finger on the interesting methodological problem which is whether we should look at the problems of turbulent flow round buildings, and turbulent flow over aircraft near the ground, in a deterministic or probabilistic kind of way. It certainly seems to be the trend amongst the people interested in structures, as Mr. Scruton pointed out this morning, to go for the statistical sort of approach, in which little is done to examine the tail of the probability density distribution of velocity or pressure. But the other day I visited the Royal Aircraft Establishment of Bedford in England and was intrigued to find that there the approach of the engineers, who are trying to predict sudden loads on aircraft caused by gusts near the ground, is to look at UV-traces of turbulence and from the trace of big gusts, attempting to calculate their structure. Thus, by this semi-deterministic method they claim (this is Mr. Jones) that you can construct models of the kind of gust that occurs in the tail of the probability distribution function. One might describe these people as "gust-imaginers". I wonder what the view of the panel is on this difference in approach between the aeronautical and structural engineers and whether such a difference occurs in other countries?

Prof. Cermak: I too had the opportunity to discuss with Drs. Burnham, Jones and McPherson the approach they are using to describe turbulent events for their gust analysis and I am in agreement with them that the distribution function for the maximum or the extreme difference in velocity fluctuations as a function of the time interval between the occurrences is important information from the standpoint of control analysis. I would try to promote this approach to not only getting information that is of use to the designer but for use in understanding the actual structure of the turbulence which the turbulence spectra hides from us.

Prof. Libby: I would like to make a comment and then ask a couple of questions that follow from the comment. First, I, as an aeronautical chap, have derived a great benefit from this meeting despite the difficulties that Mr. Scruton has mentioned; but, I think it is true that we aeronautical people have not really had a chance to make many comments about some of the matters discussed. Two questions I have really derived from things that I know about the turbulent boundary layers as they arise in aeronautical applications and the questions will be, whether or not these things are well known to the atmospheric people.

The first thing relates to the question of heterogeneity of boundary conditions, the importance of which has been impressed upon us at several occasions. I was particularly struck by Prof. Panofsky's remark that the boundary layer coming off the land and engaging the sea remembers the land for 100 kilometers. That is the number that I recall. Now in aeronautical applications it is well known that if one has a turbulent, two-dimensional and incompressible boundary layer, subjects it to a favorable pressure gradient, then to an adverse one and then to another favorable pressure gradient of the same sort that it originally had, the boundary layer on the second favorable gradient is not the same as the first one. It does in fact have a distinct memory. This sort of phenomena has led the aeronautical people to have models of turbulent transport which are not dependent upon only local conditions and I think almost everything that we heard these days concerned transport in the atmosphere depending upon only local conditions. Now the aeronautical people have cooked up "non-local" models e.g. in the U.K., I think Bradshaw's work is perhaps well known, and there is a review of these matters in Kovasznay's recent article in Physics of Fluids, the one which was a supplement reporting the results of a Japanese meeting on turbulence.

The other question of heterogeneity I would like to remark on is the problem that Prof. Cermak talked about, namely a boundary layer presumably flowing over a surface of one thermal characteristic and then entering a region of a different thermal characteristic. This is a very old problem in the aeronautical litterature and if I had to do a calculation of that problem, I would certainly refer to Spalding's work where he showed us a very good way of tackling it. So, my first question is: Are all these things well known to the atmospheric people?

The second question is as follows: the aeronautical people know very well that if they have a boundary layer flowing on a surface, there is a very distinct interface between the region which is turbulent and the region which is essentially potential flow namely the external flow. This is a highly convoluded interface usually described by so-called intermittency factor which is 1 if the flow is totally turbulent and 0 if there is no turbulence and, of course, this has some sort of a smooth curve in a boundary layer from 1 at the wall to 0 well beyond the mean location of the boundary layer thickness. Now in these days we have heard absolutely nothing about that interface and my question is: Do the atmospheric people know about it and have they observed it?

Prof. Panofsky: I can only speak for myself and not for the atmospheric people generally. I certainly know about the last thing that Dr. Libby mentioned, that is the interface between the turbulent and laminar regions and the kind of shape it has, from other meetings similar to this. Perhaps Dr. Scorer ought to talk about this later. There are a number of situations I think and one does not explain the conditions just by local situations.

Prof. Scorer: On the subject of local determinacy I think the assumption that everything is determined locally is made because the theory is quite difficult enough. In those situations where it is possible to do better than that, better has been done. I would like to say this in defense of meteorologists. I think they are very well informed on aerodynamics. If the aerodynamicists produce a technique they will try it out. In most cases where it is all determined locally as in a Monin-Obukhov type of analysis it is not practicable to do anything more complicated.

On the subject of intermittency there is a distinction here between aerodynamics and atmospheric dynamics in that we are not usually concerned with the upwind edge of things. The phenomenon of intermittency doesn't occur in the atmosphere in the same way in experimental aerodynamics. If you have a flat plate with flow on to it and you look at the edge of the boundary layer, it has this intermittancy. But it does not usually look like that in the atmosphere because there is always a turbulent boundary layer upwind, even in air arriving at the coast line. In any case we are most of the time concerned with the situation far downstream. We have the Ekman layer type of phenomenon where you have got a sort of equilibrium situation. You can measure a sort of intermittency in the atmosphere (e.g. between clouds when flying among cumulus clouds). After a period with a smooth trace you will get some turbulence, which is obviously turbulence, on entering a cloud. But, this is not the same thing as your intermittency. It is a quite different phenomenon.

Prof. Panofsky: I would like to worry a little about this last point. In the case of free air turbulence when one has these slanting shear layers one has turbulent regions and then next to it regions which are effectively edges of the turbulent layer. I would not be a bit surprised if the aerodynamics at the edge of the turbulent free shear layer, is very similar to what you have been talking about.

Prof. Libby: I don't think that I made clear to Prof. Scorer what I am talking about; the

intermittency that I am asking about has nothing to do with starting edges. If one would have a turbulent boundary layer 3000 miles long it would still have an interface between the potential flow and the flow which is interior and turbulent. It has nothing to do with the sort of intermittency that is associated with transition for example.

Prof. Scorer: I will come back on that immediately. The thing that determines the edges of turbulence in the atmosphere is usually the density stratification. It extends up to a certain level and then it meets a lid. By searching hard you might find the kind of intermittency you refer to but the external flow is not potential flow - it is stratified and contains a lot of vorticity. Perhaps Prof. Lettau has a better answer for this.

Prof. Lettau: I would like to come to the rescue of the meteorologist. If you look at a series of weather maps you find lots of pressure gradients opposing themselves. At a given point you may have today a pressure gradient from the south and tomorrow one from the north. The major difference in comparison with wind tunnel boundary layers is that ambient flow in the atmosphere is to a very good degree geostrophic and not potential flow. These facts cause quite different conditions in energetics of flow as well as of turbulent disturbances. The type of intermittency that we do have to work with in the continuous planetary boundary layer all around the world is mainly caused by changes in pressure gradient and hydrostatic stratification, from day to day, even from hour to hour, but quite different from the kind of intermittency in the wind tunnel for unchanged (controlled) driving force of the ambient flow.

Prof. Cermak: I would like to make a couple of comments in response to Dr. Libby's questions -- in reverse order from that in which they were posed. On the matter of intermittency I would like to refer to some measurements being made by one of our staff members, Prof. Sandborn with hot-wires in the atmosphere. He tells me that he observes intermittency the same as he does in the wind-tunnel boundary layers. This, I think, is comforting to know. Another factor -- I think I mentioned this as some of the basic problems that we ought to be investigating -- there is, in many instances, at the top of what we call a planetary boundary layer in the atmosphere a flow which is actually turbulent with a considerable amount of turbulent energy. Therefore, we don't have as for the ordinary aeronautical boundary layer a flow which is turbulence-free above the turbulent boundary layer. You mentioned something about the work of Dr. Spalding. I think one of the difficulties in applying Dr. Spalding's analysis to the problems we have been talking about is that in the atmosphere we are concerned with situations where the heated section of boundary may cause buoyancy forces which produce motions which are strong compared with those due to the forced convection. Therefore, the whole flow pattern becomes dependent upon the local boundary condition and the work of Spalding is no longer applicable. There was some concern about the long distance to which the land-formed boundary layer and its effects are observed out at sea. It seems to me that this may be associated with the large scale longitudinal vortices sometimes observed in boundary layers formed over land.

Prof. Panofsky: My statement about the length to which the solid ground is felt out to sea was actually based on a theory by Dr. Peter Taylor of Toronto who talked about this in England. This is not based on observations. What essentially happens is that he makes a model with a change of roughness. An internal boundary layer develops which at the beginning has a slope of about one in ten and then becomes flatter. The boundary layer is about 1 km thick and it takes about a hundred kilometres horizontally until the whole boundary layer is modified. I don't know of any observations of this.

I would like to come back to the other question of intermittency and that is really

ng along with what Dr. Cermak said before. There is a definite situation when one gets a y definite lid on a turbulent layer, and that is under stable conditions when the Richard- number near the ground is quite small and increases with height. So, somewhere between or 40 metres the Richardson number becomes critical. You can see this in terms of dis- sion under these conditions; contaminants from a ground source disperses vertically, but se from an elevated source do not disperse vertically. So there is actually a fairly rp boundary between the subcritical Richardson number flow and the supercritical Richard- number laminar flow. In this region there is indeed intermittency, as shown e.g. in a ent paper by Slade in Journal of Applied Meteorology.

. Korkegi: My question is directed to Prof. Cermak and concerns his laminar modeling of e atmospheric turbulent shear layer. This model looks quite clever of course and I would ke to compliment Prof. Cermak for it. In the laminar Reynolds number you have the kinema- viscosity and in the corresponding turbulent Reynolds number you have the eddy viscosity. , roughly speaking, the kinematic viscosity will barely vary across the layer assuming nsity and temperature variations a small, but the eddy viscosity varies considerably. I wonder if you can comment on discrepancies in the modeling due to this difference in scosity variation.

of. Cermak: I am glad you brought up this subject because unfortunately there was not ally time enough to go into much detail. I would like to point out that this type of mo- ling certainly does not represent a universally good approximation. This type of modeling appropriate only if we consider the ratio of the integral scale of turbulence to a re- rence length of the obstacle, say a mountain, to be of the same order of magnitude as the tio of the mean-free-path length (molecular tion in the model fluid) to the scaled down ference length of the model. In a sense we are considering the turbulent atmosphere to be- ve as a sticky fluid grossly approximated by a constant eddy viscosity. Therefore, I would ain caution that this appears to be a useful concept only when the mean flow field is domi- ted by the boundary geometry, i.e., a mountain-valley-complex under stably stratified at- spheric conditions. In other words, this concept is appropriate only if spatial variation the mean flow field in the horizontal is more intense than in the vertical direction.

. Korkegi: There is still the mountain or the building that would be a perturbation in- de of a boundary layer. So whereas the local Reynolds number in a laminar boundary layer uld be made to match the local turbulent Reynolds number in the atmosphere at correspon- ng points within the layers, the Reynolds number equivalence will no longer hold and there ll be considerable departure within the respective shear layers away from this point. So, en though one might take the local Reynolds numbers to be equivalent based on the size of e di rbance or the roughness -- mountain or building for the atmospheric layer -- , they ll not be equivalent as one goes up into the atmospheric shear layer. I think there is me question as to how good the matching really is.

of. Scorer: I am very much in sympathy with Prof. Cermak's idea but please people must t think that we are naive about it. The point is that when you do these experiments you e not looking on those occasions for a very precise quantitative answer. We are looking r qualitative enlightenment and if you can make mechanisms visible which are not visible the ll scale you have a better chance a) of understanding the qualitative way and b) setting up the right equations for them by making the right sort of assumptions subse- ently.

. Korkegi: In answer to Prof. Scorer, I am not questioning the desirability of modeling e atmosphere in a wind tunnel; but rather, the technique. It is somewhat doubtful to me

that the equivalence provided by laminar modeling is any better than that provided by a turbulent boundary layer even though its Reynolds number is much smaller than that of the atmosphere.